

*N73-27176*

JSC 08021.  
Contract NAS9-13027

*CR -133964*

Final  
Report

June 1973

---

**Attached  
Manipulator  
System Design  
and Concept  
Verification for  
Zero-g Simulation**

**CASE FILE  
COPY**

**MARTIN MARIETTA**

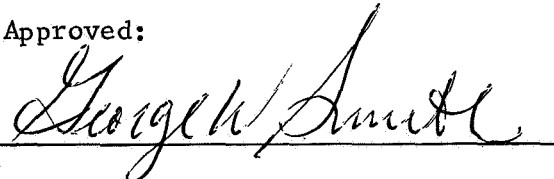


ATTACHED MANIPULATOR SYSTEM  
DESIGN AND CONCEPT VERIFI-  
CATION FOR ZERO-G SIMULATION

R. Booker	F. Greeb
W. Burkitt	C. Johnson
P. Corveley	G. Kyrias
P. Cramer	J. Lazar
O. Duwaik	D. Lorenz
C. Flatau	D. Rittenhouse
P. Garber	R. Skidmore
C. Grant	J. Yatteau

Shepard B. Brodie  
Program Manager

Approved:



GEORGE W. SMITH, Manager  
Manned Experiments & Life Sciences

MARTIN MARIETTA CORPORATION  
P. O. Box 179  
Denver, Colorado 80201



## FOREWORD

This document presents the results of work performed by the Martin Marietta Corporation while under contract to NASA L. B. Johnson Space Center. This final report was prepared as partial fulfillment of Contract NAS9-13027, Attached Manipulator System Design and Concept Verification for Zero-G Simulation. The NASA Technical Monitor for the contract was Mr. Richard B. Davidson, of the Spacecraft Design Division, Engineering Technology Branch.



## CONTENTS

---

	<u>Page</u>
I. INTRODUCTION AND SUMMARY. . . . .	I-1
II. DESIGN REQUIREMENTS . . . . .	II-1
A. Characteristics and System Description. . . . .	II-1
B. Manipulator Trajectory Definition . . . . .	II-5
C. Manipulator Reach Capabilities. . . . .	II-23
III. SERVO DESIGN OF A 2-DEGREE OF FREEDOM X REFERENCE FRAME BILATERAL FORCE REFLECTING POSITION-POSITION CONTROL SYSTEM	
A. Control Law Equations . . . . .	III-1
B. Servo System Design . . . . .	III-71
C. Test Results. . . . .	III-102
IV. MANIPULATOR . . . . .	IV-1
A. Joints. . . . .	IV-1
B. Counterbalance Analysis and Optimization. . . . .	IV-61
C. Counterbalance Linkage. . . . .	IV-83
D. Overall Manipulator Design. . . . .	IV-104
V. CONTROL DEVICES . . . . .	V-1
A. Existing Human Factors Controller Data. . . . .	V-4
B. Controller Design Evaluations . . . . .	V-27
C. Recommendations and Conclusions . . . . .	V-53
VI. DYNAMICS. . . . .	VI-1
A. Rigid Body Analysis . . . . .	VI-2
B. Vibration Analysis. . . . .	VI-16
C. Nonlinear Flexible Body Analysis. . . . .	VI-31
D. Summary and Recommendations . . . . .	VI-42
E. References. . . . .	VI-44
APPENDICES	
A. Derivation of the Rigid Body Equation of Motion. . . . .	A-1
B. 7 DOF Joint Ordering Breadboard . . . . .	B-1
C. Video Synthesizer . . . . .	C-1
D. Breadboard Digital Program. . . . .	D-1
E. Manipulator Trajectory Data . . . . .	E-1
F. Mechanical Design of Bilateral Breadboard . . . . .	F-1



# Figure

I-1	AMS Technology Questions. . . . .	I-2
II-1	AMS With Articulated Counterbalance . . . .	II-3
II-2	Simulator Layout, Payload Deployment and Stowage . . . . .	II-4
II-3	One-Eighth Scale Shuttle and Manipulator Mockup. . . . .	II-6
II-4	Scale Model Manipulator Configuration . . .	II-7
II-5	Capture Concept 1 - Down Shuttle Centerline	II-9
II-6	Capture Concept 1 - Down Shuttle Centerline	II-10
II-7	Capture Concept 2 - Over Wing . . . . .	II-12
II-8	Capture Concept 2 - Over the Wing . . . . .	II-13
II-9	Capture Concept 3 - Vertical Over Shoulder Centerline. . . . .	II-14
II-10	Capture Concept 3 - Vertical Over Shoulder Centerline. . . . .	II-15
II-11	Capture Concept 4 - Across Cargo Bay. . . .	II-16
II-12	Capture Concept 4 - Across Cargo Bay. . . .	II-17
II-13	Capture Concept 5 - Across Manipulator Shoulder. . . . .	II-18
II-14	Capture Concept 6 - Across Pilot Station. .	II-19
II-15	Capture Concept 7 - Across Pilot Station. .	II-20
II-16	Cargo Deployment. . . . .	II-22
II-17	Maximum Joint Movements for 7 Capture Con- cepts (6-DOF Slave) . . . . .	II-24
II-18a	Cargo Bay Levels. . . . .	II-25
II-18b	Manipulator Reach Zones . . . . .	II-26
II-18c	Manipulator Reach Zones . . . . .	II-27
II-19a	Docked Satellite Reach Envelopes. . . . .	II-29
II-19b	Docked Satellite Reach Envelopes (Two Manipulators) . . . . .	II-30
II-20	Module Replacement. . . . .	II-32
III-1	Two Way Information Flow in Bilateral Force Reflecting Manipulator System . . . . .	III-2
III-2	Bilateral Force Reflecting Manipulator With One to One Joint Coupling . . . . .	III-3
III-3	Master and Slave Operating in Two Different Axis Systems. . . . .	III-5
III-4	X Reference Frame Position-Position Bi- lateral Force Reflecting Control System . .	III-7
III-5	Two DOF Master and Slave Breadboard Arms. .	III-9
III-6	Control System for Two DOF Breadboard . . .	III-10
III-7	Joint Angles and Tip Position Labelling for Master. . . . .	III-11
III-8	Master Torques and Forces at Equilibrium. .	III-15



III-9	Equilibrium Torques and Forces on Master Upper Segment. . . . .	III-16
III-10	Equilibrium Torques and Forces on Master Lower Segment. . . . .	III-17
III-11	Two Axis System Showing Derivation of Coordinate Transformation Matrix . . . .	III-22
III-12	Master Shoulder Servo System . . . . .	III-29
III-13	Piecewise Linearized $S(X(1))$ Function Around Origin. . . . .	III-33
III-14	Linearized Form of Master Shoulder Servo Loop . . . . .	III-34
III-15	Master Elbow Servo System. . . . .	III-36
III-16	Linearized Form of Master Elbow Servo Loop	III-37
III-17	Slave Shoulder Servo System. . . . .	III-38
III-18	Linearized Form of Manipulator Shoulder Servo Loop . . . . .	III-39
III-19	Slave Elbow Servo System . . . . .	III-40
III-20	Linearized Form of Manipulator Elbow Servo Loop . . . . .	III-41
III-21	Schematic of Two Degree of Freedom Breadboard Arms . . . . .	F-2
III-22	Gearing Characteristics of Two DOF Breadboard Arms . . . . .	F-8
III-23	Weight Summary of Two DOF Breadboard Arms	F-13
III-24	Backdrive Characteristics of Breadboard Arm Joint. . . . .	F-14
III-25	Forward and Backdrive Characteristics of Breadboard Arm Joint . . . . .	F-15
III-26	Pan and Air Bearing Design . . . . .	F-17
III-27	Two DOF Manipulator with Air Bearing Load . . . . .	III-72
III-28	Bode Plots of Uncompensated Open Loop Linearized Master Shoulder Servo Systems	III-78
III-29	Bode Plots of Compensated Open Loop Linearized Master Shoulder Servo Loop. .	III-79
III-30	Bode Plots of Compensated Open Loop Linearized Master Shoulder Servo System with 60 hz Notch Filter. . . . .	III-81
III-31	Compensated Master Shoulder Linearized Servo Subsystem. . . . .	III-80
III-32	Bode Plots of Uncompensated Open Loop Linearized Master Elbow Servo System . .	III-84
III-33	Bode Plots of Compensated Open Loop Linearized Master Elbow Servo System . .	III-85
III-34	Bode Plots of Compensated Open Loop Linearized Master Elbow with 60 hz Notch Filter . . . . .	III-87

III-35	Compensated Master Elbow Linearized Servo System. . . . .	III-88
III-36	Bode Plots of Uncompensated Open Loop Linearized Slave Shoulder Servo System. .	III-90
III-37	Bode Plots of Compensated Open Loop Linearized Slave Shoulder Servo System. .	III-91
III-38	Bode Plots of Compensated Open Loop Linearized Slave Shoulder Servo System with hz Notch Filter. . . . .	III-92
III-39	Compensated Slave Shoulder Linearized Servo Subsystem . . . . .	III-94
III-40	Bode Plots of Uncompensated Open Loop Linearized Slave Elbow Servo System . . .	III-97
III-41	Bode Plots of Compensated Open Loop Linearized Slave Elbow Servo System . . .	III-98
III-42	Bode Plots of Compensated Open Loop Linearized Slave Elbow Servo System with 60 hz Notch Filter. . . . .	III-100
III-43	Compensated Slave Elbow Linearized Servo Subsystem . . . . .	III-101
III-44	Force Reflecting Ratio, Configuration 1 .	III-105
III-45	Force Reflecting Ratio, Configuration 2 .	III-106
III-46	Force Reflecting Ratio, Configuration 3 .	III-107
III-47	Force Reflecting Ratio, Configuration 4 .	III-108
III-48	Force Reflecting Ratio, Configuration 5 .	III-109
III-49	Compliance, Figure 1. . . . .	III-110
III-50	Compliance, Figure 2. . . . .	III-111
III-51	Tracking - Part A, Figure 1 . . . . .	III-113
III-52	Tracking - Part A, Figure 2 . . . . .	III-114
III-53	Tracking - Part A, Figure 3 . . . . .	III-115
III-54	Tracking - Part A, Figure 4 . . . . .	III-116
III-55	Tracking - Part A, Figure 5 . . . . .	III-117
III-56	Tracking - Part A, Figure 6 . . . . .	III-118
III-57	Tracking - Part A, Figure 7 . . . . .	III-119
III-58	Tracking - Part A, Figure 8 . . . . .	III-120
III-59	Tracking - Part A, Figure 9 . . . . .	III-121
III-60	Tracking - Part A, Figure 10 . . . . .	III-122
III-61	Tracking - Part B, Figure 1 . . . . .	III-123
III-62	Tracking - Part B, Figure 2 . . . . .	III-124
III-63	Tracking - Part B, Figure 3 . . . . .	III-125
III-64	Tracking - Part B, Figure 4 . . . . .	III-126
III-65	Tracking - Part B, Figure 5 . . . . .	III-127
III-66	Tracking - Part B, Figure 6 . . . . .	III-128
III-67	Tracking - Part B, Figure 7 . . . . .	III-129
III-68	Tracking - Part B, Figure 8 . . . . .	III-130
III-69	Tracking - Part B, Figure 9 . . . . .	III-131
III-70	Breadboard Manipulator with Maze Test Board . . . . .	III-139

IV-1	Harmonic Drive Concept. . . . .	IV-4
IV-2	Harmonic Drive, USM Model 8M. . . . .	IV-6
IV-3	Spur Gear Drives - Schematics . . . . .	IV-7
IV-4	External Drive Breadboard Design. . . . .	IV-8
IV-5	Internal Drive Breadboard Design. . . . .	IV-9
IV-6	Joint Breadboard Test Set-up. . . . .	IV-11
IV-7	External Drive Under Low-Load Test. . . . .	IV-15
IV-8	Internal Drive Under Low-Load Test. . . . .	IV-16
IV-9	Harmonic Drive-Static Breakaway Torques . . . . .	IV-18
IV-10	External Drive-Static Breakaway Torques . . . . .	IV-19
IV-11	Internal Drive-Static Breakaway Torques . . . . .	IV-20
IV-12	Static Breakaway Efficiencies . . . . .	IV-21
IV-13	Torsion Deflection of Three Drives. . . . .	IV-22
IV-14a	External Drive Under Low Load Dynamic Test	IV-24
IV-14b	Test Set-up-Harmonic Drive During Accel- eration Test. . . . .	IV-25
IV-15a	Harmonic Drive-Dynamic Torque Losses. . . . .	IV-27
IV-15b	External Drive-Dynamic Torque Losses. . . . .	IV-28
IV-15c	Internal Gear Drive-Dynamic Torque Losses . . . . .	IV-29
IV-15d	Harmonic Drive-Torque Losses. . . . .	IV-30
IV-15e	External Drive-Friction and Inertia Torque Losses. . . . .	IV-31
IV-15f	Internal Gear Drive-Torque Losses . . . . .	IV-32
IV-16	Gear Ratio vs Peak Power, 1200 ft 1b Gear Assembly. . . . .	IV-39
IV-17	Gear Ratio vs Output Speed, 1200 ft 1b Gear Assembly . . . . .	IV-39
IV-18	Duty Cycle vs Motor Torque, 1200 ft 1b Gear Assembly . . . . .	IV-40
IV-19	Gear Ratio vs Friction, 1200 ft 1b Gear Assembly. . . . .	IV-40
IV-20	Gear Ratio vs Joint Weight, 1200 ft 1b Gear Assembly . . . . .	IV-41
IV-21	Gear Ratio vs Reflected Inertia, 1200 ft lbs Gear Assembly . . . . .	IV-41
IV-22	Maximum Speed vs Sensitivity. . . . .	IV-44
IV-23	Maximum Speed vs Weight . . . . .	IV-44
IV-24	Maximum Speed vs Ripple . . . . .	IV-45
IV-25	Maximum Speed vs Breakaway Torque . . . . .	IV-45
IV-26	Gear Ratio vs Peak Power, 650 ft 1b Gear Assembly. . . . .	IV-48
IV-27	Gear Ratio vs Output Speed, 650 1b Gear Assembly. . . . .	IV-48
IV-28	Duty Cycle vs Motor Torque, 650 ft 1b Gear Assembly . . . . .	IV-49
IV-29	Gear Ratio vs Friction, 650 ft 1b Gear Assembly. . . . .	IV-49



IV-30	Gear Ratio vs Joint Weight, 650 ft lb Gear Assembly . . . . .	IV-50
IV-31	Gear Ratio vs Reflected Inertia, 650 ft lb Gear Train . . . . .	IV-50
IV-32	Gear Ratio vs O.D., 650 ft lb Gear Assem- bly . . . . .	IV-51
IV-33	AMS Shoulder Pitch Joint Assembly . . . .	IV-54
IV-34	AMS Shoulder Roll Joint Assembly. . . . .	IV-57
IV-35	AMS Elbow Yaw Joint Assembly. . . . .	IV-59
IV-36	Articulated Counterbalance Concept. . . .	IV-61
IV-37	Four Body AMS Model . . . . .	IV-63
IV-38	Counterbalanced AMS . . . . .	IV-66
IV-39	Counterbalanced AMS Components. . . . .	IV-68
IV-40	Yoke Size Constraints . . . . .	IV-71
IV-41	Counterbalance - Shoulder Clearance . . .	IV-74
IV-42	Counterbalance Dimensions . . . . .	IV-78
IV-43	Increase in Moment of Inertia . . . . .	IV-79
IV-44	Yoke Dimensions . . . . .	IV-80
IV-45	Counterbalance Design Selection . . . . .	IV-81
IV-46	Counterbalance Selection vs Wrist Weight.	IV-82
IV-47	Counterbalance Linkage Concepts . . . . .	IV-86
IV-48	Multi-Cable Test Set-up at Full Load Condition . . . . .	IV-87
IV-49	Starting Torque vs Load Torque. . . . .	IV-88
IV-50	Counterbalance Bar Linkage Concept. . . .	IV-90
IV-51	Four-Bar Test Set-up With Load. . . . .	IV-91
IV-52	Four Bar with Counterweight . . . . .	IV-92
IV-53	Four Bar Test Set-up Showing Crank Assem- bly . . . . .	IV-93
IV-54	Test Set-up of Counterbalancing System. .	IV-94
IV-55	Trip Bar Counterbalancing Breadboard Test Set-up . . . . .	IV-96
IV-56	Closeup View of the Cranking Mechanism of a Triple Bar Counterbalancing Breadboard.	IV-97
IV-57	Friction Variation with Arm Position. . .	IV-98
IV-58	Typical Bearing Data. . . . .	IV-98
IV-59	Breakaway Torque Losses . . . . .	IV-99
IV-60	Selected Three Bar Counterbalance Linkage Scheme. . . . .	IV-100
IV-61	Three Bar Counterbalance Geometry and Loads . . . . .	IV-101
IV-62	Typical Double Shear Pin Connection . . .	IV-103
IV-63	Attached Manipulator System (AMS) "Slave" Assembly. . . . .	IV-105
IV-64	AMS Manipulator Model Fully Extended. . .	IV-107
IV-65	AMS Manipulator Model with Yoke Mounted in Vertical Position. . . . .	IV-108

IV-66	AMS Manipulator Model with Yoke Mounted in Horizontal Position. . . . .	IV-109
IV-67	AMS Manipulator Model Counterbalance. . .	IV-110
IV-68	AMS Manipulator Model Showing Counterbalance Linkage Cabling at Elbow. . . . .	IV-111
IV-69	AMS Manipulator Model Terminal Device . .	IV-112
V-1	Manipulator Controller Development. . . .	V-3
V-2	Anthropometry of Flying Personnel . . . .	V-5
V-3	Arm Reach Envelopes . . . . .	V-8
V-4a	Arm Positions and Directions of Movement, Side View . . . . .	V-10
V-4b	Arm Positions and Directions of Movement, Top View. . . . .	V-10
V-5	Maximum Push and Pull Force . . . . .	V-13
V-6	Pilots Average Arm Movements. . . . .	V-15
V-7	"Difference limens" for various control types . . . . .	V-19
V-8	Average Error in Degrees. . . . .	V-21
V-9	Controller Nonlinearities . . . . .	V-23
V-10a	Elbow Type 6 DOF Position Controller. . .	V-36
V-10b	Elbow Type 6 DOF Position Controller. . .	V-37
V-11a	6 DOF Vertical Slider Position Controller	V-39
V-11b	6 DOF Vertical Slider Position Controller	V-40
V-12	Controller Mockups. . . . .	V-44
V-13	6 DOF Elbow Type Controller Movement Volume. . . . .	V-45
V-14	Elbow Type Position Controller. . . . .	V-46
V-15	Replica Stiction Force Ratio. . . . .	V-47
V-16	6 DOF Sliding Base Position Controller. .	V-49
V-17a	6 DOF Vertical Slider Position Controller Front Mounted . . . . .	V-54
V-17b	6 DOF Vertical Slider Position Controller Side Mounted. . . . .	V-55
V-18	Sliding Base Controller, Top View . . . .	V-50
V-19	6 DOF Slider (Vertical) Bilateral Con- troller . . . . .	V-56
V-20	Controller Hand Grip. . . . .	V-29
VI-1	Rigid Body Payload Deployment Task. . . .	VI-7
VI-2	Payload Velocity and Shoulder Pitch Accel- eration for 3 Min. Task Time and 2 ft Stopping Distance . . . . .	VI-9
VI-3	Shoulder Pitch Rate and Angle for 3 Min. Task Time and 2 ft Stopping Distance. . .	VI-10
VI-4	Shuttle Pitch Rate and Angle. . . . .	VI-11
VI-5	SAMS Joint Torques. . . . .	VI-12
VI-6	AMS Joint Torques . . . . .	VI-13
VI-7	Joint Torques vs Stopping Distance. . . .	VI-14
VI-8	Joint Torque Selection. . . . .	VI-15
VI-9	Mathematical Model of Structural Elements	VI-17
VI-10	Normalized Mode Shapes, AMS Loaded and Extended. . . . .	VI-23

VI-11	Normalized Mode Shapes, AMS Unloaded and Extended. . . . .	VI-24
VI-12	Uncoupled Vibrational Analysis Structural Model . . . . .	VI-27
VI-13	Frequencies and Modes of Upper Arm. . . . .	VI-28
VI-14	Frequencies and Modes of Lower Arm. . . . .	VI-29
VI-15	Payload Handling Task for Rigid/Flexible AMS Comparison. . . . .	VI-34
VI-16	Payload Trajectory for Rigid and Flexible AMS . . . . .	VI-35
VI-17	Payload X Position vs Time. . . . .	VI-36
VI-18	Payload Y Position vs Time. . . . .	VI-38
VI-19	Rigid and Flexible AMS Shoulder Torque Requirement . . . . .	VI-39
VI-20	Rigid and Flexible AMS Elbow Torque Requirement. . . . .	VI-40
VI-21	Rigid and Flexible AMS Wrist Torque Requirement. . . . .	VI-41
A-1	Generalized AMS Model. . . . .	A-2
A-2	Augmented Body 2 . . . . .	A-5
A-3	Reference Frames . . . . .	A-10
B-1	Joint Ordering Mechanism . . . . .	B-5
B-2	Joint Ordering Mechanism as a Master Controller . . . . .	B-6
B-3	Telescoping 6 DOF Controller (Modified from 6 DOF Joint Ordering Mechanism) . . . .	B-7
C-1	Color Video Monitor Displays . . . . .	C-4
C-2	Video Synthesizer Block Diagram. . . . .	C-5

# Table

II-1	Joint Design Characteristics. . . . .	II-1
II-2	Static Deflections. . . . .	II-2
III-1	Definition of Variable Names Appearing in Figure III-6. . . . .	III-12
III-2	Motor Characteristics . . . . .	III-73
III-3	Gear Train Ratio. . . . .	III-74
III-4	Inertia Properties. . . . .	III-74
III-5	Bandwidth Measurements, Unloaded, MM = 1/2. .	III-133
III-6	Bandwidth Measurements, Unloaded, MM = 1/4. .	III-133
III-7	Bandwidth Measurements, Unloaded, MM = 1/8. .	III-134
III-8	Bandwidth Measurements, Loaded, MM = 1/2. . .	III-134
III-9	Bandwidth Measurements, Loaded, MM = 1/4. . .	III-135
III-10	Bandwidth Measurements, Loaded, MM = 1/8. . .	III-135
III-11	Sample Rates, Unloaded, MM = 1/2. . . . .	III-136
III-12	Sample Rates, Unloaded, MM = 1/8. . . . .	III-136
III-13	Sample Rates, Unloaded, MM = 1/4. . . . .	III-137
III-14	Maze Task Times . . . . .	III-140
IV-1	Measured and Calculated Joint Data. . . . .	IV-13
IV-2	Sample Data Sheet - Static Tests. . . . .	IV-14
IV-3	Sample Data Sheet - Dynamic Test. . . . .	IV-23
IV-4	Mass Moment of Inertia. . . . .	IV-26
IV-5	Input Data for Counterbalance Optimization Computer Program. . . . .	IV-75
IV-6	Evaluation of Alternative Methods in Counter- balance Linkage Methods . . . . .	IV-85
V-1	Arm Strength in Pounds. . . . .	V-11
V-2	Grip Strength & Endurance . . . . .	V-14
V-3	Angular Torque (in./lbs.) . . . . .	V-16
V-4	Hand Grasp Data . . . . .	V-17
V-5	Torque Relationships. . . . .	V-20
VI-1	Inertia and Geometry Data for Rigid Body Dynamics Program. . . . .	VI-5
VI-2	Degree of Freedom Table . . . . .	VI-18
VI-3	Beam Stiffness Data . . . . .	VI-18
VI-4	Distributed Mass. . . . .	VI-20
VI-5	Concentrated Mass . . . . .	VI-20
VI-6	Modal Frequencies (cps) . . . . .	VI-22



## I. INTRODUCTION AND SUMMARY

The goal of the Attached Manipulator System (AMS) program is the development of Shuttle related long-boom teleoperator technology. The purpose of the AMS is to simulate and demonstrate zero-g Shuttle manipulator cargo handling operations. It is not the design or development of the Shuttle Attached Manipulator System (SAMS); however, every effort is being made, to insure that the AMS will be functionally similar to the SAMS.

The objective of this contract is the investigation of the primary AMS technology questions, verification of AMS design concepts, and the preliminary design of critical components. The technology questions examined in this effort are those shown in Figure I-1. All technology questions have been answered satisfactorily and design concepts have been successfully verified. Preliminary designs of all critical components have been completed, which meet all functional and configurational requirements.

Martin Marietta is confident that the AMS is technically feasible and that a detail design and fabrication program can now be successfully undertaken.

Chapter II, Design Requirements, enumerates the configurational and functional requirements of the AMS and its subsystems. The overall AMS manipulator design is discussed and a typical simulation layout is shown. An analysis was made of the Shuttle manipulator movement requirements using an eighth scale Shuttle and 50 ft (scaled) manipulator model. Seven satellite capture trajectories were evaluated, along with various cargo placement and satellite servicing tasks. A scaled 40-ft long x 15-ft diameter payload mockup was used for cargo handling tasks. Both 6 and 7 degree of freedom (DOF) manipulator configurations were evaluated. Each joint angle was continuously monitored and recorded throughout each operational trajectory. Manipulator tip position and terminal device attitude, in relation to the manipulator shoulder, were computed for each trajectory. The results of the analysis were used to select tasks for further evaluation using our 6 DOF simulator (SOS). Position controller movements were related to the manipulator trajectories.

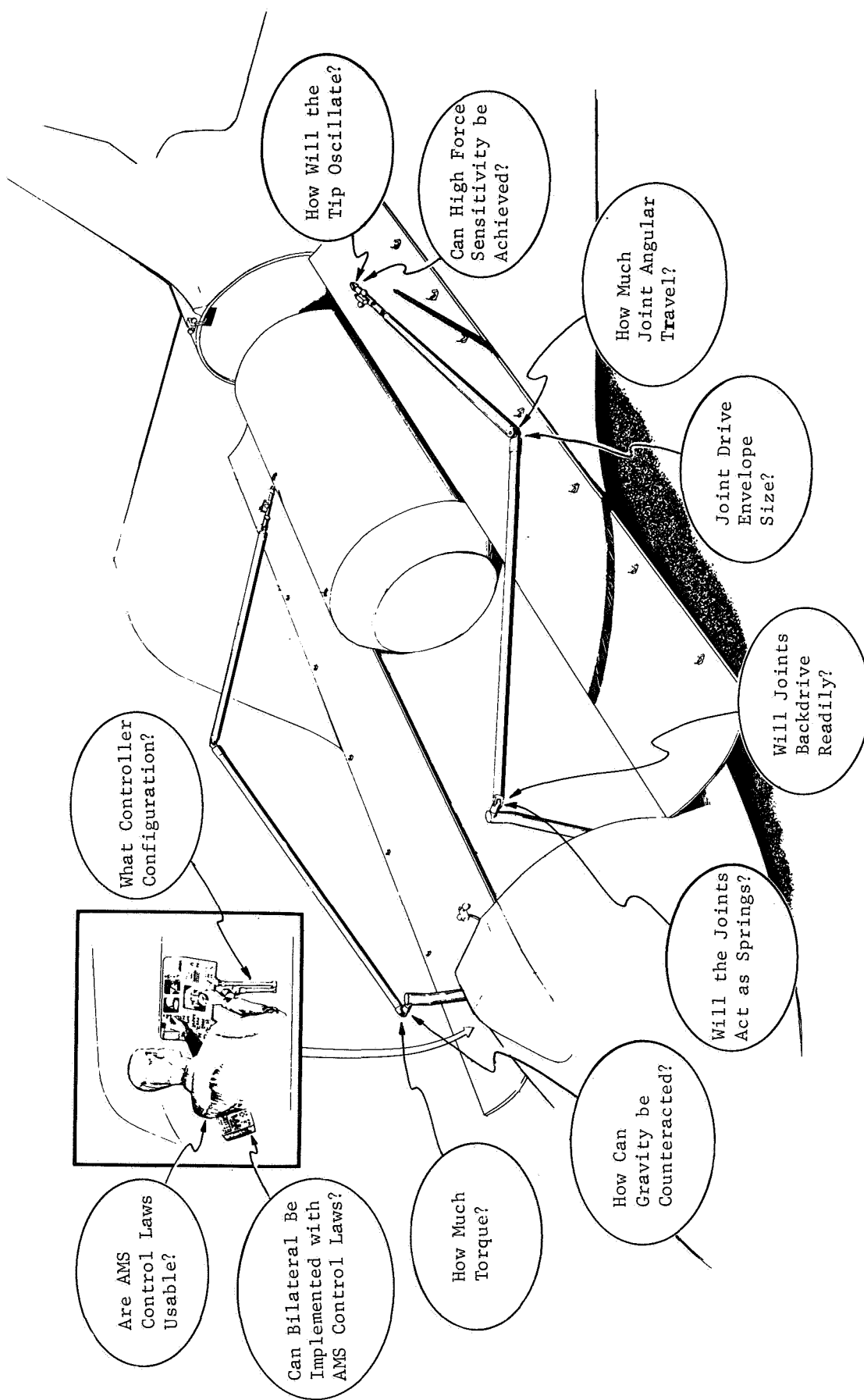


Figure I-1 AMS Technology Questions

Chapter III, Control System Breadboard, describes a new manipulator control technique. The control scheme permits a bilateral system with great master-slave size disparity to incorporate coordinate transformations, variable gain ratios, and position indexing between input controller and output manipulator. The translational control law equations are derived, and the servo system design procedures using both frequency and time domain techniques are presented. A two DOF master-slave breadboard was designed, built, and tested. The breadboard verified the control technique to be feasible, and the hardware test results were used to document (1) bilateral operation, (2) coordinate transformations, (3) variable gain ratios, (4) position indexing, and (5) stability. The coordinate transformations, variable gain ratios, and position indexing operated satisfactorily, and the force reflecting ratio was shown to be truly independent of these features. The master and slave tip to tip tracking properties were excellent, and it was demonstrated how man-in-the-loop serves as an adaptive filter for stabilizing a bilateral system handling a large payload. The unloaded manipulator bandwidth varied from 3.0 Hz to 1.6 Hz as the variable gain ratio was raised from  $MM = 1/2$  to  $MM = 1/8$ . The loaded manipulator (306 lbs air bearing load at the manipulator tip) bandwidths for these same variable gain ratios varied from 0.2 to 0.1 Hz. The sampled analog system revealed the tolerable sample rate to range from 10 msec for  $MM = 1/2$  to 32 msec for  $MM = 1/8$ . A simple unilateral-bilateral comparison of a maze task indicated the bilateral mode to be two to seven times more efficient for the particular tests conducted.

In Chapter IV we discuss the manipulator joints, counterbalance, and overall manipulator design. Two gear train concepts were designed and breadboarded full scale. Comprehensive tests were conducted with these and with a purchased harmonic drive. Results showed an internal (ring) gear with double drives to be superior in torsional stiffness, efficiency, and compactness of size.

A gear train ratio/motor size selection scheme is developed which is used to preliminarily design the manipulator shoulder pitch joint and elbow joint. In addition, the preliminary design of the shoulder roll drive is discussed.

A counterbalance optimization technique is developed and is used to arrive at a counterbalance design incorporating a 2900 lb counterweight as one resulting in the least increase

in moment of inertia while satisfying certain design constraints. A near full-scale breadboard of the counterbalance linkage is described and test results presented. This linkage concept was selected from many alternatives and the selection rational is tabulated.

Lastly, this chapter presents the design layout of the AMS manipulator and shows a 15% scale model which proves the articulated counterbalance principle.

Chapter V, Control Devices, describes our evaluation of position control devices. This evaluation followed an orderly, systematic approach, consisting of four phases: requirements development, design evaluations, dynamic simulations and a recommended final design. Primary emphasis was placed on the development of a 6 DOF position controller that could be indexed and have variable movement ratios between the controller and the manipulator. Both unilateral and bilateral position controllers were evaluated, as well as two 3 DOF Apollo-type rate controllers. MMC's 6 DOF Space Operations Simulator was used for dynamic tracking and capture, and cargo handling task evaluations. The recommended controller configuration is a 6 DOF, floor mounted unit, which has a pitch and yaw shoulder and a vertical telescoping section. It has a 3 DOF attitude balanced, gimbal arrangement at the wrist. The controller evaluation criteria was based primarily on human factors and mechanical design considerations. The evaluation did not compare computational requirements of the candidate controller configurations. A full-scale model of the telescoping controller was fabricated.

Chapter VI contains a detailed account of the dynamical analyses of the AMS. Three parallel efforts are described. First, the mathematical model and corresponding computer program describing the rigid body behavior of the SAMS and the AMS is presented. This program was used to compare the performance of the AMS with that of the SAMS for identical payload handling tasks. The results are used to arrive at AMS joint torque requirements of 1200, 650, and 300 ft-lbs for the shoulder, elbow, and wrist joints, respectively. The differences in performance between the SAMS and the AMS are also discussed.

Next, two types of AMS vibration analyses are presented. Using preliminary design data, the frequencies and mode shapes of the counterbalanced and non-counterbalanced versions of the

AMS are compared. The results predict fundamental frequencies on the order of 1 Hz for the unloaded AMS and .02-.03 Hz for the loaded manipulator (60,000 lb payload).

Finally, using an existing Martin Marietta computer program, the nonlinear (large joint excursions) flexible behavior of the AMS is studied. Results comparing rigid and flexible AMS motions for a simplified payload handling task indicate oscillations (about the rigid body trajectory) with approximately a 3 in. amplitude (peak-to-peak) and a frequency of .05 Hz.

This final report describes all work done under Contract NAS9-13027. This report includes all of the material from the Final Report Briefing, with the exception of some charts prepared as part of company-funded research task.

The design drawings and associated lists are bound separately from this report.



## II. DESIGN REQUIREMENTS

### A. CHARACTERISTICS AND SYSTEM DESCRIPTION

#### 1. Requirements

The intended use of the AMS in a zero-gravity simulation facility is for dynamic response testing and for demonstration of the capability to deploy payloads, retrieve and stow orbiting payloads, and service satellites.

The AMS design requirements include both configuration and functional requirements. The former include: (1) 40-ft total arm length, (2) upper and lower arm segments of 18.5 ft each, (3) aluminum tubes 12 in. outside diameter, (4) seven degrees of freedom plus terminal device, (5) shoulder: pitch, yaw and roll; elbow: yaw; wrist: yaw, pitch and roll, (6) joint torque and travel characteristics (Table II-1), (7) counterbalanced to overcome gravitational effect on joints, and (8) 6 degrees of freedom position controller.

The functional requirements include: (1) operation unloaded in any plane, (2) operation loaded in horizontal plane, (3) reach capability governed only by the joint angular travel, (4) fail-safe joint brakes, (5) 5 minute deployment time (65,000 lbs), (6) 2-ft stopping distance, loaded (65,000 lbs), (7) 0.2 ft stopping distance, unloaded, (8) 2 ft/sec unloaded tip velocity, (9) 0.2 ft/sec loaded (65,000 lbs) tip velocity, (10) 30 lbs static tip force (tangential with arm extended), (11) bilateral, force reflecting control system with indexing, selectable coordinate system, and variable control ratios, (12) 4 in. static tip deflection due to motor loading; 4 in. due to gravity and, (13) backdriveable joints.

TABLE II-1 JOINT DESIGN CHARACTERISTICS

	Pitch	Yaw	Roll	Yaw	Yaw	Pitch	Roll
Angular Travel (deg)	$\pm 200$	$\pm 150$	$\pm 200$	- 2 + 164	$\pm 120$	$\pm 120$	$\pm 200$
Stall Torque (ft-lb)	1200	1200	650	650	300	300	200

## 2. Manipulator Design

Figure II-1 is the AMS with articulated counterbalance. The design incorporates a wide yoke at the shoulder yaw joint. This provides a balanced 40-ft manipulator whose shoulder or elbow joint torques need not, in any orientation, overcome the force of gravity on either the upper or lower arm and whose motion is completely unrestricted either loaded or unloaded. This design produces an AMS whose moment of inertia (unloaded) about the shoulder is increased a maximum of only 30% due to the counterbalance mass. In the loaded case (65,000) the increase is only a fraction of a percent. Therefore, the dynamic operating characteristics have been only slightly altered from the uncounterbalanced (zero-g) arm.

The tip deflections for an upper and lower arm tube wall thickness of 0.18 in. and 0.08 in., respectively, are given in Table II-2. These numbers are based on joint stiffness as determined from geartrain tests.

Table II-2 Static Deflections

Component	Loading		
	Torque Motor (Stall)	Gravity	Total
Beams	1.05 in.	3.31 in.	4.36 in.
Joints	2.70 in.	0	2.70 in.
Total	3.75 in.	3.31 in.	7.06 in.

Maximum Horizontal Deflection →

Maximum Vertical Deflection with no Vertical Torque Force →

Maximum Vertical Deflection with Torque Force Up →

## 3. Simulator Layout

Figure II-2 shows a simulator concept for payload deployment, and stowage. It is based on an airbearing facility with an operator's console and test director's console. It is this AMS simulation configuration that produces the terminology for the degrees of freedom for the manipulator, since with the Shuttle as reference, the shoulder first joint becomes a pitch drive, the elbow a yaw and so forth.

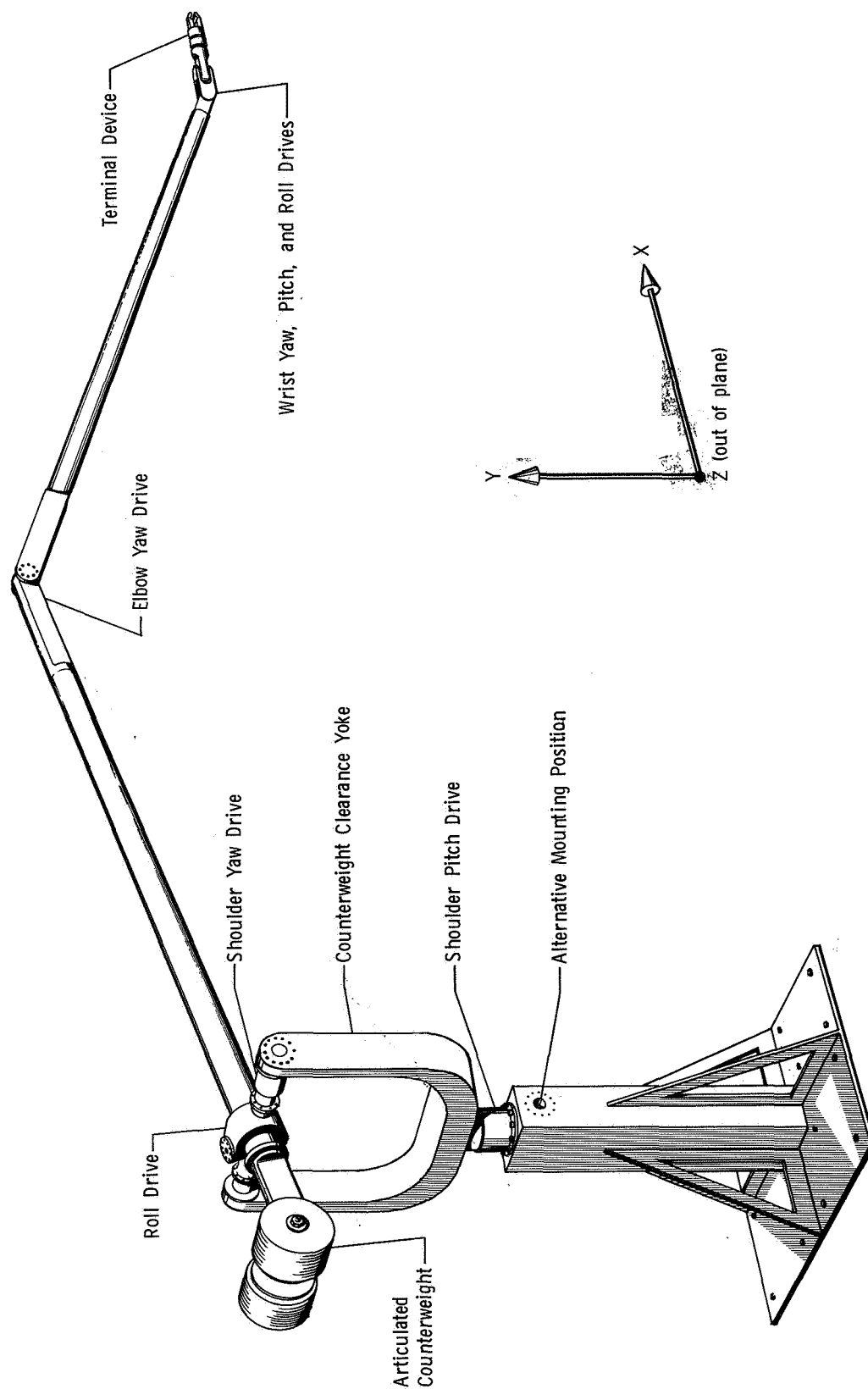


Figure II-1 AMS With Articulated Counterbalance

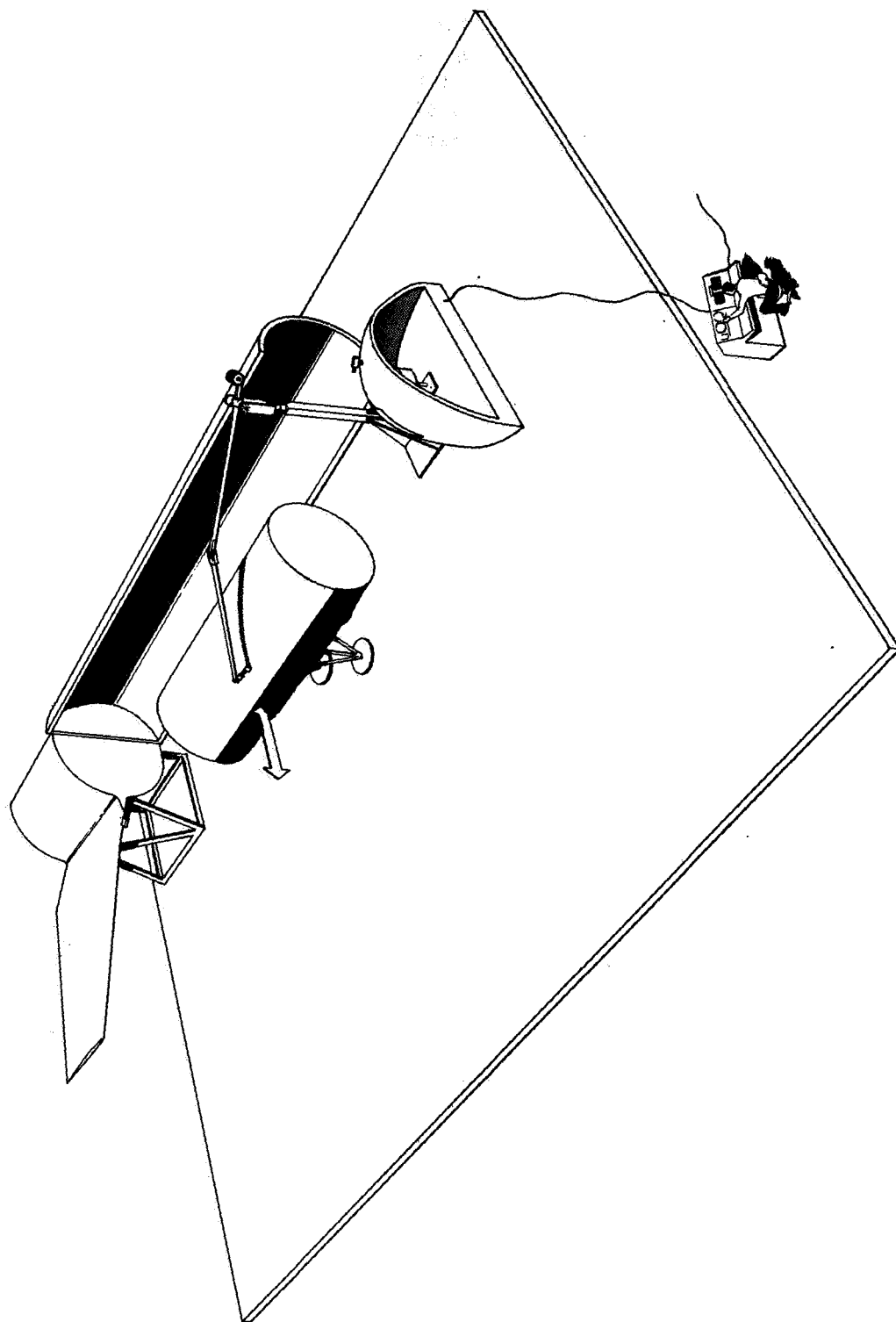


Figure II-2 Simulator Layout, Payload Deployment and Stowage

## B. MANIPULATOR TRAJECTORY DEFINITION

The purpose of this analysis was to determine desirable Shuttle manipulator movement trajectories and manipulator characteristics when related to typical payload tasks. This data was required to establish design requirements for the manipulator, operational limitations for this configuration and establish operational requirements for the position controller. Initially the maximum joint angular travel limits for each joint was derived from the data analytically established in a prior contract\*. These joint characteristics were incorporated into a scaled 50-ft manipulator (which was the shuttle baseline length) to allow evaluation through various operational trajectories. The following manipulator tasks were simulated.

- (1) Seven Capture Trajectories,
- (2) Cargo Placement,
- (3) Cargo Deployment,
- (4) Cargo Bay Reach Envelopes,
- (5) Docked Satellite Reach Envelope, and
- (6) Module Replacement.

To date, much of the manipulator movement data has been derived from simple desk-top models or by computer analysis. The desk-top models show gross movements but lack accuracy. They also have no way of recording joint movements and tip trajectories. Computer analysis are generally limited to point to point translations and do not account for Shuttle obstacles such as cargo bay doors, the docking port and flight deck. An eighth scale mockup of the Shuttle was used since it was large enough to allow high fidelity and small enough not to be cumbersome. The total mockup was approximately 10 ft long. (Figure II-3). The Shuttle and cargo mockups were constructed of foam-core and plywood. The manipulator was made of aluminum and steel. Each joint has potentiometers to measure the joint angles and a friction brake for locking in position. The manipulator is scaled for 50 ft from the shoulder centerline to the center point of the terminal device and has seven degrees of freedom. The joint ordering, starting at the shoulder, is pitch, yaw, roll with yaw at the elbow and yaw, pitch, roll at the wrist. (See Figure II-4)

Continuous joint angle data was taken during each run on a standard 8 channel Brush recorder. Joint angle data was not taken while reach envelopes were being evolved, since the reach limits themselves were the desired results. The raw strip chart

\* NAS9-11932 "Preliminary Design of a Shuttle Docking and Cargo Handling System"

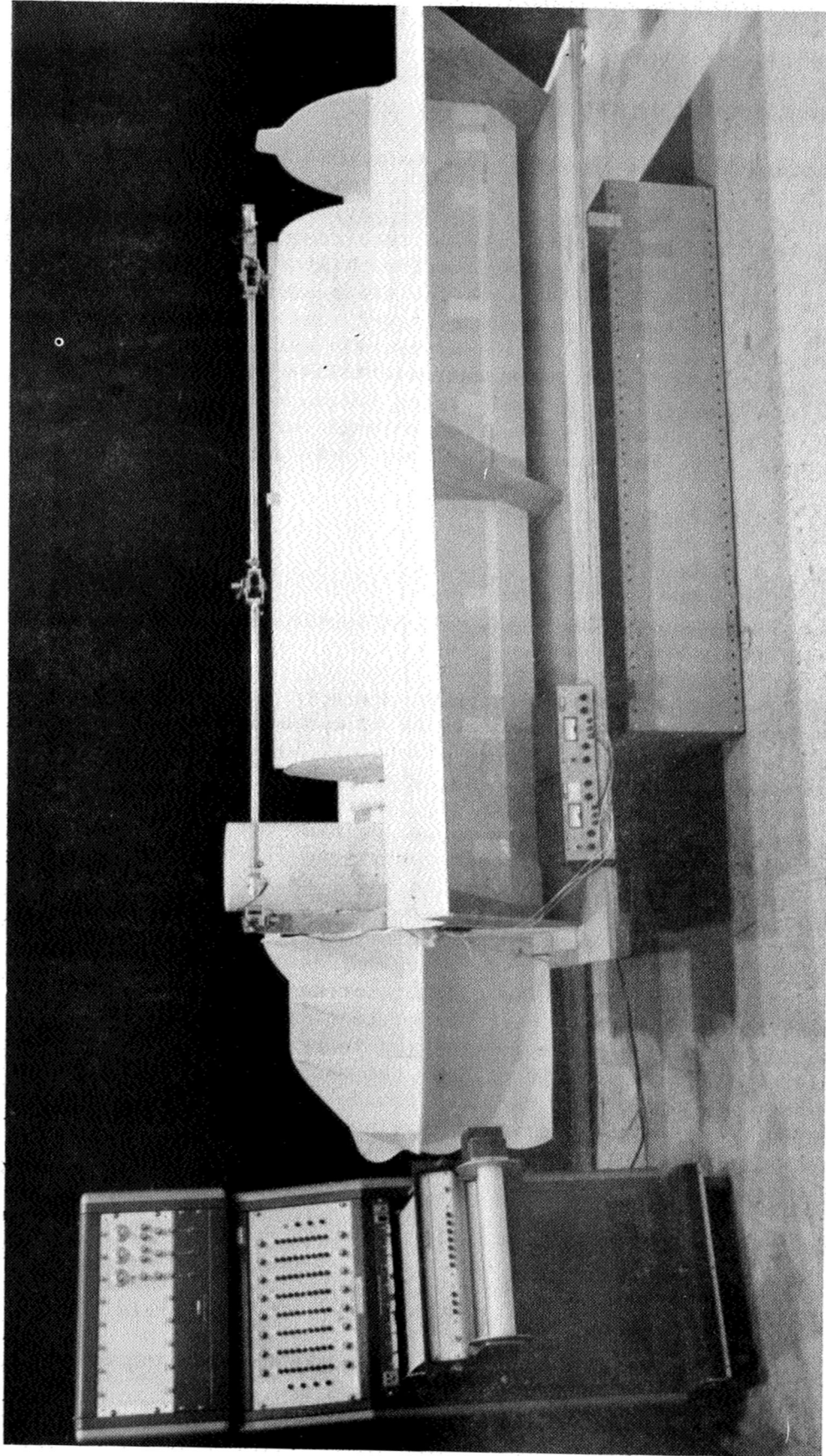


Figure II-3 One-Eighth Scale Shuttle and Manipulator Mockup

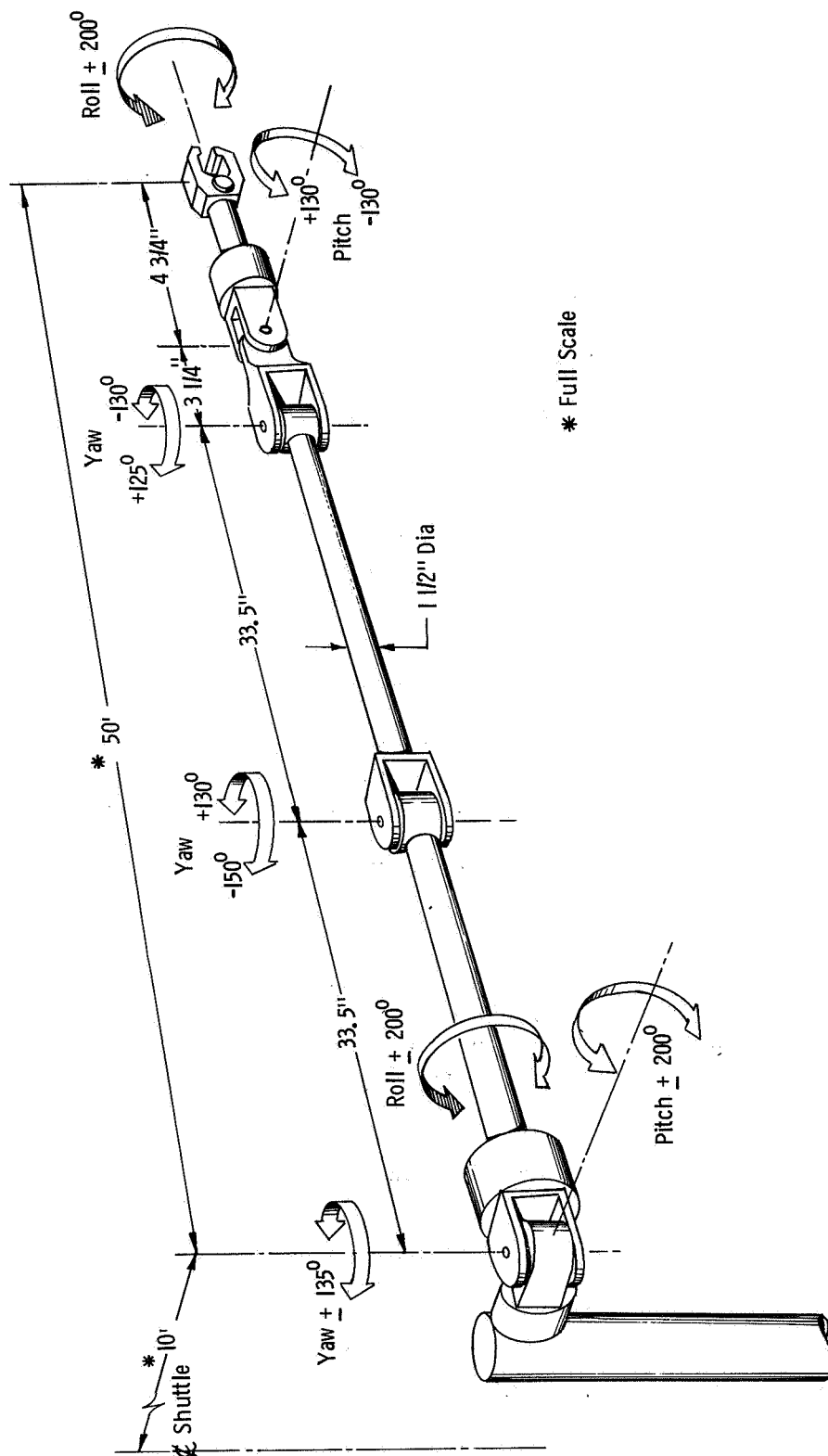


Figure II-4 Scale Model Manipulator Configuration



data was digitized and computer printouts were made showing all seven joint angles throughout each run with the corresponding terminal device positions, which were computed for the X, Y, Z Shuttle coordinates (based at the shoulder). Gross manipulator positions were noted beside the data, such as initial condition (I.C.), forward capture position, rear capture position, etc.

## 1. Capture Trajectories

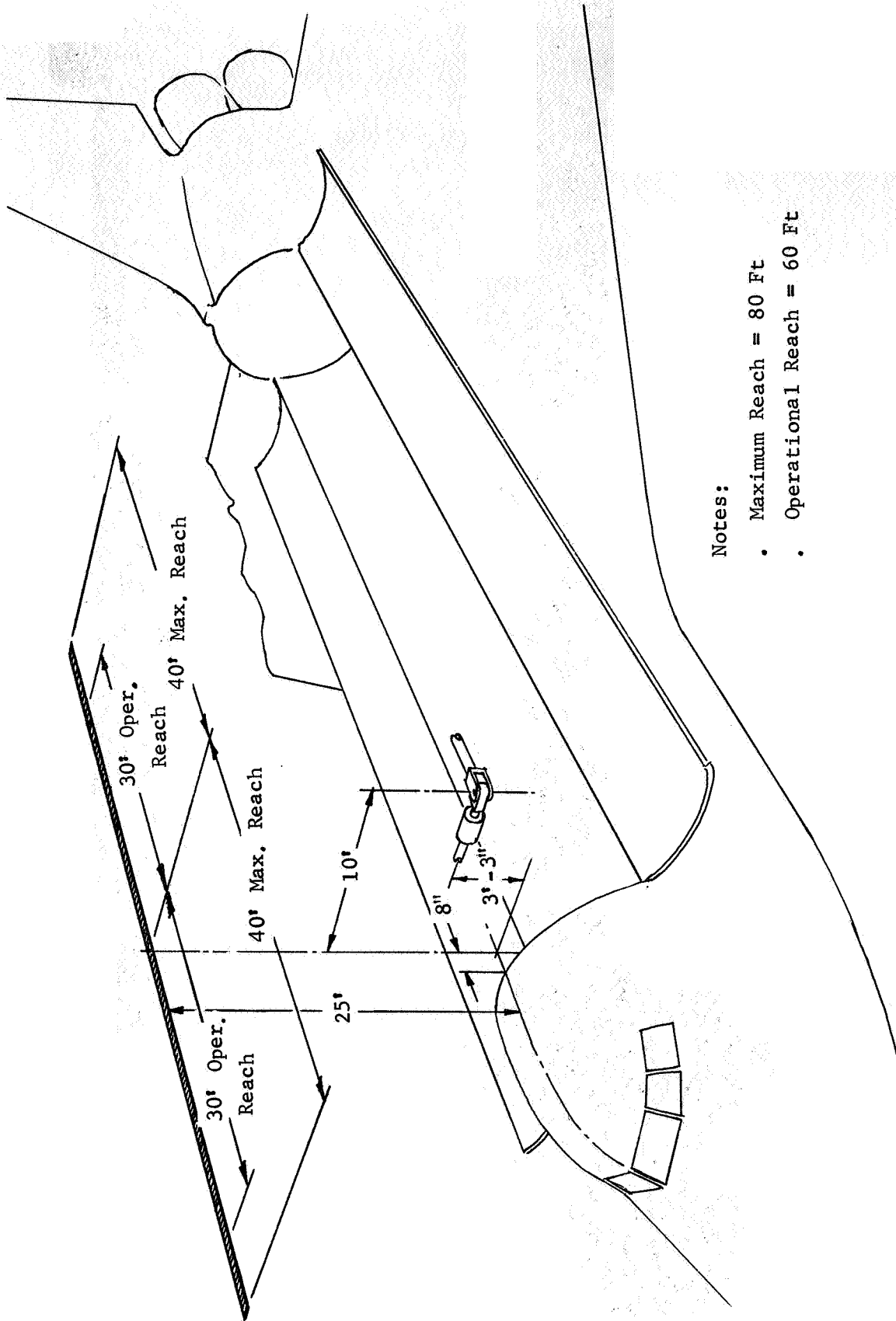
Seven basic capture trajectories were analyzed (See Figures II-5 to II-15. At the time of the study, the baseline for satellite capture was a flyby technique where the Shuttle was flown to within a capture envelope, then deactivate the Shuttle attitude control system\*\*, reached out and attach the manipulator to the satellite. The satellite was to be attitude stabilized and have a relative velocity no greater than .25 ft/sec. This capture philosophy dictated capture paths for the satellite relative to the Shuttle. The intent of the analysis was to determine which one looked best from the manipulator movement standpoint. Twenty-five feet was selected for the minimum distance between the Shuttle and a passing satellite. Throughout all the trajectory evaluations the manipulator elbow joint was bent away from the Shuttle structure. The maximum path length was established by accurately placing an aluminum angle the length of the proposed trajectory and positioning the manipulator to each extreme. This was derived by extending the manipulator until the elbow was within  $10^{\circ}$  of being straight out. The operational path length is 75% of the maximum travel. This means, primarily, that if you do not have the payload stopped by the limit of the operational travel (reach), it should be released.

Each capture trajectory was evaluated with the manipulator configured for a full 7-DOF and also with the shoulder roll locked at  $0^{\circ}$  for 6-DOF. All capture task manipulator maneuvers, started from the I.C. condition shown in Figure II-4 then were extended to the forward maximum reach and then maneuvered along the guide to the rear position.

Capture Concept 1 - Down Shuttle Centerline - This concept would be relatively easy for the pilot to do the initial alignment. However, the satellite is on a collision course with the tail. See Figure II-5 and II-6. The trajectory is directly over the operator's windows for good direct vision. The maximum reach\* is quite long - 80 ft. The post capture stowage maneuver is very short since the satellite is directly over the cargo bay

\* "reach" is used here to denote the length of the path.

\*\* Main (large) thruster system.



Notes:

- Maximum Reach = 80 Ft
- Operational Reach = 60 Ft

Figure II-5 Capture Concept 1 - Down Shuttle Centerline

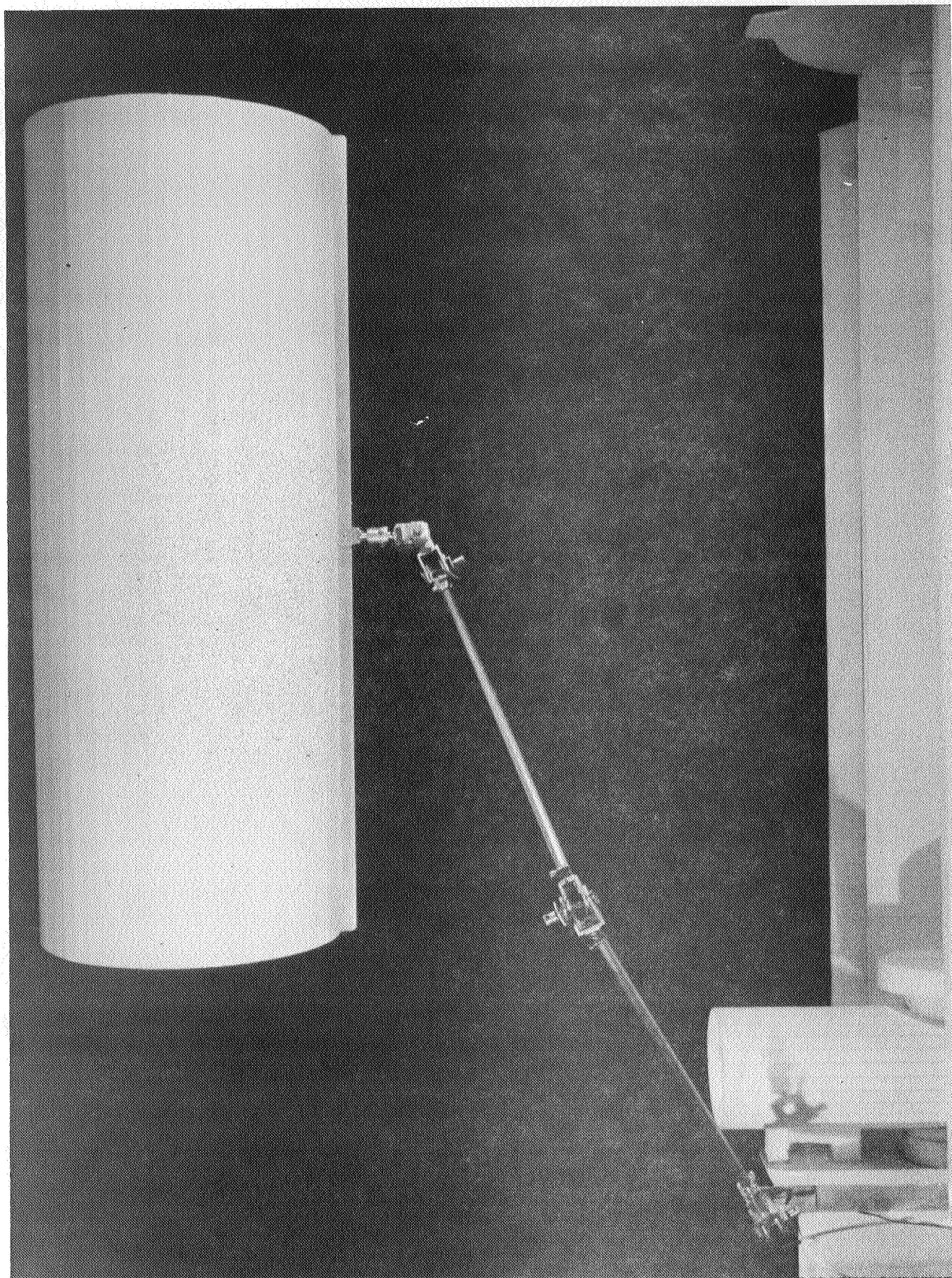


Figure II-6 Capture Concept 1 - Down Shuttle Centerline

when the relative velocity between Shuttle and payload is stopped.

Capture Concept 2 - Over the Wing - The satellite trajectory in this concept is from nose to tail, over the wing (Figure II-7 and II-8). This concept also allows the Shuttle pilot good visibility for initial alignment. The trajectory is not on a collision course with the Shuttle. The maximum reach, 84 ft, was the longest of all of the concepts evaluated. The manipulator operator could have good direct vision, depending on the Shuttle window configuration. The manipulator elbow required 150° of travel in the negative (yaw) direction.

Capture Concept 3 - Vertical Over Shoulder Centerline - This concept relates to the Z docking maneuver, which was not well-defined at the time. As can be seen in Figure II-9, this concept limits the maximum reach to 40 ft, which is the shortest of all the trajectories evaluated. Because of the combination of a 26 ft operational reach limit and the direct collision course with the Shuttle, this concept is considered very poor when compared to the others. The downward reach is limited by the manipulators elbow to bend back on itself. In this case, the limit was 150°. This is shown in Figure II-10.

Capture Concept 4 - Across Cargo Bay - This concept (Figure II-11 and II-12) allows excellent direct vision to the manipulator operator if the docking module is not installed in the cargo bay. The trajectory is across the cargo bay in the Shuttle Y Axis. Maximum reach is average, (65 ft) and no gross manipulator angular motions were required.

Capture Concept 5 - Across Manipulator Shoulder - This concept (Figure II-13) provides good direct vision potential for the manipulator operator, good maximum reach and non-collision course. The trajectory is poor from the Shuttle pilot's standpoint. Initial alignment might be difficult. With the capture path 25 ft above the Shuttle skin and the manipulator segment lengths used, the elbow moves into the capture path as the terminal device passed through the Shuttle centerline. By moving the capture path up 5 ft (to 30 ft) this is avoided.

Capture Concepts 6 and 7 - Across Pilot's Station - Concepts 6 and 7 (Figures II-14 and II-15) are nearly the same except trajectory 7 is 8 ft lower in the Z-axis than 6. These concepts were evaluated to show capture trajectories which would be adequately far from the Shuttle vehicle to allow a 60 ft payload to slowly rotate about its cg, after capture, and not collide with the Shuttle. Both concepts place the terminal





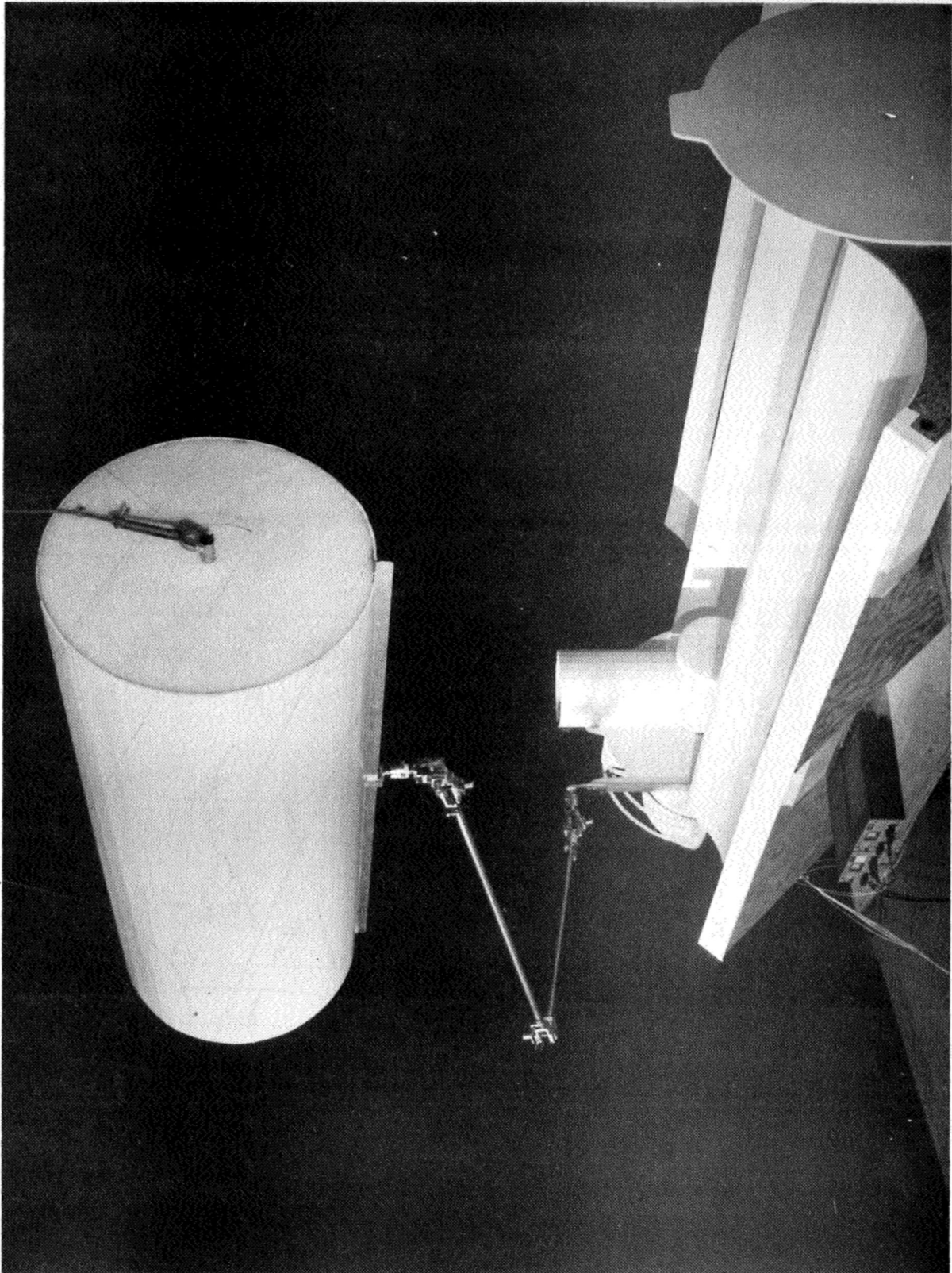


Figure II-8 Capture Concept 2 - Over the Wing

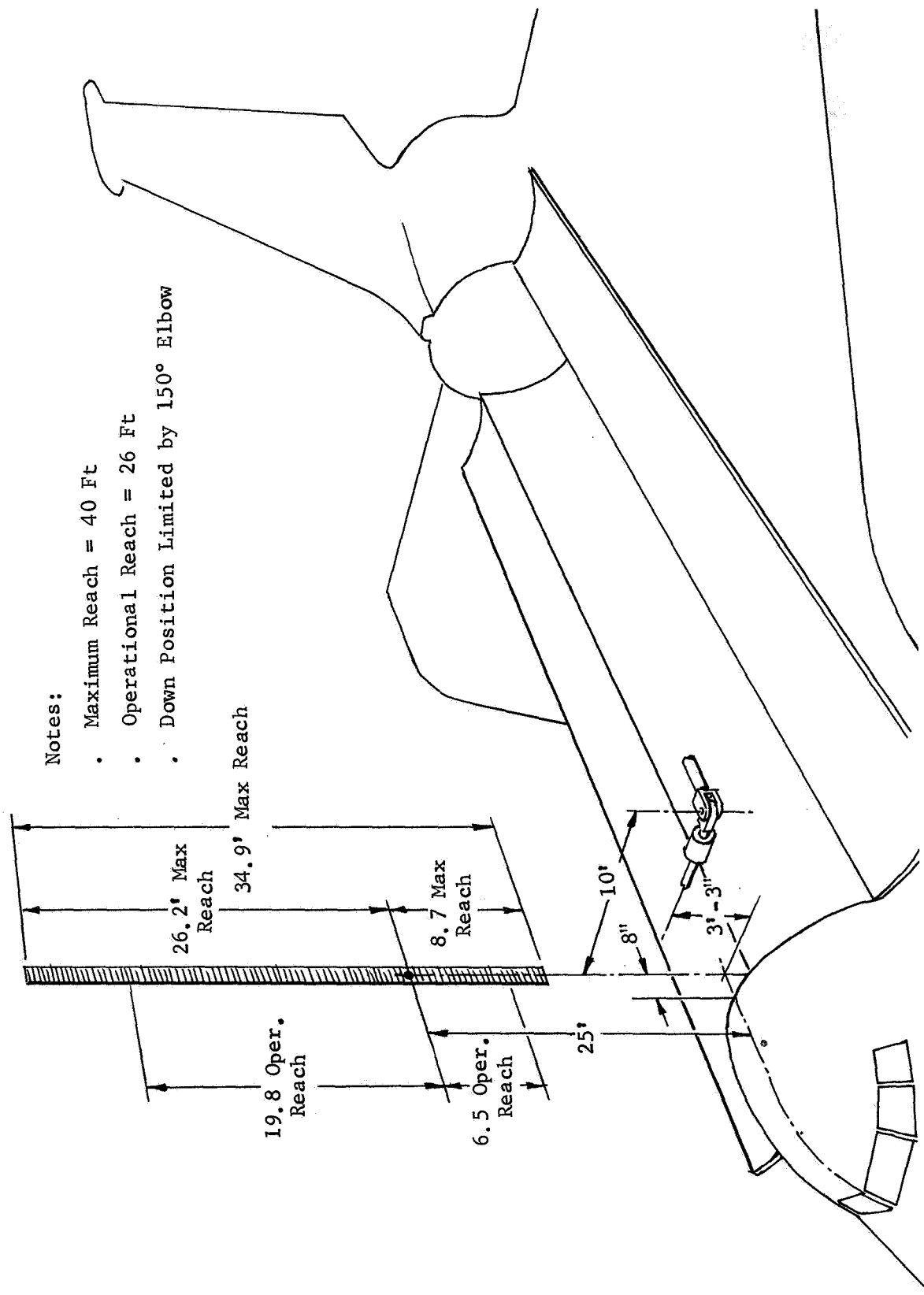


Figure II-9 Capture Concept 3 - Vertical Over Shoulder Centerline

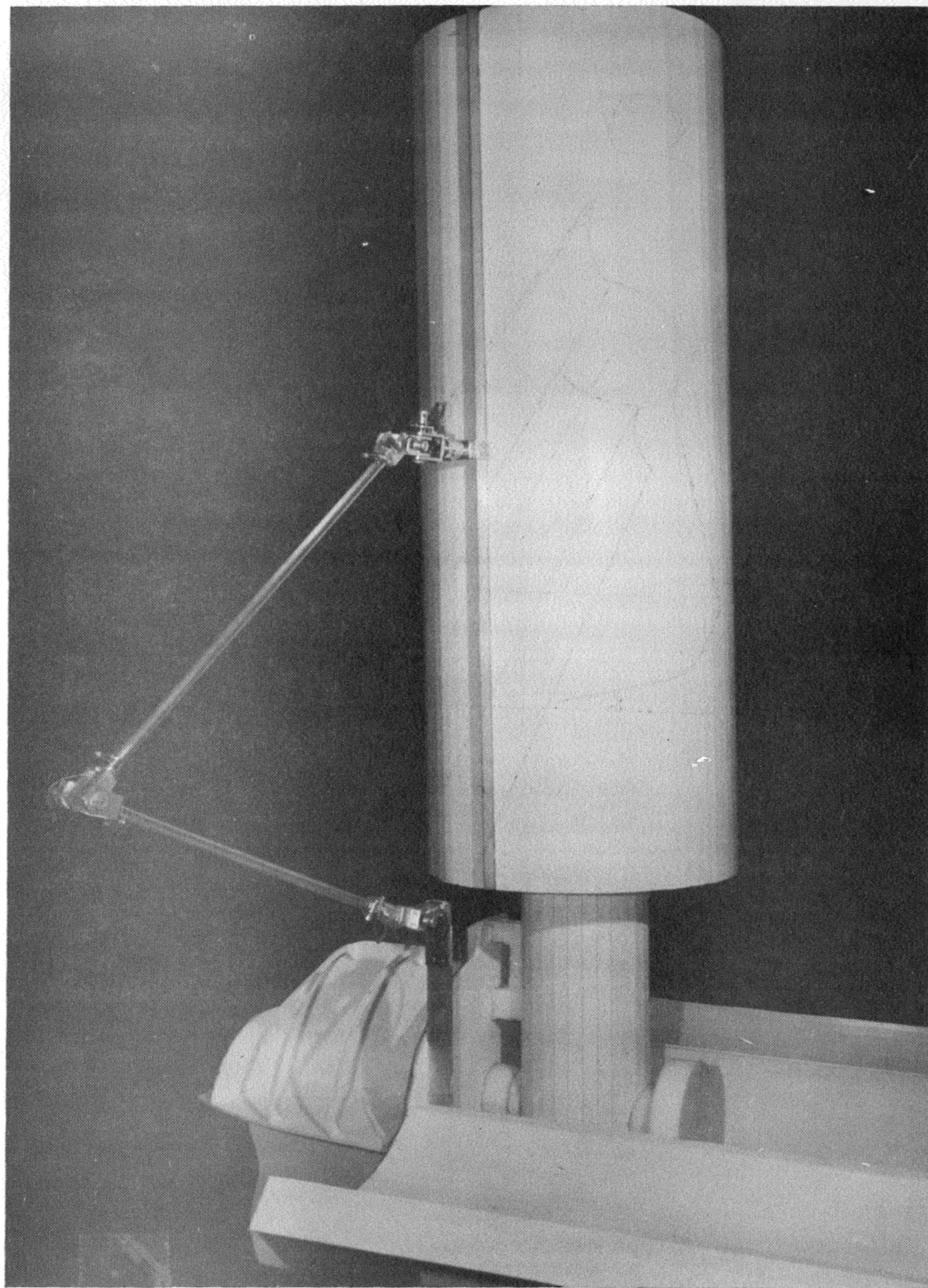
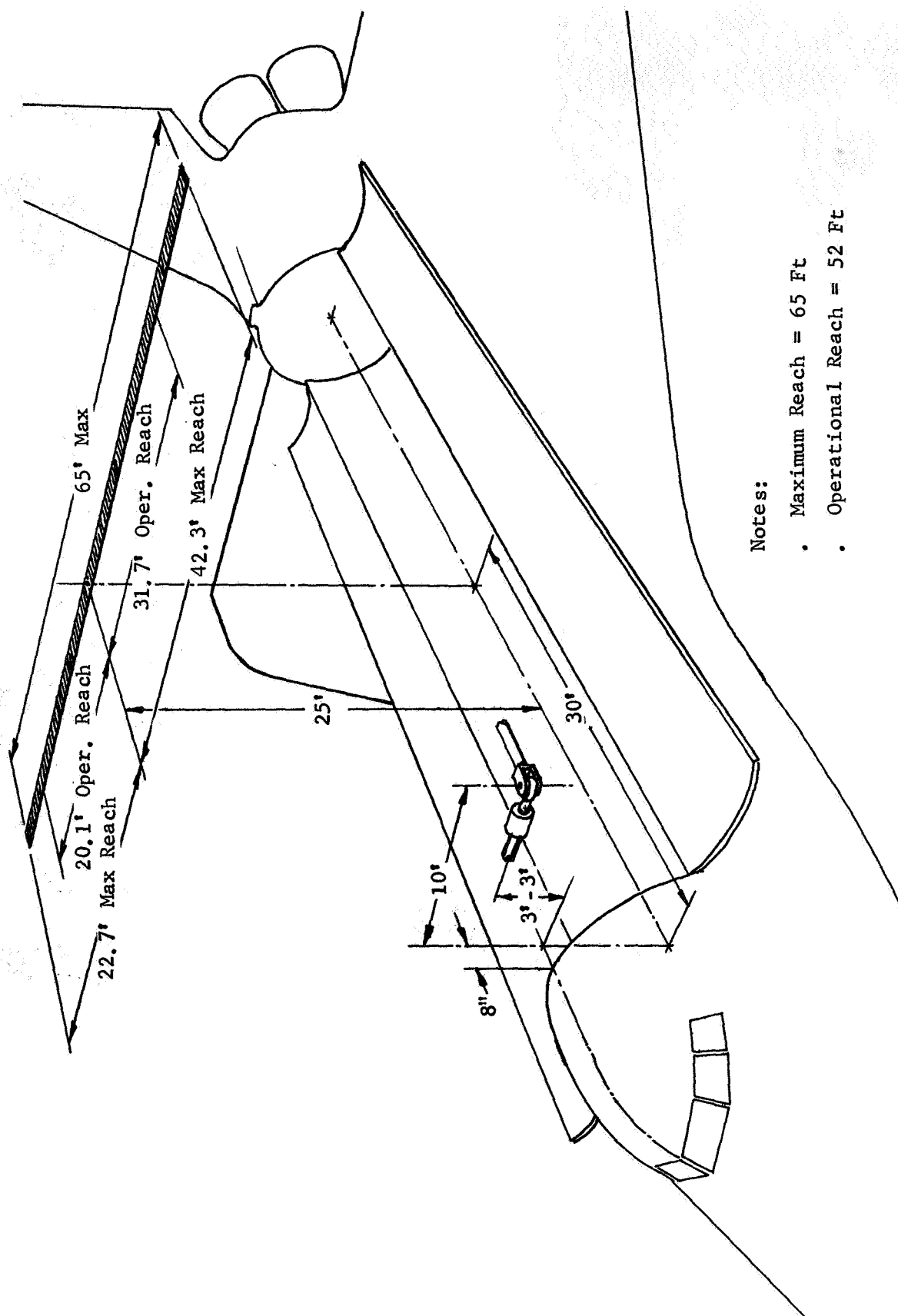


Figure II-10 . Capture Concept 3 - Vertical Over Shoulder Centerline





Notes:

- Maximum Reach = 65 Ft
- Operational Reach = 52 Ft

Figure II-11 Capture Concept 4 - Across Cargo Bay

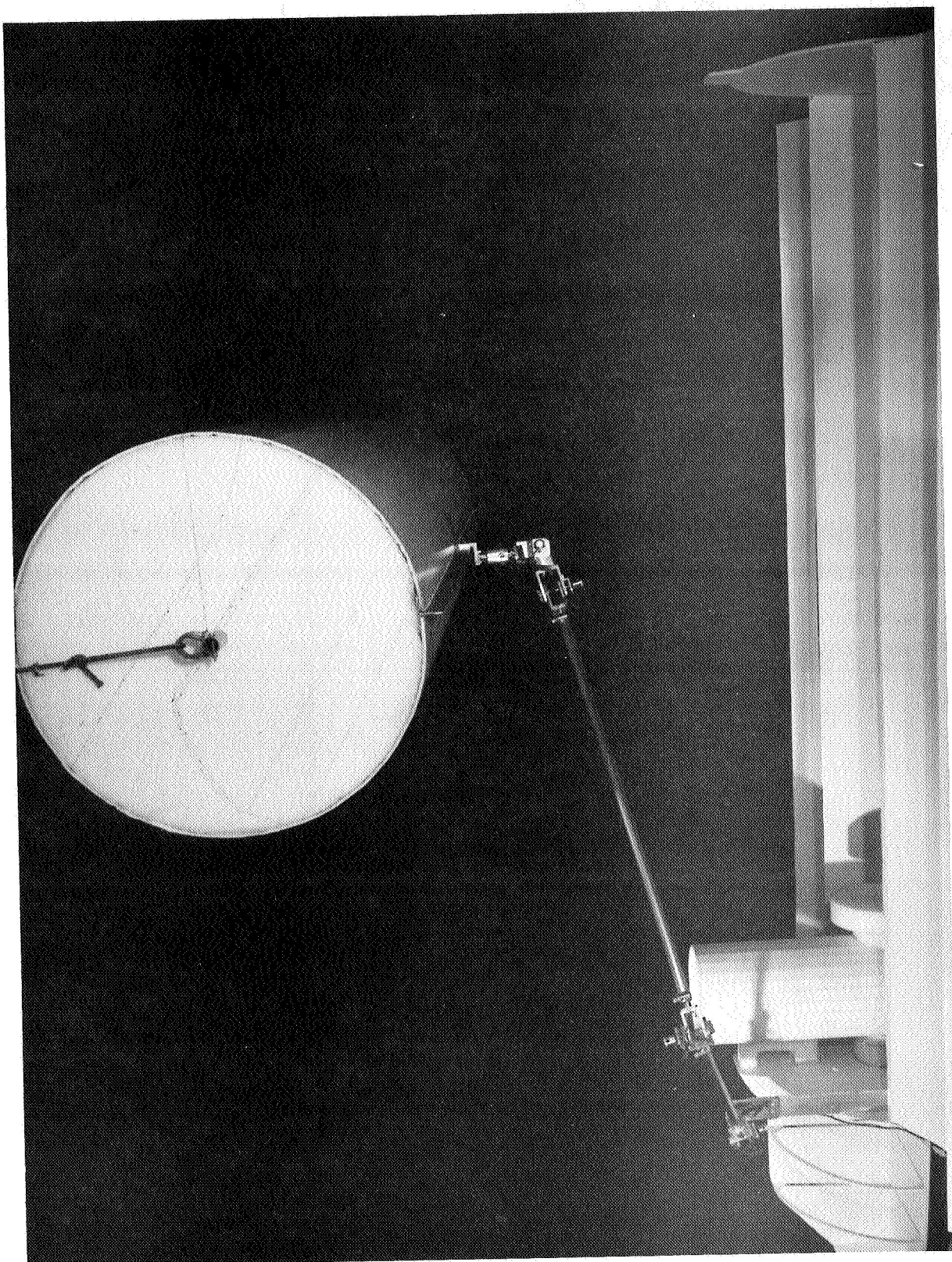


Figure II-12 Capture Concept 4 - Across Cargo Bay

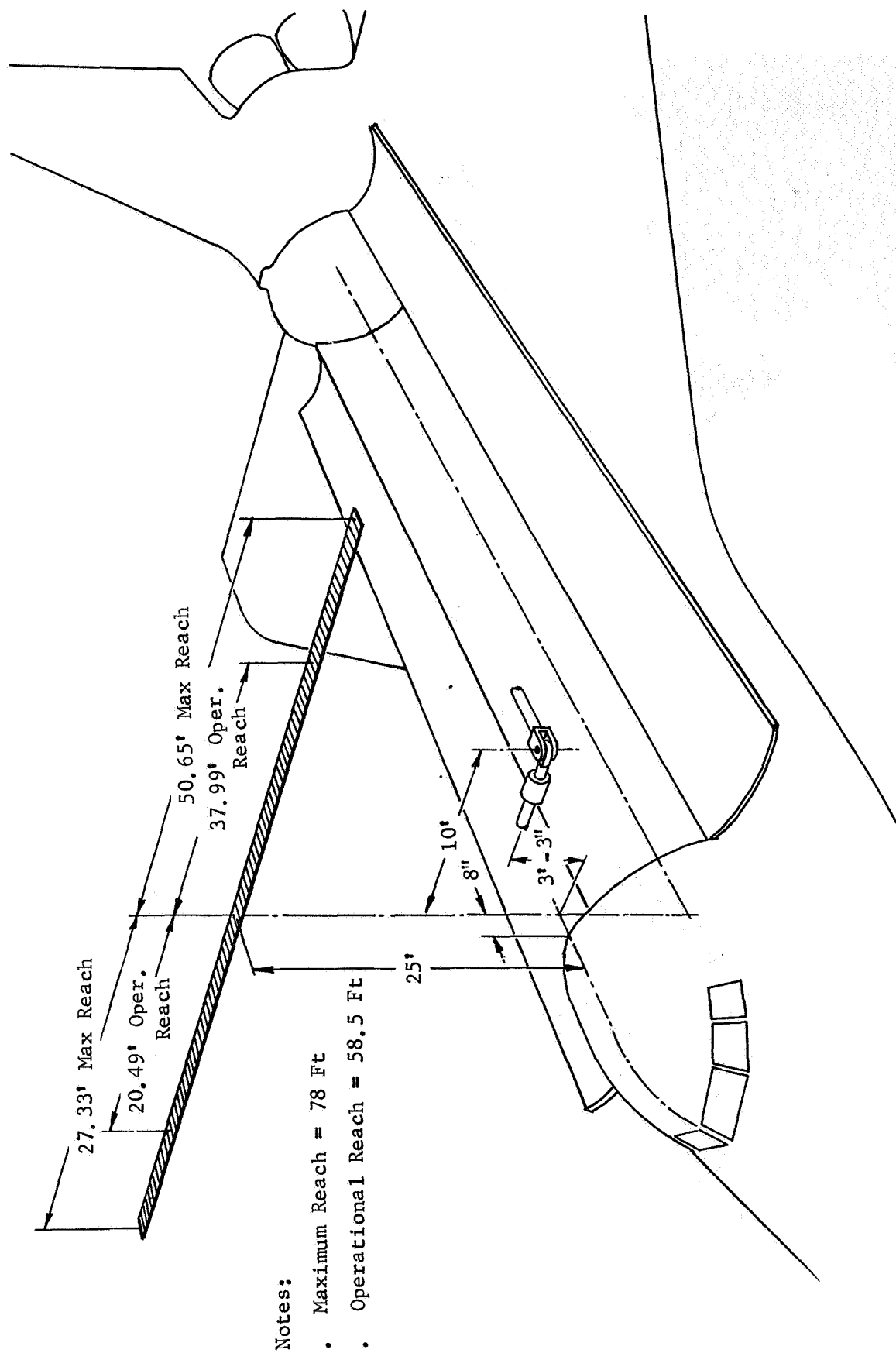


Figure II-13 Capture Concept 5 - Across Manipulator Shoulder

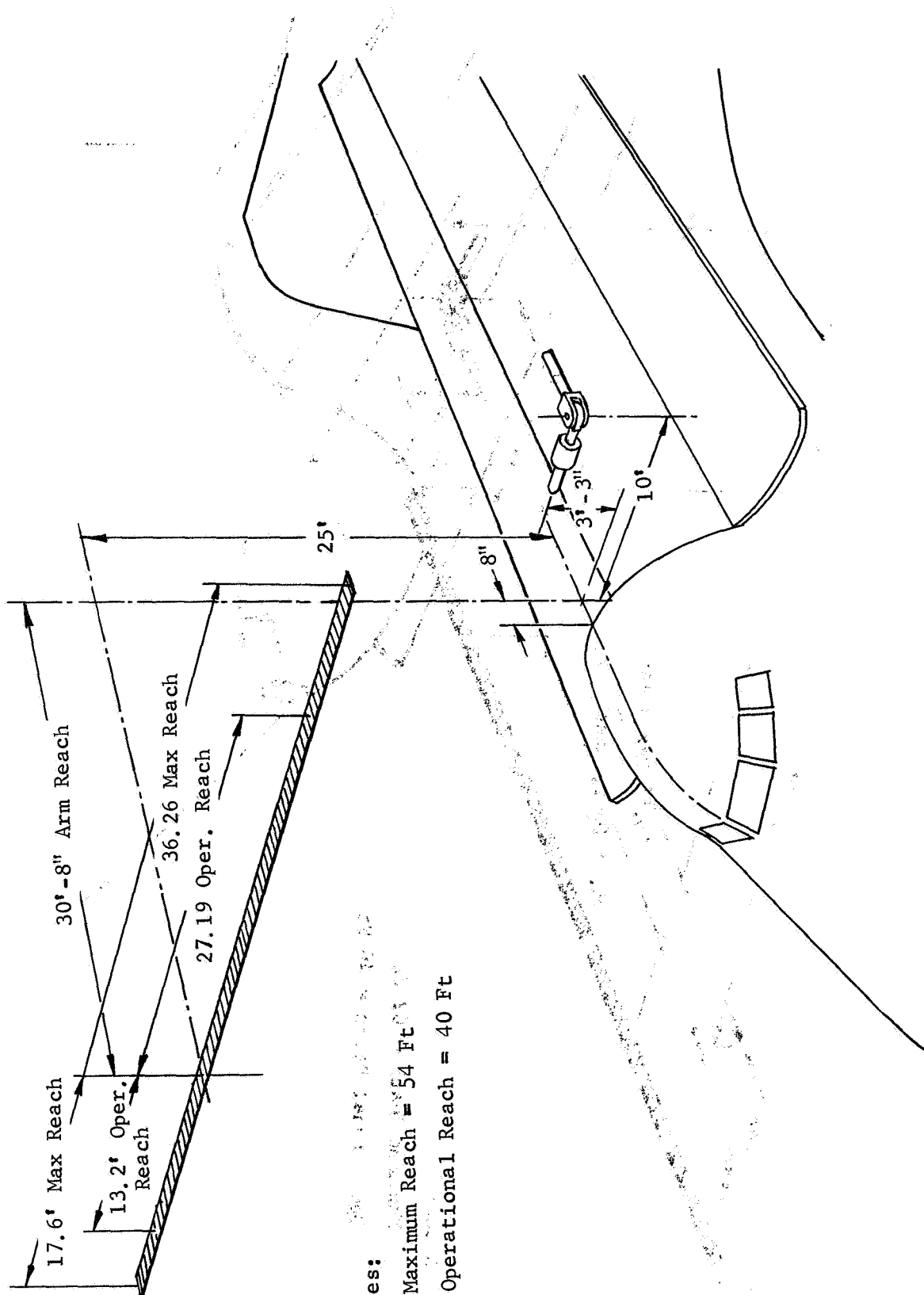


Figure II-14 Capture Concept 6 - Across Pilot Station

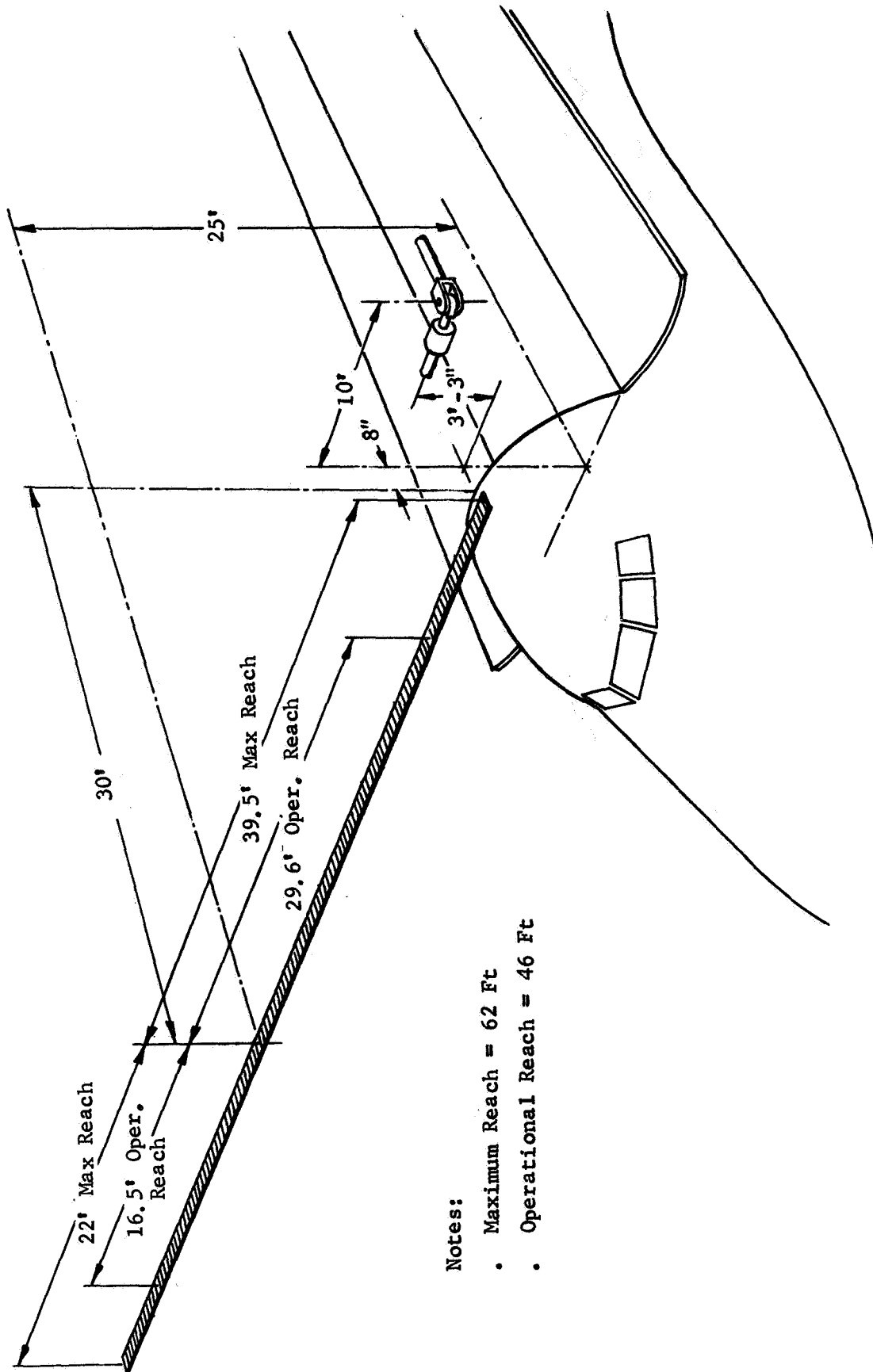


Figure II-15 Capture Concept 7 - Across Pilot Station

device in front of the Shuttle nose. Both 6 and 7 allow excellent Shuttle pilot direct vision (especially 7) but none for the manipulator operator. The post capture maneuvers are significant. A translation of 45 ft in the X-direction alone would require additional time for a 60K payload.

## 2. Cargo Placement

A cargo placement evaluation was made for each capture concept. The cargo mockup was scaled for a 15-ft diameter by 40-ft long satellite. The starting point for each placement was the end of the operational reach for each capture trajectory. This point was carefully determined for each trajectory, the terminal device was attached to the cargo mockup and the mockup was slowly maneuvered into the cargo bay. Joint angles were recorded and all of the maneuvers required no more than 6-DOF in the manipulator.

## 3. Cargo Deployment

The cargo deployment task consists of:

- (1) Maneuver the manipulator to the upper center of the 40 ft satellite mockup, in the cargo bay,
- (2) Attach the terminal device to the center of the mockup (Figure II-16),
- (3) Maneuver satellite straight up to clear cargo bay by approximately 10 ft,
- (4) Roll satellite  $180^{\circ}$ ,
- (5) Extend manipulator straight up, in Shuttle Z axis, to operational limit, and
- (6) Release satellite.

Joint angles were recorded for this maneuver and 7-DOF (roll at the shoulder) was not required.

## 4. Capture and Cargo Placement

- a. None of the capture concepts, placement or deployment of the large cargo requires the 7th-DOF (roll at the shoulder)(a 7-DOF requirement is discussed in Section C).



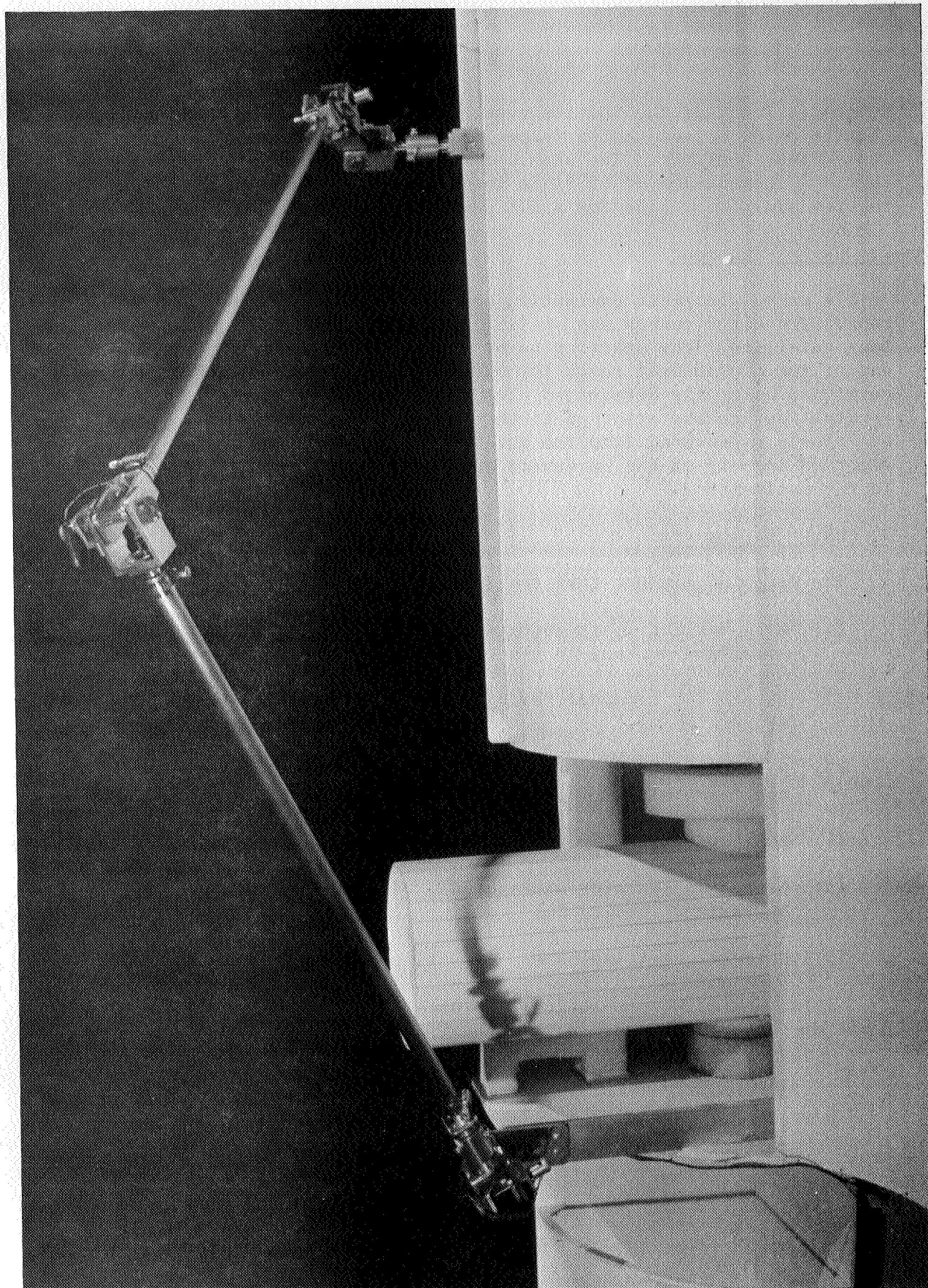


Figure II-16 Cargo Deployment

- b. Having roll at the shoulder did not increase the capture trajectory reach envelopes.
- c. At no time during these manipulator maneuvers did the elbow rotate to the positive direction. The elbow was only required to bend as a human arm does.
- d. Capture concept 2, over the wing, was selected as the most desirable of the 7 evaluated. It gave the longest reach, and provided good direct vision potential for both the pilot and the manipulator operator. No gross translations were required after satellite capture, since the deceleration zone is nearly over the cargo bay. The satellite is not on a collision course with any part of the Shuttle vehicle. This concept was used for dynamic capture task evaluations on our Space Operations Simulator.
- e. Maximum joint angular travel requirements are shown in Figure II-17.
- f. Joint angle travel profiles and associated tip position data are contained in Appendix E.

### C. MANIPULATOR REACH CAPABILITIES

For the 6 and 7-DOF manipulator, reach zones in the cargo bay were determined. The manipulator was scaled for 50 ft long and 12 inches in diameter. Four levels in the cargo bay were evaluated. These all related to the cargo bay door hinge line. The top level was 3 ft above the hinge line. Level 2 was at the hinge line. Levels 3 and 4 were 3 ft and 6 ft below the hinge line, respectively. The task was to establish a zone on each level where the terminal device could reach straight down, touch the level and maneuver straight up as though it were attached to cargo. It quickly became obvious that roll at the shoulder was required.

First, all levels were evaluated with a 6-DOF manipulator, with the shoulder roll locked at  $0^\circ$ . As can be seen in Figures II-18a thru c on level 1 and 2 and the reach zones are somewhat the same and appear operationally adequate. On levels 3 and 4 however, the reach zone is limited by the outer segment of the manipulator arm hitting the hinge line as greater shoulder pitch is required to move the terminal device down into the cargo bay. The reach limits were derived by allowing the lower arm to come



SLAVE JOINT	SLAVE MODEL JOINT LIMIT	1 DOWN SHUTTLE CENTERLINE	2 OVER WING	3 VERTICALLY OVER OPERA- TOR'S STATION	4 ACROSS CARGO BAY	5 ACROSS SLAVE SHOULDER	6 ACROSS PILOT STATION	7 ACROSS PILOT STATION
WRIST ROLL	$\pm 200^{\circ}$	$117^{\circ}$	$126^{\circ}$	$0^{\circ}$	$15^{\circ}$ $-27^{\circ}$	$193^{\circ}$	$194^{\circ}$	$198^{\circ}$
WRIST PITCH	$\pm 130^{\circ}$	$72^{\circ}$ $-63^{\circ}$	$83^{\circ}$ $-76^{\circ}$	$9^{\circ}$	$81^{\circ}$	$32^{\circ}$ $-14^{\circ}$	$61^{\circ}$	$-74^{\circ}$
WRIST YAW	$+125^{\circ}$ $-130^{\circ}$	$97^{\circ}$	$45^{\circ}$	$125^{\circ}$	$72^{\circ}$ $-41^{\circ}$	$112^{\circ}$ $-45^{\circ}$	$67^{\circ}$ $-36^{\circ}$	$59^{\circ}$ $-34^{\circ}$
ELBOW YAW	$+130^{\circ}$ $-150^{\circ}$	$-135^{\circ}$	$-153^{\circ}$	$-156^{\circ}$	$-99^{\circ}$	$-144^{\circ}$	$-103^{\circ}$	$-118^{\circ}$
SHOULDER ROLL	$\pm 200^{\circ}$ Locked Out	---	---	---	---	---	---	---
SHOULDER YAW	$\pm 135^{\circ}$	$38^{\circ}$	$124^{\circ}$	$33^{\circ}$ $-9^{\circ}$	$72^{\circ}$ $-41^{\circ}$	$108^{\circ}$ $-43^{\circ}$	$59^{\circ}$ $-39^{\circ}$	$61^{\circ}$ $-42^{\circ}$
SHOULDER PITCH	$\pm 200^{\circ}$	$169^{\circ}$	$180^{\circ}$	$99^{\circ}$	$25^{\circ}$	$95^{\circ}$	$160^{\circ}$	$171^{\circ}$

Figure II-17 Maximum Joint Movements for 7 Capture Concepts (6-DOF Slave)

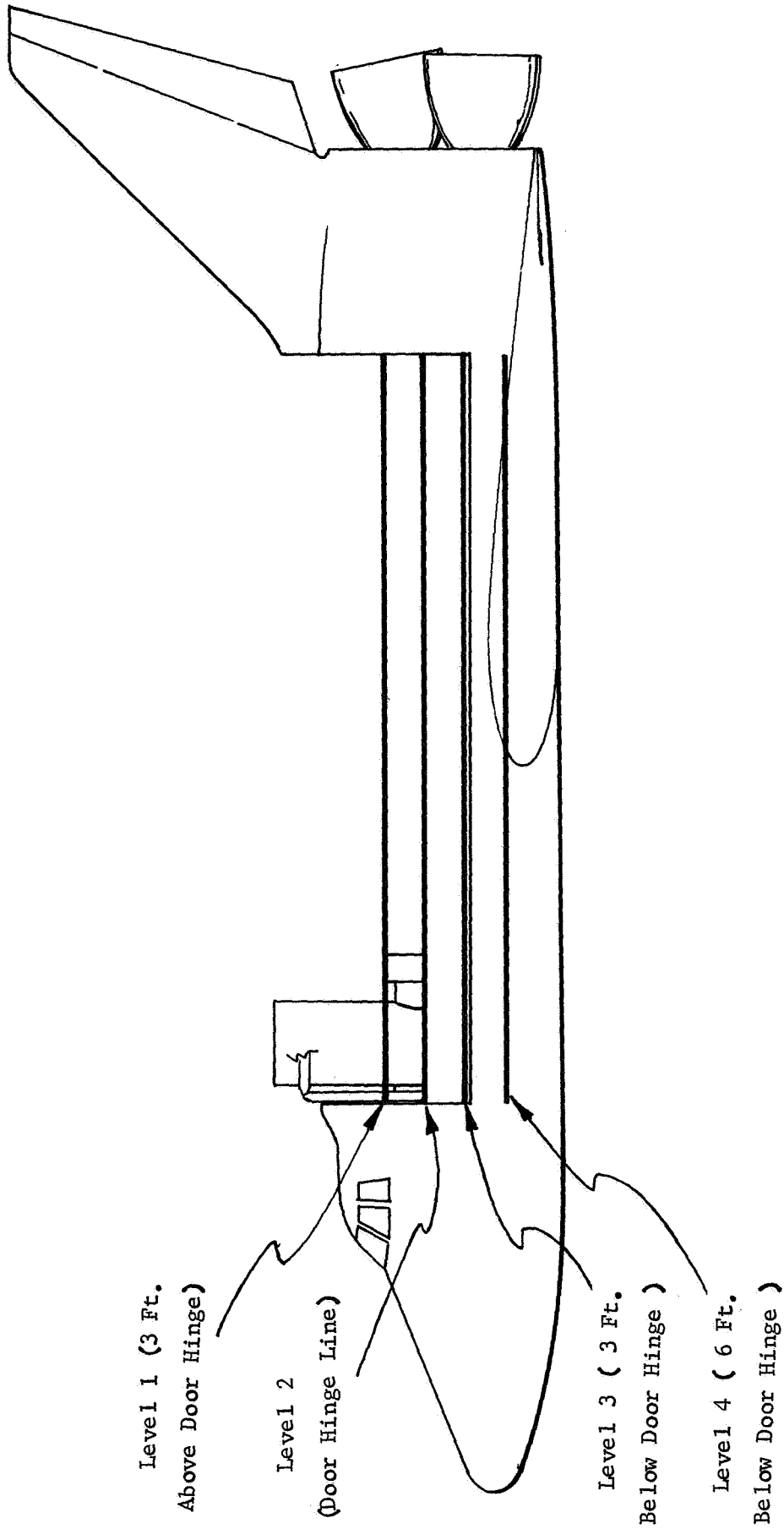
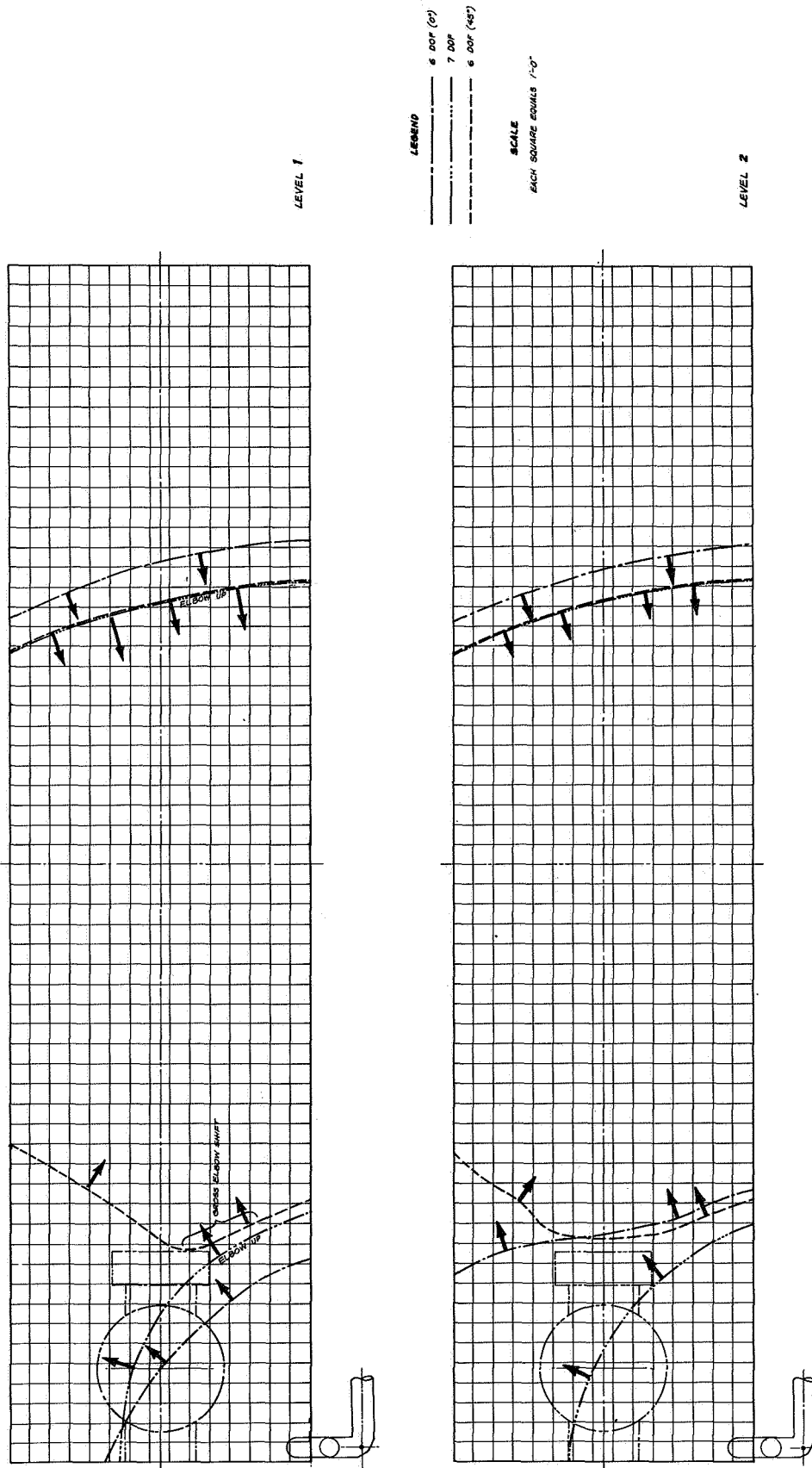
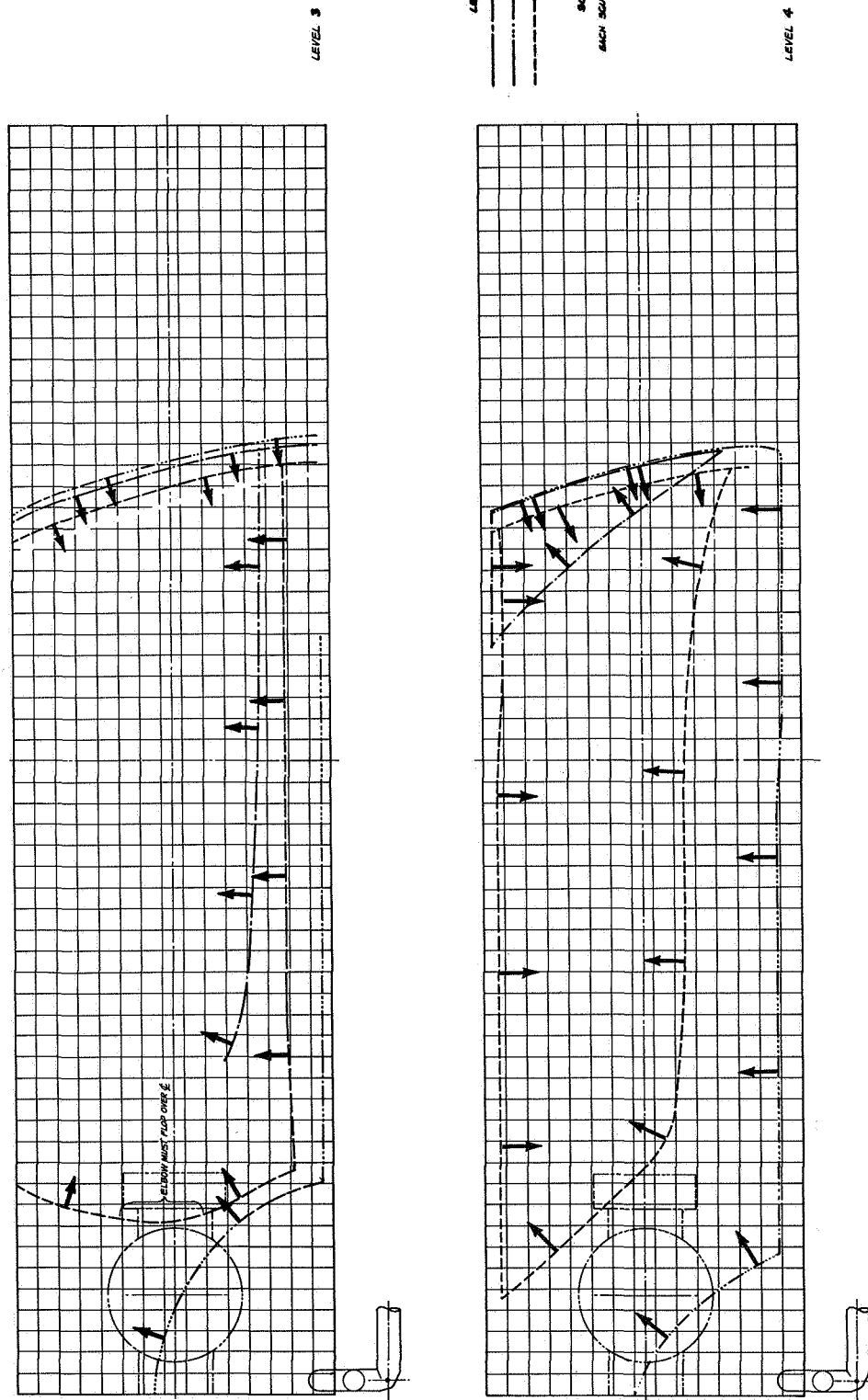


Figure II-18a Cargo Bay Levels



Note: Arrows Indicate Direction of Enclosed Reach Zones

Figure II-18b Manipulator Reach Zones



Note: Arrows Indicate Direction of Enclosed Reach Zones

Figure II-18c Manipulator Reach Zones

down to within one foot (scaled) of the hinge line. As shown in Figure II-18c levels 3 and 4, with 6-DOF and shoulder roll at  $0^{\circ}$ , the task of reaching below the hinge line rapidly deteriorates, until on level 4, the contact zone becomes a small triangle at the rear of the reach zone. This appears unacceptable.

Next, using a full 7-DOF, the shoulder roll angle was carefully recorded to determine its travel. Obviously, the full 7-DOF gave the greatest movement volume since the elbow was free to be positioned straight up. During the tests, the shoulder roll fluxuated between  $28^{\circ}$  and  $64^{\circ}$  while the tip of the slave was moved around the cargo bay. Since reaching into the cargo bay was the only requirement for the 7th-DOF, it was concluded that it may be possible to have two discrete positions for the shoulder roll, and perhaps have a more simplified roll joint control. The roll joint was set in  $10^{\circ}$  increments between  $25^{\circ}$  and  $65^{\circ}$  and reach zones were again evaluated. The data showed that at about  $45^{\circ}$  the best compromise was obtained, if a single roll angle (in addition to zero) was to be selected. With this concept the manipulator operator would control the shoulder roll with a switch to select  $0^{\circ}$  or  $45^{\circ}$  as the task required. The reach profiles are also shown for the shoulder roll at  $45^{\circ}$  in Figures II-18B& C.

#### 1. Docked Satellite Reach Envelopes

This task was to determine the reach zones on the surface of a 15-ft diameter by 40-ft long satellite, docked to the Z axis docking port. This data relates to satellite maintenance, and where the manipulator can reach to do a useful task. The reach zones represent not only the terminal device touching the area, with the wrist roll axis orthogonal to the payload surface, but also being able to move away orthogonally for 5 ft. This would represent pulling a module out. Figure II-19a shows the areas reachable (shaded) in a plan view of the cylinder outer skin. Three reach envelopes are shown for the manipulator configured in 6-DOF (shoulder roll at  $0^{\circ}$ ), 6-DOF (shoulder roll at  $45^{\circ}$ ) and a full 7-DOF. Figure II-19b shows the overlapping zones when two symmetrically mounted manipulators are used. The zone limits were established by either the manipulator upper arm hitting the mockup or by joint limits being reached.

#### 2. Module Replacement

The module replacement task consisted of reaching to the center of the cargo bay, at the hinge line, attaching the terminal

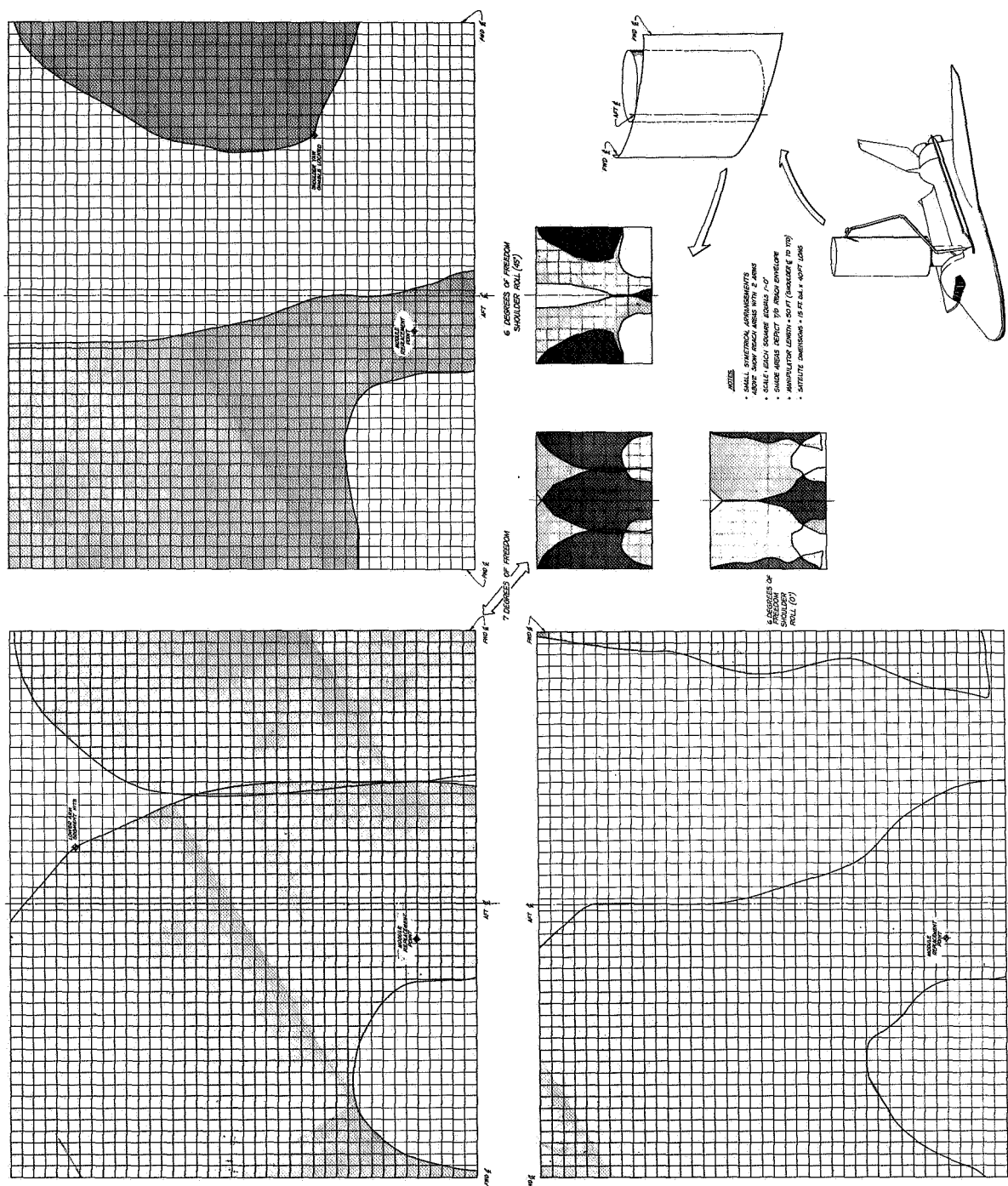


Figure II-19a Docked Satellite Reach Envelopes

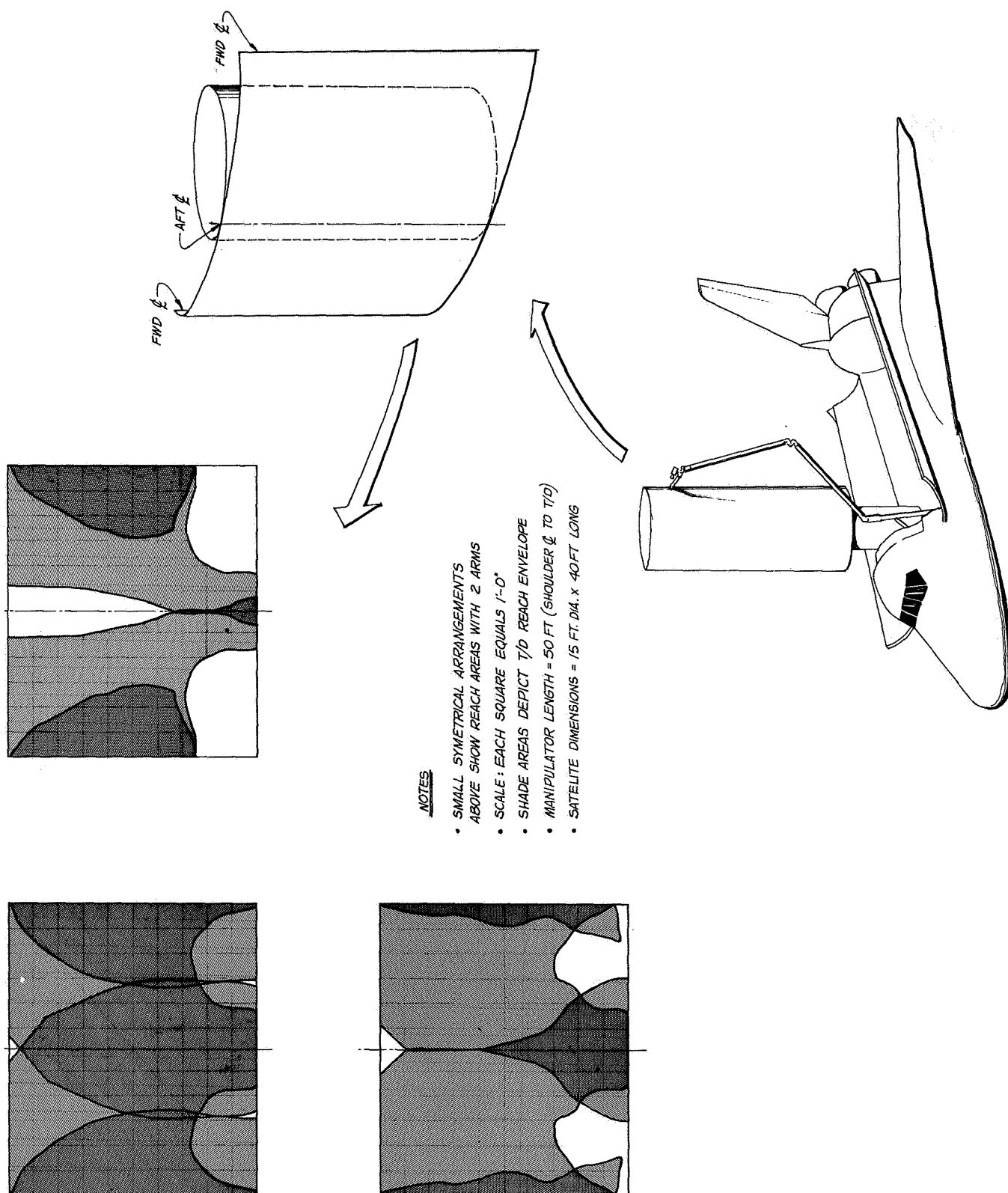


Figure II-19b Docked Satellite Reach Envelopes (Two Manipulators)

device to a module mockup, lifting the module straight up, rotating 90° and inserting it into the satellite mockup (See Figure II-20). This task was easily done with a 6-DOF (shoulder roll at 0°) manipulator configuration.



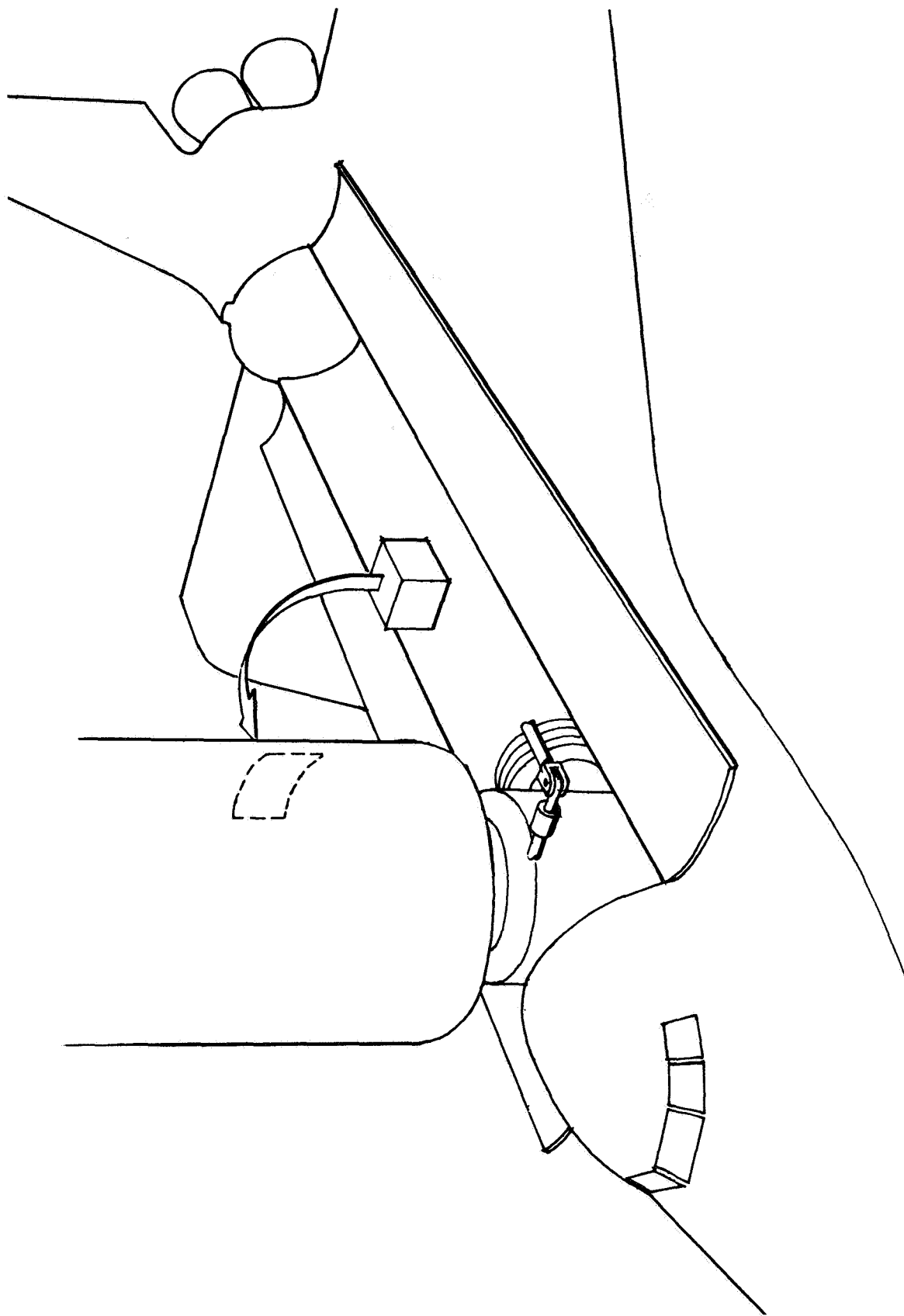


Figure II-20 Module Replacement

### III. SERVO DESIGN OF A 2-DEGREE OF FREEDOM X REFERENCE FRAME BILATERAL FORCE REFLECTING POSITION-POSITION CONTROL SYSTEM

#### A. CONTROL LAW EQUATIONS

##### 1. Objective

The objective of this section is the control law design of a 2-DOF bilateral force reflecting control system for use in a manipulator system breadboard incorporating a 2-DOF master and a 2-DOF slave.

The 2-DOF breadboard control system is for concept verification prior to the detail design of a 6-DOF control system for the AMS.

The control system must include the following features:

1. Bilateral force reflecting operation,
2. Size disparity between master and slave,
3. Different coordinate systems for master and for slave,
4. Position indexing for the master, and
5. Variable control gain ratios between master and slave.

##### 2. Existing Bilateral Manipulator

To develop an understanding and appreciation of the control scheme being designed, a brief discussion will be given here of the control principles of existing bilateral manipulators and why these principles cannot be directly applied to a manipulator possessing the aforementioned capabilities.

Bilateral force reflecting manipulators, incorporating a geometrically similar master controller as the control input device, possess, in addition to the forward position loop which makes the manipulator follow the master movements, feedback to the master from the manipulator. The servo parameter used for this feedback may be either position or force. Figure III-1 depicts this two way information flow between master and slave. To be more explicit, Figure III-1 can be shown in greater detail, Figure III-2, to reveal that existing bilateral manipulator systems with master replica controllers have two

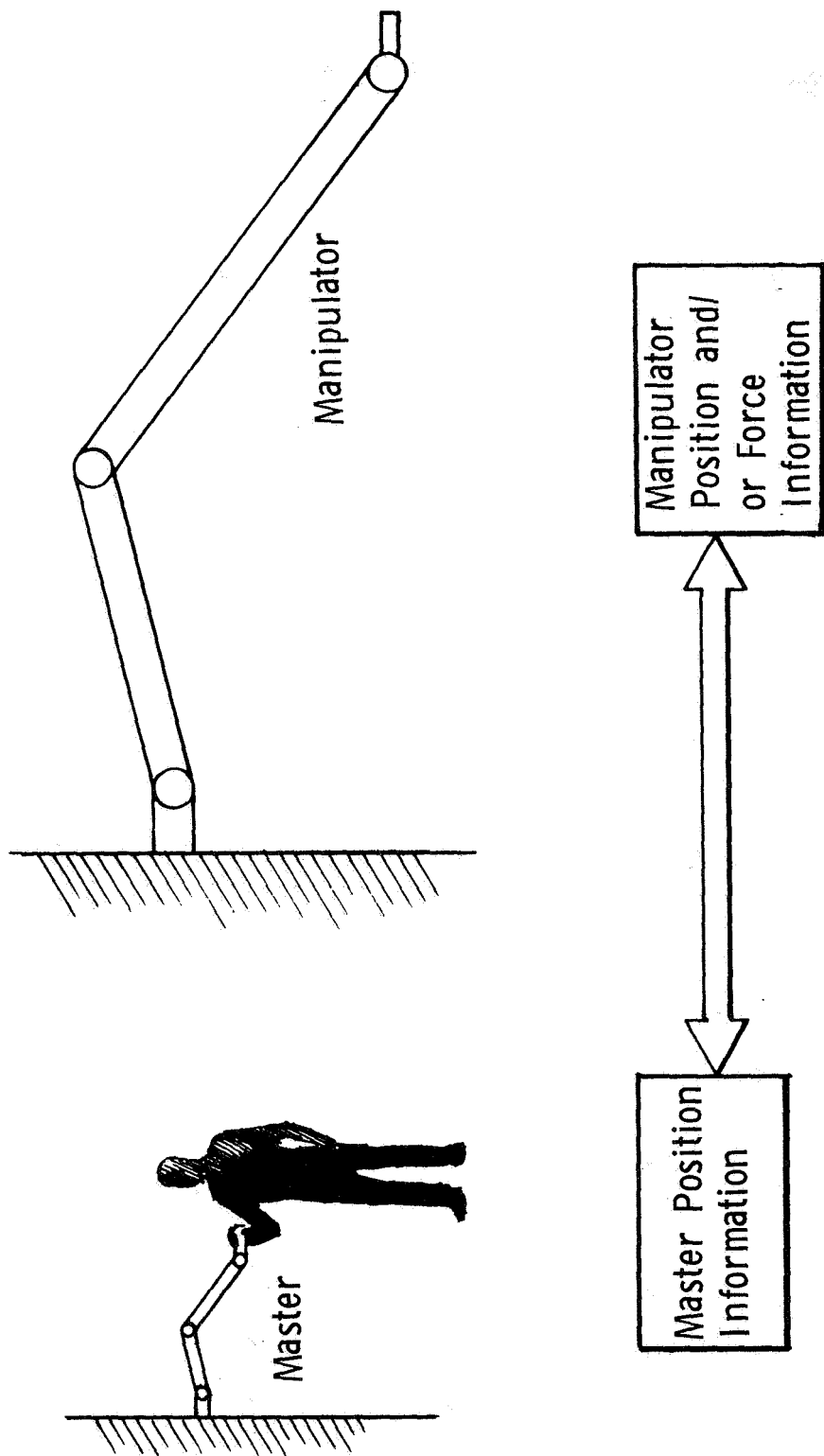


Figure III-1 Two Way Information Flow in Bilateral Force Reflecting Manipulator System

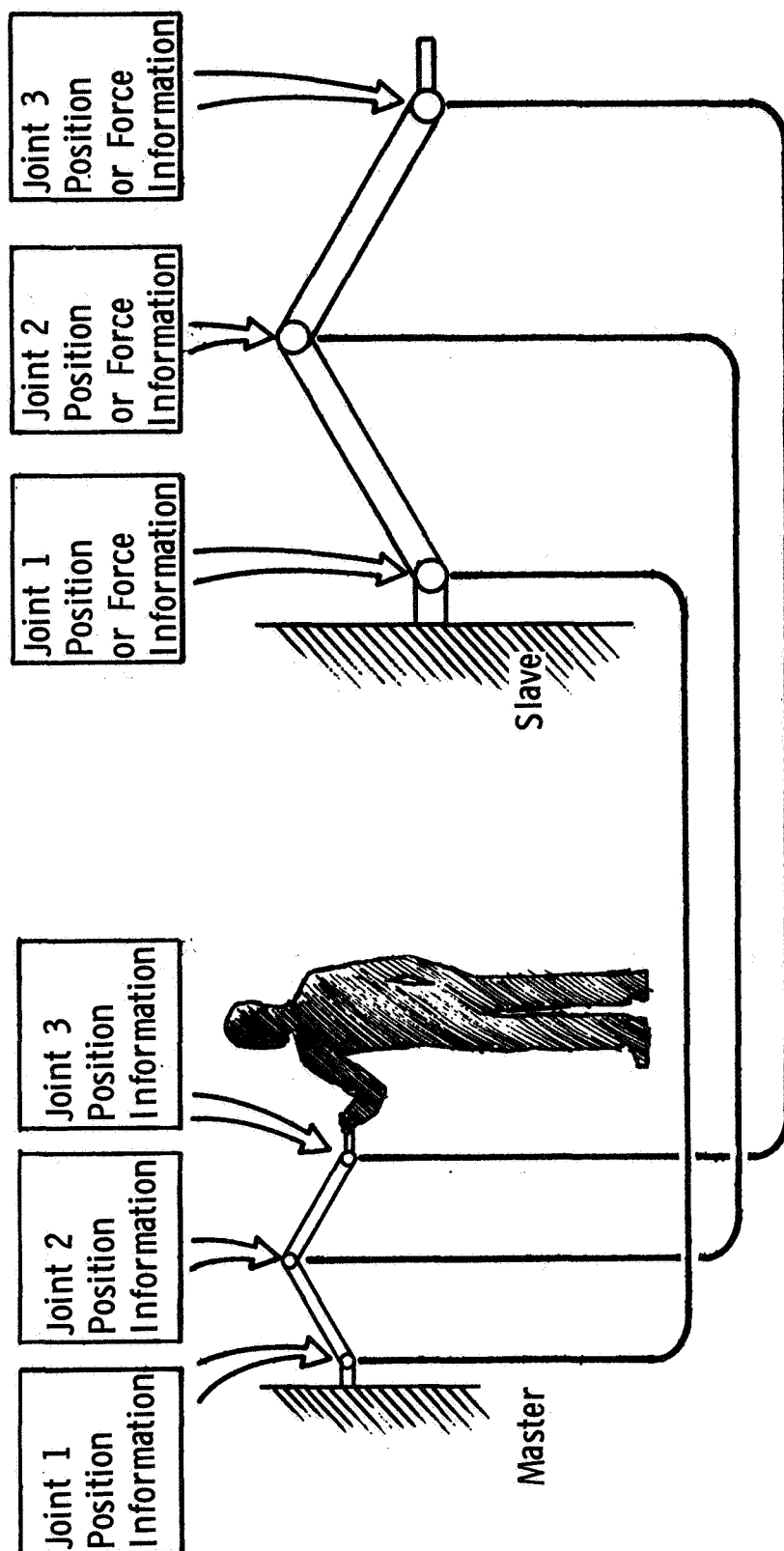


Figure III-2 Bilateral Force Reflecting Manipulator With One to One Joint Coupling

way information flow only on a one-to-one joint basis. That is, master and slave have the same number of degrees of freedom and each joint on the master is electrically coupled to and only to its counterpart joint on the manipulator. Thus, each master-slave joint pair track each other in angular positions at some prescribed ratio.

To understand the inability of a one-to-one joint coupled system to perform multi-mode and coordinate indexed functions, consider the situation shown in Figure III-3. Represented is the master operating in Shuttle axis (axis system one) and the manipulator operating in its own terminal device TV camera axis (axis system two). If it is desired that the manipulator move forward in the  $X_2$  direction, the master must be moved forward in the  $X_1$  direction. It is easily seen that the ratio of movement between any joint on the master and its counterpart on the manipulator is a function of manipulator position. In fact, the situation could easily arise whereas all joints on the master are in motion and only one or two joints on the manipulator are activated to produce the commanded trajectory. Thus, one-to-one joint coupling is totally inapplicable for coordinate indexing. Likewise, for multi-mode operation (operation in which the tip position of the master and the tip position of the slave move with respect to each other in some set ratio, and this ratio can be selected by the operator) one-to-one joint coupling is impractical (considering now motion ratios other than 1:1, and large master-slave size disparity). This is easily seen if it is realized that the motion ratio for a master-slave joint pair is a function of position if the tip motion ratio between the input and output devices is to remain constant.

In order to surmount the abovementioned problems, the comparison of individual joint positions in a one-to-one joint coupled system must be abandoned and a new quantity of comparison devised. This new quantity is the XYZ (henceforth referred to as  $\underline{X}$ ) tip position of the master and manipulator. By doing all comparisons in the  $\underline{X}$  reference frame, the capabilities of coordinate indexing, multi-mode operation, and position indexing are easily obtainable as will be shown below.

### 3. Basic Control Scheme

Figure III-4 shows the block diagram of the  $\underline{X}$  reference frame position-position bilateral force reflecting control scheme under consideration. It was stated previously that the

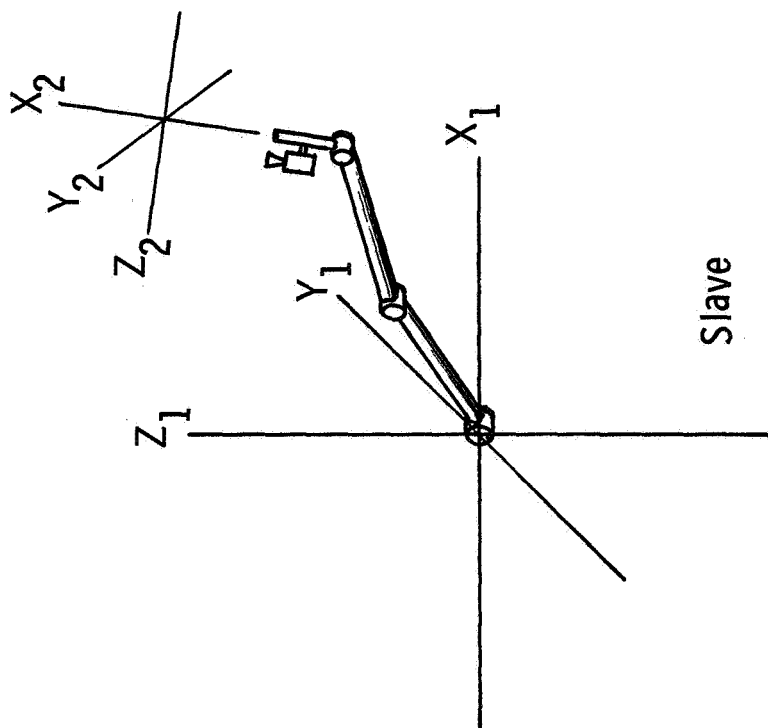
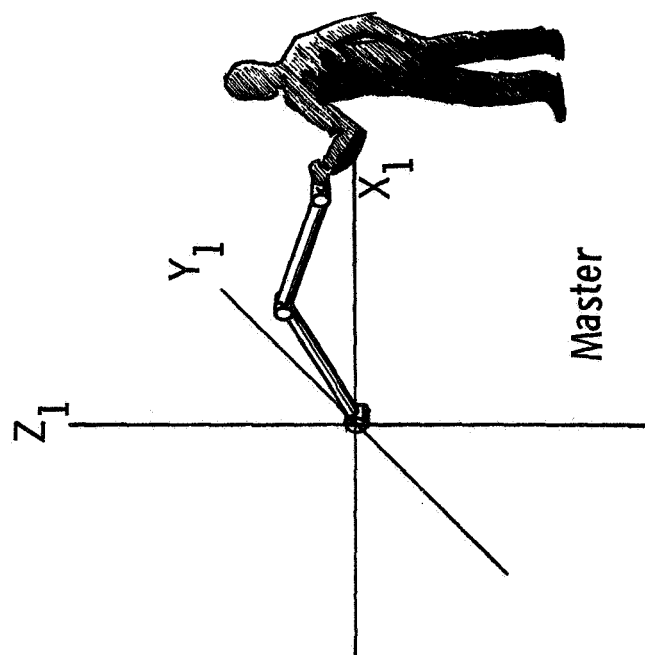


Figure III-3 Master and Slave Operating in Two Different Axis Systems

feedback parameter for a bilateral manipulator system could be either position or force. As evidenced by Figure III-4, the parameter of position has been selected to illuminate the inherent problems associated with force measuring devices such as strain gauges.

As seen from Figure III-4, the first step in the control laws is the calculation of the  $\underline{X}_c$  tip position of the master and the  $\underline{X}_m$  tip position of the manipulator. After these tip position values are obtained, they are operated on by coordinate transformation matrices, gain or attenuation functions (to obtain the proper multi-mode value), and can readily be summed with bias voltages to provide position indexing. The resulting  $\underline{X}'_c$  and  $\underline{X}'_m$  values are compared to produce  $\pm \underline{X}$  position error signals. These signals are multiplied by appropriate gain matrices (the magnitude of these gain functions determine the compliance or stiffness of the control system) and are then summed with  $\underline{X}_c$  and  $\underline{X}_m$  tip velocity terms which produce the needed system damping. The resulting signals represent  $\underline{X}$  tip forces that the master and slave must apply to their environment. These force signals are then operated on by torque distribution matrices with the result being the desired signal levels to be sent to the individual servo motors at each master and slave joint.

Although this  $\underline{X}$  reference frame control technique does provide a bilateral manipulator system with the desired performance qualities, it also introduces two system complications, these being:

1. The resultant control system is highly nonlinear, and
2. The master and slave must be interfaced with either an analog or digital computer.

The effects of these two complications will be discussed further.

#### 4. Two DOF Control Laws

a. Purpose of Two DOF Breadboard - Figure III-4 represents the translation  $\underline{X}$  reference frame control logic for a bilateral force reflecting manipulator with coordinate indexing, multi-mode operation, and position indexing. For a six DOF manipulator, controlling the tip translations is only half the job, terminal device rotational control must likewise be considered.

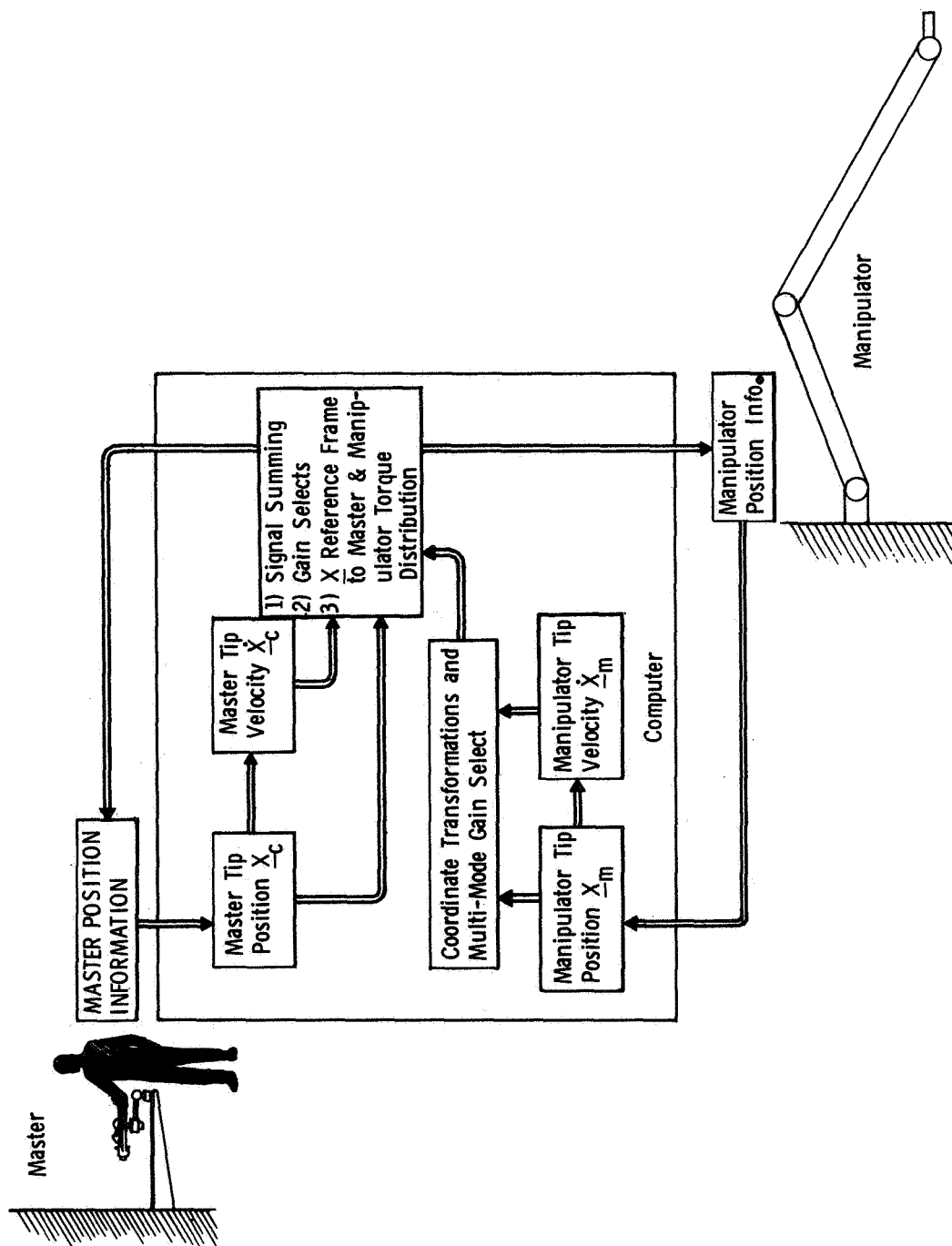


Figure III-4  $\underline{X}$  Reference Frame Position-Position Bilateral Force Reflecting Control System



It is conceived that rotational and translational control will be similar in that the terminal device orientation of both the master and slave will be computed with respect to some inertial orientation and then compared to produce a  $\theta$  orientational error signal in much the same fashion that a  $X$  positional error signal is computed for translational control. The details of rotational control have not been considered but it is believed that a slightly more complicated technique will be needed for rotational as compared to translational control. Therefore, this initial investigation will deal primarily with the problems of translational control and hopefully the solutions to these problems will expedite the eventual design of the rotational part of the system.

To "prove the concept", in hardware, of the translational control technique, a two, instead of three, DOF breadboard was selected. This decision was made for two reasons: (1) all the computer calculations needed for three DOF are also needed for two DOF, and therefore the simpler situation can prove the workability of both cases, and (2) a two DOF manipulator needs no counterbalancing mechanism and thus is quite cost effective.

Figure III-5 shows the two DOF master and slave breadboard arms. The master has segment lengths of one foot with the manipulator segment lengths being two feet. The actual size of the arms was not critical but a master-slave size disparity was important to prove the validity of the control equations. As indicated by Figure III-4, the two arms shown will be interfaced by computer (analog first then digital) that will perform the needed calculations.

b. Shortcomings of Two DOF Breadboard - To fully understand what is to be expected from the design of the two DOF breadboard, the questions it will not answer must be made clear: (1) Figure III-5 shows there are no terminal devices on the end of either the master or slave, and therefore, as mentioned earlier, no rotational control techniques are included, (2) One of the major unknowns of the full length AMS manipulator is the effect of low frequency structural oscillations that presumably can be excited in the manipulator beams. The two DOF breadboard is not designed to investigate this problem, for as seen in Figure III-5, the beam structures are relatively short and very rigid. In a separate section this problem is addressed by using the results of the breadboard design to write a computer program for the design of a full length two DOF manipulator which is integrated with another program describing the manipulator flexible body dynamics. These two combined programs are used to investigate

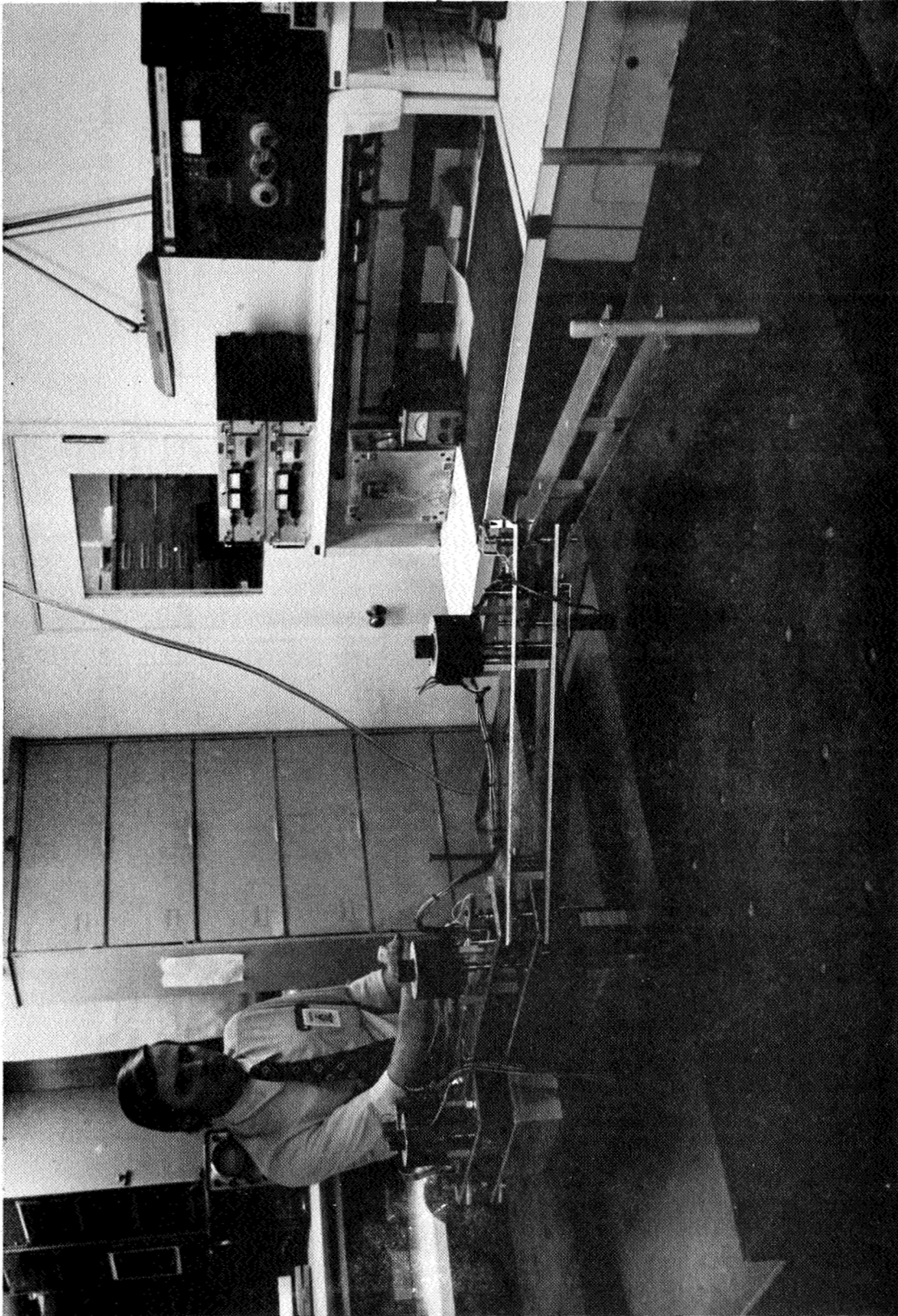


Figure III-5 Two DOF Master and Slave Breadboard Arms

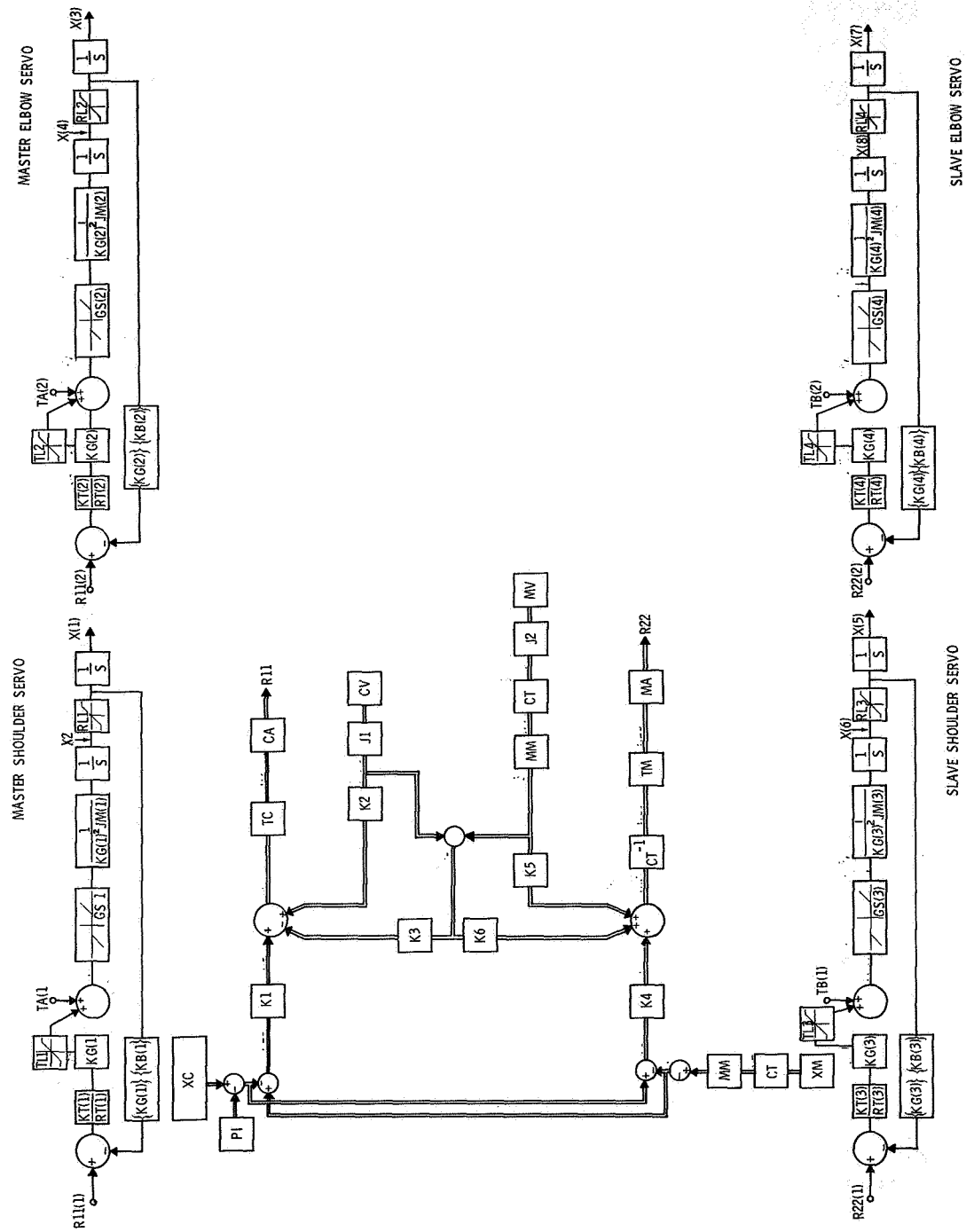


Figure III-6 Control System for Two DOF Breadboard

the effects of structural oscillations on the control system, and will, if necessary, aid in the design of an active damping system.

### c. Block Diagram of Two DOF Control System -

Figure III-6 represents the block diagram of the control system for the two DOF breadboard. This diagram includes all joint components (servo motors, tachometer generators, gears, potentiometers, etc.) of both the master and slave along with all the signal channelling and necessary computer accomplished computations. Double lined signal routes represent two separate signals, and many of the gain functions are actually gain matrices, as will be described below. A considerable number of the variable names are included only as an aid in computer programming and will not be defined, whereas the more important quantities are defined in Table III-1. Those elements that cannot be clearly explained by the use of Figure III-6 and Table III-1 are briefly discussed in further detail below.

#### 1. XC

XC is a two dimensional vector denoting the X and Y tip position of the master. This tip position is calculated from a knowledge of the master shoulder,  $X(1)$ , and elbow,  $X(3)$ , angular positions. From Figure III-7 it is seen that XC is calculated as follows:

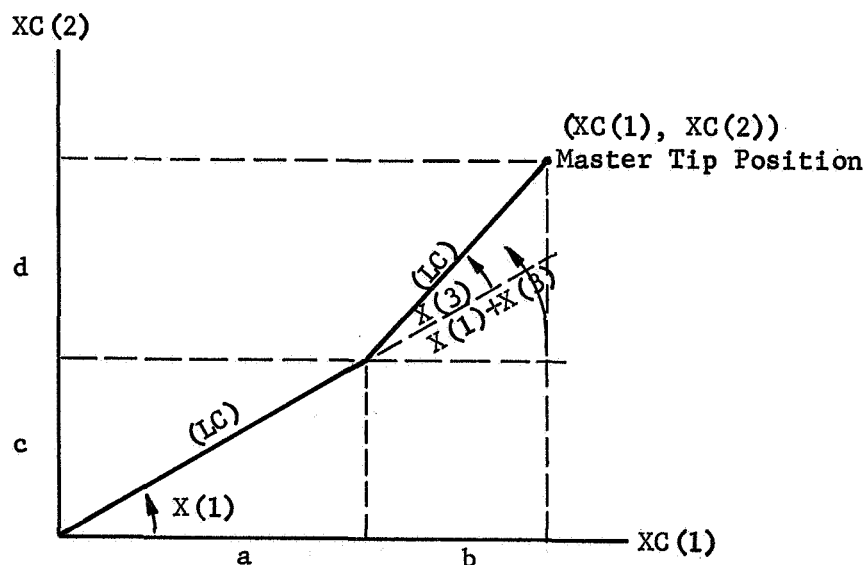


Figure III-7 Joint Angles and Tip Position Labelling for Master

Table III-1 Definition of Variable Names Appearing in Figure III-6.

GS(i)	= Motor and Gear Train Stiction Valves
KT(i)	= Motor torque sensitivity constants
RT(i)	= Total resistance of motor winding and output impedance of driver amplifier
KG(i)	= Gear train ratio
KB(i)	= Motor viscous damping constants
<u>XC</u>	= X and Y tip position of Master
<u>XM</u>	= X and Y tip position of manipulator
K1, K2, K3, K4, K5, K6	= diagonal gain matrices
TC	= Torque distribution matrix for the Master
TM	= Torque distribution matrix for the manipulator
CA, MA	= Diagonal gain matrices
J1, J2	= Jacobian matrices relating joint rates to tip rates
CT	= Coordinate transformation matrix
MM	= Diagonal gain matrix used to select different multi-mode values
<u>PI</u>	= Position index bias signals
<u>CV</u>	= Master joint rates
<u>MV</u>	= Manipulator joint rates
X(1)	= Master shoulder joint position
X(2)	= Master shoulder joint rate
X(3)	= Master elbow joint position
X(4)	= Master elbow joint rate
X(5)	= Manipulator shoulder joint position
X(6)	= Manipulator shoulder joint rate
X(7)	= Manipulator elbow joint position
X(8)	= Manipulator elbow joint rate
TA(i)	= Master input disturbance torques
TB(i)	= Manipulator input disturbance torques
R11(i)	= Master servo motor drive signals
R22(i)	= Manipulator servo motor drive signals
TL(i)	= Motor-gear train torque limit values
RL(i)	= Motor-gear train rate limit values
$\frac{1}{s}$	= Denotes integration

$$\underline{XC} = \begin{bmatrix} XC(1) \\ XC(2) \end{bmatrix} = \begin{bmatrix} (a+b) \\ (c+d) \end{bmatrix}$$

$$a = (LC)\cos(X(1))$$

$$b = (LC)\cos(X(1) + X(3))$$

$$c = (LC)\sin(X(1))$$

$$d = (LC)\sin(X(1) + X(3))$$

$$\underline{XC} = \begin{bmatrix} XC(1) \\ XC(2) \end{bmatrix} = \begin{bmatrix} (LC) [\cos(X(1)) + \cos(X(1) + X(3))] \\ (LC) [\sin(X(1)) + \sin(X(1) + X(3))] \end{bmatrix}$$

## 2. XM

XM is a two dimensional vector denoting the X and Y tip position of the manipulator. This tip position is calculated from a knowledge of the manipulator shoulder, X(5), and elbow, X(7), angular position. The derivation for XM is identical to that for XC and therefore, by comparison,

$$\underline{XM} = \begin{bmatrix} XM(1) \\ XM(2) \end{bmatrix} = \begin{bmatrix} (LM) [\cos(X(5)) + \cos(X(5) + X(7))] \\ (LM) [\sin(X(5)) + \sin(X(5) + X(7))] \end{bmatrix}$$

## 3. PI

PI is a two dimensional vector representing the X and Y bias voltages needed for positional indexing. When the master is position indexed from location XC<sub>1</sub> to location XC<sub>2</sub>, the

difference between these two tip position locations is calculated and used as a bias value that is summed with XC.

4. K1

K1 is a diagonal 2 x 2 gain matrix with the two diagonal elements equal. The K1 elements determine the X forward loop gain of the master servos and thus are inversely proportional to the master servo compliance.

5. K2

K2 is a diagonal 2 x 2 gain matrix with the two diagonal elements equal. The K2 elements determine how much positive tip rate feedback is incorporated into the master servo system. Positive rate feedback can be (but may not necessarily be) used to overcome the viscous damping of the servo motor and thus make the master easier to move.

6. K3

K3 is a diagonal 2 x 2 gain matrix with the two diagonal elements equal. The K3 elements determine how much differential tip rate feedback is used in the master servo system. Differential rate feedback is used to help stabilize the system and acts to give good transient damping yet does not degrade "easy of movement" for steady state conditions.

7. K4

K4 is K1's counterpart for the manipulator arm.

8. K5

K5 is K2's counterpart for the manipulator arm.

9. K6

K6 is K3's counterpart for the manipulator arm.

10. TC

TC is the master torque distribution matrix and is one of the more important parts of the overall control system. The inputs to TC are signals that represent force values the master is to exert on its environment. These force values

must be transformed into torque values that the shoulder and elbow servo motors can produce. To derive this matrix, consideration is given to the external applied forces and internal generated torques that act on the master in equilibrium, as pictured in Figure III-8.

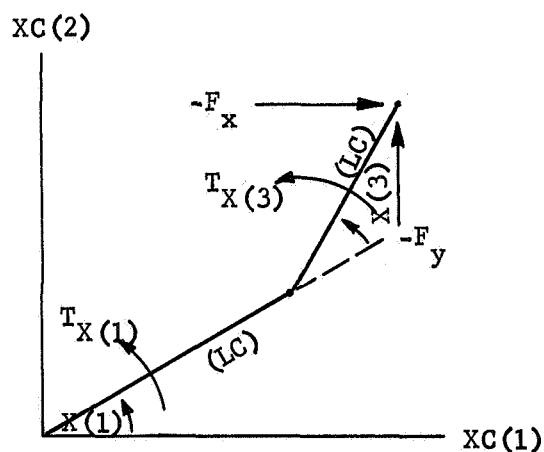


Figure III-8 Master Torques and Forces at Equilibrium

Considering first only the elbow to tip segment of the master as shown in Figure III-9, the equilibrium torques about point E are summed to give,

$$\sum T_E = 0 = T_{X(3)} - (F_y)(LC)\cos(X(1) + X(3)) + (F_x)(LC)\sin(X(1) + X(3)),$$



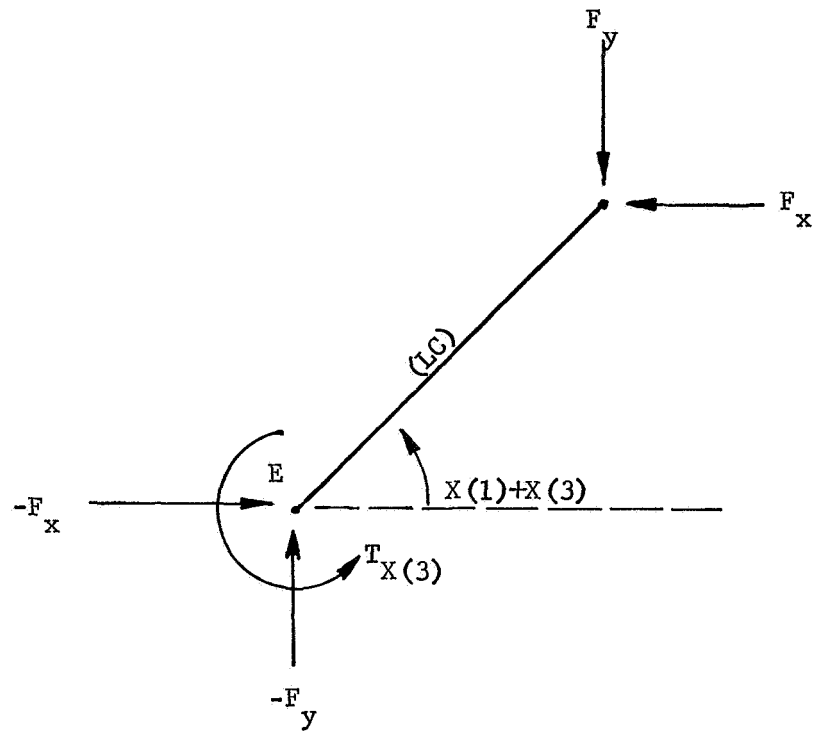


Figure III-9 Equilibrium Torques and Forces on Master Upper Segment

or

(1)

$$T_{X(3)} = (-LC)\sin(X(1) + X(3))(F_x) + (LC)\cos(X(1) + X(3))(F_y).$$

Accounting now for the equilibrium conditions of the elbow to shoulder segment, as shown in Figure III-10,

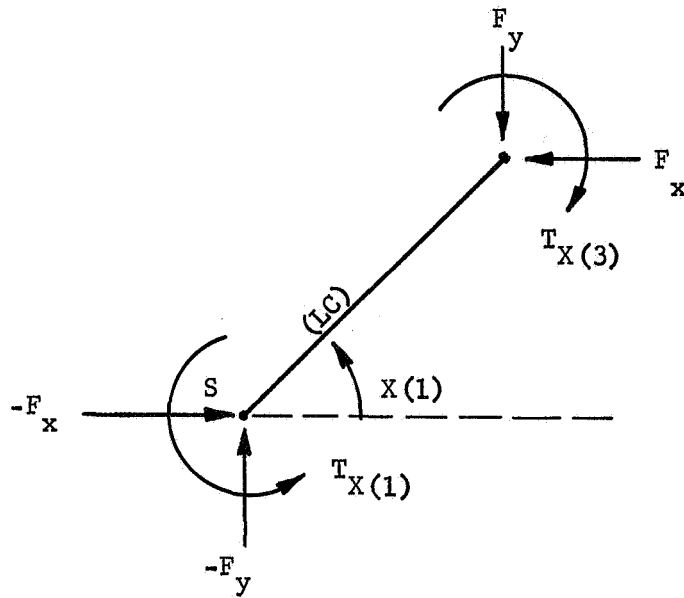


Figure III-10 Equilibrium Torques and Forces on Master Lower Segment

the torques about point S are summed to give,

$$\sum T_s = 0 = T_{X(1)} - (F_y)(LC)\cos(X(1)) + (F_x)(LC)\sin(X(1)) - T_{X(3)}.$$

Solving for  $T_{X(1)}$  and substituting from equation (1) yields

$$T_{X(1)} = (-LC) \left[ \sin(X(1)) + \sin(X(1) + X(3)) \right] (F_x) + (LC) \left[ \cos(X(1)) + \cos(X(1) + X(3)) \right] (F_y). \quad (2)$$

Putting equations (1) and (2) in matrix form gives:

$$\begin{bmatrix} T_{X(1)} \\ T_{X(3)} \end{bmatrix} = \begin{bmatrix} (-LC) \left[ \sin(X(1)) + \sin(X(1) + X(3)) \right] & (LC) \left[ \cos(X(1)) + \cos(X(1) + X(3)) \right] \\ (-LC) \sin(X(1) + X(3)) & (LC) \cos(X(1) + X(3)) \end{bmatrix} \begin{bmatrix} F_x \\ F_y \end{bmatrix}.$$

This equation relates the tip forces, in equilibrium, that the master applies to its environmental when the shoulder and elbow torque motor are producing  $T_{X(1)}$  and  $T_{X(3)}$  units of torque, respectively. Therefore, the TC matrix is given by

$$TC = \begin{bmatrix} (-LC) \left[ \sin(X(1)) + \sin(X(1) + X(3)) \right] & (LC) \left[ \cos(X(1)) + \cos(X(1) + X(3)) \right] \\ (-LC) \sin(X(1) + X(3)) & (LC) \cos(X(1) + X(3)) \end{bmatrix}.$$

#### 11. TM

TM is the manipulator torque distribution and is derived in the same fashion as TC. The TM matrix is given by:

$$TM = \begin{bmatrix} (-LM) \left[ \sin(X(5)) + \sin(X(5) + X(7)) \right] & (LM) \left[ \cos(X(5)) + \cos(X(5) + X(7)) \right] \\ (-LM) \sin(X(5) + X(7)) & (LM) \cos(X(5) + X(7)) \end{bmatrix}.$$

#### 12. J1

J1 is the Jacobian matrix relating master joint rates to the X, Y tip rates. It was shown that the master tip position is given by:

$$XC(1) = (LC) \left[ \cos(X(1)) + \cos(X(1) + X(3)) \right] \quad (3)$$

$$YC(1) = (LC) \left[ \sin(X(1)) + \sin(X(1) + X(3)) \right] \quad (4)$$

If the first derivative of these equations with respect to time are denoted by

$$\frac{d[XC(1)]}{dt} = XCD(1)$$

$$\frac{d[XC(2)]}{dt} = XCD(2)$$

and letting

$$\frac{d[X(1)]}{dt} = X(2)$$

$$\frac{d[X(3)]}{dt} = X(4),$$

the time derivatives of equations (3) and (4) are

$$XCD(1) = \frac{\partial XC(1)}{\partial X(1)} X(2) + \frac{\partial XC(1)}{\partial X(3)} X(4)$$

$$XCD(2) = \frac{\partial XC(2)}{\partial X(1)} X(2) + \frac{\partial XC(2)}{\partial X(3)} X(4).$$

Evaluating these equations yields in matrix form

$$\underline{\underline{XCD}} = \begin{bmatrix} XCD(1) \\ XCD(2) \end{bmatrix} = \begin{bmatrix} (-LC) \left[ \sin(X(1)) + \sin(X(1)+X(3)) \right] & (-LC) \sin(X(1)+X(3)) \\ (LC) \left[ \cos(X(1)) + \cos(X(1)+X(3)) \right] & (LC) \cos(X(1)+X(3)) \end{bmatrix} \begin{bmatrix} X(2) \\ X(4) \end{bmatrix}.$$

From this equation it is seen that the J1 Jacobian matrix is

$$J1 = \begin{bmatrix} (-LC) \left[ \sin(X(1)) + \sin(X(1)+X(3)) \right] & (-LC) \sin(X(1)+X(3)) \\ (LC) \left[ \cos(X(1)) + \cos(X(1)+X(3)) \right] & (LC) \cos(X(1)+X(3)) \end{bmatrix}.$$

### 13. J2

J2 is the Jacobian matrix relating manipulator joint rates to X, Y tip rates. By analogy to J1, it is derived to be

$$J2 = \begin{bmatrix} (-LM) \left[ \sin(X(5)) + \sin(X(5)+X(7)) \right] & (-LM) \sin(X(5)+X(7)) \\ (LM) \cos(X(5)) + \cos(X(5)+X(7)) & (LM) \cos(X(5)+X(7)) \end{bmatrix}.$$

#### 14. MM

MM is a diagonal gain matrix with all diagonal elements equal. It is used to set the multi-mode ratio selected by the operator. As an example, suppose it is desired that the master and manipulator tip displacement ratio is 1:10; that is, for every one unit moved by the master, the manipulator moves 10 units. To obtain this ratio, the MM matrix would equal

$$MM = \begin{bmatrix} \frac{1}{10} & 0 \\ 0 & \frac{1}{10} \end{bmatrix}.$$

#### 15. CT

CT is the coordinate transformation matrix that transforms the XC tip position of the manipulator in the XC, or fixed axis system, to the value of this tip position in the XM, or operating axis system.

The CT matrix is derived as shown below. Consider the two axis systems XC and XM shown in Figure III-11.

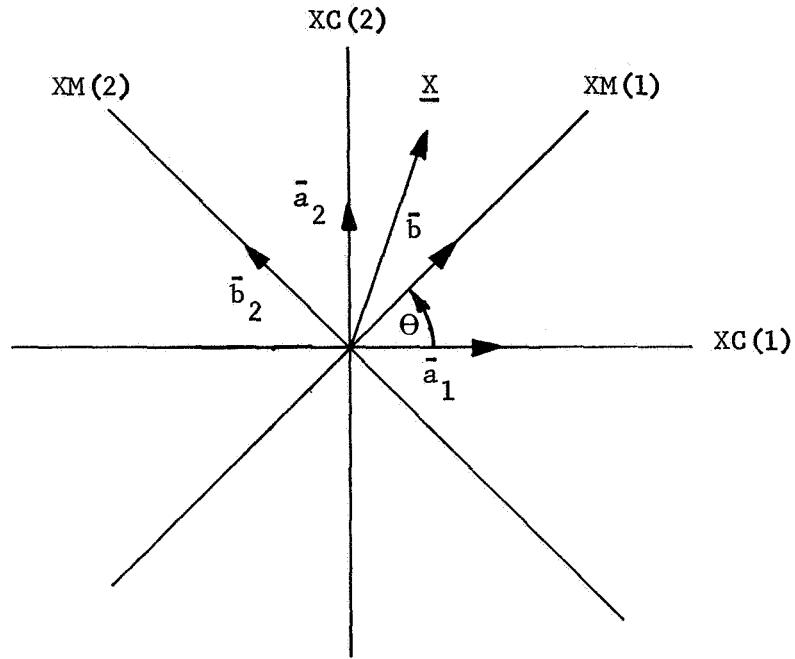


Figure III-11 Two Axis System Showing Derivation of Coordinate Transformation Matrix

- Let:
- (1)  $\underline{X}$  be vector representing manipulator tip position,
  - (2)  $\bar{a}_i$  be unit basis vectors in  $\underline{XC}$  axis,
  - (3)  $\bar{b}_i$  be unit basis vectors in  $\underline{XM}$  axis, and
  - (4)  $\theta$  be rotation angle between the axis  $\underline{XC}$  and  $\underline{XM}$ .

The  $\bar{a}_i$  can be expressed in terms of the  $\bar{b}_i$  as:

$$\bar{a}_1 = P_{11}\bar{b}_1 + P_{12}\bar{b}_2 \quad (5)$$

$$\bar{a}_2 = P_{21}\bar{b}_1 + P_{22}\bar{b}_2 \quad (6)$$

where  $P_{11} = \cos\theta$ ,  $P_{12} = -\sin\theta$ ,  $P_{21} = \sin\theta$ ,  $P_{22} = \cos\theta$ , and the vector  $\underline{X}$  can be expressed as either

$$\bar{X} = XC(1)\bar{a}_1 + XC(2)\bar{a}_2 = XM(1)\bar{b}_1 + XM(2)\bar{b}_2. \quad (7)$$

Substituting equations (5) and (6) into (7) yields

$$\bar{X} = XC(1) \begin{bmatrix} P_{11}\bar{b}_1 + P_{12}\bar{b}_2 \end{bmatrix} + XC(2) \begin{bmatrix} P_{21}\bar{b}_1 + P_{22}\bar{b}_2 \end{bmatrix} = XM(1)\bar{b}_1 + XM(2)\bar{b}_2.$$

Simplifying produces

$$(XC(1)P_{11} + XC(2)P_{21})\bar{b}_1 + (XC(1)P_{12} + XC(2)P_{22})\bar{b}_2 = XM(1)\bar{b}_1 + XM(2)\bar{b}_2,$$

and comparing coefficients of the  $b_i$  gives

$$\begin{bmatrix} XM(1) \\ XM(2) \end{bmatrix} = \begin{bmatrix} P_{11} & P_{21} \\ P_{12} & P_{22} \end{bmatrix} \begin{bmatrix} XC(1) \\ XC(2) \end{bmatrix}. \quad (8)$$

Equation 8 transforms the tip position of the manipulator in the fixed, or base axis system,  $\underline{XC}$ , into the value of this tip position in the operating or  $\underline{XM}$  axis system. Substituting for the  $P_{ij}$  yields



$$\begin{bmatrix} XM(1) \\ XM(2) \end{bmatrix} = \begin{bmatrix} \cos\theta & \sin\theta \\ -\sin\theta & \cos\theta \end{bmatrix} \begin{bmatrix} XC(1) \\ XC(2) \end{bmatrix} \quad (9)$$

and thus CT is shown to be

$$CT = \begin{bmatrix} \cos\theta & \sin\theta \\ -\sin\theta & \cos\theta \end{bmatrix}$$

## 5. Design Philosophy

a. Operational Requirements - As a guideline for the design of the electronics that will interface the master and slave arms, basic operational criteria must be specified. Some of this criteria is "general", in that no unique design numbers exist due to the systems flexibility with man "in the loop", some of the criteria is obtained from past research on bilateral force reflecting remote manipulators, and still other of the guidelines are a result of personal intuition on how this X reference frame control system should operate. The four primary operational requirements that must be considered for this, as well as any other bilateral manipulator system, are as follows.

1) Compliance - Compliance is a measure of the servo "stiffness" of a manipulator system. As has been pointed out by past work in the field, the stiffer the servo loops the more readily man-in-the-loop can adapt and control a remote manipulator. Unfortunately, there is an upper bound on how stiff a servo loop can be made due to the high gains that evolve which result in destabilizing the system. Compliance can easily be measured by rigidly attaching the manipulator to an immovable object and then applying a torque to one of the master joints. The ratio of angular displacement of the

joint to the applied torque is the compliance number for that joint. The literature has shown that a compliance of  $2 \times 10^{-3}$  rad/ft.lb is a workable number for a one-to-one joint coupled bilateral manipulator. For an  $\underline{X}$  reference frame control system, the compliance will be given as the feet displaced at the master tip in the X or Y direction to the lbs applied force of the tip in the X or Y direction for a rigidly fixed manipulator. It is hoped that the two DOF breadboard can be designed with an X and a Y compliance figure of  $0.5 \times 10^{-3}$  ft/lb. The gain matrix K1 in Figure III-6 determines the master compliance and therefore must be, to meet the  $0.5 \times 10^{-3}$  ft/lb figure, given by

$$K1 = \begin{bmatrix} 2000 & 0 \\ 0 & 2000 \end{bmatrix}.$$

2) Operating Speed - The speed at which the master and slave move (let this speed be denoted by  $\dot{\underline{X}}$ ) under the influence of an operator applied input force is a function of the system gains, gear friction, and the internal viscous damping of each servo motor. The greater the force needed to move the arms, the greater the degradation in the force feedback qualities of the system. Thus it is desirable to maximize the ratio  $\frac{\dot{\underline{X}}}{F_{\min}}$ , where  $F_{\min}$  is the minimum input force needed to set the system in motion, to its largest possible value and still maintain a workable system stability. From initial work, it appears that a value of

$$\frac{\dot{\underline{X}}}{F_{\min}} = \frac{1 \text{ ft/sec}}{1 \text{ lb}}$$

will be possible to obtain for both the X and Y directions.

3) Force Reflection - The force reflection ratio between master and slave is probably the easiest of the operational criteria to obtain. The ratio of the forces applied at the master to those applied at the manipulator is given by

$$\text{Force ratio} = \frac{K1}{K4} \quad (10)$$

Actually equation (10) violates a fundamental property of matrix algebra and should be more correctly stated as

$$\text{Force ratio in X direction} = \frac{K1(1,1)}{K4(1,1)} \quad (11)$$

$$\text{Force ratio in Y direction} = \frac{K1(2,2)}{K4(2,2)} \quad (12)$$

The two D.O.F. breadboard is being designed with a force reflecting ratio of 1, and therefore equations (11) and (12) indicate that  $K1 = K4$ . From the compliance criteria  $K1$  has been defined, and thus  $K4$  is given by

$$K1 = K4 = \begin{bmatrix} 2000 & 0 \\ 0 & 2000 \end{bmatrix} \quad (13)$$

4) Stability - System stability is the most critical and the most difficult of the criteria to achieve. The system must be stable for: 1. all arm configurations, 2. operating with the multi-mode feature active, 3. master and slave operating in different axis systems, 4. master short circuited and open circuited (tip of master both held on to and not held on to by the operator), 5. manipulator short circuited and open circuited (tip of manipulator both in contact with an object or load and allowed to move free), and 6. any combination of circumstances 1. through 5. Unfortunately, there is no "cook book" procedure for a system design that will guarantee total stability. Several of the parameters in the two D.O.F. control scheme that can be varied to achieve the desired system stability will be briefly discussed below.

b. Options in Design - There are several options in the design of the two D.O.F. breadboard that can be used to obtain the desired stability. First of all, as shown in Figure III-6, differential tip rate feedback has been included to provide transient damping without effecting the steady state

$\frac{\dot{X}}{F_{min}}$  value. Thus, the gain matrices K3 and K6 are parameters that can be varied to effect stability. There exists the option of configuring the DC servo motors at each joint in either a voltage or current drive mode. In the voltage drive configuration, the internal viscous damping of each motor becomes significant and thus provides desirable stability qualities but tends to greatly degrade the

$\frac{\dot{X}}{F_{min}}$  ratio. To obtain a workable  $\frac{\dot{X}}{F_{min}}$  value, positive tip rate feedback can be introduced but this naturally has a detrimental effect on stability. In the current drive configuration, the motor internal viscous damping is negligible which yields a large value for

$\frac{\dot{X}}{F_{min}}$  but leaves the system highly understabilized. To provide the necessary stability, shaping filters and differential tip rate feedback can be used. These shaping filters, placed in the input circuit to each servo motor, are of the lead-lag variety and provide the needed gain and phase shift to stabilize each servo closed loop.

c. Methods of Analysis and Design - Both frequency and time domain techniques are being used to analyze and design the two D.O.F. control system. As a first step, the total closed loop system is divided into its four individual components. These four components undergo a piecewise linearization and a frequency domain stability analysis is conducted. The appropriate gain functions and filters are designed to assure the stability of each servo loop considered individually. Unfortunately, analyzing each linearized servo system separately does not reveal the stability qualities of the total closed loop control system. To investigate the total system behavior, time trajectories to simulated force inputs are obtained by programming the control system on the digital computer, which performs the needed integrations via a numerical integration routine. These time trajectories reveal the overall system stability qualities, and thus an iterative update design procedure is obtained between the frequency and time domains. This procedure is repeated until a control system that meets all the general operational criteria is developed.

## 6. Frequency Domain Analysis

a. Individual Joints - As seen from the definitions of Section III.A.4, the  $\underline{X}$  reference control scheme as shown in Figure III-6 is highly nonlinear. Unfortunately, nonlinear systems present some difficulties in their analysis and design due to the inapplicability of standard frequency domain techniques to such systems. In an effort to analyze, by hand, in the frequency domain, the two D.O.F. control system, the servo motors and their associated closed loops for each joint are considered individually. These individual systems are piecewise linearized and a frequency domain design is conducted on the various gains and shaping filters to assure stability. After this is done, the complete system is reunited and time trajectories are obtained to investigate the total nonlinear closed loop system behavior.

1. Consider first the master shoulder joint servo motor and its various inputs as shown in Figure III-12. To investigate the stability of this system with respect to an input disturbance torque,  $U_1$ , the manipulator and master elbow joints are held fixed, and therefore the rate inputs  $U_4$ ,  $U_5$ , and  $U_6$  are zero and the position inputs  $U_2$  and  $U_3$  are constant for any particular arm configuration. To calculate the open loop transfer function for this system, for

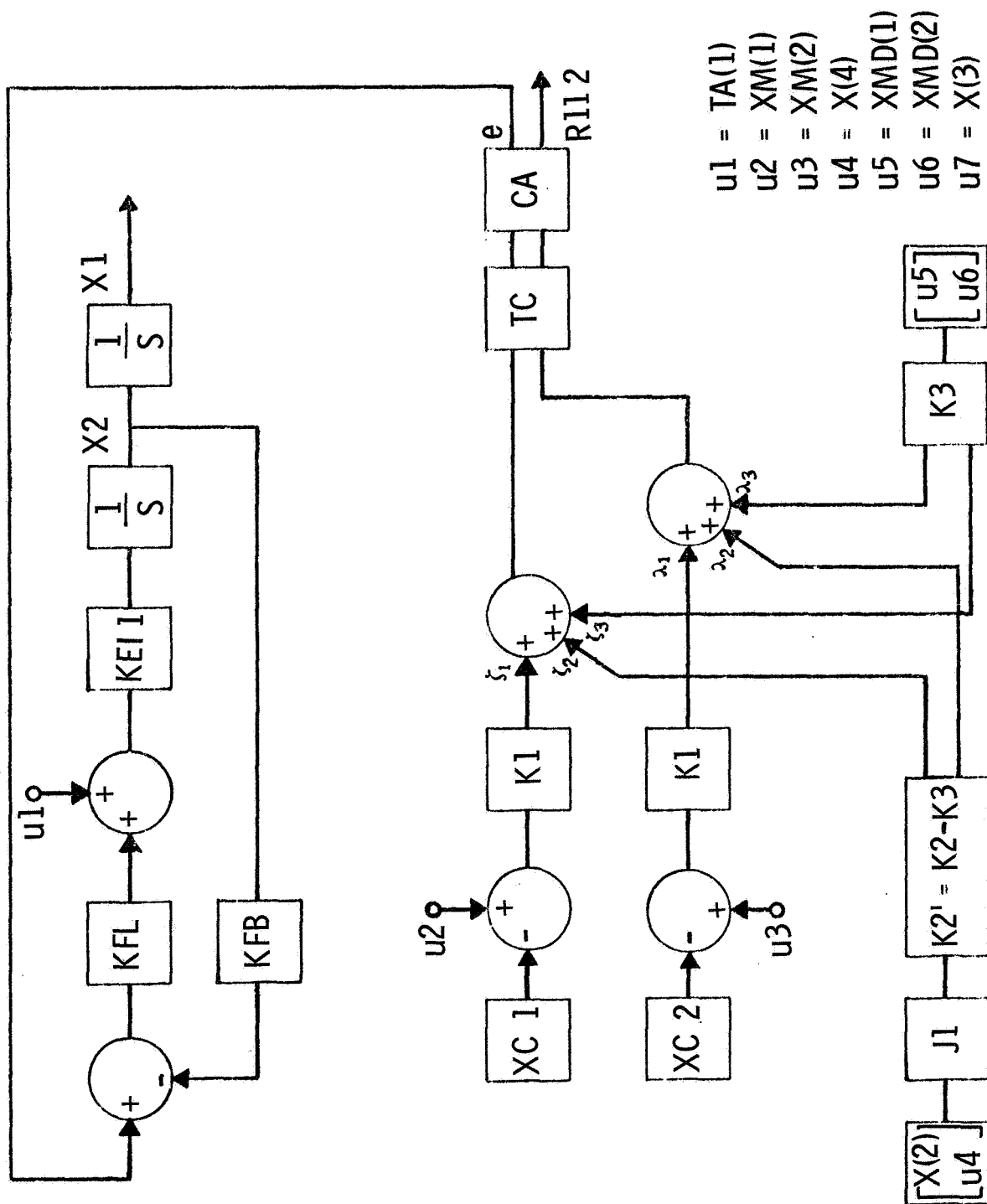


Figure III-12 Master Shoulder Servo System

all permissible locations the master shoulder joint can obtain under normal operation, the signal content at point e in Figure III-12 must be known. To obtain this information, each of the  $\delta_i$  and  $\lambda_i$  must be determined.

Letting:  $U1 = U1$

$$U2 = (LC) \left[ C(X_{10}) + C(X_{10} + U7) \right]$$

$$U3 = (LC) \left[ S(X_{10}) + S(X_{10} + U7) \right]$$

$$U4 = U5 = U6 = 0$$

$$U7 = X(3)$$

$$X(1) = X_{10} + X(1)$$

$$X_{10} = \text{initial condition on } X(1)$$

$$C = \text{COSINE}$$

$$S = \text{SINE}$$

and from the variable definitions of Section III.A.4 the  $\delta_i$  and  $\lambda_i$  are seen to be

$$\zeta_1 = (-LC)(K1) \left[ C(X_{10} + X(1)) + C(X_{10} + X(1) + U7) \right] + (K1)(LC) \left[ C(X_{10}) + C(X_{10} + U7) \right]$$

$$\zeta_2 = (-K2')(LC) \left[ S(X_{10} + X(1)) + S(X_{10} + X(1) + U7) \right] X(2)$$

$$\zeta_3 = 0$$

$$\lambda_1 = (-LC)(K1) \left[ S(X_{10} + X(1)) + S(X_{10} + X(1) + U7) \right] + (LC)(K1) \left[ S(X_{10}) + S(X_{10} + U7) \right]$$

$$\lambda_2 = (LC)K2' \left[ C(X_{10} + X(1)) + C(X_{10} + X(1) + U7) \right] X(2)$$

$$\lambda_3 = 0.$$

Forming the sums  $\sum_{i=1}^3 \zeta_i$  and  $\sum_{i=1}^3 \lambda_i$ , and operating on these signals with the torque distribution matrix TC and the gain matrix CA results in e given by

$$\begin{aligned}
 e = & (CA) (-LC) \left[ S(X_{10} + X(1)) + S(X_{10} + X(1) + U7) \right] \text{ times} \\
 & \begin{bmatrix} (-LC) (K1) \left[ C(X_{10} + X(1)) + C(X_{10} + X(1) + U7) \right] \\ + (K1) (LC) \left[ C(X_{10}) + C(X_{10} + U7) \right] \\ - (K2') (LC) \left[ S(X_{10} + X(1)) + S(X_{10} + X(1) + U7) \right] X(2) \end{bmatrix} \\
 & + (CA) (LC) \left[ C(X_{10} + X(1)) + C(X_{10} + X(1) + U7) \right] \text{ times} \\
 & \begin{bmatrix} (-LC) (K1) \left[ S(X_{10} + X(1)) + S(X_{10} + X(1) + U7) \right] \\ + (LC) (K1) \left[ S(X_{10}) + S(X_{10} + U7) \right] \\ + (LC) (K2') \left[ C(X_{10} + X(1)) + C(X_{10} + X(1) + U7) \right] X(2) \end{bmatrix}.
 \end{aligned}$$

Simplifying

$$\begin{aligned}
 e = & (CA) (K1) (LC)^2 \left[ \begin{bmatrix} S(X_{10}) + S(X_{10} + U7) \\ - \left[ C(X_{10}) + C(X_{10} + U7) \right] \end{bmatrix} \begin{bmatrix} C(X_{10} + X(1)) + C(X_{10} + X(1) + U7) \\ S(X_{10} + X(1)) + S(X_{10} + X(1) + U7) \end{bmatrix} \right] \\
 & + (CA) (K2') (LC)^2 X(2) \left[ \left[ S(X_{10} + X(1)) + S(X_{10} + X(1) + U7) \right]^2 + \left[ C(X_{10} + X(1)) + C(X_{10} + X(1) + U7) \right]^2 \right].
 \end{aligned}$$



Simplifying

$$e = (CA) (K2') (LC)^2 X(2) \left[ 1 + 1 + 2S(X_{10} + X(1))S(X_{10} + X(1) + U7) + 2C(X_{10} + X(1))C(X_{10} + X(1) + U7) \right. \\ \left. + (CA) (K1) (LC)^2 \left[ \begin{aligned} &S(X_{10})C(X_{10} + X(1)) - C(X_{10})S(X_{10} + X(1)) + \\ &S(X_{10})C(X_{10} + X(1) + U7) - C(X_{10})S(X_{10} + X(1) + U7) + \\ &S(X_{10} + U7)C(X_{10} + X(1)) - C(X_{10} + U7)S(X_{10} + X(1)) + \\ &S(X_{10} + U7)C(X_{10} + X(1) + U7) - C(X_{10} + U7)S(X_{10} + X(1) + U7) \end{aligned} \right] \right].$$

Simplifying

$$e = (CA) (K2') (LC)^2 X(2) [2 + 2C(U7)] \\ + (CA) (K1) (LC)^2 [S(-X(1)) + S(-X(1) - U7) + S(U7 - X(1)) + S(-X(1))].$$

Simplifying

$$e = (2) (CA) (K2') (LC)^2 [1 + C(U7)] X(2) \\ - (CA) (K1) (LC)^2 [2S(X(1)) + 2S(X(1))C(U7)].$$

Simplifying

$$e = (2) (CA) (K2') (LC)^2 [1 + C(U7)] X(2) \tag{14} \\ - (2) (CA) (K1) (LC)^2 [1 + C(U7)] S(X(1)).$$

The above equation reveals that  $e$  is composed of a linear term in rate,  $X(2)$ , and a nonlinear term in position,  $S(X(1))$ . Remembering that equation (14) was derived for any position of the master shoulder joint, and as was shown in Section A.4.c. the system will have a small compliance number,  $X(1)$  will vary only small amounts around  $X_{10}$  for all expected values of  $U1$ . Therefore  $S(X(1))$  can be linearized around the origin as shown in Figure III-13 to result in

$$S(X(1)) = K_s X(1),$$

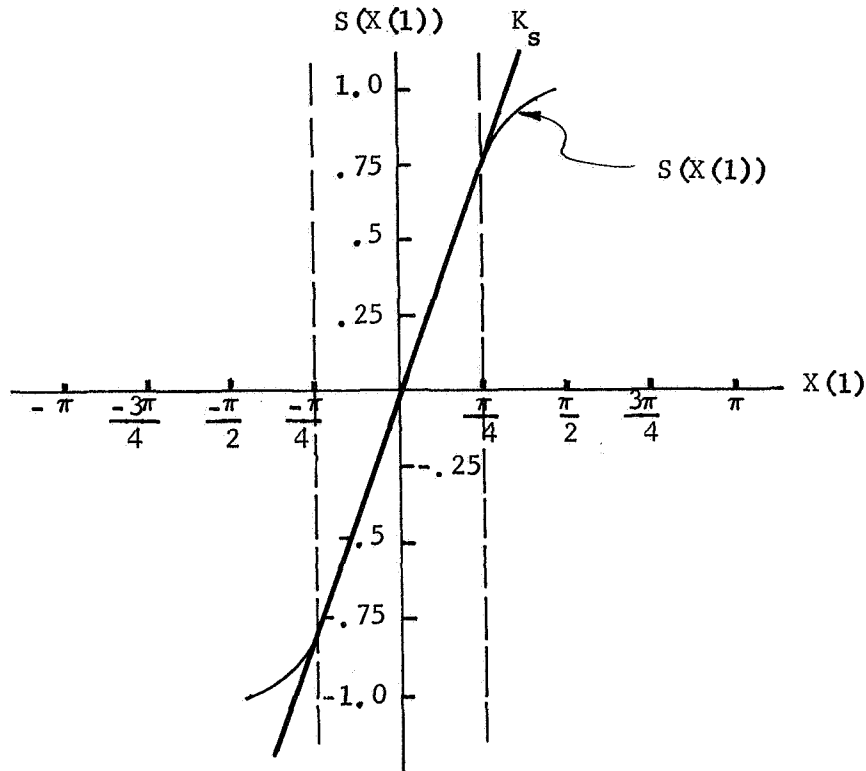


Figure III-13 Piecewise Linearized  $S(X(1))$  Function Around Origin

where  $K_s$  is the slope of the piecewise linearized curve. Under this linearization, equation (14) becomes

$$\begin{aligned} e = & (2)(CA)(K_2') (LC)^2 [1+C(U7)] X(2) \\ & - (2)(CA)K_1 (LC)^2 (K_s) [1+C(U7)] X(1); \end{aligned}$$

and Figure III-12 can be simplified as shown in Figure III-14.

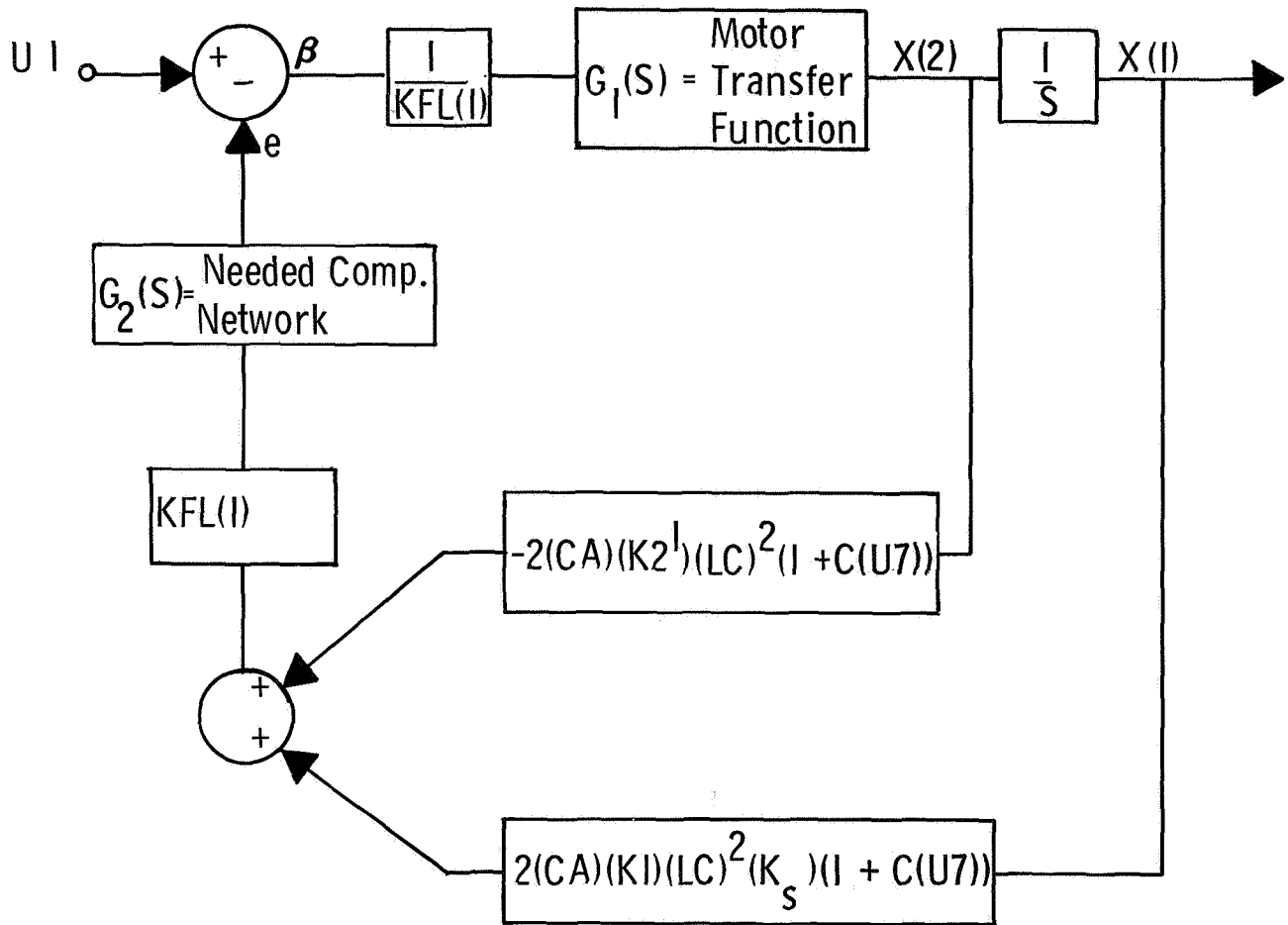


Figure III-14 Linearized Form of Master Shoulder Servo Loop

Letting  $G_2(S) = 1$ , the open loop transfer function  $e/\beta$  is easily calculated to be

(15)

$$e/\beta = \frac{(2)(1+C(U7))(K1)(K_s)}{(KFL(1))(KFB(1))} \left[ \frac{1 + \frac{s}{(K1)(K_s)}}{\frac{(-K_2^1)}{s(1 + \frac{s}{(KFL(1))(KEI(1))(KFB(1))})}} \right]$$

From a knowledge of the servo motor parameters and the system gains  $K1$ ,  $K2$ , and  $K3$ , equation (15) reveals open loop charac-

teristics and can be used to determine the needed compensating filter to assure relative stability. This technique can therefore be used to stabilize the master shoulder servo closed loop system considered, it is remembered, only as a subsystem and thus does not guarantee satisfactory performance when the servo is operated as a member of the total system.

The master elbow servo system, Figure III-15 can be treated in an identical fashion as above to determine its relative stability about any position the elbow can achieve under normal operation. The value of  $e$ , derived in the same manner as that of equation (14), becomes

$$e = (CA) (K_2') (LC)^2 X(4) - (CA) (LC)^2 (K_1) S(X(3)). \quad (16)$$

Once again approximating  $S(X(3))$  in the region of the origin by  $K_s X(3)$  yields

$$e = (CA) (K_2') (LC)^2 X(4) - (CA) (LC)^2 (K_1) (K_s) X(3).$$

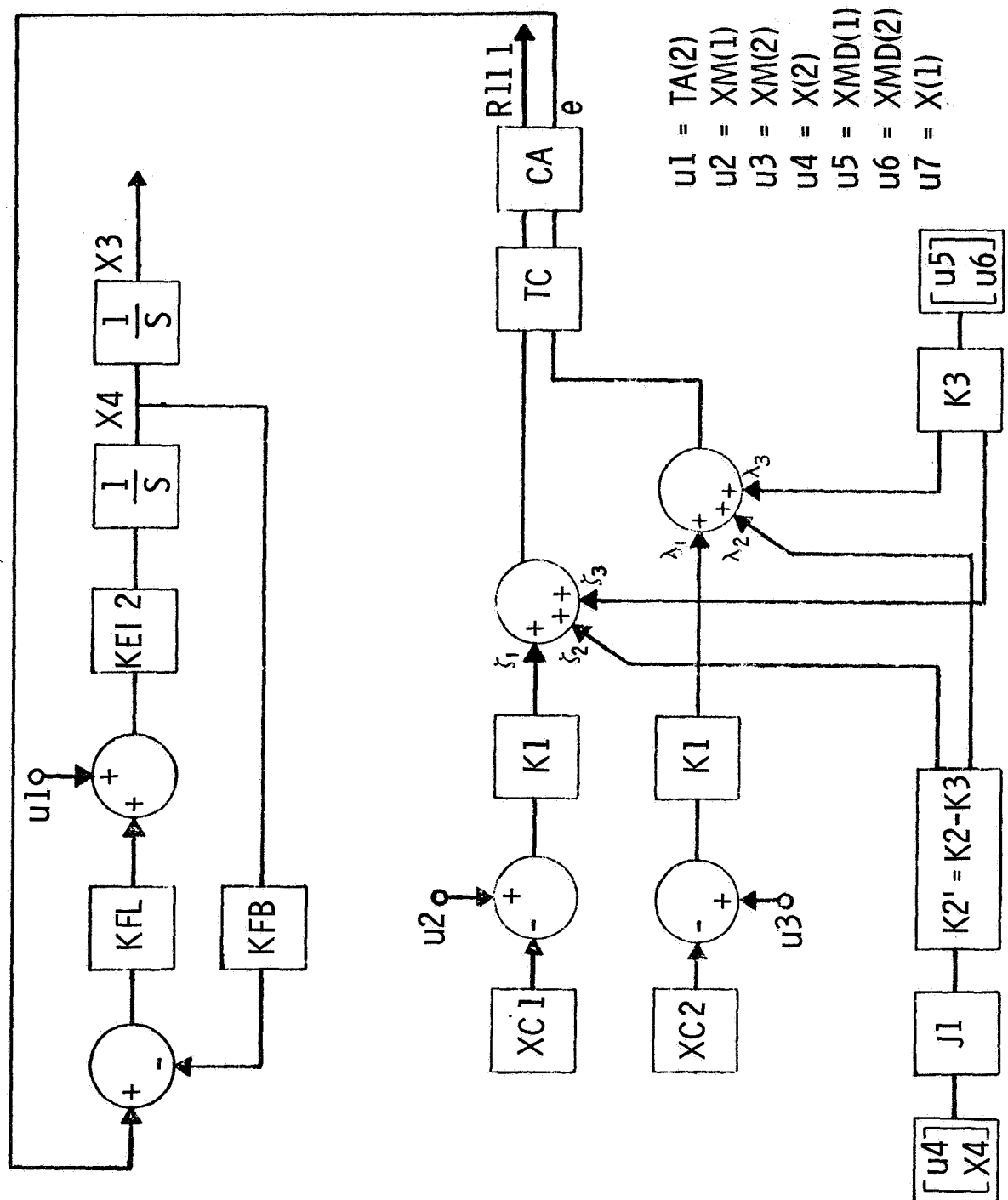
Figure III-15 can now be reconstructed as shown in Figure III-16.

Letting  $G_2(S) = 1$ , the open loop transfer function  $e/\beta$  is easily calculated to be

$$e/\beta = \frac{(K_1) (K_s)}{(K_{FB}(2)) (K_{FL}(2))} \left[ \frac{1 + \frac{S}{(K_1) (K_s)}}{\frac{(-K_2')}{S}} \right] \left[ \frac{S}{S (1 + \frac{S}{(K_{FL}(2)) (K_{EI}(2)) (K_{FB}(2))})} \right] \quad (17)$$

Proceeding with a similar analysis on the individual manipulator joints as was conducted above on the master joints, the manipulator shoulder servo loops exists as shown in Figure III-17.  $e$  is calculated to be

$$e = (MA) (MM) (2) (K_5') (LM)^2 [1 + C(U7)] X(6) - (MA) (MM) (2) (K_4) (LM)^2 [1 + C(U7)] S(X(5)) \quad (18)$$



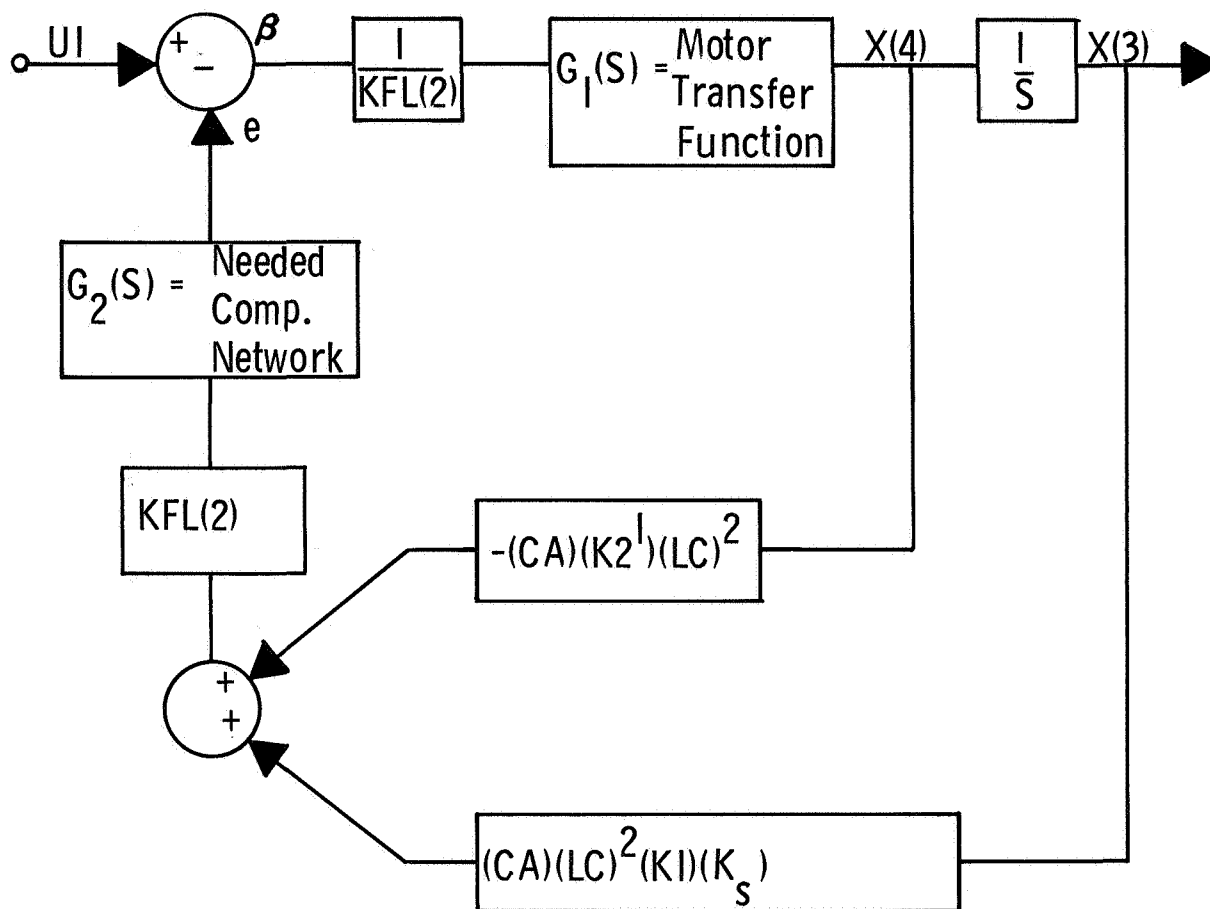


Figure III-16 Linearized Form of Master Elbow Servo Loop

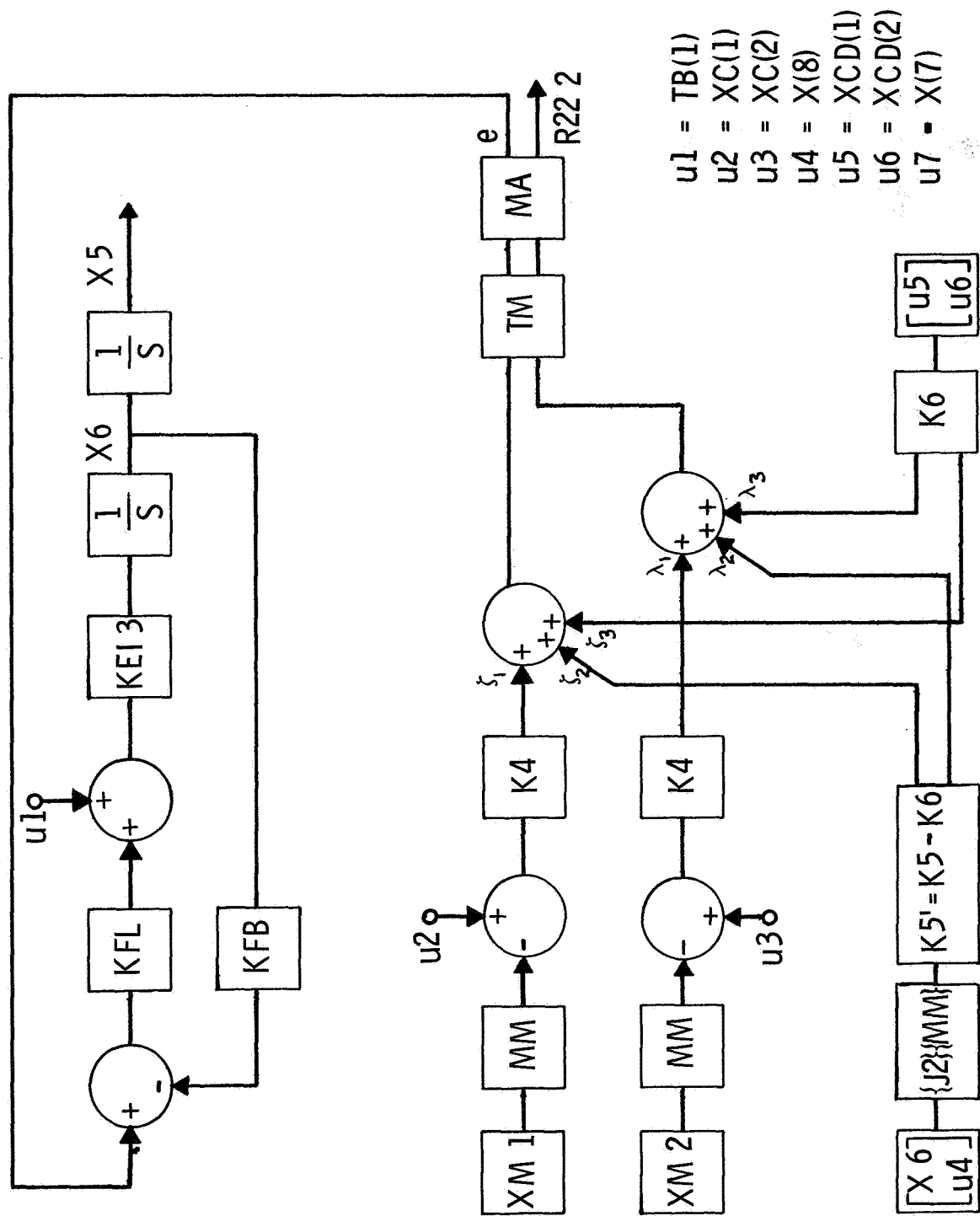


Figure III-17 Slave Shoulder Servo System

Letting  $S(X(5)) = K_s X(5)$

for small values of  $X(5)$ , Figure III-17 can be redrawn as shown in Figure III-18

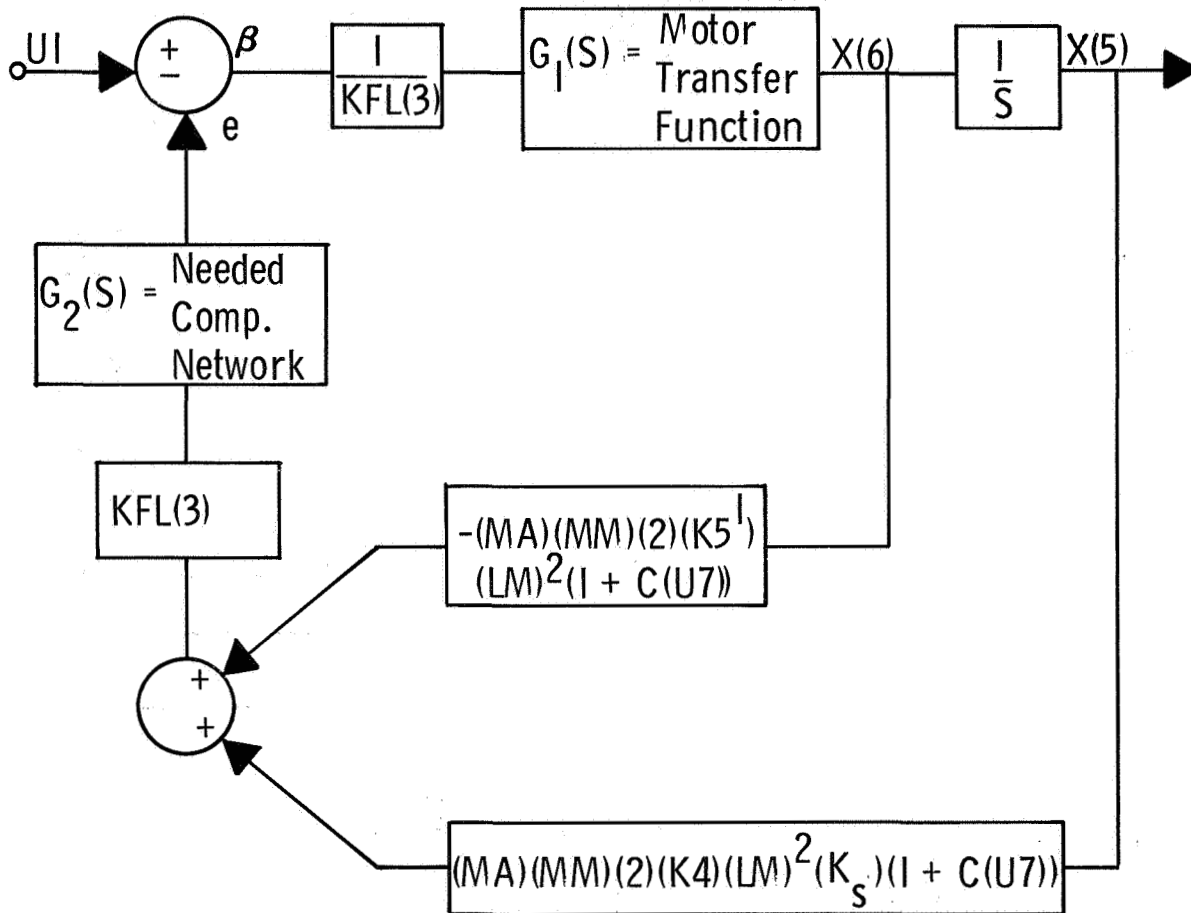


Figure III-18 Linearized Form of Manipulator Shoulder Servo Loop

Letting  $G_2(S) = 1$ , the open loop transfer function  $\frac{e}{\beta}$  is calculated to be (19)

$$\frac{e}{\beta} = \frac{2(LM)^2(1+C(U7))(K4)(K_s)(MM)}{(KFL(3))(KFB(3))} \left[ \frac{1 + \frac{S}{(K4)(K_s)}}{\frac{(-K_5)}{S}} \right] \left[ \frac{S}{S(1 + \frac{S}{(KFL(3))(KEI(3))(KFB(3))})} \right]$$

D. The manipulator elbow servo subsystem is shown in Figure III-19.  $e$  is derived to be

$$e = (MA)(MM)(K5)(LM)^2 X(8) - (MA)(MM)(LM)^2 (K4) S(X(7)). \quad (20)$$



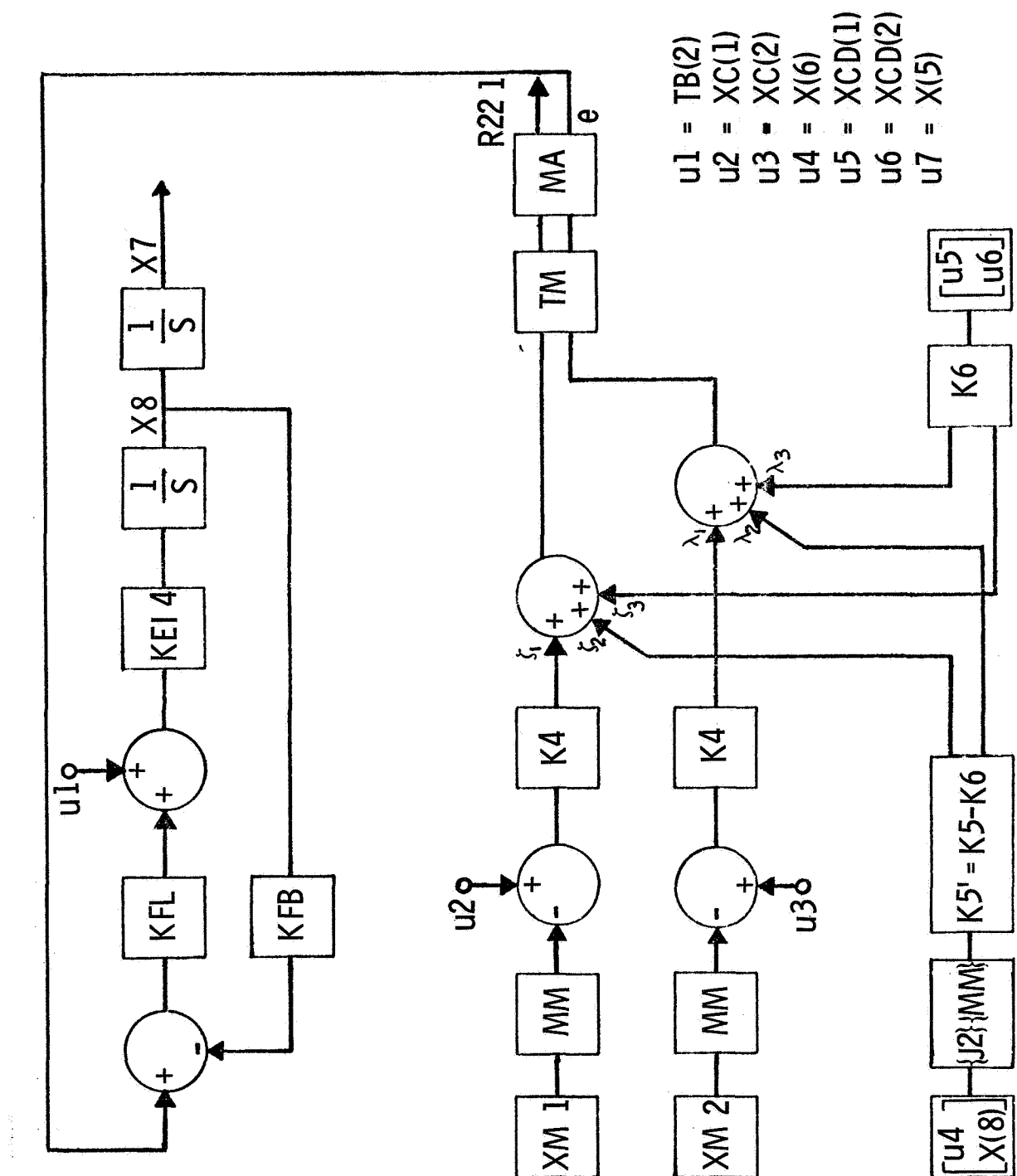


Figure III-19 Slave Elbow Servo System

Letting  $S(X(7)) = K_s X(7)$

for small values of  $X(7)$ , Figure III-19 can be reconstructed as shown in Figure III-20

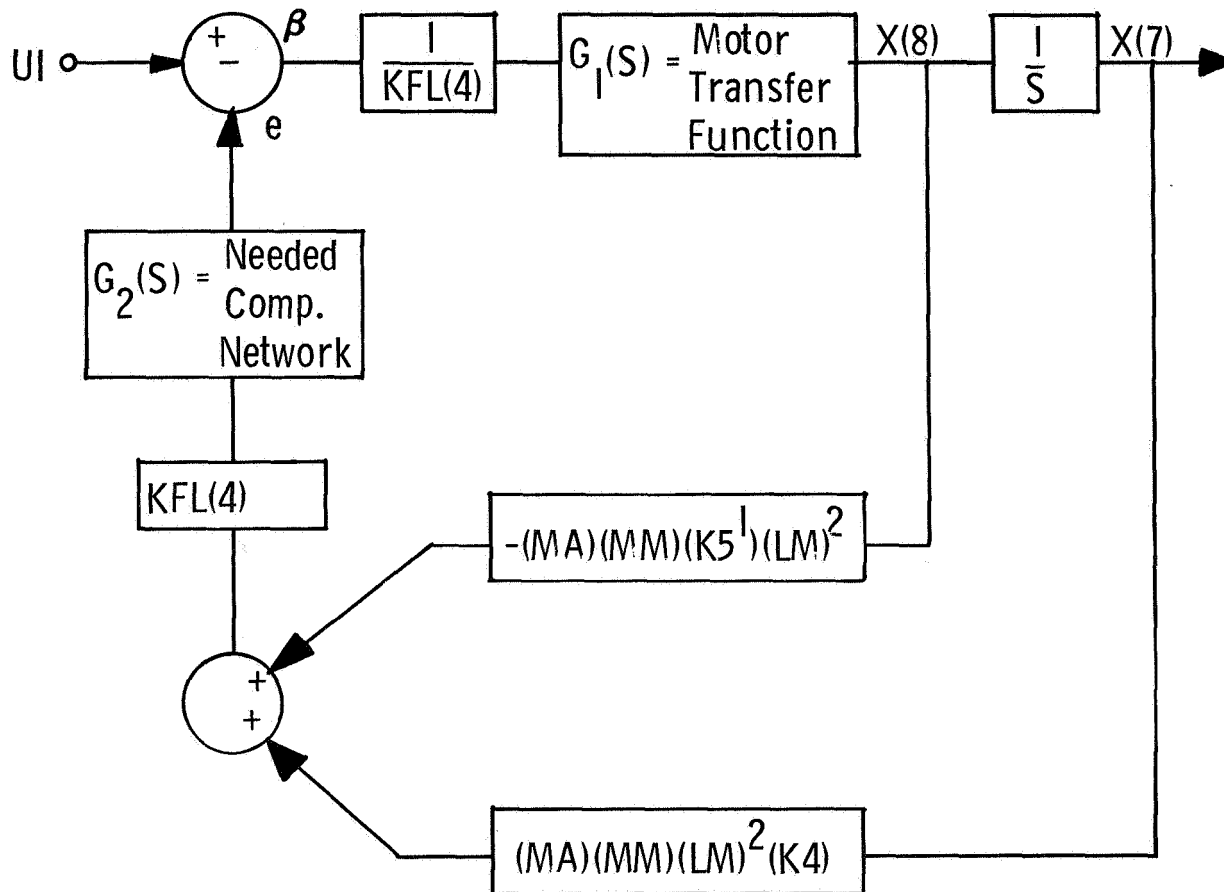


Figure III-20 Linearized Form of Manipulator Elbow Servo Loop

Letting  $G_2(s) = 1$ , the open loop transfer function  $e/\beta$  is given by

$$e/\beta = \frac{(LM)^2 (MM) (K4) (K_s)}{(KFB(4))(KFL(4))} \left[ \frac{1 + \frac{S}{(K4)(K_s)}}{S \left( 1 + \frac{S}{(KFL(4))(KEI(4))(KFB(4))} \right)} \right] \quad (21)$$

## 7. Time Domain Analysis

The final analysis of the total system becomes somewhat difficult in that now no piece of the system can be held rigid while another piece is analyzed. A complete system linearization must be performed for both the forced and unforced situations. This linearization results in investigating the system behavior around equilibrium points, of which there are an infinite number, and provides a linearized system with time varying coefficients for the forced case. Almost to the point of being facetious, it can be said that this type of analysis becomes horrendous for an eighth order system (sixteenth order if all compensating filters are included). Therefore an easier method for determining the behavior of the total closed loop system must be found. If the frequency domain is now abandoned and attention is given to the time domain, it is realized that an easier method does exist. This easier technique consists of examining the systems time trajectories for various inputs, or forcing functions, and is described in detail in the following section.

a. Digital Program - To obtain time trajectories for the resultant motion to various input forcing functions for the system of Figure III-6, the servo motors and control laws are modelled and programmed, in Fortran IV, with the resultant program designed for execution on a CDC 6400 computer. The system motion is described by eight first order nonlinear differential equations. The time solutions to these equations are obtained by iterative integration using the Kutta Merson integration routine. The inputs to the program are: 1. all system variables, 2. all initial conditions, and 3. the external forces applied at the tip of the master and manipulator; the outputs are: 1. motion of all joints, 2. rate of all joints, 3. tip motion of master and slave, 4. tip rates, and 5. torques generated by all servo motors. The program can simulate the servo motors connected in either the voltage or current drive modes and includes the nonlinearities introduced by motor torque and rate limits. See Appendix D for program listing.

The program consists of five major parts. Each of these parts provides the functions as described below.

Part I:

1. reads in all data
2. writes out all input data
3. defines the coordinate transformation matrix CT
4. computes the composite servo parameters  $KFL(i)$  (forward loop),  $KEI(i)$  (reflected inertia), and  $KFB(i)$  (servo viscous damping)
5. calls numerical integration routine
6. stores results of numerical integration routine
7. prints out time histories in tabular form
8. plots each time history on a separate graph

Part II:

Part II is the Kutta-Merson numerical integration subroutine.

One of the formal parameters passed into this subroutine is the name of another subroutine which contains the eight first order differential equations that describe the motion of the master-slave system.

Part III:

Part III is the "FIRDER" subroutine that defines the eight first order differential equations that describe the system. The program input data, read by the main program (Part I), is passed into this subroutine by means of common block storage.

Part IV:

Part IV is a short subroutine that seeks out the minimum and maximum values of each trajectory to be plotted.

Part V:

Part V is a scale subroutine that scales all axes for trajectory plotting.

b. Results of Digital Program

As stated previously, the first output function of the program is to print out all input data. A sample print out follows.

TWO DIMENSIONAL BILATERAL MANIPULATOR PROGRAM

INPUT DATA

K1	2000.000	0.	K2	6.500	0.
	0.	2000.000		0.	6.500
K3	20.000	0.	K4	2000.000	0.
	0.	20.000		0.	2000.000
K5	6.500	0.	K6	20.000	0.
	0.	6.500		0.	20.000
CA	.799	0.	MA	.799	0.
	0.	.799		0.	.799
MM	1.000	0.			
	0.	1.000			
GS	0.	0.		0.	0.
PI	0.	0.			
RR	0.	0.			
KT	.149	.149		.149	.149

RL	1.500	1.500	1.500	1.500			
TL	28.125	28.125	28.125	28.125			
RT	11.900	11.900	11.900	11.900			
KG	100.000	100.000	100.000	100.000			
KB	.200	.200	.200	.200			
JM	0.	0.	0.	0.			
RA =	0.						
LC =	1.000	LM =	2.000				
STIME =	1.000						
NEQ = 8	STEP =	.005					
T =	0.						
X(1)	.523	X(2)	0.	X(3)	-1.045	X(4)	0.
X(5)	1.122	X(6)	0.	X(7)	-2.244	X(8)	0.
FC	0.	1.000					
FM	0.	0.					
END OF INPUT DATA							

Those values in this print out that have not been previously defined in Table III-1 are:

1. KT = torque sensitivity value of each servo motor
2. RL = rate limit for each joint
3. TL = torque limit for each servo-gear train combination
4. RT = total resistance of motor winding and driver amplifier output impedance for each servo motor
5. KG = gear train reduction value
6. KB = viscous damping of servo motor
7. JM = reflected inertia at each joint due to load at tip of master or slave
8. RA = coordinate axis rotation angle
9. LC = length of master arm segments
10. LM = length of manipulator arm segments
11. STIME = length of run time for program
12. NEQ = number of first order differential equations to be handled by numerical integration subroutine
13. STEP = print out interval
14. T = initial time
15. X(i) = initial values of joint positions
16. FC = X and Y tip forces applied to master
17. FM = X and Y tip forces applied to manipulator

The tabular print out of the time functions will not be presented as that information can more readily be shown by the trajectory plots. To avoid a lengthy explanation of each plotted function, three examples

will be given that show the plotted results of actual computer runs.

#### A. Example I

This example demonstrates the force reflecting properties of the system. The servo motors are modeled in the voltage drive mode, a moderate amount of differential tip rate feedback is included, and the external applied forces on the tip of the master and manipulator are (10 lbs, 10 lbs) and (-10 lbs, -10 lbs), respectively. The master and manipulator tips are initially placed at (1.7 ft, 0). Since equal and opposite external forces are placed on the master and manipulator, it is expected that the system will undergo initial transients with the steady state condition revealing no motion and the individual joint servo motors actuated to oppose the external applied forces. As seen by the time trajectories, this is indeed the case.

In the following plots, angular position is given in radians, angular rate in radians/second, tip position in feet, tip rate in feet/second, and torques in foot lbs.

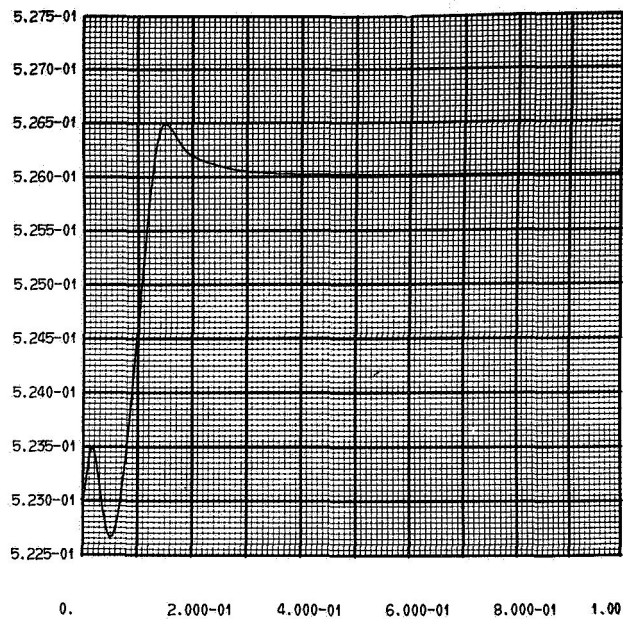


# TWO DIMENSIONAL BILATERAL MANIPULATOR PROGRAM

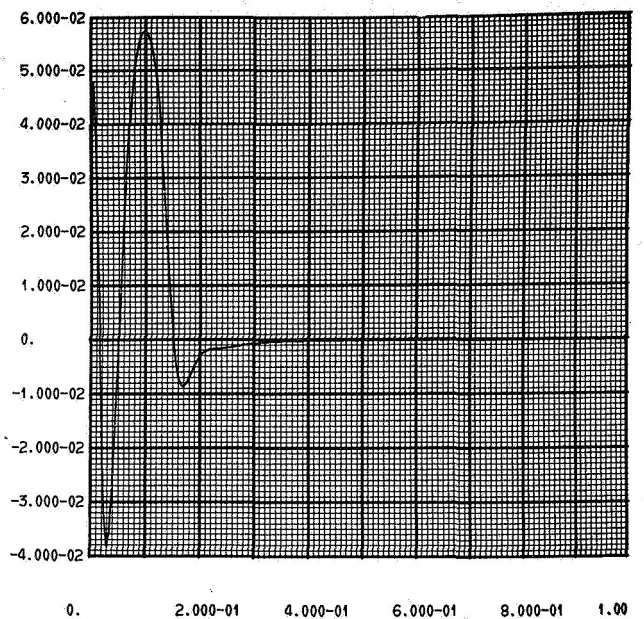
## INPUT DATA

K1	2000.000	0.	K2	0.	0.
	0.	2000.000		0.	0.
K3	20.000	0.	K4	2000.000	0.
	0.	20.000		0.	2000.000
K5	0.	0.	K6	20.000	0.
	0.	0.		0.	20.000
CA	.799	0.	MA	.799	0.
	0.	.799		0.	.799
MM	1.000	0.			
	0.	1.000			
GS	0.	0.		0.	0.
PI	0.	0.			
RR	0.	0.			
KT	.149	.149		.149	.149
RL	1.500	1.500		1.500	1.500
TL	28.125	28.125		28.125	28.125
RT	11.900	11.900		11.900	11.900
KG	100.000	100.000		100.000	100.000

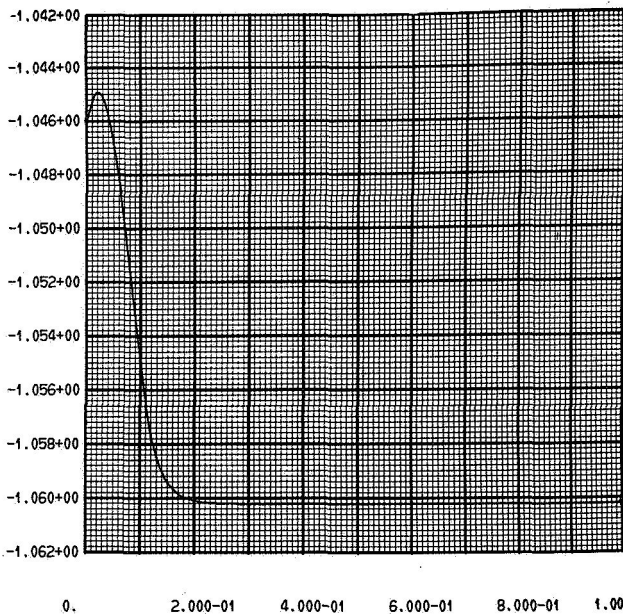
KB	.200	.200	.200	.200			
JM	0.	0.	0.	0.			
RA =	0.						
LC =	1.000	L1 =	2.000				
STIME =	1.000						
NEQ =	8	STEP =	.005				
T =	0.						
X(1)	.523	X(2)	0.	X(3)	-1.046	X(4)	0.
X(5)	1.122	X(6)	0.	X(7)	-2.244	X(8)	0.
FC	10.000		10.000				
FM	-10.000		-10.000				
END OF INPUT DATA							



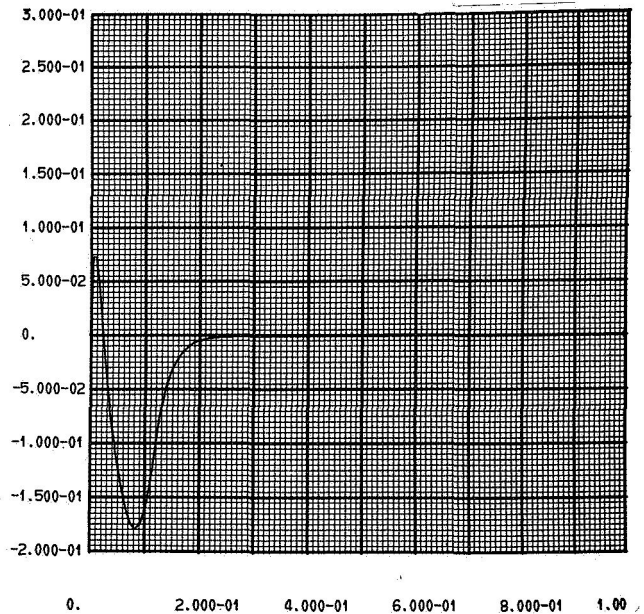
X(1) VS TIME  
1 MASTER SHOULDER POSITION X(1)



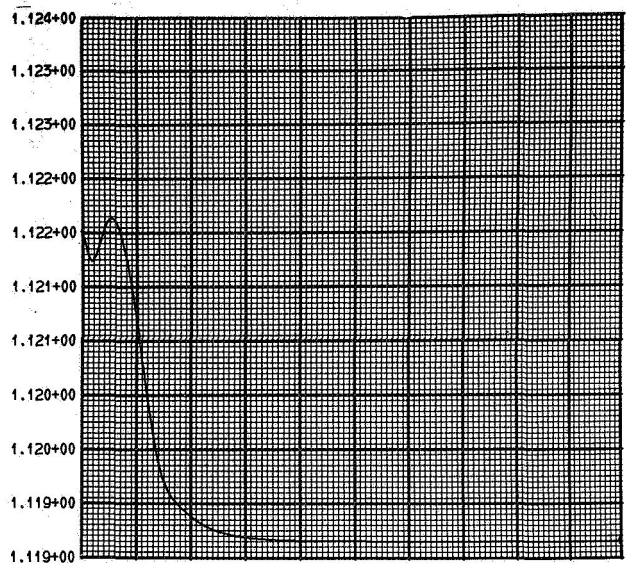
X(2) VS TIME  
1 MASTER SHOULDER VELOCITY X(2)



X(3) VS TIME  
1 MASTER ELBOW POSITION X(3)



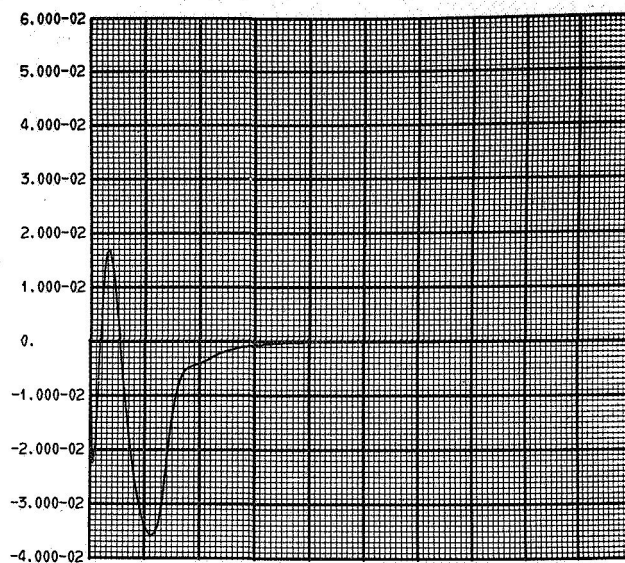
X(4) VS TIME  
1 MASTER ELBOW VELOCITY X(4)



0. 2.000-01 4.000-01 6.000-01 8.000-01 1.00

X(5) VS TIME

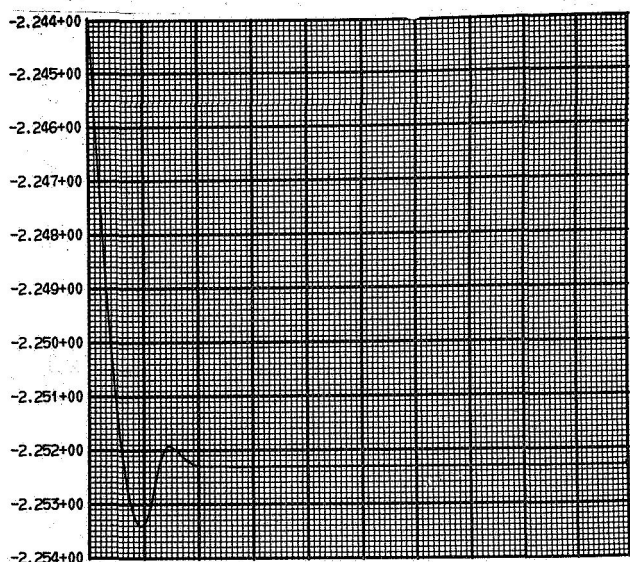
1 SLAVE SHOULDER POSITION X(5)



0. 2.000-01 4.000-01 6.000-01 8.000-01 1.00

X(6) VS TIME

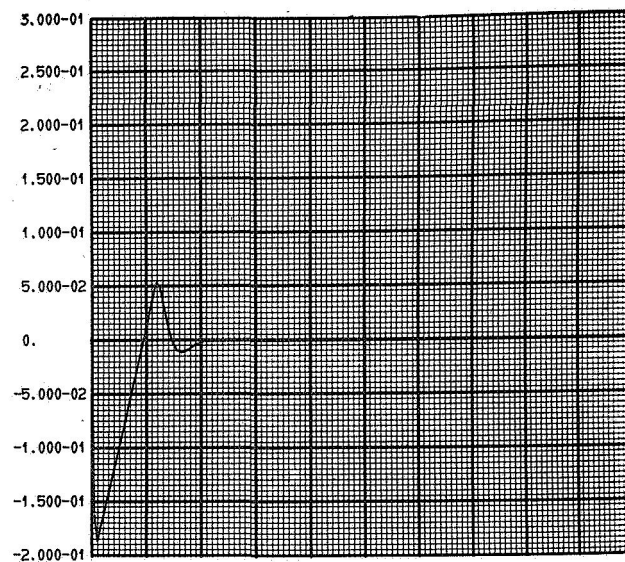
1 SLAVE SHOULDER VELOCITY X(6)



0. 2.000-01 4.000-01 6.000-01 8.000-01 1.00

X(7) VS TIME

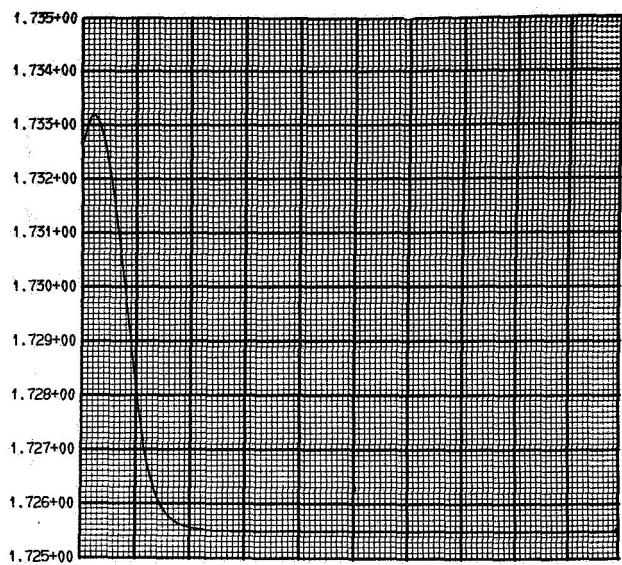
1 SLAVE ELBOW POSITION X(7)



0. 2.000-01 4.000-01 6.000-01 8.000-01 1.00

X(8) VS TIME

1 SLAVE ELBOW VELOCITY X(8)



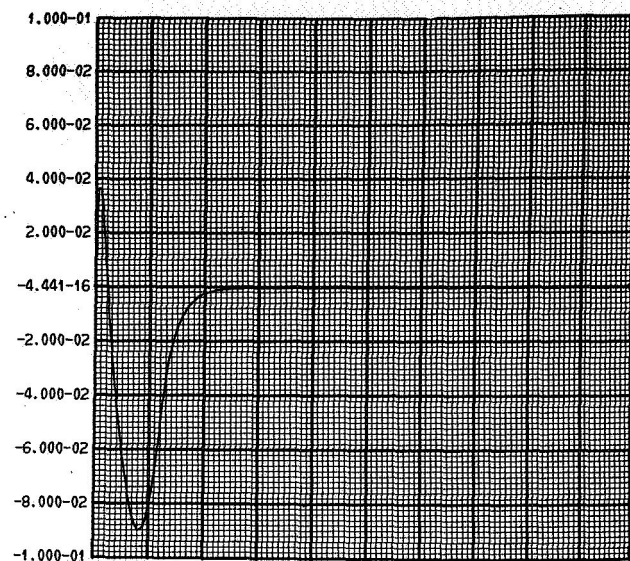
0. 2.000-01 4.000-01 6.000-01 8.000-01 1.00

XC(1) VS TIME

1

MASTER X TIP POSITION

XC(1)



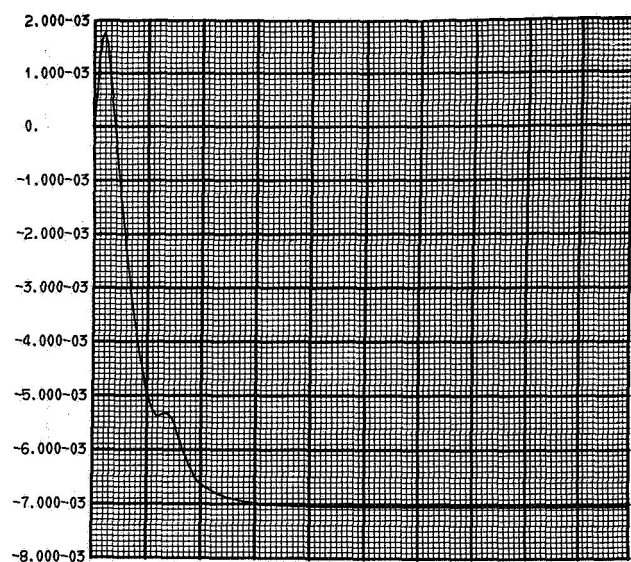
0. 2.000-01 4.000-01 6.000-01 8.000-01 1.00

XCD(1) VS TIME

1

MASTER X TIP VELOCITY

XCD(1)



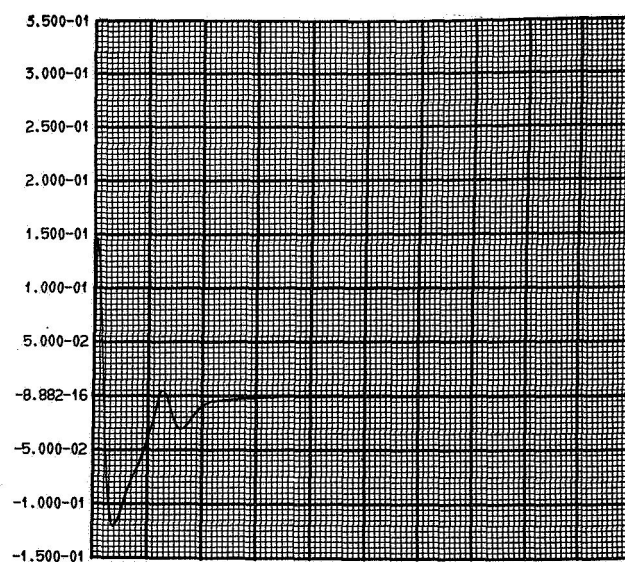
0. 2.000-01 4.000-01 6.000-01 8.000-01 1.00

XC(2) VS TIME

1

MASTER Y TIP POSITION

XC(2)



0. 2.000-01 4.000-01 6.000-01 8.000-01 1.00

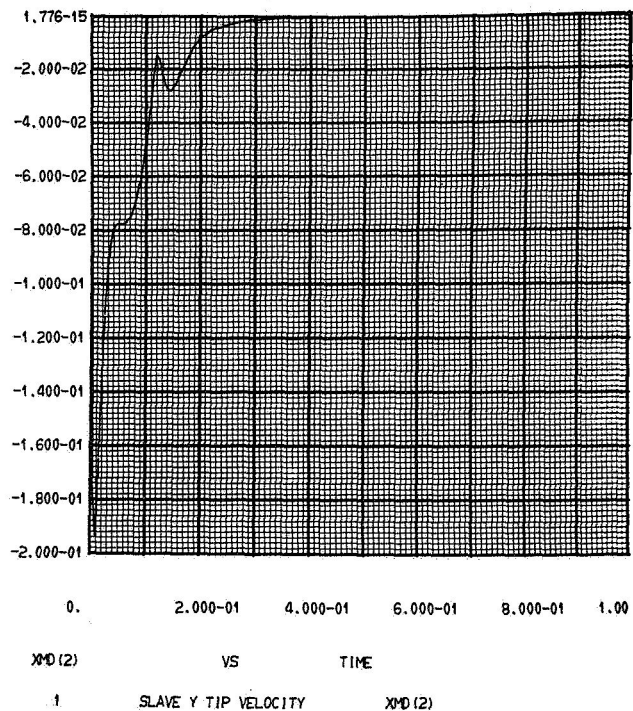
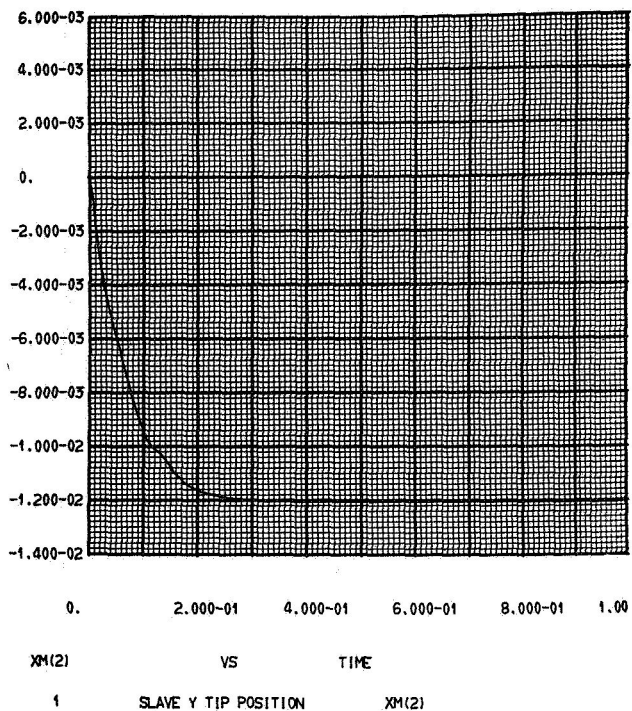
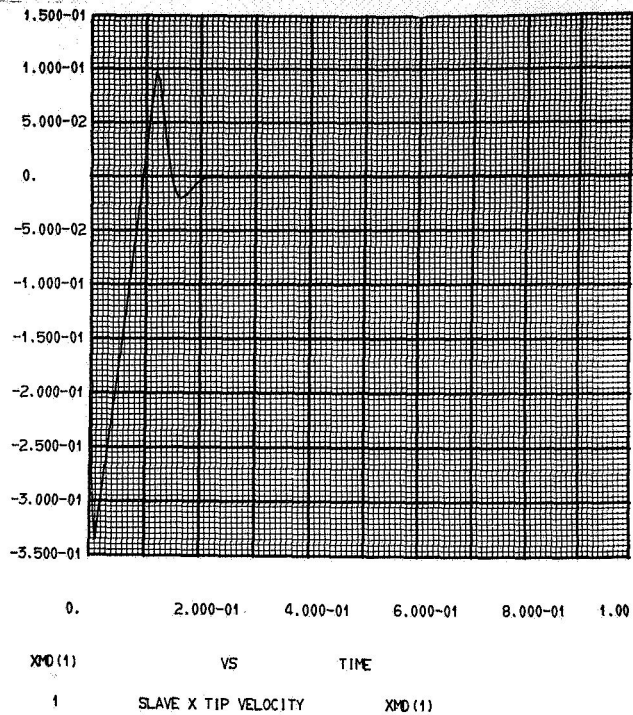
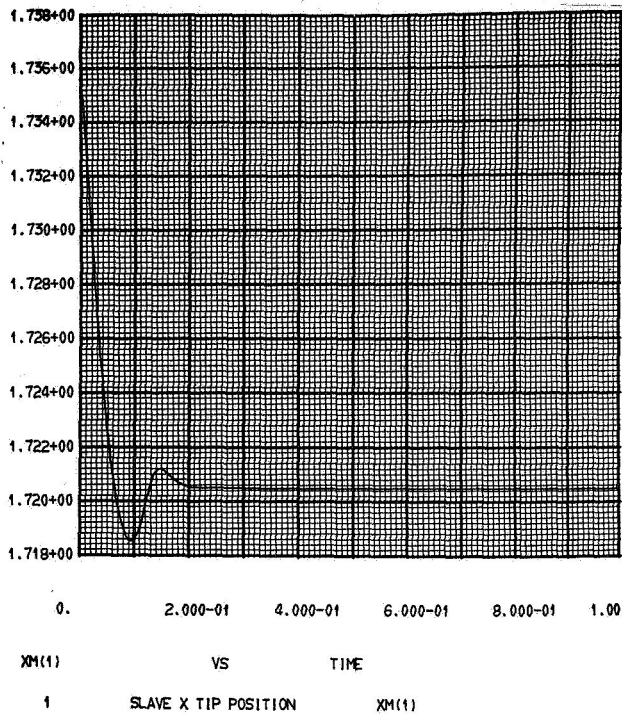
XCD(2) VS TIME

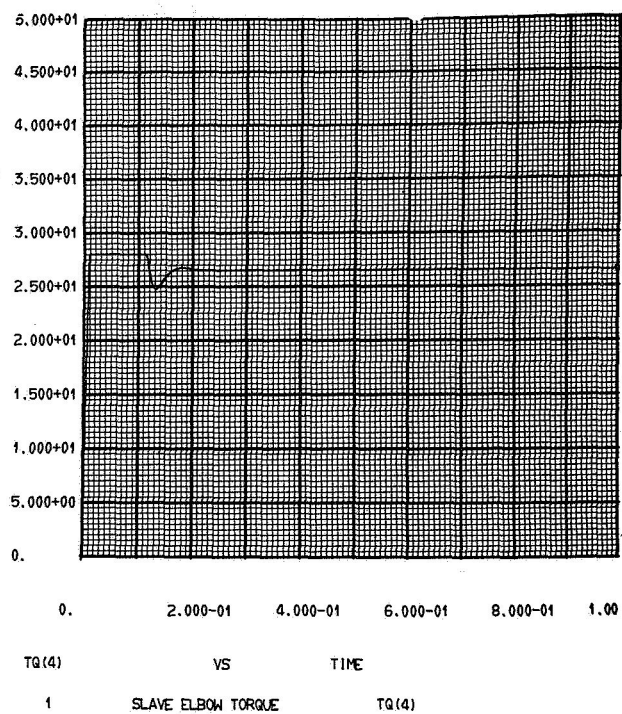
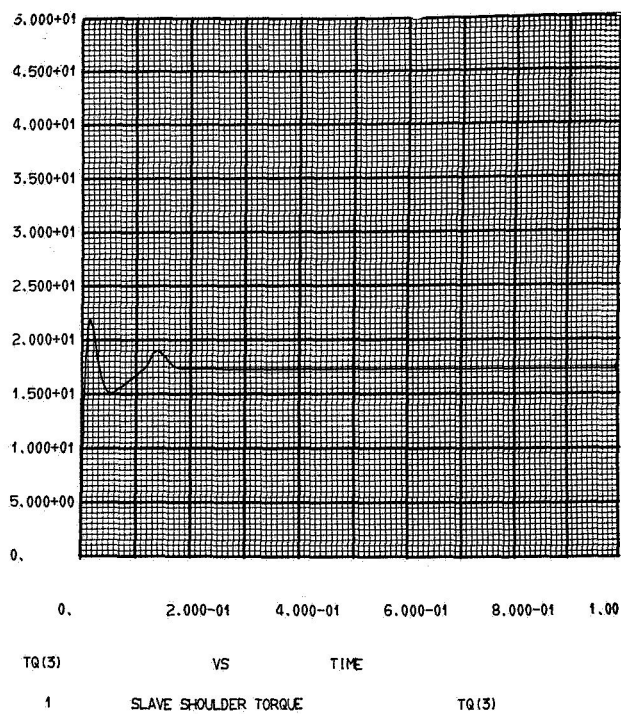
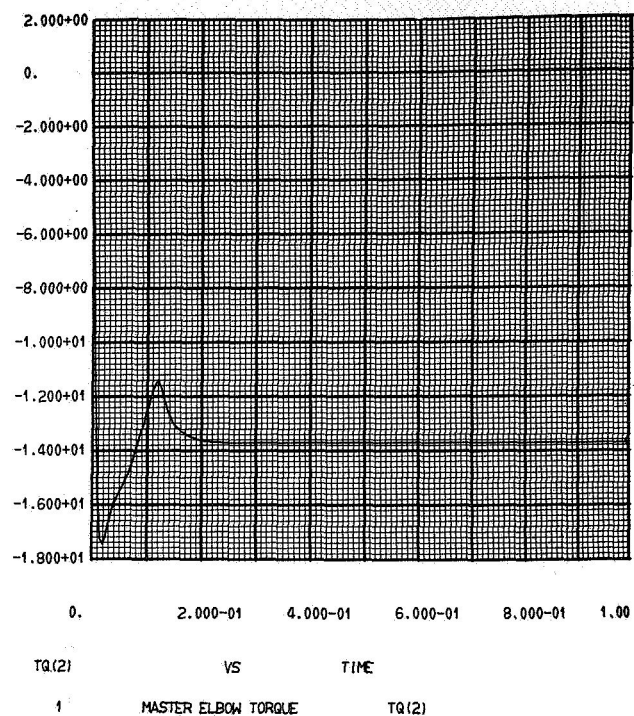
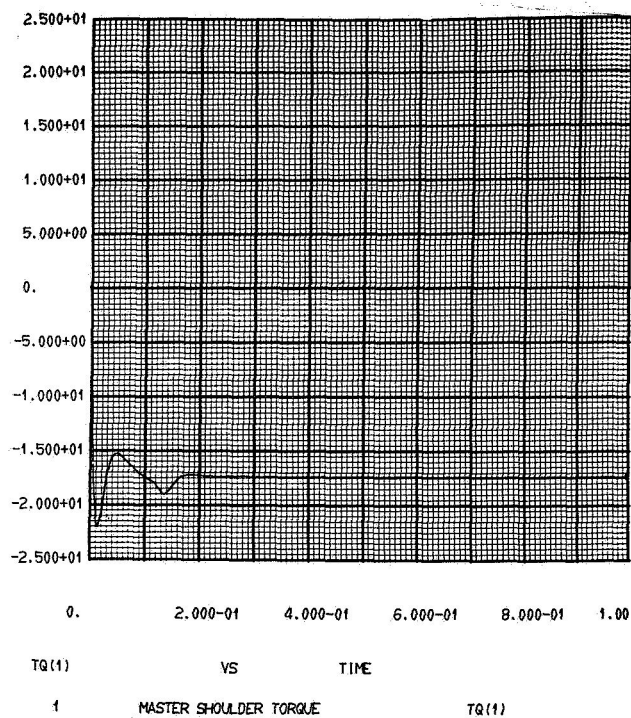
1

MASTER Y TIP VELOCITY

XCD(2)







b. Example II -

In this example the servo motors are modeled in the voltage drive mode, there is no differential or positive tip rate feedback, the external applied forces on the Master are (0, 1 lb), and external forces on the manipulator are (0, 0). Both arms are initially placed at (1.7 ft, 0). As seen from the time trajectories, this system is considerably underdamped and has a very poor  $\frac{X}{F_{\min}}$  ratio.

$$\frac{X}{F_{\min}}$$



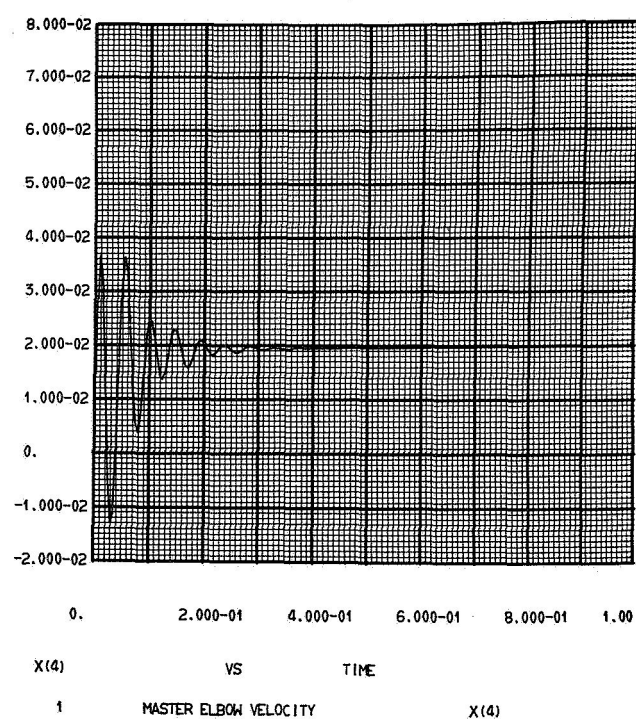
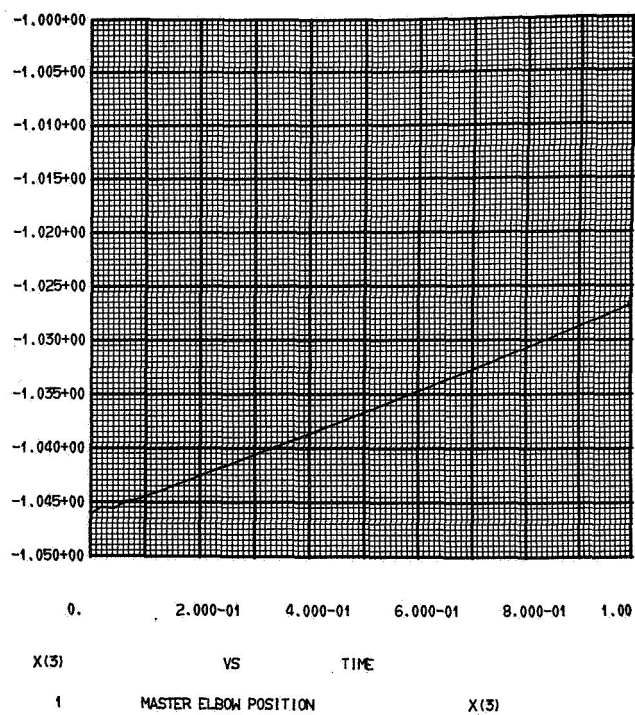
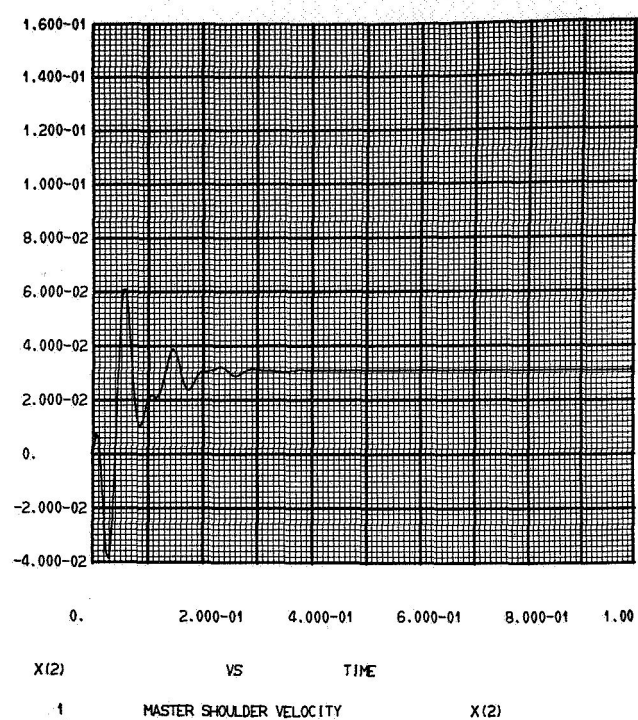
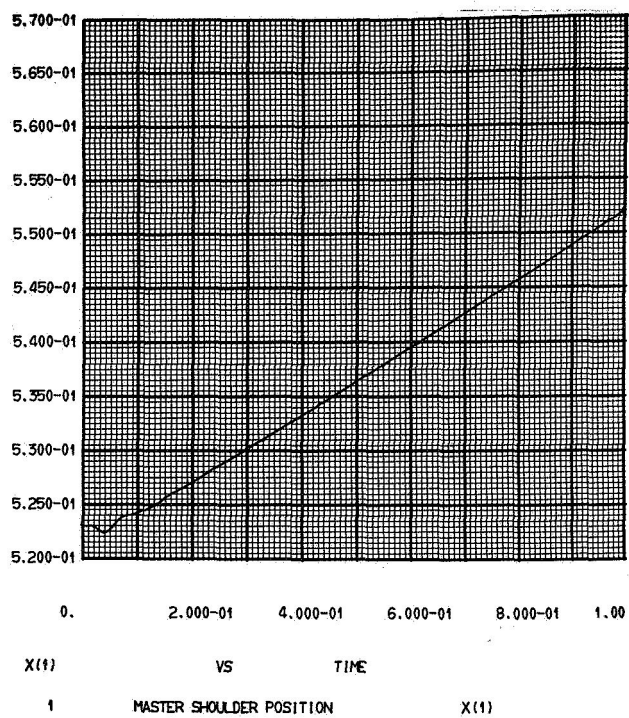
# TWO DIMENSIONAL BILATERAL MANIPULATOR PROGRAM

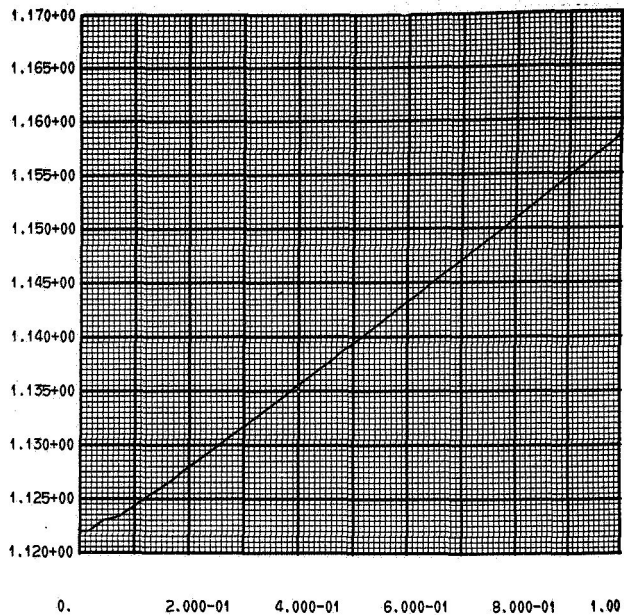
## INPUT DATA

K1	2000.000	0.	K2	0.	0.
	0.	2000.000		0.	0.
K3	0.	0.	K4	2000.000	0.
	0.	0.		0.	2000.000
K5	0.	0.	K6	0.	0.
	0.	0.		0.	0.
CA	.799	0.	MA	.799	0.
	0.	.799		0.	.799
MM	1.000	0.			
	0.	1.000			
GS	0.	0.		0.	0.
PI	0.	0.			
RR	0.	0.			
KT	.149	.149		.149	.149
RL	1.500	1.500		1.500	1.500
TL	28.125	28.125		28.125	28.125
RT	11.900	11.900		11.900	11.900
KG	100.000	100.000		100.000	100.000

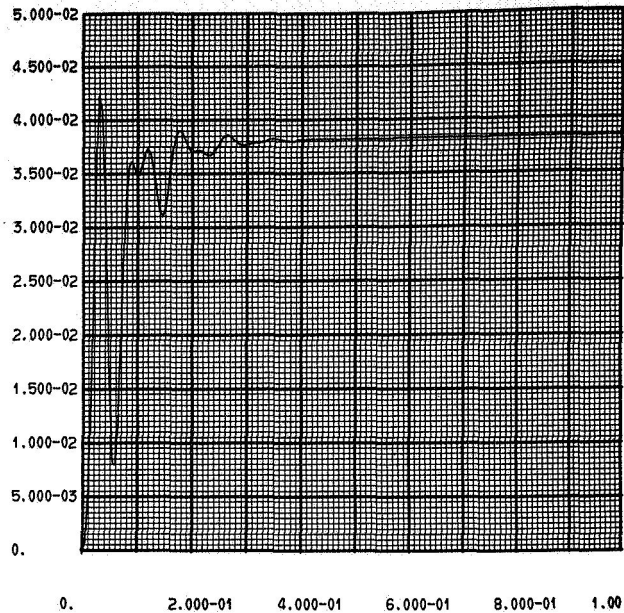
KB	.200	.200	.200	.200			
JM	0.	0.	0.	0.			
RA =	0.						
LC =	1.000	LM = 2.000					
STIME =	1.000						
NEQ = 8	STEP = .005						
T =	0.						
X(1)	.523	X(2)	0.	X(3)	-1.046	X(4)	0.
X(5)	1.122	X(6)	0.	X(7)	-2.244	X(8)	0.
FC	0.	1.000					
FM	0.	0.					

END OF INPUT DATA

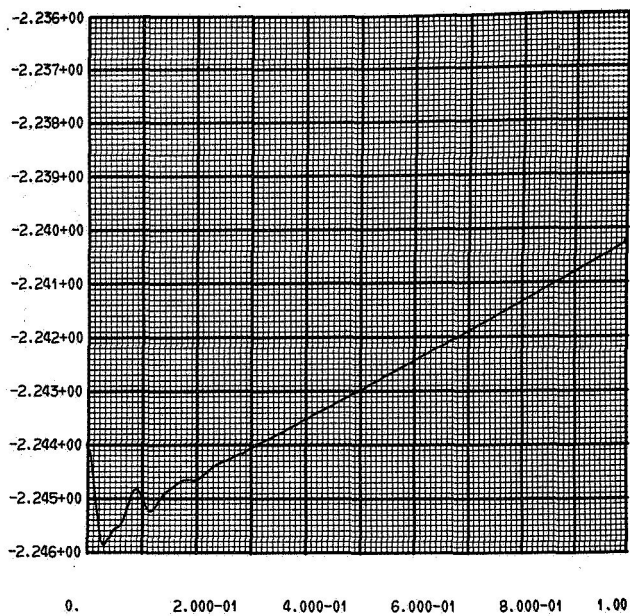




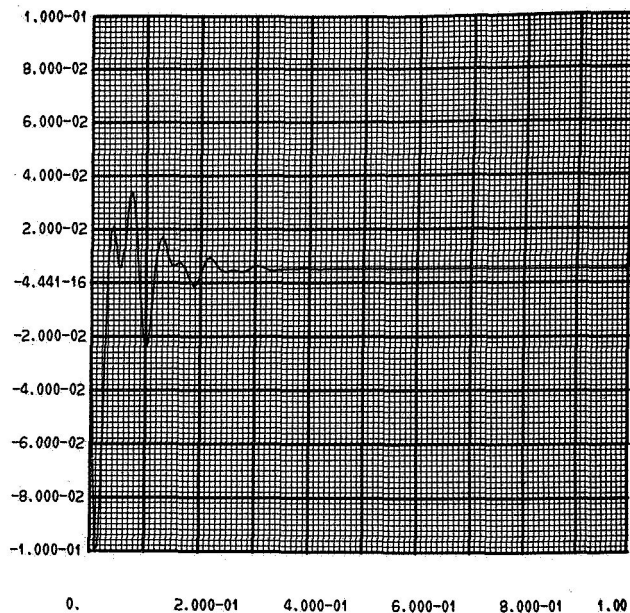
X(5) VS TIME  
1 SLAVE SHOULDER POSITION X(5)



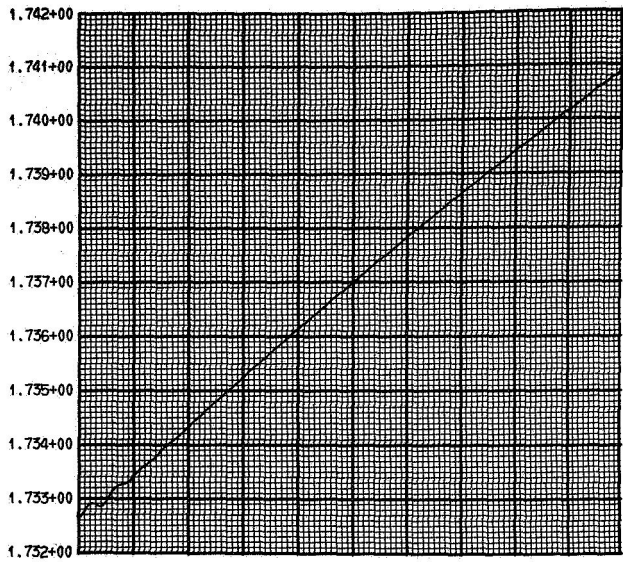
X(6) VS TIME  
1 SLAVE SHOULDER VELOCITY X(6)



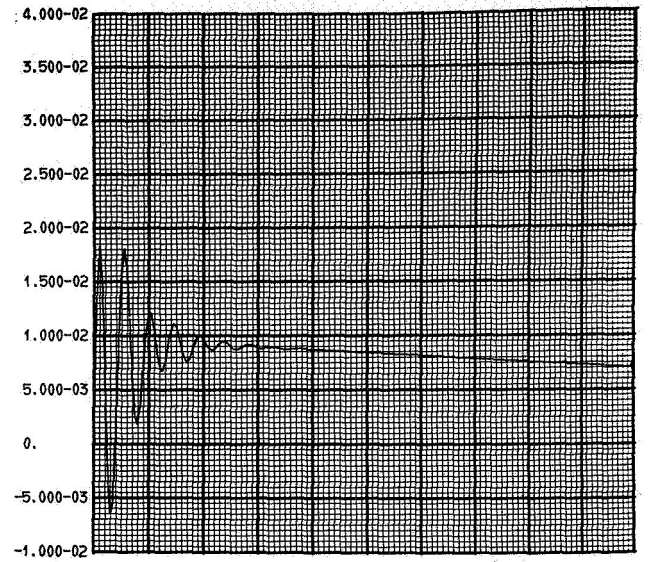
X(7) VS TIME  
1 SLAVE ELBOW POSITION X(7)



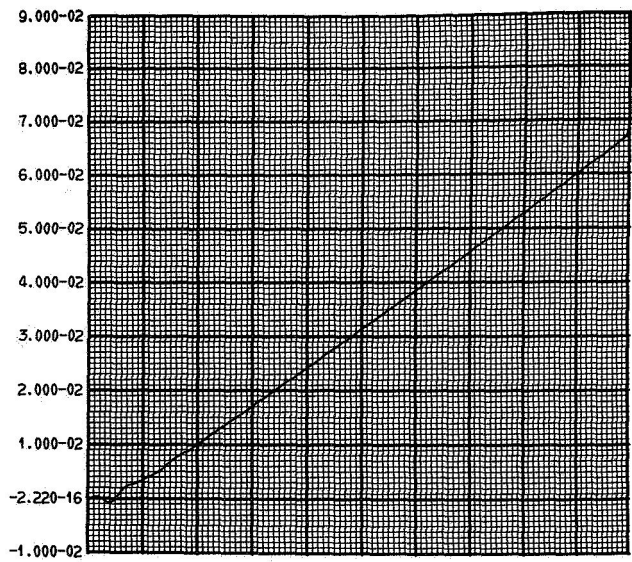
X(8) VS TIME  
1 SLAVE ELBOW VELOCITY X(8)



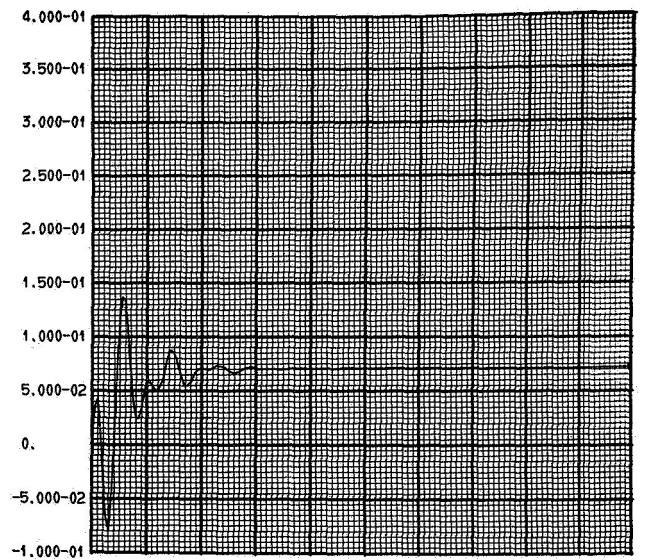
XC(1) VS TIME  
1 MASTER X TIP POSITION XC(1)



XCD(1) VS TIME  
1 MASTER X TIP VELOCITY XCD(1)

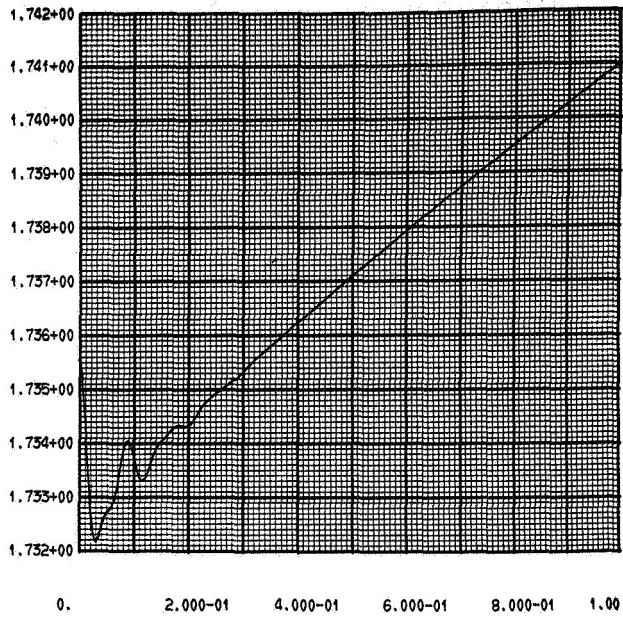


XC(2) VS TIME  
1 MASTER Y TIP POSITION XC(2)

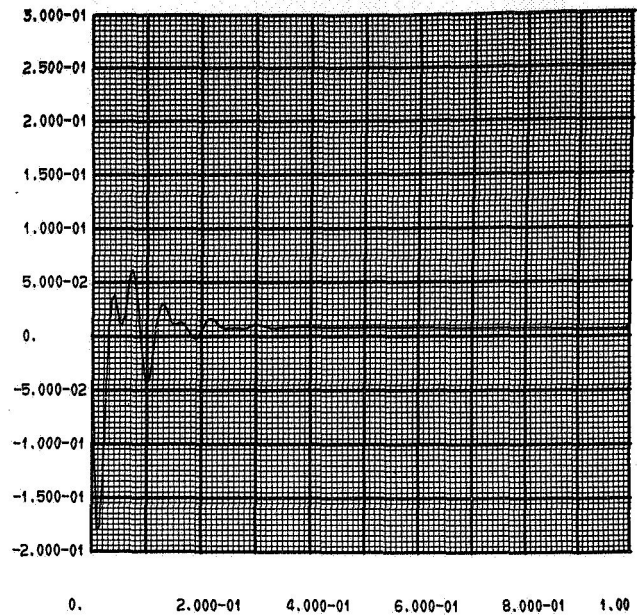


XCD(2) VS TIME  
1 MASTER Y TIP VELOCITY XCD(2)

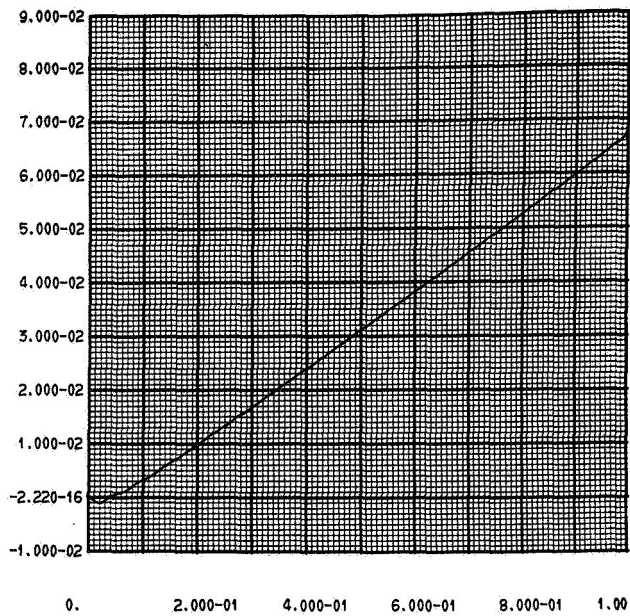




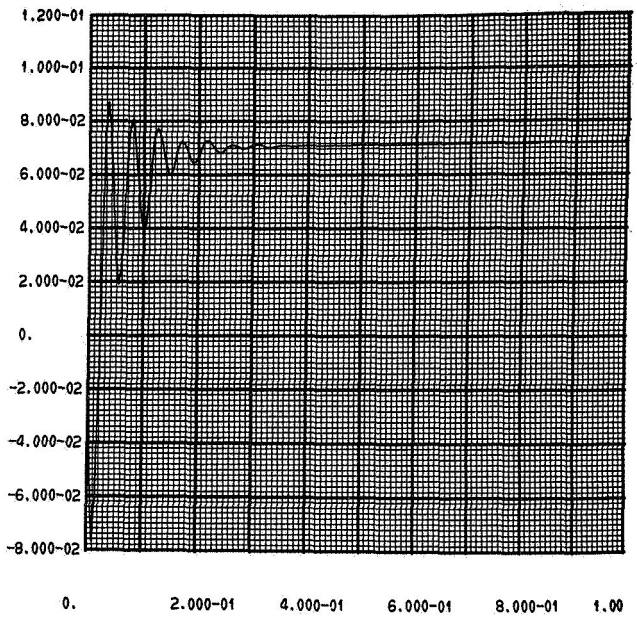
XM(1) VS TIME  
1 SLAVE X TIP POSITION XM(1)



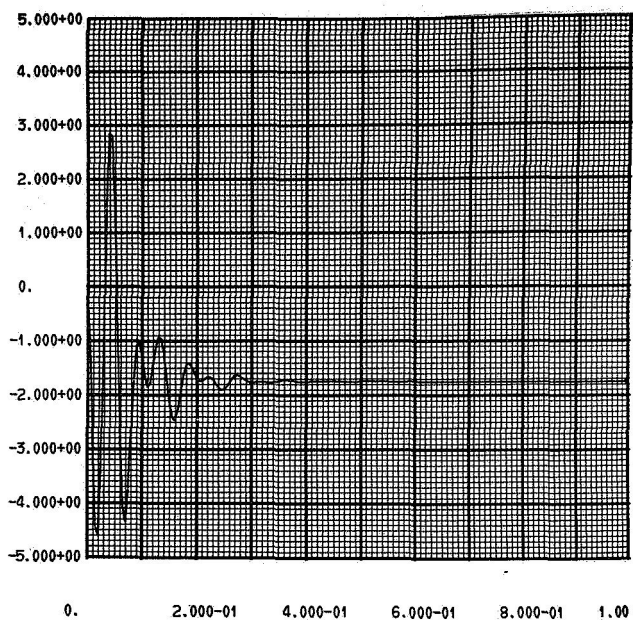
XM(1) VS TIME  
1 SLAVE X TIP VELOCITY XM(1)



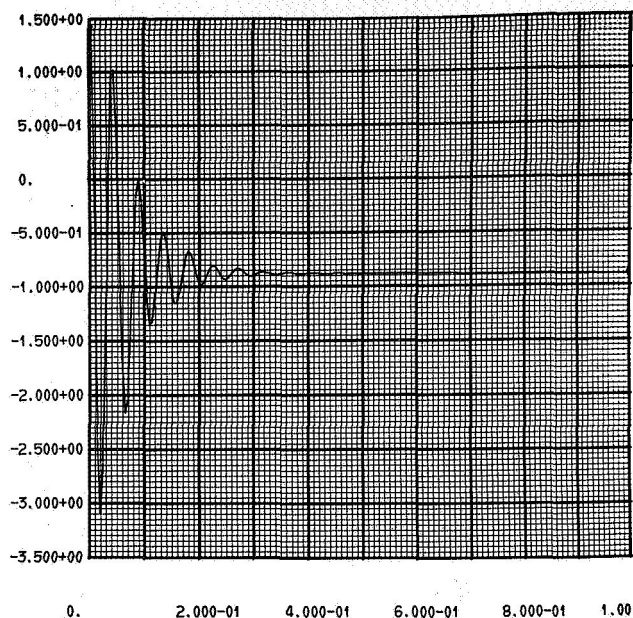
XM(2) VS TIME  
1 SLAVE Y TIP POSITION XM(2)



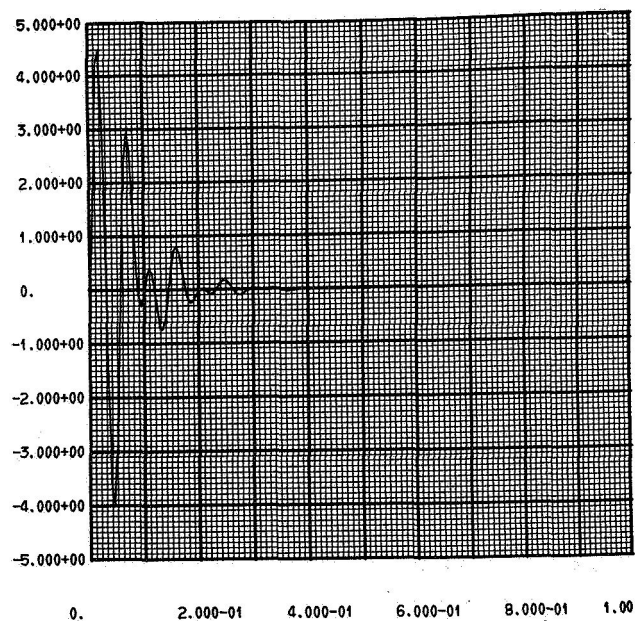
XM(2) VS TIME  
1 SLAVE Y TIP VELOCITY XM(2)



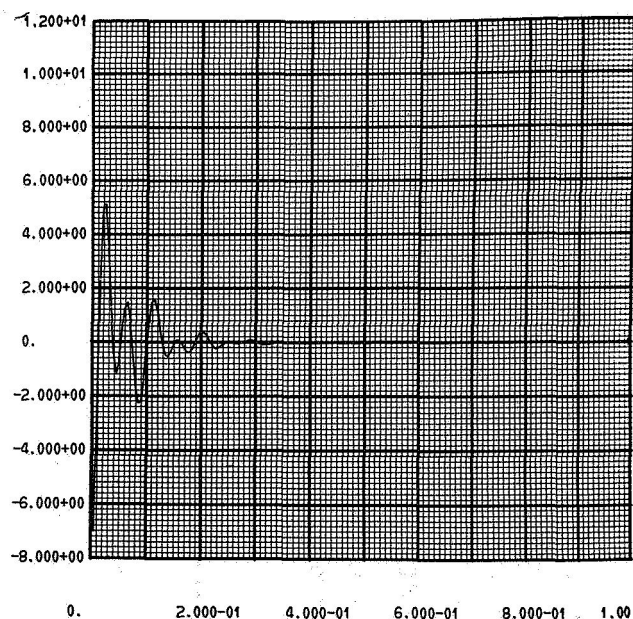
TQ(1) VS TIME  
1 MASTER SHOULDER TORQUE TQ(1)



TQ(2) VS TIME  
1 MASTER ELBOW TORQUE TQ(2)



TQ(3) VS TIME  
1 SLAVE SHOULDER TORQUE TQ(3)



TQ(4) VS TIME  
1 SLAVE ELBOW TORQUE TQ(4)

c. Example III -

In this example the servo motors are modeled in the current drive mode, there is no differential or positive tip rate feedback, the external applied forces on the Master are (0, 1 lb), and the external forces on the manipulator are (0, 0). Both arms are initially placed at (1.7 ft, 0). As seen from the time trajectories, the system is totally unstable due to the almost complete absence of any internal damping.

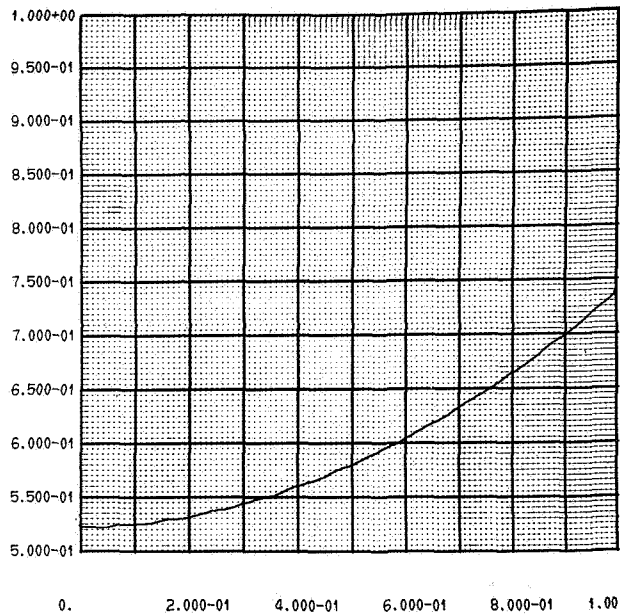


# TWO DIMENSIONAL BILATERAL MANIPULATOR PROGRAM

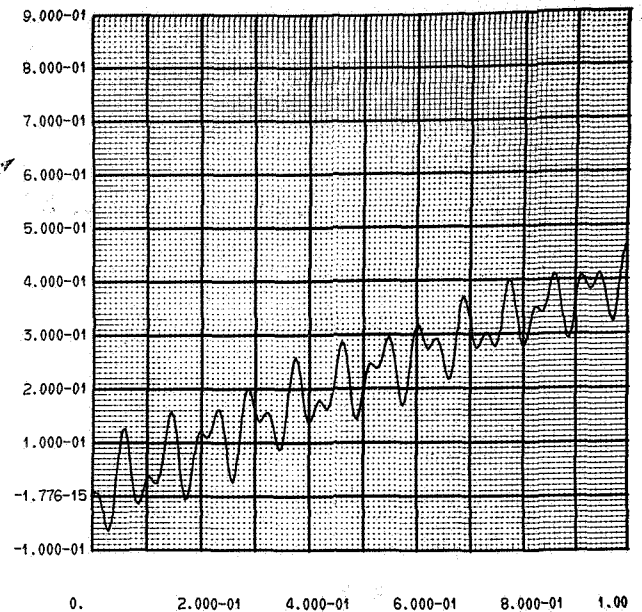
## INPUT DATA

K1	2000.000	0.	K2	0.	0.
	0.	2000.000		0.	0.
K3	0.	0.	K4	2000.000	0.
	0.	0.		0.	2000.000
K5	0.	0.	K6	0.	0.
	0.	0.		0.	0.
CA	.06720	0.	MA	.06720	0.
	0.	.06720		0.	.06720
MM	1.000	0.			
	0.	1.000			
GS	0.	0.		0.	0.
	0.	0.		0.	0.
PI	0.	0.			
	0.	0.			
RR	0.	0.			
	0.	0.			
KT	.149	.149		.149	.149
	.149	.149		.149	.149
RL	1.500	1.500		1.500	1.500
	1.500	1.500		1.500	1.500
TL	28.125	28.125		28.125	28.125
	28.125	28.125		28.125	28.125
RT	11.900	11.900		11.900	11.900
	11.900	11.900		11.900	11.900
KG	100.000	100.000		100.000	100.000
	100.000	100.000		100.000	100.000

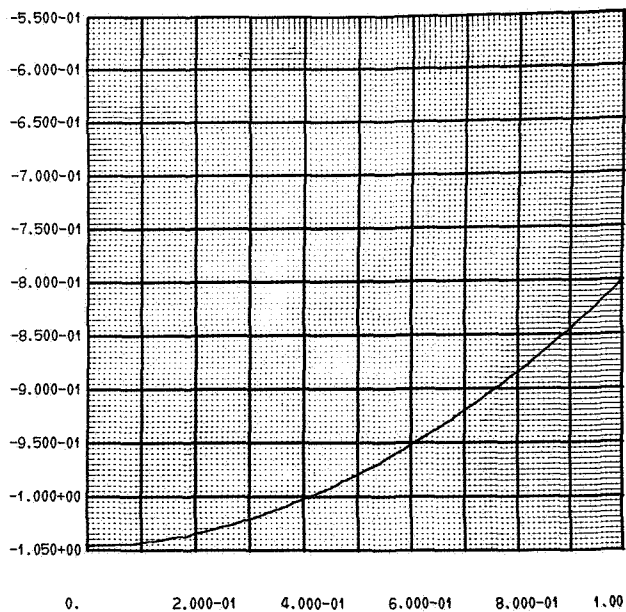
KB	.00042	.00042	.00042	.00042			
JM	0.	0.	0.	0.			
RA =	0.						
LC =	1.000	LM =	2.000				
STIME =	1.000						
NEQ = 8	STEP =	.005					
T =	0.						
X(1)	.523	X(2)	0.	X(3)	-1.046	X(4)	0.
X(5)	1.122	X(6)	0.	X(7)	-2.244	X(8)	0.
FC	0.		1.000				
FM	0.		0.				
END OF INPUT DATA							



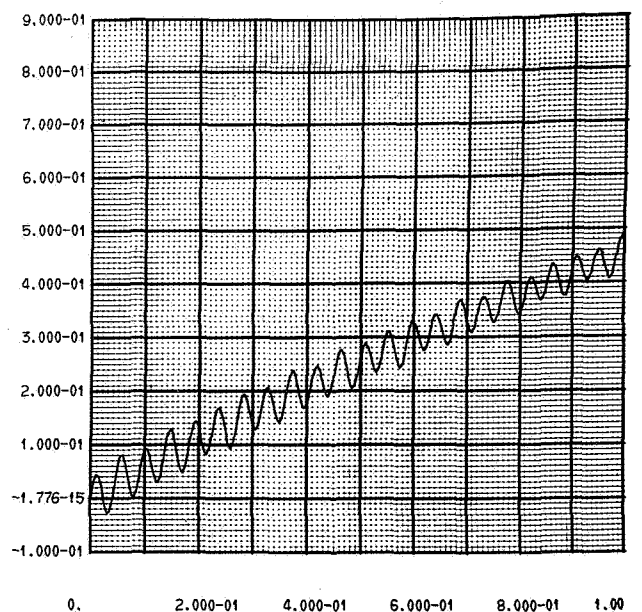
X(1) VS TIME  
1 MASTER SHOULDER POSITION X(1)



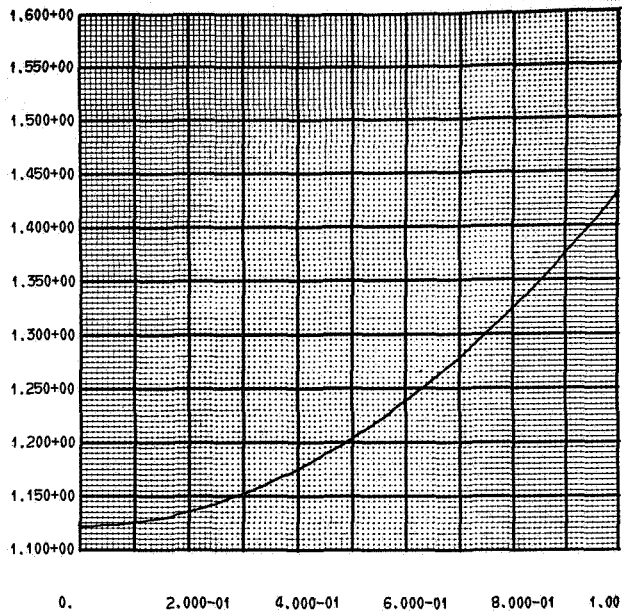
X(2) VS TIME  
1 MASTER SHOULDER VELOCITY X(2)



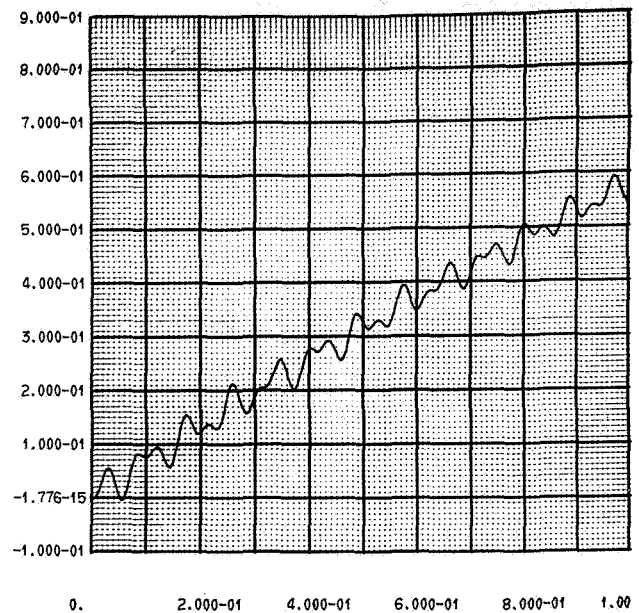
X(3) VS TIME  
1 MASTER ELBOW POSITION X(3)



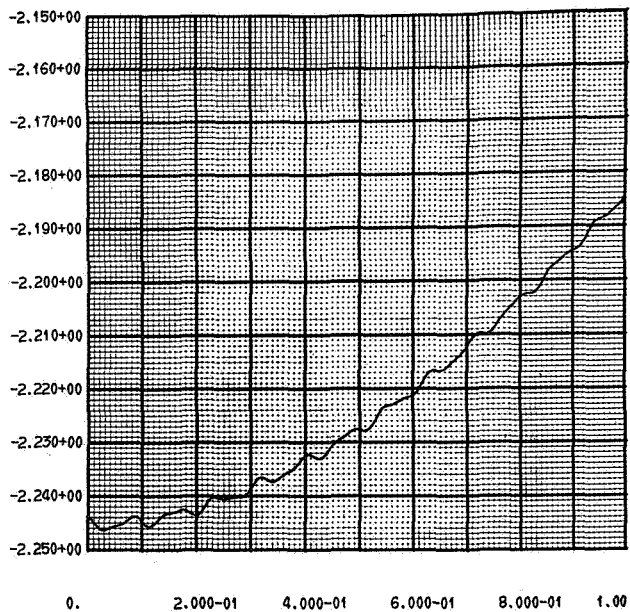
X(4) VS TIME  
1 MASTER ELBOW VELOCITY X(4)



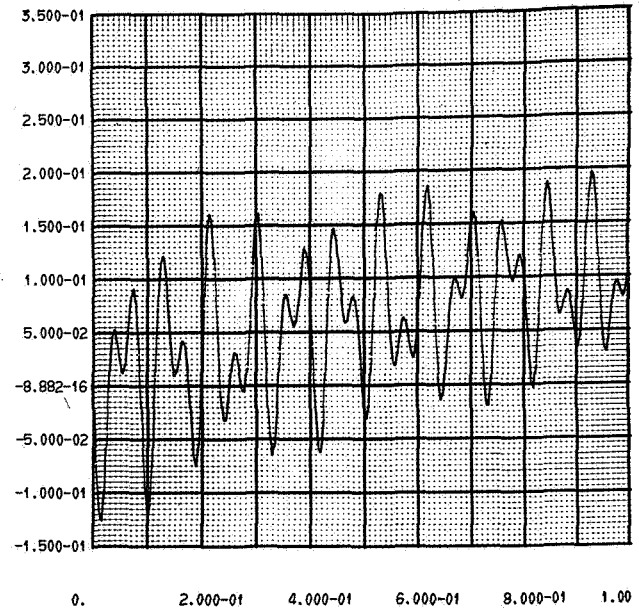
X(5) VS TIME  
1 SLAVE SHOULDER POSITION X(5)



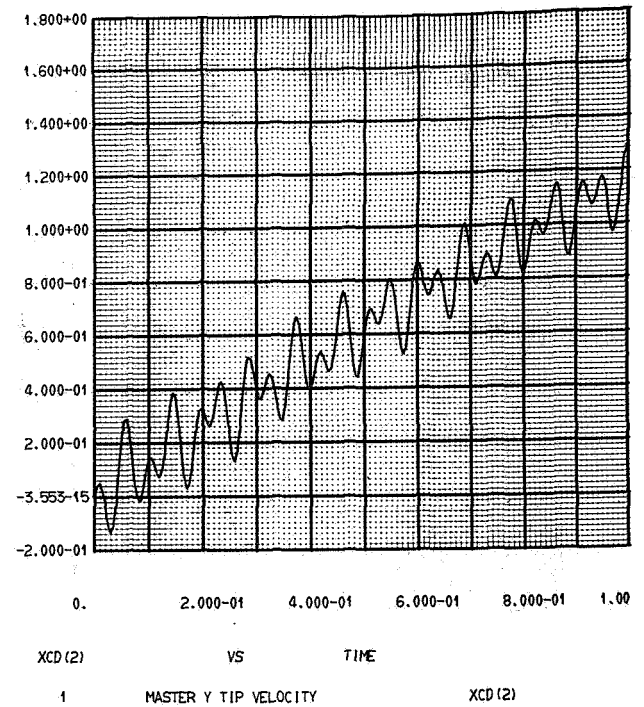
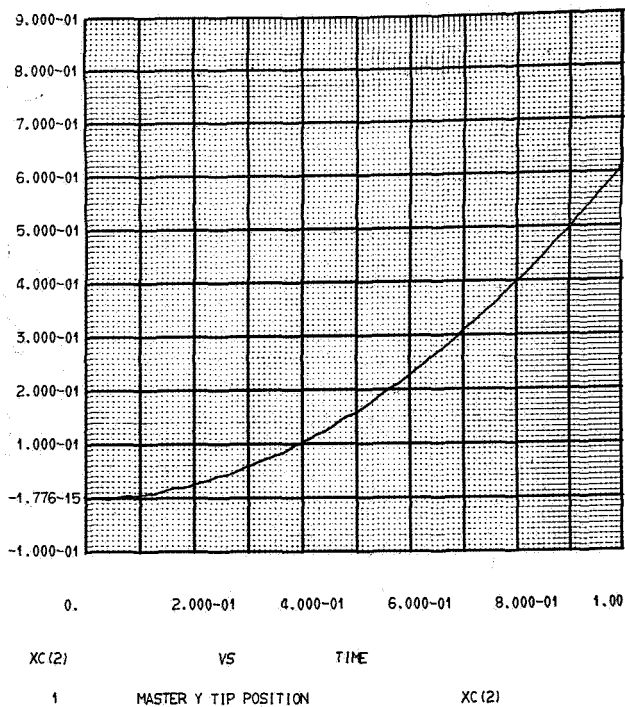
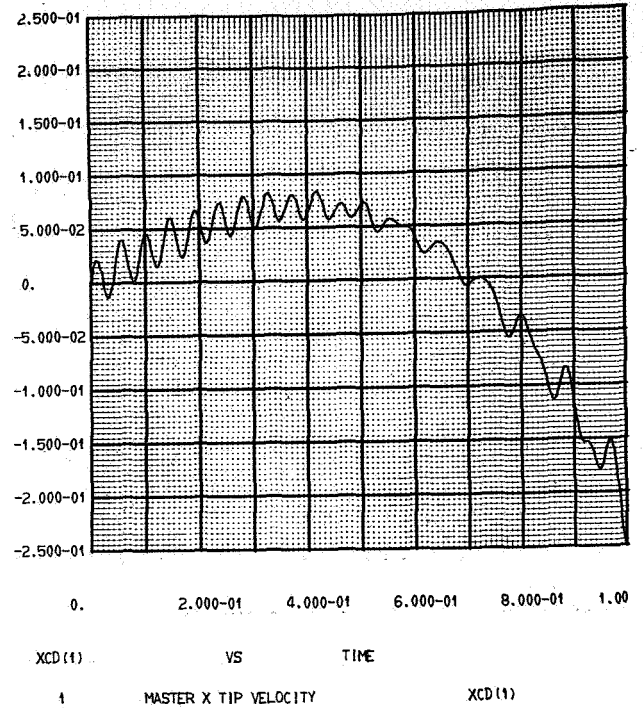
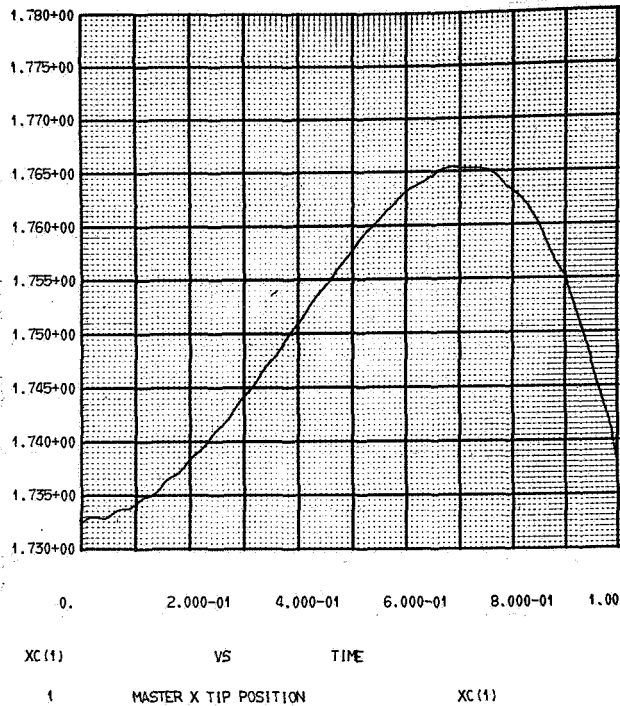
X(6) VS TIME  
1 SLAVE SHOULDER VELOCITY X(6)

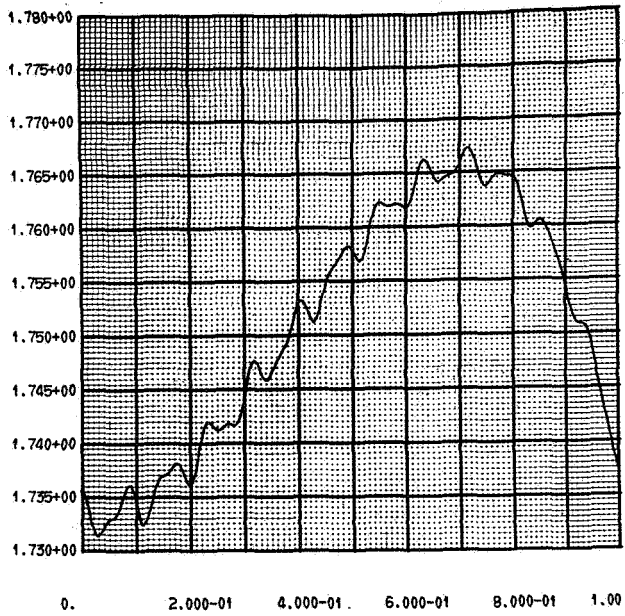


X(7) VS TIME  
1 SLAVE ELBOW POSITION X(7)

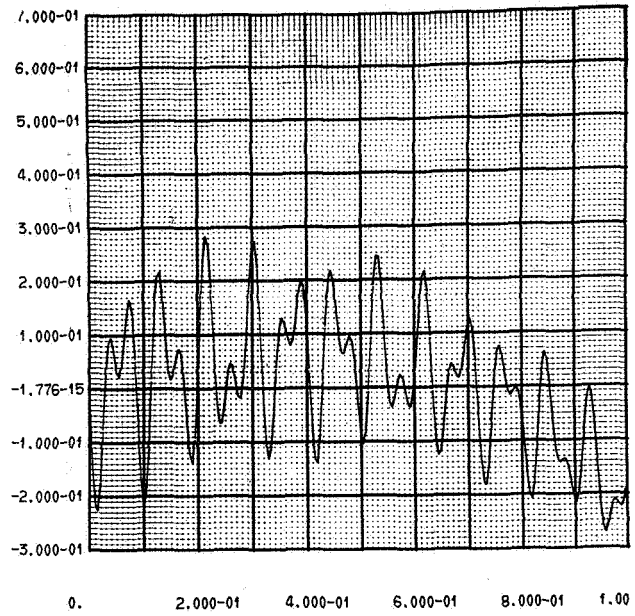


X(8) VS TIME  
1 SLAVE ELBOW VELOCITY X(8)

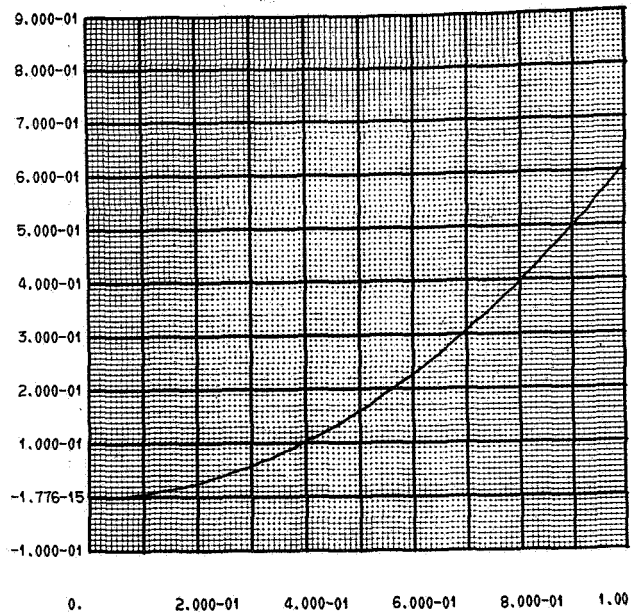




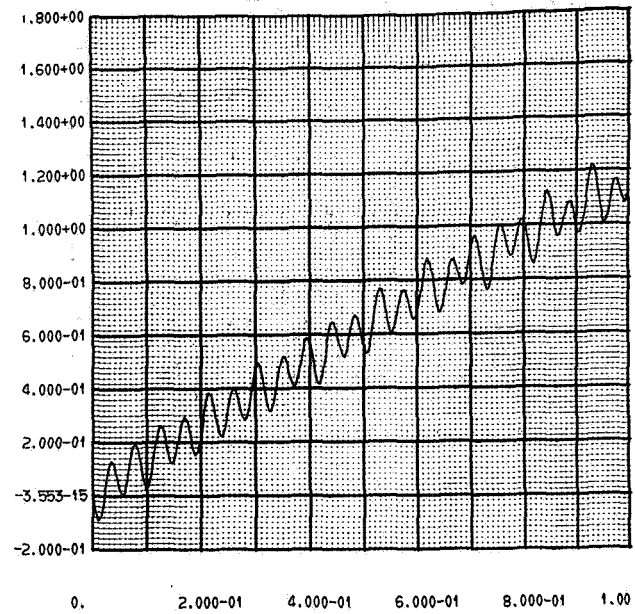
XM(1) VS TIME  
1 SLAVE X TIP POSITION XM(1)



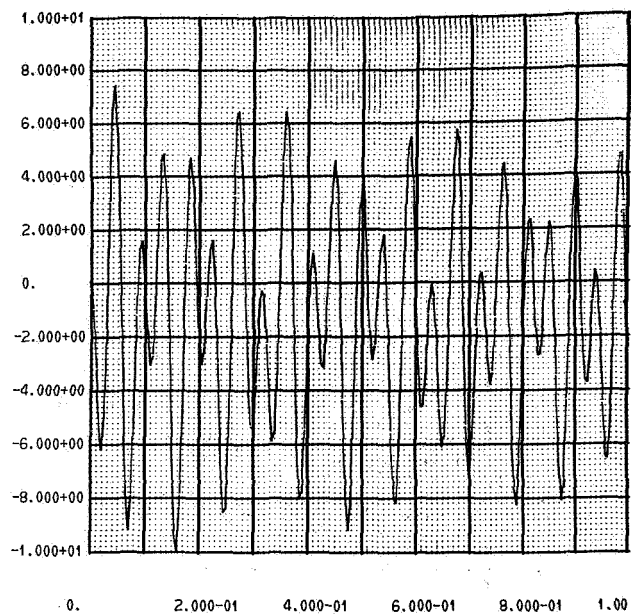
XMD(1) VS TIME  
1 SLAVE X TIP VELOCITY XMD(1)



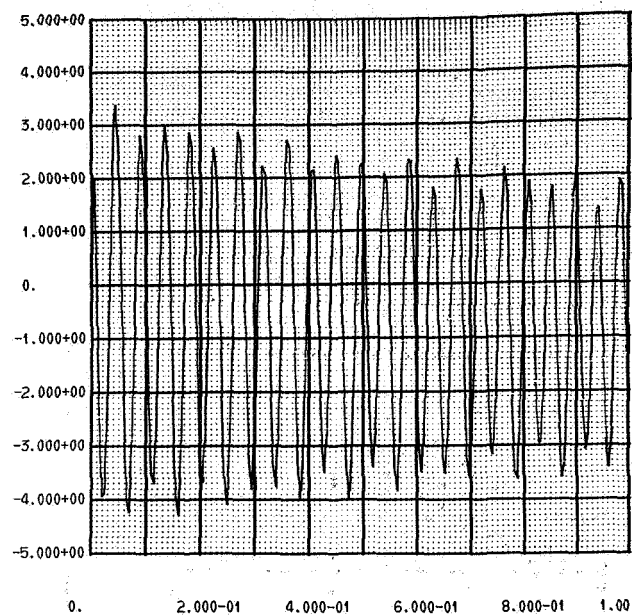
XM(2) VS TIME  
1 SLAVE Y TIP POSITION XM(2)



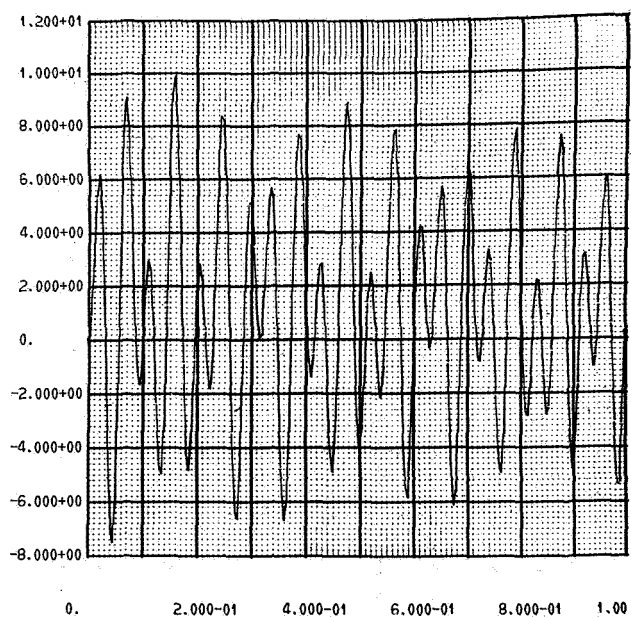
XMD(2) VS TIME  
1 SLAVE Y TIP VELOCITY XMD(2)



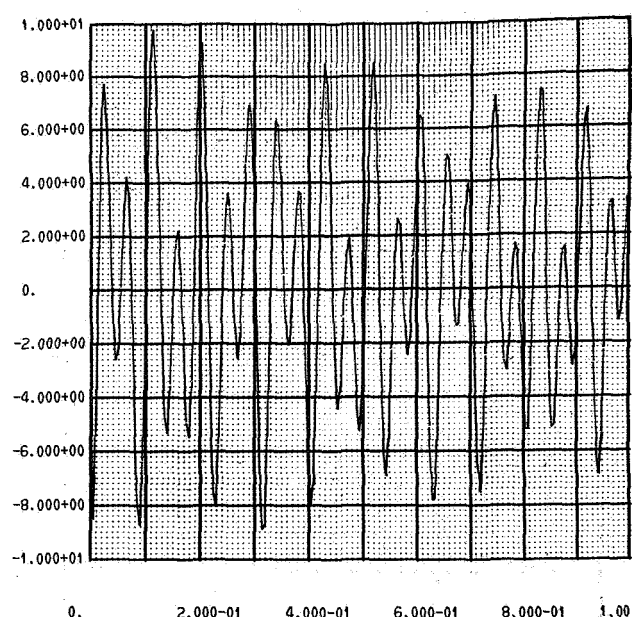
TQ(1) VS TIME  
1 MASTER SHOULDER TORQUE TQ(1)



TQ(2) VS TIME  
1 MASTER ELBOW TORQUE TQ(2)



TQ(3) VS TIME  
1 SLAVE SHOULDER TORQUE TQ(3)



TQ(4) VS TIME  
1 SLAVE ELBOW TORQUE TQ(4)

## B. SERVO SYSTEM DESIGN

### 1. Two DOF Breadboard Controller-Manipulator Physical Characteristics

Before proceeding to the actual design and analysis of the two D.O.F. control system, the physical characteristics of the breadboard hardware will be reviewed so that these characteristics can be used in transforming the previously discussed control law generalities into the needed electronics to interface input controller and output manipulator.

Figure III-27 depicts the completed arms with motors, tachometers, and potentiometers. All physical dimensions are given on the schematic of Figure III-21\* and will therefore be omitted here. In contrast to Figure III-21, the potentiometer at each joint was moved from the output shaft to the shaft that is one mesh removed from the input drive. As with many designs, hindsight was greater than foresight in that the center to center distances for each gear mesh were not made adjustable and the overall gear trains resulted with appreciable backlash. This backlash accompanied with high loop gains (low compliance bilateral system) resulted in intolerable nonlinear limit cycling. To alleviate this problem, higher turn potentiometers were obtained and placed closer to the input shafts. Normally the price paid for this type of solution is a degradation in tip position accuracy, but tip accuracy is only meaningful for a manipulator system with computer commanded inputs. Since the breadboard manipulator was designed to operate with man-in-the-loop, tip accuracy was meaningless, and thus no penalty was paid for this particular solution to reduce the backlash effects.

The mechanical parameters of interest to the servo system design are:

1. Motor characteristics
2. Gear characteristics
3. Inertia properties

It is noted that no optimization procedure was used for selecting the motor and gear train at each joint. For the sake of expediency, the same Inland prehousing Tach-Torquer was used for both joints of master and slave and initially the same gear train was used for all joints. As indicated below,

\* Mechanical design of the breadboard and Figures III-21 through III-26 are contained in Appendix F.



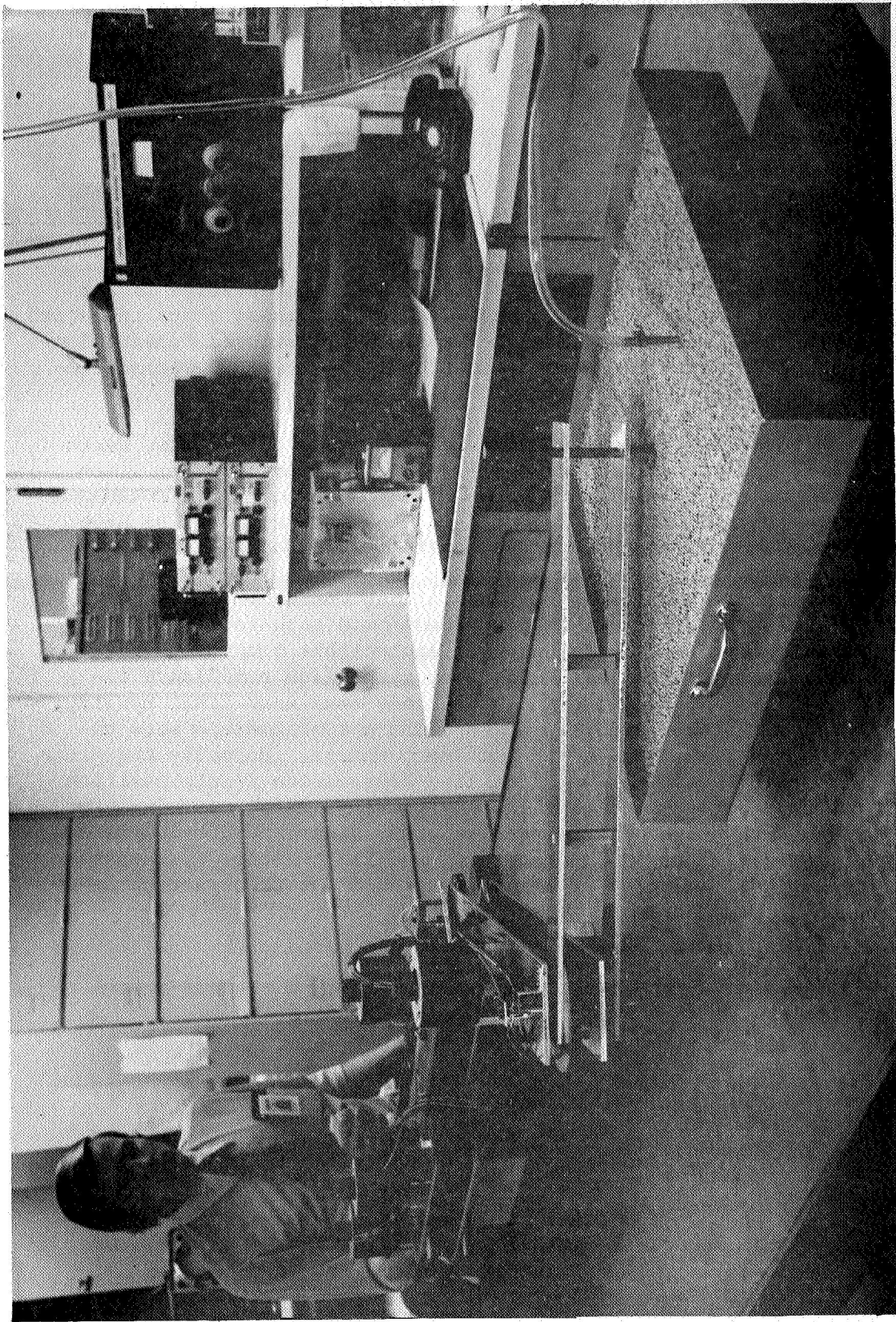


Figure III-27 Two DOF Manipulator With Air Bearing Load

the master shoulder and elbow gear ratios were modified slightly to reduce friction levels and yield an input controller with an 8 lb tip force capability.

Tables III-2, III-3, and III-4 summarize the motor, gear, and inertia properties associated with each joint. The inertia numbers are actual measured values and represent the inertia reflected to the output shaft of all rotating members (beam structure, gears, shafts, motor rotor, potentiometer shaft, etc.) associated with a particular joint.

Table III-2

<u>Motor Characteristics</u> (All joints have same motor)	
Manufacture:	Inland
Model:	NT2173
Peak Torque:	0.281 ft lbs
Power Input, at Peak Torque:	57 watts
Viscous Damping, Infinite Impedence Source:	0.0000625 ft lbs/rad/sec
DC Resistance:	11.8 ohms
Volts at Peak Torque:	22.4 volts
Amps at Peak Torque:	1.9 amps
Torque Sensitivity:	0.149 ft lbs/amp

Table III-3

<u>Gear Train Ratio</u>	
Joint	Gear Ratio
Master Shoulder	62:1
Master Elbow	29:1
Slave Shoulder	100:1
Slave Elbow	100:1

Table III-4

<u>Inertia Properties</u>		
Joint		Inertia Reflected to Output Shaft
Master Shoulder	Elbow = 0°	0.90 ft lbs sec <sup>2</sup>
	Elbow = 90°	0.86 ft lbs sec <sup>2</sup>
Master Elbow		0.434 ft lbs sec <sup>2</sup>
Slave Shoulder	Elbow = 0°	1.97 ft lbs sec <sup>2</sup>
	Elbow = 90°	1.62 ft lbs sec <sup>2</sup>
Slave Elbow		0.781 ft lbs sec <sup>2</sup>

## 2. Control System Design

As indicated in the above discussion, after the control laws have been formulated that yield a system with all the required operational qualities, the foremost problem in the control system design becomes that of developing the compensating circuitry that will provide an unconditionally stable servo system.

As revealed by the above time trajectories, using tachometric feedback as the primary stabilizing technique produces very undesirable effects for a bilateral force reflecting system. Since it is desired to minimize the forces needed to produce motion in the master controller when the slave is free to move, any negative tachometric feedback present in the system tends to increase the required input force. Thus, with tachometric feedback, a force to velocity ratio exists for all non steady state conditions, and if differential tachometric feedback is not used, a force to velocity ratio will exist also for all steady state conditions. This force to velocity relationship is clearly undesirable for a bilateral system since it tends to degrade the operator's sense of feel for inertial and externally applied forces acting on the slave member. Tachometric feedback has other undesirable qualities in that although it can be used to stabilize a system, it cannot simultaneously optimize other system parameters such as bandwidth, rise time, resonant frequency, etc.

Due to these considerations, the use of tachometric feedback was abandoned and it was decided to use network compensators (lead-lag filters) for stabilizing all portions of the system. The design of compensating filters for each of the servo subsystems was accomplished by frequency domain techniques as described below.

a. Master Shoulder Joint - Figure III-12 represents the master shoulder servo system with its various signal inputs. For a given initial position (equilibrium point) of the master and slave, this system can be linearized as previously described to yield the linearized system shown in Figure III-14, where

$$G_1(s) = \frac{(KFL(1))(KEI(1))}{s + (KFL(1))(KEI(1))(KFB(1))} \quad (22)$$

and

$$G_2(s) = \text{needed compensating filter.}$$

To find the needed transfer function for  $G_2(s)$ , the open loop transfer function  $e/\beta$  must be obtained. From Figure III-14  $e/\beta$  is seen to be

$$e/\beta = \frac{(2)(1+C(U7))(K1)(K_s)}{(KFL(1))(KFB(1))} \left[ \frac{1 + \frac{S}{(K1)(K_s)}}{(-K_2')} \frac{S}{S(1 + \frac{S}{(KFL(1))(KEI(1))(KFB(1))})} \right] \quad (23)$$

Taking worst case condition for the Bode gain of equation (23),  $(C(U7) = 1)$ , and remembering no tachometric feedback is to be used, and setting  $K_s = 1$ ; the above equation becomes

$$e/\beta = \frac{4(K1)}{(KFL(1))(KFB(1))} \left[ \frac{1}{S(1 + \frac{S}{(KFL(1))(KEI(1))(KFB(1))})} \right] \quad (24)$$

Since the values for  $KFL(1)$ ,  $KFB(1)$ , and  $KEI(1)$  are given by the motor, gear, and inertia characteristics of the master shoulder joint, the remaining unknown in equation (24) is  $K1$ , the master system forward loop gain. It was originally hoped that  $K1$  could be set as high as 2000; although this is theoretically feasible, it was found that the computer 231R analog computer used to program the control equations has a significant 60 Hz noise problem and  $K1$  could not be raised much beyond 300. Using this value of  $K1$ , the values from Tables III-2, III-3, and III-4 and the definitions in Table III-1, the variables of equation (24) are given by:

$$\begin{aligned} K1 &= 300 \\ KG(1) &= 62.2 \\ KFL(1) &= 9.28 \\ KFB(1) &= 0.02615 - \text{current drive, infinite impedance source} \\ KEI(1) &= 1.09 - \text{worst case inertia, elbow} = 0^\circ \\ LC &= 1 \\ CA &= 0.108 \end{aligned} \quad (25)$$

and  $e/\beta$  becomes

$$e/\beta = 6612 \quad \frac{1}{s(1 + \frac{s}{0.263})} \quad (26)$$

Figure III-28 depicts the Bode plots of the gain and phase curves for the transfer function of equation (26), and reveals, as expected, the intolerable stability parameters of:

$$\text{Gain Margin (GM)} = -18\text{db}$$

$$\text{Phase Margin (PM)} = 0^\circ$$

Figure III-28 reveals that lead compensation is needed in the  $\omega = 50$  rad/sec vicinity in order to yield workable values for GM and PM. Inserting the network filter

$$G_2(s) = \frac{1 + \frac{s}{16.4}}{1 + \frac{s}{54.7}} \quad (27)$$

with a zero to pole ratio of 0.3, the Bode plots of the open loop transfer function become shifted as shown in Figure III-29. From this figure it is seen that the gain and phase margins now have the acceptable values of:

$$\text{GM} = 30\text{db} \quad (28)$$

$$\text{PM} = 24^\circ$$

Due to the high gain crossover frequency in Figure III-28, the compensating network of equation (27) has "tail-end" effects that extend into the 60 Hz frequency range. Since, as stated earlier, the analog computer used generates 60 Hz noise, it was decided to insert the 60 Hz notch filter

$$G_f = \frac{s^2 + 396s + (381)^2}{s^2 + 792s + (381)^2} \quad (29)$$

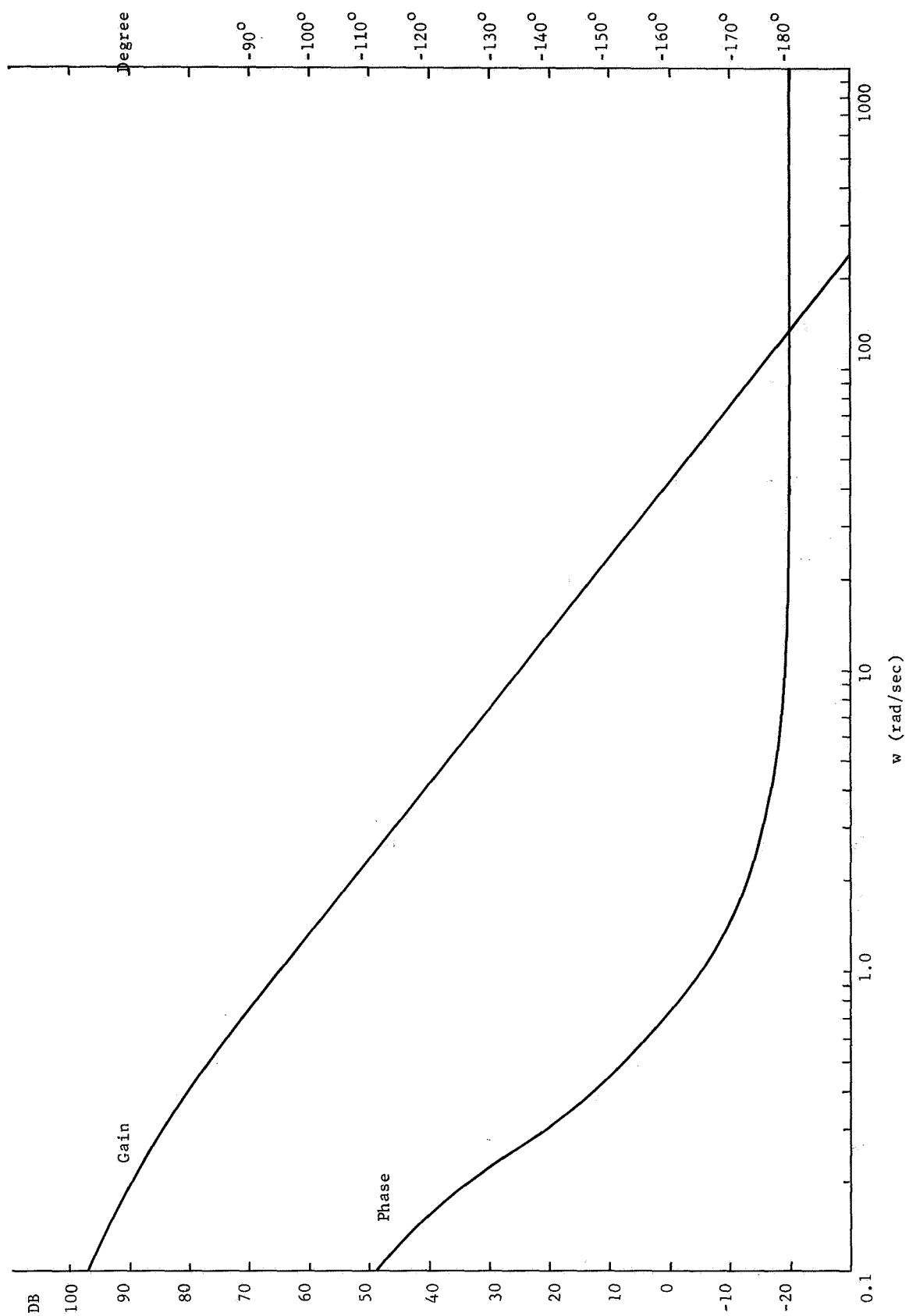


Figure III-28 Bode Plots of Uncompensated Open Loop Linearized Master Shoulder Servo Systems

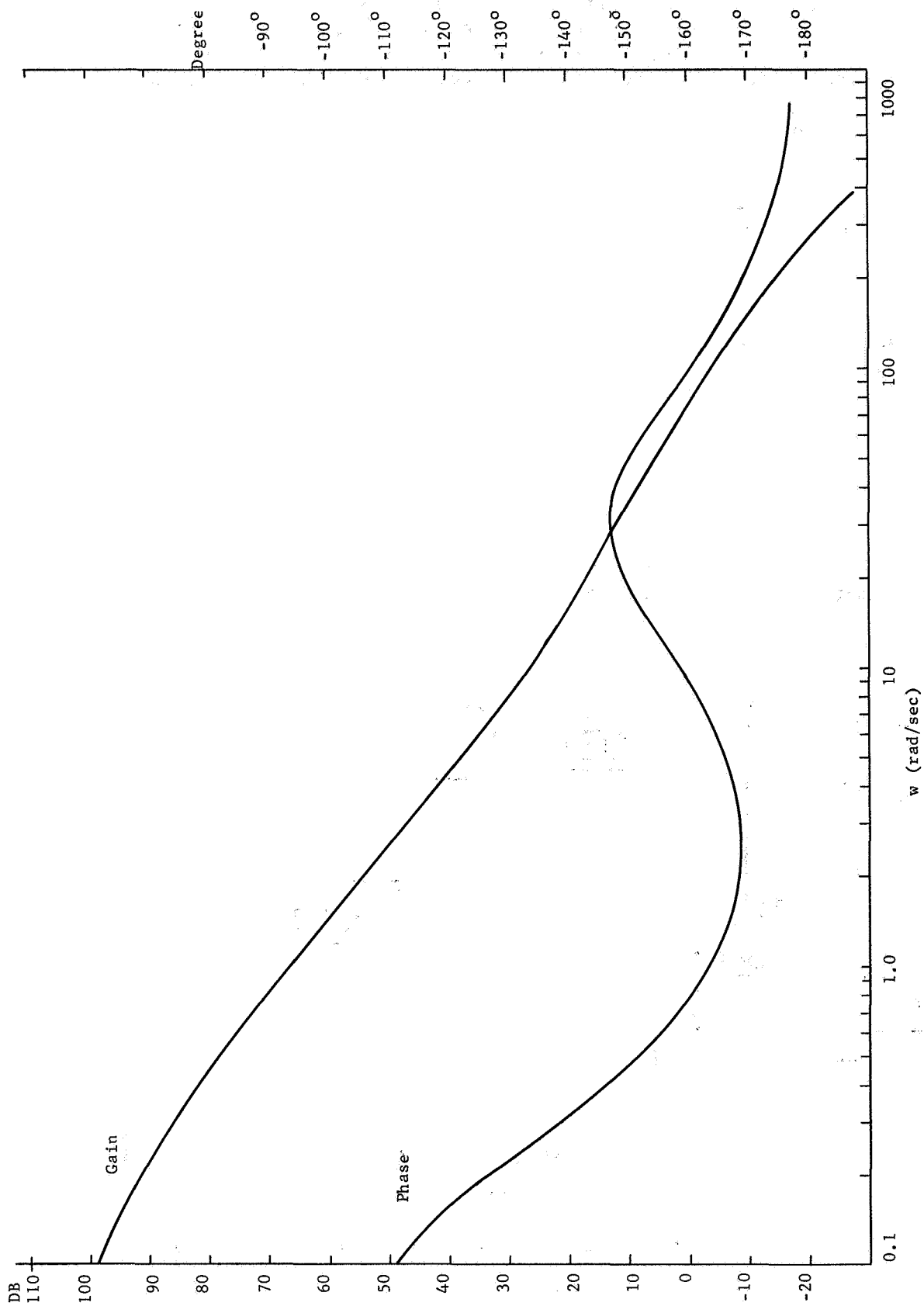


Figure III-29 Bode Plots of Compensated Open Loop Linearized Master Shoulder Servo Loop



in order to reduce the dither generated in the servo motors. It is noted that this filter has a notch ratio of only 0.5. Lower notch ratios could not be used due to the undesirable phase shift characteristics introduced in the gain crossover region. With the noise filter introduced in the circuit, the lead compensator of equation (27) must be modified to retain allowable values of GM and PM. This modified filter

$$G_2(s) = \frac{1 + \frac{s}{17}}{1 + \frac{s}{85}} \quad (30)$$

has a zero to pole ratio of 0.2 and yields total open loop gain and phase curves given by Figure III-30. From these curves it is seen that the final compensated linearized system has the following stability margins,

$$\begin{aligned} \text{GM} &= 12\text{db} \\ \text{PM} &= 23^\circ \end{aligned} \quad (31)$$

Summarizing these results, the compensated master shoulder linearized servo subsystem is given as shown in Figure III-31.

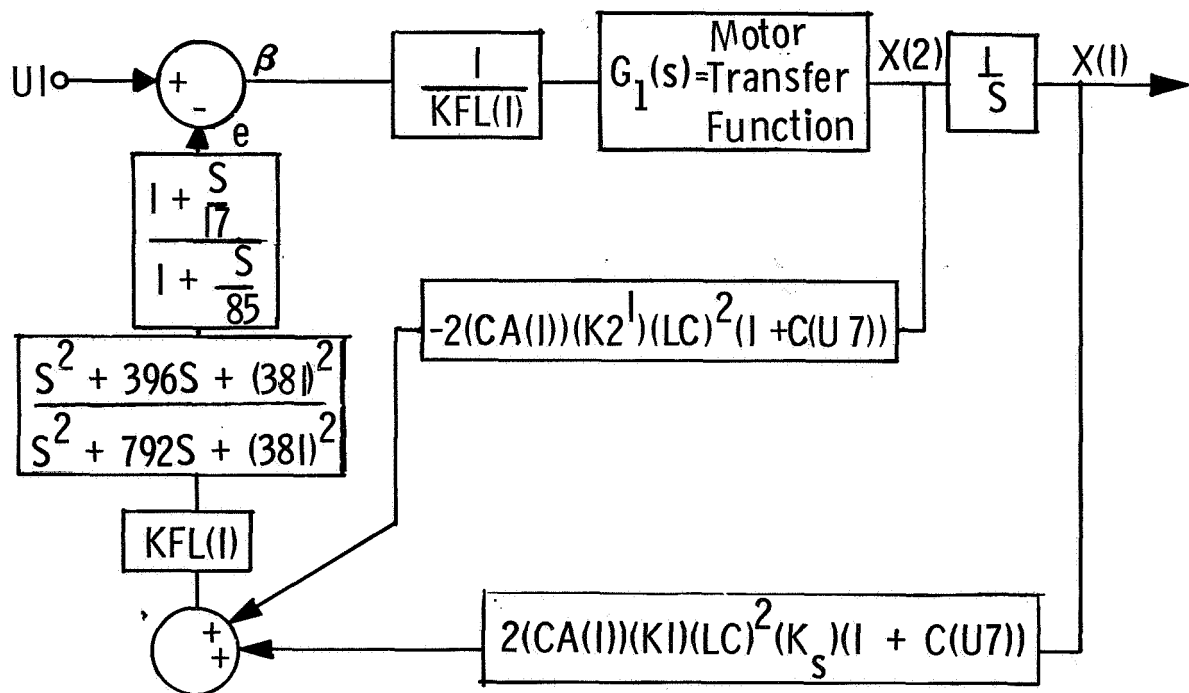


Figure III-31 Compensated Master Shoulder Linearized Servo Subsystem

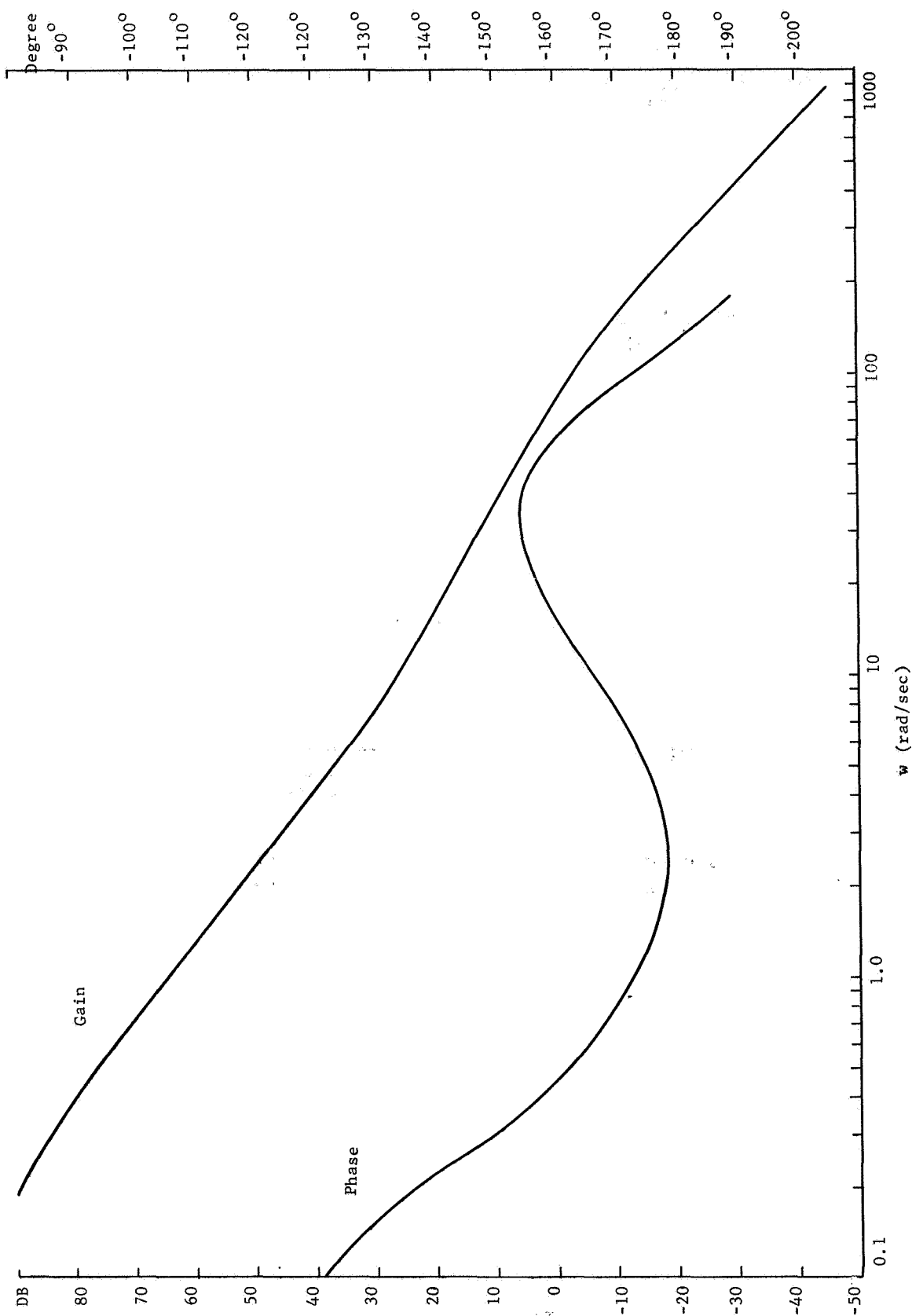


Figure III-30 Bode Plots of Compensated Open Loop Linearized Master Shoulder Servo System with 60 Hz Notch Filter

b. Master Elbow Joint - Figure III-15 represents the master elbow servo subsystem and its associated signal inputs. Proceeding as in the above section, this system is linearized about any initial master-slave position to produce the linearized system show in Figure III-16.

where

$$G_1(s) = \frac{(KFL(2))(KEI(2))}{s + (KFL(2))(KEI(2))(KFB(2))} \quad (32)$$

and

$$G_2(s) = \text{needed compensating filter.}$$

The open loop transfer function  $e/\beta$  is seen to be

$$e/\beta = \frac{(K1)(K_s)}{(KFB(2))(KFL(2))} \left[ \frac{1 + \frac{s}{(K1)(K_s)}}{s \left( 1 + \frac{s}{(KFL(2))(KEI(2))(KFB(2))} \right)} \right] \quad (33)$$

From the discussion of Section III.C.2 and Tables III-1, III-2, III-3, III-4, the variables of equation (33) are given by

$$\begin{aligned}
K_1 &= 300 \\
K_s &= 1 \\
KG(2) &= 29.6 \\
KFB(2) &= 0.0124 \\
KFL(2) &= 4.41 \\
CA &= 0.227 \\
-K_2' &= 0 \\
LC &= 1 \\
KEI(2) &= 2.31
\end{aligned}$$

and  $e/\beta$  becomes

$$e/\beta = 7312 \left[ \frac{1}{s(1 + \frac{s}{0.124})} \right] \quad (34)$$

Figure III-32 represents the Bode plots of  $e/\beta$  and reveals that the uncompensated system has stability margins of

$$\begin{aligned}
GM &= -23\text{db} \\
PM &= 0^\circ.
\end{aligned} \quad (35)$$

Inserting the lead compensator

$$G_2(s) = \frac{1 + \frac{s}{11.2}}{1 + \frac{s}{37.3}} \quad (36)$$

in the circuit yields the Bode plots of Figure III-33 and the system is now seen to have

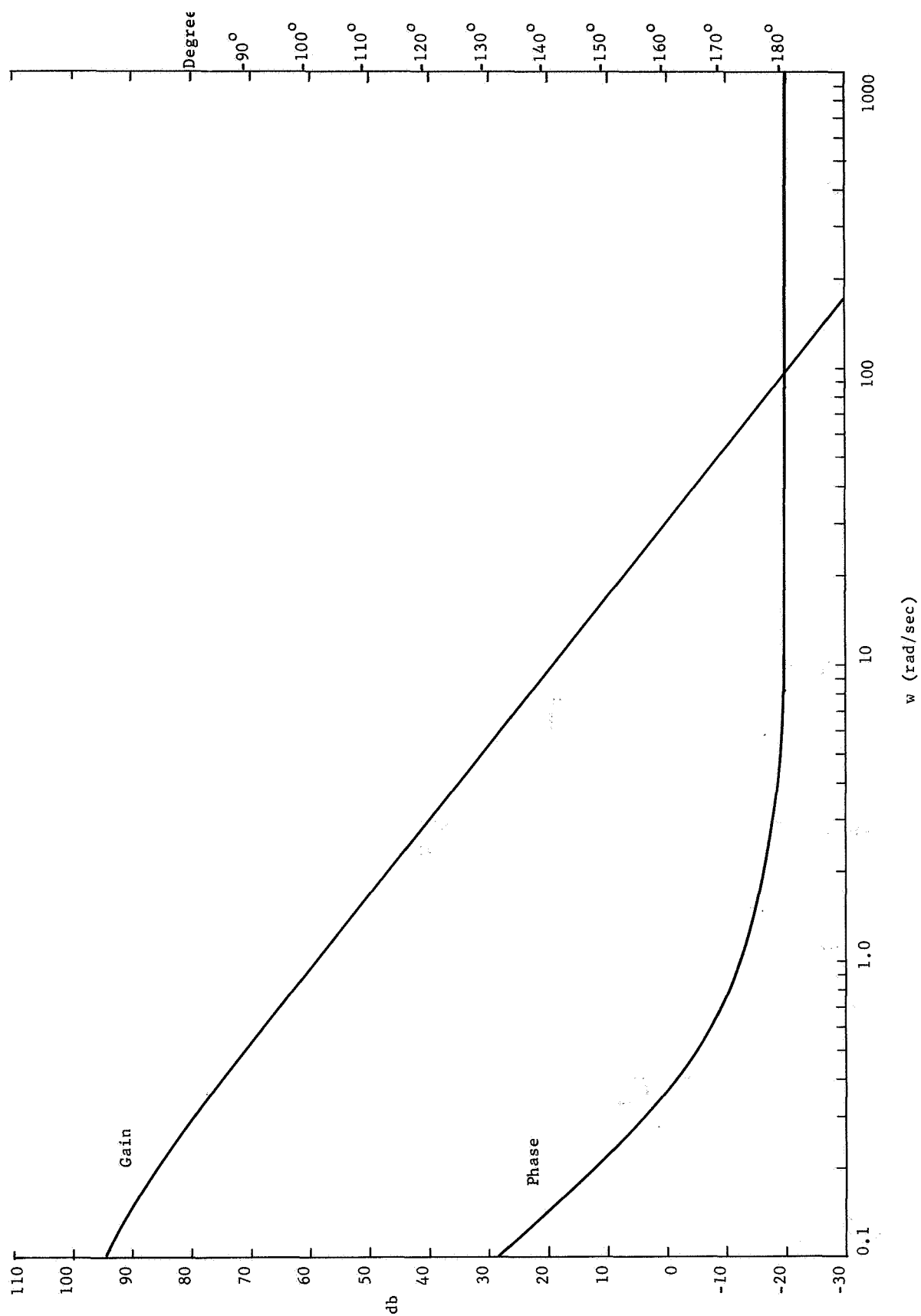


Figure III-32 Bode Plots of Uncompensated Open Loop Linearized Master Elbow Servo System.

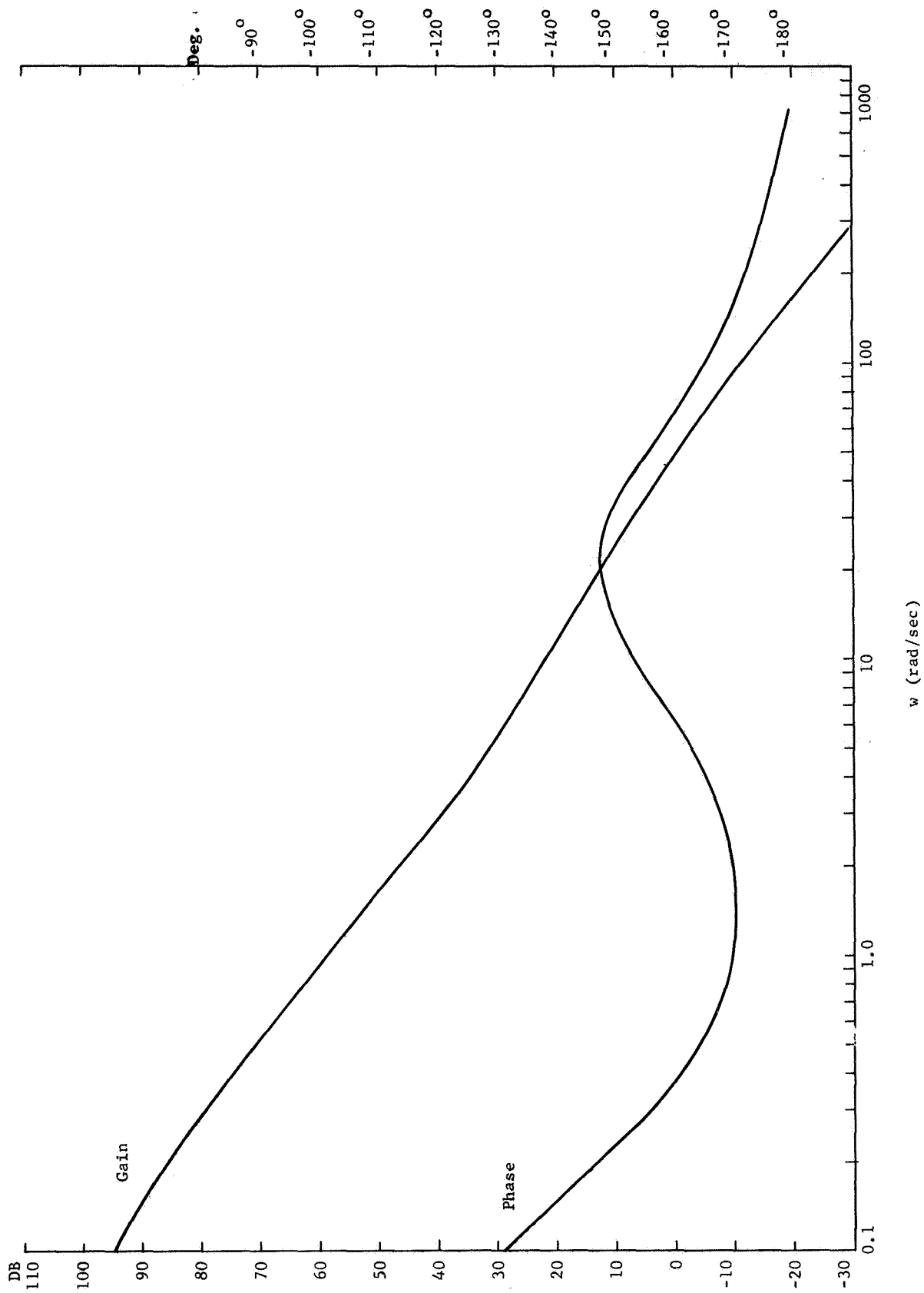


Figure III-33 Bode Plots of Compensated Open Loop Linearized Master Elbow Servo System

$$\begin{aligned} \text{GM} &= 30\text{db} \\ \text{PM} &= 24^\circ. \end{aligned} \tag{37}$$

Once again attenuating the 60 Hz noise with the notch filter

$$G_f = \frac{s^2 + 396s + (381)^2}{s^2 + 792s + (381)^2} \tag{38}$$

and modifying  $G_2(s)$  to

$$G_2(s) = \frac{1 + \frac{s}{14}}{1 + \frac{s}{70}} \tag{39}$$

yields the Bode plots of Figure III-34 for the total compensated system. Figure III-34 reveals the open loop stability margins to be

$$\begin{aligned} \text{GM} &= 16\text{db} \\ \text{PM} &= 28^\circ \end{aligned} \tag{40}$$

and Figure III-35 represents the completely compensated master elbow linearized servo subsystem,

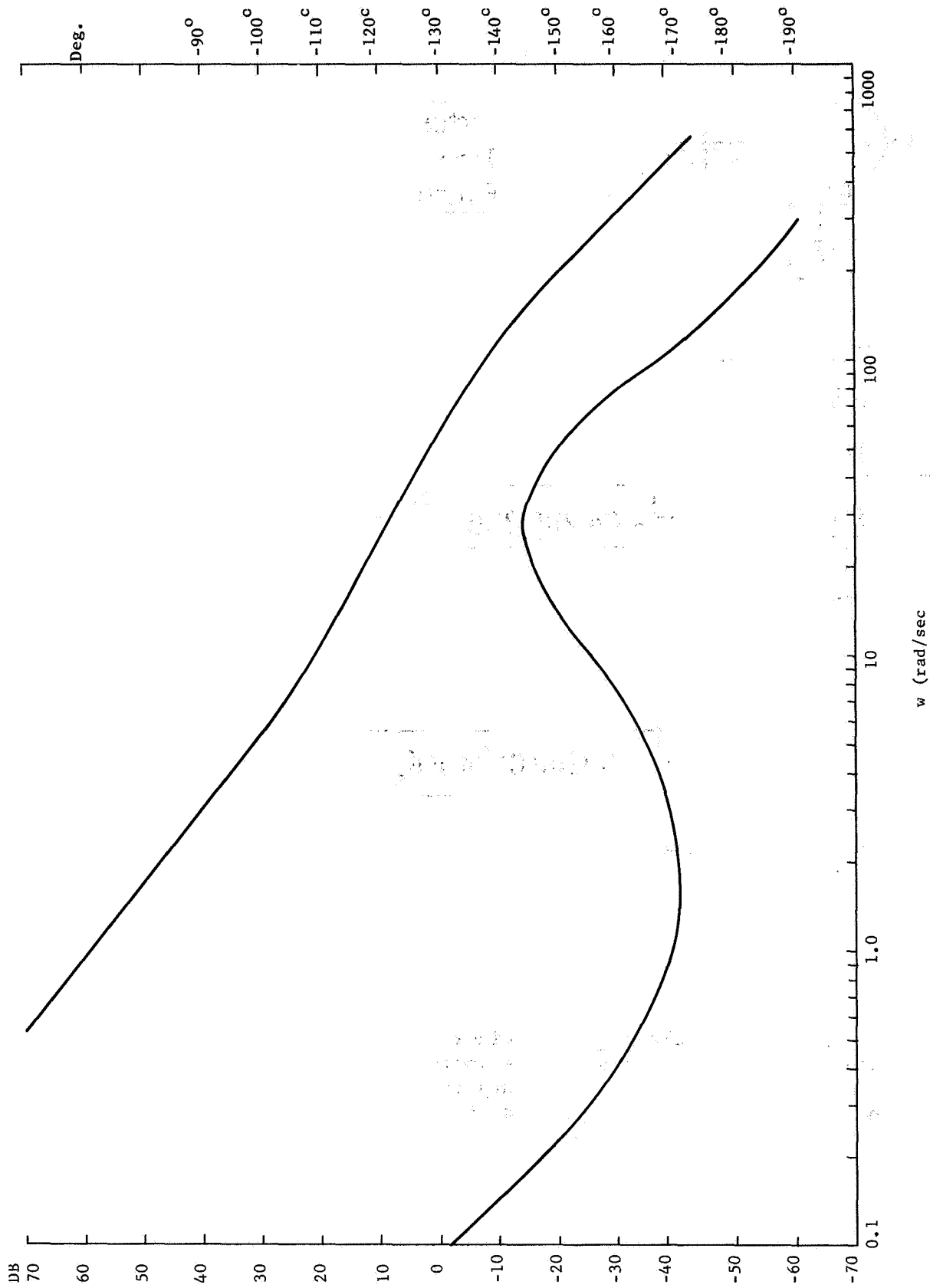


Figure III-34 Bode Plots of Compensated Open Loop Linearized Master Elbow  
With 60 Hz. Notch Filter



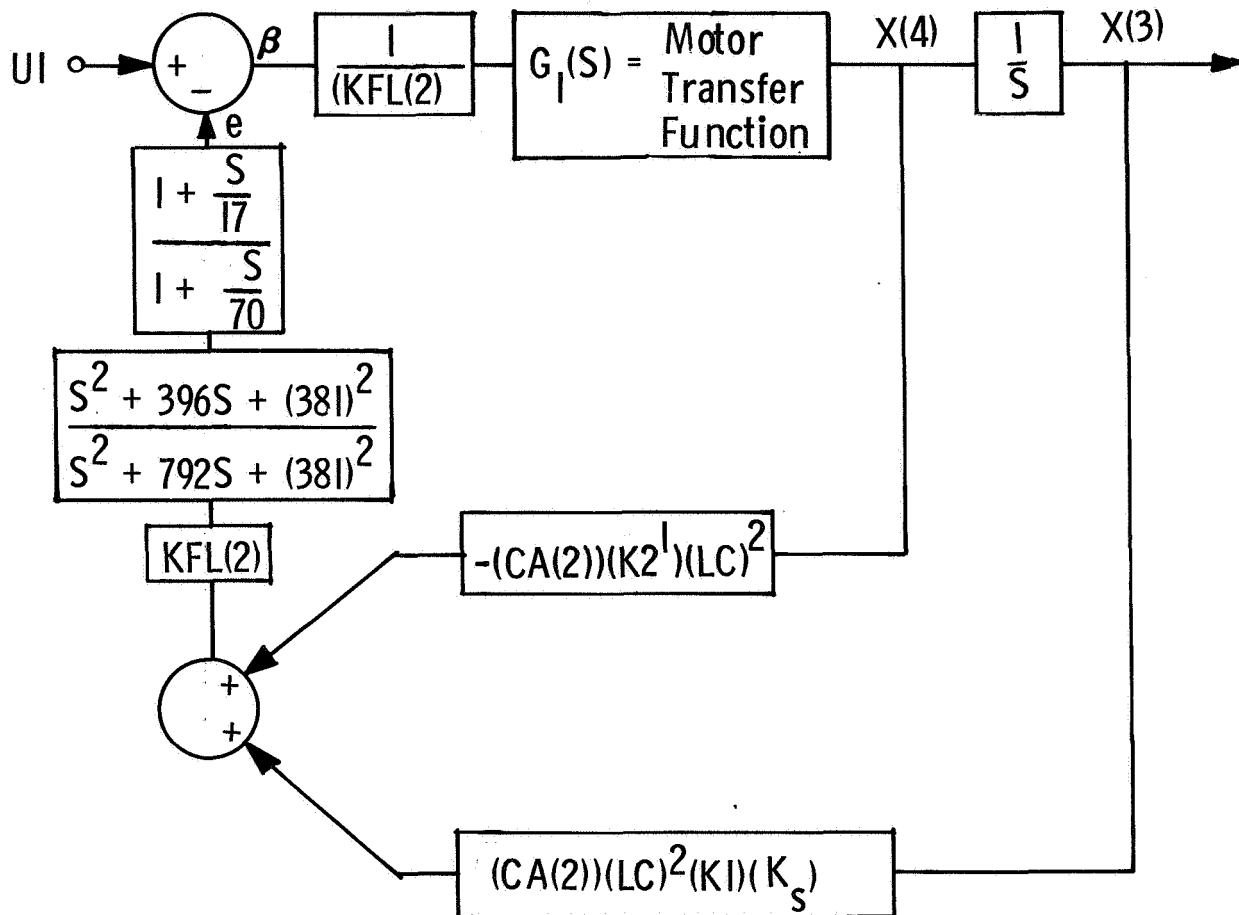


Figure III-35 Compensated Master Elbow Linearized Servo System

c. Slave Shoulder Joint - Figure III-17 depicts the slave shoulder servo subsystem and its various signal inputs. Linearizing this system around any initial master-slave position results in the system of Figure III-18,

where

$$G_1(s) = \frac{(KFL(3)) (KEI(3))}{s + (KFL(3)) (KEI(3)) (KFB(3))} \quad (41)$$

and

$$G_2(s) = \text{needed compensating filter.}$$

The open loop transfer function is

$$e/\beta = \frac{2(LM)^2 (1 + C(U7)) (K4) (K_s) (MM)}{(KFL(3)) (KFB(3))} \left[ \frac{1 + \frac{s}{(-K_5')}}{\frac{s}{(K4) (K_s)}} \right] \frac{1}{s (1 + \frac{s}{(KFL(3)) (KEI(3)) (KFB(3))})}.$$

From Section III.C.2 and Tables III-1, III-2, III-3, III-4, the variables of equation (41) are defined to be

$$K4 = 300$$

$$K_s = 1$$

$$KG(3) = 100$$

$$MB(3) = 0.042$$

$$KFL(3) = 14.9$$

$$KEI(3) = 0.508 = \text{worst case inertia, elbow} = 0^\circ$$

$$MA(1) = 0.0672$$

$$K5' = 0$$

$$LM = 2$$

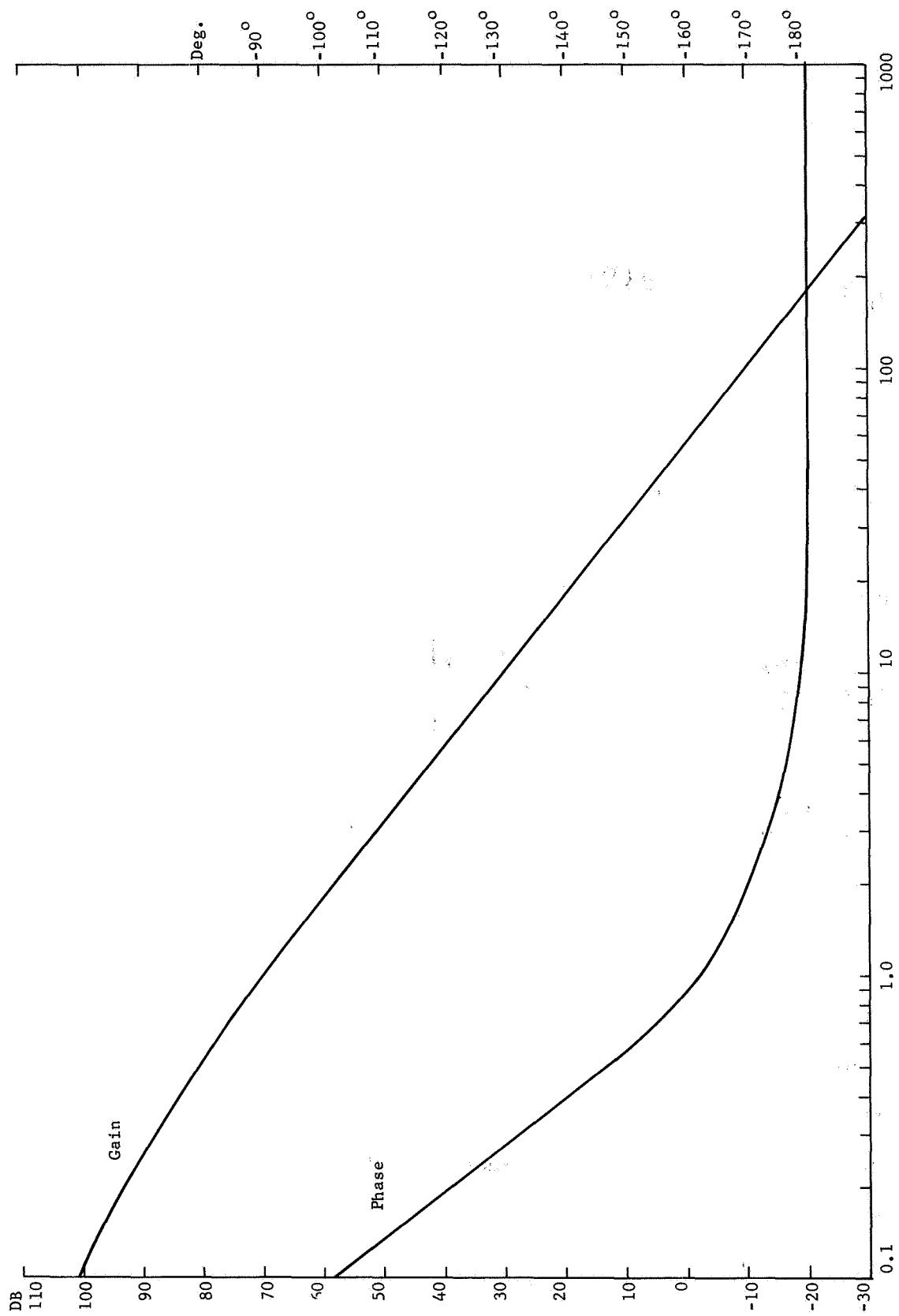


Figure III-36 Bode Plots of Uncompensated Open Loop Linearized Slave Shoulder Servo System

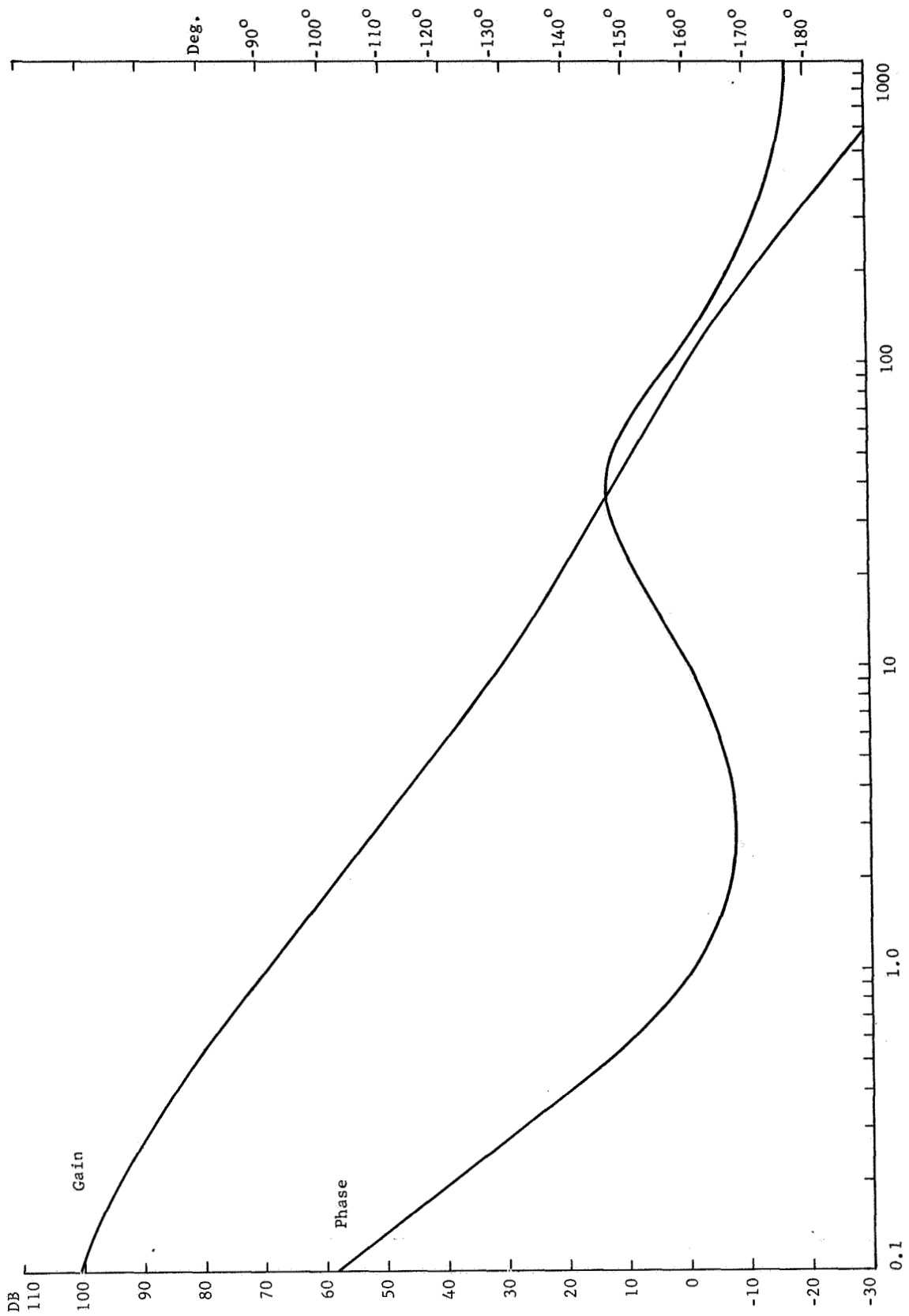


Figure III-37 Bode Plots of Compensated Open Loop Linearized Slave Shoulder Servo System

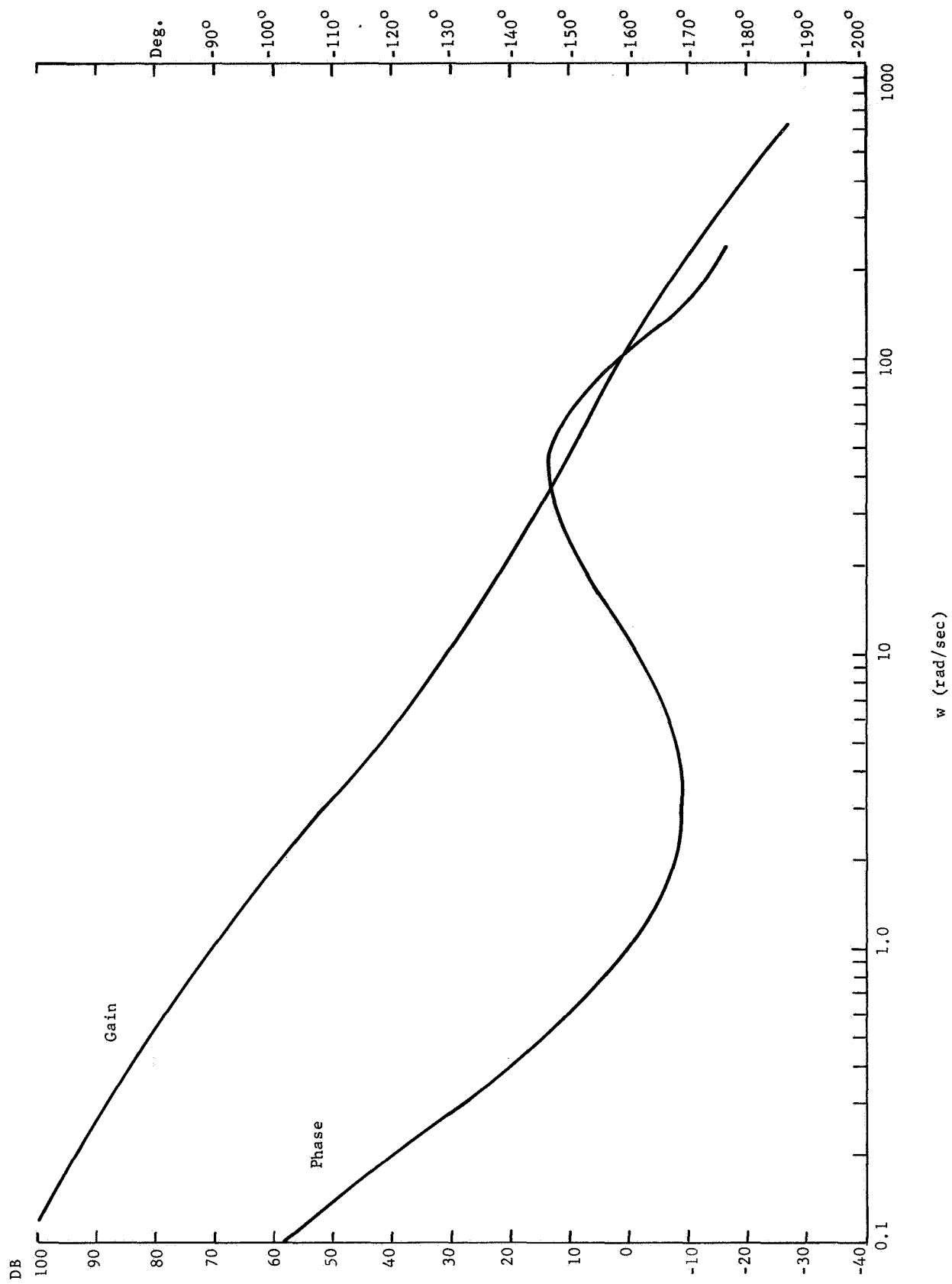


Figure III-38. Bode Plots of Compensated Open Loop Linearized Slave Shoulder Servo System with 60 Hz Notch Filter

MM = 1 worst case multi-mode value

C(U7) = 1 worst case position of slave elbow

and  $e/\beta$  becomes

$$e/\beta = 10240 \left[ \frac{1}{s \left( 1 + \frac{s}{0.33} \right)} \right] \quad (42)$$

Figure III-36 presents the Bode plots of equation (42) and reveals the uncompensated stability margins to be

$$\begin{aligned} \text{GM} &= -23\text{db} \\ \text{PM} &= 0^\circ. \end{aligned} \quad (43)$$

Inserting the filter

$$G_2(s) = \frac{1 + \frac{s}{20}}{1 + \frac{s}{66.6}} \quad (44)$$

the compensated system has Bode plots given by Figure III-37 and gain and phase margins of

$$\begin{aligned} \text{GM} &= 30\text{db} \\ \text{PM} &= 22^\circ. \end{aligned} \quad (45)$$

Attenuating the 60 Hz noise with

$$G_f(s) = \frac{s^2 + 396s + (381)^2}{s^2 + 792s + (381)^2} \quad (46)$$

and modifying  $G_2(s)$  to

$$G_2(s) = \frac{1 + \frac{s}{24}}{1 + \frac{s}{120}}$$

yields the Bode plots of Figure III-38 for the total compensated system. Figure III-38 reveals the open loop stability margins to be

$$\begin{aligned} \text{GM} &= 17\text{db} \\ \text{PM} &= 22^\circ. \end{aligned} \quad (47)$$

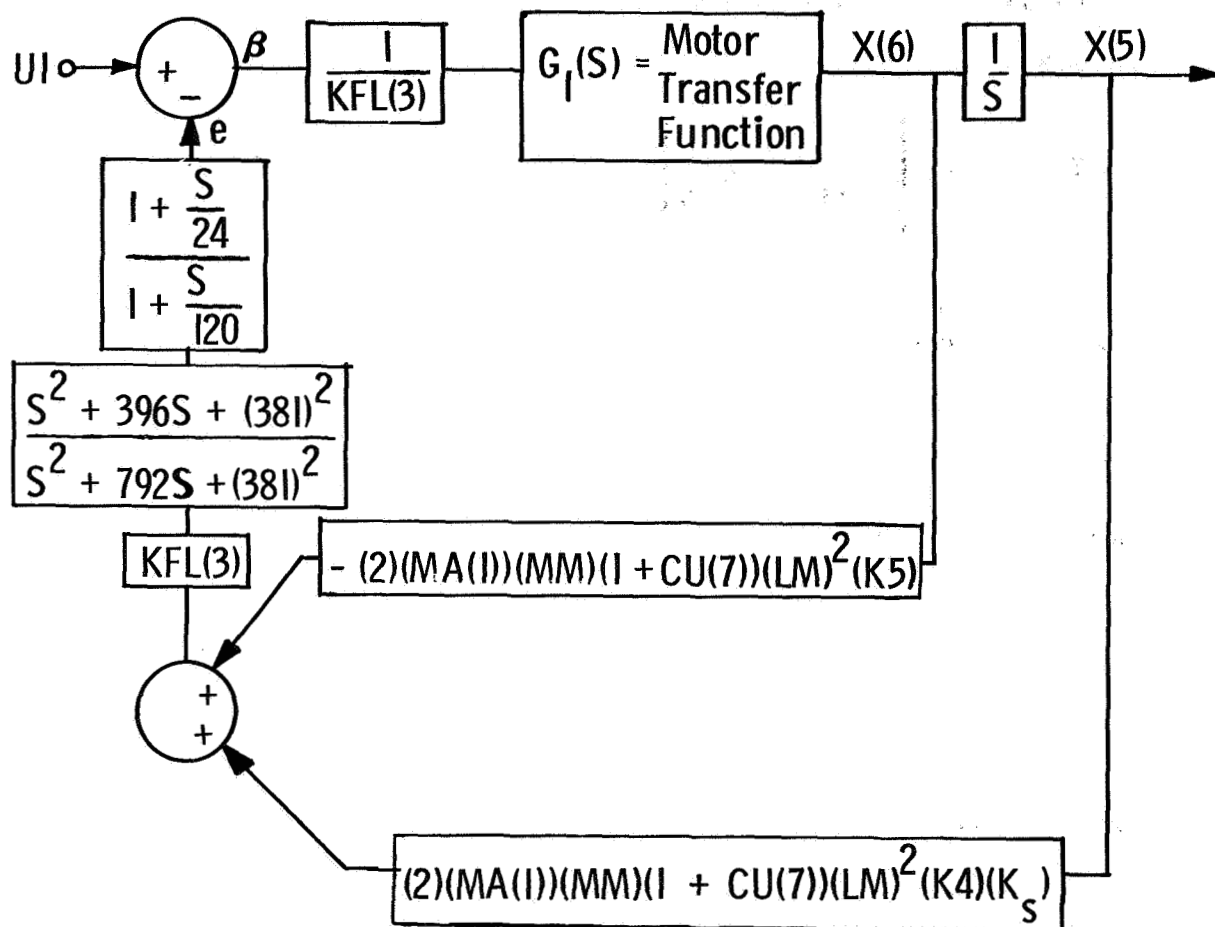


Figure III-39 Compensated Slave Shoulder Linearized Servo Subsystem

Figure III-39 shows the completely compensated slave shoulder linearized servo subsystem.

d. Slave Elbow Joint - Figure III-19 shows the slave elbow servo subsystem and its associated signal inputs. Linearizing this system around any initial master-slave position results in the system of Figure III-20,

where

$$G_1(s) = \frac{(KFL(4))(KEI(4))}{s + (KFL(4))(KEI(4))(KFB(4))} \quad (48)$$

and

$G_2(s)$  = needed compensating filter.

The open loop transfer function is given by

$$e/\beta = \frac{(LM)(MM)(K4)(K_s)}{(KFB(4))(KFL(4))} \left[ \frac{1 + \frac{S}{(K4)(K_s)}}{S \left( 1 + \frac{S}{(KFL(4))(KEI(4))(KFB(4))} \right)} \right] \quad (49)$$

From Section III.C.2 and Tables III-1, III-2, III-3, III-4, the variables of equation (48) are given by

$$K4 = 300$$

$$K_s = 1$$

$$KG(4) = 100$$

$$KFB(4) = 0.042$$

$$KFL(4) = 14.9$$

$$KEI(4) = 1.28$$

$$MA(2) = 0.0672$$

$$K5^* = 0$$

$$LM = 2$$

$$MM = 1$$



and  $e/\beta$  becomes

$$e/\beta = 2556 \left[ \frac{1}{s \left( 1 + \frac{s}{0.922} \right)} \right] \quad (50)$$

Figure III-40 shows the Bode plots of equation (50) and reveals the uncompensated stability margins of

$$\begin{aligned} \text{GM} &= -3\text{db} \\ \text{PM} &= 0^\circ. \end{aligned} \quad (51)$$

Letting

$$G_2(s) = \frac{1 + \frac{s}{16.6}}{1 + \frac{s}{55.3}} \quad (52)$$

the Bode plots of the compensated system are given by Figure III-41 and the gain and phase margins become

$$\begin{aligned} \text{GM} &= 30\text{db} \\ \text{PM} &= 22^\circ \end{aligned} \quad (53)$$

Attenuating the 60 Hz noise with

$$G_f(s) = \frac{s^2 + 396s + (381)^2}{s^2 + 792s + (381)^2} \quad (54)$$

and redesigning  $G_2(s)$  to

$$G_2(s) = \frac{1 + \frac{s}{17}}{1 + \frac{s}{83}} \quad (55)$$

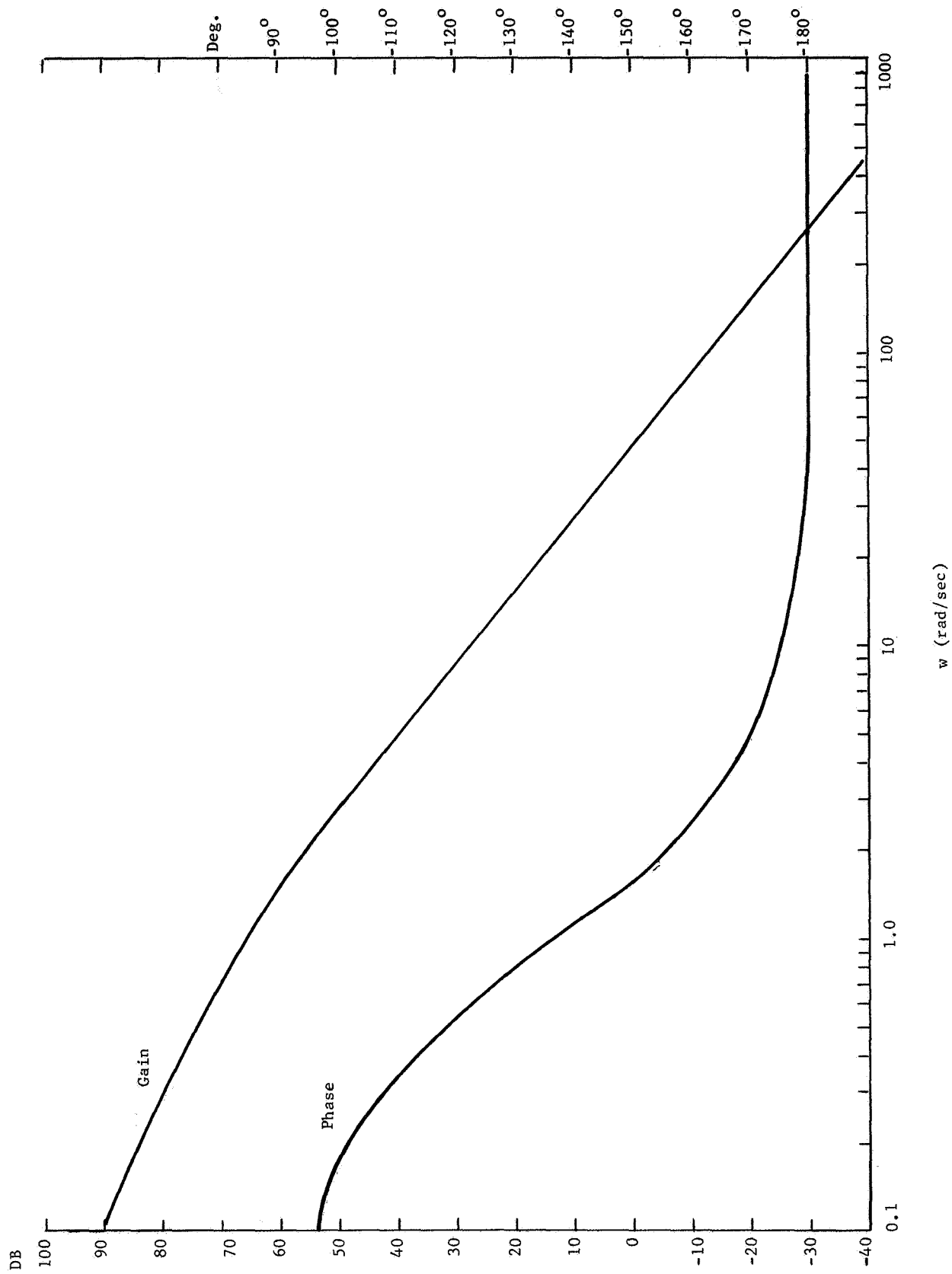


Figure III-40 Bode Plots of Uncompensated Open Loop Linearized Slave Elbow Servo System

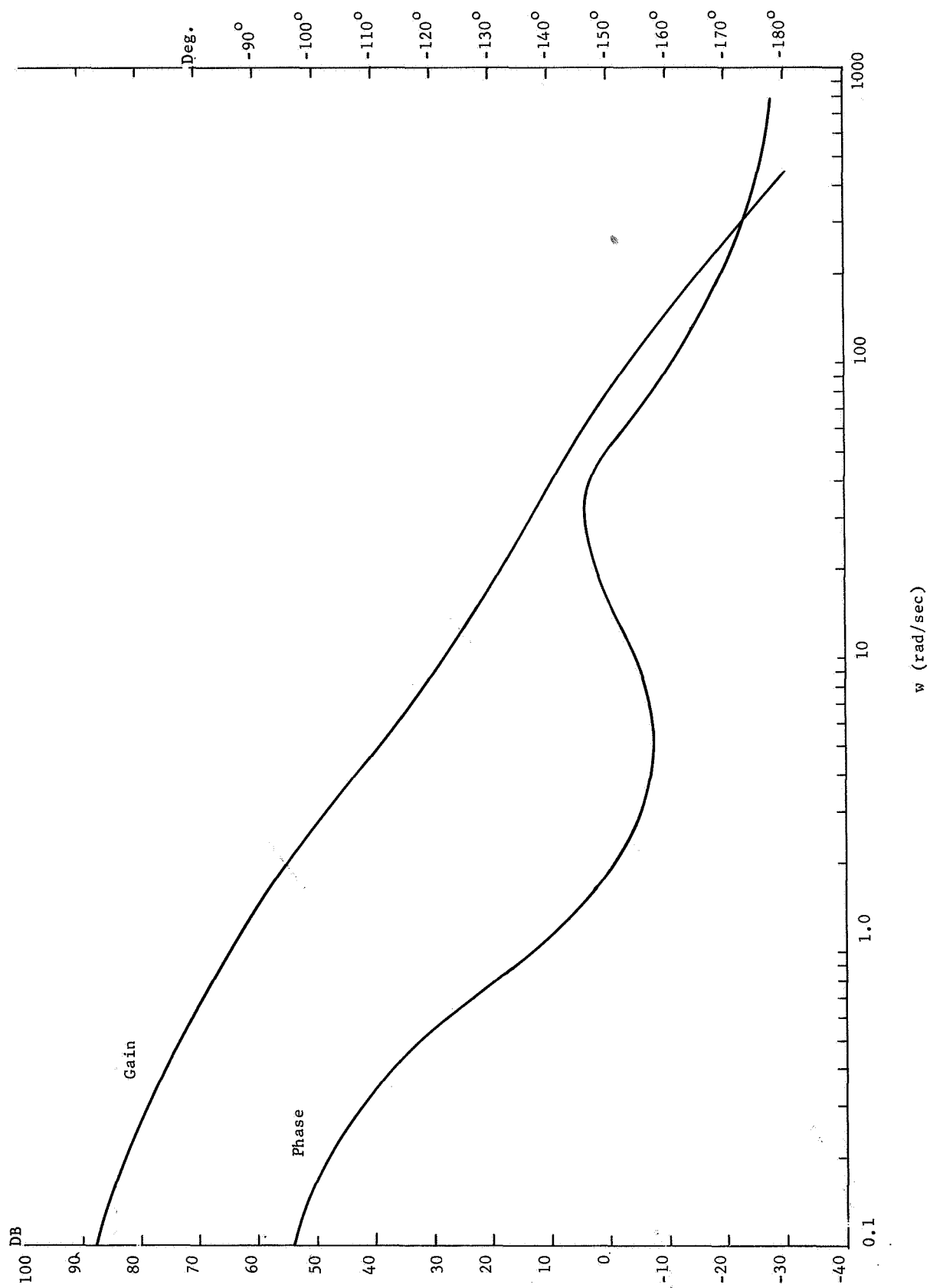


Figure III-41 Bode Plots of C ompensated Open Loop Linearized Slave Elbow Servo System

yields the Bode plots of Figure III-42 with gain and phase margins of

$$\begin{aligned} \text{GM} &= 10\text{db} \\ \text{PM} &= 16^\circ. \end{aligned} \tag{56}$$

The totally compensated slave elbow servo subsystem is represented by Figure III-43.

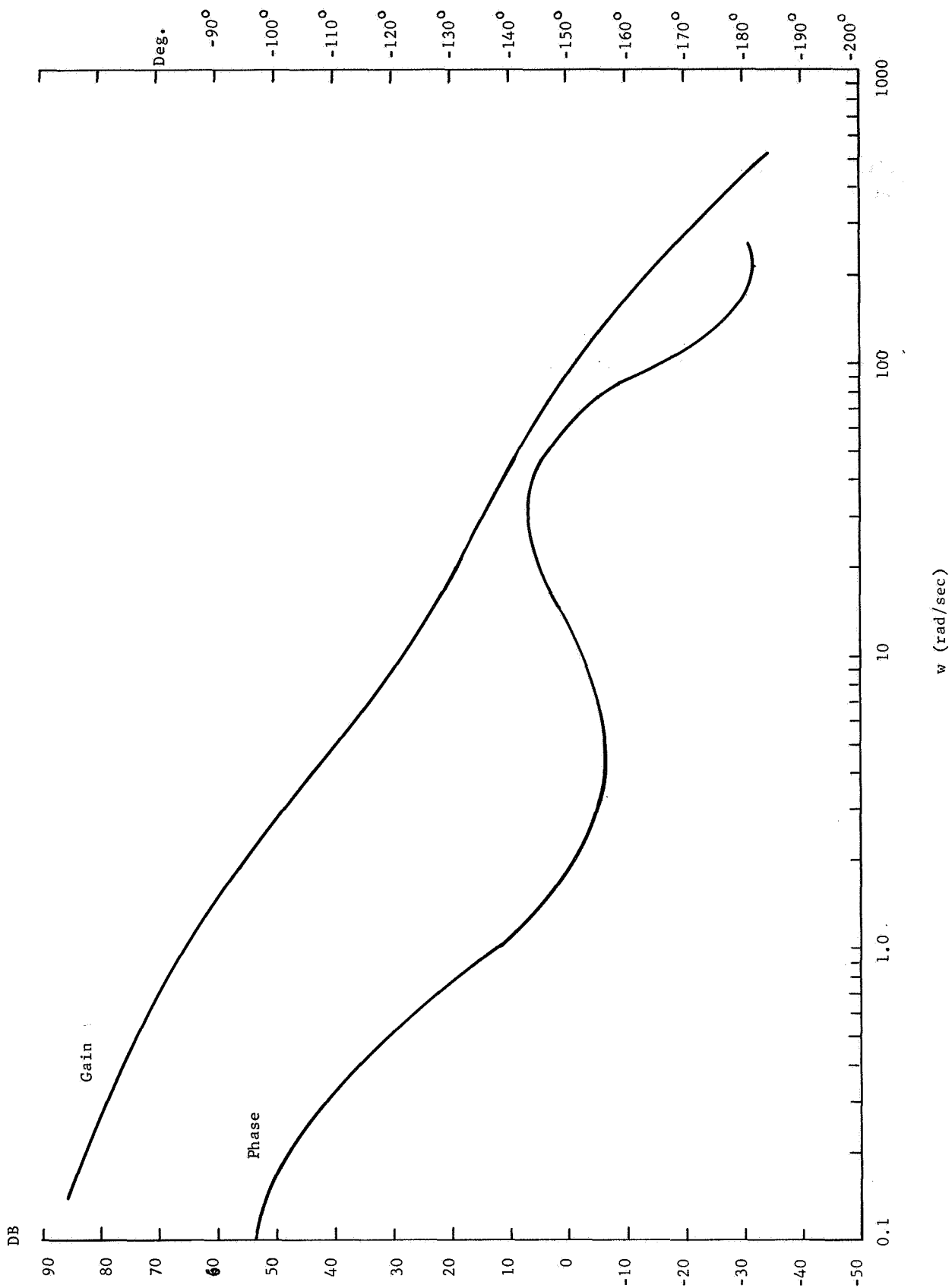


Figure III-42 Bode Plots of Compensated Open Loop Linearized Slave Elbow Servo System with 60 hz Notch Filter

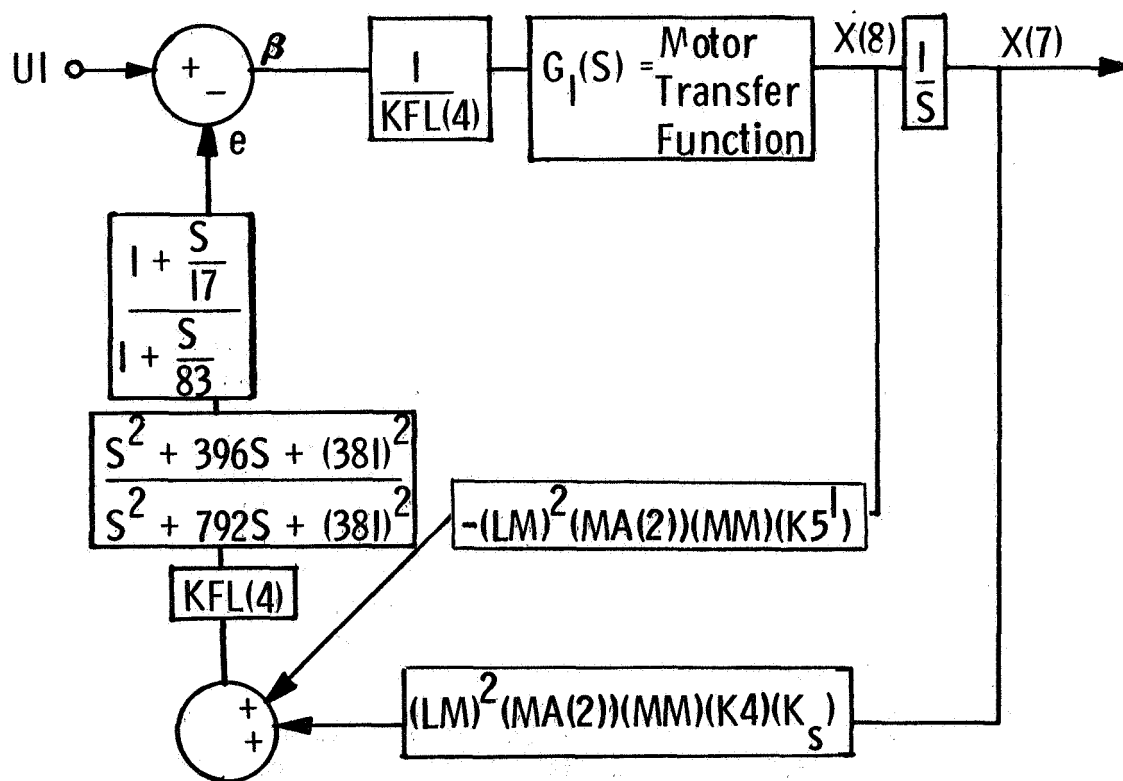


Figure III-43 Compensated Slave Elbow Linearized Servo Subsystem

## C. TEST RESULTS

### 1. Two DOF Breadboard Test Plan

The test plan for the two DOF breadboard must be a procedure that demonstrates, or investigates, all the foreseen and unforeseen operational characteristics of breadboard hardware and electronics. The investigation of the operability of the breadboard is divided into five general areas:

1. Bilateral operation
2. Coordinate transformations
3. Position indexing
4. Variable gain ratio
5. Stability

By necessity, the documentation of the tests conducted in these five areas will be both objective and subjective. Many of the system's characteristics can be determined by well defined definite procedures that are conducted via man-not-in-the-loop techniques. The characteristics determined in this manner reveal the basic operational qualities of the system.

Since the breadboard manipulators are bilateral force reflecting that require inputs from a human operator, the man-in-the-loop characteristics of the system must likewise be determined. Man has his own unique transfer function (this function differing from person to person) that results in a servo system having man-not-in-the-loop basic operational qualities that differ markedly from the man-in-the-loop complex operational qualities. To document these complex operational qualities the investigator must subjectively evaluate system performance for various bilateral tasks.

The following test plan will investigate the five aforementioned areas by determining the following properties of the system.

1. Unpowered hardware characteristics
2. Force reflecting properties
3. Coordinate indexing capabilities

4. Position indexing capabilities
5. Variable gain ratio operation
6. Stability (man-not-in-the-loop)
7. Stability (man-in-the-loop)
8. Large payload handling characteristics
9. Bandwidth
10. Unilateral operation
11. Unilateral - bilateral task time comparisons

## 2. Bilateral Operation

Of primary importance in any bilateral manipulator is the mechanical aspects of both master and slave. Although the theoretical characteristics of the breadboard hardware are given in the mechanical section of this report, following are the actual measured values of stiction, inertia, and backlash for each joint of master and slave.

### a. Stiction

Master elbow:	$T_S = 0.56 \text{ ft lbs}$
Master shoulder:	$T_S = 1.06 \text{ ft lbs}$
Slave elbow:	$T_S = 1.77 \text{ ft lbs}$
Slave shoulder:	$T_S = 1.52 \text{ ft lbs}$

### b. Inertia

Master elbow:	$I = 0.43 \text{ ft lbs sec}^2$
Master shoulder:	$I_{\text{elbow}} = 0^\circ = 0.90 \text{ ft lbs sec}^2$
	$I_{\text{elbow}} = 90^\circ = 0.86 \text{ ft lbs sec}^2$
Slave elbow:	$I = 0.78 \text{ ft lb sec}^2$
Slave shoulder:	$I_{\text{elbow}} = 0^\circ = 1.97 \text{ ft lbs sec}^2$
	$I_{\text{elbow}} = 90^\circ = 1.62 \text{ ft lbs sec}^2$



### c. Backlash

Master elbow: B = 5.51 min

Master shoulder: B = 7.44 min

Slave elbow: B = 2.98 min

Slave shoulder: B = 6.09 min

To document the force reflecting properties of the breadboard, the force reflection ratio was measured, in the X and Y directions, for various arm positions (all with position indexing) with differing variable gain ratio values and with master and slave operating in different coordinate systems. The forward loop gains K1 and K4 are equal for all measurements and thus theoretically the force reflection ratio should be 1:1 for all test cases. As seen from the slopes of the following graphs, the force reflecting ratio is very nearly 1:1 for all measurements with any inconsistencies arising from measurement and analog computer gain setting inaccuracies.

For each of the following test cases (Figures III-44 through III-48), the initial slave position and the indexed master position are given, the values of the variable position gain ratio MM and the coordinate transformation rotation angle RA are noted, and plots of the force reflecting ratio in the X and Y direction are included.

### 3. Compliance

The compliance of a bilateral manipulator system is a measure of its servo stiffness. For the two DOF breadboard control system, the compliance, in either the X or Y direction, is inversely equal to the forward loop gain K1. The compliance is measured by immobilizing the slave and measuring the displacement to force ratio in both the X and Y directions. Figures III-49 and III-50 reveal the measured compliance to be very near its theoretical value and indicate that system compliance, like the force reflecting ratio, is independent of the variable gain ratio MM, the coordinate transformation roll angle RA, and the position indexing vector PI.

### 4. Tracking - Part A

To document the operability of position indexing, variable

MM = 1/4  
RA = 0°

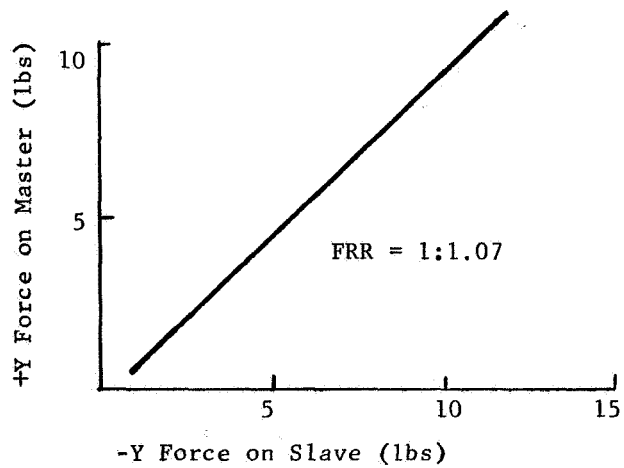
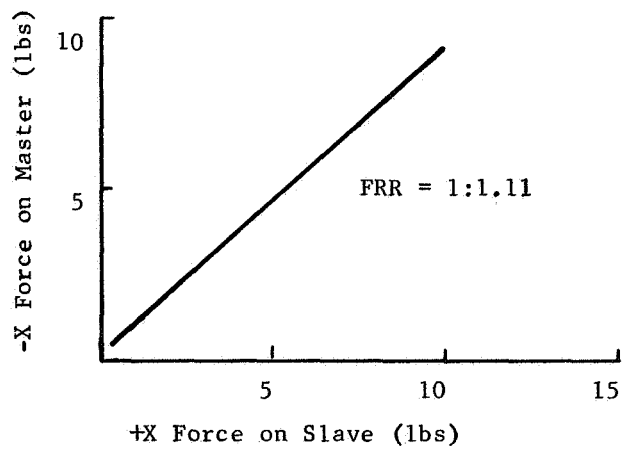
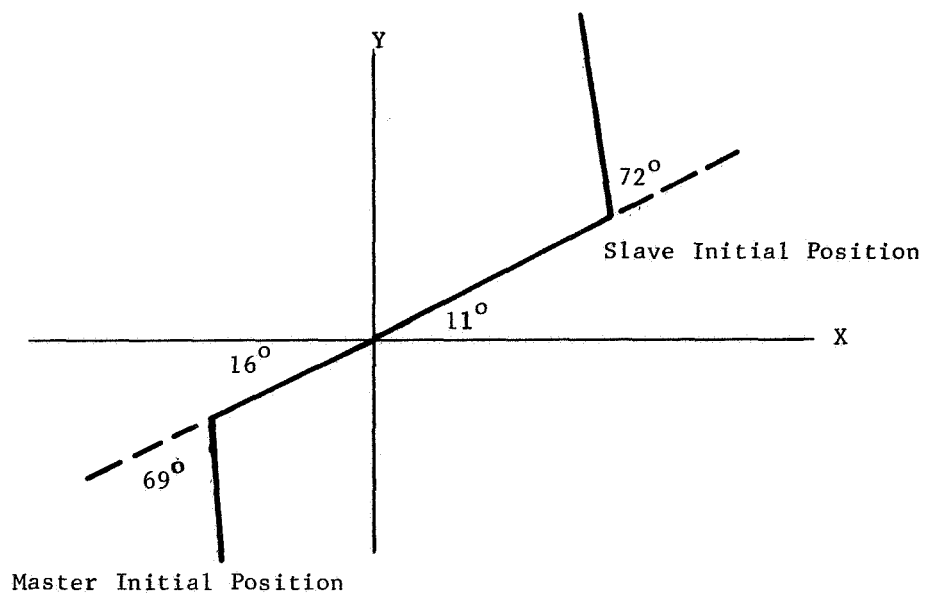


Figure III-44 Force Reflecting Ratio, Configuration 1

MM = 1/4  
RA = 0°

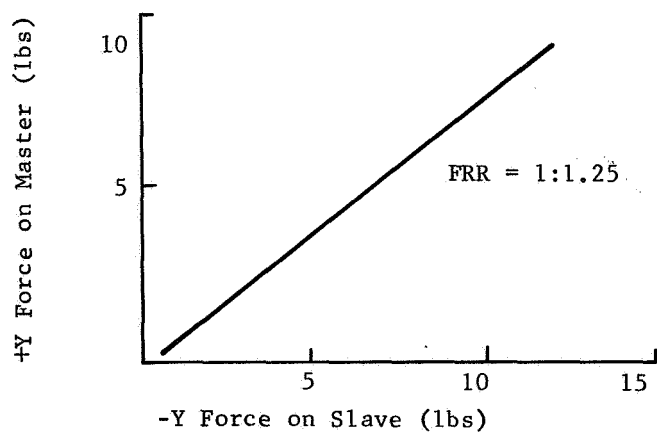
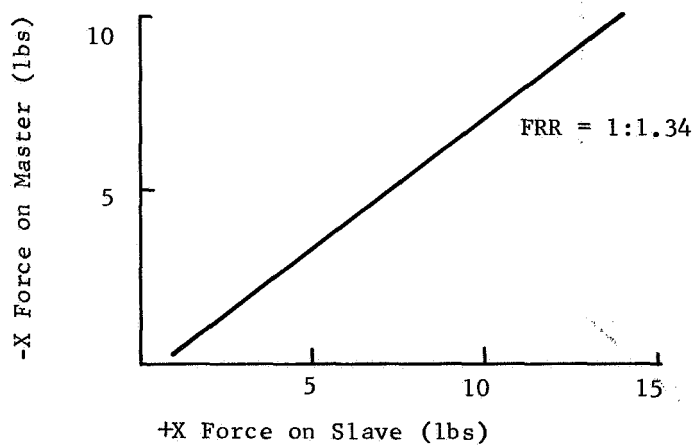
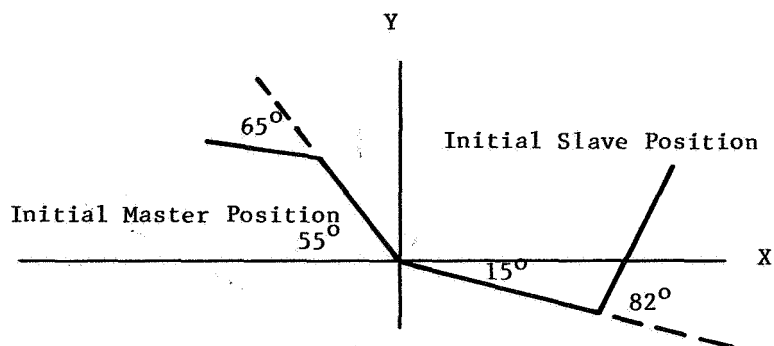


Figure III-45 Force Reflecting Ratio, Configuration 2

MM = 1/8

RA = 0°

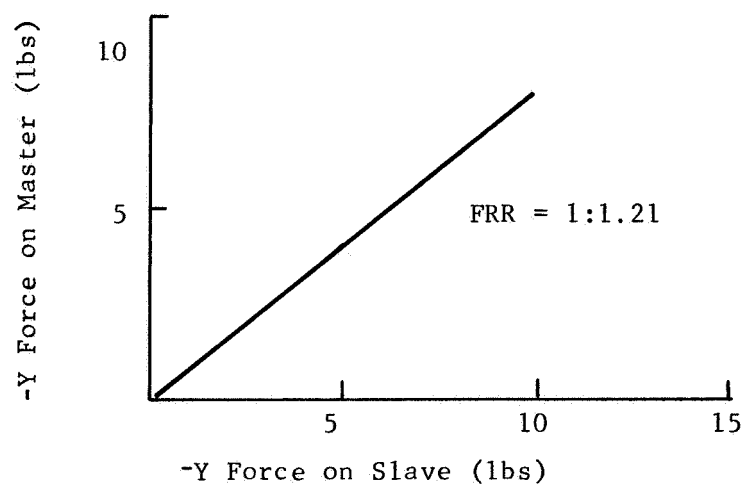
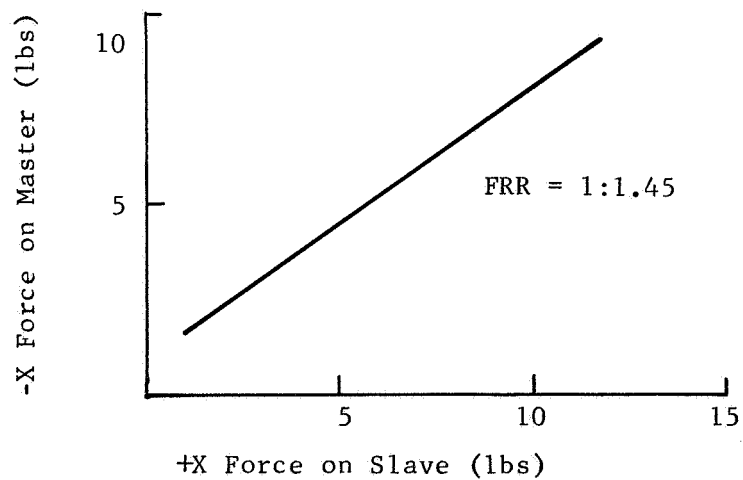
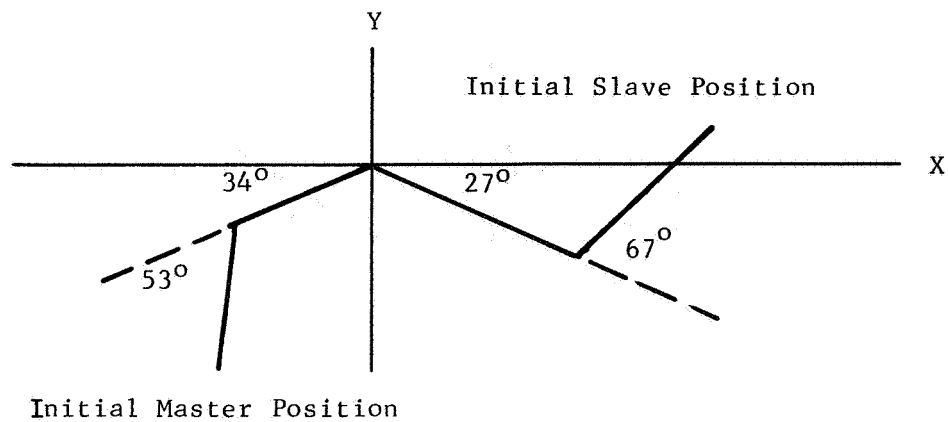


Figure III-46 Force Reflecting Ratio, Configuration 3

MM = 1/6

RA = 0°

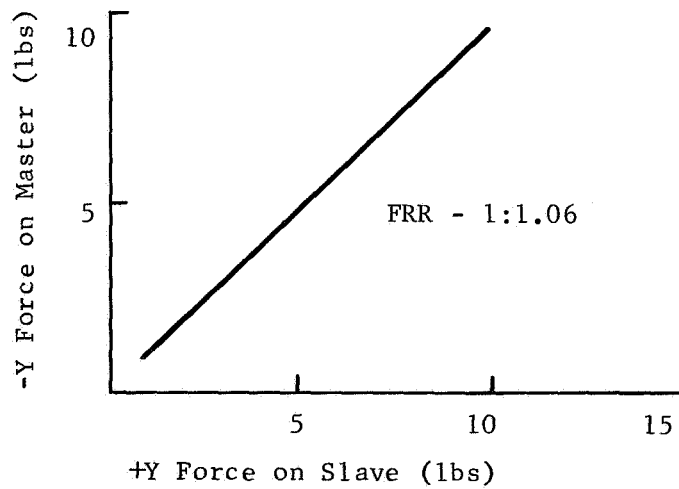
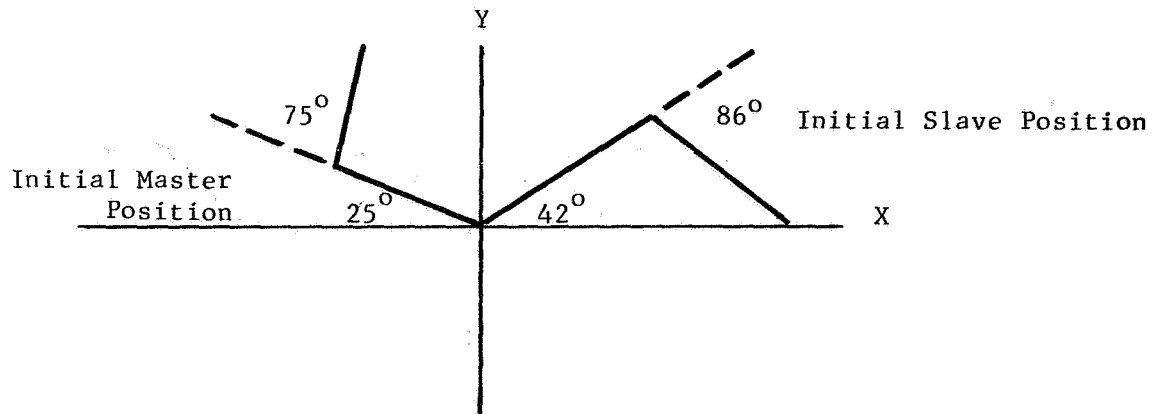


Figure III-47 Force Reflecting Ratio, Configuration 4

MM = 1/4

RA = 90°

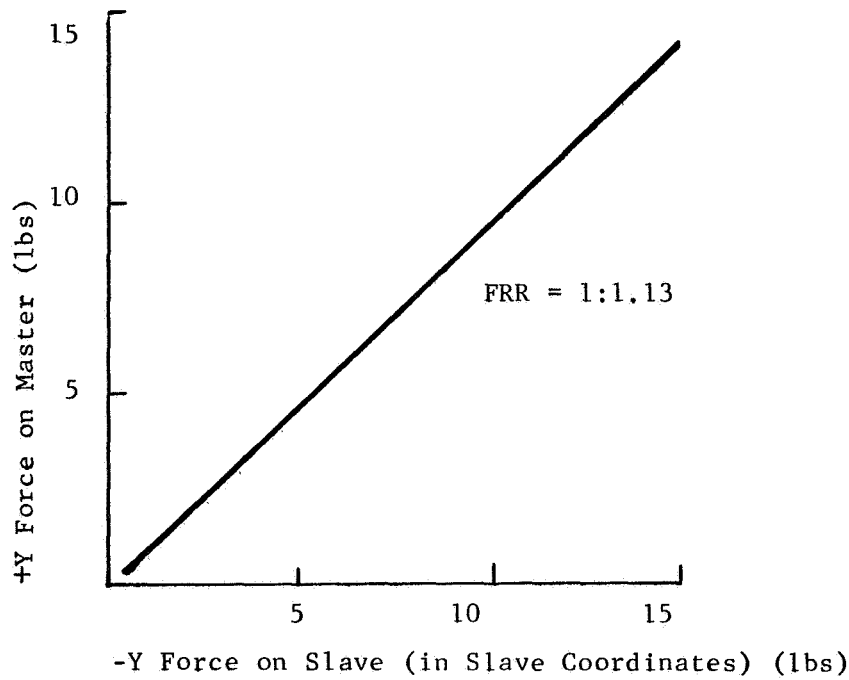
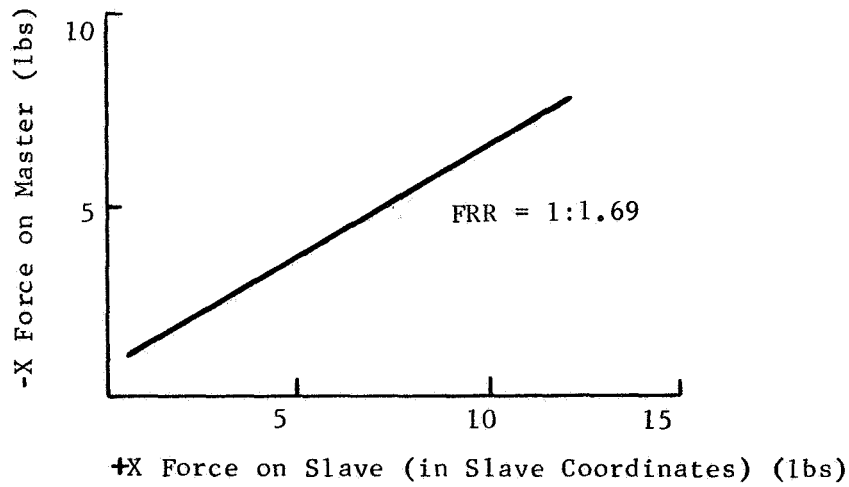
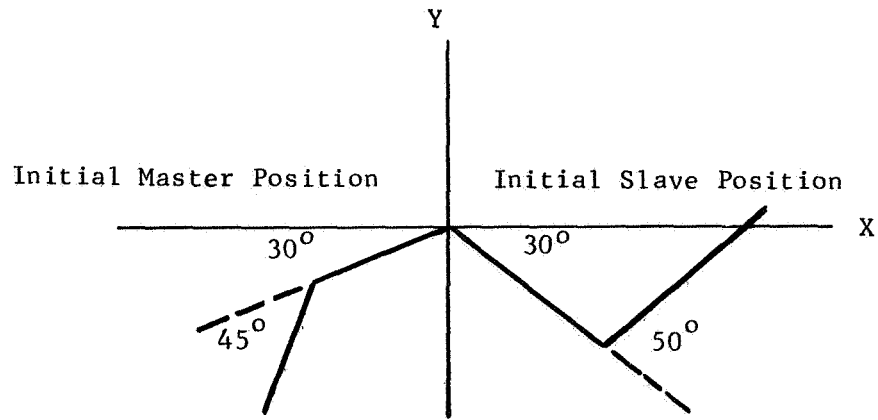


Figure III-48 Force Reflecting Ratio, Configuration 5

MM = 1/4

RA = 90°

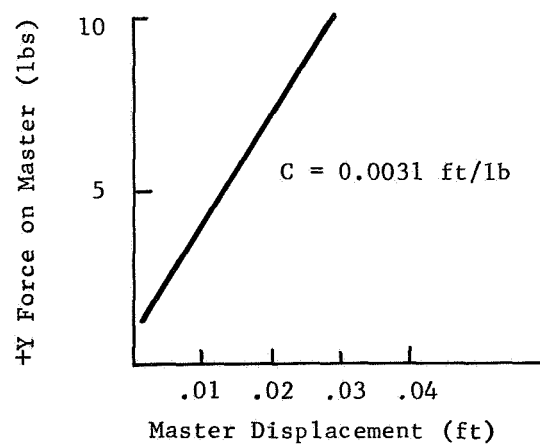
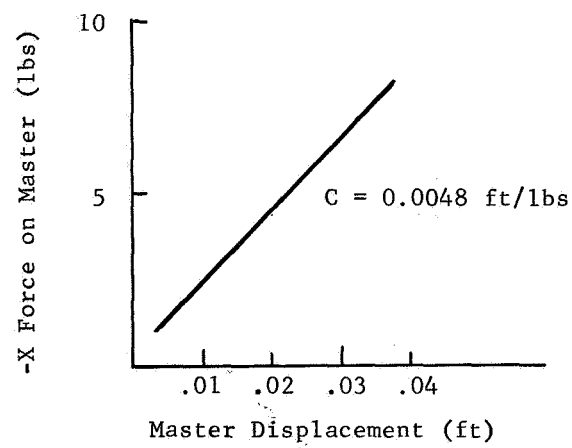
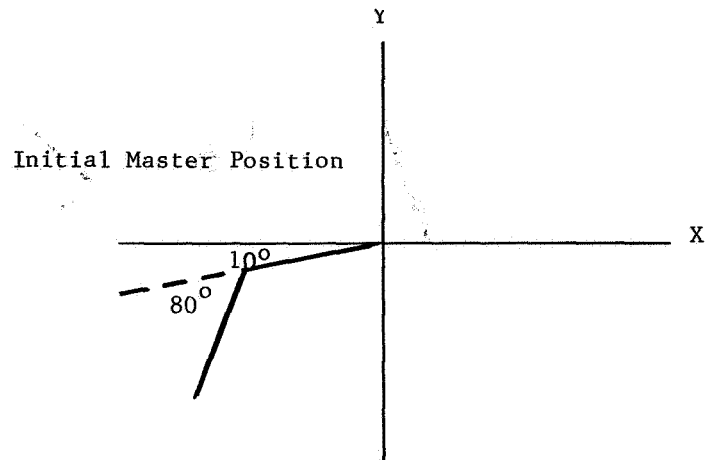


Figure III-49 Compliance, Figure 1

MM = 1/8  
RA = 0°

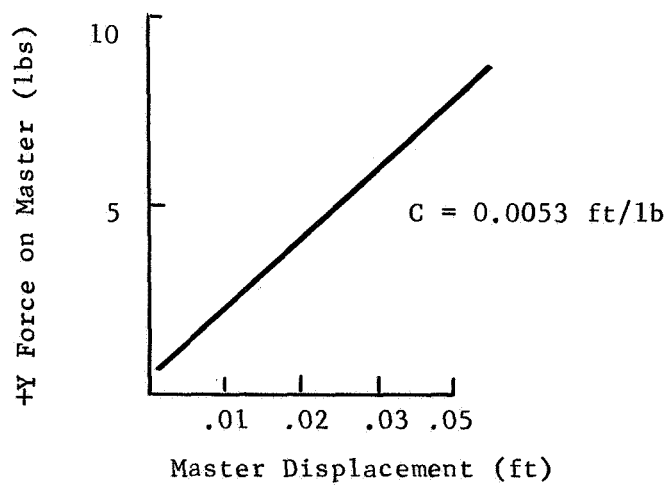
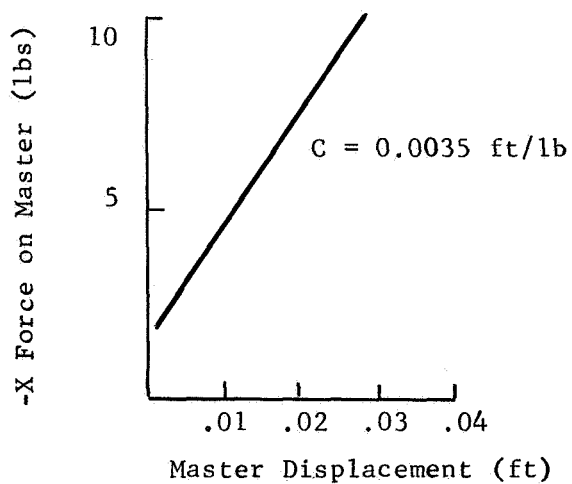
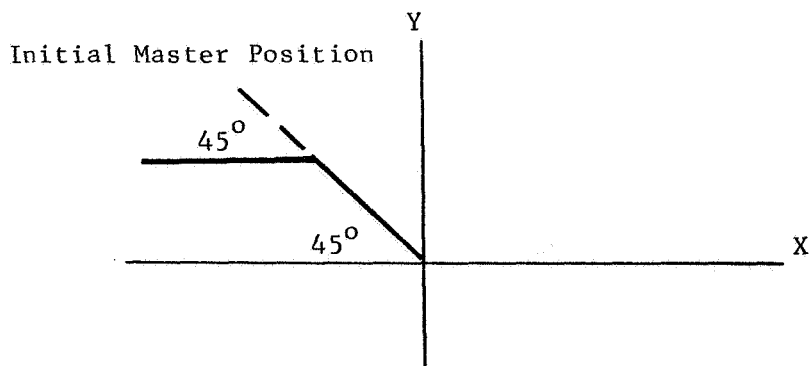


Figure III-50 Compliance, Figure 2



gain ratios, and coordinate transformations between master and slave, the following tracking curves are presented. Various MM, RA, and PI values are introduced into the system, the tip of the master is then moved, in a straight line along a guiding bar, in the X and Y direction and the tracking capability of the tip of the slave is recorded. The following curves (Figures III-51 through III-60) plot master and slave tip position as a function of time. Each figure indicates the master-slave initial positions, the direction in which the tip of the master was moved, and the appropriate values of MM and RA. As revealed by the traces, the tracking properties of the system are excellent with respect to all three properties (position indexing, variable gain ratios, and coordinate transformations) and there is no detectable "cross talk" between pure X and pure Y motions.

#### 5. Tracking - Part B

As a second part to the tracking problem, it was desired to investigate the transient behavior and stability properties of the breadboard system to man in the loop inputs. Input trajectories similar to those in the preceding section were provided, only now the object was to stop the tip of the master at some predetermined point. The trajectory was terminated by either driving the master to a peg or visually recognizing the end point scribe. The system was tested both unloaded and loaded with a 306 lbs weight (described in mechanical section) floating on an air bearing attached to the end of the slave arm (Figure III-27). The 306 lbs weight was used to provide large slave inertial loading and both unilateral and bilateral testing was accomplished with the load attached.

As seen from the following traces (Figures III-61 through III-69), the unloaded system has excellent man-in-the-loop tracking and stability qualities for all combinations of inputs and system parameters considered. For large inertial loads on the slave, it is seen that the slave is highly underdamped for unilateral (no force feedback to the operator) operation. This marginal stability is to be expected since the system was not designed for unilateral operation with high inertial loading. When operated in the bilateral mode with the large inertia load, it is noted that the system has both excellent track and stability qualities. The payload can be brought to the desired end point, deaccelerated and stopped by the operator with little to no overshoot. This bilateral handling quality for large payloads is likewise to

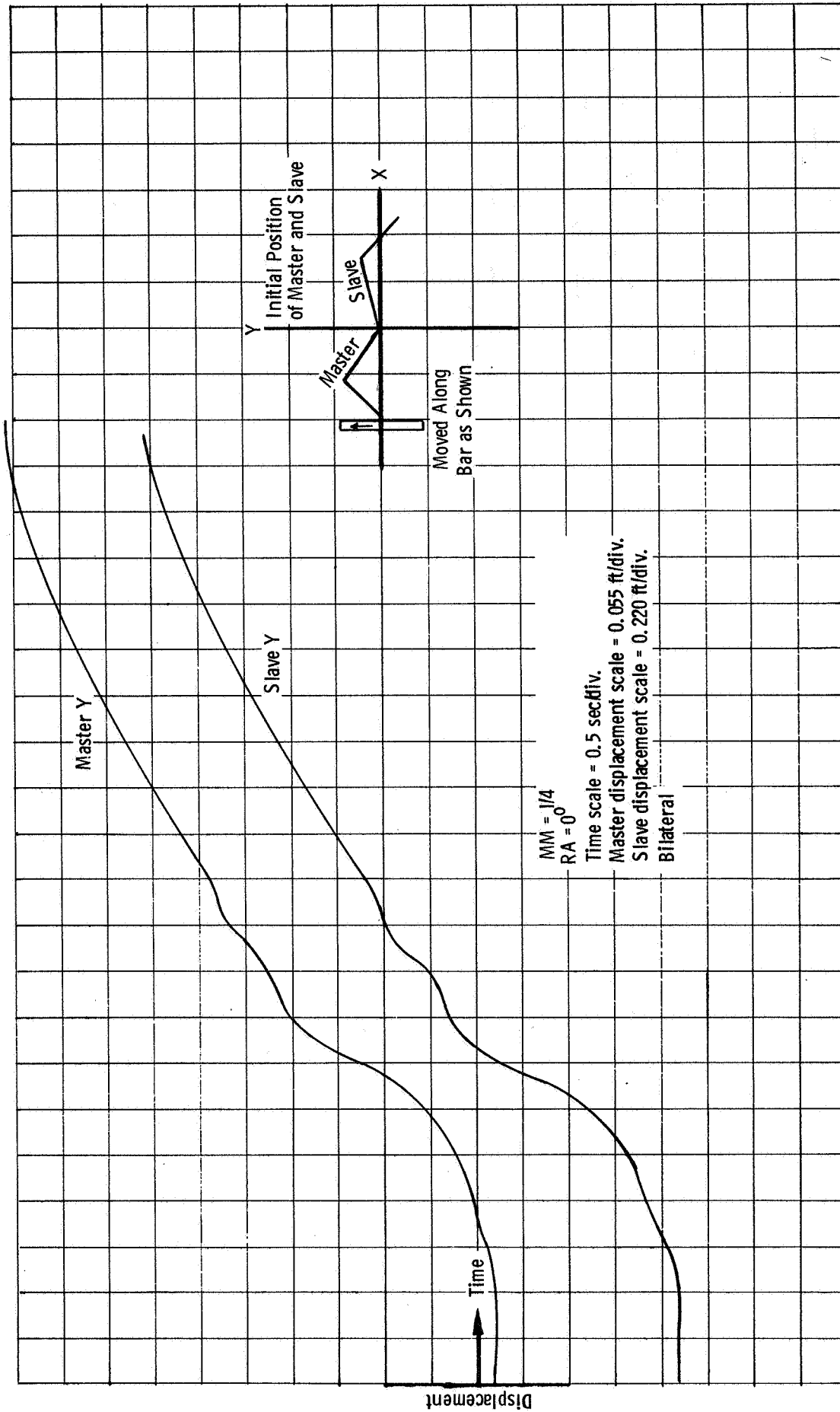


Figure III-51 Tracking - Part A, Figure I

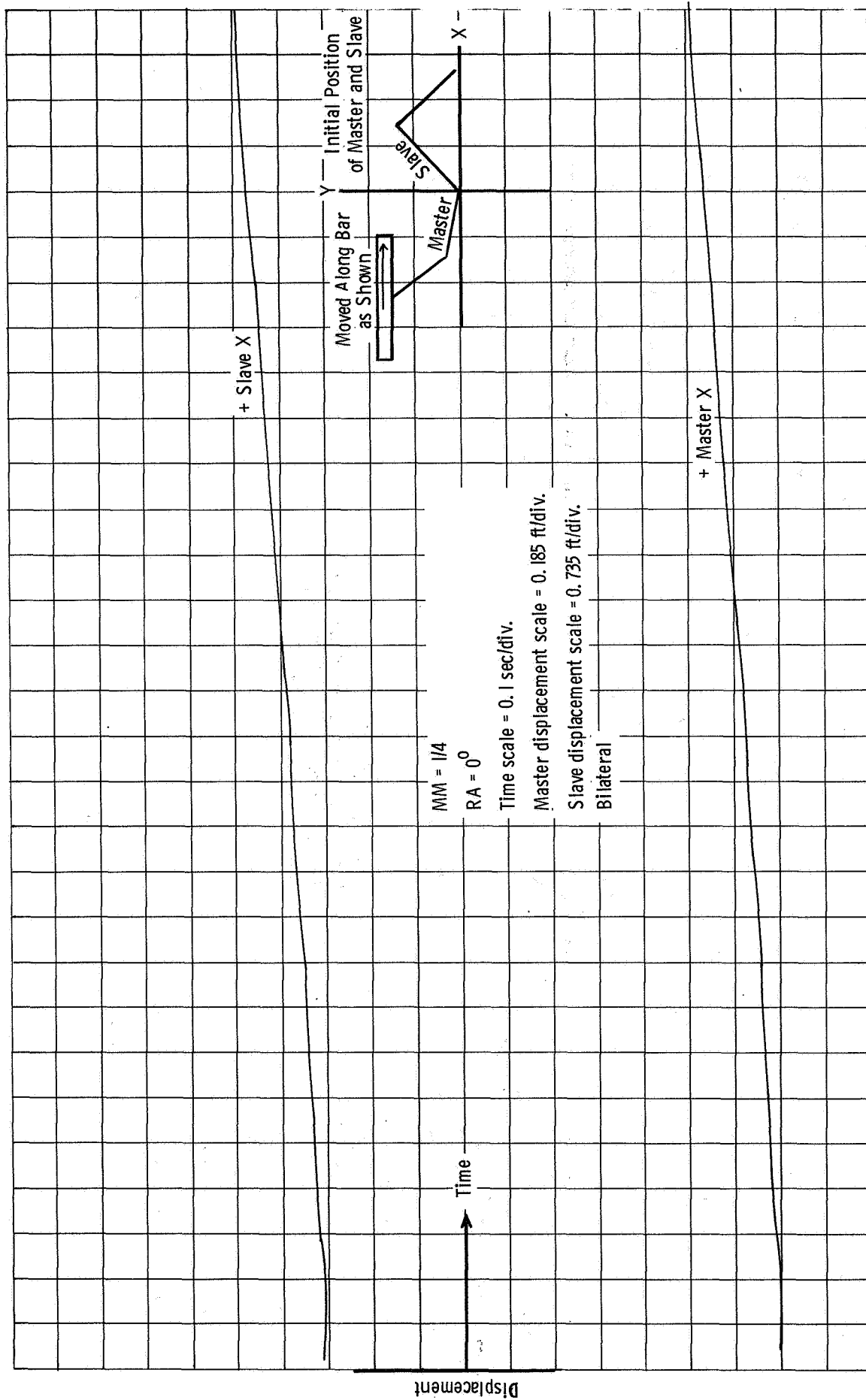


Figure III-52 Tracking - Part A, Figure 2

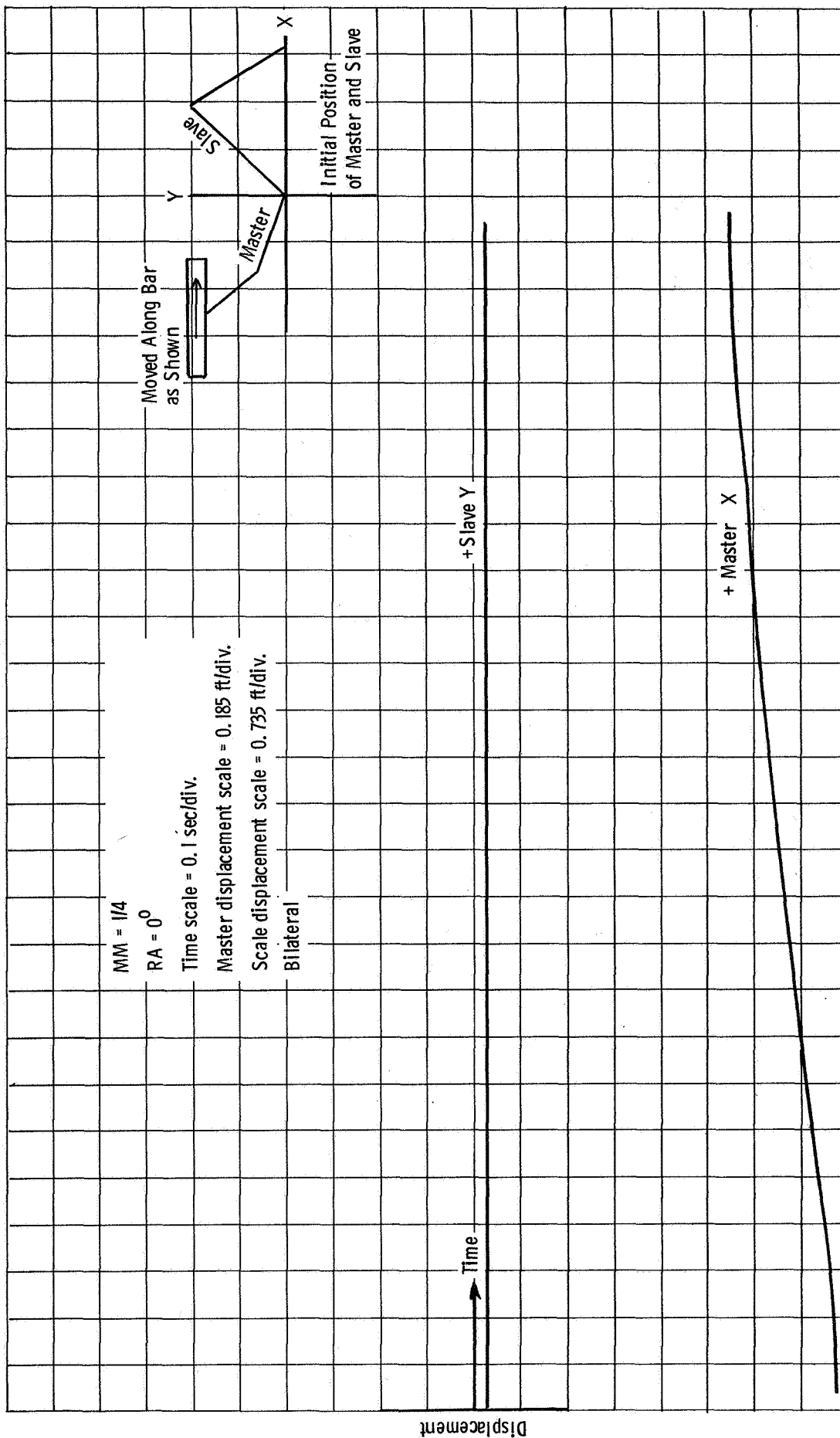


Figure III-53 Tracking - Part A, Figure 3

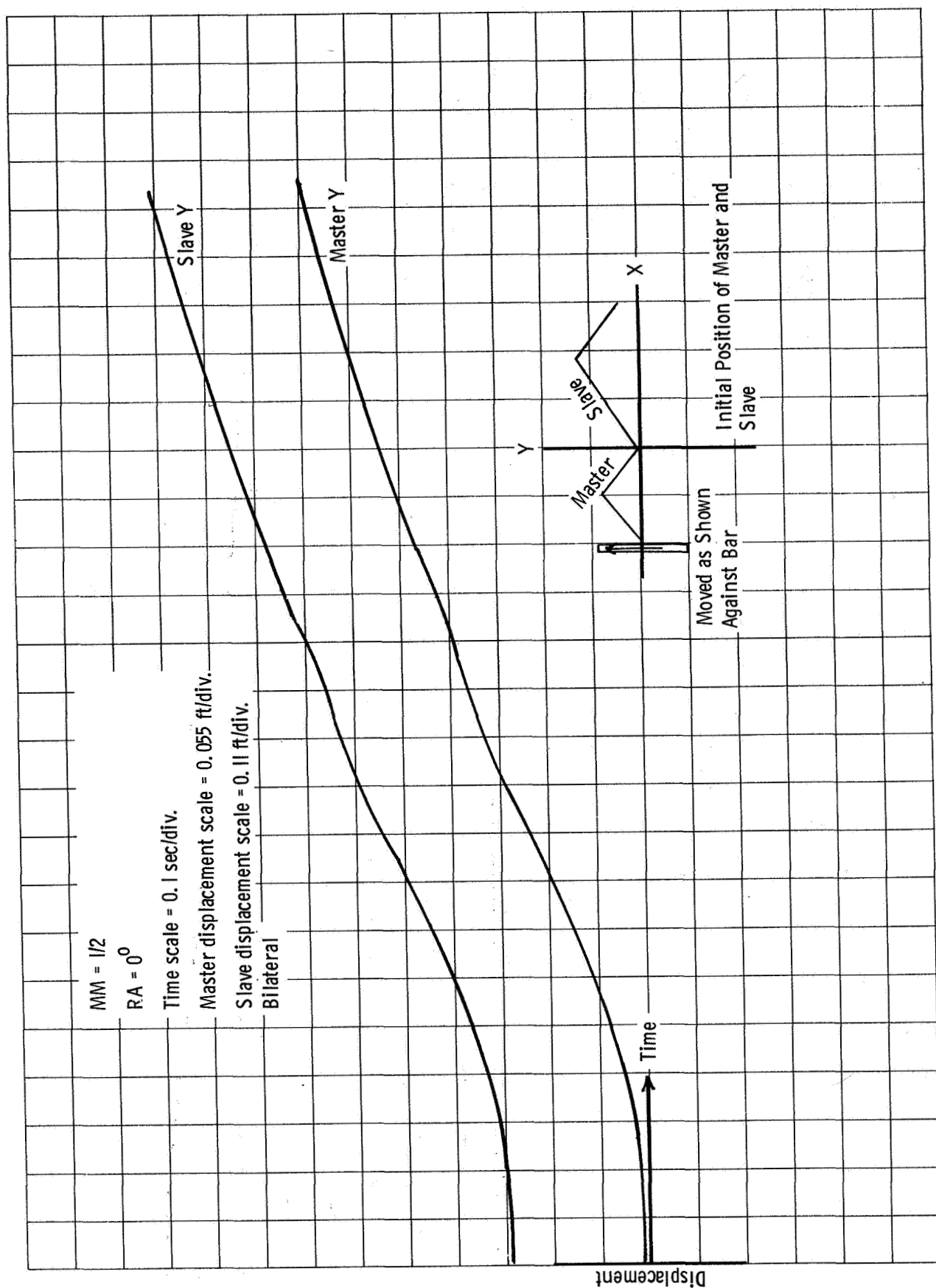


Figure III-54 Tracking - Part A, Figure 4

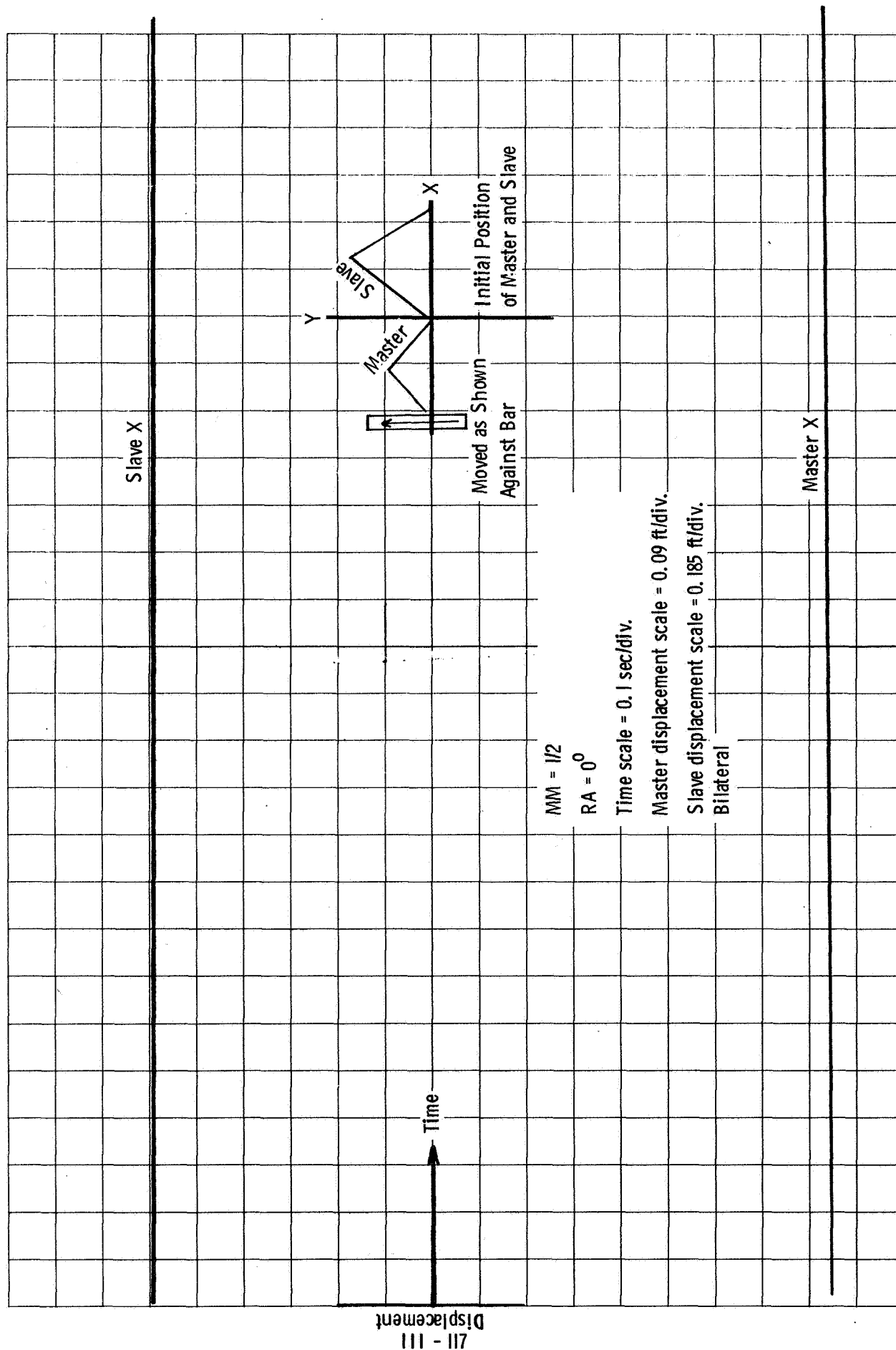


Figure III-55 Tracking-Part A, Figure 5

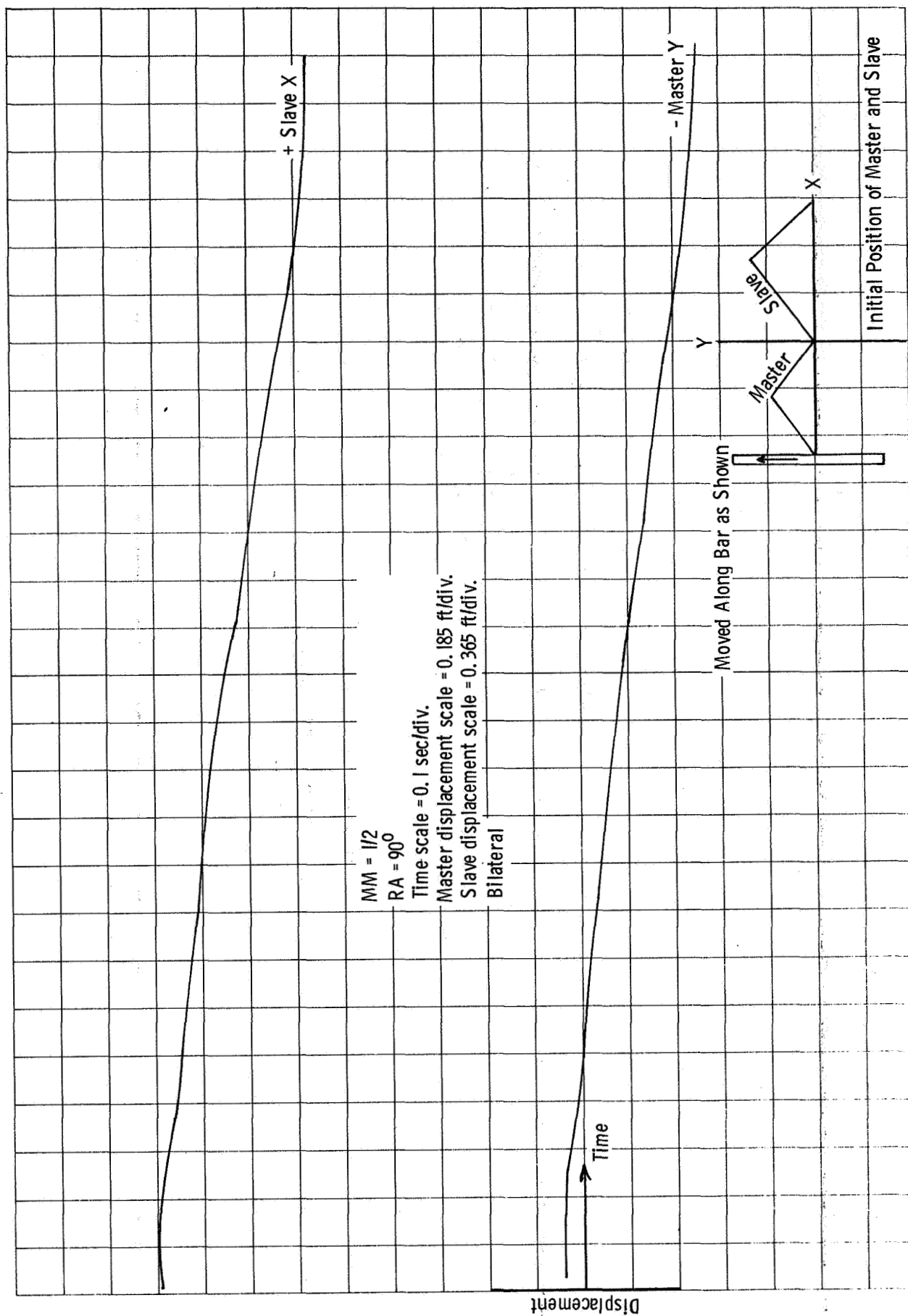


Figure III-56 Tracking - Part A, Figure 6

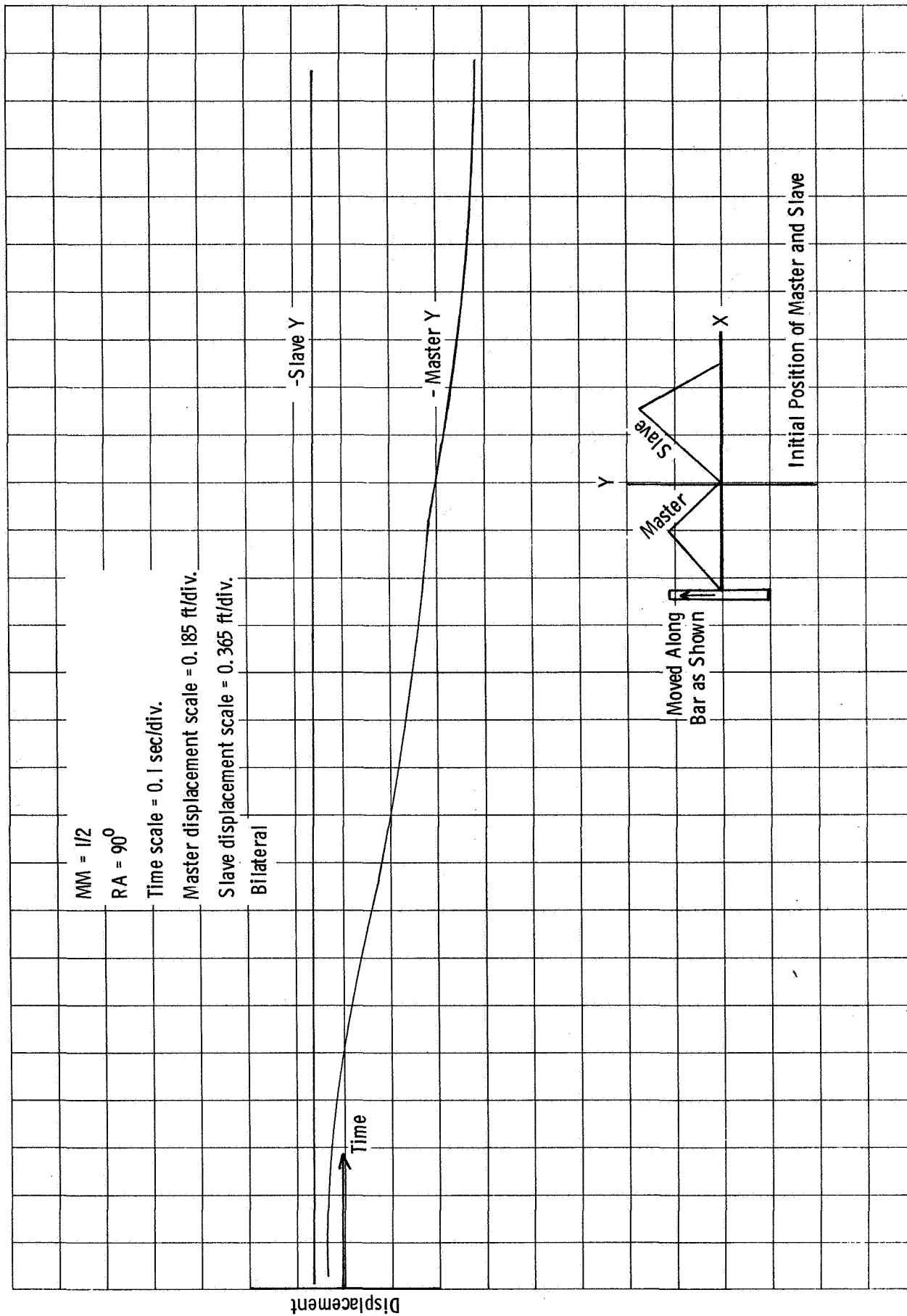


Figure III-57 Tracking-Part A, Figure 7



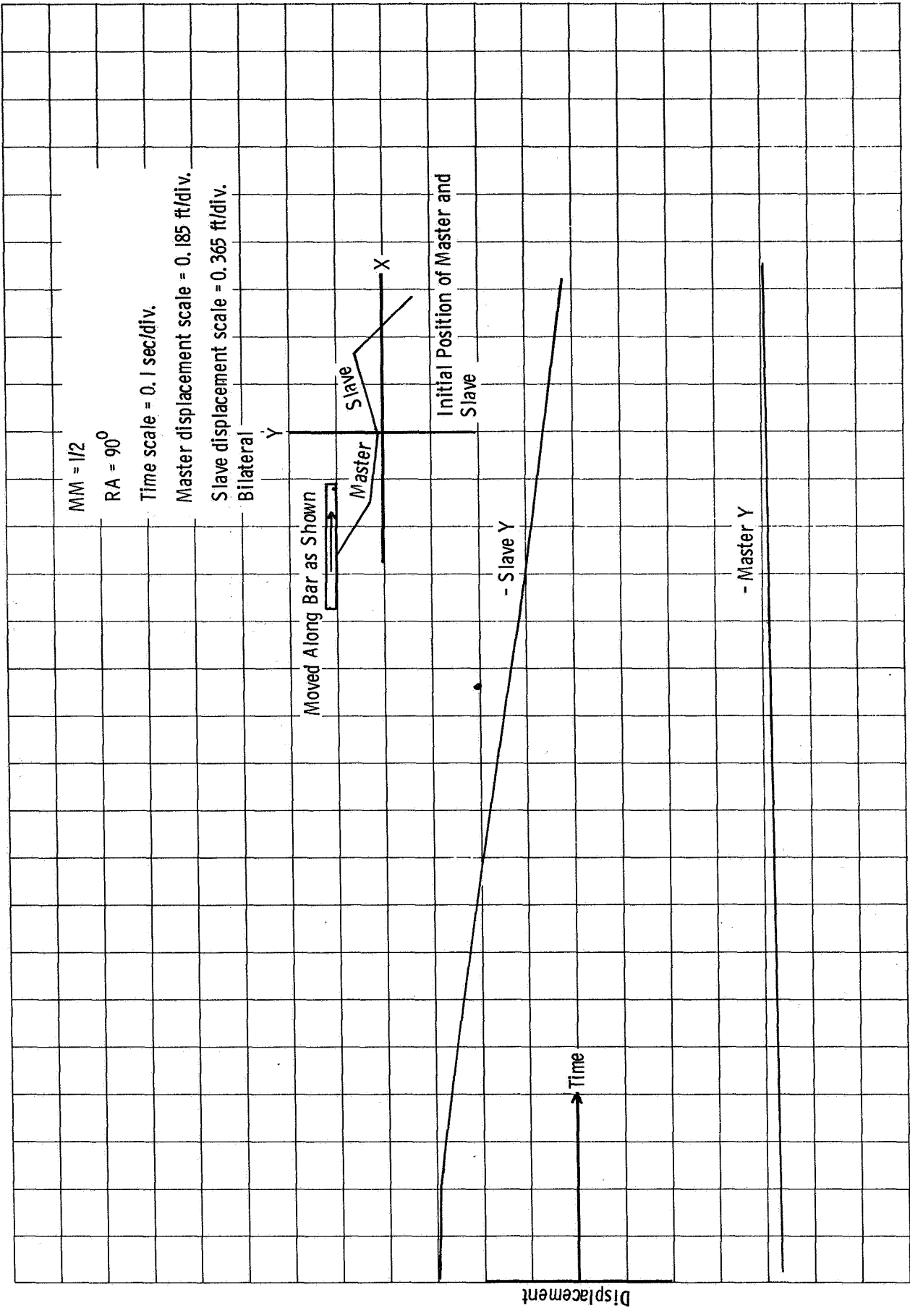


Figure III-58 Tracking - Part A, Figure 8

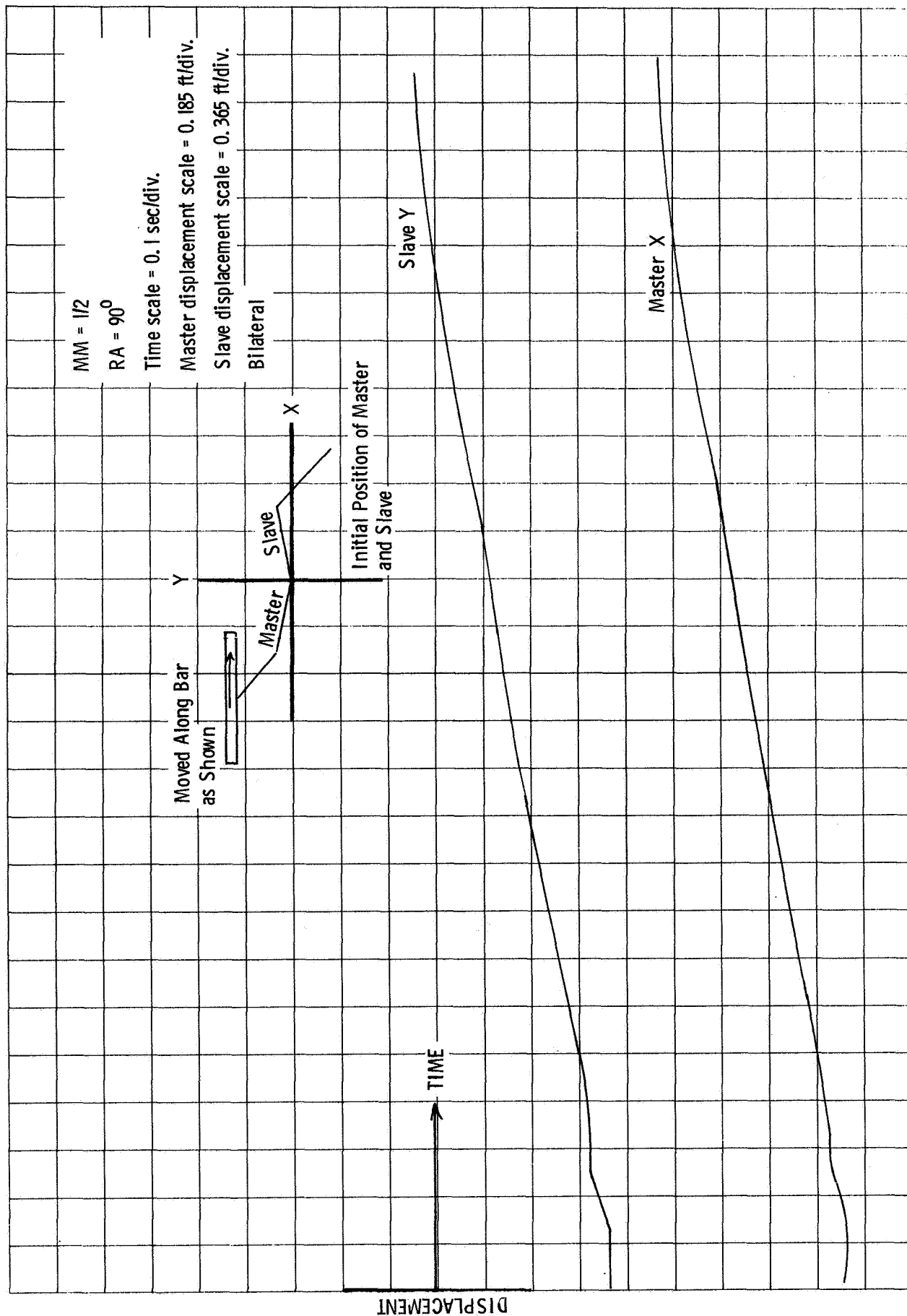


Figure III-59 Tracking - Part A, Figure 9

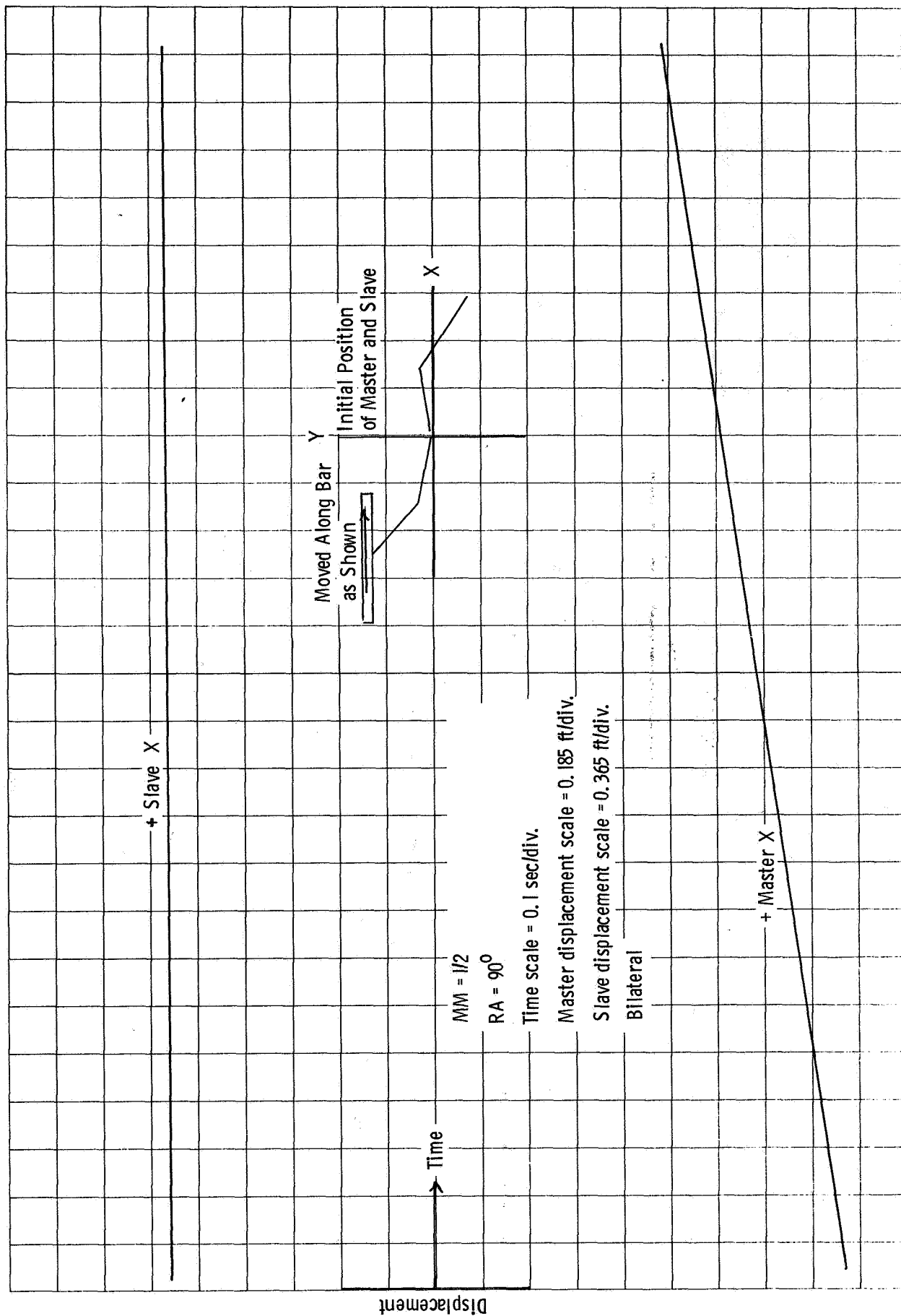


Figure III-60 Tracking - Part A, Figure 10

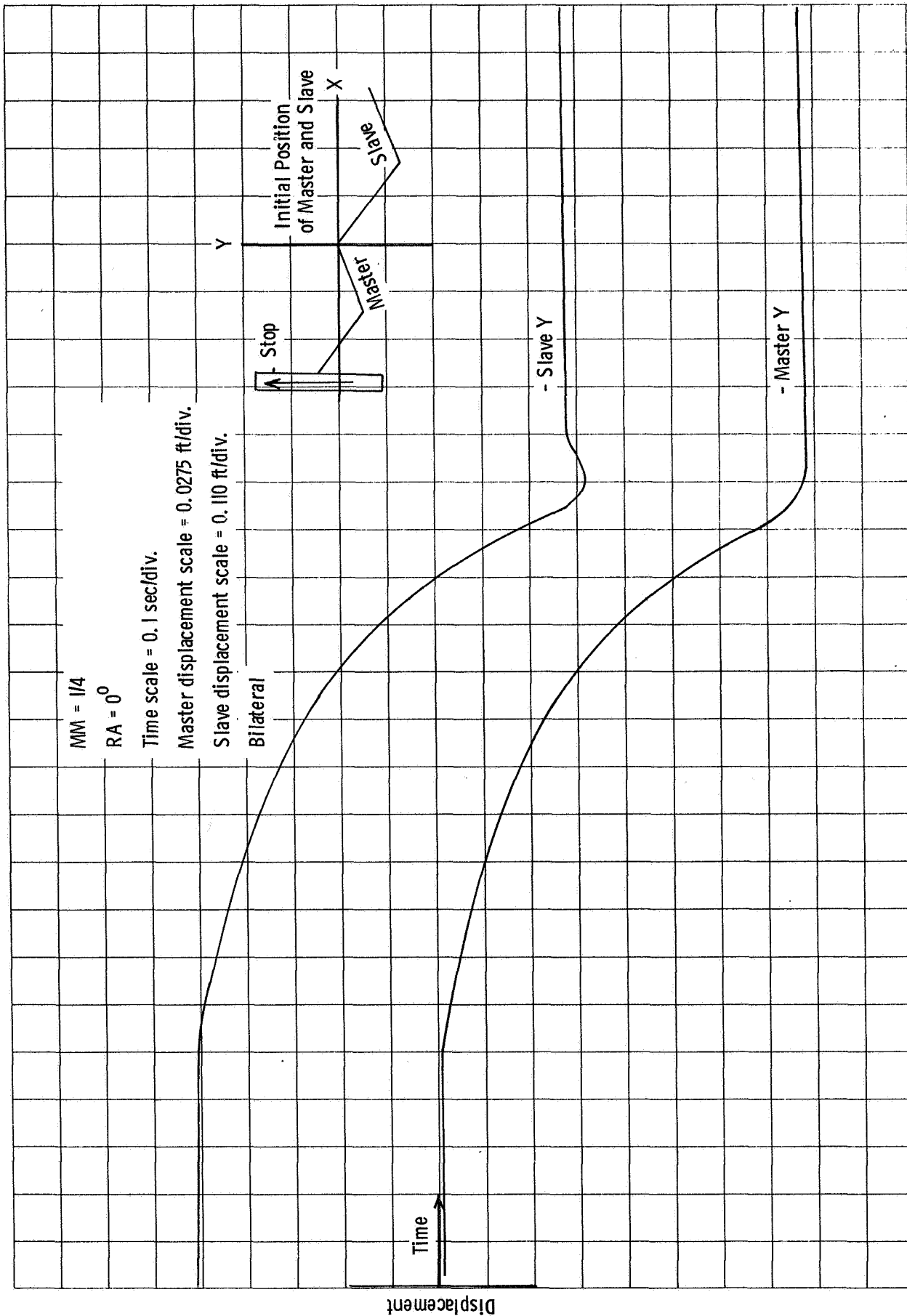


Figure III-61 Tracking - Part B, Figure I

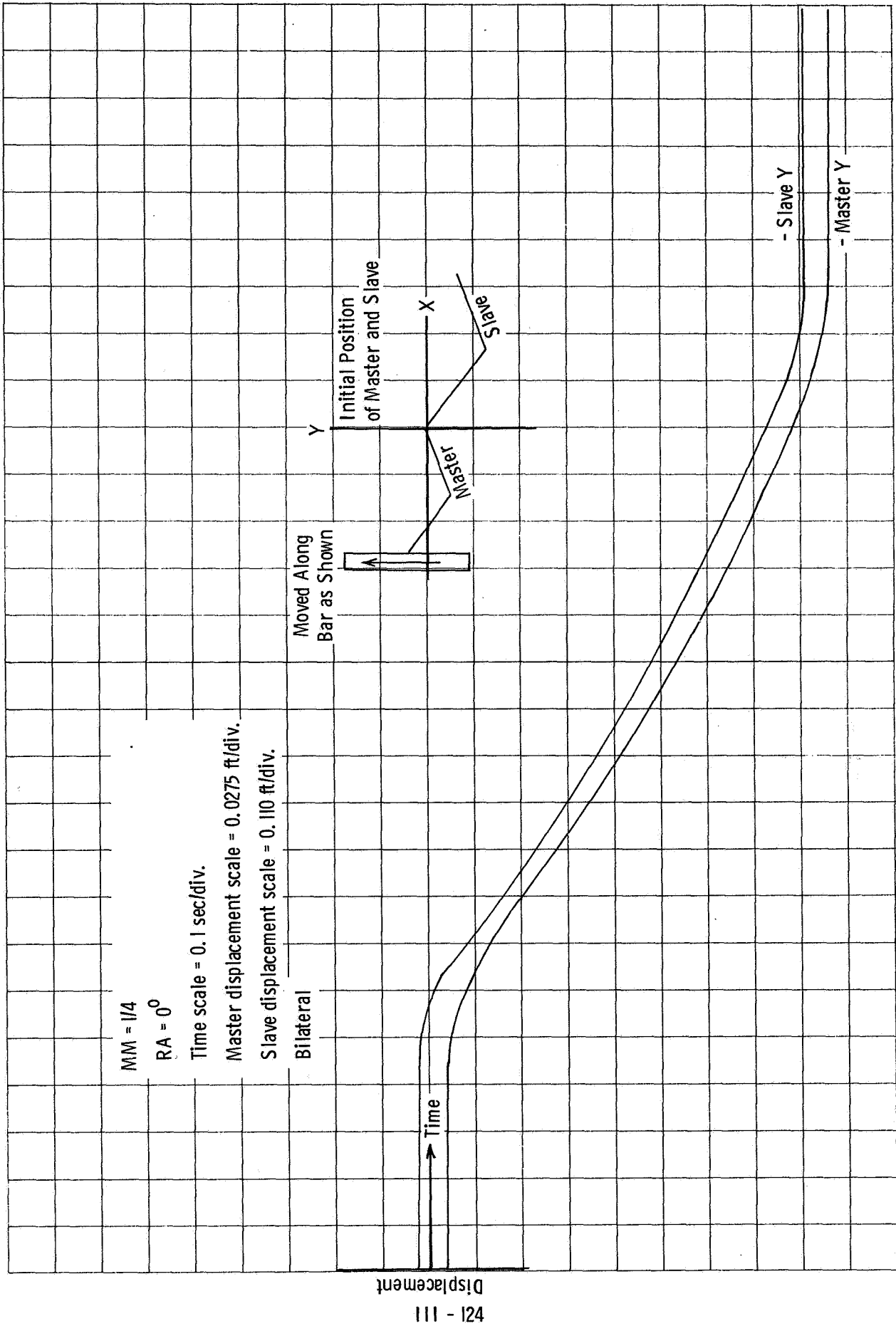


Figure III-62 Tracking - Part B, Figure 2

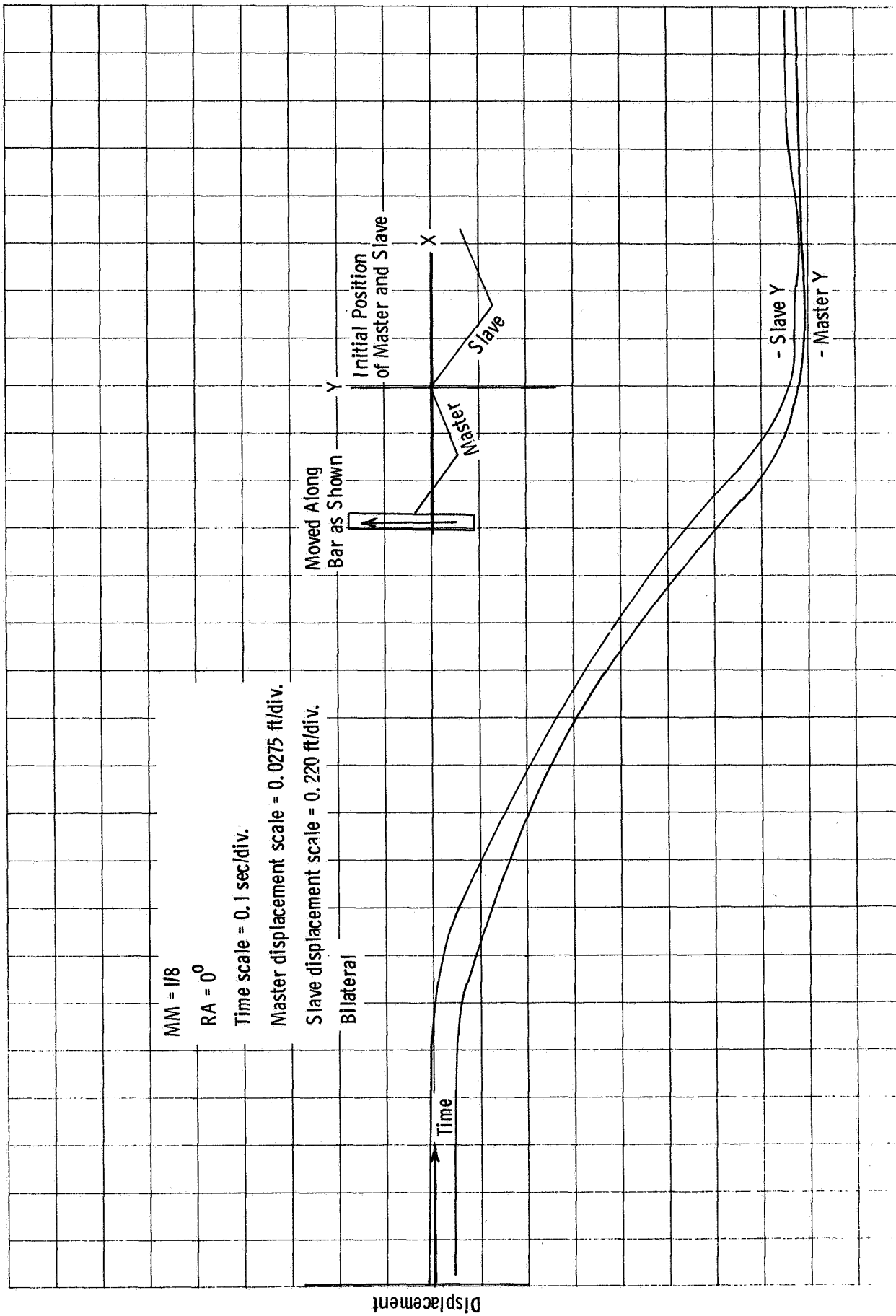


Figure III-63 Tracking - Part B, Figure 3

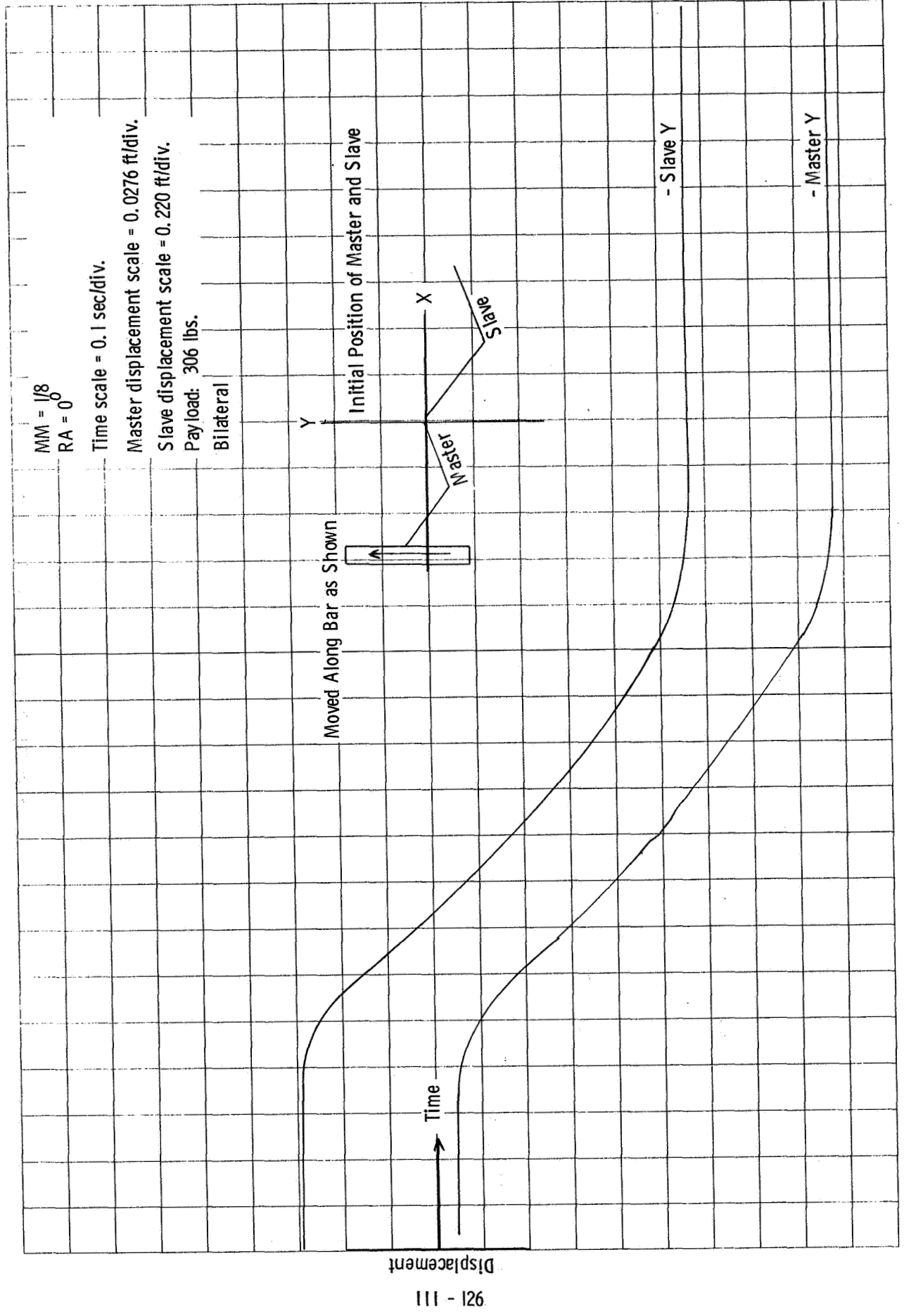


Figure III-64 Tracking - Part B, Figure 4

MM = 1/4, RA = 0°

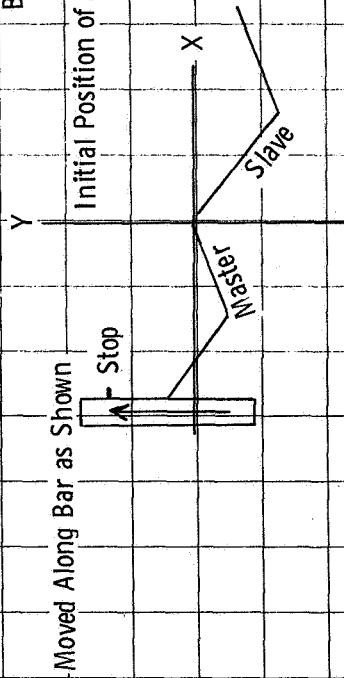
Time scale = 0.5 sec/div.

Master displacement scale = 0.0275 ft/div.

Slave displacement scale = 0.110 ft/div.

Payload: 306 lbs

Bilateral - held against stop



Displacement

Time

- Slave Y

- Master Y

Figure III-65 Tracking - Part B, Figure 5



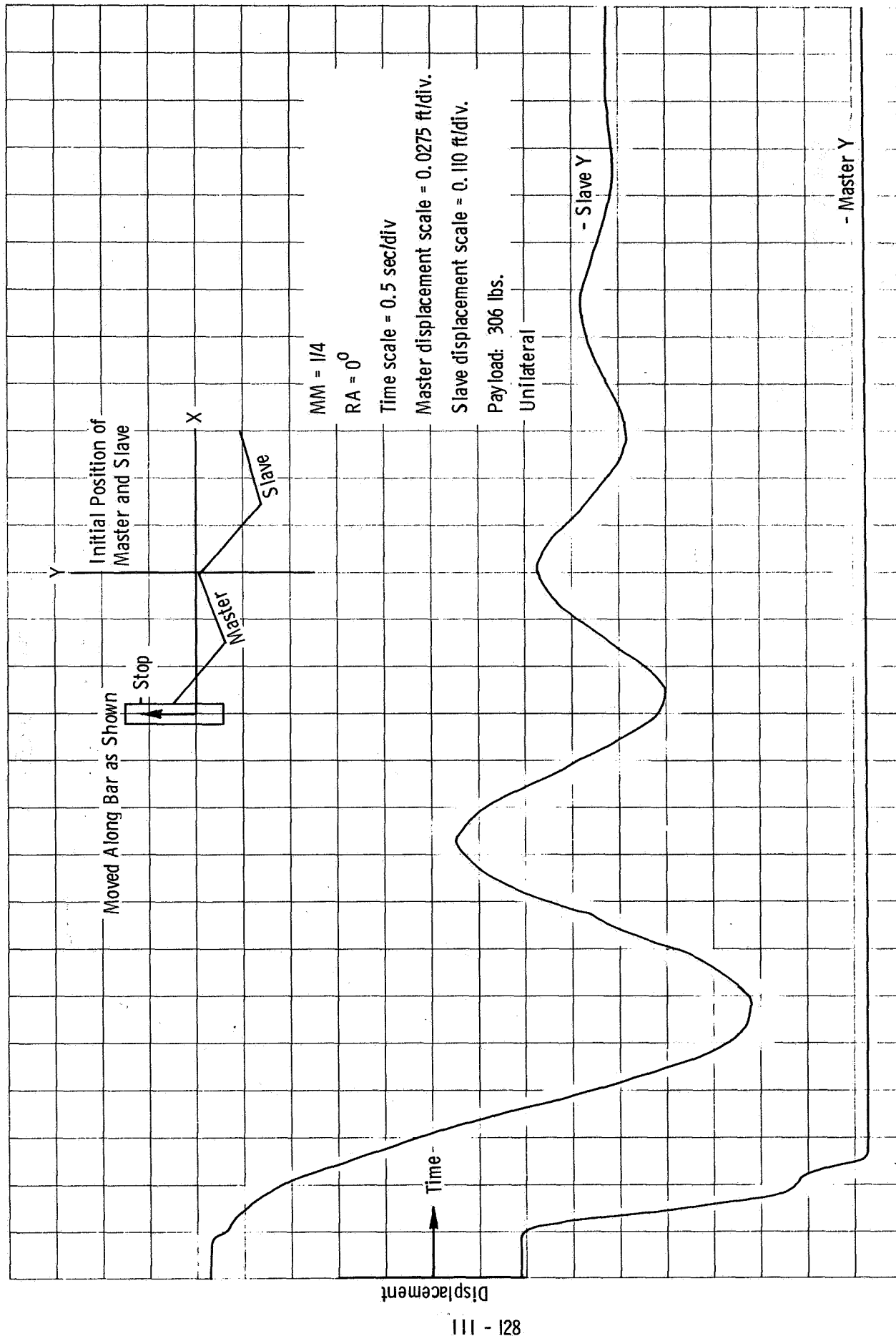


Figure III-66 Tracking - Part B, Figure 6

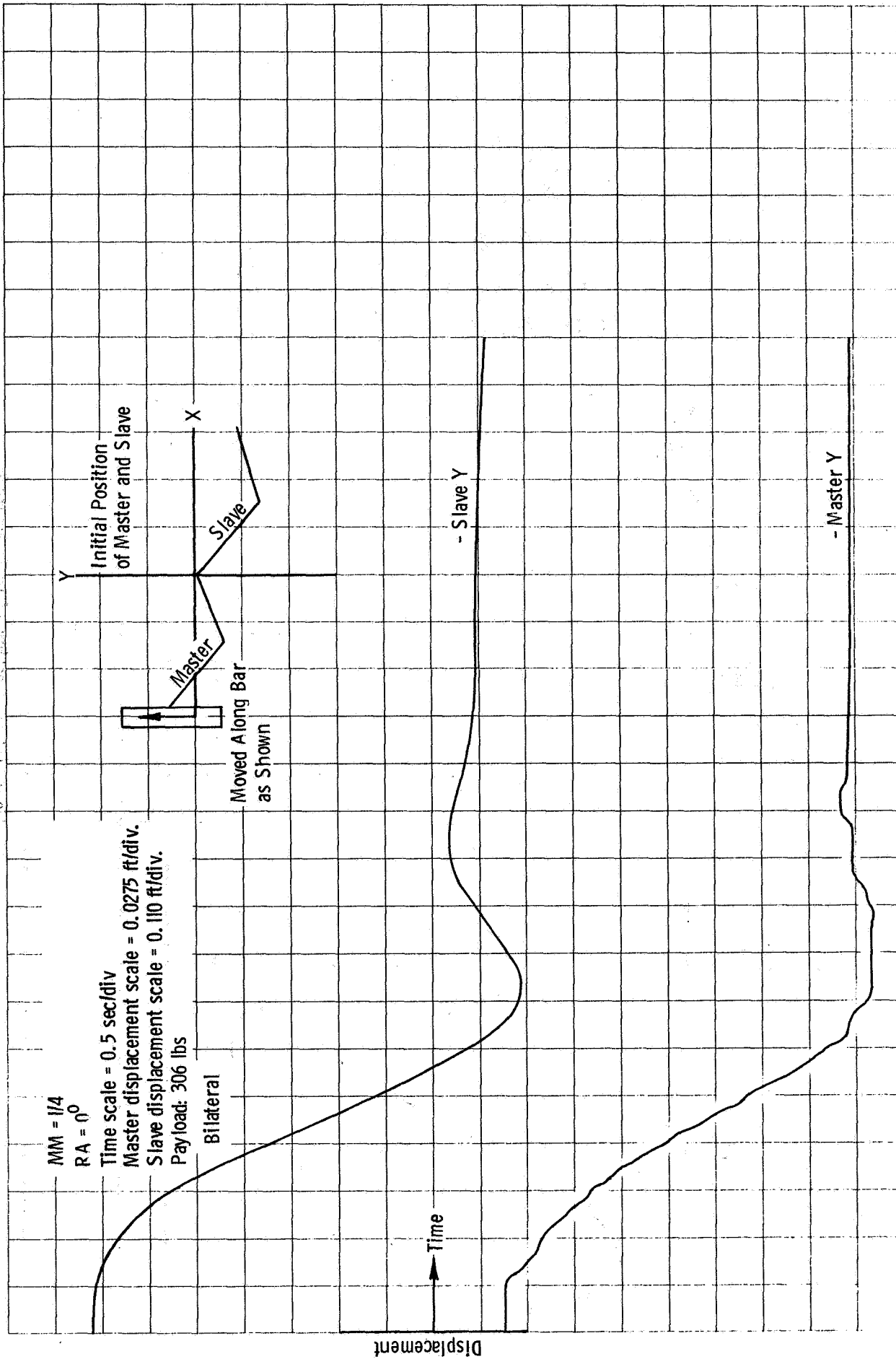


Figure III-67 Tracking - Part B, Figure 7

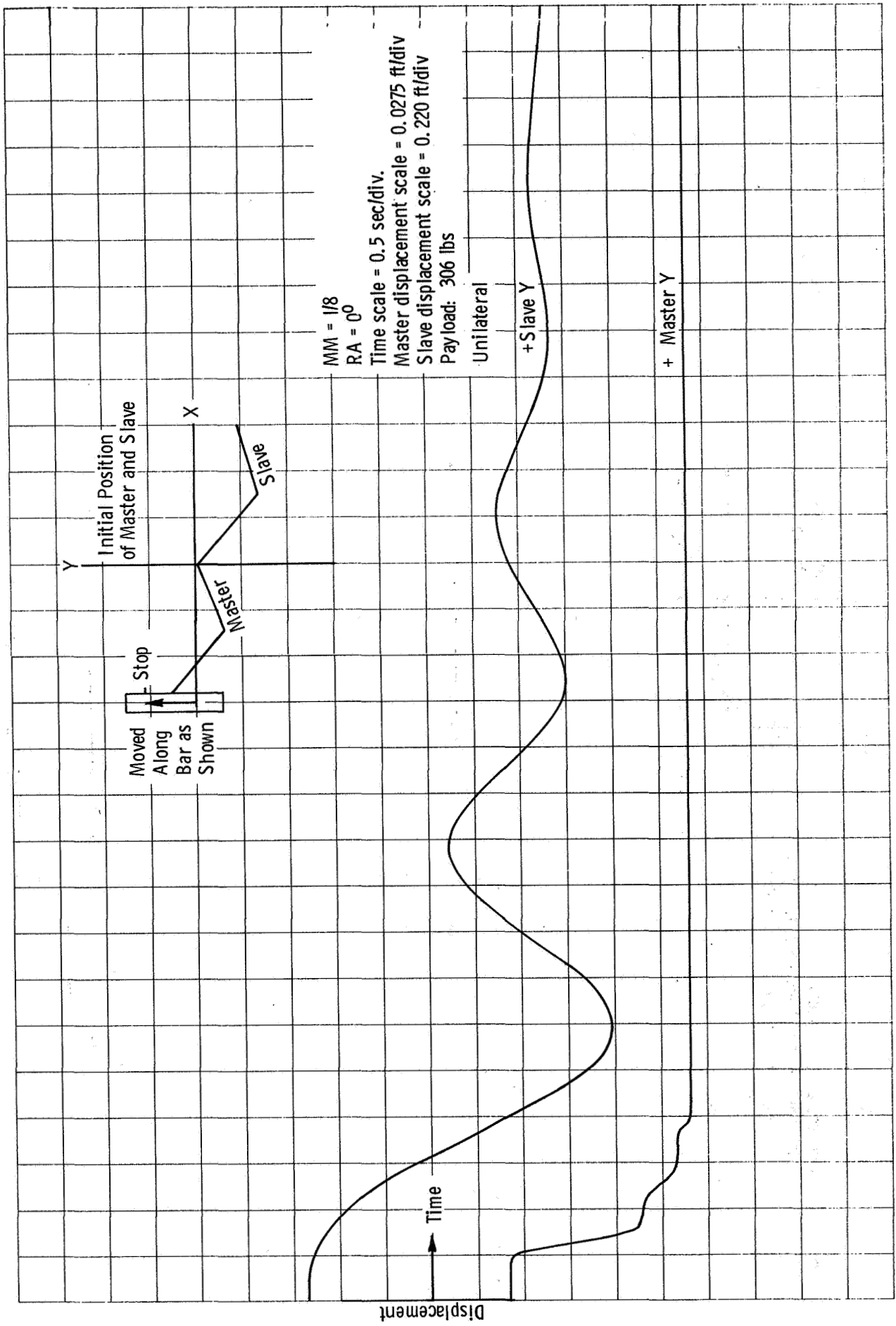


Figure III-68 Tracking - Part B, Figure 8

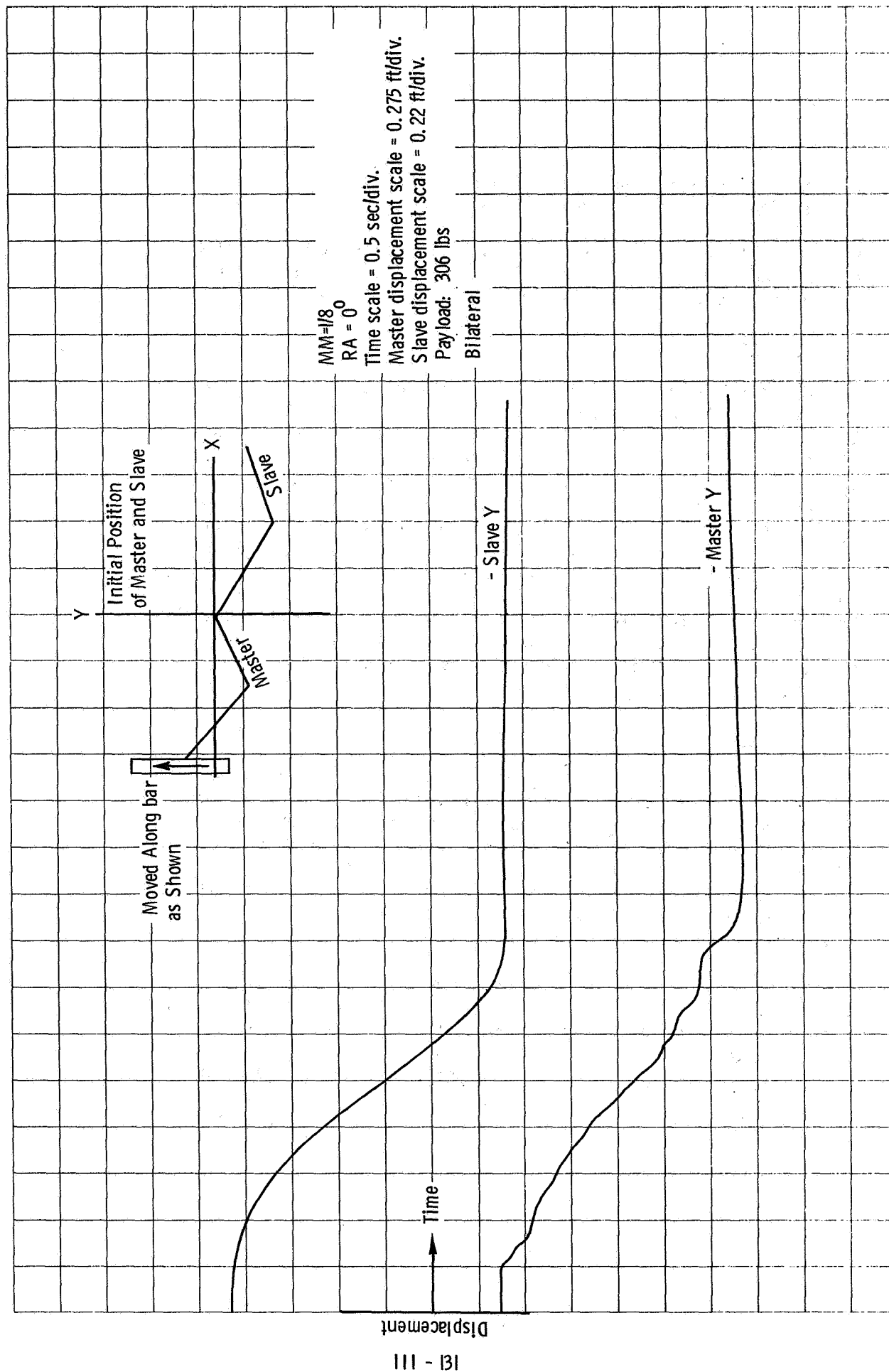


Figure III-69 Tracking - Part B, Figure 9

be expected since equilibrium point oscillations are nulled by the fastest, or dominant member of the system

- this member being the master controller. Thus, even though designed for unloaded operation, the bilateral feature allows the operator to compensate the system to yield a large payload handling capability.

## 6. Bandwidth

The bandwidth of any bilateral manipulator is determined by the slowest responding member of the system - this member being the slave arm. Thus, the bandwidth of the breadboard manipulator was determined by applying inputs on the tip of the master and recording the resulting motion at the tip of the slave. A pure Y oscillating input of  $\pm 0.092$  ft was used to excite the master tip and slave motion was observed for MM values of  $1/2$ ,  $1/4$ , and  $1/8$ . Bandwidth measurements were made for the slave both unloaded and loaded (306 lbs weight and air bearing attached to slave tip), and Tables III-5 through III-10 reveal the unloaded system capable of responding to frequencies ranging between 3.0 Hz and 1.6 Hz and the bandwidth of the loaded system ranges between 0.2 Hz and 0.1 Hz.

## 7. Sample Times

In an attempt to secure preliminary information as to the needed sample rate for the digital interface of the two DOF breadboard manipulator, sample and hold circuits were inserted in the drive channels to each of the joint servo motors. Although sampling the output signals is certainly not equivalent to a true digital interface, it does reveal the nature of system dependency upon sample rate and does give an insight into needed computational time.

Since sample rate is dependent upon system bandwidth, worst case conditions (unloaded slave arm) were investigated. Variable gain ratio values of  $MM = 1/2$ ,  $1/4$ , and  $1/8$  were used and both pure Y sinusoidal ( $\pm 0.092$  ft) and man-in-the-loop inputs were applied to the master controller. As seen from Tables III-11, III-12, and III-13, both the objective and subjective conclusions as to system stability indicate allowable sample rates vary from 7 msec ( $MM = 1/2$ ) to 61 msec or slower for  $MM \leq 1/8$ .

Table III-5. Bandwidth Measurements, Unloaded, MM = 1/2

MM = 1/2		
RA = 0°		
Pure Y input on master		
Frequency	Input Y <sub>c</sub>	Output Y <sub>m</sub>
0.05 hz	± 0.092 ft	± 0.20 ft
0.1 hz	± 0.092 ft	± 0.17 ft
0.2 hz	± 0.092 ft	± 0.18 ft
0.8 hz	± 0.092 ft	± 0.19 ft
1.0 hz	± 0.092 ft	± 0.19 ft
1.4 hz	± 0.092 ft	± 0.20 ft
1.6 hz	± 0.092 ft	± 0.21 ft
1.8 hz	± 0.092 ft	± 0.23 ft
2.0 hz	± 0.092 ft	± 0.21 ft
2.2 hz	± 0.092 ft	± 0.19 ft
2.4 hz	± 0.092 ft	± 0.18 ft
2.6 hz	± 0.092 ft	± 0.16 ft
2.8 hz	± 0.092 ft	± 0.15 ft
3.0 hz	± 0.092 ft	± 0.13 ft

Table III-6. Bandwidth Measurements, Unloaded, MM = 1/4

MM = 1/4		
RA = 0		
Pure Y input on master		
0.05 hz	± 0.092 ft	± 0.36 ft
0.1 hz	± 0.092 ft	± 0.37 ft
0.4 hz	± 0.092 ft	± 0.36 ft
0.8 hz	± 0.092 ft	± 0.37 ft
1.2 hz	± 0.092 ft	± 0.39 ft
1.4 hz	± 0.092 ft	± 0.41 ft
1.6 hz	± 0.092 ft	± 0.49 ft
1.8 hz	± 0.092 ft	± 0.42 ft
2.0 hz	± 0.092 ft	± 0.39 ft
2.4 hz	± 0.092 ft	± 0.30 ft
2.8 hz	± 0.092 ft	± 0.27 ft
3.0 hz	± 0.092 ft	± 0.23 ft
3.4 hz	± 0.092 ft	± 0.17 ft

Table III-7 Bandwidth Measurements, Unloaded, MM = 1/8

MM = 1/8		
RA = 0°		
Pure Y input on master		
Frequency	Input Y <sub>c</sub>	Output Y <sub>m</sub>
0.05 hz	± 0.092 ft	± 0.84 ft
0.1 hz	± 0.092 ft	± 0.77 ft
0.2 hz	± 0.092 ft	± 0.75 ft
0.4 hz	± 0.092 ft	± 0.77 ft
0.6 hz	± 0.092 ft	± 0.75 ft
0.8 hz	± 0.092 ft	± 0.80 ft
1.0 hz	± 0.092 ft	± 0.75 ft
1.2 hz	± 0.092 ft	± 0.75 ft
1.4 hz	± 0.092 ft	± 0.75 ft
1.6 hz	± 0.092 ft	± 0.60 ft
1.8 hz	± 0.092 ft	± 0.48 ft
2.0 hz	± 0.092 ft	± 0.45 ft

Table III-8 Bandwidth Measurements, Loaded, MM = 1/2

MM = 1/2		
RA = 0°		
306 lb load on slave		
Pure Y input on master		
Frequency	Input Y <sub>c</sub>	Output Y <sub>m</sub>
0.05 hz	± 0.092 ft	± 0.27
0.07 hz	± 0.092 ft	± 0.21
0.10 hz	± 0.092 ft	± 0.21
0.13 hz	± 0.092 ft	± 0.21
0.16 hz	± 0.092 ft	± 0.19
0.19 hz	± 0.092 ft	± 0.21
0.22 hz	± 0.092 ft	± 0.23
0.25 hz	± 0.092 ft	± 0.24
0.3 hz	± 0.092 ft	Uncontrollable

Table III-9 Bandwidth Measurements, Loaded, MM = 1/4

MM = 1/4

RA = 0°

306 lbs load on slave

Pure Y input on master

Frequency	Input $Y_c$	Output $Y_m$
0.02 hz	+ 0.092 ft	
0.05 hz	+ 0.092 ft	+ 0.43 ft
0.07 hz	+ 0.092 ft	+ 0.42 ft
0.09 hz	+ 0.092 ft	+ 0.42 ft
0.11 hz	+ 0.092 ft	+ 0.43 ft
0.13 hz	+ 0.092 ft	+ 0.43 ft
0.15 hz	+ 0.092 ft	+ 0.44 ft
0.17 hz	+ 0.092 ft	+ 0.48 ft
0.2 hz	+ 0.092 ft	+ 0.52 ft
0.24 hz	+ 0.092 ft	Uncontrollable

Table III-10 Bandwidth Measurements, Loaded, MM = 1/8

MM = 1/8

RA = 0°

306 lbs load on master

Pure Y input on master

Frequency	Input $Y_c$	Output $Y_m$
0.05 hz	+ 0.092 ft	+ 0.92 ft
0.07 hz	+ 0.092 ft	+ 0.77 ft
0.09 hz	+ 0.092 ft	+ 0.87 ft
0.12 hz	+ 0.092 ft	+ 1.02 ft
0.15 hz	+ 0.092 ft	Uncontrollable



Table III-11 Sample Rates, Unloaded, MM = 1/2

MM = 1/2			
RA = 0°			
No load			
Frequency	Input	Output	Sample Time
Normal Oper.	Human Oper.	Very good	0.4 msec
Normal Oper.	Human Oper.	Very good	5.0 msec
Normal Oper.	Human Oper.	Good	6.0 msec
Normal Oper.	Human Oper.	Fair	7.0 msec
Normal Oper.	Human Oper.	Fair	10.0 msec
Normal Oper.	Human Oper.	Unstable	15.0 msec

Table III-12 Sample Rates, Unloaded, MM = 1/8

MM = 1/8			
RA = 0°			
No load			
Frequency	Input	Output	Sample Time
Normal Oper.	Human Oper.	Very good	0.4 msec
Normal Oper.	Human Oper.	Very good	9.5 msec
Normal Oper.	Human Oper.	Very good	14.8 msec
Normal Oper.	Human Oper.	Very good	20.0 msec
Normal Oper.	Human Oper.	Very good	25.0 msec
Normal Oper.	Human Oper.	Very good	32.0 msec
Normal Oper.	Human Oper.	Good	41.0 msec
Normal Oper.	Human Oper.	Good	50.0 msec
Normal Oper.	Human Oper.	Fair	61.0 msec
Normal Oper.	Human Oper.	Fair	80.0 msec
Normal Oper.	Human Oper.	Poor	100 msec
Normal Oper.	Human Oper.	Unstable	120 msec

Table III-13 Sample Rates, Unloaded, MM = 1/4

MM = 1/4

RA = 0°

No Load

Pure Y input on master

Frequency	Input $Y_c$	Output $Y_m$	Sample Time
0.1 hz	+ 0.092 ft	+ 0.41 ft	0.4 msec
0.1 hz	+ 0.092 ft	+ 0.40 ft	0.8 msec
0.1 hz	+ 0.092 ft	+ 0.40 ft	2.6 msec
0.1 hz	+ 0.092 ft	+ 0.40 ft	4.2 msec
0.1 hz	+ 0.092 ft	+ 0.40 ft	6.0 msec
0.1 hz	+ 0.092 ft	+ 0.34 ft	9.5 msec
0.1 hz	+ 0.092 ft	+ 0.40 ft	14.4 msec → Starting to chatter
0.1 hz	+ 0.092 ft	+ 0.34 ft	19.5 msec
0.1 hz	+ 0.092 ft	+ 0.34 ft	30.0 msec
0.1 hz	+ 0.092 ft	+ 0.34 ft	45.0 msec → Totally unstable
1.2 hz	+ 0.092 ft	+ 0.40 ft	0.4 msec
1.2 hz	+ 0.092 ft	+ 0.40 ft	7.6 msec
1.2 hz	+ 0.092 ft	+ 0.40 ft	10.8 msec
1.2 hz	+ 0.092 ft	+ 0.38 ft	16.4 msec
1.2 hz	+ 0.092 ft	+ 0.38 ft	25.0 msec
1.2 hz	+ 0.092 ft	+ 0.42 ft	33.0 msec → Starting to go
1.2 hz	+ 0.092 ft	+ 0.42 ft	44.0 msec unstable
1.2 hz	+ 0.092 ft	+ 0.47 ft	50.0 msec → Unstable
2.0 hz	+ 0.092 ft	+ 0.44 ft	0.4 msec
2.0 hz	+ 0.092 ft	+ 0.34 ft	1.8 msec
2.0 hz	+ 0.092 ft	+ 0.44 ft	11.2 msec
2.0 hz	+ 0.092 ft	+ 0.36 ft	16.4 msec
2.0 hz	+ 0.092 ft	+ 0.44 ft	25.0 msec
2.0 hz	+ 0.092 ft	+ 0.49 ft	37.0 msec → Starting to go
2.0 hz	+ 0.092 ft	+ 0.44 ft	52.0 msec unstable
Normal Oper.	Human Oper.	Very good	0.4 msec
Normal Oper.	Human Oper.	Very good	6.0 msec
Normal Oper.	Human Oper.	Very good	11.2 msec
Normal Oper.	Human Oper.	Very good	16.4 msec
Normal Oper.	Human Oper.	Fair	20.4 msec
Normal Oper.	Human Oper.	Fair	25.0 msec
Normal Oper.	Human Oper.	Poor	30.0 msec

## 8. Maze Times

Figure III-70 depicts the breadboard manipulator being used to negotiate a probe through a maze. This test was included in the system documentation procedures to reveal to those unfamiliar with manipulator systems one of the advantages of bilateral over unilateral operation. Four test subjects were used and each was directed to guide the probe through the maze in the fastest possible time under both unilateral operation and bilateral operation with and without visual feedback. As seen from Table III-14, virtually no difference in task times was noted, for any of the subjects, between bilateral operation with and without visual feedback. Also seen from the table, the difference in times to complete the task between the unilateral mode and bilateral mode varied with the experience of the operator, with unilateral times ranging from 2 to 7 times greater than bilateral times.

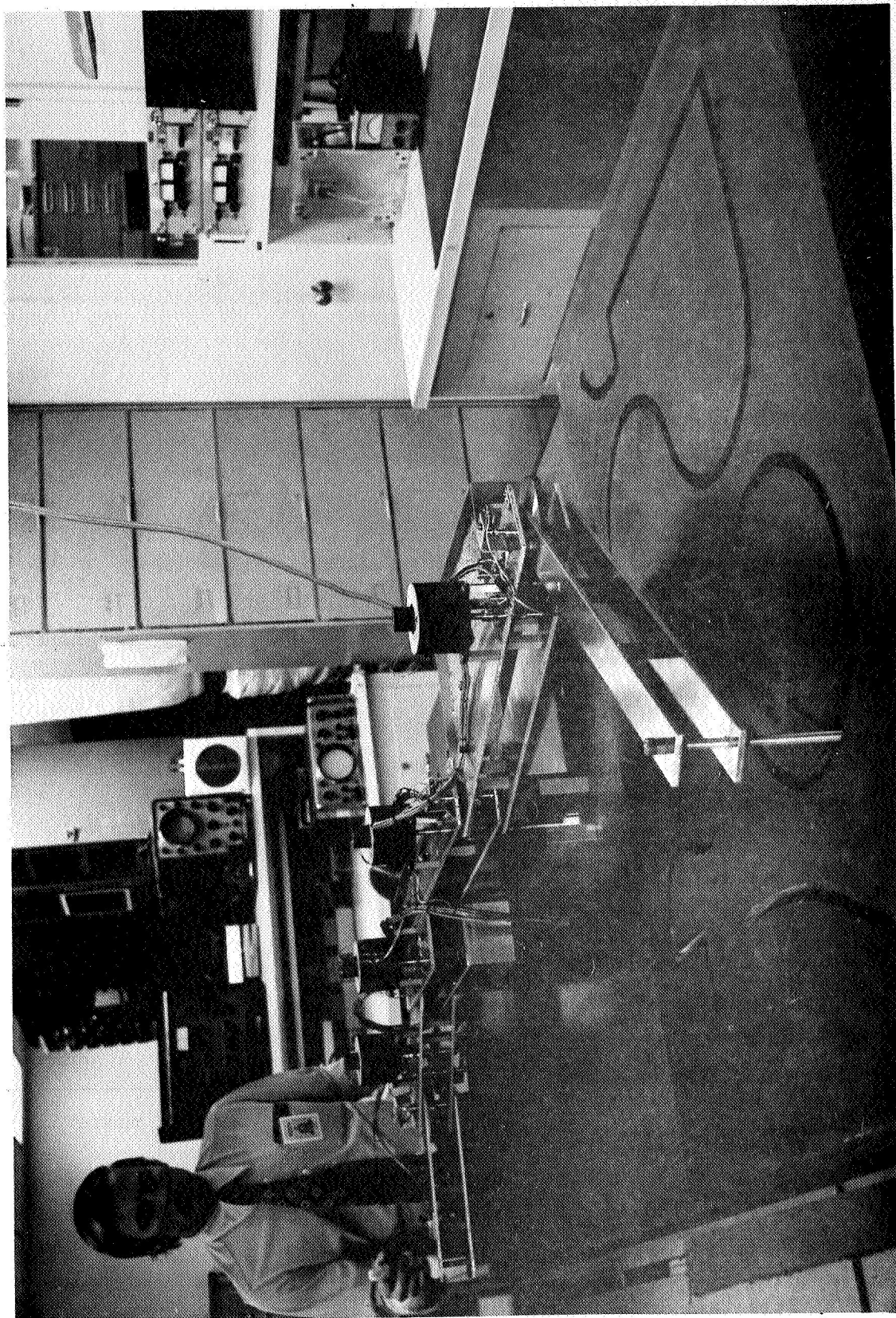


Figure III-70 Breadboard Manipulator With Maze Test Board

Table III-14 Maze Task Times

Unilateral (seconds)	Bilateral No Visual (seconds)	Bilateral With Visual (seconds)	Subject I, very experienced
24.0	8.00	6.25	MM = 1/4. RA = 0°
19.0	6.50	8.00	
14.5	7.00	7.10	
16.5	11.00	7.00	
15.0	8.50	6.75	
13.5	7.50	7.50	
Subject II, experienced			
59.0	8.9	8.5	MM = 1/4 RA = 0°
19.9	8.4	9.7	
36.8	7.3	6.9	
51.4	7.8	9.8	
	7.5	8.0	
	7.3	7.5	
Subject III, not experienced			
41.4	58.6 lost <sup>+</sup>	10.0	MM = 1/4 RA = 0°
37.7 index*	11.3	9.0	
Out of maze**	15.2	9.6	
42.6	13.3	8.6	
47.1	11.6	8.7	
	9.0	8.4	
Subject IV, experienced			
43.4	10.0	9.0	MM = 1/4 RA = 0°
61.1	9.5	9.4	
54.7	8.7	10.7	
59.2	8.7	10.6	
	12.4	10.8	
	9.8	11.0	

\* It was the option of all subjects to position index the master controller at will.

\*\* Due to Subject III's inexperience, exceedingly high forces were applied in the unilateral mode and the probe was forced out of the maze.

<sup>+</sup> In the bilateral mode with no visual feedback, the subject, on his first run, became momentarily lost and had to hunt by trial and error for the proper path.

## E. SUMMARY

A control technique has been presented that allows a bilateral force reflecting manipulator to incorporate coordinate transformation, multi-mode operation, and position indexing. The technique uses an  $\underline{X}$  reference frame control scheme which results in a highly nonlinear system. Servo system compensation design is based on linearized control law equations and the procedures for deriving the needed filter networks are presented.

To "prove the concept", in hardware, of the  $\underline{X}$  reference frame technique, a two DOF master-slave breadboard was fabricated. The breadboard master and slave were interfaced with a EAI 231R analog computer on which the control law equations and compensating network were programmed.

Testing of the breadboard system revealed the  $\underline{X}$  reference frame force reflecting properties were truly independent of coordinate transformations, multi-mode operation, and position indexing. The coordinate transformations and multi-mode features operated perfectly, and it was realized that position indexing was not only a nicety but a necessity for teleoperators with a large master-slave size disparity. The X, Y tip compliance of the system was 0.003 ft/lb; although originally it was hoped that a smaller compliance figure could be obtained, the achieved value did yield a workably stiff servo system. The tip to tip tracking properties were excellent, and it was demonstrated how man-in-the-loop serves as an adaptive filter for stabilizing a bilateral system handling a large payload. The tip to tip bandwidth of the unloaded system was experimentally determined to range from 3.0 to 1.6 Hz, with the loaded system (306 lbs inertia load on tip of manipulator) having a bandwidth ranging from 0.2 to 0.1 Hz. It was concluded that if the analog system were sampled, the tolerable sample rate varied from 10 msec ( $MM = 1/2$ ) to 32 msec ( $MM = 1/8$ ). To demonstrate one advantage of a bilateral system, a maze was negotiated with a probe attached to the end of the manipulator. Comparing unilateral and bilateral task times revealed the bilateral mode to be two to seven times more efficient.

#### IV. MANIPULATOR

This chapter discusses three main areas: joints, counterbalance, and overall manipulator design. The work on joints includes gear train breadboards, gear ratio/motor selection and final design. The latter is based on commercial quality components but has incorporated several space version requirements; i.e., envelope size, torque, etc.

A counterbalance mechanism breadboard was designed and tested. Alternative techniques and final recommended design is discussed. An optimization technique was used to minimize the effect of the counterbalance on the arm dynamics and aid in the yoke design.

The last section, overall manipulator design, includes a layout drawing of the 40 ft counterbalanced AMS. The design incorporates a counterweight clearance yoke which allows complete manipulator movement.

##### A. JOINTS

###### 1. Design Requirements and Joint Alternatives

Many techniques have been used and proposed over the years for providing the required torques and speeds for manipulator joints. Most systems were not weight or efficiency critical and many design configurations gave satisfactory results. However, for a system, with potential utilization in space, where a high degree of control is required, certain optimization is mandatory. This does not imply increasing mechanism complexity. It does mean that the design parameter tradeoffs must be considered more thoroughly; those such as weight, efficiency, reliability, backdriveability, inertia, backlash, torsional elasticity, envelope volume, and so forth. The backdriveability requirement has a very strong influence on the selection of a torque multiplier system.

It should be noted that the criteria for selecting the torque values and the drive types for the AMS is not related to the presence of gravity. The gravity load is overcome by counterbalancing (Section B). Therefore, the selection of a drive type is applicable for the SAMS as well as the AMS.

Several candidate speed reduction techniques for use in space manipulator joints have been shown in the past. Each has apparent advantages and disadvantages. The approach of this technology investigation is to (1) select three alternative gear train types, (2) design and fabricate a full size breadboard of each gear train, (3) test each for static and dynamic friction, backdriveability, torsional deflection (wind-up), and backlash, (4) analyze the data and select the preferred gear train type, and (5) design three AMS joints based on the selected gear train type. The 1200 ft-lb shoulder joint was the one selected to breadboard.

With regard to a choice of overall ratio for the gear train breadboards several factors were considered. DC torque motors are available in a wide range of torques so that it was equally possible to use a low torque motor with a high gear ratio or a high torque motor with a low gear ratio. The need to have high backdriveability means that motor reflected friction must be low, which indicates a low gear ratio. In addition, if there are more meshes there are more sources of gear friction and thus a higher gear reflected friction. Based on previously designed and fabricated breadboard arms it was known that a simple spur gear system could be backdriven if the ratio was in the vicinity of 100 or 200 to 1, with up to four gear meshes. Beyond this, no concrete information was available. Most Harmonic Drives are limited to a ratio of 200:1 in a single stage.

Based on the above reasoning a gear train ratio of 200:1 was selected for the joint breadboards. An effort (parallel to the breadboard fabrication) was conducted to analytically tradeoff the gear train ratio vs motor size. The results of this analysis (discussed in part 3 of this section) points to a gear ratio of approximately 100:1 for the 1200 ft-lb shoulder joint. Since this ratio is relatively close to that used in the breadboards, the latter test results are valid for comparison of gear train types for use on the AMS.

The three gear train types selected for breadboarding are: (1) a harmonic drive, (2) a spur gear system with external spur gears throughout, and (3) a double spur gear system with the final (output) member an internal spur (or ring) gear. The latter two are referred to as the "external" and the "internal" drives, respectively.



## 2. Breadboards

a. Design and Fabrication - The external and internal systems were designed and built by MMC. The harmonic drive was purchased from United Shoe Machinery (USM) Corporation. High strength, accurate gears were purchased for the internal and external drives. Standard commercial gears do not have the accuracy and strength which are necessary for a design which can meet the final envelope and backlash requirements. For example, the safe tooth loading of both cast iron or soft steel gears (commercial types) is in the order of 20,000 lbs per square inch. Using high strength steel, safe tooth loading can be about 80,000 lbs per square inch. This strength factor of four reduces the width of the gears, thus producing significantly smaller envelope sizes.

Because of the 200:1 reduction ratio and the 12.0 inches envelope limitation for the drive housing in the test breadboard drive and furthermore the desire for no more than 3 meshes, it was necessary to use enlarged shaped teeth pinions with 13 teeth. This way a full beam strength was achieved for the pinion teeth in contrast to what one would get with an undercut teeth pinion.

In the two spur gear systems the following design guidelines were used:

- 1) Weight of test breadboards was not limited,
- 2) Unground gears were used,
- 3) Simplicity was a prime goal,
- 4) Aluminum housings and external drive shafts with keyways were used for ease of connecting input and output torque loads,
- 5) Approximately 12 inch overall joint diameter,
- 6) Low backlash of less than 0.005 inches on output gear teeth, and
- 7) Gears manufactured to AGMA-9 quality specifications, using standard hobbing methods for cutting.

It should be noted that more rigid tolerance specifications (such as AGMA-10 to 14 could reduce backlash, but funding constraints prevented this on these breadboards. For comparative evaluation a higher backlash was considered allowable.

Harmonic drive - The harmonic drive uses an eccentric input drive to deflect a circular spline, engaging many small teeth at one time. Each rotation of the input advances the drive by one tooth, thus achieving a 200:1 ratio in one mesh. A model 8M (USM) harmonic drive was purchased for the breadboard tests. This drive has a 200:1 speed reduction ratio, and is rated for 1200 ft-lbs on the output shaft. The harmonic drive concept is shown in Figure IV-1. The unit used for test was an off-the-shelf model (Figure IV-2), although its components were selected (by the vendor) for best fit. Prior to the test the oil was removed from the drive leaving only a light oil film. The input shaft seal was also removed to decrease the friction level.

External Drive - A simple three mesh system was designed, each mesh ratio approximately 6:1 with a total reduction of 199:1. This system consists of 20° spur gears in a single train. The backlash in this system was controlled with good dimensional tolerance and with some small adjustments available during final assembly.

In developing the gear and pinion specifications the basic Lewis Equation was used throughout. The velocities to be encountered are so low that the dynamic effects are inconsequential. Also, the pitch line velocity is so small that the Barth modification does not make any significant contribution. The major factor of importance is the safe tooth load stress which is dependent on the characteristics of the gear material. The material chosen was SAE4340 steel. Although full strength is not reached until RC45 or greater we allowed a relaxation of this to RC38 to enable final machining without grinding, after heat treatment.

The breadboard concept and detail design is shown in Figures IV-3 and IV-4.

Internal Drive - The internal gear system is driven by a standard spur pinion, but then branched off into two spur gear trains driving a common ring gear. This drive uses adjustments in the double pinion drive to allow for assembly of the gears.

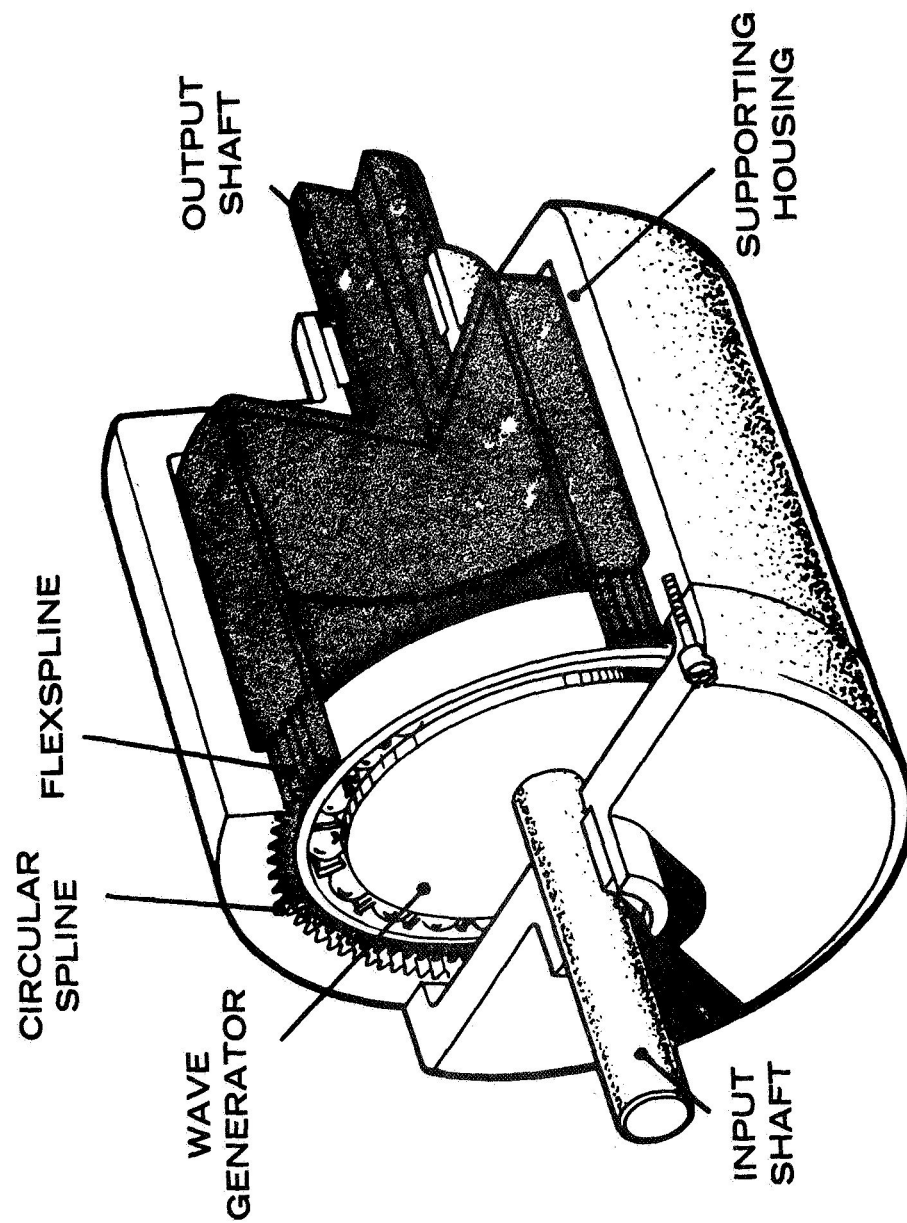


Figure IV-1 Harmonic Drive Concept

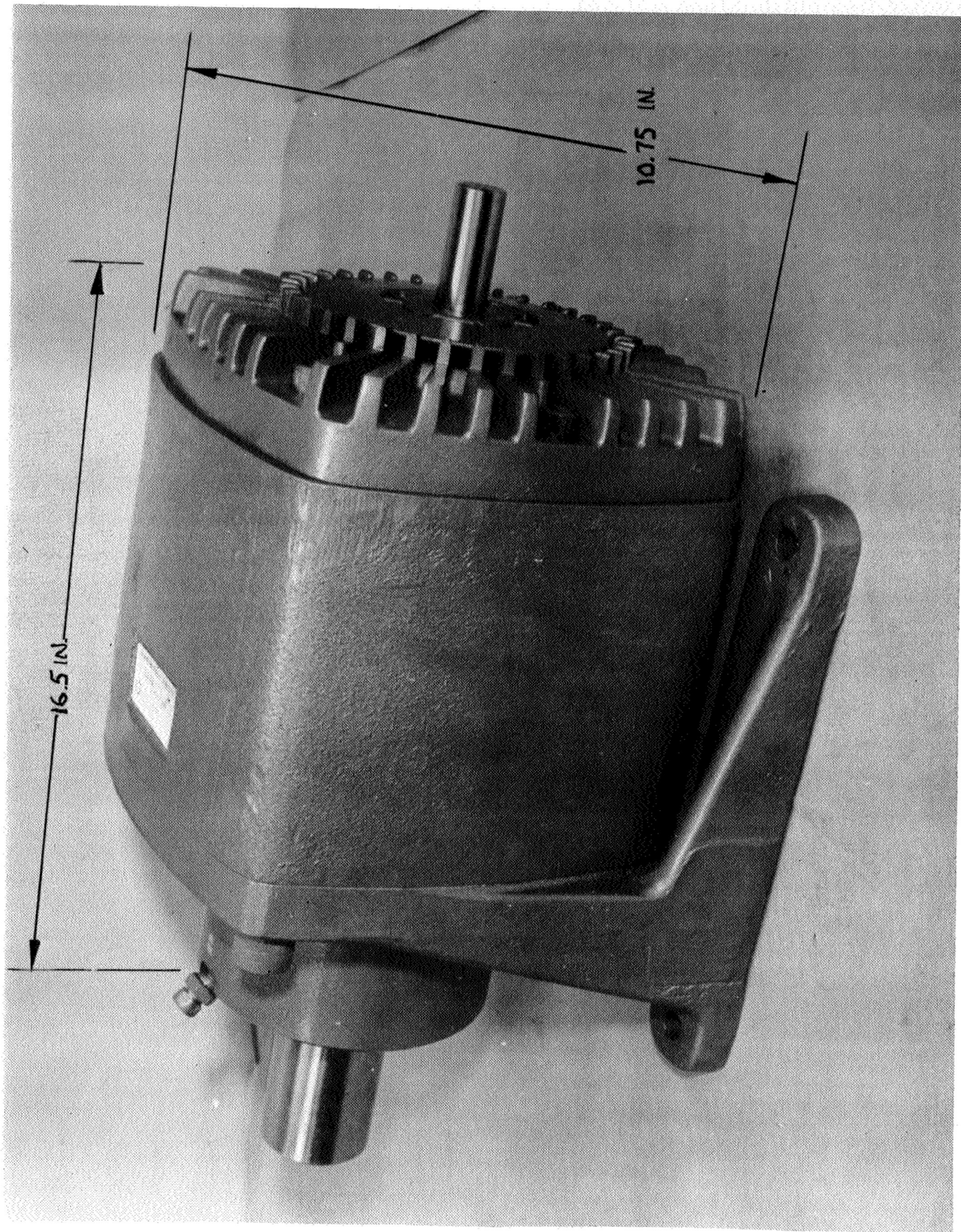


Figure IV-2 Harmonic Drive, USM Model 8M

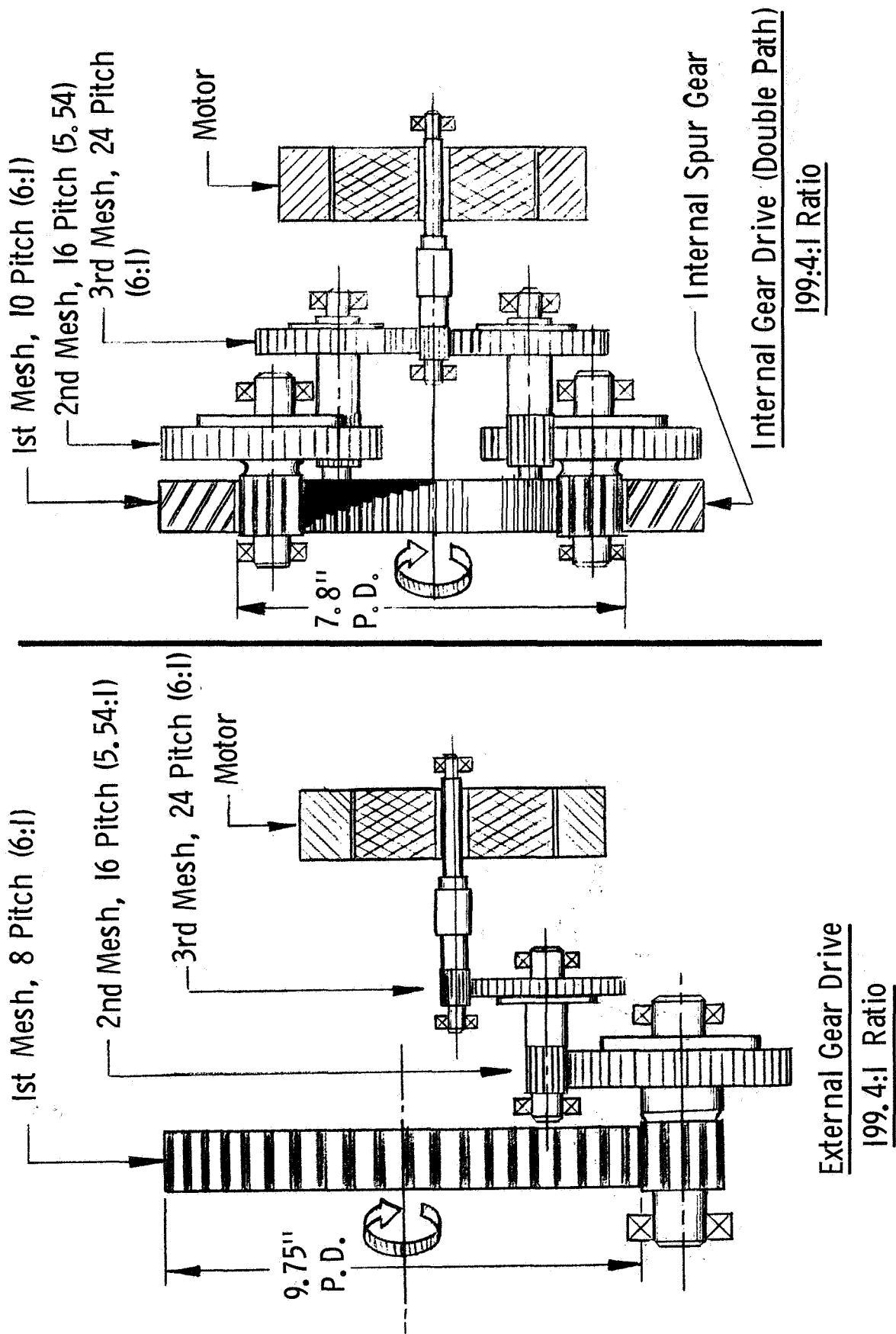


Figure IV-3 Spur Gear Drives - Schematics

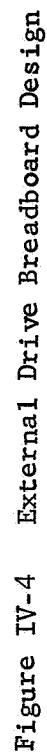




Figure IV-5 Internal Drive Breadboard Design

The internal drive also has three meshes, each approximately 6:1, giving a total reduction of 199:1. The external drive discussion above regarding the Lewis and Barth relationships, and the material selected also applies to the internal drive. The internal drive breadboard concept and detail design is shown in Figures IV-3 and IV-5.

b. Testing and Test Results - The following parameters are those evaluated and measured in the test program.

- 1) Drive torsional elasticity (windup) through the total loading range (0 to 1200 ft-lbs),
- 2) Breakaway (stiction) torque through the total loading range (driving forward and backward),
- 3) Frictional running torque loss at several accelerations and velocities through the total loading range,
- 4) Running efficiency at several accelerations and velocities through the total loading range,
- 5) Backlash at input and output shaft, and
- 6) Miscellaneous operating characteristics of each drive observed during the test.

1) Test Set-up - Figure IV-6 is a schematic of the test apparatus. No motors or exterior gear drives were used. The drive mount is approximately 12 feet above the floor. The output shaft is equipped with a balanced arm from which weights are suspended. These weights produce an output torque up to 1200 ft-lbs. On the input shaft is a pulley of known diameter over which is wound nylon cord from which the input weight is applied. The input load is accurately weighed. For the dynamic tests, a timer is wired to a limit switch at the input pulley and a limit switch at the stop point approximately 12 feet below the input pulley. On release of the input weight the upper switch starts the timer. When the drop weight strikes the stop, the lower switch stops the timer. The timer is readable within 2 milliseconds. By accurately measuring the distance the weight falls, accelerations and velocities can be accurately determined. The maximum output velocities expected in manipulator operation are expected to be about 2 ft/sec unloaded and 0.2 ft/sec fully loaded. These



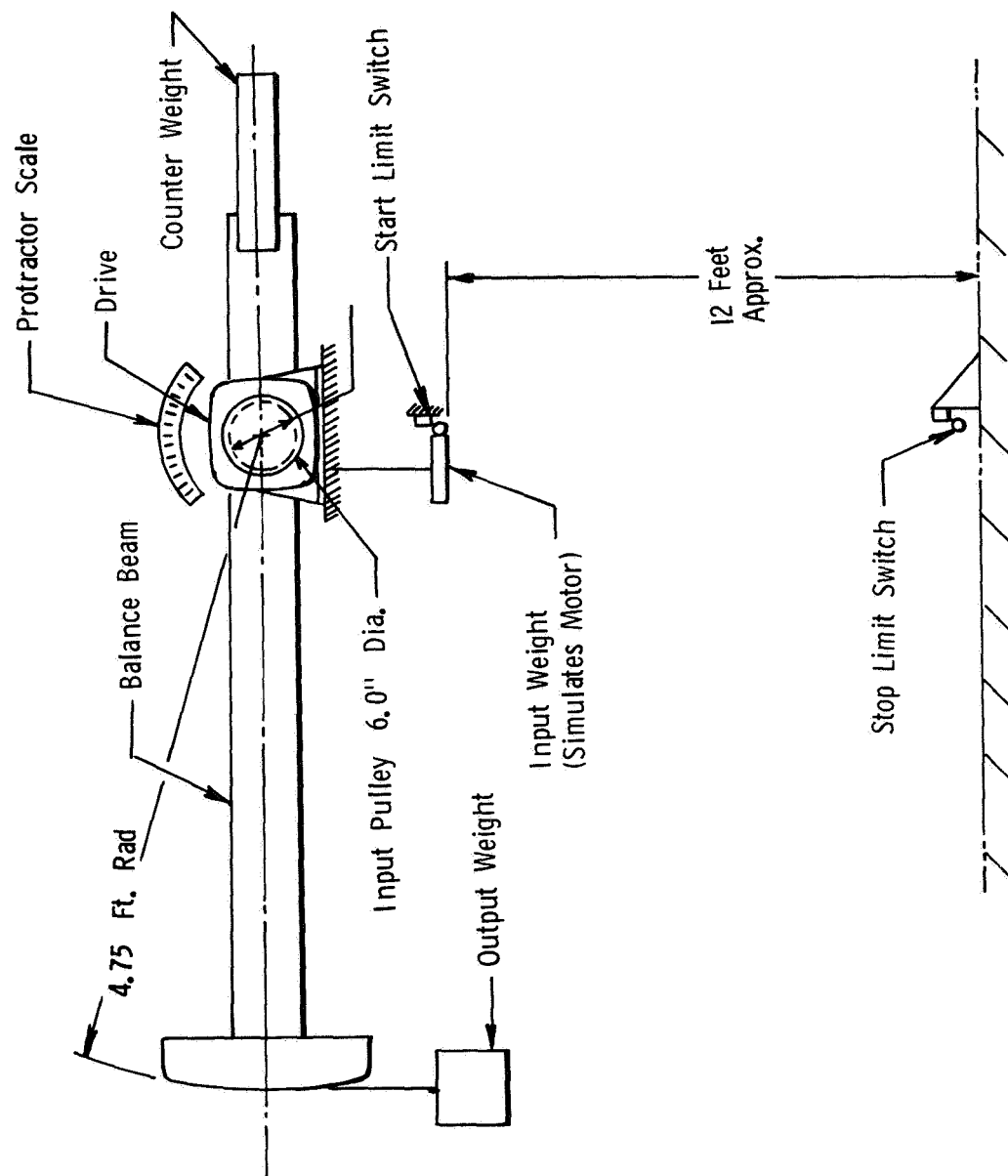


Figure IV-6 Joint Breadboard Test Set-up

accelerations and velocities were within the range obtained with the test set-up.

Table IV-1 shows the parameters that were measured during the tests and those that were calculated later. A digital computer program was written and used to reduce the data.

2) Static Tests - Backlash and torsional windup at the input shaft were measured by a calibrated protractor located at the input shaft. A pointer fixed to the input shaft shows the angle traveled from the time weights were first applied till the time breakaway occurs. Backlash was first measured by manually rotating the input shaft while the output shaft is locked. Backlash at the output shaft was measured while the input shaft was locked.

Table IV-2 shows a sample static breakaway torque test data sheet used for each drive for the forward drive mode. A weight was placed at the end of the balance beam to simulate output torque. This weight is recorded as output weight. A weight was applied at the input pulley until movement of the balance beam was detected on the dial indicator. This weight is recorded as input weight. At the same time, the windup angle was read at the input shaft to determine the windup angle. Torque on the input shaft was computed based on the weight and input pulley diameter of 6 inches. This torque multiplied by 200, the gear ratio for harmonic drive and 199.3 for spur drives, provides the theoretical output torque. The output torque is the output weight times the beam length of 4.75 ft. The actual output torque divided by the theoretical output torque is the static breakaway efficiency in percent. Actual drive static friction in ft-lbs is theoretical output torque less actual output torque. Backdrive static breakaway torque tests were run identical to the forward drive test. The data is handled identical to the forward drive test except windup data was not obtainable.

By comparing input torque applied, to the output torque, static breakaway torque efficiency is determined. By subtracting the output torque from the input torque times the gear ratio, the actual friction torque of the drive is derived.

Figures IV-7 and IV-8 show the external and internal drives set up for testing.

Table IV-1 Measured and Calculated Joint Data

Test	Measured Data	Calculated Data
Backlash	Protractor reading in degrees	
Torsional Elasticity (Windup)	Protractor reading in degrees	Deflection of components in drive and balance beam
Static Break- away Torque Forward and Backward	Input pulley torque Output shaft torque	Drive breakaway friction torque Drive static efficiency
Dynamic driving characteristics	Weight applied to output Weight applied to input Input weight fall distance Input weight fall time	Mass moment of inertia of: a. Input pulley b. Balance beam c. Drive Distance Travelled by: a. Input pulley (radians) b. Balance beam (radians) c. Output weight Acceleration of: a. Input weight (ft/sec <sup>2</sup> ) b. Input pulley (rad/sec <sup>2</sup> ) c. Output weight (ft/sec <sup>2</sup> ) d. Balance beam (rad/sec <sup>2</sup> ) Final Velocity of: a. Input weight (ft/sec) b. Input pulley (rad/sec) c. Balance beam (rad/sec) d. Output weight (ft/sec) Drive Running Friction Drive Torque Loss Due to inertia

Table IV-2 Sample Data Sheet - Static Tests

Measurement	Test Number					
	1	2	3	4	5	6
Drop Weight (lbs)	.0125	5.437	10.406	16.094	22.406	27.313
Output Weight (lbs)	0	50	100	150	200	250
		D A T A				
Torsional Windup - Degrees (Input Shaft)	0	15	33	40	65	115
		D A T A				

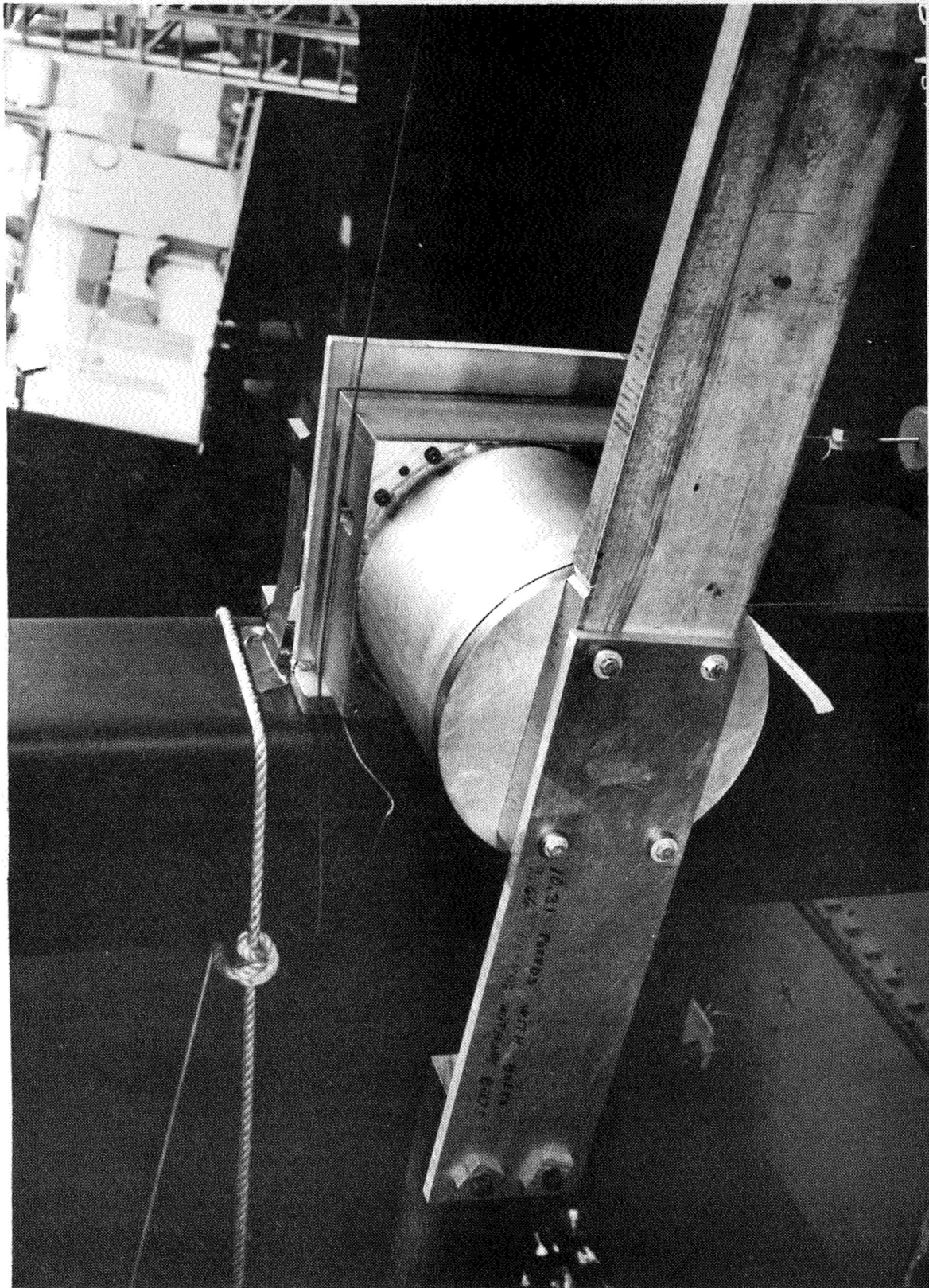


Figure IV-7 External Drive Under Low-Load Test



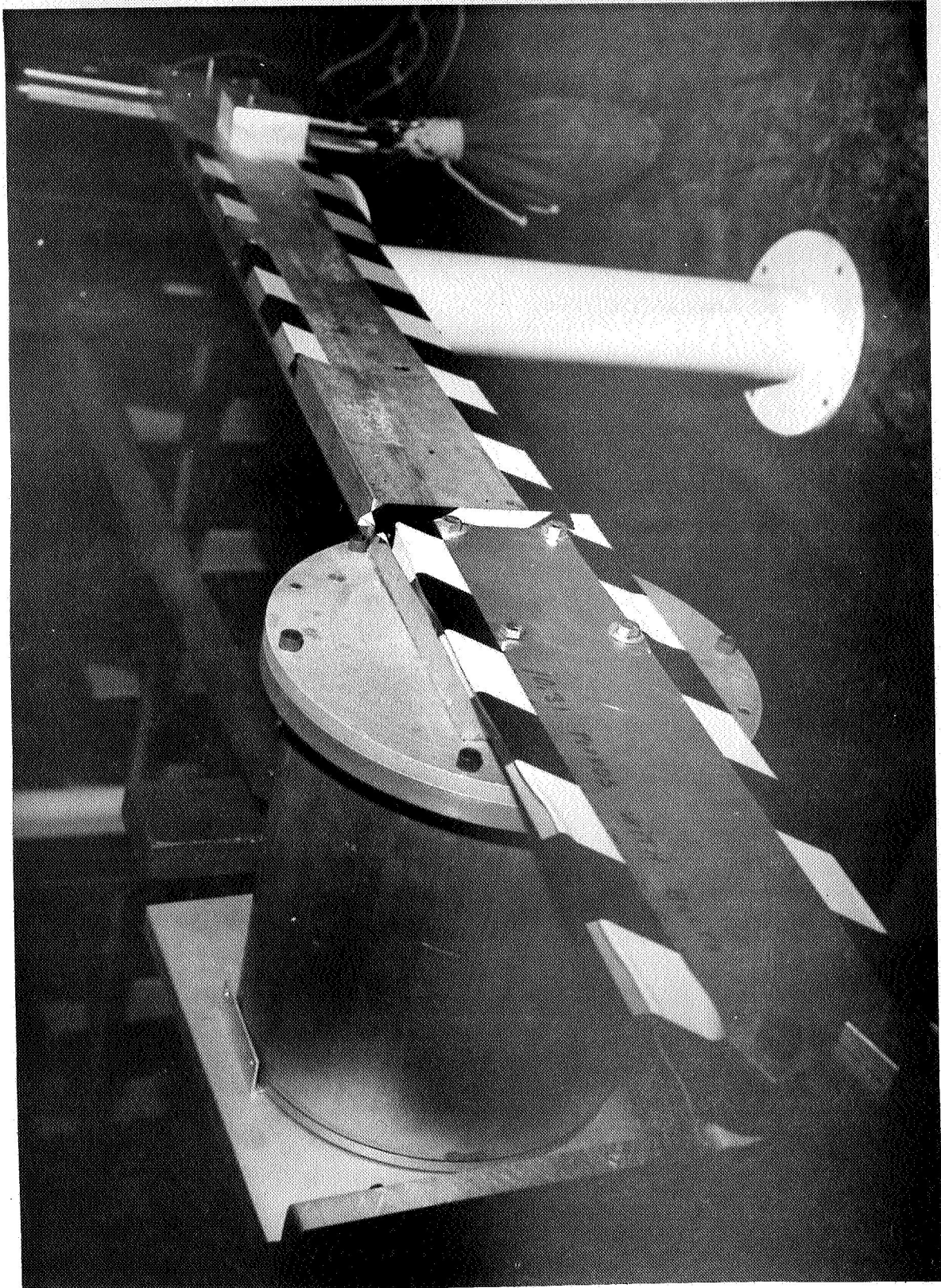


Figure IV-8 Internal Drive Under Low-Load Test

Static breakaway torque values over the full range of output torques applied to the drive were obtained by the following procedure.

- 1) Apply load to end of balance beam to simulate torque on drive output shaft,
- 2) Set height gage under pin located on end of balance beam,
- 3) Carefully add lead shot to container attached to cord on input pulley, and
- 4) When the dial indicator shows movement of the output weight, record the weight applied to the input side of the drive.

Static test results are plotted in Figures IV-9 through IV-13.

3) Dynamic Tests - A sample data sheet is shown in Table IV-3. Three tests were run at each output shaft load (50, 100, 150, 200 and 250 pounds). The drop weight was increased for each test to provide three different acceleration and velocity points. Each test was repeated four times, recording drop distance and time of drop. The average time and drop distance of the four drops was used for the analysis of each test.

By knowing the distance traveled by the input weight and in what time period, distance traveled and elapsed time can be computed for the input shaft, output shaft and output weight. From these times and distances, average accelerations, final velocities, dynamic torque, kinetic energy values and efficiencies can be determined for each individual component of the system.

Figure IV-14 a and b show two typical dynamic test setups.

Table IV-4 lists the mass moments of inertia. These inertias are reflected to the input shaft for forward driving and reflected to the output for backdriving.

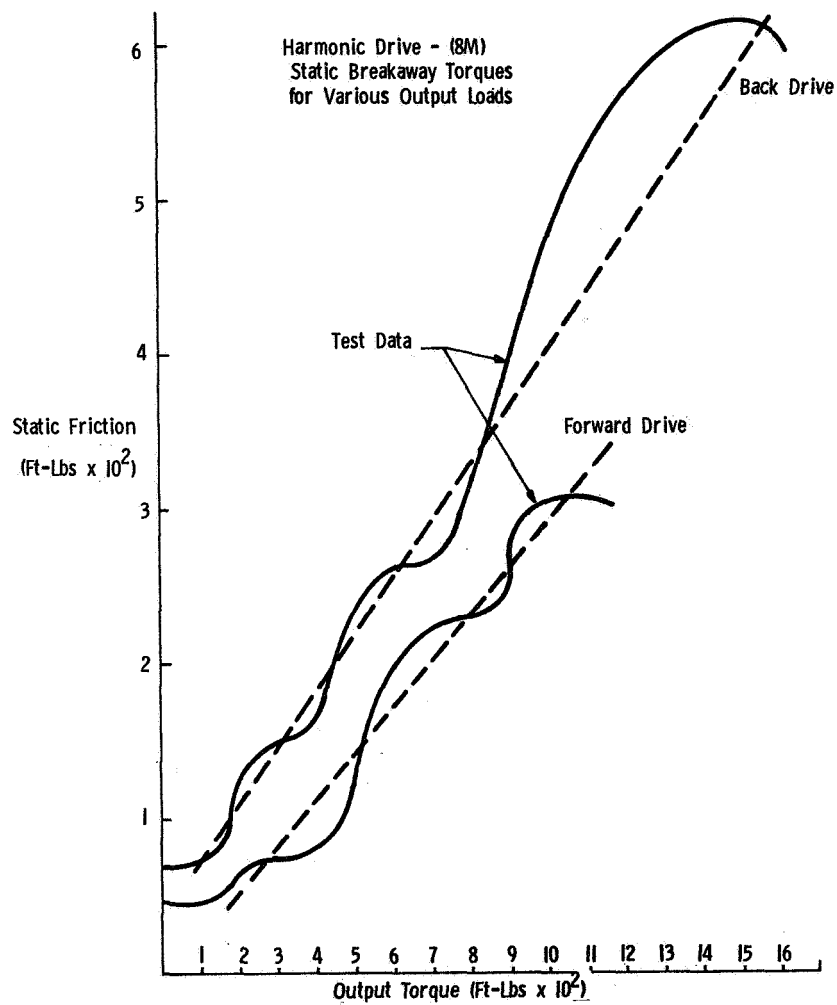


Figure IV-9 Harmonic Drive-Static Breakaway Torques



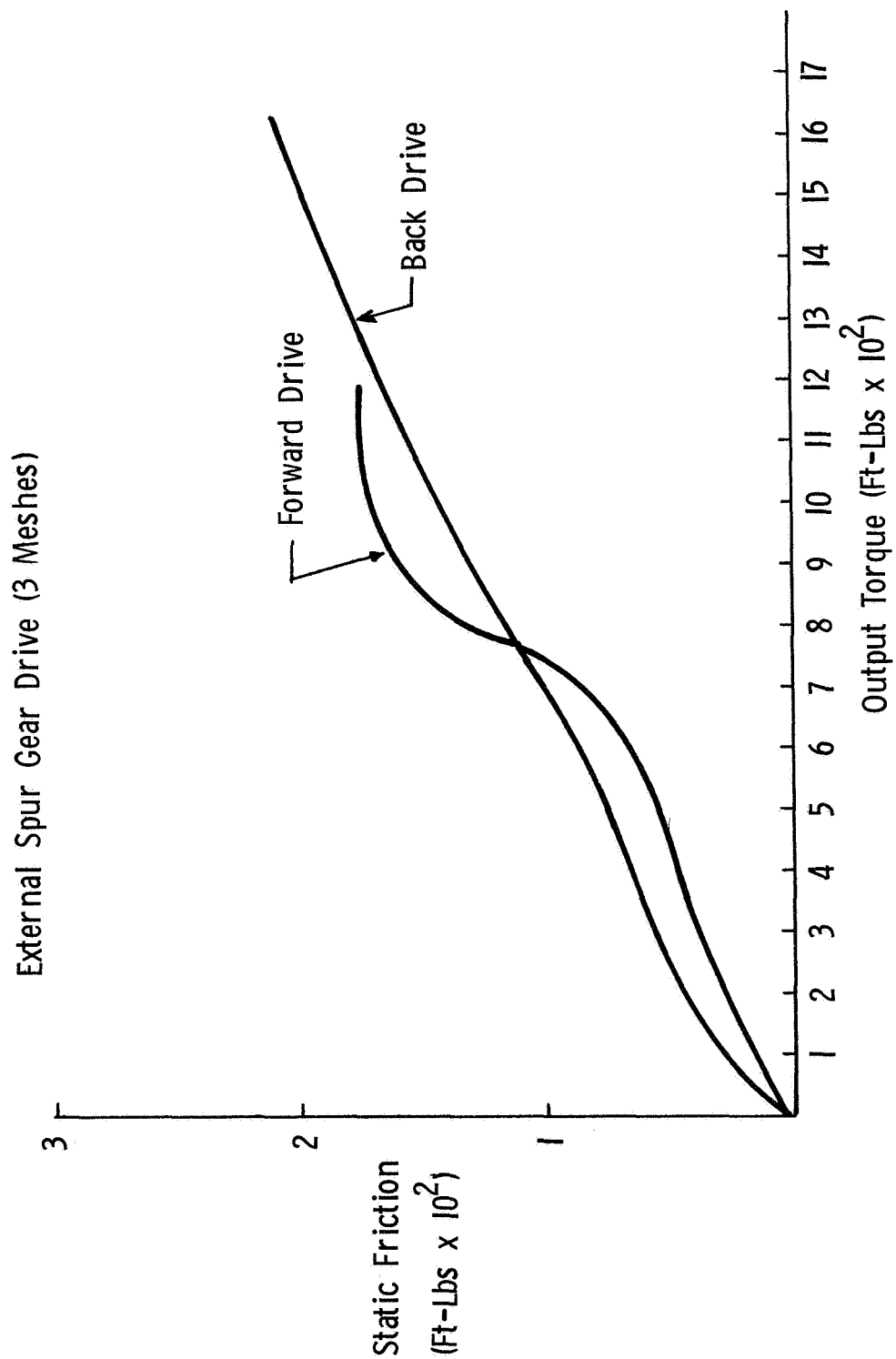


Figure IV-10 External Drive-Static Breakaway Torques

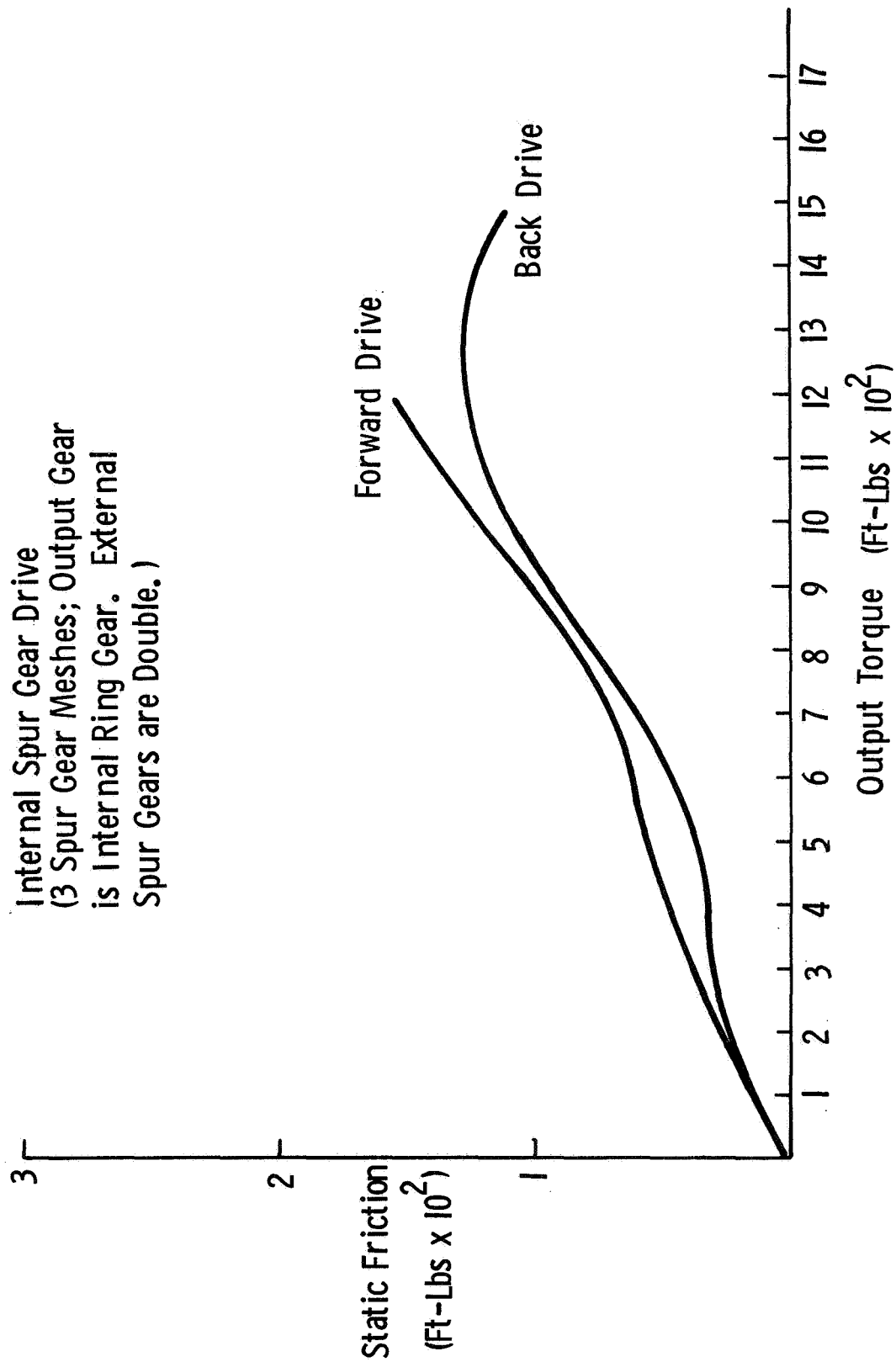


Figure IV-11 Internal Drive-Static Breakaway Torques

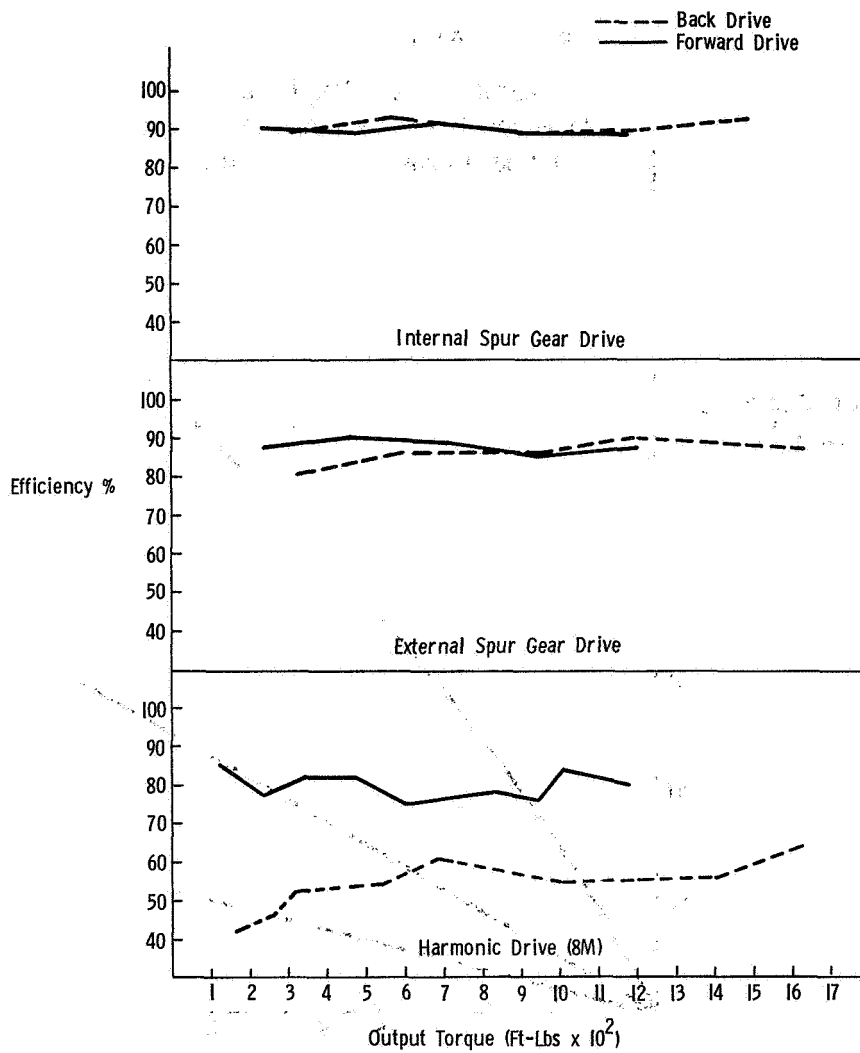


Figure IV-12 Static Breakaway Efficiencies

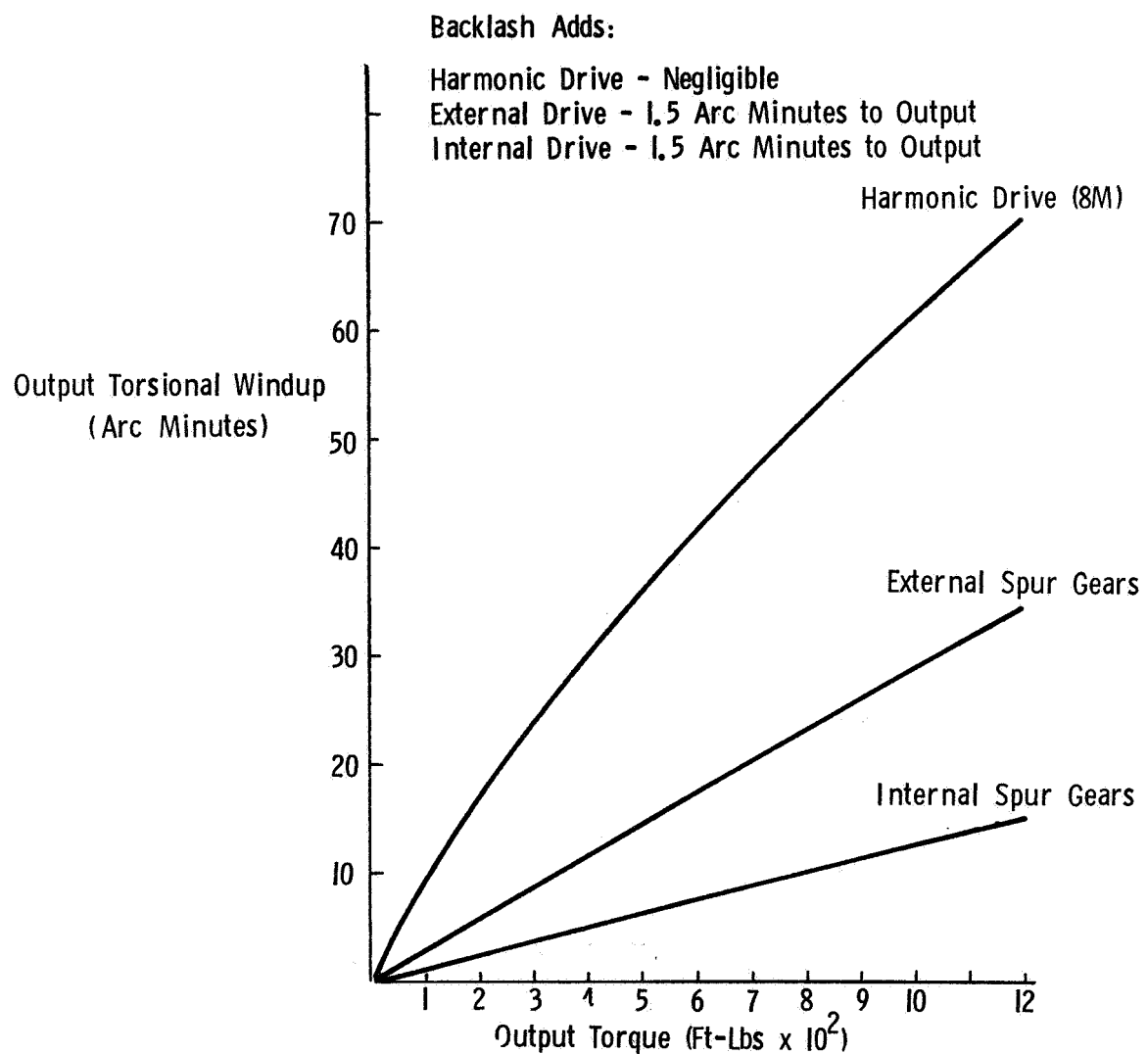


Figure IV-13 Torsion Deflection of Three Drives

Table IV-3 Sample Data Sheet - Dynamic Test

Harmonic Drive						
Measurement	#1	#2	#3	#4	#5	#6
Drop Weight(Pounds)	7.75	9.75	15.75	12.25	14.25	16.00
Output Weight(Pounds)	50	50	50	100	100	100
Drop Time (Sec) and Distance (Ft-In)	$\frac{2.313}{12' - 0''}$	$\frac{1.598}{12' - 0''}$	$\frac{1.163}{12' - 1/4''}$	$\frac{4.146}{12' - 1/2''}$	$\frac{2.106}{12' - 1/4''}$	$\frac{1.687}{12' - 3/4''}$
	$\frac{2.228}{12' - 1/2''}$	$\frac{1.609}{12' - 1/4''}$	$\frac{1.160}{12' - 0''}$	$\frac{3.725}{12' - 1/2''}$	$\frac{2.190}{12' - 1/4''}$	$\frac{1.780}{12' - 7/8''}$
	N/A	$\frac{1.590}{12' - 7/16''}$	$\frac{1.160}{12' - 0''}$	$\frac{3.796}{12' - 1/2''}$	$\frac{2.170}{12' - 1/2''}$	$\frac{1.756}{12' - 1/2''}$
	$\frac{2.143}{11' - 11 - 7/8''}$	$\frac{1.589}{12' - 5/8''}$	$\frac{1.172}{12' - 5/8''}$	$\frac{3.913}{12' - 1/2''}$	$\frac{2.162}{12' - 1/4''}$	$\frac{1.708}{12' - 1/2''}$
Average $\frac{\text{Time}}{\text{Dist}}$	$\frac{2.189}{12' - .232''}$	$\frac{1.597}{12' - .328''}$	$\frac{1.164}{12' - .219''}$	$\frac{3.895}{12' - .500''}$	$\frac{2.147}{12' - .312''}$	$\frac{1.733}{12' - .656''}$

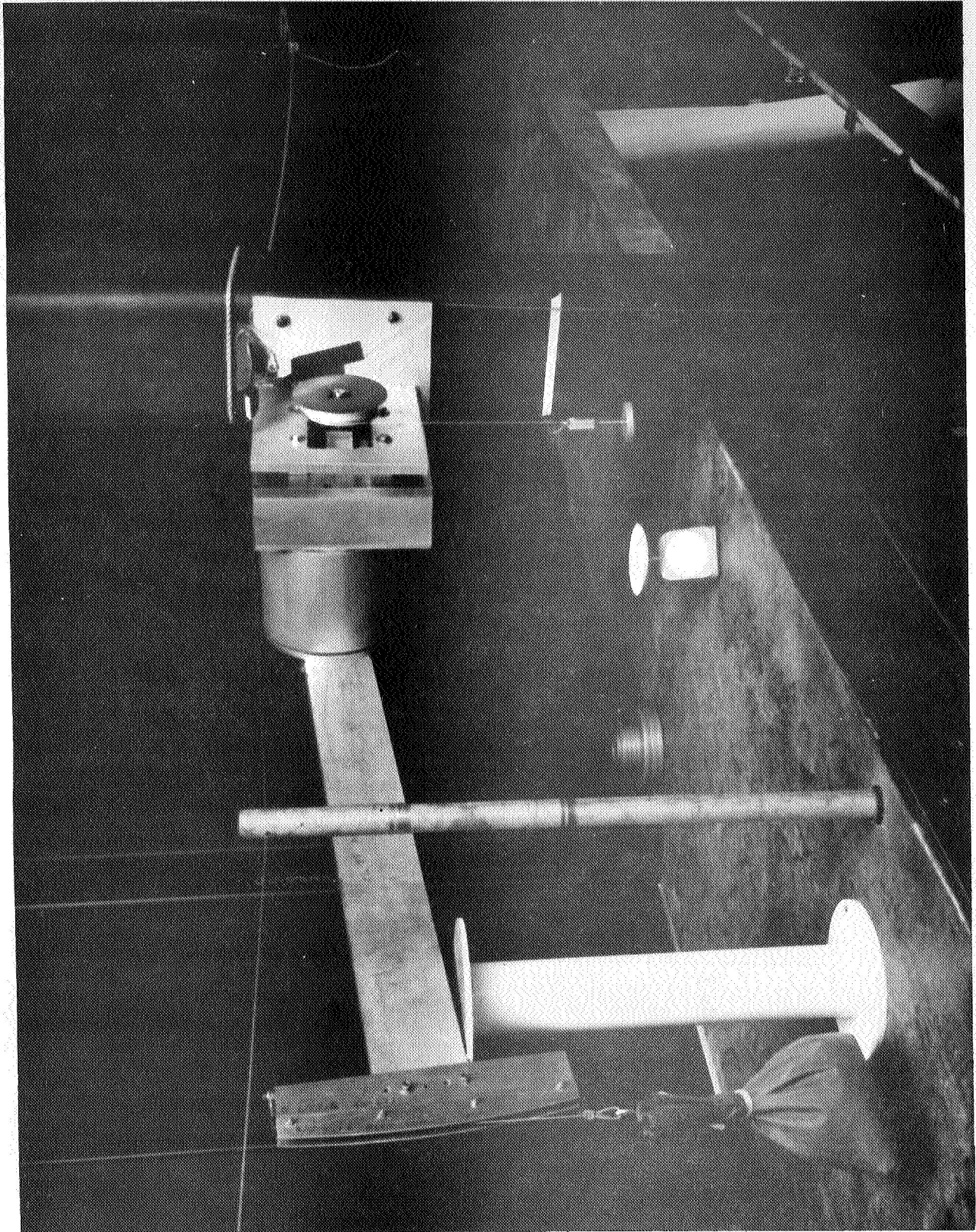


Figure IV-14a External Drive Under Low Load Dynamic Test



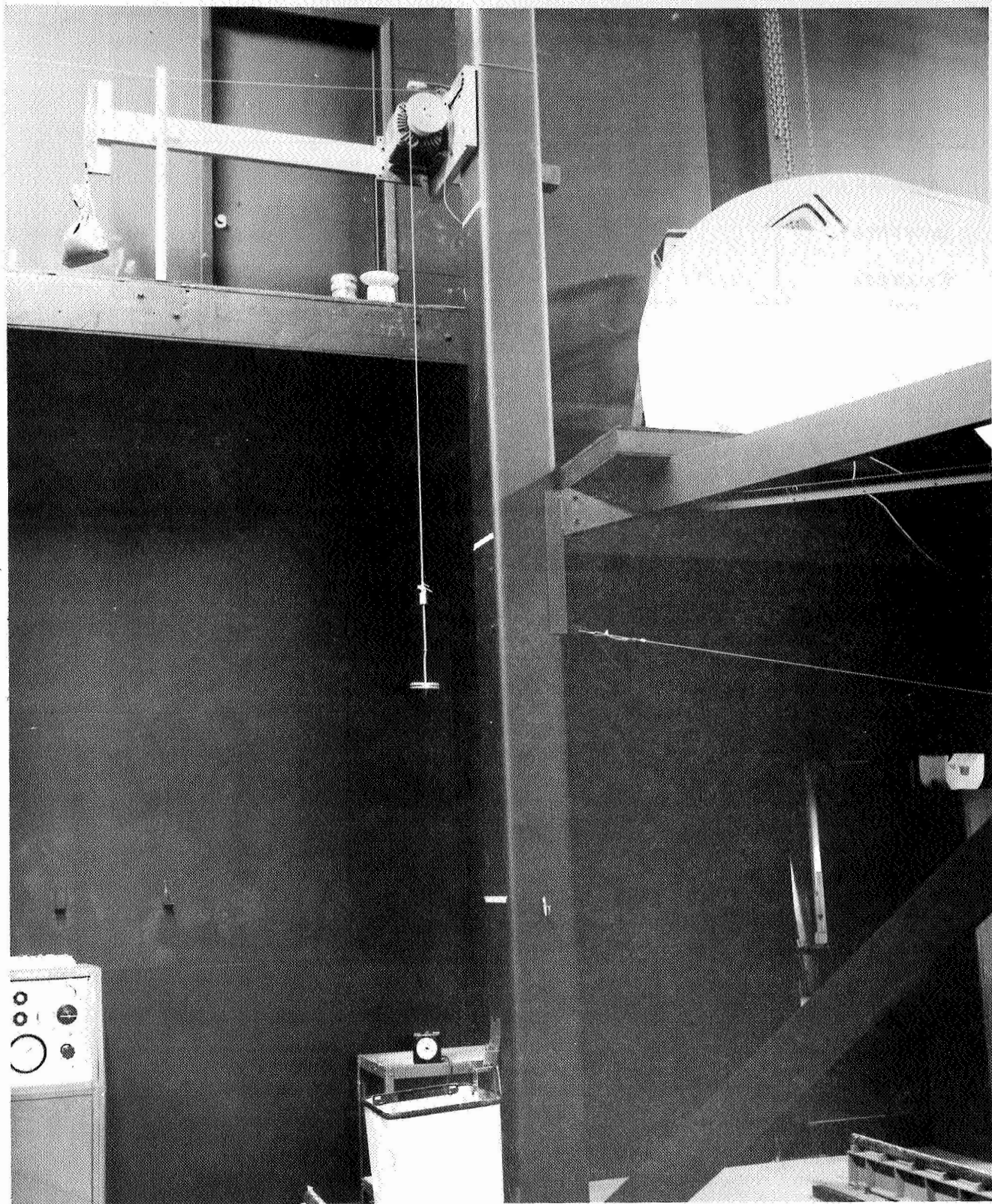


Figure IV-14b Test Set-up-Harmonic Drive During Acceleration Test

Table IV-4 Mass Moment of Inertia

Drive Type	Forward Drive (Slug-Ft <sup>2</sup> )	Back Drive (Slug-Ft <sup>2</sup> )
Harmonic	$.565 \times 10^{-2}$	226.006
Internal	$.2801 \times 10^{-4}$	1.11413
External	$.1755 \times 10^{-4}$	.6938

The mass moment of inertia of the balance beam and input pulley were calculated to complete the information necessary for energy balance and dynamic torque determinations.

Figures IV-15a through IV-15f show the dynamic data for all drives.

#### 4) Conclusions

Harmonic Drive - This drive requires approximately 30% additional torque be applied over actual output torque to overcome the static friction of the drive. This value applies regardless of the output load. At zero output load, 50 ft-lbs (output value) was required to initially move the drive. Periodic drag was noted at approximately every 15° of input shaft rotation. This drag could be referred to as cogging. As the drive was accelerated, the cogging effect was not as noticeable.

There was no detectable backlash associated with this drive. The spring deflection (windup) of the drive was substantial and is a serious characteristic to consider for its effect on the control system. At 1200 ft-lbs output torque applied, the input shaft turned approximately 235° before movement of the output shaft was detected. An angle of 235° at the input shaft represents 1° 10' windup at the output shaft. Part of this windup can be eliminated by increasing the diameter of the output shaft but the majority would remain as inherent to this type of drive. It has been proposed also that 50% reduction in windup could be accomplished by using a 3 lobe cam instead 2; and some additional lessening of windup by tightening cam fit.



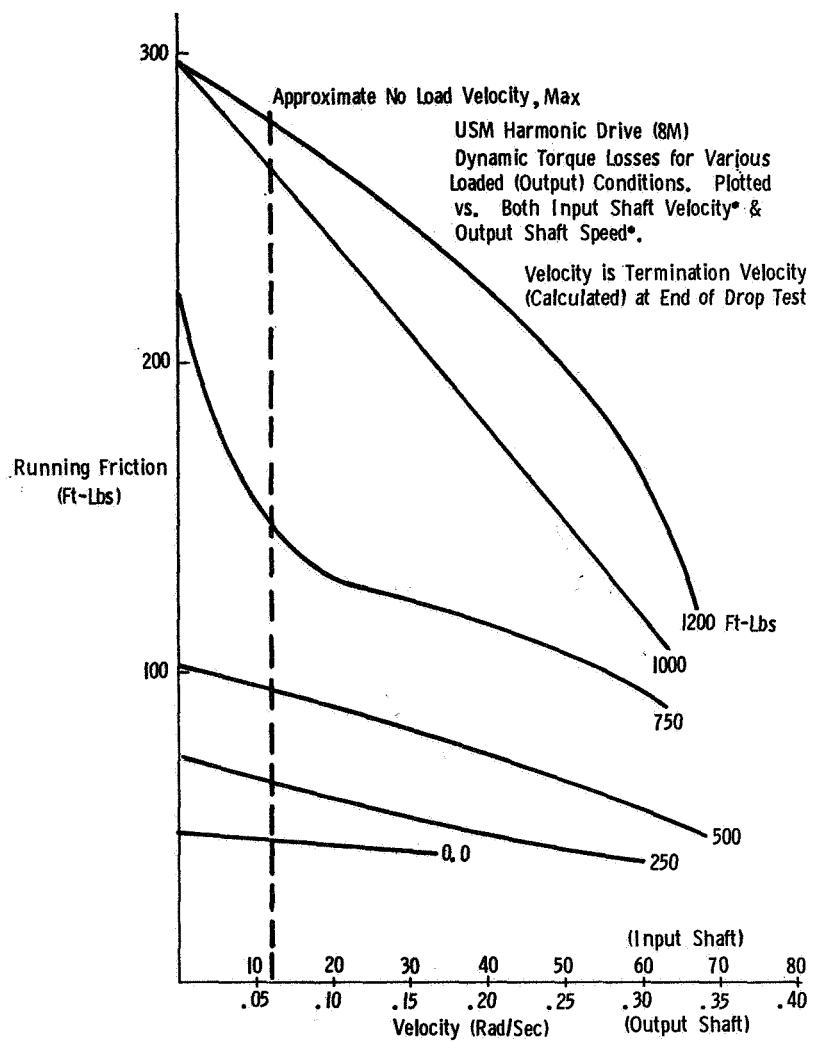


Figure IV-15a Harmonic Drive-Dynamic Torque Losses

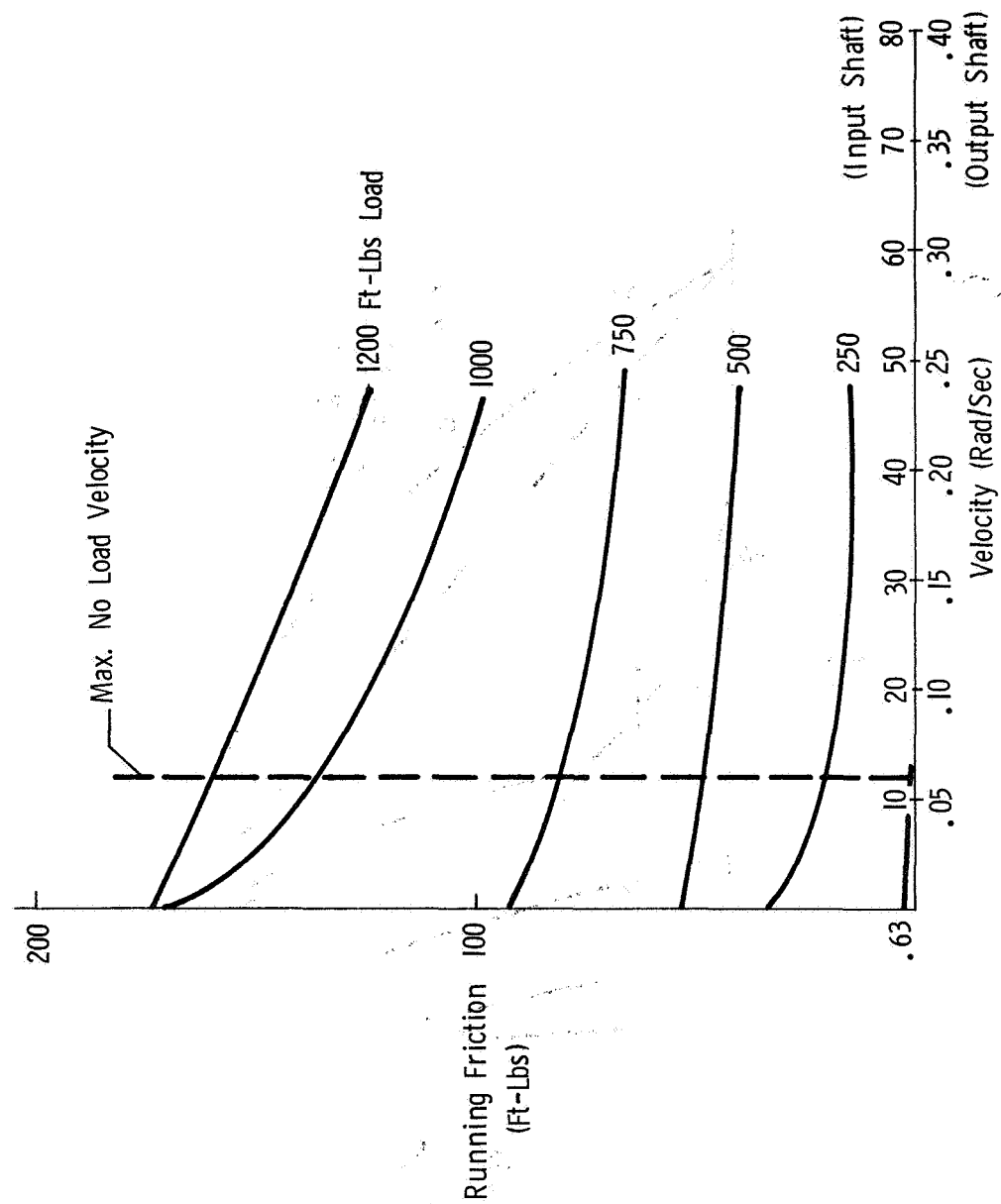


Figure IV- 15b External Drive-Dynamic Torque Losses

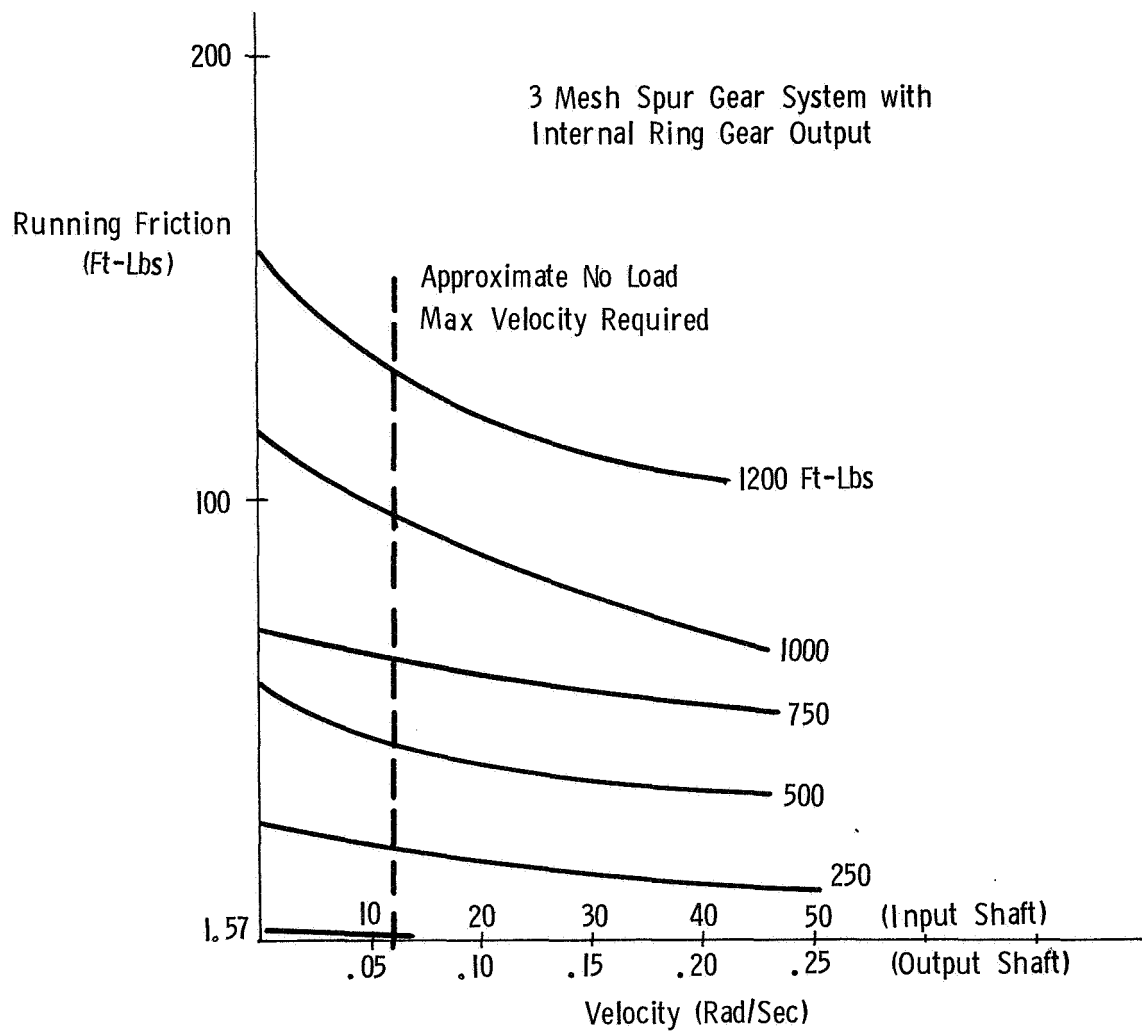


Figure IV-15c Internal Gear Drive-Dynamic Torque Losses

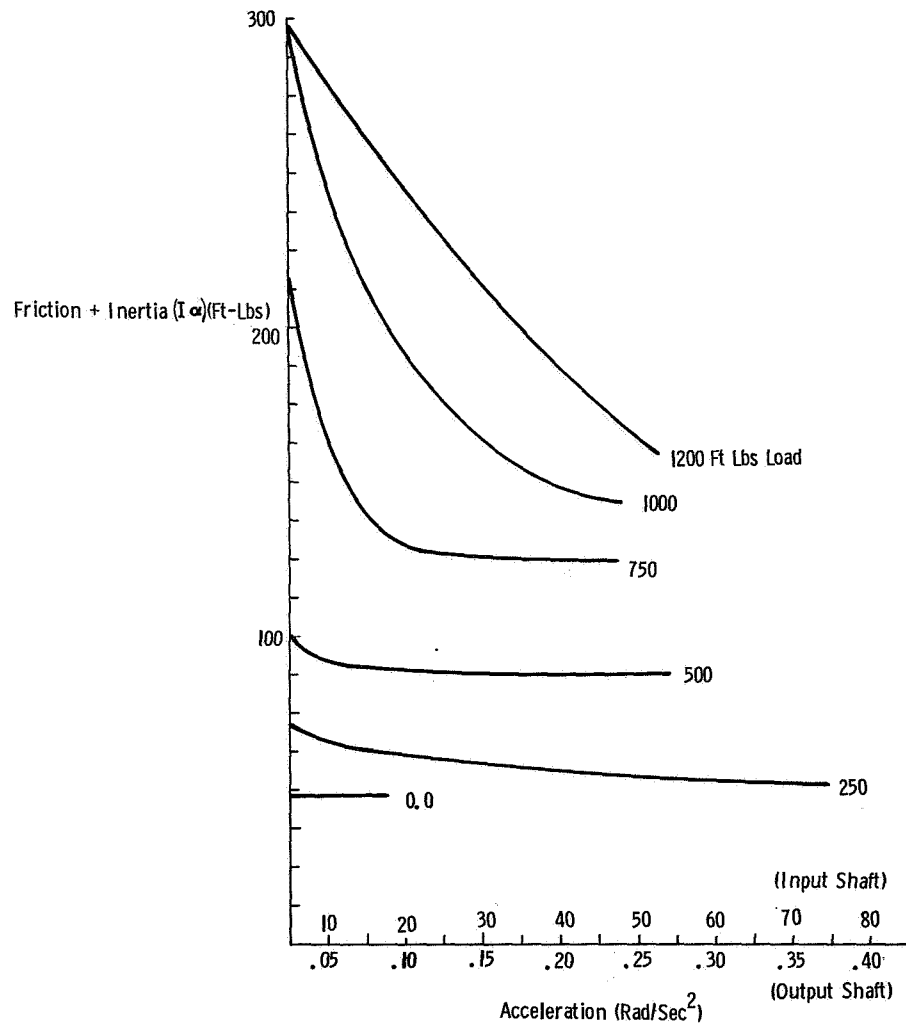


Figure IV-15d Harmonic Drive-Torque Losses

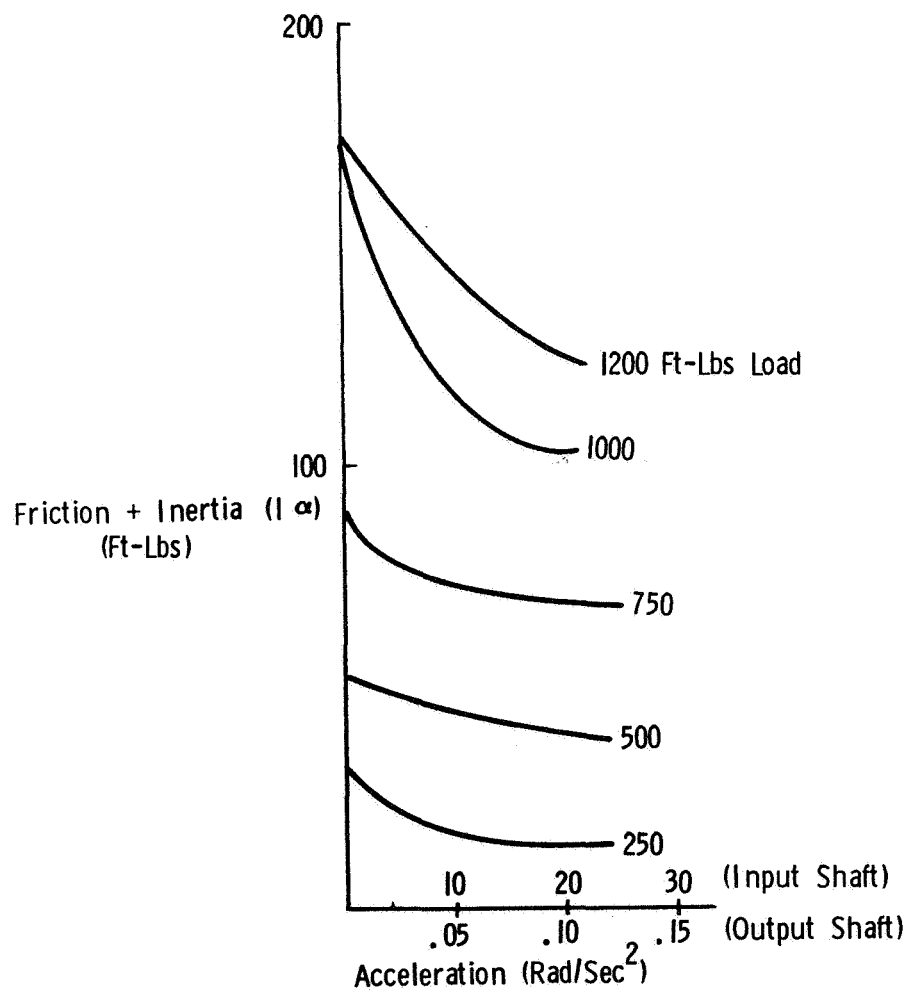


Figure IV-15e External Drive-Friction and Inertia Torque Losses

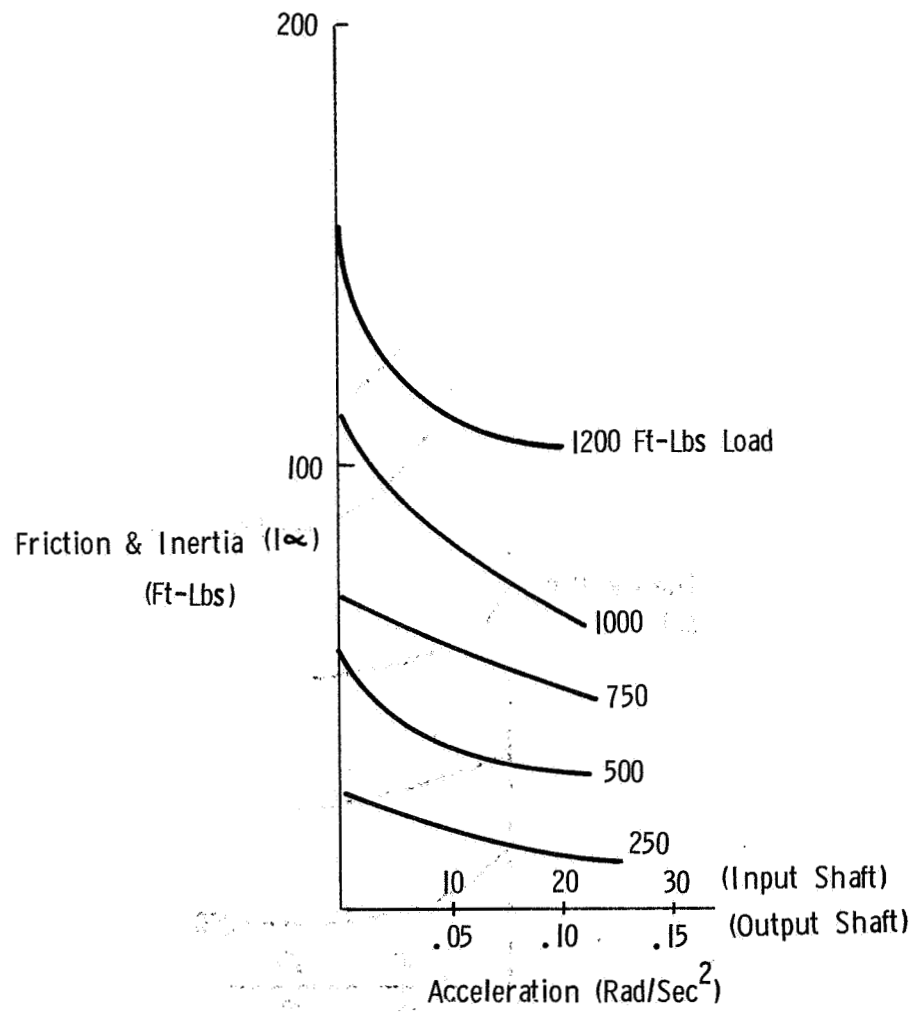


Figure IV-15f Internal Gear Drive-Torque Losses

The drive efficiency based on work-in vs work-out in the dynamic range is low in the low velocity range where this drive will be operated. With higher velocities, the efficiency improves to the 80 to 90% range.

At the higher velocities, frictional torque of the drive diminishes substantially from the static breakaway value. However, due to the high moment of inertia, torque to accelerate the gearing is high.

External Drive - The static breakaway friction of this drive was over 40% less than the harmonic drive. No cogging was observed. Torsional deflection at maximum output torque was 115° at the input shaft or 35 arc minutes at the output shaft. An evaluation of deflection shows that the majority of this is attributable to bearing deflection and looseness. Close tolerance, good quality angular contact or tapered bearings can improve this situation.

Backlash in this drive varied from 1.8 to 3.0 arc minutes at the output shaft. This variation is caused by gear eccentricities and bearing deflection. The drive was designed to allow for unlimited adjustment of the output gear to the pinion and minor adjustments in the other gear centers. During final assembly it was noted that the output spur gear was substantially eccentric. Backlash could be adjusted to a small angle only at one point on the gear.

Dynamic torque losses vary from 5% of the output torque at 250 ft-lbs to 10% at 1200 ft-lbs output torque. This is substantially less than the 20% figure for the Harmonic Drive at high and low output torques.

This drive exhibited excellent backdrivability characteristics. Static breakaway efficiencies were nearly as good during backdriving as forward driving. No cogging or draggy spots were noted.

Internal Drive - Improvement in the static and dynamic friction was noted over the external drive. Backdrive efficiencies were as good as the forward efficiencies. Backlash is 1.8 arc minutes at the output shaft (measured at the completion of the load tests). Torsional windup of about 15 arc minutes, less than half the external drive, was

the most noted difference over the external drive. As with the external drive, the use of close tolerance angular contact bearings will reduce this deflection even more. No cogging was noted.

The results of this test program clearly suggest that the double drive, internal spur gear system is the best choice of drive for the shoulder joint (and probably for all the joints) of the manipulator arm. In addition to the operational performance advantages of this drive, it can be packaged more compactly than the external spur gear system. The torque motor can easily be located within the drive housing.

### 3. Motor-Gear Ratio Selection Considerations

a. Introduction - To optimize the selection of the motor and gear ratio to be used at the shoulder and elbow gimbals of the 1-G manipulator, the following operational criteria were considered: 1. Power, 2. Speed, 3. Duty Cycle, 4. Friction, 5. Weight, and 6. Inertia. Each requirement is briefly discussed and curves are presented that depict the effect the requirement has on the motor-gear ratio selection. The included curves are drawn for 1200 ft lb (shoulder) and 650 ft lb (elbow) gear assemblies and consist of points that represent various Inland and Magtech DC torque motors that give, when combined with the indicated gear ratio, the desired stall torque value. Since the curves were generated from existing motor catalogue data, they can be used only to indicate general trends, and thus the effects a particular parameter has on the gear ratio selection cannot be definitely defined. The plotted data can be used only to bracket or give upper or lower bounds to the gear ratio that yields an acceptable motor-gear assembly.

The shoulder gimbal is considered first, and based upon the arguments presented herein, a recommended gear ratio and torque motor selection is presented. A brake compatible with the chosen motor is indicated and a suitable tachometer generator is selected via considerations and graphs similar to those used to determine the acceptable motor-gear ratio.

Curves applicable to the elbow gimbal are also presented and the elbow joint components are selected based upon results derived from the trends indicated by these curves.



## b. Shoulder 1200 lb Joint Assembly

### 1. Power

A General rule of thumb for the larger torque motors ( $> 6$  ft lbs) is to avoid output shaft powers greater than  $1/2$  the rated motor peak power. This precaution is a result of commutation problems that arise if shaft power exceeds  $1/2 P_p$ . If it is desired to apply 1200 ft lbs to a shaft rotating at 0.07 rad/sec, then a servo motor with a peak power rating of  $(2) \times (1200 \text{ ft lbs}) \times (0.07 \text{ rad/sec}) \times$

$$\left( \frac{1.3 \text{ watts}}{\text{ft lb/sec}} \right) = 218 \text{ watts must be used.}$$

Examining the gear train vs peak power curves for Inland and Magtech motors, it is seen that a gear ratio of 65:1 or less should be used with a Magtech motor.

It is also noticed from the curves that ratios of 70:1 or less should not be used with Inland motors to avoid servos with excess power ratings. Likewise, ratios of 10:1 or less should be avoided with Magtech motors to eliminate over designing.

Conclusions: Gear Train vs Peak Power curves indicate a general trend that reveals the following gear ratio bounds for the two motors considered:

- |            |                                  |
|------------|----------------------------------|
| 1. Inland  | 70:1 $\longleftrightarrow$ 170:1 |
| 2. Magtech | 10:1 $\longleftrightarrow$ 65:1  |

### 2. Speed

For the 1200 ft lb gear assembly under consideration, the maximum desired no load speed is 0.07 rad/sec. From the graphs of gear train vs output speed for the Inland and Magtech motors, it is seen that all gear ratios of 90:1 or less satisfy the speed requirement for Inland motors, and ratios of 77:1 or less satisfy the requirement for Magtech motors.

Note from the curves that as the gear ratio decreases, the output speed increases. At first thought, one might think that a lower gear ratio limit must be specified to avoid overdesign; this is, of course, true, but the limit must be derived from power considerations and not solely from the gear train vs speed curves.

Conclusion:

1. Inland  $\leq 90:1$

2. Magtech  $\leq 77:1$

3. Duty Cycle

Since a duty cycle criteria has not been established for the 1-G simulator, to meet any future duty cycle requirement a near 100% full torque on time must be designed for.

A general trend for D.C. servo motors is - the larger the motor the higher the duty cycle.

Thus, motors of at least a certain size must be selected to allow for even the most stringent operating conditions. Upon examining the duty cycle vs motor size curves, there appears to be a great difference between the duty cycles for Inland and Magtech.

This is actually not the case since the two companies differ in their laboratory procedures for measuring motor heat dissipation. Magtech claims to arrive at their  $^{\circ}\text{C}/\text{watt}$  ultimate temperature rise figures with the motor placed in a typical installation configuration, while Inland makes temperature measurements with the motor attached to no heat sink metal such as a shaft and housing.

Since the Magtech values are quoted to be "typical", it is assumed that Inland motors will yield comparable values under similar test conditions.

Examining the Magtach duty cycle curve, it appears that a motor capable of 12 ft lbs stall torque or greater should be selected to assure a 100% or greater duty cycle. This requirement results in a gear train ratio of 100:1 or less for a 1200 ft lb gear assembly.

Conclusion:

1. Magtech  $\leq 100:1$

#### 4. Friction

Friction in D.C. torque motors has two sources: 1. brush commutator friction and 2. magnetic retarding torques (such as hysteresis drag and cogging). Brush drag accounts for 20-40% of the total friction with magnetic effects contributing the other 60-80%. Magtech motors have slightly higher magnetic friction which is a result of their design philosophy to build motors with a high torque to weight ratio .

Observing the Gear Train vs Friction curves for a 1200 ft lb gear assembly, it is seen that friction levels at the output gear shaft are fairly independent of gear ratio for ratios between 4:1 and 90:1.

Although as stated above, Magtech does have higher friction levels, no general trend from either curve is noticed and therefore no conclusions will be drawn on restrictions as to gear ratio.

#### 5. Weight

Although the larger the torque motor the greater the weight is an obvious fact; when the weight of motor and gear train are considered together for a 1200 ft lb gear assembly, a definite trend develops. As noticed from the Gear Train vs Weight curves for Magtech and Inland motors, gear ratios greater than 35:1 and less than 200:1 produce a total gear assembly weight that is almost gear ratio invariant. Below a 35:1 ratio the total assembly weight starts to increase rapidly. These two facts are a consequence of gear weight dominance for high gear ratios and motor weight dominance for low gear ratios. The former fact of a dominant gear weight yielding a constant total assembly weight is a result of the large output gear weight being fairly independent of the gear ratio for ratios between 35:1 and 200:1 for Inland and 55:1 and 200:1 for Magtech.

##### Conclusion:

1. Magtech  $\geq 55:1$
2. Inland  $\geq 55:1$

#### 6. Inertia

The inertia of the motor rotor is reflected to the output

gear shaft as a function of the square of the associated gear ratio. For a 1200 ft lb gear assembly, it is seen from the Gear Train vs Inertia curves that the reflected rotor inertia for Inland and Magtech motors does not increase rapidly as the gear ratio is increased from 30:1 to 90:1, but remains fairly constant due to the smaller rotor inertias for the smaller motors. At first this result would seem to indicate that a gear ratio between 30:1 and 90:1 would be optimal from the inertia standpoint. Although this is partially true, the value of this optimization fades when the reflected motor inertia is compared with the load inertia. For the 1200 ft lb shoulder gear assembly under consideration, the unloaded arm<sub>4</sub> inertia about the shoulder joint is approximately  $1.03 \times 10^4$  ft lb sec<sup>2</sup> and the loaded arm inertia is approximately  $3.2 \times 10^6$  ft lb sec<sup>2</sup>. When these numbers are compared with the average reflected motor<sub>2</sub> inertia for gear ratios between 30:1 and 90:1 of 70 ft lb sec<sup>2</sup>, it is realized that even the unloaded arm presents inertia loads two orders of magnitude greater than the reflected motor inertia. Therefore, any optimization restriction on gear ratio values with respect to motor inertia is somewhat superficial.

Conclusion: For gear ratios less than 90:1, reflected motor inertia is insignificant with respect to load inertias.

## 7. Summary

Criteria	Indicated Gear Ratio Range
1. Power	Inland: 70:1 ↔ 170:1 Magtech: 10:1 ↔ 65:1
2. Speed	Inland: Less than 90:1 Magtech: Less than 77:1
3. Duty Cycle	Inland: Less than 100:1 Magtech: Less than 100:1
4. Friction	No conclusions
5. Weight	Inland: Greater than 35:1 Magtech: Greater than 55:1
6. Inertia	Inland: Less than 90:1 Magtech: Less than 90:1

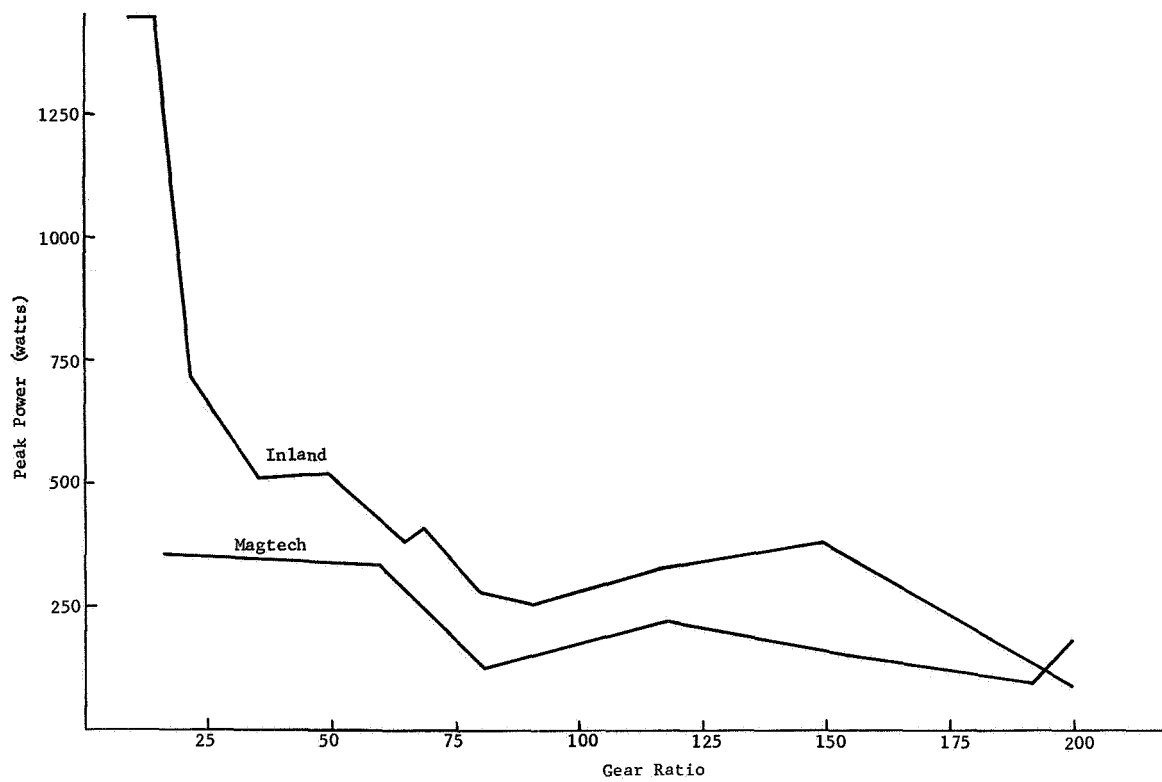


Figure IV-16 Gear Ratio vs Peak Power, 1200 ft lb Gear Assembly

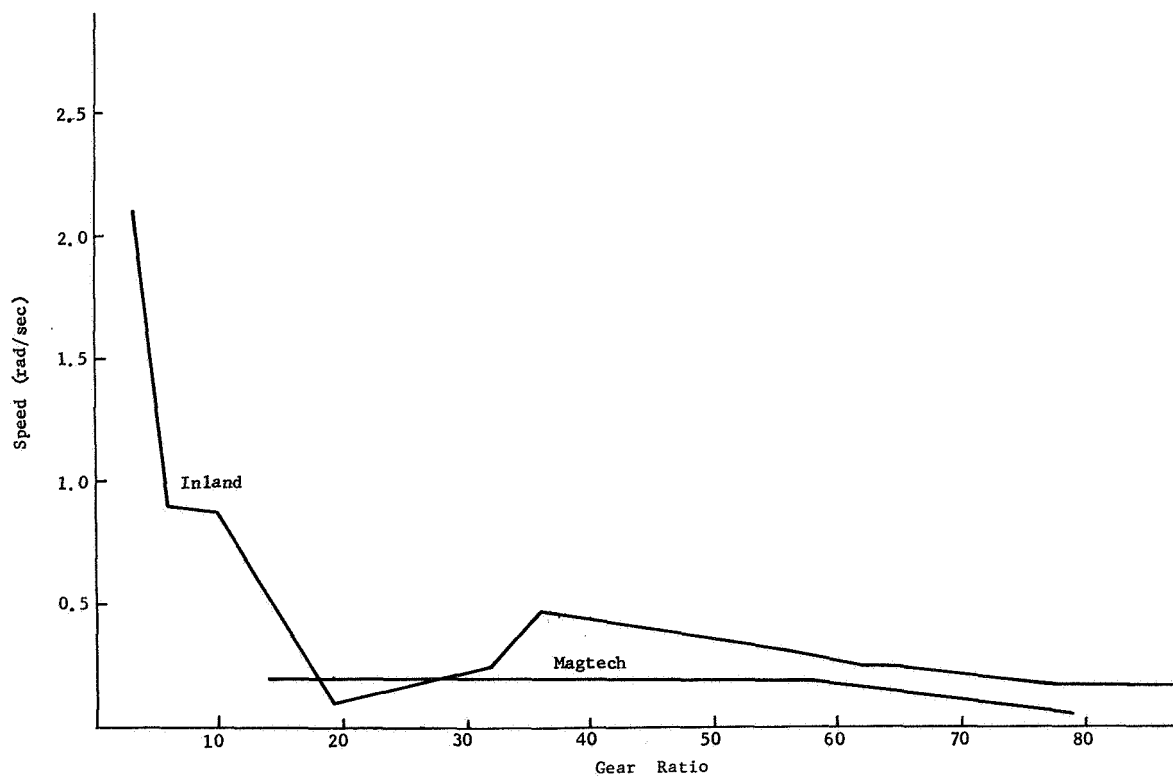


Figure IV-17 Gear Ratio vs Output Speed, 1200 ft lb Gear Assembly

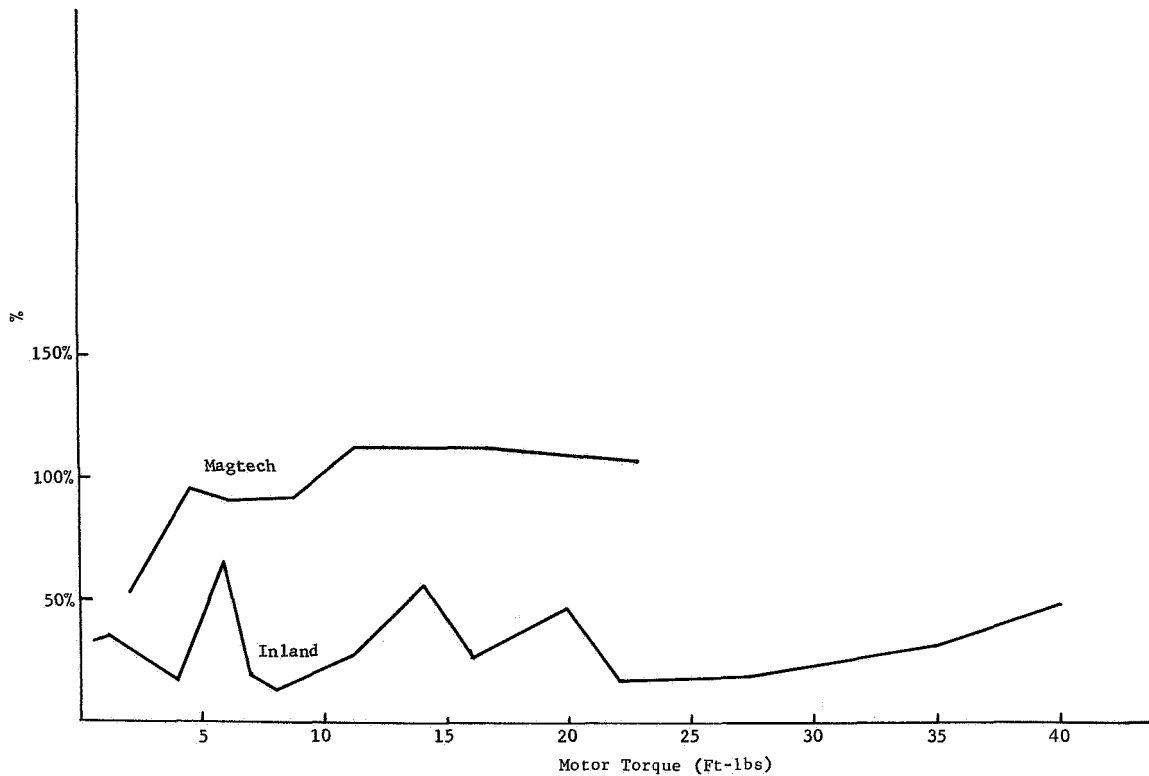


Figure IV-18 Duty Cycle vs Motor Torque, 1200 ft lb Gear Assembly

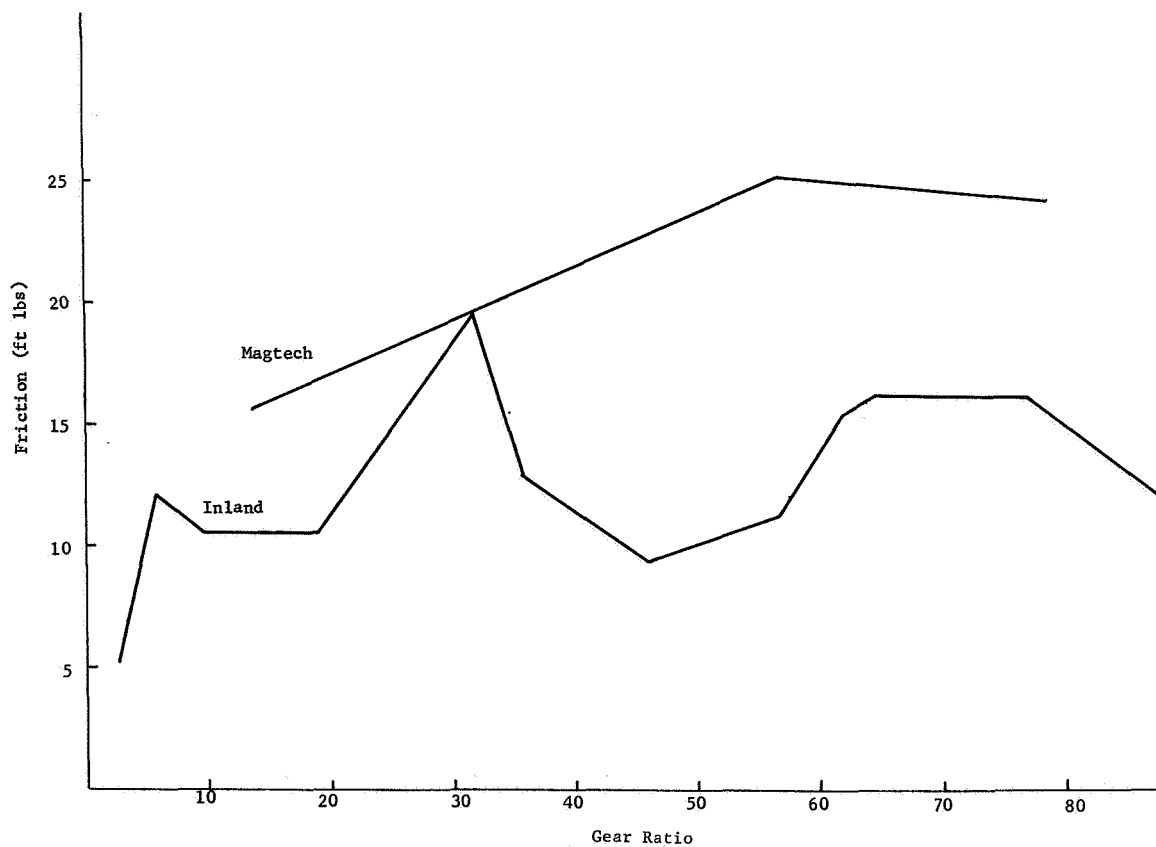


Figure IV-19 Gear Ratio vs Friction, 1200 ft lb Gear Assembly

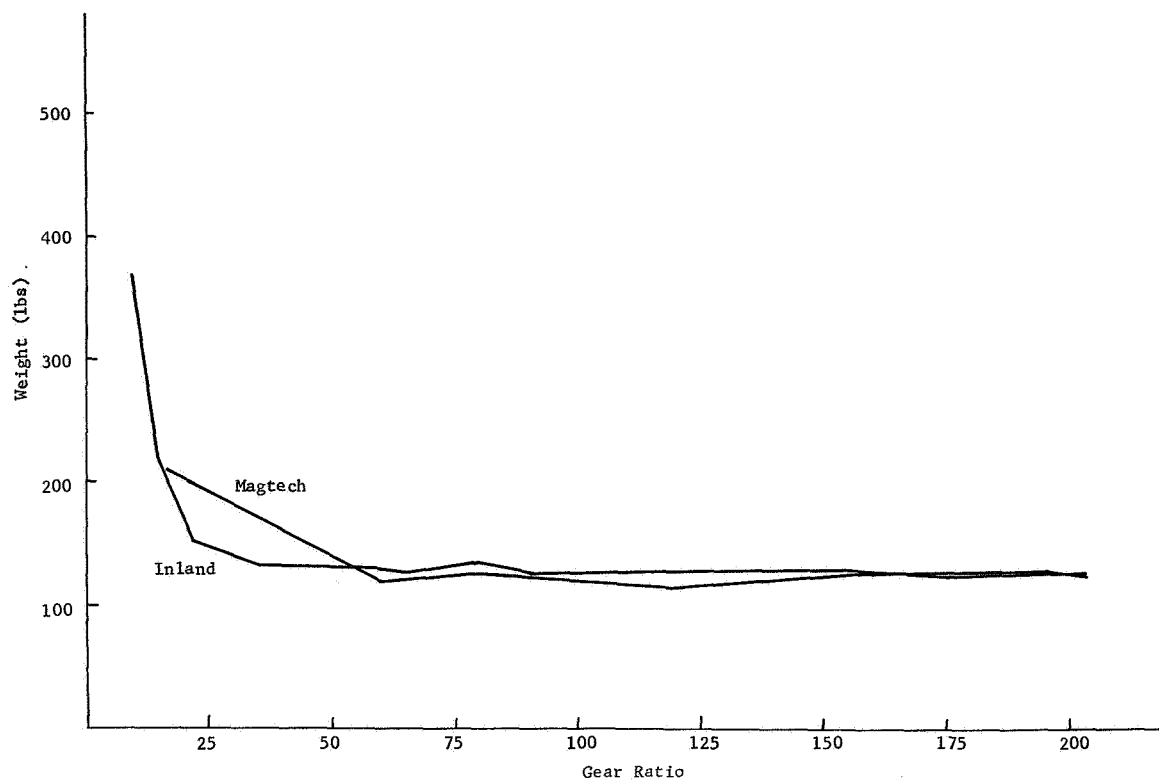


Figure IV-20 Gear Ratio vs Joint Weight, 1200 ft lb Gear Assembly

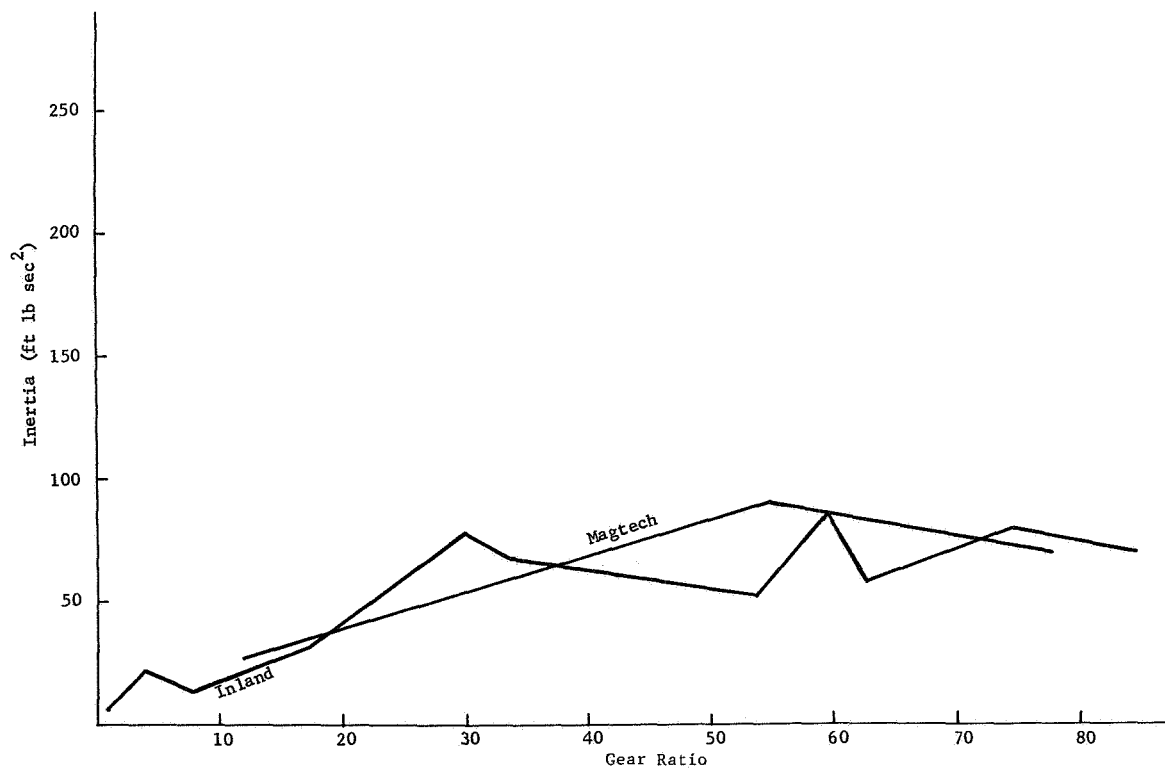


Figure IV-21 Gear Ratio vs Reflected Inertia, 1200 ft lbs Gear Assembly

Attempting to average these results for all the criteria yields,

Motor Brand	Indicated Gear Ratio Range
Inland	70:1 $\longleftrightarrow$ 90:1
Magtech	55:1 $\longleftrightarrow$ 65:1

It is reiterated once again these results are based only on trends and do not represent a hard fast rule.

In an attempt to pick one brand of motor over the other, it is remembered that Magtech has higher torque to weight ratios and Inland has lower static friction torque values. Since it was shown that for gear ratios greater than 55:1 the gear weight was dominant, it appears that variations in motor weight are insignificant for this range of gear ratios. Thus it is suggested that Inland motors be selected on the basis of their providing somewhat lower magnetic cogging.

#### Motor, Gear Selection

Using the above information as a guide, the following motor, gear selection is offered as a candidate for one of the 1200 ft lb shoulder joints of the 1-G simulator.

Gear Ratio: 85.7:1

D.C. Torque Motor: Inland T-5745

No load speed:	14 rad/sec
Motor friction:	0.15 ft lbs
Motor inertia:	0.01 ft lbs sec <sup>2</sup>
Motor peak power:	274 watts
Motor temp. rise:	1.3°C/watt
Motor weight:	15 lbs
Motor constant:	0.88 ft lb/ watt
Motor power rate:	19600 ft lbs/sec <sup>2</sup>
OD:	7.2 inches
ID:	3.95 inches



Motor-Gear Assembly:

Stall torque: 1200 ft lbs  
Max. output speed: 0.16 rad/sec  
Reflected friction: 12.8 ft lbs  
Reflected inertia: 73.4 ft lbs sec<sup>2</sup>  
Total weight: 124 lbs

Brake: Simplatrol PMB-103

Holding torque: 16.6 ft lbs  
Weight: 3.8 lbs

c. Tachometer Generator Considerations - Upon comparing Inland and Magtech tachometer generators there appears to be no outstanding advantage of one brand over the other. Although only Magtech generators are considered below due to a more extensive Magtech tach generator catalogue, this by no means implies that an Inland product would not be suitable.

The various tach generator parameters discussed below are compared as a function of a maximum generator speed since this is the most well defined parameter in the selection process. For the motor-gear train selected previously, the no load motor speed is 14 rad/sec. Tach generators having maximum speed capabilities slightly less and slightly greater than this value are considered to reveal general trends in the various parameters.

1) Sensitivity - It is seen from the Max. Speed vs Sensitivity curve that the generator sensitivity rises sharply for max. speeds below 15 rad/sec. Since a high sensitivity is desirable, it is concluded that a tach generator with the lowest possible maximum speed that is compatible with the torque motor selection should be used.

2) Weight - From the Max. Speed vs Weight curve the general trend indicates the lower the maximum speed the greater

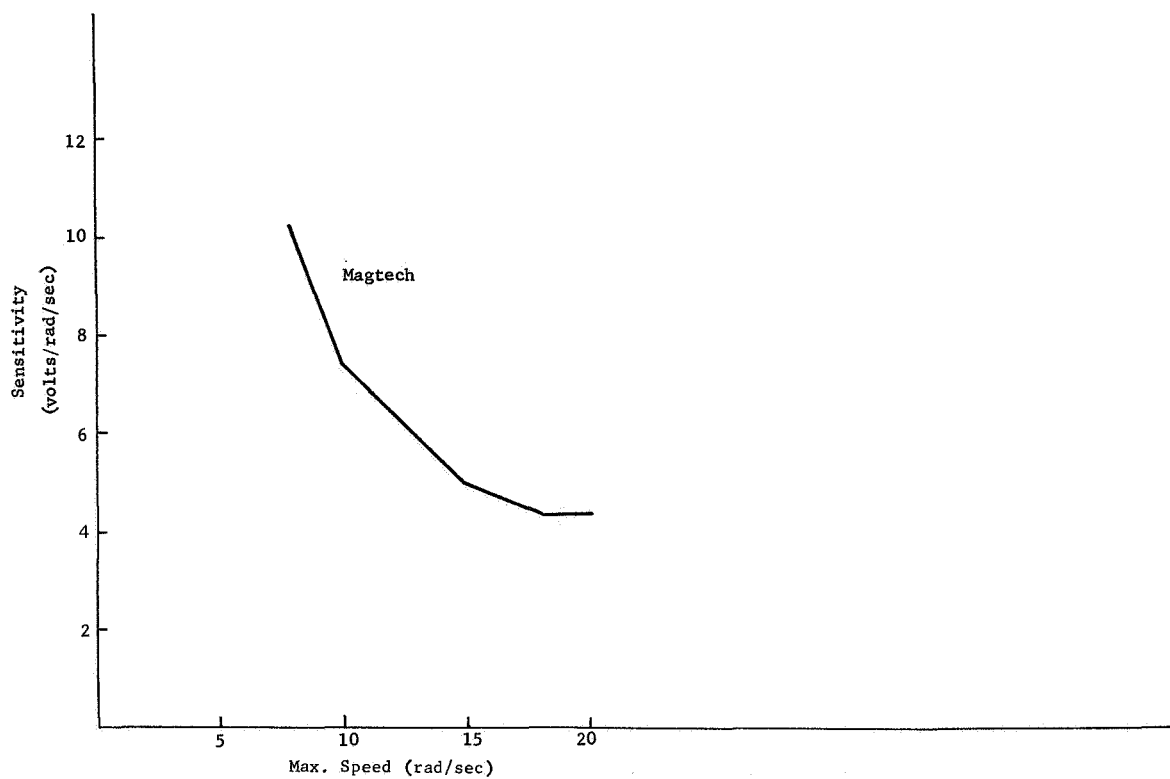


Figure IV-22 Maximum Speed vs Sensitivity

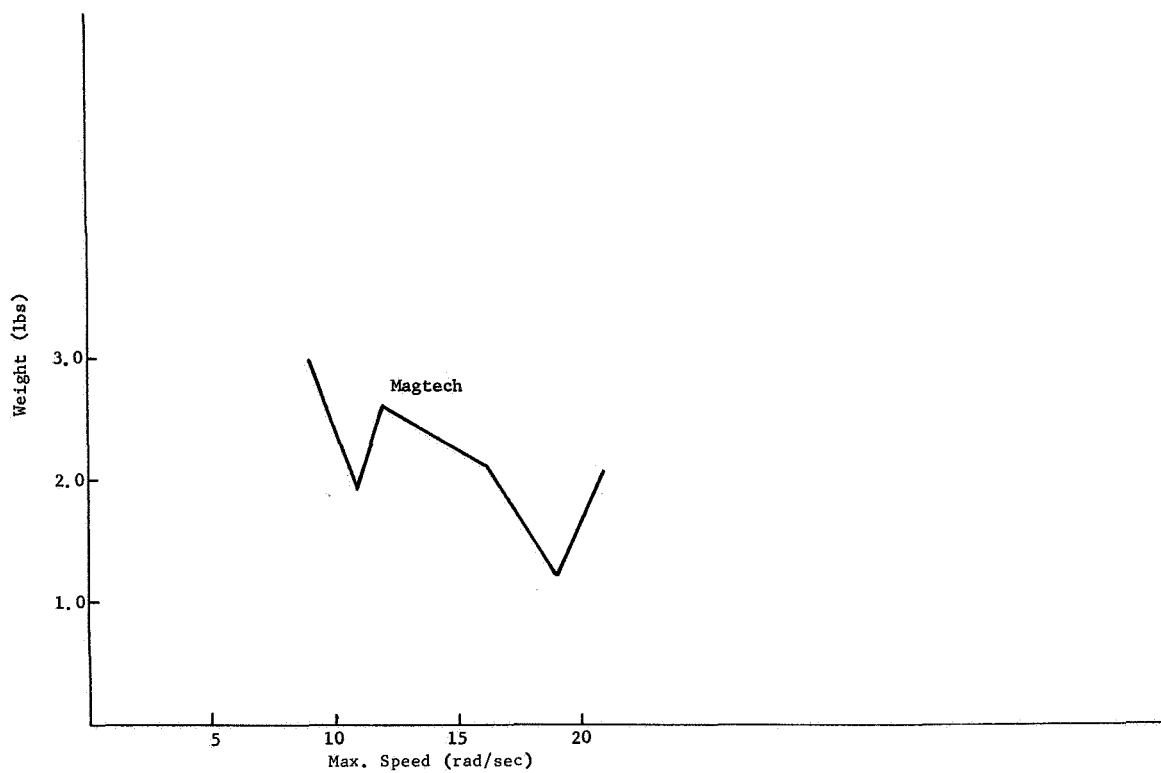


Figure IV-23 Maximum Speed vs Weight

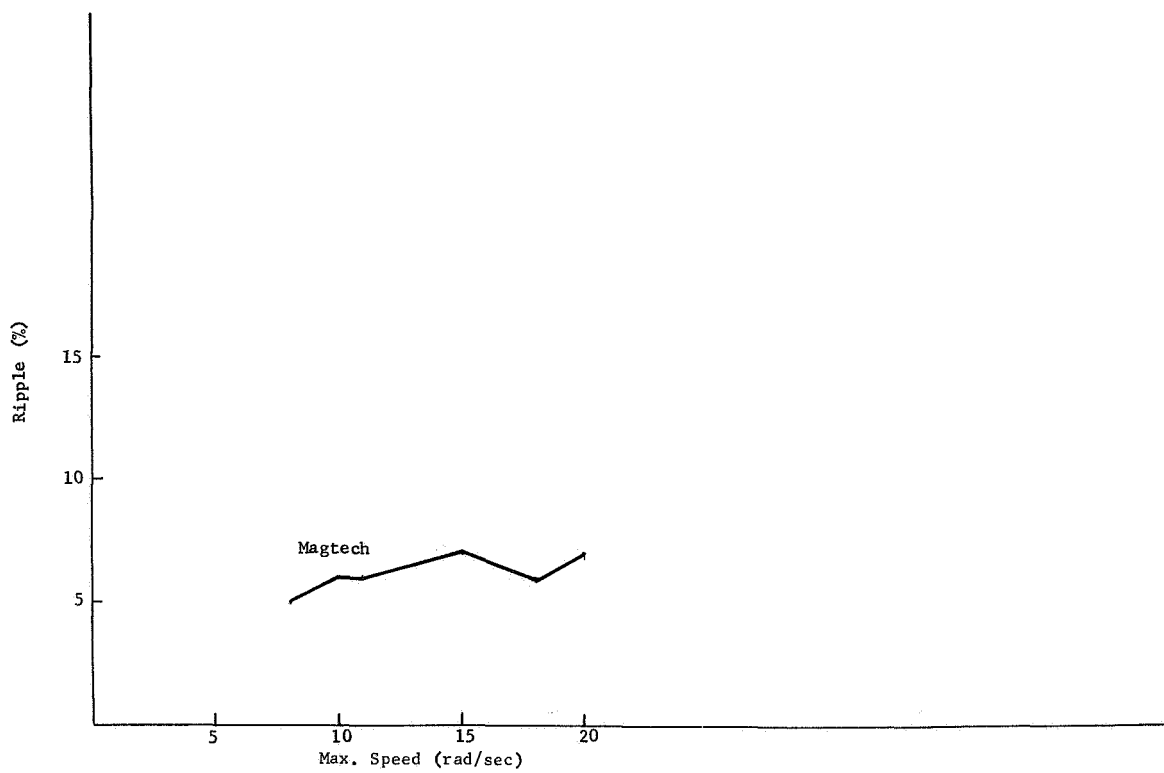


Figure IV-24 Maximum Speed vs Ripple

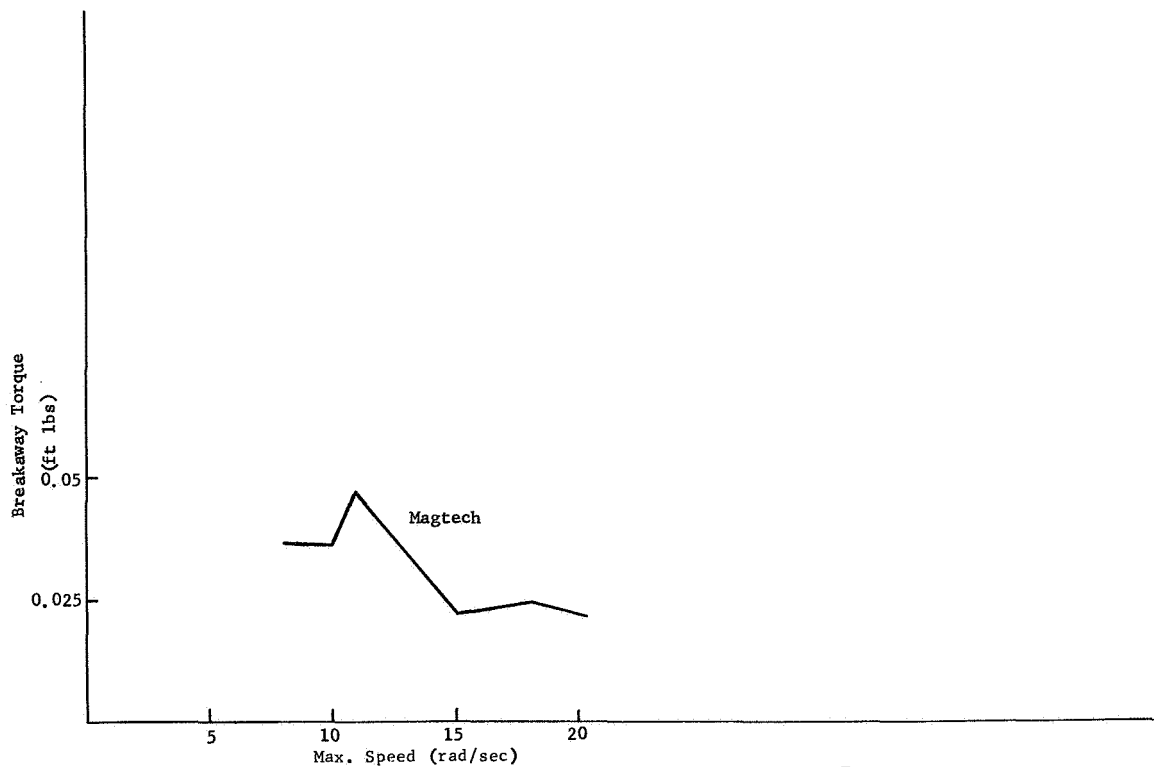


Figure IV-25 Maximum Speed vs Breakaway Torque

the weight. This seems to indicate a high speed generator should be used to minimize weight, although this is true to some extent, the tach weight is negligible compared to the total gear assembly weight, and therefore weight conservation is not a dominant factor for generator selection.

3) Ripple - The Max. Speed vs Ripple curve indicates that ripple varies only between 5 to 7% for max. speed values between 8 and 20 rad/sec. Therefore % ripple does not appear to be a limiting factor.

d. Breakaway Torque - The Max. Speed vs Breakaway Torque curve reveals that generally higher speed tachs have a lower static friction value. Although this seems to indicate a high speed generator should be selected with respect to friction torque, it is noted that breakaway torque differs only by 0.025 ft lbs for speed ranges between 8 and 20 rad/sec and the total friction values range only between 0.02 and 0.047 ft lbs. These values compared with a motor friction of 0.14 ft lbs are small, and therefore breakaway torque does not constitute a major parameter to be optimized.

#### 4. Summary

From the above discussion, it is believed that sensitivity is the dominant parameter in the selection of a tachometer generator. Since sensitivity varies inversely with maximum speed, a generator should be picked that has a max. speed compatible with the selected torque motor no load speed. As an example, and this is by no means unique, of a tachometer that meets the above criteria, the following selection is offered.

#### Tachometer Generator: Magtech 3730B-134

Max. Speed:	15 rad/sec
Sensitivity:	5.0 V/rad/sec
Ripple:	7%
Breakaway Torque:	0.021 ft lbs
Moment of Inertia:	0.00031 ft lb sec <sup>2</sup>
Weight:	2.06 lbs
OD:	3.73 inches
ID:	1.34 inches

Elbow 650 ft lb Joint Assembly - The elbow gimbal components were chosen in the same fashion as were those of the shoulder. The following curves show the relationship between gear ratio and:

1. Power
2. Speed
3. Duty Cycle
4. Friction
5. Weight
6. Inertia
7. Motor outside diameter

The trends of these curves indicate the following criteria - gear ratio relationships.

<u>Criteria</u>	<u>Indicated Gear Ratio Range</u>
1. Power	Inland: less than 144:1 Magtech: less than 35:1
2. Speed	Inland: less than 100:1 Magtech: less than 40:1
3. Duty Cycle	Inland: no conclusion Magtech: no conclusion
4. Friction	Inland: less than 94:1 Magtech: less than 86:1
5. Weight	Inland: greater than 35:1 Magtech: greater than 35:1
6. Inertia	Inland: less than 144:1 Magtech: less than 100:1
7. Motor Outside Diameter	Inland: greater than 44:1 Magtech: greater than 40:1

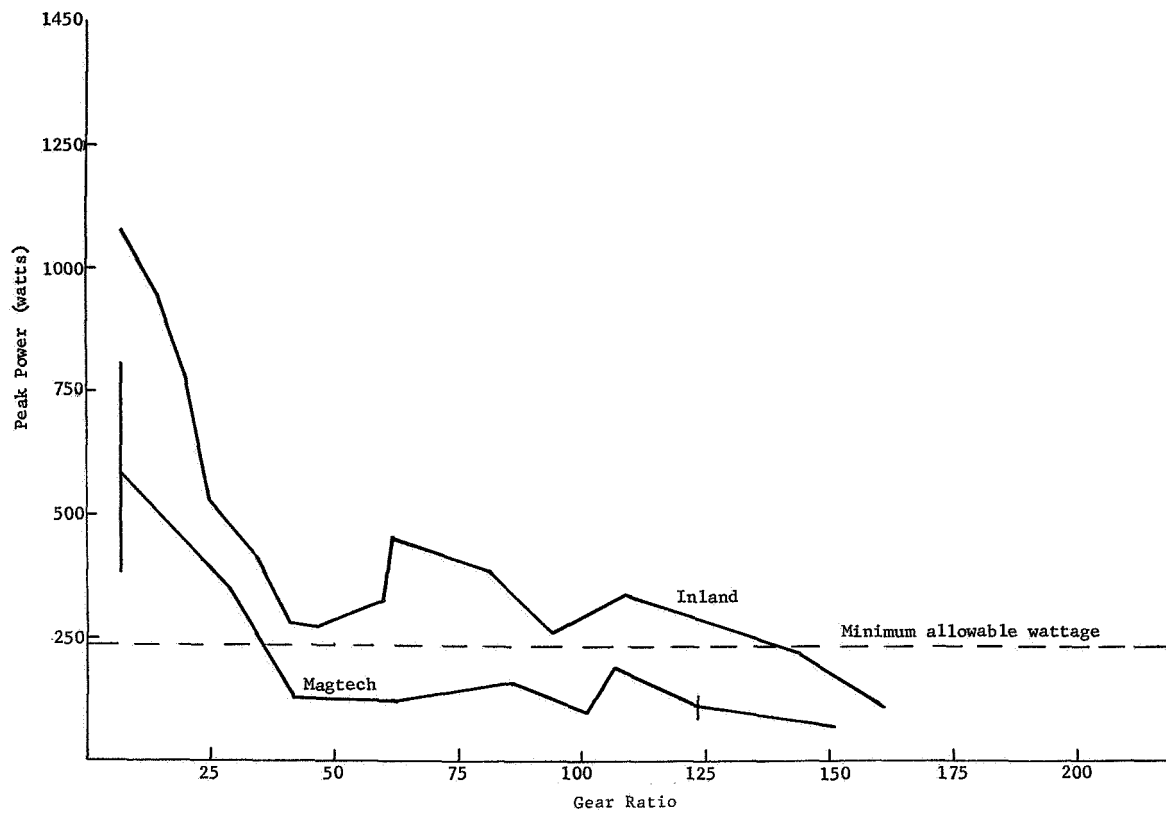


Figure IV-26 Gear Ratio vs Peak Power, 650 ft lb Gear Assembly

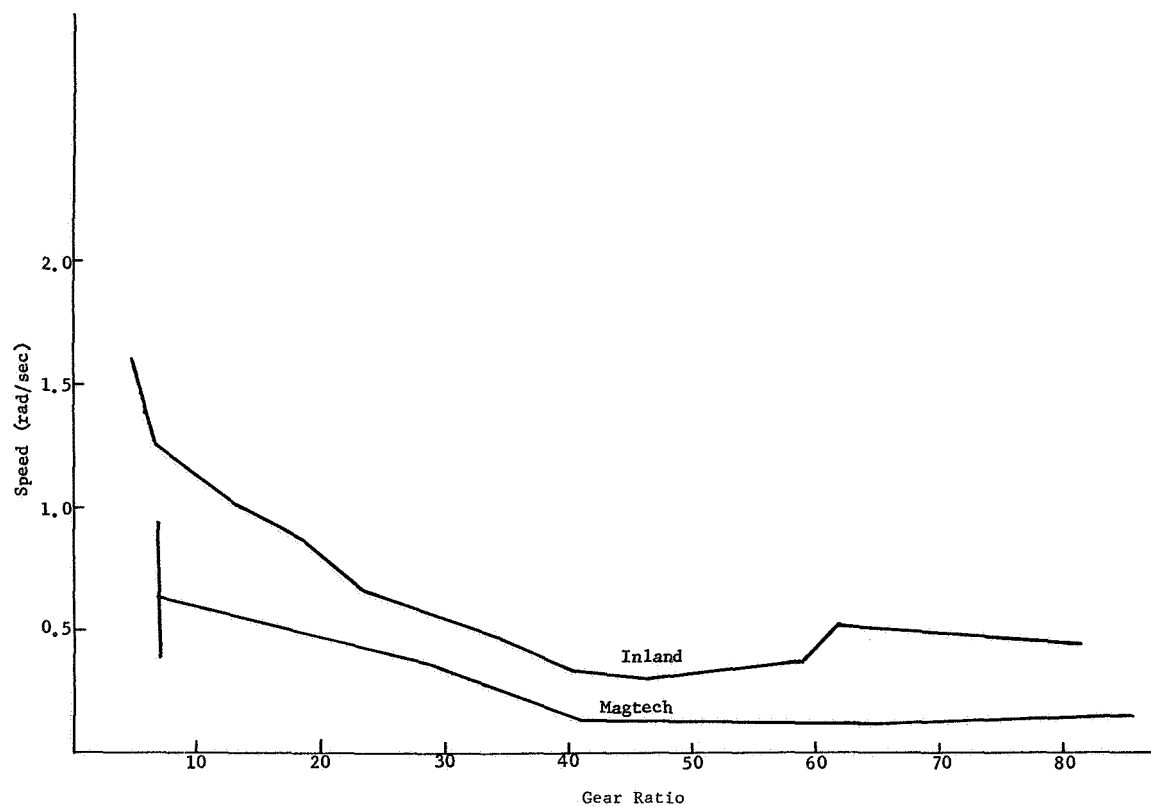


Figure IV-27 Gear Ratio vs Output Speed, 650 lb Gear Assembly

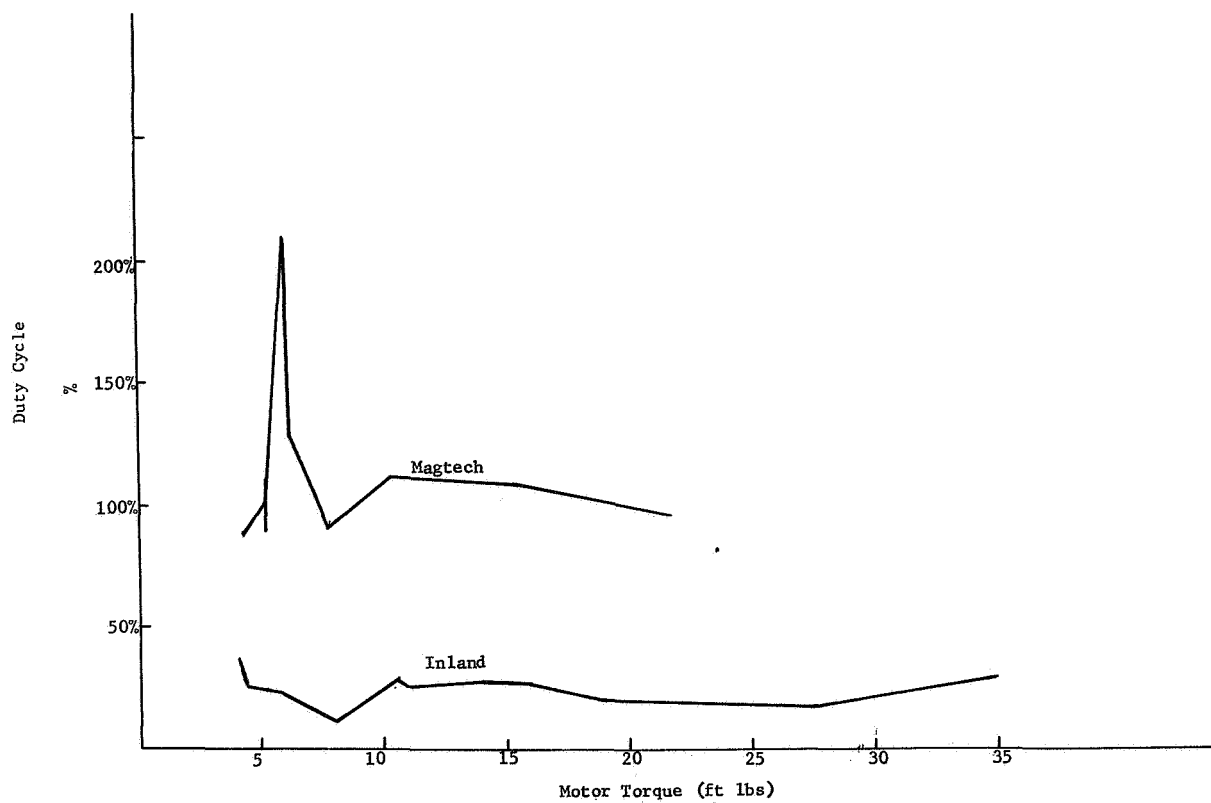


Figure IV-28 Duty Cycle vs Motor Torque, 650 ft lbs Gear Assembly

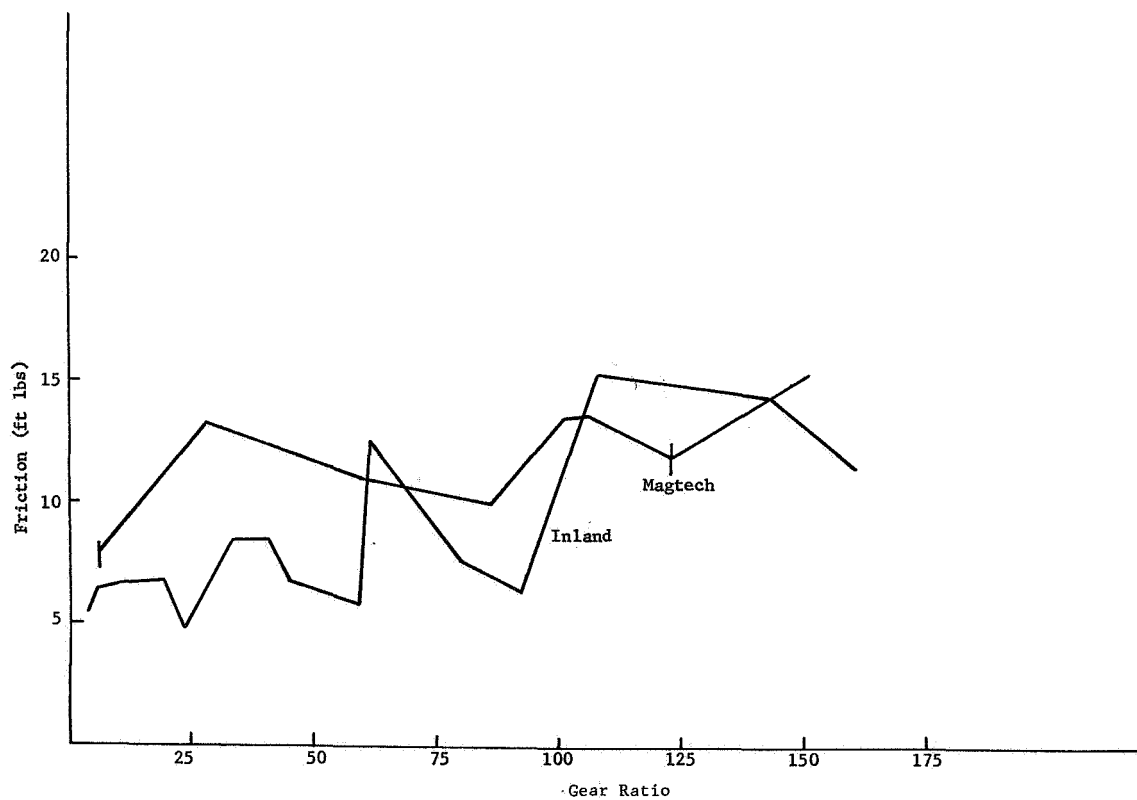


Figure IV-29 Gear Ratio vs Friction, 650 ft lb Gear Assembly

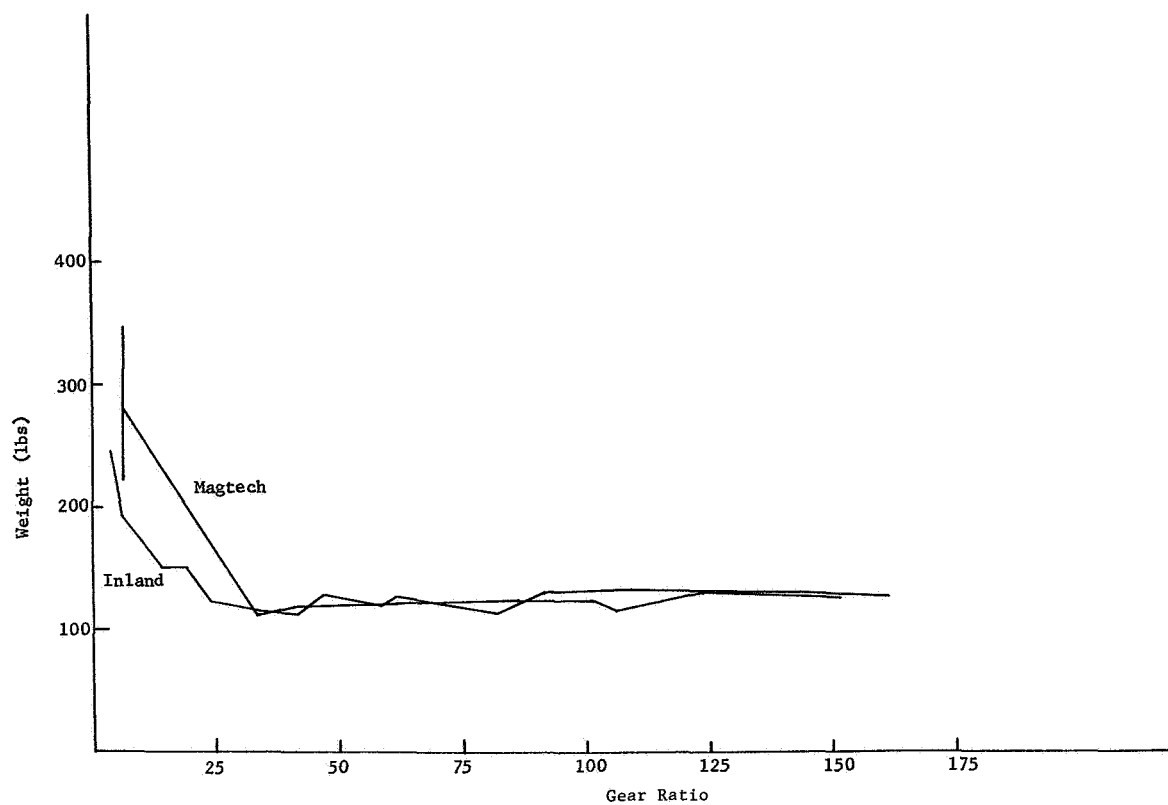


Figure IV-30 Gear Ratio vs Joint Weight, 650 ft lb Gear Assembly

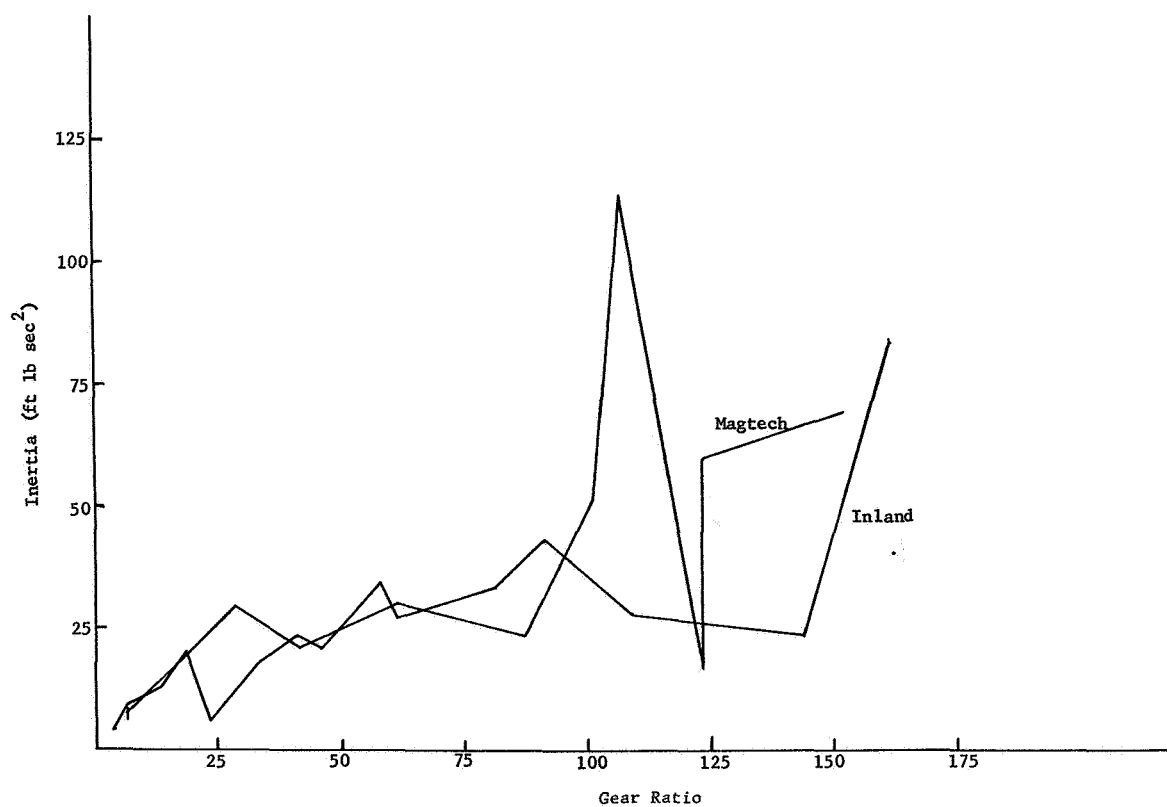


Figure IV-31 Gear Ratio vs Reflected Inertia, 650 ft lb Gear Train



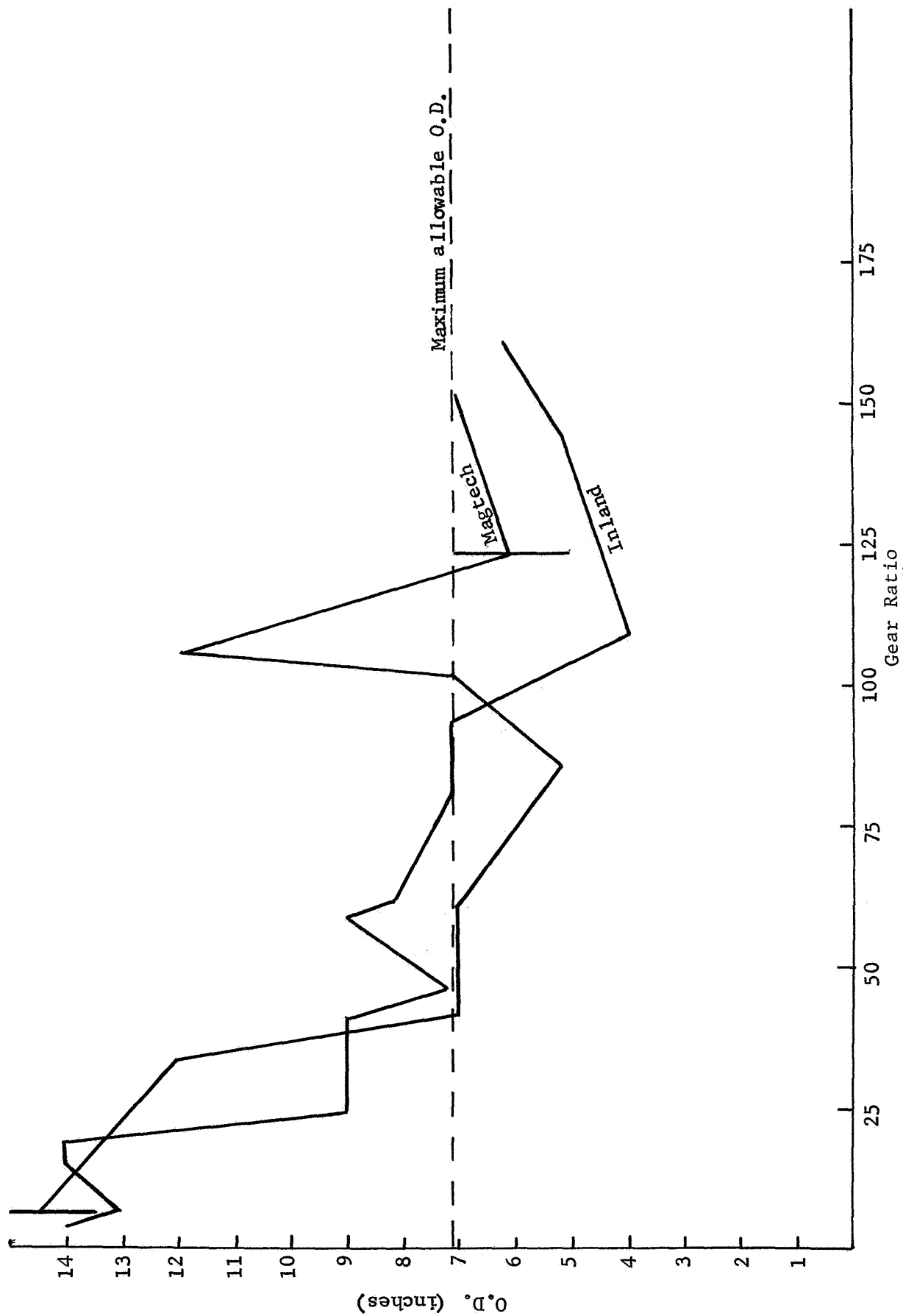


Figure IV-32 Gear Ratio vs O.D., 650 ft lb Gear Assembly

Attempting to average these results for all the criteria yields,

<u>Motor Mfg.</u>	<u>Indicated Gear Ratio Range</u>
Inland	44:1 $\longleftrightarrow$ 94:1
Magtech	No obvious conclusion

Once again selecting an Inland motor in the above indicated range results in the following suggested components.

Gear Ratio: 46.4:1

D.C. Torque Motor: Inland T-5745

Motor-Gear Assembly:

Stall torque: 650 ft lbs

Max. output speed: 0.3 rad/sec

Reflected friction: 6.9 ft lbs

Reflected Inertia: 21.5 ft lbs sec<sup>2</sup>

Total weight: 124 lbs

As revealed above, the same motor was selected for both shoulder and elbow joints; thus, the same brake and tachometer generator can be used for both joints. Reiterating, these two elements are:

Brake: Simplatrol PMB-103

Tachometer Generator: Magtech 3730B-134

#### 4. Joint Design for AMS

This section discusses the final design approach for three joints and some of the included components. The design arrangements are the result of analyzing many previous designs, the limiting envelopes required, directed toward weight optimization, stresses and loads in important members, and of course the breadboard tests and technology studies of motor/gearing combinations. Assembly sequence is also a very important factor in considering the arrangement.

Each joint contains a DC servo motor, DC fail-safe magnetically operated brake, tachometer generator, all preferably on a common shaft, a potentiometer, gearing as the torque multiplier, yoke type hinging to provide maximum load carrying bearing support, and precision bearings located biaxially (at end of shafts - non-cantilevered loads) wherever space permits.

Every effort has been made to standardize on components wherever possible to reduce costs, to simplify maintenance and to minimize adverse effects on the control system.

Addition weight optimization will be necessary in the detail component design. Aluminum castings should be considered for the large housings where some machining areas may be difficult or impossible for reducing weight.

For the final AMS and SAMS gears a full hardness would be recommended. This may require grinding after heat treat if it is determined that there would be significant distortion of critical tolerances. It would reduce costs if grinding could be avoided. Shaping, hobbing and/or shaving may be sufficient. A hardness of from RC38 to RC45 should also provide good tooth wear characteristics for the type of service expected.

The three joints preliminarily designed are the shoulder pitch and roll and elbow yaw. These are discussed in the following paragraphs.

Shoulder Pitch - The design of this drive is shown on Figure IV-33. It incorporates the type of internal gearing system proven by the tests, however, in a smaller packaging arrangement. The gearing ratio was selected at approximately 96:1 which when used with the proper motor 14 ft-lb produces an optimum design capable of providing the required 1200 ft.lb

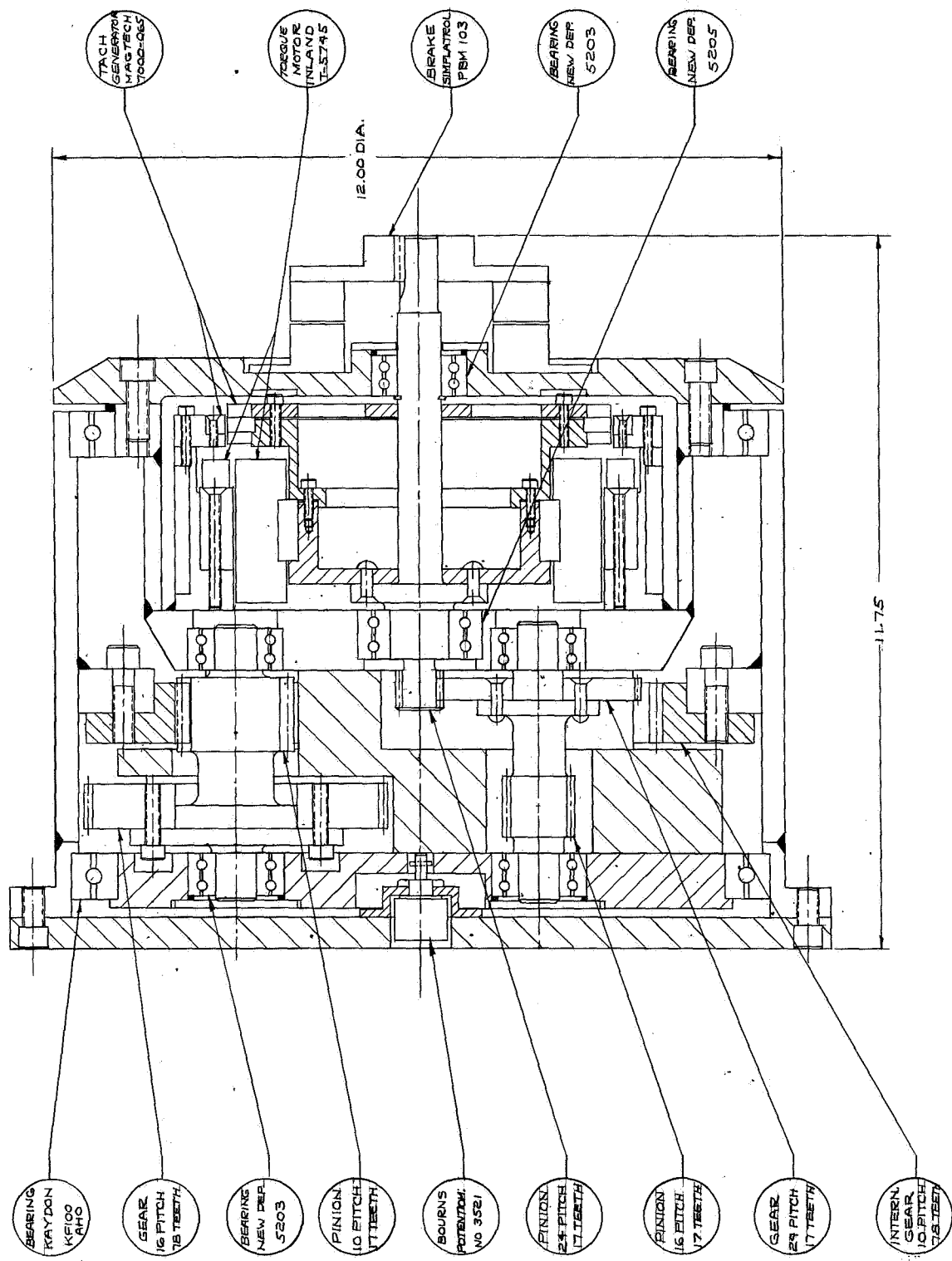


Figure IV-33 AMS Shoulder Pitch Joint Assembly

output torque plus losses. (See Section A.3 for gear train ratio and motor selection.)

The selected motor Inland T5945 weighs 16 lbs and will provide 14 lb ft at stall. The armature is held onto the shaft by end clamping (standard practice) and will have a partial aluminum support for lighter weight. Provision is made in the housing for wire routing to a common penetration. Particular attention has been given for the provision of proper sequence of field "keeper" removal to prevent magnet damage.

Tach generator (Magnetic Technology No. 7000-065) installation and support is similar to the motor however somewhat larger and thinner to enable assembly within the envelope. Both tachometer generator and motor will have the required non-magnetic material clearances of approximately 0.25 inches.

The fail-safe brake that fulfills the requirement is a Simplatrol PMB103. This will provide a braking torque of slightly greater than the motor stall torque. This type has been used previously in the MMC test articles. Many others similar in size and capacities are available. There was some speculation concerning the use of a new type of fail-safe brake, from the same company, that can be pulse operated to open and close, thereby eliminating "operational period" power consumption. However, for simulator use the standard brake was selected. For space use the pulse operated system (nearly the same size but requiring external electronics) should be investigated further. Axial alignment of the brake is relatively unimportant except for dynamic balancing problems, therefore, it can be placed in a cantilevered mode if necessary and also driven through a coupling.

The gearing is designed using high strength SAE 4340 steel at a hardness of RC38 to RC45 for strength and wear characteristics necessary for a simulator, however, also sufficiently capable for space use. Precision tolerances in housings, bearings and gearing (and shafting) will permit backlashes on the order of .002 in. to be fully realizable. Selected gear pitches: 1st mesh: 24; 2nd mesh: 16; 3rd mesh: 10 will provide smooth torque transmittal, yet be sufficiently strong for small impact loads, and continuous duty at rated loads.

The internal ring gear is the identical pitch as that used in the test apparatus. Tooth finishes should be held to 30 rms for best wear.

Wherever possible multiple gears should be made on one shaft with spacing only sufficient for tooth cutting relief for shaping, hobbing or grinding tools. One of our gear/pinion combinations does require a two piece fabrication due primarily as an aid in fitting in the dual output system to allow for proper orientation of teeth throughout. For this gear it is planned that the gears be machined separately, however, assembled and pinned (riveted) together for positioning and holding in shear. If the fabrication or development proves the necessity for gear grinding (warping from heat treat) the other dual gear/pinions could also be fabricated in two pieces.

Access to components and isolation of electrical components from gearing is desirable although not mandatory. This reasoning has also been imposed wherever practicable.

The bearings will be the permanently lubricated double shielded type. It is recommended that a dry lubricant baked, burnished, (or possibly impregnated type) be used, and a thin application of a lubriplate or silicone grease also be considered. Wherever grease may be thrown out double shields will be provided. This situation is unlikely because of the slow speeds involved. Care must be exercised to prevent oil film build-up on brushes and brake faces in particular.

Bearings selected for this design are readily available. One promising approach selected is extensive use of double row angular contact bearings which help on alignment and pre-load. Other precision bearings (angular contact) could also be acceptable. Joint housings will be high strength aluminum such as 6061 T-6 or equivalent.

No internal mechanical stops for rotation are required for this joint. The motor provides the prime stop force via the control system; fail-safe braking provides stopping forces in the event of power loss.

This joint was designed to obtain a packaging so that it could also be used for the shoulder yaw and so that it would be applicable to the space version.

Shoulder Roll - Figure IV-34 shows a layout for this joint. The design applies specifically to the AMS because of the necessity of including the counterbalance bar scheme (See Section C) within the tubing. For the space version it would



be intended that a roll design would be incorporated within the tube.

The AMS roll joint is of utmost simplicity. Easy backdriveability is not a requirement, therefore, a worm drive was selected. This offers two advantages: a) a very high single mesh ratio and b) deletion of a holding fail-safe brake because of the inherent high friction capability of a properly designed worm gearing system.

It is planned that the 14 ft lb DC torque motor used in the shoulder pitch be used here for commonality. Certainly this represents a maximum size and could be reduced if necessary. However, for the roll joint of the AMS configuration, weight is not critical. Counterbalancing has been considered and is easily accommodated in a symmetrical envelope if necessary. Added inertia is not significant compared to the main arm segments.

Elbow Yaw - The same motor Inland T-5745 as those in the shoulder joints used here with a 53:1 gear ratio, after counterbalancing mechanisms and gearing friction losses are accounted for, we have (with some margin) the required 650 ft lbs torque. Use of gearing and counterbalancing breadboard test data provided guidance in determining conservative allowances for frictional losses here.

Figure IV-35 is a layout of the elbow joint. The counterbalancing mechanism crankshaft disks (See Section C), driven by the connecting bars are shown in dashed lines. These occupy considerable envelope space, even though minimized in size, and caused the resultant gearing arrangement with the ring gear drive in the yoke. It was desirable to provide a dual gear drive here as in the breadboard, however, the counterbalancing mechanism prevented this and a compromise was made using only one drive pinion. Several gearing and bearing arrangements were investigated. The resultant design appeared best because of minimal housing extension and its attendant lower weight. Also the desirability of having the motor and tachometer generator and motor drive pinion on the same shaft with the brake was achieved.

The ring gear used in the yoke drive is slightly larger than that used for the shoulder, however, it does allow use of a larger pinion for single drive tooth strength, and with a larger number of pinion teeth undercutting is avoided. Back-



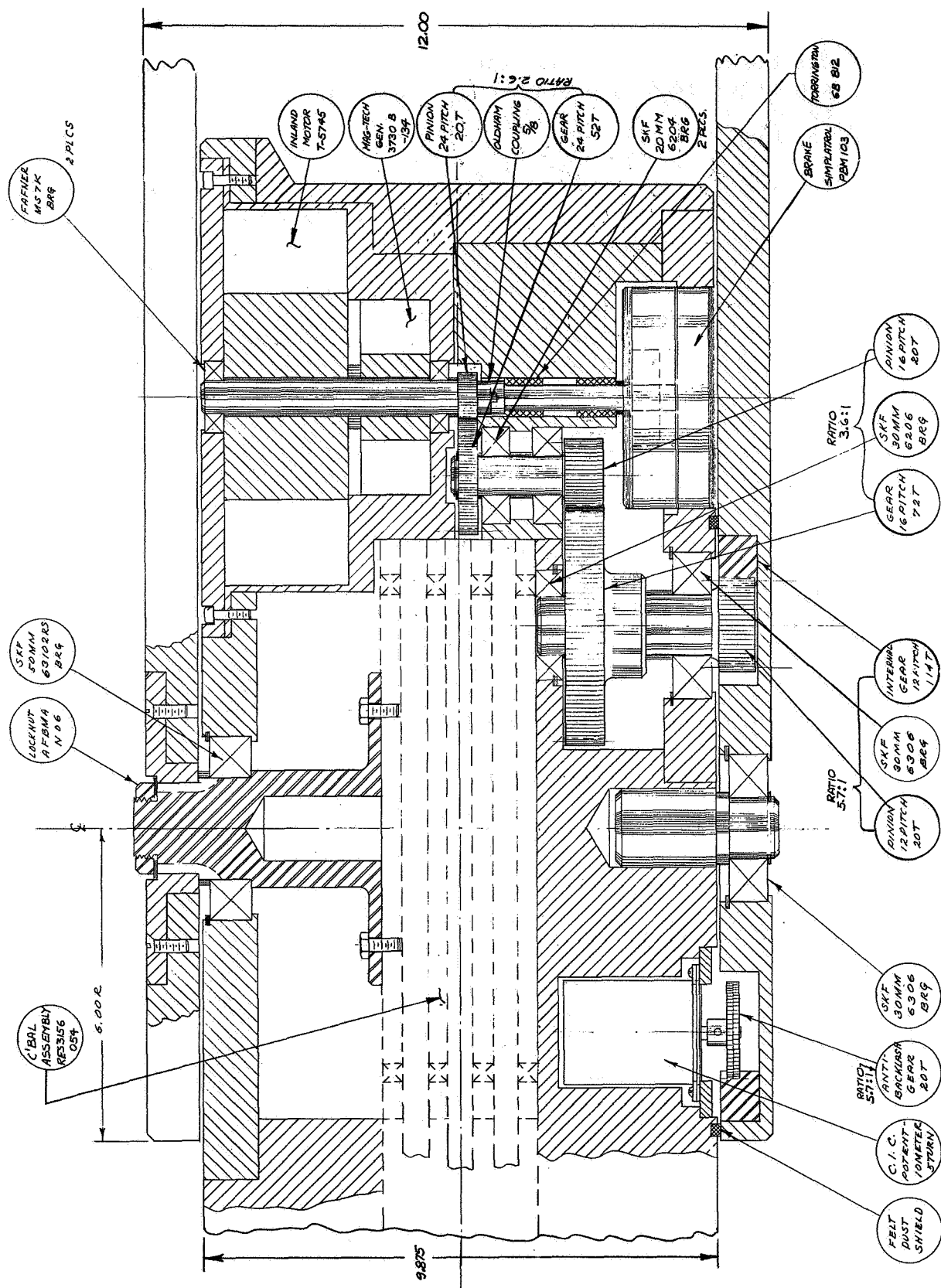


Figure IV-35 AMS Elbow Yaw Joint Assembly

driving will be very easy with the 53:1 ratio. Dust protection can be provided by a plastic or rubber lip. Normally (for space version) all gearing would be internal to the main housing.

All bearings can easily handle the loads while retaining the necessary alignment with minimal deflections. Double sealed bearings will be used which should be good for the life of the simulator. Preloading will also be employed either externally or in double row angular contact.

The tachometer generator selected is Magnetic Technology 3730 B-134 the same as that used for the shoulder roll.

A Simplatrol fail-safe brake model PMB-103, (identical to that specified for the Shoulder Pitch) is provided. This will provide 16.7 ft-lb which is slightly greater than stall torque of the motor.

Generally the yoke/hinge configuration and envelope is applicable to both the AMS and SAMS except for the elongation of the housing beyond the hinge centerline to contain the motor, tach generator brake and part of the gearing. The yoke/hinge allows articulation from approximately  $-2^{\circ}$  to  $+164^{\circ}$  minimum. Yoke design shown here has been partially enclosed with the angled flange that provides added joint stiffness and strength.

## B. COUNTERBALANCE ANALYSIS AND OPTIMIZATION

A prerequisite to realistic AMS operation in a 1-g environment is some means by which the torques about the AMS joints, due to gravitational forces, can be nullified. One way to accomplish this is to extend the upper arm back past the shoulder joint for some distance and attaching an articulated counterweight at the end of this extension (see Figure IV-36).

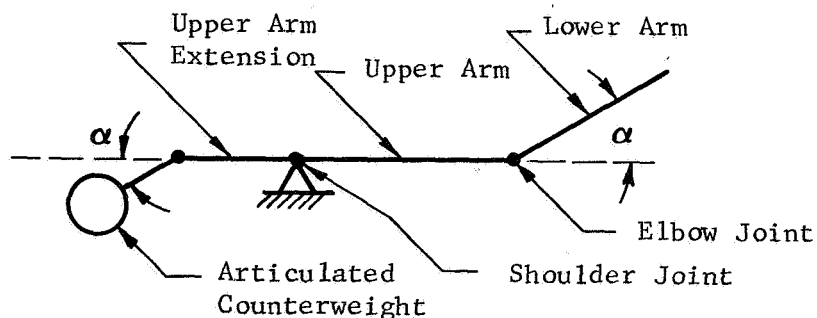


Figure IV-36 Articulated Counterbalance Concept

The term articulated implies that the counterweight is physically connected to the elbow joint in such a way that the orientation of the counterweight relative to the upper arm is identical to the orientation of the lower arm relative to the upper arm (the angle,  $\alpha$ , in Figure IV-36). A detailed discussion of how one actually achieves such articulation is contained in Section C of this chapter.

It will be shown in what follows that, by proper selection of the counterbalance inertia properties and geometry, it is possible to negate the gravitational torques about the shoulder and elbow of the AMS, simultaneously, regardless of AMS orientation (neglecting perturbations due to changes in wrist orientation).

It will become apparent in the sequel that there are an infinity of counterbalance geometry and inertia combinations that satisfy the counterbalance equations. It is therefore necessary to further investigate the details of the AMS design in order to arrive at a meaningful criterion for selection of counterbalance inertia properties and geometry. One means of selection can be found by examining the increase in shoulder pitch moment of inertia for each of the multitude of counterbalance possibilities; for, although the gravitational torques are cancelled in each case, the shoulder and elbow motors are required to drive the additional counterbalance inertia. Thus, it would seem desirable to choose the counterbalance mass and geometry that minimizes the increase in inertia. The necessary equations and corresponding digital computer program to accomplish this task are described below along with results for a range of AMS design data. Finally, some conclusions are drawn about the counterbalance design.

### 1. Counterbalance Equations

We begin by assuming there are no unbalanced gravity forces on the payload or the support structure (i.e., it is assumed that both of these bodies are supported by the floor). For this reason, one need only consider counterbalancing the unloaded AMS. To further simplify matters, we assume the wrist does not require counterbalancing and therefore lump the mass of the wrist at the end of the lower arm.

The foregoing assumptions result in a reduction of the six body model shown in Figure A-1 (see Appendix A) to the four body model shown in Figure IV-37. It is noted that the gravity vector,  $\bar{g}$ , is assumed parallel to  $\bar{e}_{63}$ .

Now the counterbalance design philosophy is to choose the mass properties of body 1 and the location of hinge 1 (see Figure IV-37) in such a way that the torque motors at hinges 2 and 3 need not counteract any gravity torques, regardless of AMS orientation.

The necessary counterbalance relations can be obtained from Equations (A-1) - (A-12) in Appendix A. For the static case and with the gravity vector parallel to  $\bar{e}_{63}$ , these equations become (for the four bodies shown in Figure IV-37).

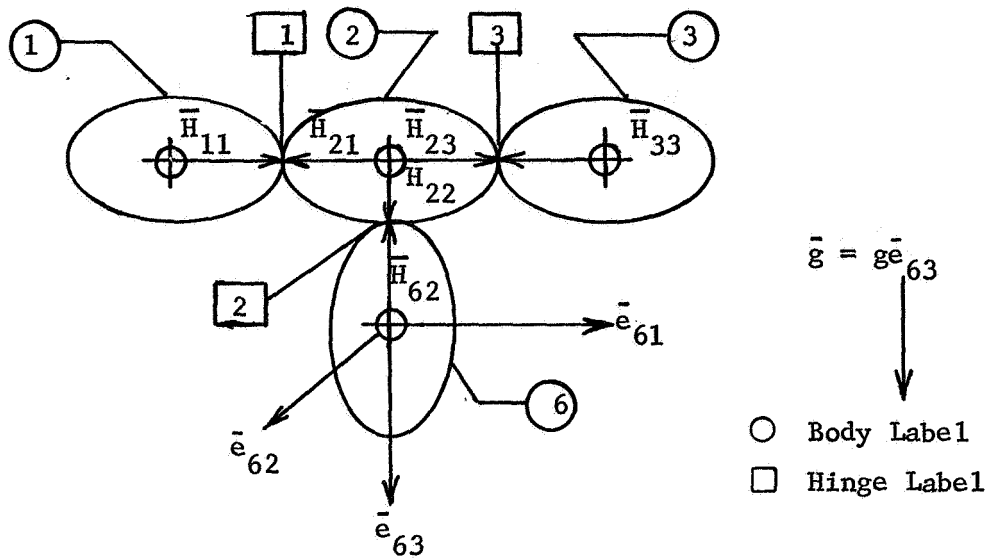


Figure IV-37 Four Body AMS Model

$$\bar{F}_{11}^H = -m_1 g \bar{e}_{63} \quad (\text{IV-1})$$

$$\bar{F}_{33}^H = -m_3 g \bar{e}_{63} \quad (\text{IV-2})$$

$$\bar{F}_{22}^H = -(m_1 + m_2 + m_3) g \bar{e}_{63} \quad (\text{IV-3})$$

$$\bar{F}_6^H = -(m_1 + m_2 + m_3 + m_6) g \bar{e}_{63} \quad (\text{IV-4})$$

where  $\bar{F}_6^H$  in Eq. (IV-4) represents the force of the floor on the support structure. Solving Eqs. (A-7) - (A-9) (See Appendix A) for  $\bar{T}_{11}^H$ ,  $\bar{T}_{33}^H$ , and  $\bar{T}_{22}^H$ , and using the above expressions for the hinge forces, one is left with

$$\bar{T}_{11}^H = m_1 g (\bar{H}_{11} \times \bar{e}_{63}) \quad (\text{IV-5})$$

$$\bar{T}_{33}^H = m_3 g (\bar{H}_{33} \times \bar{e}_{63}) \quad (\text{IV-6})$$

$$\begin{aligned} \bar{T}_{22}^H = g \left[ m_1 (\bar{H}_{11} - \bar{H}_{21} + \bar{H}_{22}) + m_3 (\bar{H}_{33} - \bar{H}_{23} + \bar{H}_{22}) \right. \\ \left. + m_2 \bar{H}_{22} \right] \times \bar{e}_{63} \quad (\text{IV-7}) \end{aligned}$$

Now it is assumed that the orientation of body 1 relative to body 2 is identical to that of body 3 relative to body 2 and it is further assumed that

$$\begin{aligned}
 \bar{H}_{11} &= H_{11} \bar{e}_{31} \\
 \bar{H}_{21} &= -H_{21} \bar{e}_{21} \\
 \bar{H}_{22} &= -H_{22} \bar{e}_{21} \\
 \bar{H}_{23} &= H_{23} \bar{e}_{21} \\
 \bar{H}_{33} &= -H_{33} \bar{e}_{31}
 \end{aligned}
 \tag{IV-8}$$

Equation (IV-8) reflect the assumption that the joints lie on the centerlines of the tubes comprising the lower and upper arm segments.

Since the motor at joint 3 must drive both bodies 1 and 3, the counterbalance conditions can be written

$$\bar{T}_{11}^H + \bar{T}_{33}^H = 0
 \tag{IV-9}$$

$$\bar{T}_{22}^H = 0
 \tag{IV-10}$$

Substituting from Eq. (IV-8) into (IV-5) and (IV-6), Equation (IV-9) can be written

$$(m_1 g H_{11} - m_3 g H_{33}) \bar{e}_{31} \times \bar{e}_{63} = 0$$

which will be satisfied regardless of the AMS orientation if one requires

$$m_1 H_{11} - m_3 H_{33} = 0 \quad (\text{IV-11})$$

Similarly, Eq. (IV-10) can be written

$$(m_1 g H_{11} - m_3 g H_{33}) \bar{e}_{31} \times \bar{e}_{63} + \left[ m_1 g (H_{21} - H_{22}) - m_3 g (H_{23} + H_{22}) - m_2 g H_{22} \right] \bar{e}_{21} \times \bar{e}_{63} = 0 \quad (\text{IV-12})$$

From Eq. (IV-11) it follows that the first term in Eq. (IV-12) vanishes, and therefore Eq. (IV-12) will be satisfied if,

$$m_1 (H_{21} - H_{22}) - m_3 (H_{23} + H_{22}) - m_2 H_{22} = 0 \quad (\text{IV-13})$$

Thus, Equations (IV-11) and (IV-13) are the necessary conditions for the AMS to be counterbalanced in any orientation.

It is more meaningful to write Eqs. (IV-12) and (IV-13) in terms of the counterbalanced AMS design quantities shown in Figure IV-38. These quantities are as follows:  $L_{\text{CBLA}}$  is the distance from the counterbalance elbow (CBE) to the mass center of the counterbalance lower arm (CBLA);  $M_{\text{CBLA}}$  is the mass of CBLA, and  $M_{\text{CBE}}$  is the mass of the CBE;  $L_{\text{CBUA}}$  is the length of the counterbalance upper arm (CBUA), and  $M_{\text{CBUA}}$  is the mass of the CBUA;  $L_{\text{UA}}$  is the length of the upper arm (UA) and  $M_{\text{UA}}$  is the mass of the UA;  $M_{\text{E}}$  is the mass of the elbow and  $M_{\text{LA}}$  is the mass of the lower arm;  $L_{\text{LA}}$  is the length of the lower arm and  $M_{\text{W}}$  is the mass of the wrist (assumed to be concentrated at the wrist joint). In terms of this notation, Eqs. (IV-11) and (IV-13) can be written

$$M_{\text{CBLA}} L_{\text{CBLA}} = (M_{\text{LA}} + 2M_{\text{W}}) \frac{L_{\text{LA}}}{2} \quad (\text{IV-14})$$

$$(M_{\text{CBLA}} + M_{\text{CBE}} + \frac{M_{\text{CBUA}}}{2}) L_{\text{CBUA}} = (\frac{M_{\text{UA}}}{2} + M_{\text{E}} + M_{\text{LA}} + M_{\text{W}}) L_{\text{UA}} \quad (\text{IV-15})$$

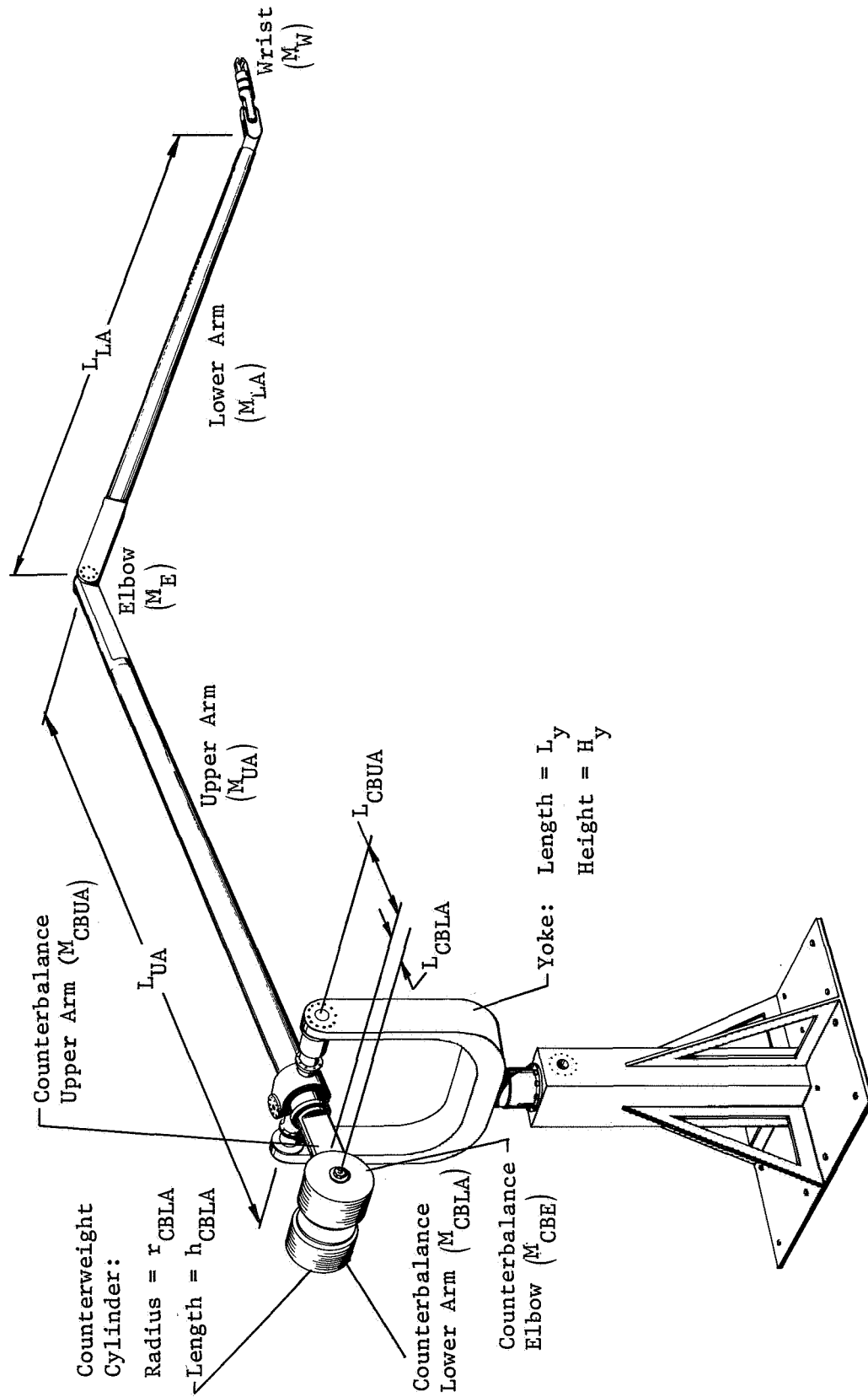


Figure IV-38 Counterbalanced AMS



Equations (IV-14) and (IV-15) are the so-called counterbalance equations that must be satisfied for cancellation of the gravity torques at the shoulder and elbow joints. It is noted that these two equations contain three unknowns:  $M_{CBLA}$ ,  $L_{CBLA}$ , and  $L_{CBUA}$ . The mass,  $M_{CBUA}$ , can be determined from  $L_{CBLA}$  and the remaining terms can be obtained from preliminary design data. Thus, Eqs. (IV-14) and (IV-15) can be used to determine  $L_{CBLA}$  and  $L_{CBUA}$  once  $M_{CBLA}$  has been selected, but these equations offer no clue as to the proper selection of  $M_{CBLA}$ . What is needed then is a third relationship that will pinpoint the selection of  $M_{CBLA}$ .

## 2. Selection Criterion for the Counterbalance Mass

The necessary third equation to supplement Eqs. (IV-14) and (IV-15) is obtained in what follows by minimizing an expression for the increase in shoulder pitch moment of inertia caused by the addition of the counterbalance mechanism. Toward this end, the counterbalanced AMS in Figure IV-38 is idealized as shown in Figure IV-39.

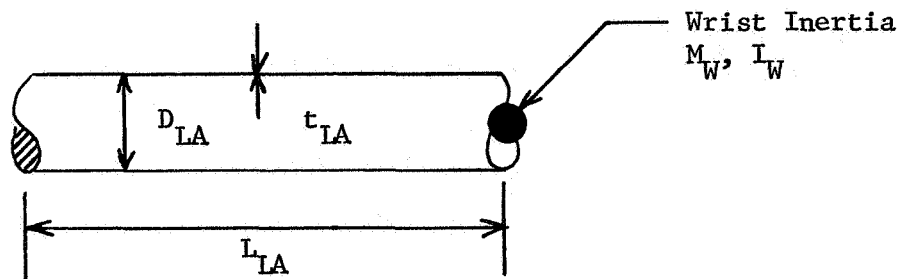
The lower arm is taken to be a thin-walled tube of diameter  $D_{LA}$ , thickness  $t_{LA}$ , length  $L_{LA}$  and density  $\rho_{LA}$ . The wrist is modelled as a concentrated mass  $M_W$  and moment of inertia  $I_W$  located at the end of the lower arm.

The upper arm is also a thin-walled tube of diameter  $D_{UA}$ , thickness  $t_{UA}$ , length  $L_{UA}$  and density  $\rho_{UA}$ . The elbow motor, gear train, etc. are all lumped together in a concentrated mass  $M_e$  and moment of inertia  $I_e$  located at the end of the upper arm. In one of the counterbalance schemes (see Section C of Chapter IV), several rods pass through the hollow upper arm connecting the lower arm to the CBLA. These rods are modelled as a single solid cylinder of diameter  $D_{CR}$ , density  $\rho_{CR}$  and length  $L_{UA}$ . Later, if rods are not used,  $\rho_{CR}$  can be taken as zero.

The counterbalance upper arm (CBUA) is simply an extension of the upper arm model over a length  $L_{CBUA}$ . The hardware connecting the CBUA to the CBLA is accounted for by a concentrated mass  $M_{CBE}$  and moment of inertia  $I_{CBE}$ .

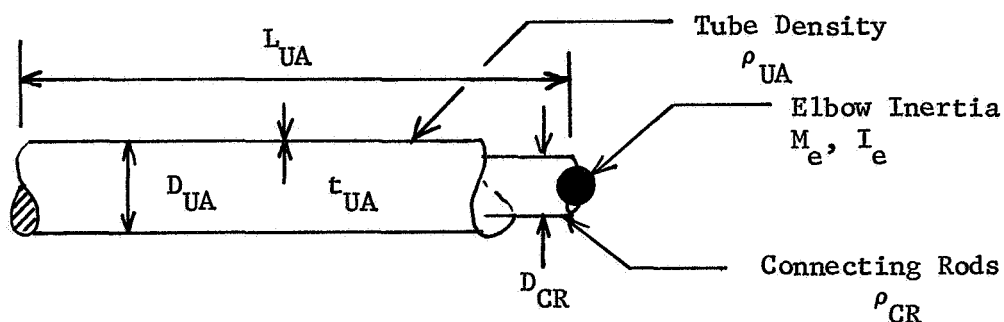
The CBLA is modelled as two solid cylinders of radius  $r_{CBLA}$ , height  $h_{CBLA}$ , and density  $\rho_{CBLA}$ . The distance from the CBE to the mass center of the CBLA (the axis of the two cylinders) is called  $L_{CBLA}$ .

Lower Arm  
and Wrist

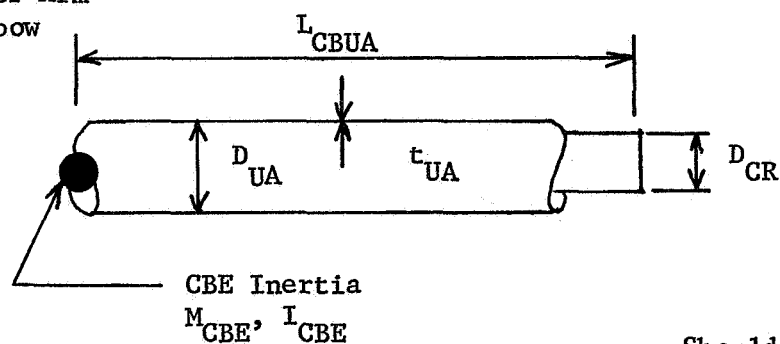


Tube Density  
 $\rho_{LA}$

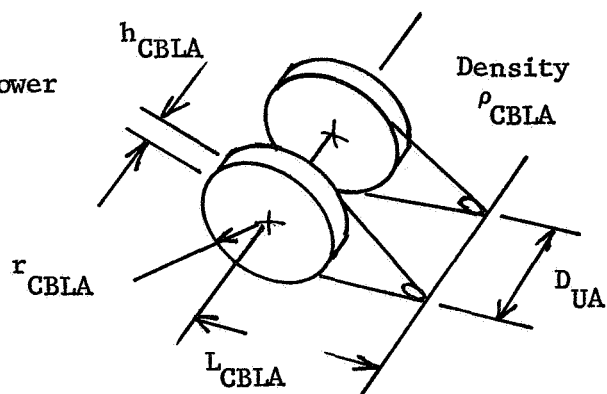
Upper Arm  
and Elbow



CB Upper Arm  
and Elbow



CB Lower  
Arm



Shoulder Yoke

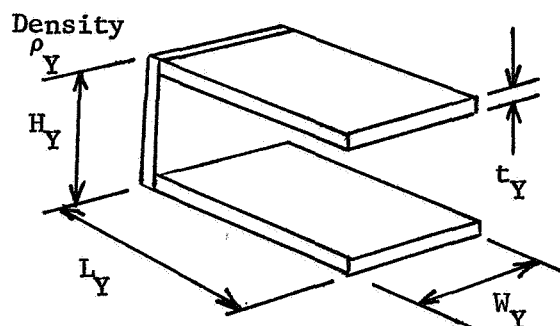


Figure IV-39 Counterbalanced AMS Components

Finally, three rectangular plates are used to represent the shoulder yoke. Two of the plates are of length  $L_y$ , width  $W_y$ , and thickness  $t_y$ . The back plate is of height  $H_y$  and of thickness  $t_y$ . All of the plates have a density  $\rho_y$ .

The maximum increase in shoulder pitch moment of inertia due to the counterbalance mechanism occurs when the AMS is fully extended. Only the contribution of the CBLA, CBUA, and the yoke to the increase in moment of inertia need be considered. The connecting rods in the upper arm represent an increase in moment of inertia, but their contribution does not depend on the mass,  $M_{CBLA}$ , and hence need not be considered when minimizing the increase in shoulder moment of inertia. The functional dependence of the other contributions (on  $M_{CBLA}$ ) will become clear in what follows.

The moment of inertia of the CBLA about the shoulder pitch axis,  $I_{CBLA}$ , is computed as follows

$$I_{CBLA} = M_{CBLA} (L_{CBLA} + L_{CBUA})^2 + M_{CBLA} \frac{r_{CBLA}^2}{2} \quad (IV-16)$$

where  $r_{CBLA}$  is determined from  $M_{CBLA}$ ,  $h_{CBLA}$  and  $CBLA$  as follows

$$r_{CBLA} = \left( \frac{M_{CBLA}}{2 \pi h_{CBLA} \rho_{CBLA}} \right)^{1/2} \quad (IV-17)$$

The moment of inertia of the CBUA about the shoulder pitch axis,  $I_{CBUA}$ , can be written

$$\begin{aligned} I_{CBUA} = & M_{UA1} \left( \frac{D_{UA}^2}{8} + \frac{L_{CBUA}^2}{12} \right) + M_{UA2} \left( \frac{D_{CR}^2}{16} + \frac{L_{CBUA}^2}{12} \right) \\ & + \left( M_{UA1} + M_{UA2} \right) \frac{L_{CBUA}^2}{4} + I_{CBE} + M_{CBE} L_{CBUA}^2 \end{aligned} \quad (IV-18)$$

where  $M_{UA1}$  is the mass of the hollow tube:

$$M_{UA1} = \pi D_{UA} t_{UA} L_{CBUA} \rho_{UA} \quad (IV-19)$$

and  $M_{UA2}$  is the mass of the connecting rods

$$M_{UA2} = \frac{\pi D_{CR}^2 L_{CBUA} \rho_{CR}}{4} \quad (IV-20)$$

In computing the moment of inertia of the yoke, the shoulder pitch axis is assumed to pass through the center of the back plate, parallel to the edge of length  $L_y$ . The pitch moment of inertia of the yoke about the shoulder pitch axis is then

$$I_y = 2M_{y1} W_y^2 + M_{y2} (H_y^2 + W_y^2) \quad (IV-21)$$

where  $M_{y1}$  is the mass of one of the horizontal plates:

$$M_{y1} = \rho_y W_y L_y t_y \quad (IV-22)$$

and  $M_{y2}$  is the mass of the back plate:

$$M_{y2} = \rho_y W_y H_y t_y \quad (IV-23)$$

Now the minimum allowable dimensions of the yoke,  $H_y$  and  $L_y$ , depend on the size of the CBLA and CBUA. In particular, when the shoulder yaw angle and elbow yaw angle are both  $90^\circ$ , the height,  $H_y$ , of the yoke must be large enough to avoid any contact between the CBLA and the yoke when the shoulder roll angle turns through  $360^\circ$ . This situation is shown in Figure IV-40(a). From the figure, it can be seen that

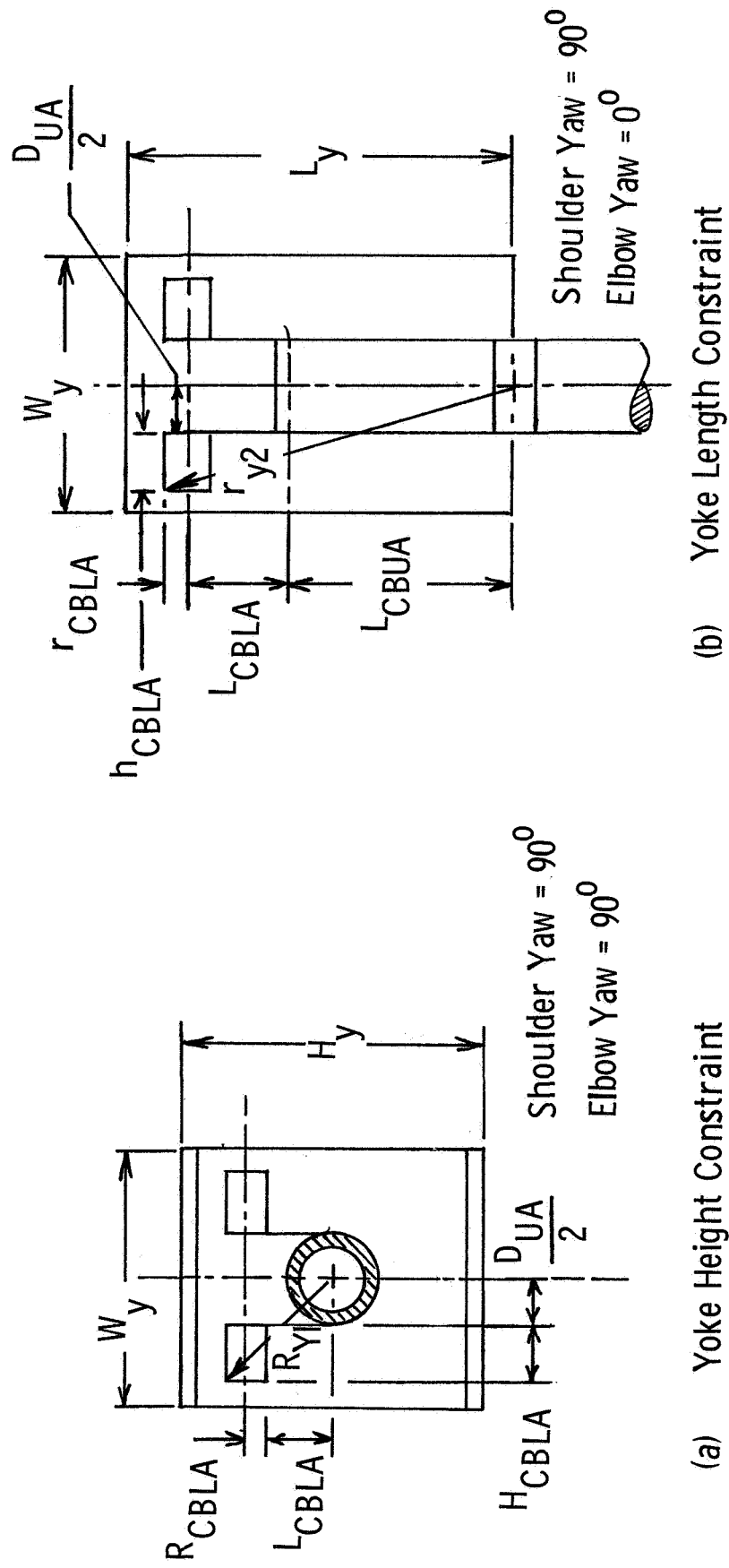


Figure IV-40 Yoke Size Constraints

$$H_y = 2r_{y1} = 2 \left[ (L_{CBLA} + r_{CBLA})^2 + (h_{CBLA} + \frac{D_{UA}}{2})^2 \right]^{1/2} \quad (IV-24)$$

Similarly, the length  $L_y$  of the yoke must be long enough to avoid any contact with the CBLA when the AMS is fully extended and the shoulder yaw angle turns through  $\pm 90^\circ$ . This condition is depicted in Figure IV-40(b). In this case, one can write

$$L_y = r_{y2} = \left[ (L_{CBUA} + L_{CBLA} + r_{CBLA})^2 + (h_{CBLA} + \frac{D_{UA}}{2})^2 \right]^{1/2} \quad (IV-25)$$

By means of Eqs. (IV-24) and (IV-25) one is able to express the yoke moment of inertia (See Eq. (IV-21)) in terms of the counterbalance dimensions (when  $W_y$ ,  $t_y$ , and  $\rho_y$  are assigned reasonable values). It is now possible to write the total increase in shoulder pitch moment of inertia,  $I_{TOTAL}$ , due to the counterbalance mechanism as

$$I_{TOTAL} = I_{CBLA} + I_{CBUA} + I_y \quad (IV-26)$$

where  $I_{TOTAL}$  is a function of  $M_{CBLA}$ ,  $L_{CBLA}$ ,  $h_{CBLA}$ ,  $L_{CBUA}$ . By solving Eqs. (IV-14) and (IV-15) for  $L_{CBLA}$  and  $L_{CBUA}$ , respectively, and substituting into (IV-26), we are left with an expression for  $I_{TOTAL}$  as a function of  $M_{CBLA}$  and  $h_{CBLA}$  only. In principal, one could set the appropriate partial derivatives equal to zero and obtain two equations for  $h_{CBLA}$  and  $M_{CBLA}$  that minimize  $I_{TOTAL}$ . Because Eqs. (IV-14) and (IV-15) have been used for  $L_{CBLA}$  and  $L_{CBUA}$ , the solution,  $h_{CBLA}$  and  $M_{CBLA}$ , of the two equations will be consistent with the counterbalance requirements. In practice, however, the resulting equations are highly nonlinear and hence not amenable to closed form solution. For this reason, a digital computer program has been developed to find those values of  $M_{CBLA}$  and  $h_{CBLA}$  that minimize  $I_{TOTAL}$ .

### 3. Counterbalance Optimization Computer Program

The digital computer program mentioned above is programmed with Eqs. (IV-14) - (IV-26). The input data consists of all of the quantities defined in Figure IV-39 except  $M_{CBLA}$ ,  $L_{CBLA}$ ,  $r_{CBLA}$ ,  $h_{CBLA}$ ,  $L_{CBUA}$ ,  $H_y$ , and  $L_y$ . The latter quantities represent the primary output of the computer program. In this way, it is a simple matter to incorporate any design changes of the AMS and determine the new counterbalance and yoke specifications.

The increase in shoulder moment of inertia is minimized by incrementing  $M_{CBLA}$  from some small value, and, for each value of  $M_{CBLA}$ , finding the value of  $h_{CBLA}$  that minimizes  $I_{TOTAL}$ . This process is continued until  $M_{CBLA}$  exceeds that value which minimizes  $I_{TOTAL}$  in both  $M_{CBLA}$  and  $h_{CBLA}$ .

By using this technique, plots of  $h_{CBLA}$ ,  $r_{CBLA}$ ,  $L_{CBLA}$ ,  $L_{CBUA}$ ,  $H_y$ , and  $L_y$  as functions of  $M_{CBLA}$  for the optimum  $h_{CBLA}$  value are obtained. In addition, plots are obtained of the percentage increase in shoulder (PISI) and elbow (PIEI) pitch moment of inertia defined by

$$PISI = \frac{I_{TOTAL}}{I_{LAS} + I_{UAS}} \times 100 \quad (IV-27)$$

$$PIEI = \frac{I_{CBLA}}{I_{LAE}} \times 100 \quad (IV-28)$$

where  $I_{LAS}$  and  $I_{UAS}$  are the pitch moments of inertia of the lower arm (including the wrist) and upper arm (including the elbow), respectively, about the shoulder joint, and  $I_{LAE}$  is the pitch moment of inertia of the lower arm and wrist about the elbow joint.

In examining the total increase in shoulder moment of inertia,  $I_{TOTAL}$ , it is helpful to express this quantity as an equivalent increase in payload weight, WEQ, defined by

$$WEQ = \frac{I_{TOTAL}}{(L_{UA} + L_{LA})^2} \times 32.174 \quad (IV-29)$$

This quantity is also plotted as a function of  $M_{\text{CBLA}}$  for the optimum  $h_{\text{CBLA}}$ .

Finally, a quantity called CLEARANCE is plotted as a function of  $M_{\text{CBLA}}$ . This length measure is the distance between the extremity of the counterbalance and the center of the shoulder joint when the elbow yaw angle is  $180^\circ$ . This distance is illustrated by Figure IV-41. It follows that any counterbalance solutions involving a negative or zero CLEARANCE are not practical.

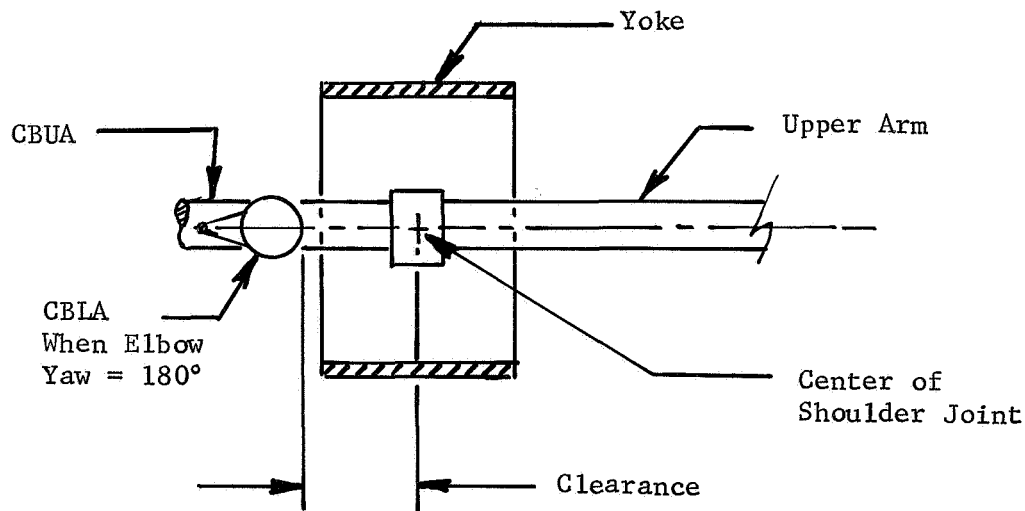


Figure IV-41 Counterbalance - Shoulder Clearance

In the next section, the input data for the counterbalance computer program is described along with the results generated by this data.

#### 4. Input Data and Results

With the exception of the yoke length and height and the geometry of the counterbalance lower arm, the quantities depicted in Figure IV-39 constitute the input data for the counterbalance optimization program. To generate the results that follow, values for these quantities were computed from preliminary design data, and these values are listed in Table IV-5.



Table IV-5 Input Data for Counterbalance Optimization Computer Program

Lower Arm and Wrist

$$D_{LA} = 12 \text{ in.}, t_{LA} = .08 \text{ in.}, L_{LA} = 222 \text{ in.}$$

$$\rho_{LA} = 3.11 \times 10^{-3} \text{ slug/in}^3, M_W = 1.55 \text{ slugs}, I_W = 1 \times 10^4 \text{ slug-in}^2$$

Upper Arm and Elbow

$$D_{UA} = 12 \text{ in.}, t_{UA} = 0.18 \text{ in.}, L_{UA} = 222 \text{ in.}$$

$$\rho_{UA} = 3.11 \times 10^{-3} \text{ slug/in}^3, D_{CR} = 2.25 \text{ in.}, \rho_{CR} = 8.4 \times 10^{-3} \text{ slug/in}^3$$

$$M_E = 2.5 \text{ slugs}, I_E = 40.5 \text{ slug-in}^2$$

Counterbalance Upper Arm and Elbow

$$M_{CBE} = 1.55 \text{ slugs}, I_{CBE} = 22.3 \text{ slug-in}^2$$

Counterbalance Lower Arm

$$\rho_{CBLA} = 1.27 \times 10^{-2} \text{ slug/in}^3$$

Shoulder Yoke

$$W_y = 18 \text{ in.}, t_y = 0.75 \text{ in.}, \rho_y = 3.11 \times 10^{-3} \text{ slug/in}^3$$

The input data reflect aluminum arms and yoke, steel connecting rods, and a lead counterbalance weight. The wrist was assumed to weigh 50 lbs and the elbow joint, 80 lbs.

The results of the computer program are shown in Figures IV-42 - IV-44. In each case, the dependent variables are plotted as functions of the counterbalance weight,  $W_{CBLA}$ .

Figure IV-42 illustrates the variation in counterbalance geometry with counterbalance weight. The lengths,  $L_{CBLA}$  and  $L_{CBLA}$ , are determined from Eqs. (IV-14) and (IV-15) and therefore represent those values for which  $W_{CBLA}$  will counterbalance the upper and lower arm segments of the AMS. The values of  $h_{CBLA}$  in Figure IV-42 are those that result in the minimum increase in shoulder pitch moment of inertia for the corresponding value of  $W_{CBLA}$ . Finally, the  $r_{CBLA}$  curve represents the radius of the counterbalance lower arm (lead cylinders) which are determined from Eq. (IV-17).

The plots of WEQ, PISI, and PIET in Figure IV-43 represent the increase in moment of inertia corresponding to the values of  $h_{CBLA}$ ,  $r_{CBLA}$ ,  $L_{CBLA}$ , and  $L_{CBLA}$  shown in Figure IV-42. These quantities are defined by Eqs. (IV-27) - (IV-29). The meaning of the quantity CLEARANCE shown in Figure IV-43 is illustrated in Figure IV-41.

Finally, Figure IV-44 depicts the length,  $L_y$ , and width,  $H_y$ , of the yoke corresponding to the counterbalance geometry shown in Figure IV-42.

The optimum counterbalance design is arrived at from Figures IV-43 and IV-44 in the following manner. Looking first at Figure IV-43, it can be seen that the increase in shoulder inertia, PISI, has a minimum value near  $W_{CBLA} = 9000$  Lbs. In addition to being unacceptably large, this value of  $W_{CBLA}$  results in a negative value of CLEARANCE (for convenience in plotting the data in Figure IV-43, negative values of CLEARANCE were plotted on the  $W_{CBLA}$  axis). A negative value of CLEARANCE implies that interference between the CBLA and the shoulder gimbal will occur when the elbow yaw angle approaches  $180^\circ$  (see Figure IV-41). Fortunately, the PISI curve is relatively flat for values of  $W_{CBLA}$  greater than 2000 Lbs. For this reason one can select a counterbalance weight, less than the optimum, without seriously changing the increase in shoulder

moment of inertia. Thus, the question remains as to what value of  $W_{CBLA}$  one should choose.

In Figure IV-44 it can be seen that the yoke dimensions increase rapidly to the left of where the two curves intersect. For this reason, it was decided to choose that value of  $W_{CBLA}$  for which  $H_y = L_y$ . For the case at hand (50 lb Wrist weight), this results in a counterbalance selection as shown in Figure IV-45. It is noted that, for the design shown in Figure IV-45, the total increase in shoulder pitch moment of inertia due to the 2900 Lb counterbalance weight, the 50 in yoke, the connecting rods, etc. is equivalent to a 42 Lb weight at the end of the wrist. When compared to the larger payloads, this increase can be considered negligible.

Throughout the foregoing investigation, it was felt that the counterbalance selection would be fairly sensitive to the wrist weight. For this reason, the procedure described above was repeated for wrist weights of 60, 70, 80, 90 and 100 Lbs. The resulting values for the yoke dimensions ( $H_y = L_y$ ) and the corresponding counterbalance weights are shown in Figure IV-46. From the figure, it can be seen that neither the counterbalance weight nor the yoke size are seriously affected by increases in wrist weight within the range shown.

In conclusion, it should be noted that the results presented above are derived from preliminary design data and should periodically be updated as the AMS design progresses. With the computer program described in Section 4, this merely entails changing the appropriate input data.

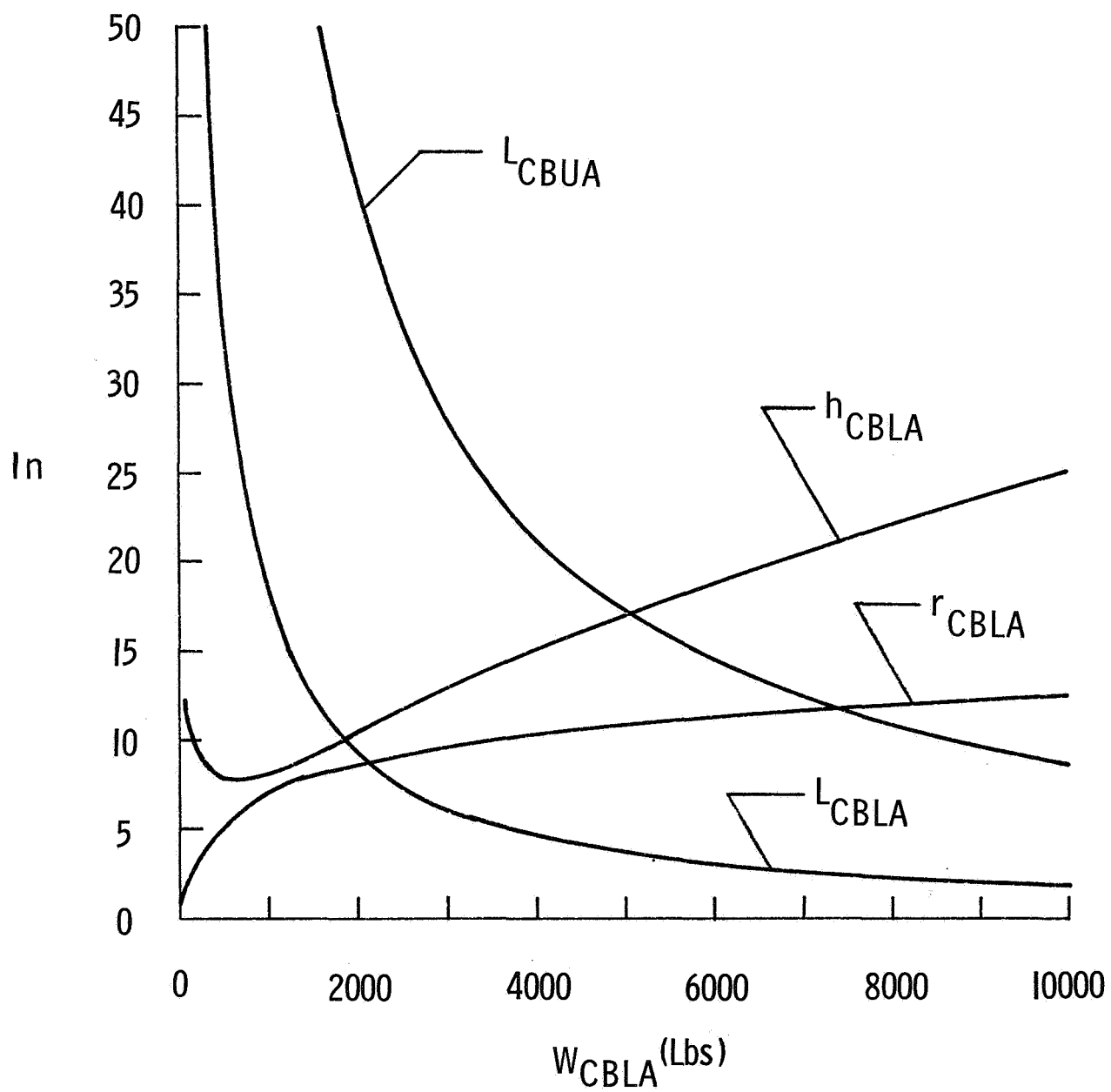


Figure IV-42 Counterbalance Dimensions

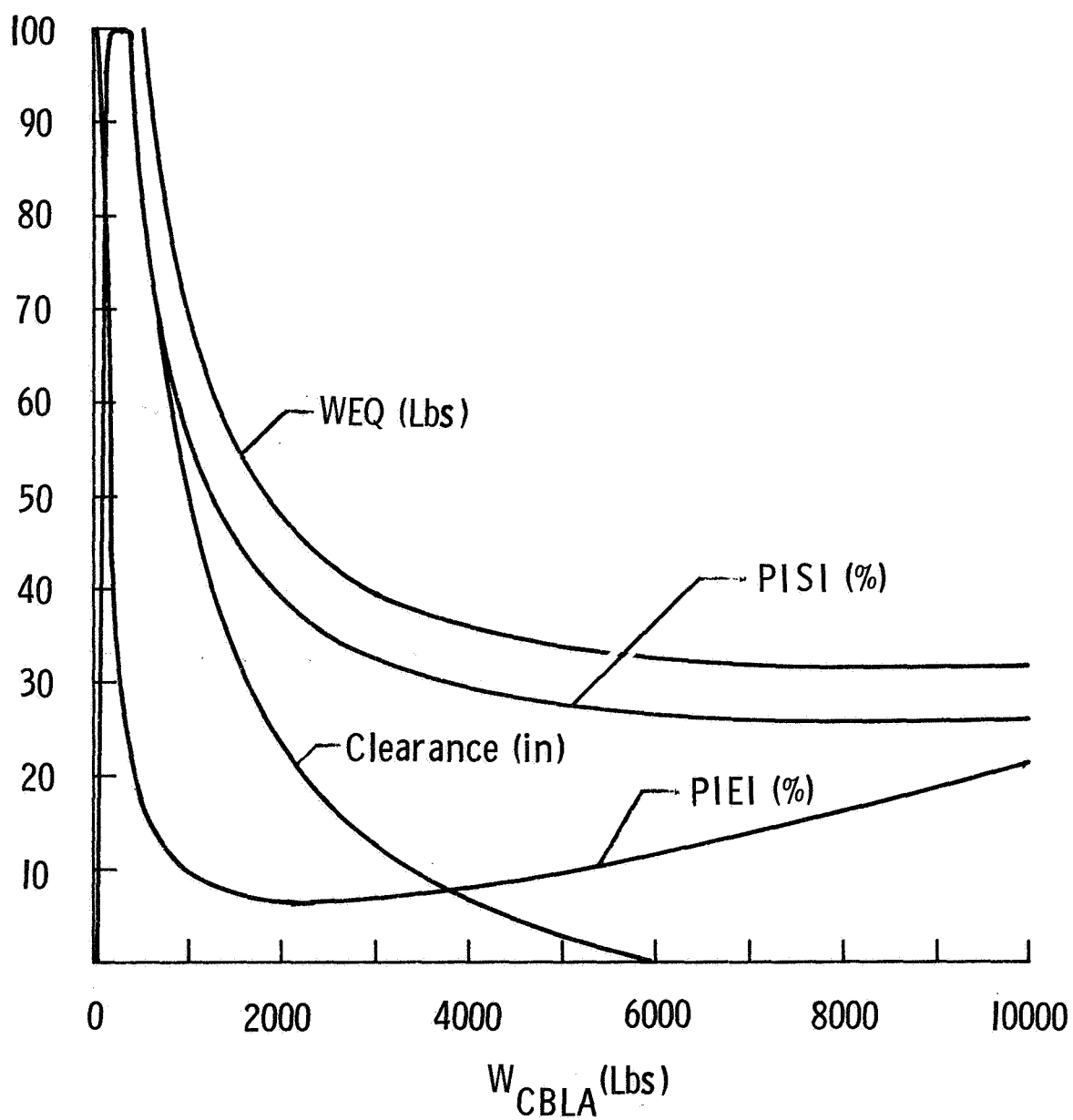


Figure IV-43 Increase in Moment of Inertia

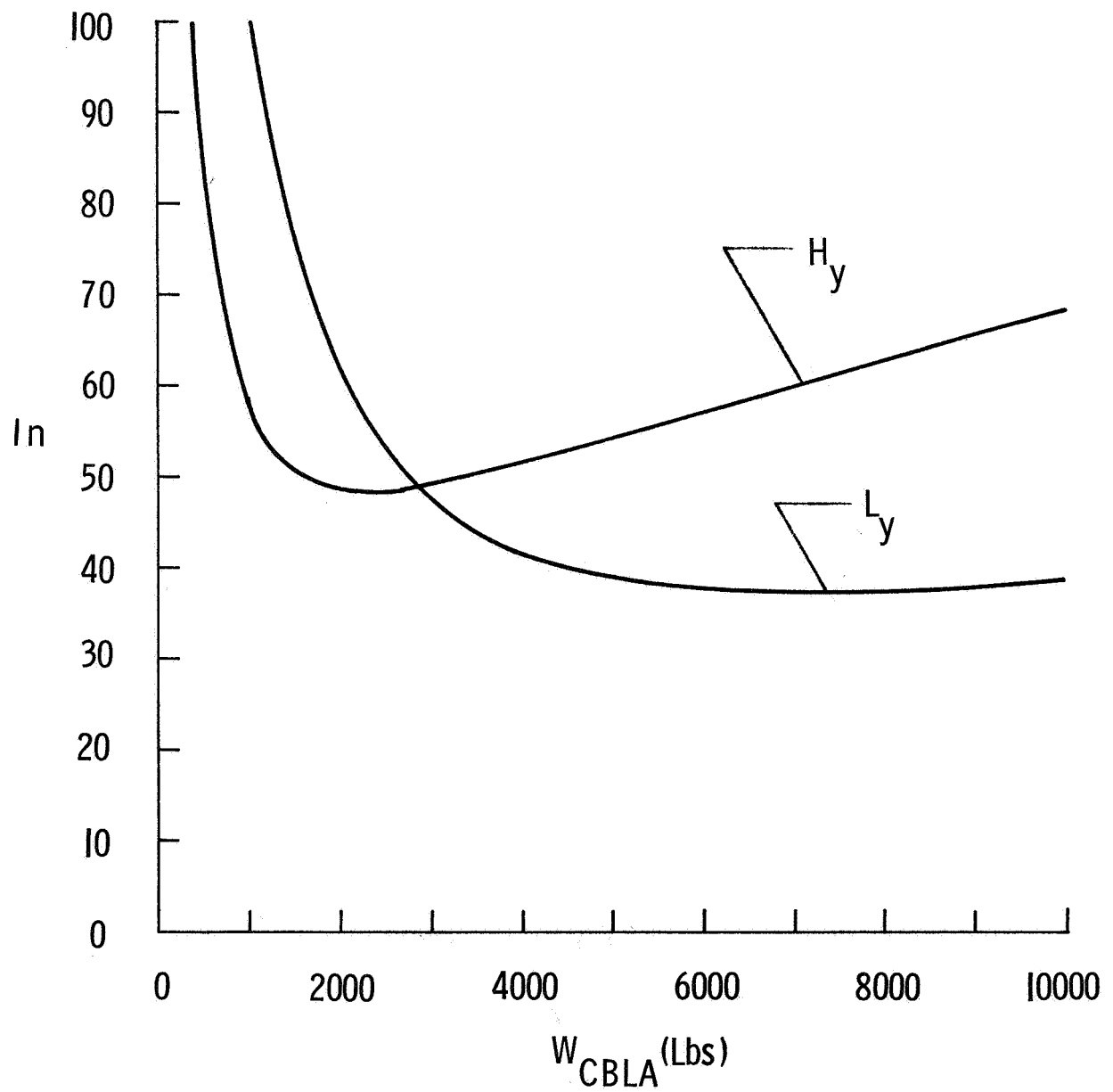


Figure IV-44 Yoke Dimensions

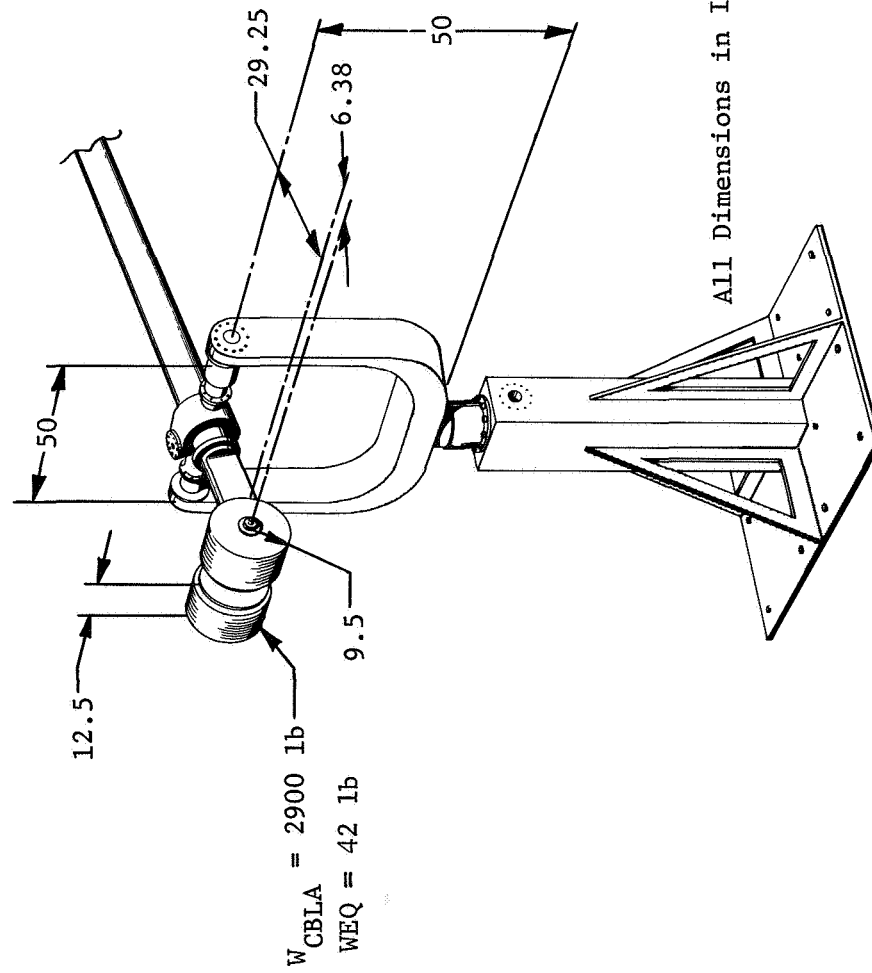


Figure IV-45 Counterbalance Design Selection

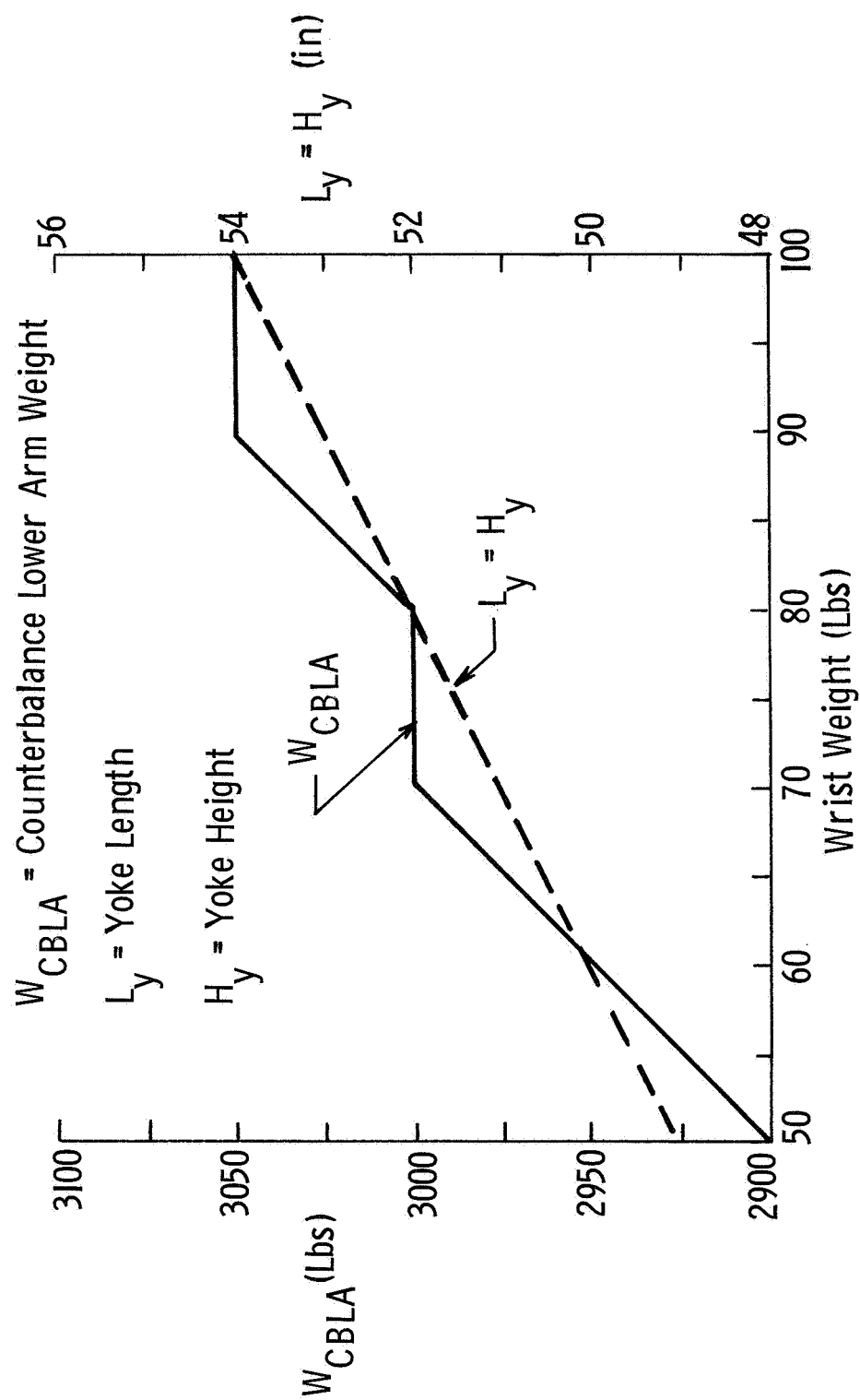


Figure IV-46 Counterbalance Selection vs Wrist Weight



## C. COUNTERBALANCE LINKAGE

### 1. Introduction

It was pointed out in the preceding section that, in order to counterbalance both the upper and lower arms simultaneously, the counterweight must pivot relative to the upper arm in concert with the rotation of the lower arm at the elbow (See Figure IV-36). What is needed, therefore, is some relatively rigid linkage (passing through the hollow upper arm) connecting the lower arm to the counterweight. In making such a connection, the gravity torque (of the lower arm and wrist) about the elbow will be transmitted to the counterweight joint where it can be nullified by proper design of the counterweight. In what follows, several techniques to accomplish the torque transmission are investigated.

Primarily because of stiffness considerations, a multi-bar linkage was selected as the most satisfactory. A prototype of such a linkage was then constructed and a number of tests were conducted. Both a description of the hardware and the test results are described in the sequel.

Finally, drawing upon the results of the analyses and tests described above, a three bar system was selected as the recommended design. Several aspects of this design are included in the following discussion.

### 2. Alternative Linkage Methods

The general requirements for the counterbalance linkage are as follows:

- (1) Within the 12 inch diameter tube,
- (2) Anticipated counterbalancing maximum torque of 2000 ft - lbs.,
- (3) High efficiency (low friction), especially breakaway,
- (4) Low inertia compared to the total arm,
- (5) High stiffness compared to tubes,

- (6) Materials should comply with standard machining and tolerance capabilities.

The alternatives considered are listed in Table IV-6, which gives a comparison of the important characteristics. Figure IV-47 shows the concept of each.

Single Cable - For simplicity this would be the ideal design, however, the restriction of pulley size by the AMS envelope and the cable manufacturer's restriction of cable size for an 8 in. dia. With a torque of 2000 ft-lbs, this cable will have a tension of 6000 lbs. If the cable's diameter is increased to accommodate larger capacities, the bending stress will increase rapidly and will make the design less reliable and subject to flexing (bending) fatigue in fewer cycles.

Multi-Cable - This is a compromise design where the load will be distributed to several 5/32 in. or 3/16 in. dia. cables which can be operated at cable manufacturer's suggested load level. This design is one of the more promising of the counterbalancing systems. A simple test setup of this system was built and data was taken at various loads. Figure IV-49 shows the setup which consisted of two stainless steel 7/32 in. dia. (7 x 19) stranded cables with pulleys. The pulleys had 9 in. pitch diameters. The goal was to obtain starting friction data including bearing friction and cable friction. The cable preloads were varied as well as the torque of the system the data below shows general characteristics of this setup.

The data indicated that the preload on the cables has minimum effect on the starting friction. The curves (Figure IV-48) also show the bearing starting friction characteristics. The strain measurements taken from this setup were not consistent with each run but the magnitude of strain was measured. At rated 170 ft-lbs torque the elongation was in the order of .18 in. to .20 in. The pulleys were 9 in. dia. The resultant strain was .003 in./in. The exact relationship between torque losses due to cable bending and bearing friction were not determined.

One disadvantage of this system is that the large wide pulley with many cables would occupy most of the elbow joint space. Also, the establishment of uniform strain in each cable without individual turn buckles may be a problem. However, the cable manufacturer recommends the use of multiple cables on a swaged fitting end with a common turn buckle. This would need further investigation.

Table IV-6 Evaluation of Alternative Methods in Counterbalance Linkage Methods

	Envelope Size at Elbow	Gogging Possibility	Strain Possible Within Envelope	Stress Level Within Envelope	Spring Constant	Reliability for Break	Inelastic Stretch	Bearing Support	Complexity	Wt & No. of Bars	Inertial Effect	Efficiency
A Single Cable	Small	None	High	Very High	Very Low	Low	Yes High	2 Necessary	Simple	Low 2	Low	High
B Multiple Cable with Bars at Middle (2)	Large	None	High	Medium	Medium	Medium	Yes Medium	2 Necessary	Simple	High 2	Low	High
C Torsion Bar with Bevel Gear Reduction	Large	Possible	Medium	Low	High	High	None	2 Necessary	Complex	High 1	High	Low
D Chain Drive with Bars at Middle	Small	Yes	Low	Low	High	Low	Yes Low	2 Necessary	Very Complex	Low 2	Low	Low
E Single Tape With Spur Gear Reduction	Small	Possible	Medium	Medium	Medium	Low	Yes Low	2 Necessary	Complex	Med 0	High	Low
F Multiple Tape with Double Pulleys at Each End	Very Large	None	Low	Low	High	High	None	2 Necessary	Complex	High 0	Low	High
G Quadruple Bar with Spur Gear Reduction	Medium	Yes	Low	Very Low	Very High	Very High	None	6 Necessary	Very Complex	Med 4	High	Low
H Multiple Bar Direct Drive	Small	Possible	Low	Very Low	Very High	Very High	None	4 Necessary	Complex	High 3	Med	High

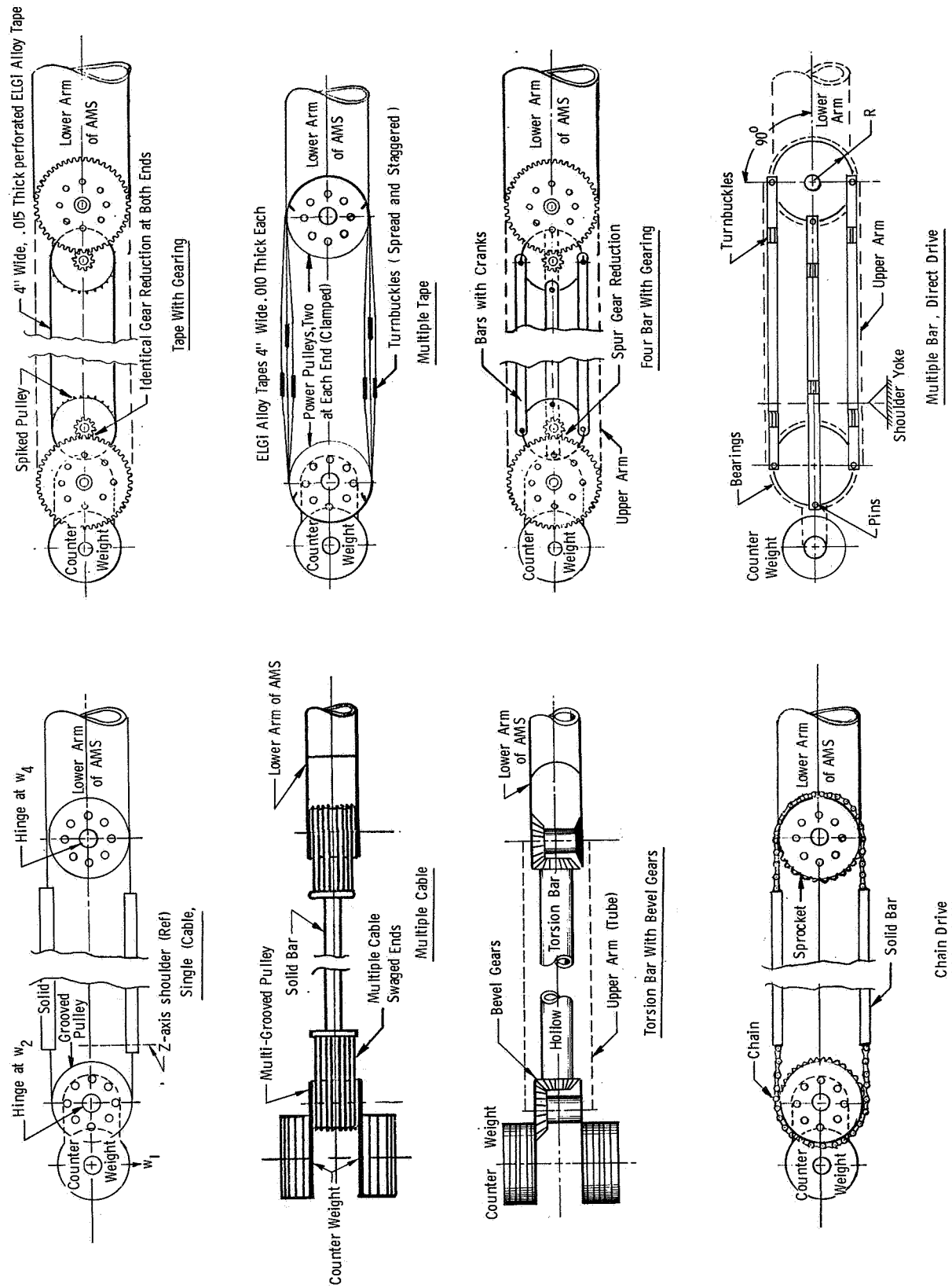


Figure IV-47 Counterbalance Linkage Concepts

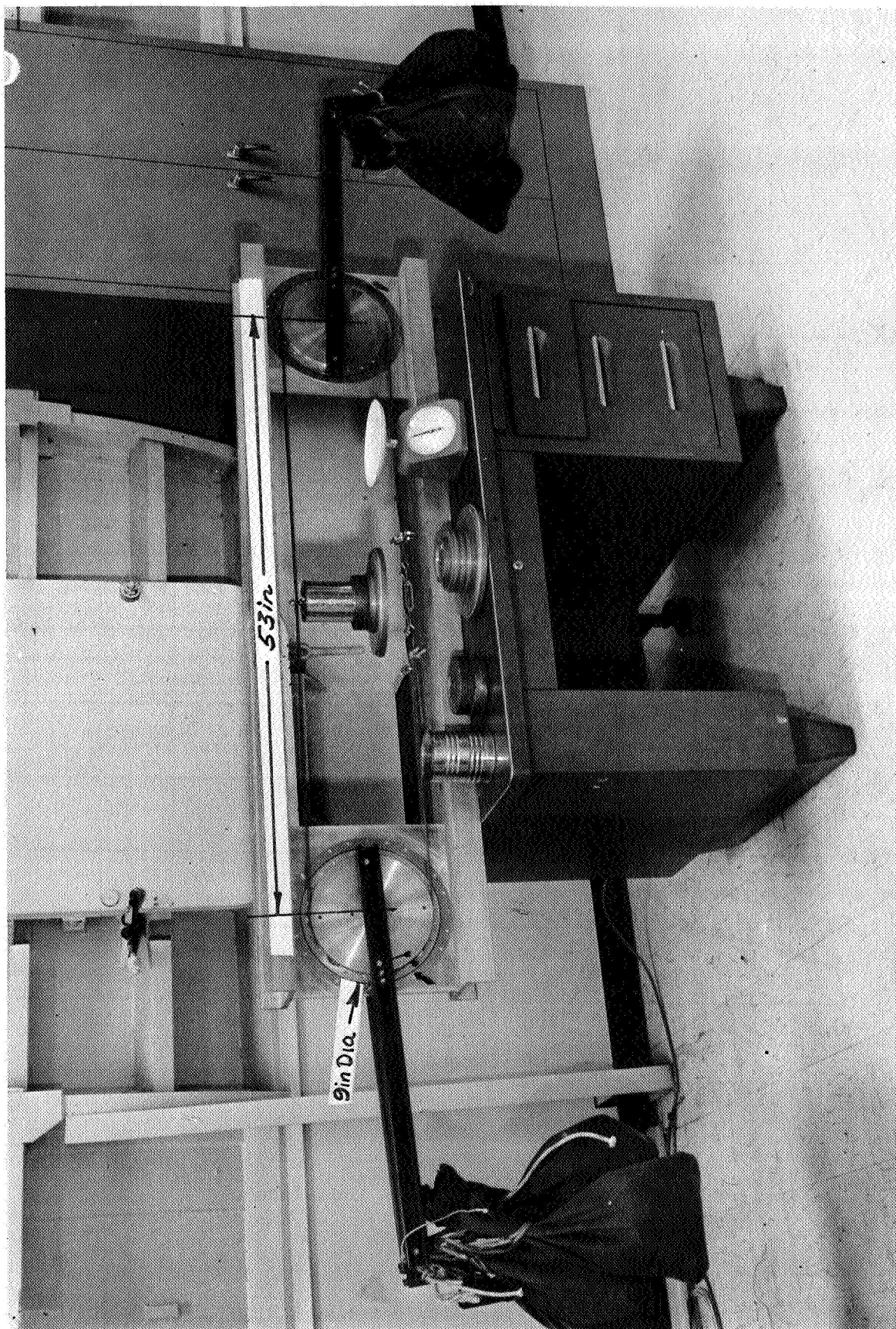


Figure IV-48 Multi-Cable Test Setup at Full Load Condition

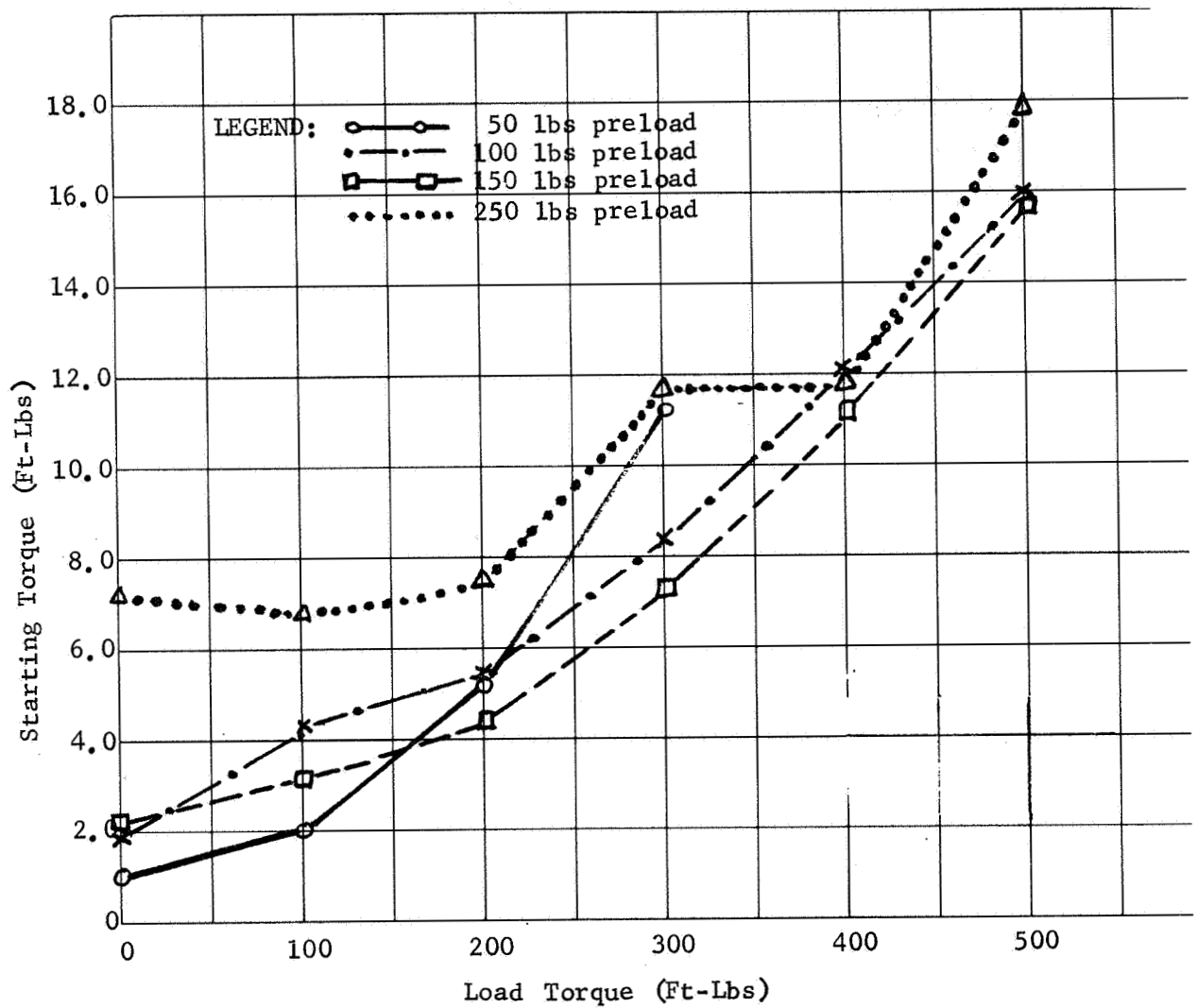


Figure IV-49 Starting Torque vs Load Torque

Torsion Bar with Bevel Gears - This system would require a large-sized torsion tube to achieve a comparative torsional strain to other systems. Even with the most efficient type of hollow torsion bar the diameter of the bar would occupy the greater portion of the center of 12 in. dia. tube which would give no other access for electrical cables, etc. In addition, the extra loss of efficiency and backlash of the two bevel-gear pairs would add to the friction level in this system.

Chain Drive - The chain-drive systems are frequently used for transmitting torque and where the strain changes and backlash are not important factors of the design. Tight chain systems are known to cog and to have lower efficiencies than loose chain systems generally used in chain drives.

Single Tape with Spur Gear Reduction - As in the case of the torsion bar, an extra gear reduction will cause backlash and low efficiency. The spiked pulleys may also cog as in the case of the chain drive. Strain is minimized as well as load in the tape by the large gear reduction. One can use a .010 in. to .015 in. thick by 4 in. wide tape for low bending stress operation.

Multiple Tape - This is a direct drive system with multi-layer tapes. It provides a good combination of bending and tensile stresses. Each tape, however, must be continuous, with turnbuckle adjustment mandatory. To accommodate the large number of turnbuckles, the 12 in. dia tube envelope is not adequate. Furthermore, the extra friction between tapes may cause efficiency problems for the system.

Quadruple Bar with Spur Gear Reduction - This four bar system will eliminate bending stresses found in tapes or cables. The bars are mounted 90° apart on plates on a common shaft with a drive pinion. The active bars are under pure tension. However, the gear reduction has additional backlash and complexity and will decrease the efficiency of the system.

Multiple Bar, Direct Drive - This system has all the good features of those discussed above and was selected for breadboarding. Four or three bars can be implemented. The disadvantage in this system is the extra weight of the bars, and some inertial increase of the system can be anticipated. The breadboard design and test results are presented below. A simplified version of this is the recommended method for the AMS and is discussed in Section 4.

### 3. Breadboard

Analytical evaluation of these several systems led to the decision to build a prototype of the multiple bar counterbalance linkage system using four bars, thereby proving the feasibility of the design. Its basic principle relies on the kinematics of the four bar linkage. Figure IV-50 depicts the concept with only one bar shown. The lower arm of the AMS now can be attached to one side of the crank (R) and to the other side a counterbalance weight is added to establish a mechanical equilibrium for the system. A torque is transferred via a tension bar to a point about 20 ft away. As the moment varies with the angular change ( $\theta$ ) of the lower arm, the tension in the bar also varies similarly, carrying the load to the counterweight up to  $90^\circ$  rotational displacement. Because of the dead center condition ( $R \cos \theta = 0$ ) the arm is unable to transfer any more moment to the counterweight and another connecting bar and crank must be introduced to the system. This bar must be out of phase from the first one. So the arm now once again is capable of transferring moment to the counterweight over the  $90^\circ$  limit. Then if the gravitational forces are inverted, a mirror image of the above bar and crank must be accommodated in the design. This four bar system was designed and fabricated as shown in Figure IV-47 (Multiple Bars, Direct Drive). It is similar to the final test article drawings no. RES3156050 and RES3150054 which are discussed in Section 4.

The multiple bars (each 1/2 in. x 2 in. x 16 ft) are attached to a separate disc plate so as to be non-interfering. Turnbuckles were provided to take up slack and pretension. Figures IV-51, IV-52, and IV-53 show the four bar system. It was mounted on a channel between two vertical columns. Figure IV-54 shows

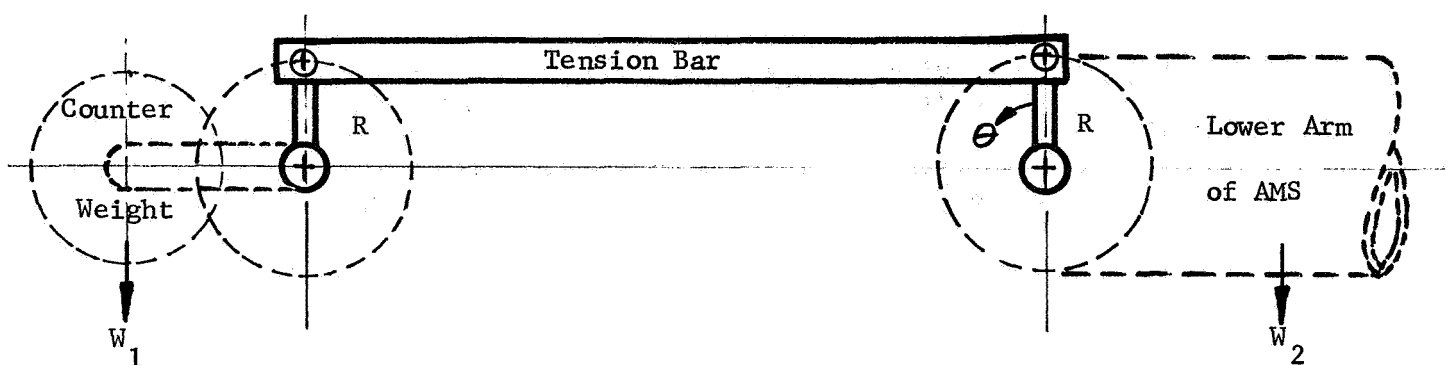


Figure IV-50 Counterbalance Bar Linkage Concept



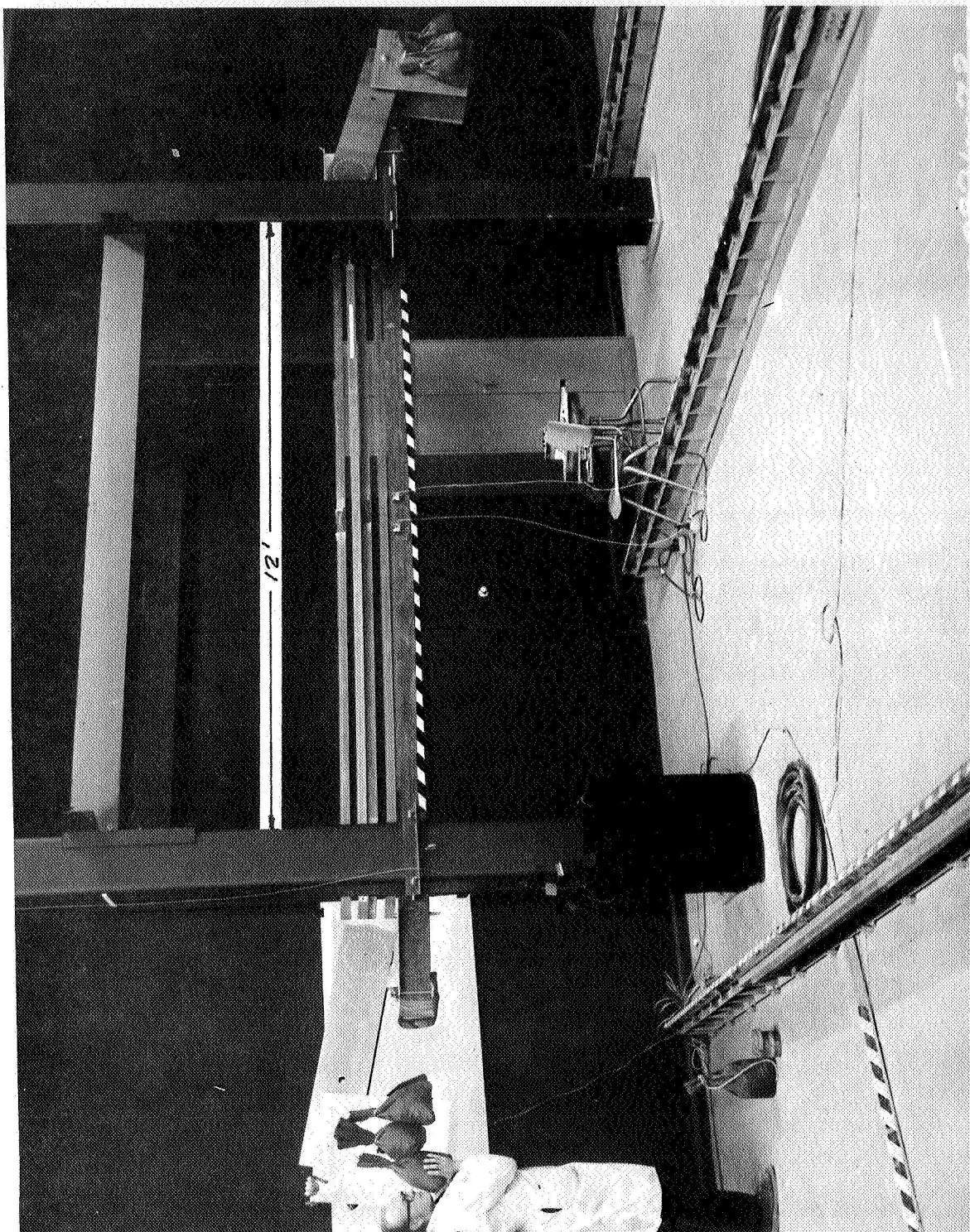


Figure IV-51 Four-Bar Test Setup With Load

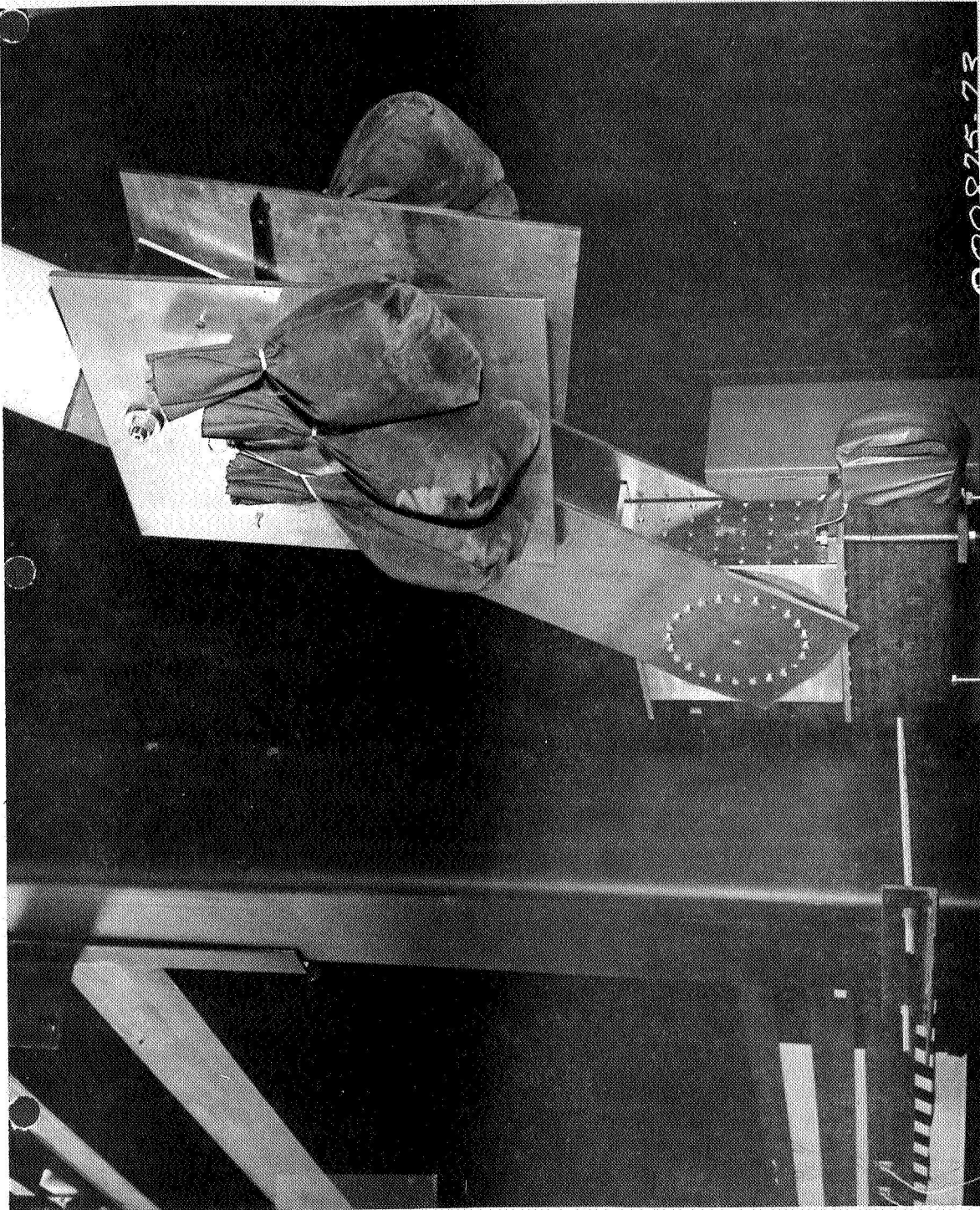


Figure IV-52 Four-Bar with Counterweight



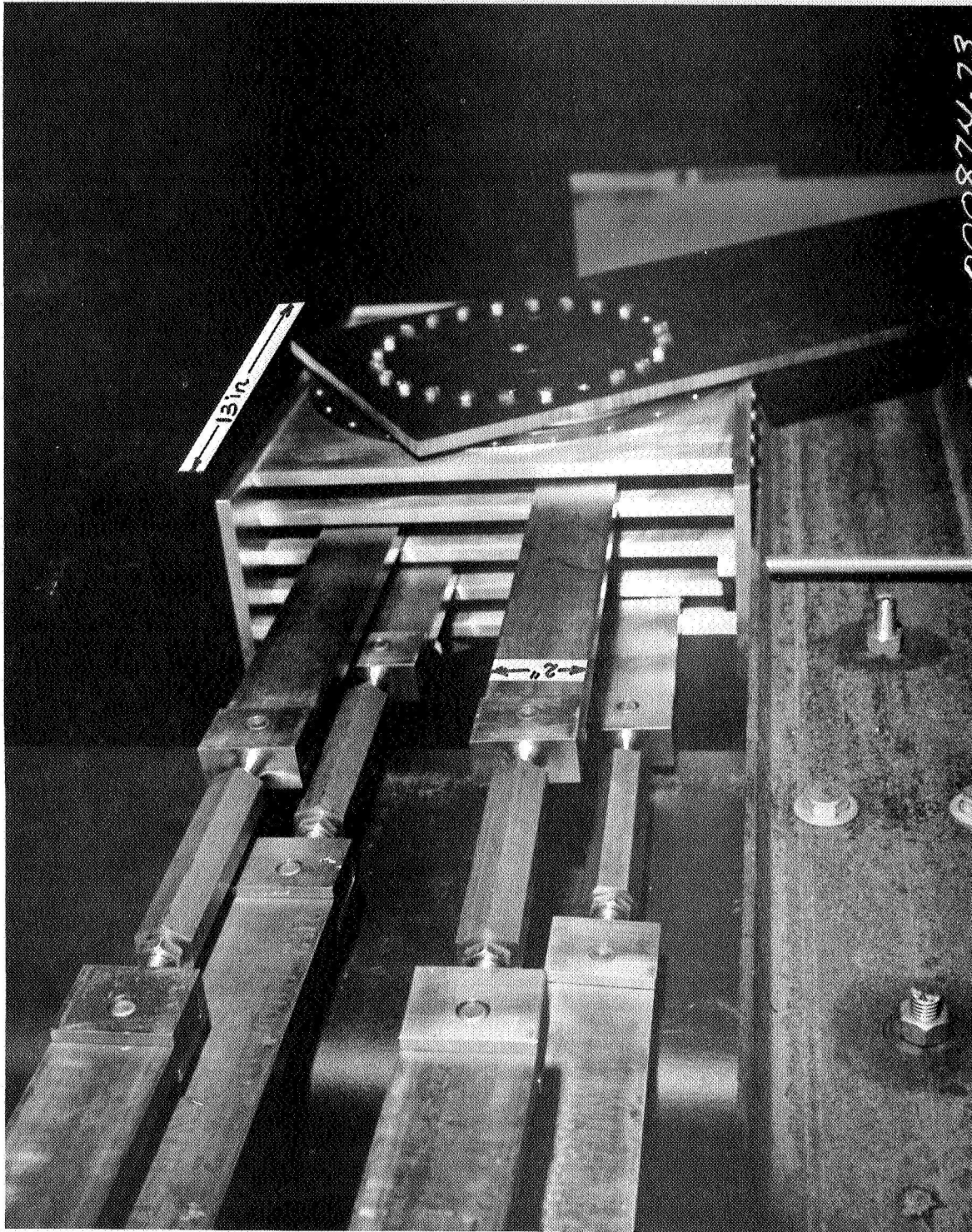


Figure IV-53 Four Bar Test Setup Showing Crank Assembly

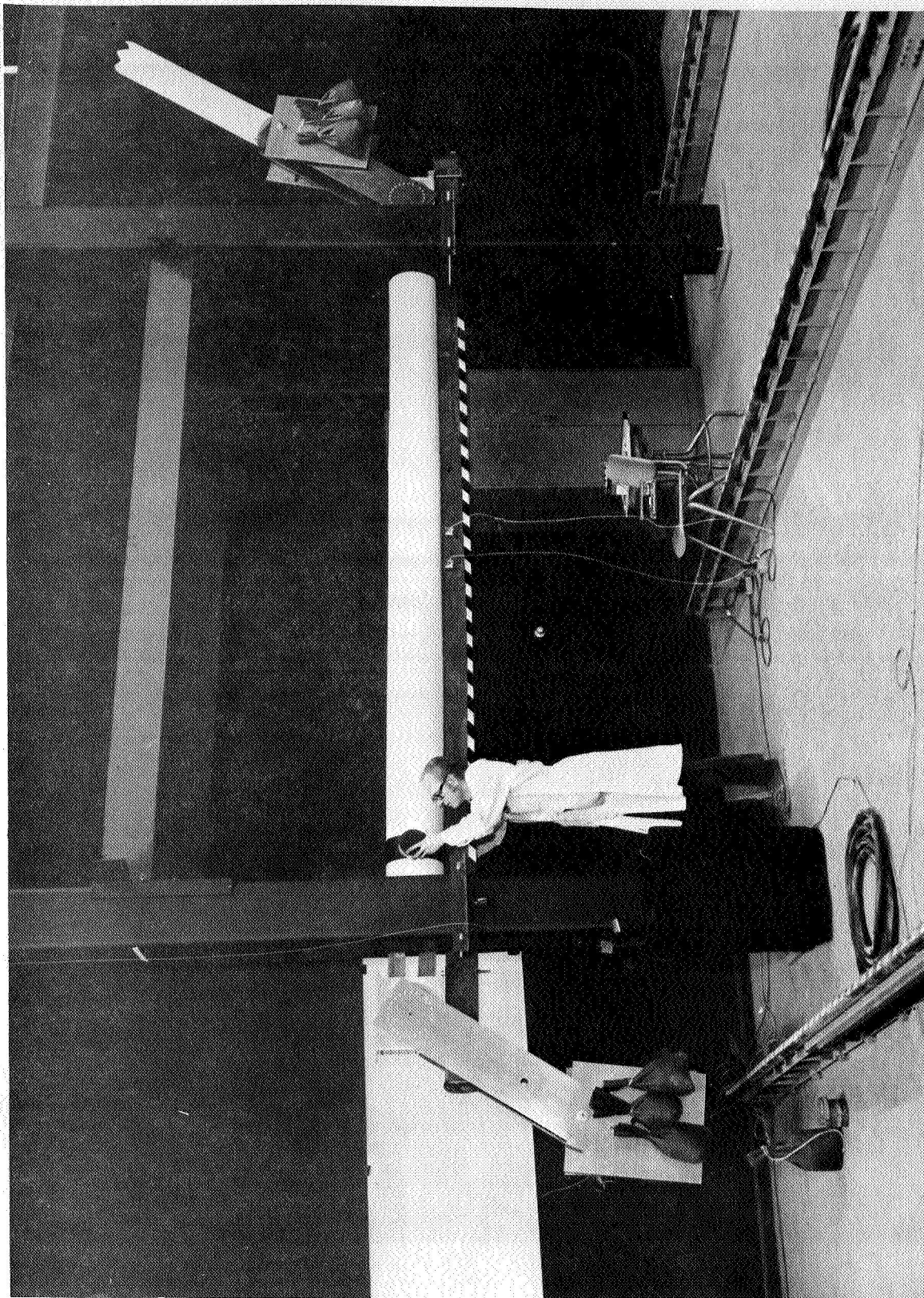


Figure IV-54 Test Setup of Counterbalancing System

the four bar system enclosed in 12 in. dia tubing to represent an approximate arm size.

Several things were learned from the four bar breadboard assembly:

- (1) Turnbuckles were difficult to adjust and align,
- (2) Three rods could do the required job (and take less space and be lighter),
- (3) Single rods without turnbuckles would aid in alignment and be easier to install.

These things prompted the modifications as shown in drawings RES3156050 and RES3156054 that represent the final test breadboard. Figures IV-55 and IV-56 show the test apparatus in its final configuration.

Torques to simulate actual AMS arm loaded conditions were obtained by simply suspending lead shot in bags in a manner so the lever arm was constant for each end (except for angular position that was easily calculated).

For each load condition, and at several angles, breakaway friction torque values were obtained by adding shot until breakaway.

#### Variation of Friction Torque with Arm Position

The curves in Figure IV-57 show the variation of bearing friction with load. The load on bearings varies with the angular position of the arm (weight or torque at  $0^\circ$  times  $\cos \theta$ ) and the data should reflect this. The bars had slight deformation in them, thereby causing some effect on the bearing load and the data obtained. Average efficiency is about 97.5%.

Starting Torque (Stiction) - One of the most important considerations of the counterbalancing system is the influence of bearing friction on starting torque. The bearings will see both axial and radial. The breadboard test system utilized the "type x" bearing by Kaydon Corporation for the large diameter supporting the drive disks and the catalog (analytical) frictional characteristics shown in Figure IV-58 apply.



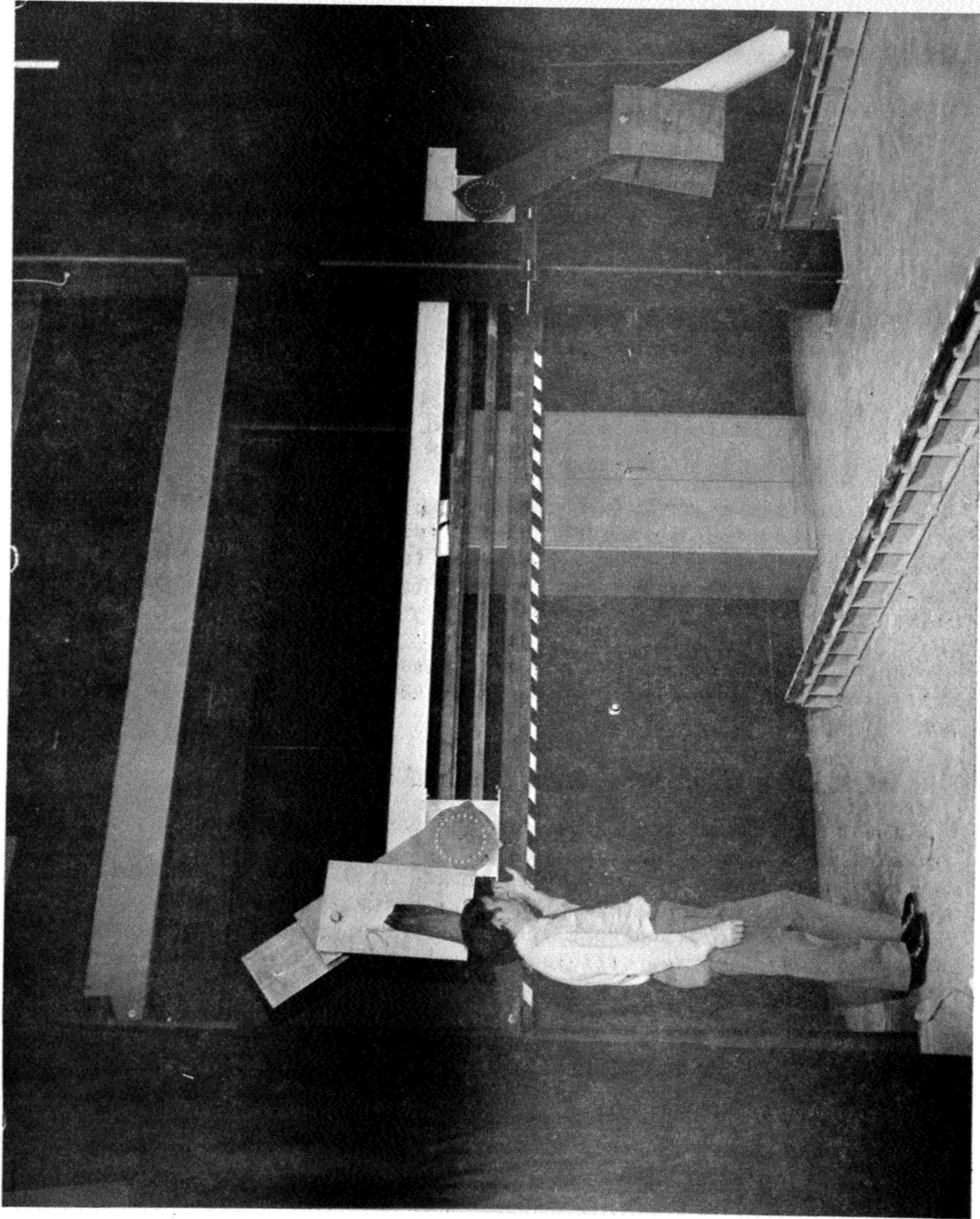


Figure IV-55 Triple Bar Counterbalancing Breadboard Test Setup

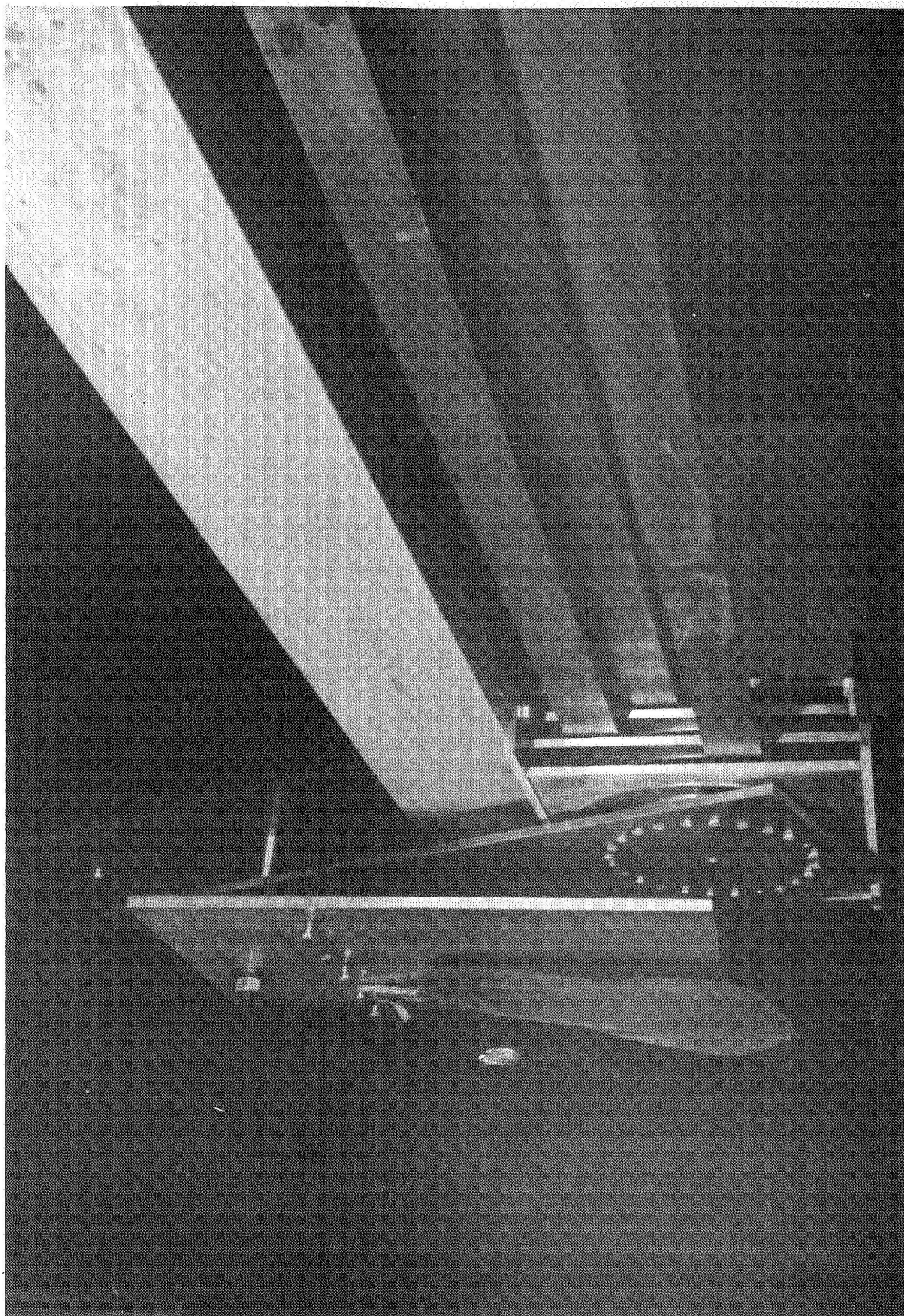


Figure IV-56 Closeup View of the Cranking Mechanism of a Triple Bar Counterbalancing Breadboard

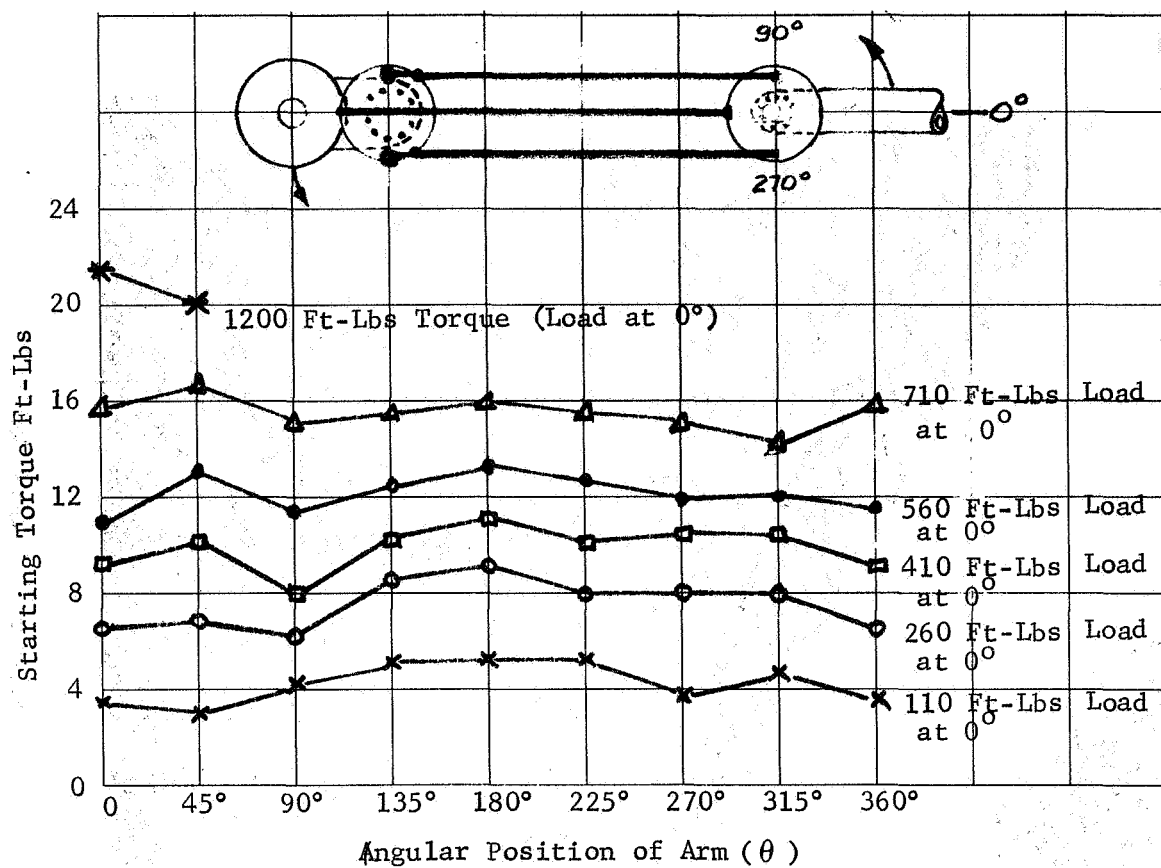


Figure IV-57 Friction Variation with Arm Position

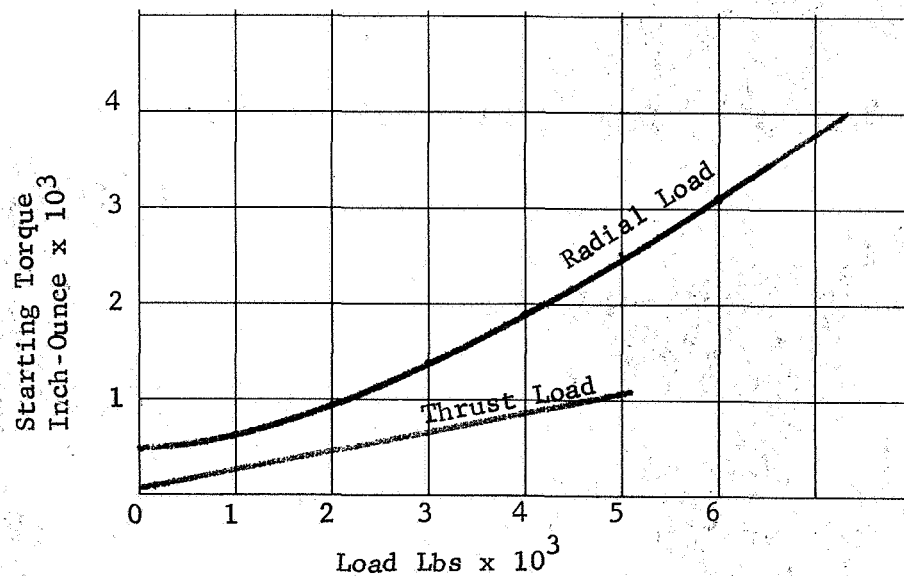


Figure IV-58 Typical Bearing Data



For comparison of experimental and analytical results assume a typical load of 1200 ft-lbs. Thrust loads are neglected for this comparison. The load on bearing (P) will be:  $P = \frac{1200}{4/12} =$

3600 lbs (Read starting Torque from Graph). This load will apply to large bearings at the arm end and the large bearings at the counterweight. Therefore, the total starting torque should be:

$\frac{2 \times 1750 \text{ in-oz}}{192} = 18.3 \text{ ft-lbs.}$  Comparing this to the measured

21.5 ft-lbs torque (Figure IV-59) it can be concluded that high percentage of the starting friction originates in the large diameter bearings. A linear extrapolation to 1600-2000 ft-lbs would appear conservative and reasonable assuming the initial bearing capacity was not exceeded.

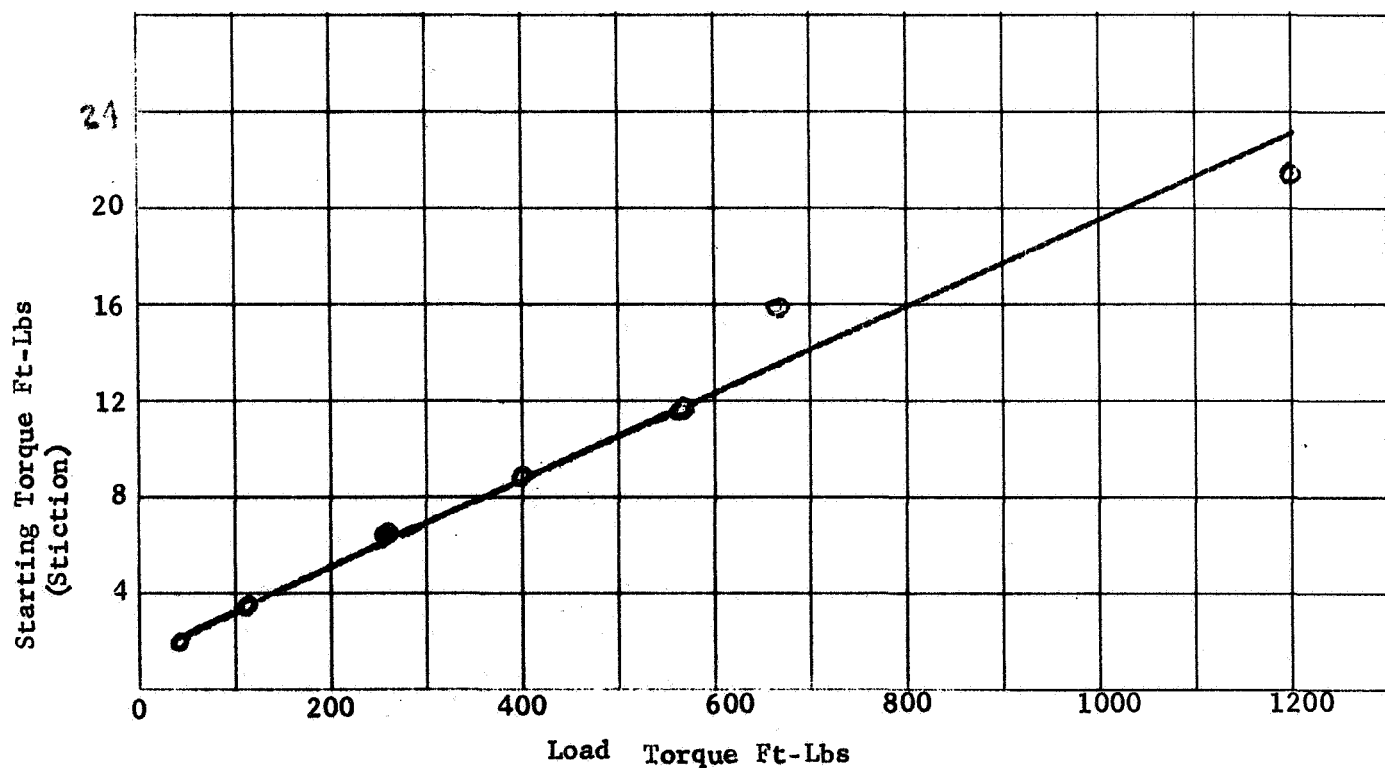


Figure IV-59 Breakaway Torque Losses

#### 4. Counterbalance Design For AMS

The final design of the recommended AMS counterbalance linkage system is presented here. It is a three bar system, each located  $120^\circ$  apart. This is the result of comparing the various alternatives, and the breadboard fabrication and test program results presented above.

The total counterbalance linkage system is shown schematically in Figure IV-60.

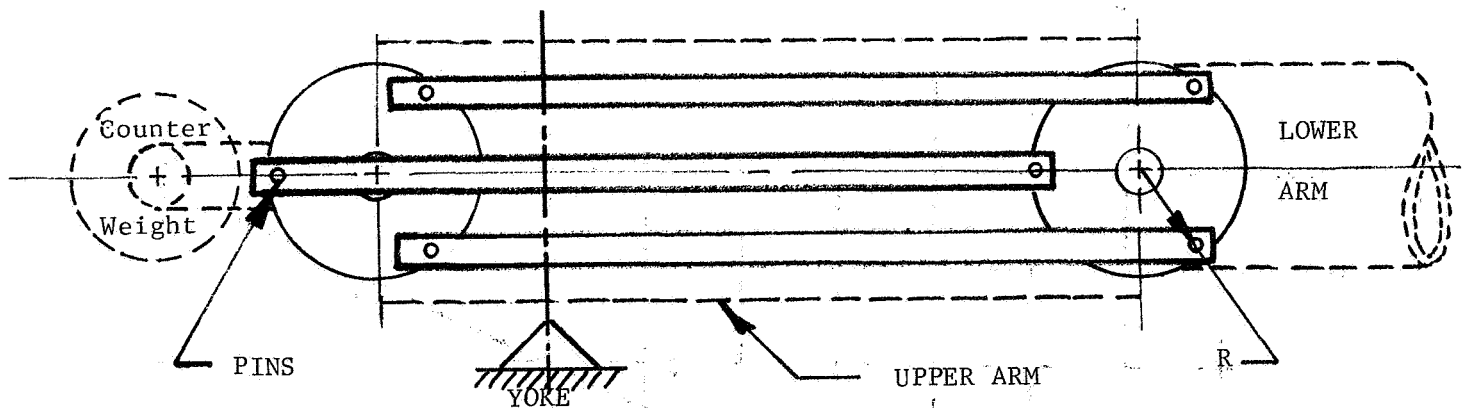


Figure IV-60 Selected Three Bar Counterbalance Linkage System

In order to avoid interference of one bar by the other each of the three bars is mounted on a separate power or crank plate. Their assemblies form a crankshaft-piston rod combination similar in concept to an automobile engine. The pin locations in the plates are  $120^\circ$  out of phase from each other (evenly divided on the diameter). The same arrangement of drive disks, etc., as shown in drawings RES3156050 and RES3156054 will be used. Space has been allowed in the elbow joint for this mechanism. (See drawing RES3156339).

The three bars will form a symmetrical assembly. The symmetry is important from the point of view of sensitivity. An out of phase bar will influence the stability of the counterbalanced equilibrium of the system. This can have a very considerable influence especially at no load condition. A short proof is presented here that if the bars are located  $120^\circ$  out of phase from each other then the moments about the center of rotation (c) caused by their weights will be in equilibrium under any angular position. This geometry is shown in Figure IV-61.

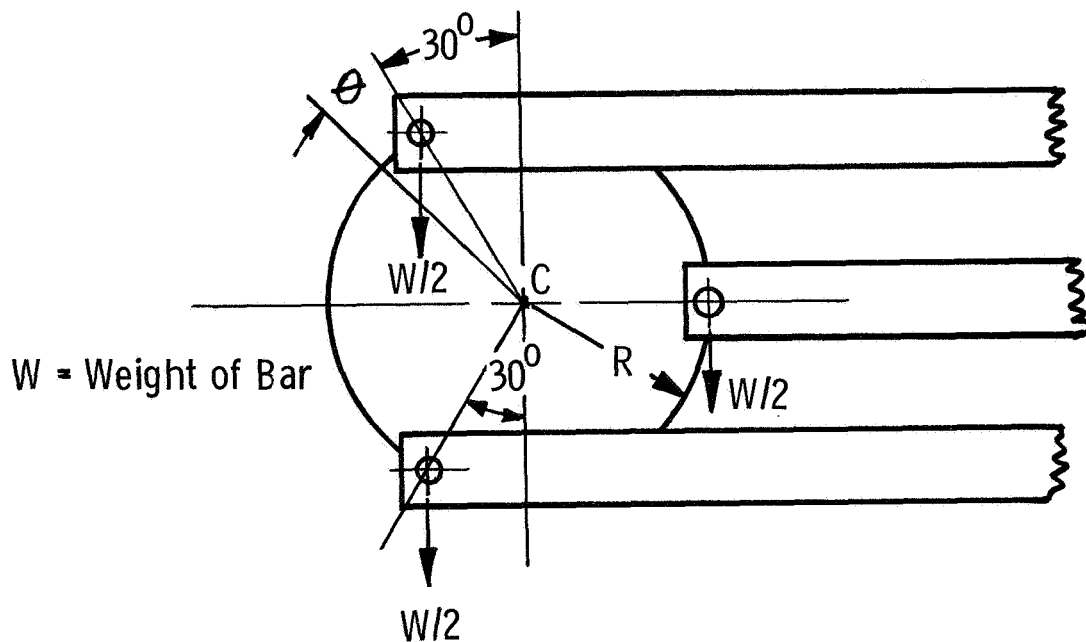


Figure IV-61 Three Bar Counterbalance Geometry and Loads

One can displace the angular position of the crank by an angle  $\theta$  then to have equilibrium, the sum of the moments around c must vanish. ( $M_c = 0$ ).

$$\frac{W}{2} R \cos \theta - \frac{W}{2} R \sin (30^\circ + \theta) - \frac{W}{2} R \sin (30^\circ - \theta) =$$

$$\begin{aligned}
&= \frac{W}{2} R(\cos\theta - \sin 30^\circ \cos \theta - \cos 30^\circ \sin\theta - \sin 30^\circ \cos\theta + \\
&\quad \cos 30^\circ/\sin) = \\
&= \frac{W}{2} R(\cos\theta - \sin 30^\circ \cos\theta - \cos 30^\circ \sin\theta - \sin 30^\circ \cos\theta + \\
&\quad \cos 30^\circ/\sin) = \\
&= \frac{W}{2} R (\cos \theta - 2 \sin 30^\circ \cos\theta) = 0
\end{aligned}$$

Therefore, the tension bars will not influence the equilibrium condition or sensitivity of the system under any angular position.

The upper arm tube diameter will be the only limitation of size of the system. The recommended system uses 8 in. drive diameter and an 11 in. overall diameter, which is a convenient size to work with inside the 12 in. structural tube of the AMS. The working volume of the three bars is 2.5 in. x 10 in.

The same 2 in. by 1/2 in. cross section cold rolled steel used for the breadboard bar was selected for each connecting bar. This can later be increased or decreased in size to vary stiffness. The magnitude of the tensile stress and strain in the bar is calculated to be 7000 psi and 0.00275 in./in., respectively.

From dynamics and buckling stress point of view the maximum compressive load should be calculated. The critical load for the above bar with hinged ends can be found from the Euler critical load formula:

$$P_{CR} = \frac{E I_z}{L^2}$$

Where:  $I_z$  = Moment of inertia of cross section with respect to the neutral axis for rectangle  $I_z = \frac{1}{12} b h^3$   $I_z = \frac{1}{48} \text{ in}^4$

$$\text{Then: } P_{CR} = \frac{2 \times 30 \times 10^6}{(240)^2 \times 48} = 108 \text{ lbs.}$$

This means, the bar has practically no load carrying capacity as a column. However, before the bar buckles the opposite tension bar will assume the torque load in tension. One might say that all of the counterbalance torque transmittal loads are carried in the bars in tension, with the compressive forces negligible.

In designing the crank pins, the forces shown in Figure IV-62 are taken into account.

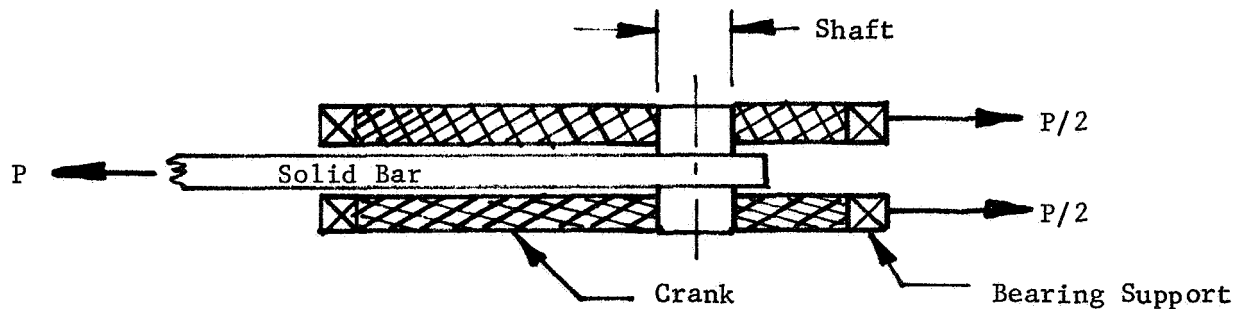


Figure IV-62 Typical Double Shear Pin Connection

Using SAE4340 steel the minimum pin size is calculated to be 0.382 in. diameter.

The drive disks at the elbow and at the opposite end will be identical, even the method of attaching the output torque tube from the drive disks to the yoke.

The bearings used in the breadboard test apparatus for outside diameter drive disk support should be entirely adequate for the final design and are shown in the elbow joint design dashed in the drawing RES3156339. Small needle bearings were used as the connecting rod bearings. More accurate bearings of the same type should be used in the final assembly.

The entire counterbalance system should operate as efficiently (97.5%) as the test apparatus.

#### D. OVERALL MANIPULATOR DESIGN

Figure IV-63 is the design layout of the AMS manipulator. The base and post are designed to allow mounting the yoke in the vertical or horizontal orientations. The counterbalancing linkage design is based on the 3-bar breadboard results. The design of the shoulder and elbow joints has been discussed in Section A. (The wrist and terminal device designs are not a requirement of this contract) Tube connections are shown in drawing RES3156301.

A model of the AMS manipulator was designed and fabricated. Figures IV-64 through IV-69 are photographs of various views. The model is scaled to approximately 15%. This permits it to be used easily on a desk top and for transporting with luggage, yet it is large enough to demonstrate concepts. The arm length from shoulder to tip is 6 ft. The base supports the arm with stability regardless of arm position or with the yoke mounted either vertically or horizontally.

A braking device was installed at each joint to enable partial friction to be applied to hold fixed in specific positions. These were clamping or pressure type arrangements for model purposes only. The counterbalance torque transmittal for the model utilized 1/16 in. diameter cable, rather than the connecting bars recommended for the full scale manipulator. This was sufficient for the 15% model. There was no sacrifice in elbow to wrist articulation due to this variation. This model proves the articulated counterbalancing concept.

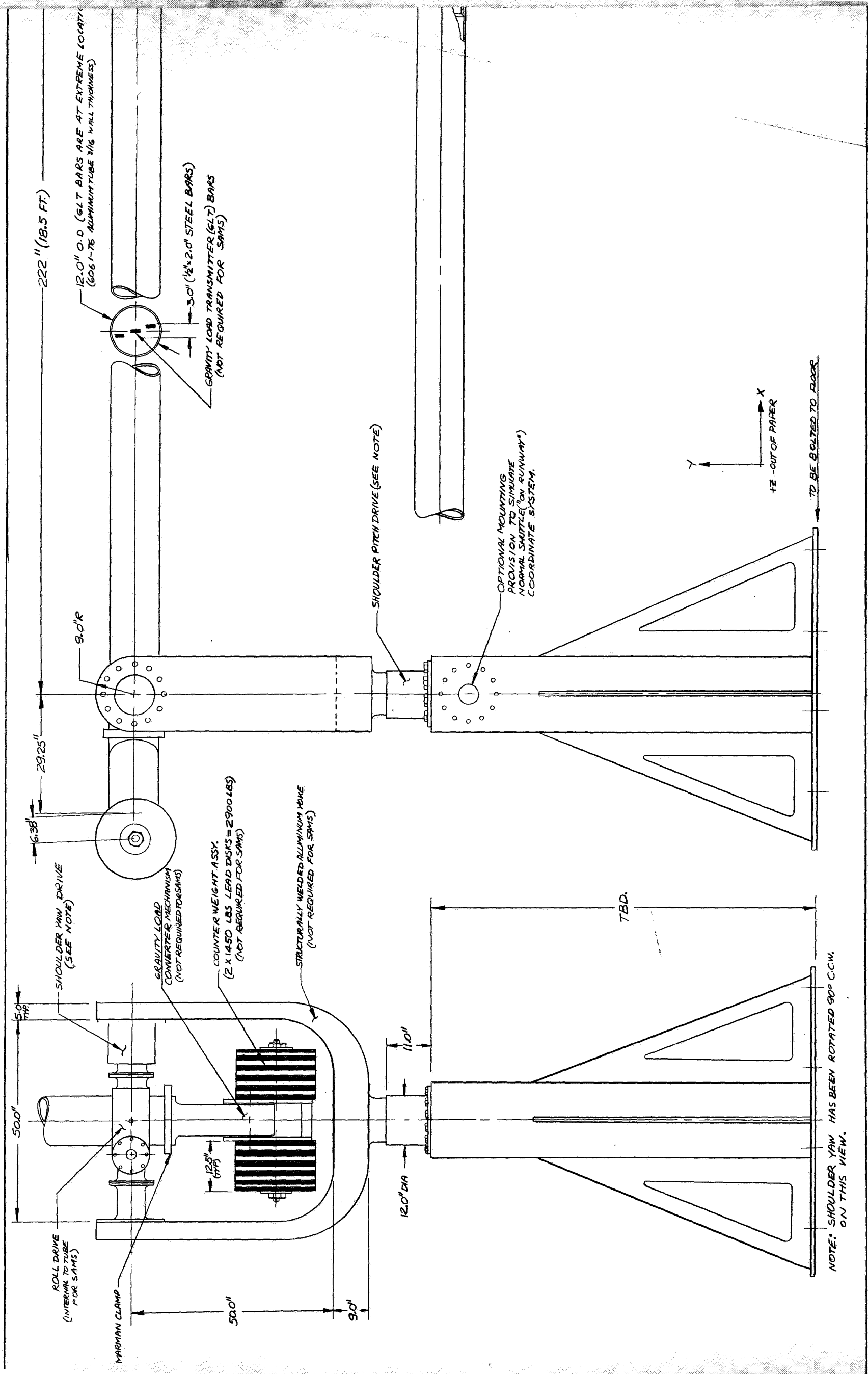


Figure IV-63 Assembly Drawing of Counterbalanced Manipulator





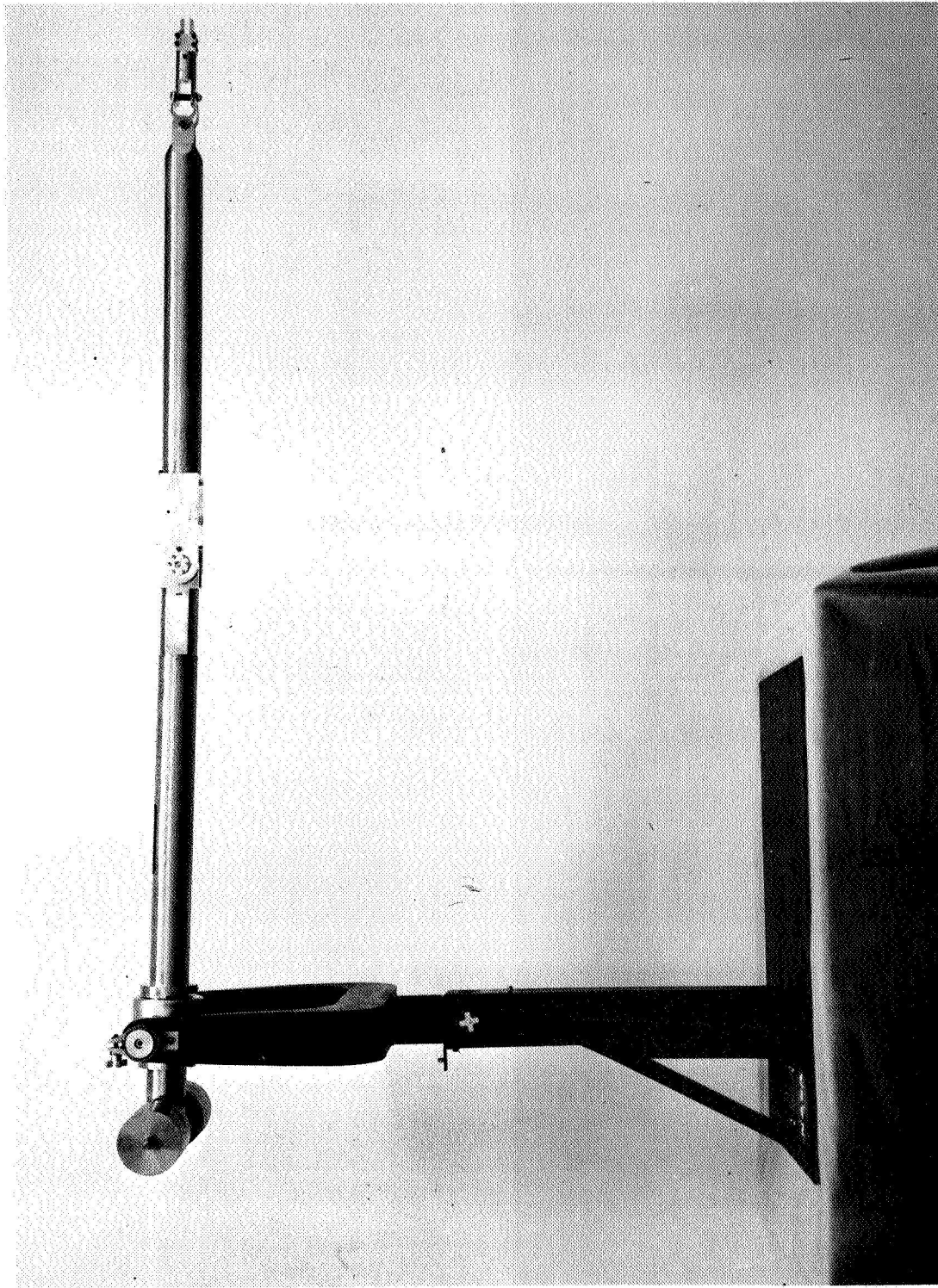


Figure IV-64 AMS Manipulator Model Fully Extended

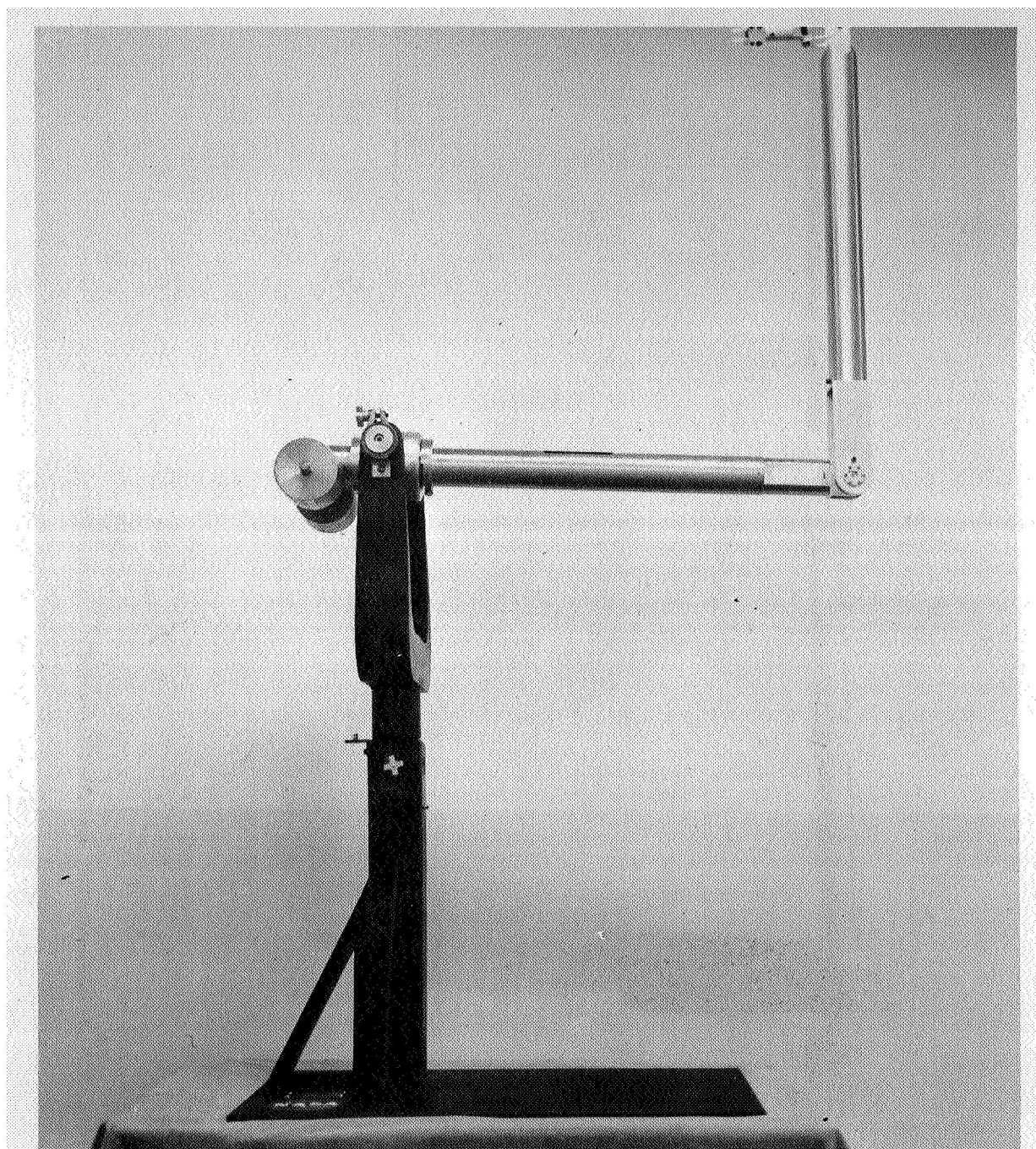


Figure IV-65 AMS Manipulator Model with Yoke Mounted in Vertical Position

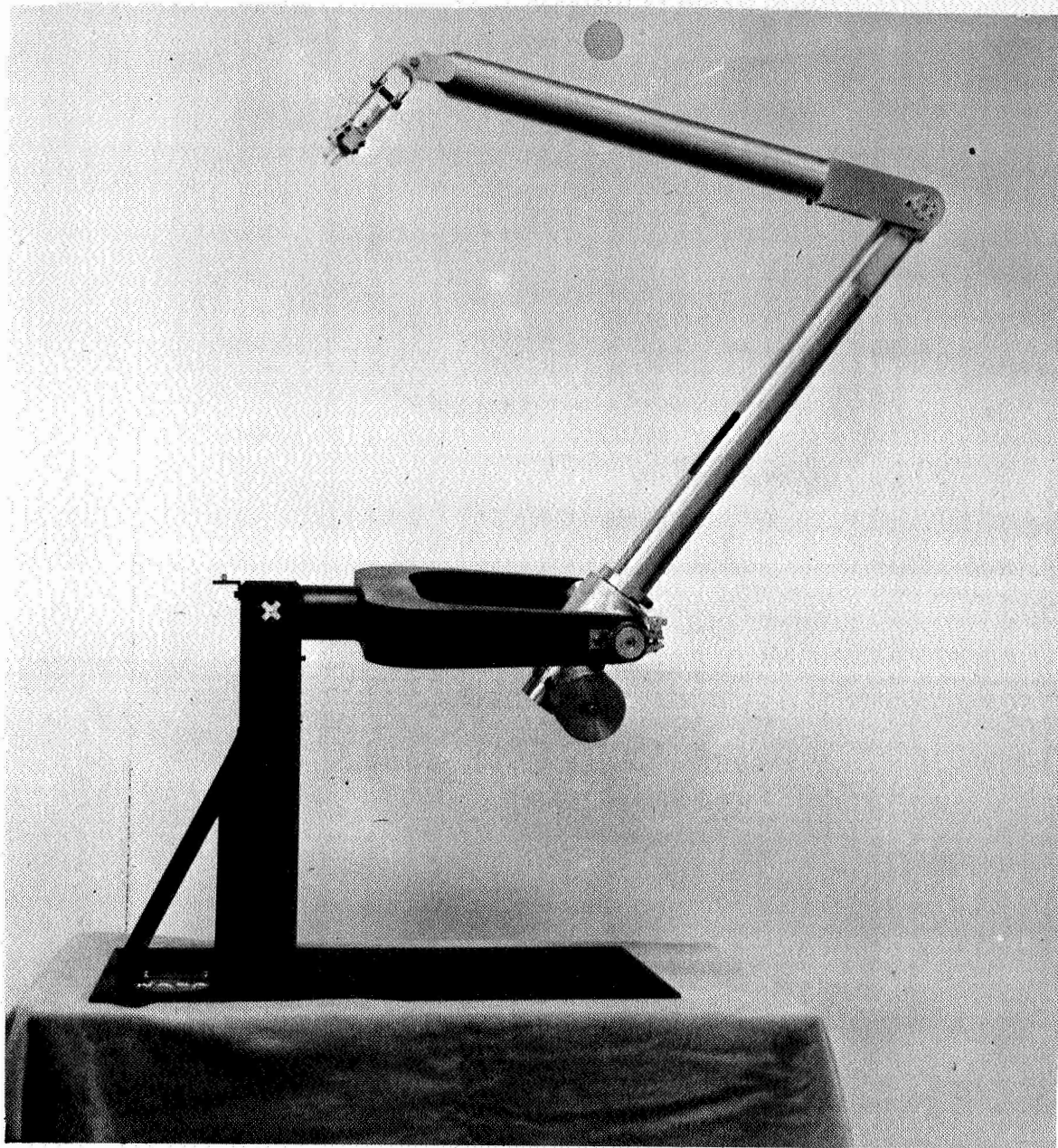


Figure IV-66 AMS Manipulator Model With Yoke Mounted in Horizontal Position



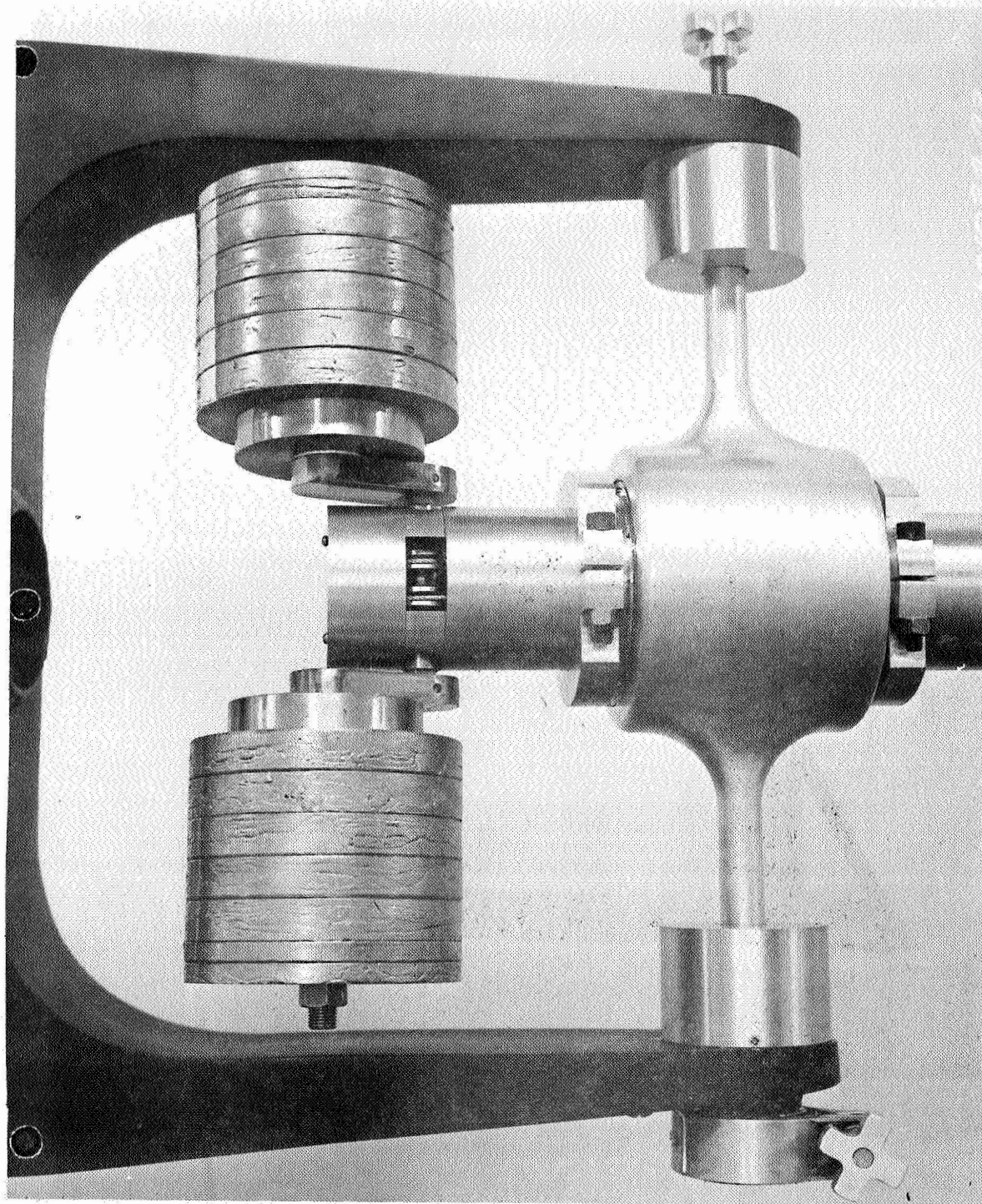


Figure IV-67 AMS Manipulator Model Counterbalance

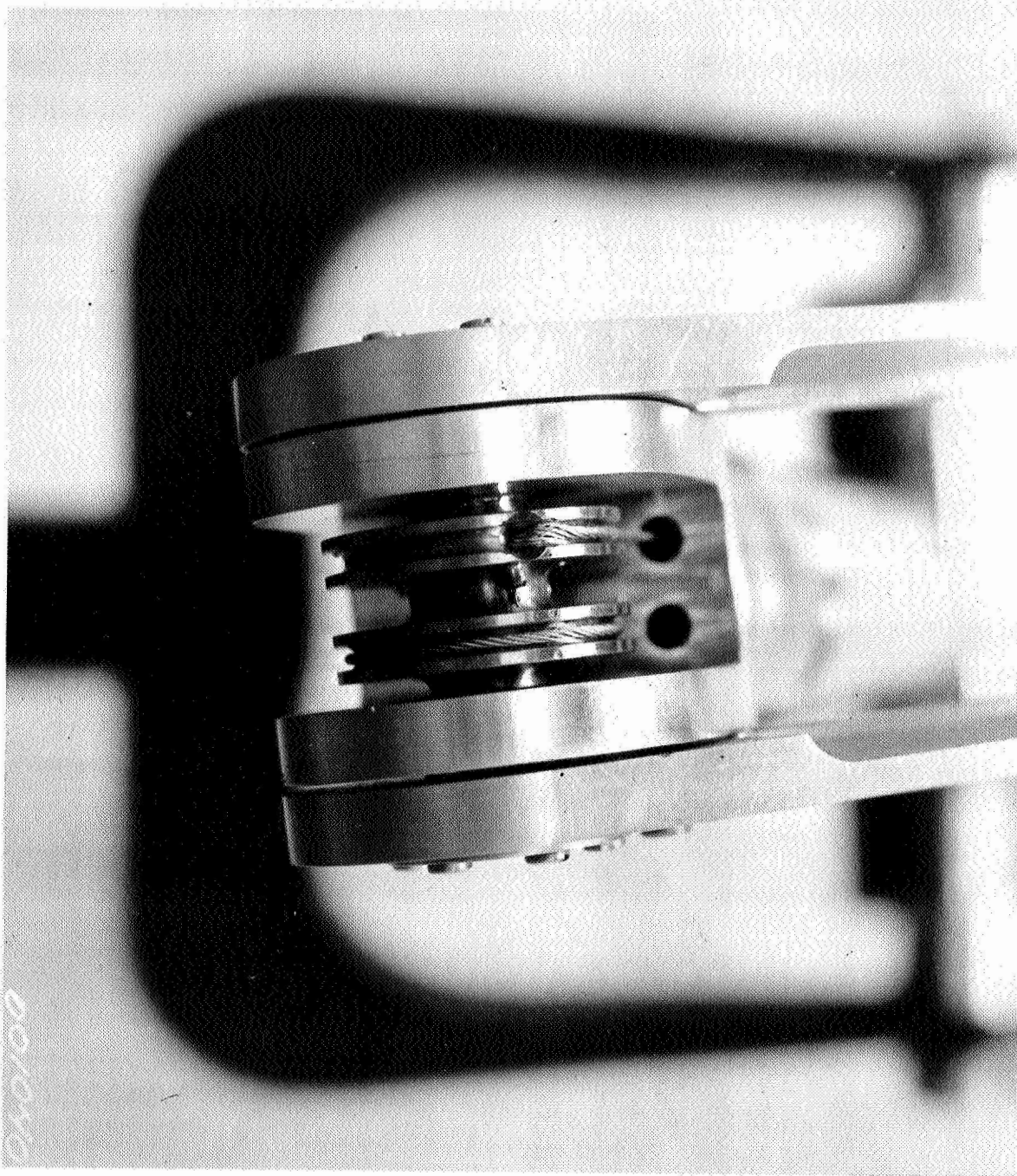


Figure IV-68 AMS Manipulator Model Showing Counterbalance Linkage Cabling at Elbow





Figure IV-69 AMS Manipulator Model Terminal Device

## V. CONTROL DEVICES

### Introduction:

The primary intent of this series of developmental evaluations and simulations is to establish design criteria and develop a preliminary configuration of a position, bilateral (force feedback), master controller for a spacecraft cargo handling manipulator system. The analysis completed, to date, represents a good definition of the problem and some preferred designs, but many areas need further work.

The design of any controller can never evolve adequately without a full understanding and integration of the total system objectives and requirements. In this case, the controller, the manipulator and the control electronics must evolve together in complete harmony. Associated with this is the problem of how much control authority is assigned to the operator (manual) and how much is automatic or computer controlled. This problem is attacked only on the basis that, for the manipulator tasks evaluated, the operator was given full manual control.

The first question one must ask at the beginning of controller design evaluation is what must the controller make the manipulator do? Our approach to the problem (as outlined in Figure V-1) is to develop "Operational Requirements" by first examining the latest NASA Shuttle Traffic Model, which provides a gross categorization of Shuttle payloads, their masses sizes and general operational characteristics. This criteria served for the basis of the next phase, "Manipulator Trajectory Definition", (Section II, B&C) which derived manipulator trajectories and reach capabilities as related to an actual shuttle and manipulator configuration.

Existing Human Engineering data was surveyed as related to position controllers. Basic data is readily available, and is shown in Section V,A. However, specific design criteria for a bilateral, position controller with indexing and selectable movement ratios must be derived from analysis and simulations.

"Design Evaluations" consisted of a combination of an analytical derivation of optimizing controller joint ordering and a hardware evaluation utilizing a variety of full scale controller mockups, semi-operational breadboards and a fully operational position controller. These controllers

were used in dynamic simulations using a video presentation which simulated tracking tasks (Appendix C) and our Space Operations Simulator which provided full 6-DOF dynamic tasks. Tracking, pre-capture and cargo handling tasks were simulated. Both rate and position controllers were utilized for manipulator control and their operational characteristics were varied for subject evaluations.

As a result of the analysis and simulations, Recommendations and Conclusions are made for the controller/manipulator system operational characteristics. A recommended 6-DOF position controller is presented along with a full scale mockup.



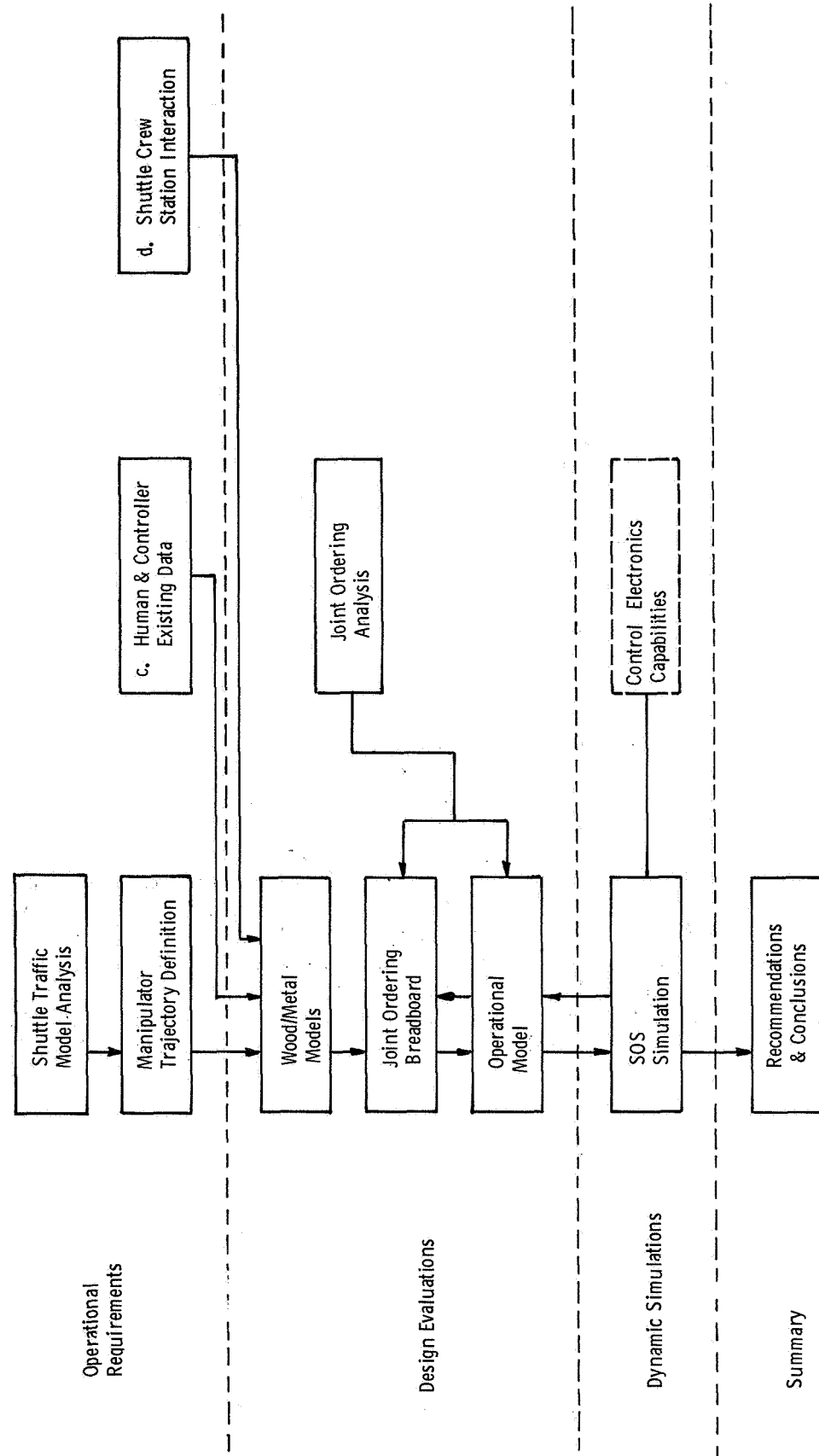


Figure V-1 Manipulator Controller Development

#### A. EXISTING HUMAN FACTORS CONTROLLER DATA

Concurrent with the Trajectory Definition study, applicable existing data on controller design and human characteristics was evaluated. Applicable data was assembled in two categories. These are:

##### Human Characteristics

- a. Anthropometric
- b. Strength
- c. Endurance
- d. Force Sensing
- e. Arm Jitter
- f. Kinesthetic Sensing

##### Control Optimization

- a. Cross Coupling
- b. Friction
- c. Stiction
- d. Backlash
- e. Deadspace
- f. Feedback Levels

##### 1. Anthropometric Reference\*

Anthropometric data for various applicable populations (flying personnel and astronauts, in particular) are well documented and readily available for design use. This data includes body segment sizes as related to the population percentile as shown in Figure V-2, joint and limb movement limits are shown in Figure V-3. For our preliminary controller configuration analysis, operator sizes between 5 and 95 percentile were used. Air Force flying personnel data was used for the preliminary design because it's readily available. However, as the position controller design is refined, actual current astronaut populations should be used.

\* Data - The data and text in this section was extracted from "Anthropometry of Flying Personnel", WADC TR52-321.

# Anthropometry of Flying Personnel



STATURE

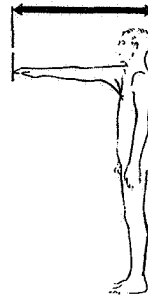
Subject stands erect looking directly forward (head oriented in the Frankfort plane). With the anthropometer arm firmly touching the scalp, measure the vertical distance from the floor to the top of the head.

Mean: 175.54 (.10) cm; 69.11 (.04) in.  
Standard Deviation: 6.19 (.07) cm; 2.44 (.03) in.  
Range: 151-197 cm; 59.45 - 77.56 in.  
v = 3.53 (.04)% N = 4062

Figure V-2a

## Percentile Values

%	CM	IN.
1	161.3	63.5
2	163.0	64.2
3	164.0	64.6
5	165.5	65.2
10	167.6	66.0
15	169.1	66.6
20	170.4	67.1
25	171.4	67.5
30	172.4	67.9
35	173.3	68.2
40	174.1	68.5
45	174.9	68.9
50	175.6	69.1
55	176.4	69.4
60	177.1	69.7
65	177.9	70.1
70	178.8	70.4
75	179.7	70.7
80	180.7	71.1
85	181.9	71.6
90	183.5	72.2
95	185.8	73.1
97	187.3	73.7
98	188.5	74.2
99	190.3	74.9



MAXIMUM REACH FROM WALL

Subject stands erect in a corner of the room, his back pressed against the rear wall and his right shoulder thrust as far forward as possible, his right arm and hand extended horizontally along the side wall. Using the scale on the side wall, measure the distance from the rear wall to the tip of the longest finger.

Mean: 98.03 (.08) cm; 38.59 (.03) in.  
Standard Deviation: 4.82 (.06); 1.90 (.02) in.  
Range: 79-117 cm; 31.10-46.06 in.  
v = 4.92 (.05)% N = 4055

Figure V-2b

## Percentile Values

%	CM	IN.
1	86.7	34.1
2	88.0	34.6
3	88.9	35.0
5	90.0	35.4
10	92.1	36.2
15	93.1	36.7
20	94.1	37.1
25	94.8	37.3
30	95.6	37.6
35	96.2	37.9
40	96.9	38.1
45	97.5	38.4
50	98.1	38.6
55	98.7	38.9
60	99.3	39.1
65	100.0	39.4
70	100.6	39.6
75	101.3	39.9
80	102.0	40.2
85	102.9	40.5
90	104.1	41.0
95	105.9	41.7
97	107.3	42.2
98	108.3	42.6
99	109.8	43.2



FUNCTIONAL REACH

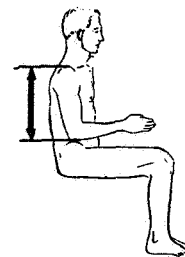
Subject stands erect in a corner of the room, his shoulders pressed against the rear wall, his right arm and hand extended horizontally along the side wall, except that the tips of his thumb and forefinger are pressed together. Using the scale on the side wall, measure the distance from the rear wall to the tip of the thumb.

Mean: 82.12 (.07) cm; 32.33 (.03) in.  
Standard Deviation: 4.14 (.05) cm; 1.63 (.02) in.  
Range: 68-103 cm; 26.77-40.55 in.  
v = 5.04 (.06)% N = 4053

Figure V-2c

## Percentile Values

%	CM	IN.
1	73.1	28.8
2	74.0	29.1
3	74.6	29.4
5	75.5	29.7
10	76.9	30.3
15	77.9	30.7
20	78.7	31.0
25	79.4	31.3
30	80.0	31.5
35	80.5	31.7
40	81.0	31.9
45	81.6	32.1
50	82.1	32.3
55	82.6	32.5
60	83.1	32.7
65	83.7	32.9
70	84.3	33.2
75	84.9	33.4
80	85.6	33.7
85	86.4	34.0
90	87.4	34.4
95	88.9	35.0
97	90.3	35.6
98	91.2	35.9
99	92.5	36.4



SHOULDER-ELBOW LENGTH

Subject sits erect, his right upper arm hanging at his side and his forearm extended horizontally. Using the anthropometer, measure the vertical distance from right acromion as marked to the bottom of the elbow.

Mean: 36.37 (.03) cm; 14.32 (.01) in.  
Standard Deviation: 1.75 (.02) cm; .69 (.01) in.  
Range: 29-46 cm; 11.42-18.11 in.  
v = 4.81 (.05)% N = 4059

Figure V-2d

## Percentile Values

%	CM	IN.
1	32.4	12.8
2	32.9	13.0
3	33.2	13.1
5	33.6	13.2
10	34.1	13.4
15	34.5	13.6
20	35.0	13.8
25	35.2	13.9
30	35.5	14.0
35	35.7	14.1
40	36.0	14.2
45	36.2	14.3
50	36.4	14.3
55	36.6	14.4
60	36.9	14.5
65	37.1	14.6
70	37.4	14.7
75	37.6	14.8
80	37.9	14.9
85	38.3	15.1
90	38.7	15.2
95	39.2	15.4
97	39.6	15.6
98	39.8	15.7
99	40.3	15.9

# Anthropometry of Flying Personnel

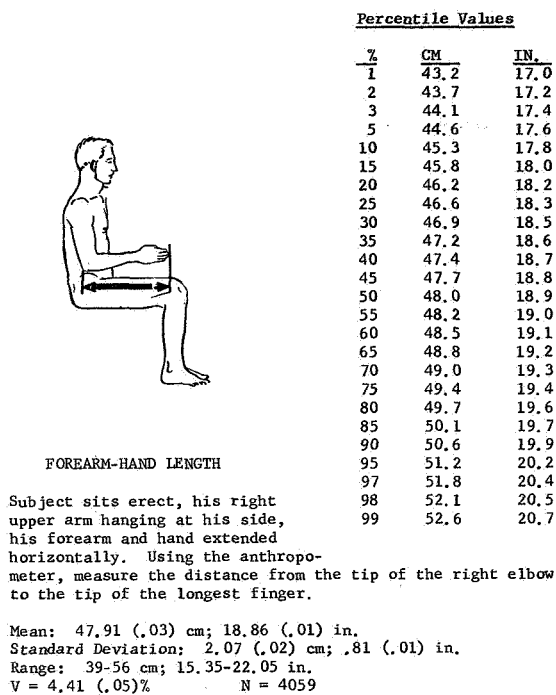


Figure V-2e

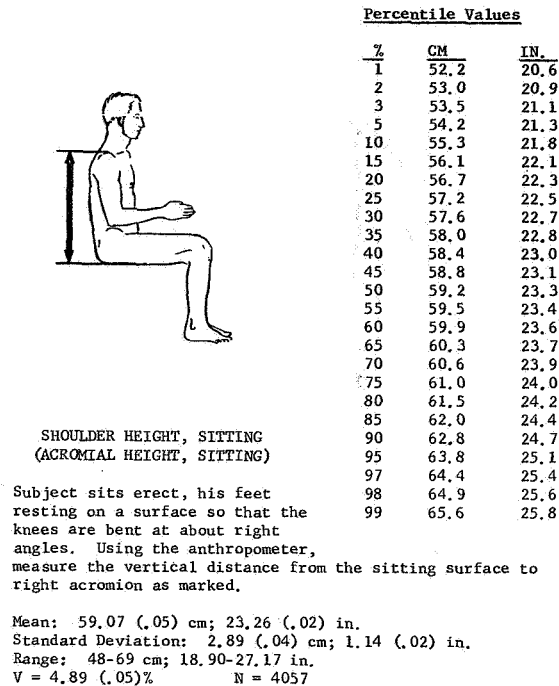


Figure V-2f

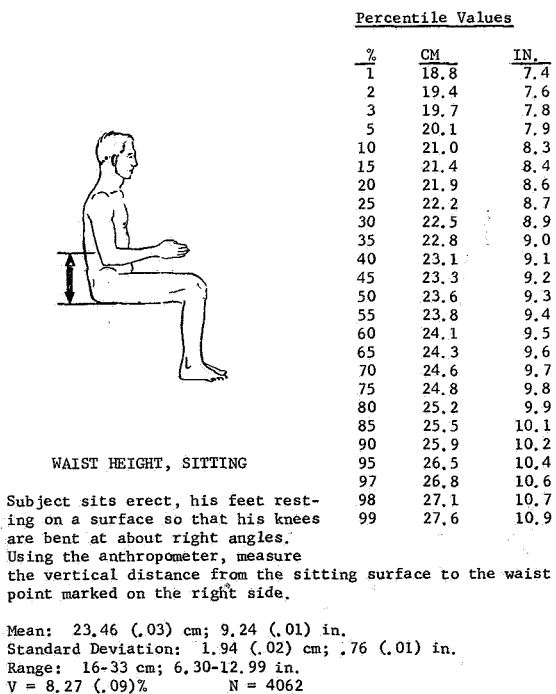


Figure V-2g

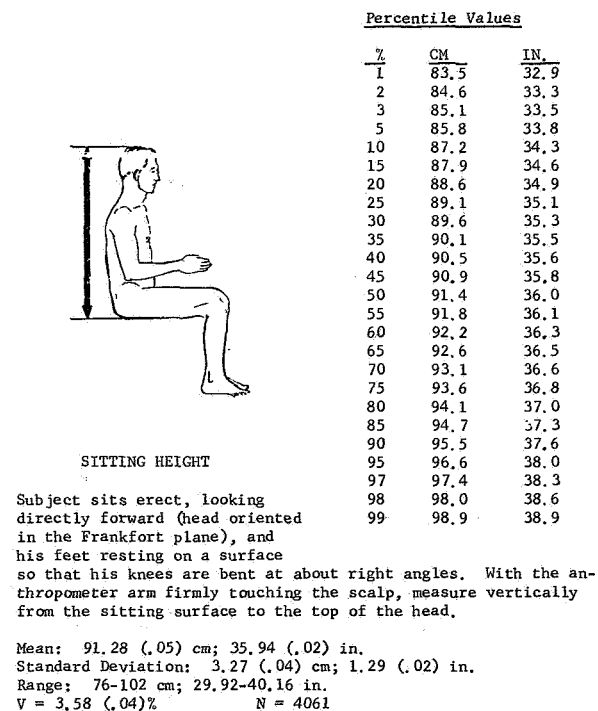


Figure V-2h

# Anthropometry of Flying Personnel

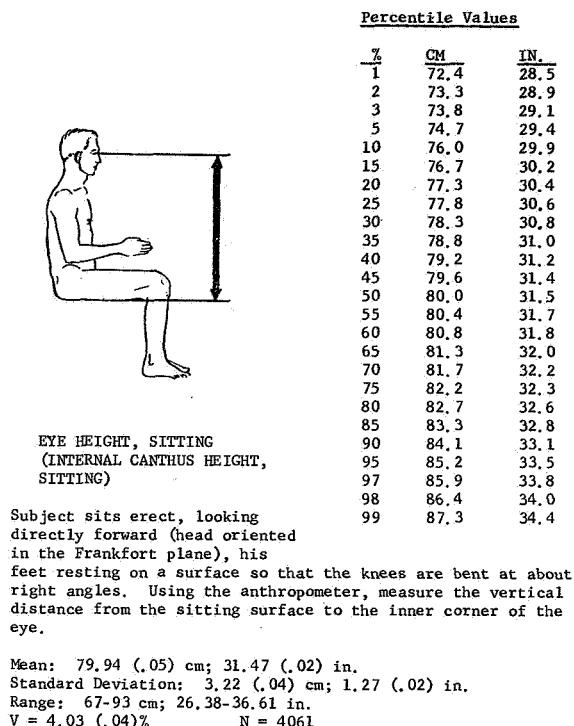


Figure V-2i

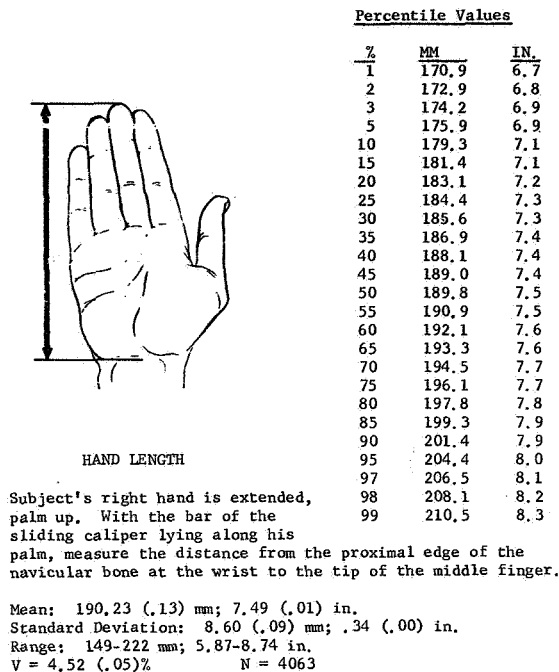


Figure V-2j

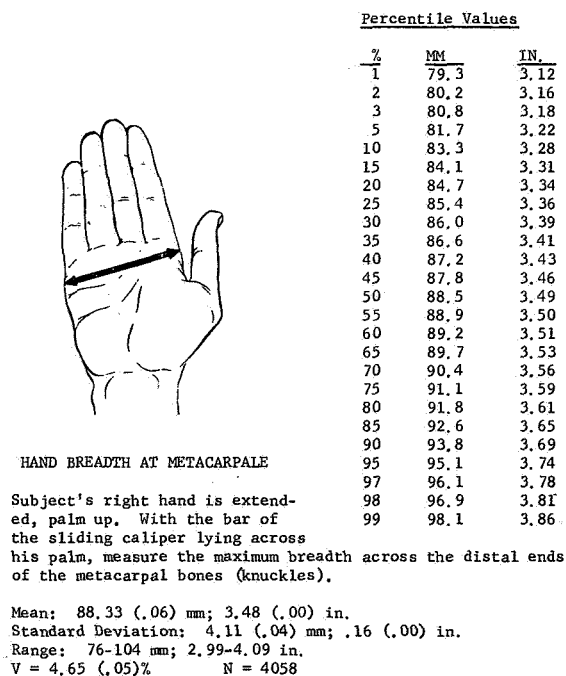


Figure V-2k

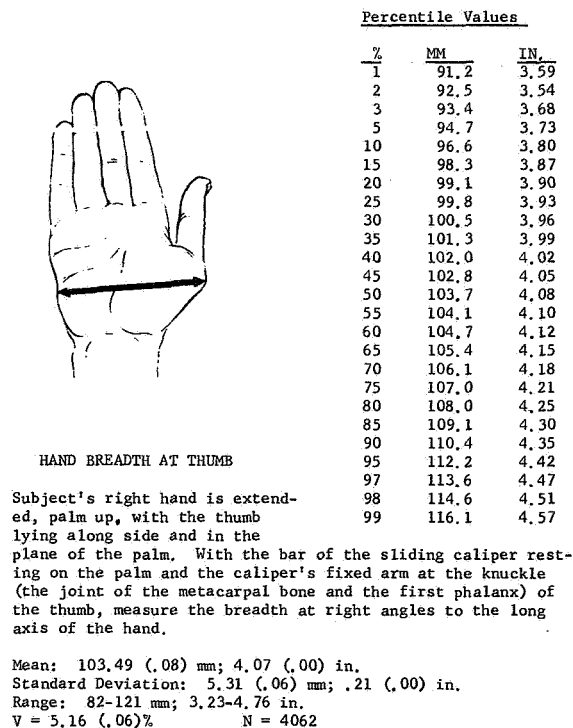


Figure v-2L

# Anthropometry of Flying Personnel

## Percentile Values

%	MM	IN.
1	25.4	1.00
2	25.9	1.02
3	26.3	1.03
5	26.7	1.05
10	27.4	1.08
15	27.9	1.10
20	28.3	1.11
25	28.6	1.13
30	28.9	1.14
35	29.1	1.14
40	29.3	1.15
45	29.5	1.16
50	29.7	1.17
55	29.9	1.18
60	30.1	1.18
65	30.3	1.19
70	30.5	1.20
75	30.7	1.21
80	31.0	1.22
85	31.4	1.24
90	31.8	1.25
95	32.5	1.28
97	33.1	1.30
98	33.5	1.32
99	34.2	1.35

## THICKNESS AT METACARPALE III

Subject's right hand is held with the fingers extended. Using the sliding caliper, measure the thickness of the knuckle (the joint of the metacarpal bone and the first phalanx) of the middle finger.

Mean: 29.67 (.03) mm; 1.17 (.00) in.  
Standard Deviation: 1.80 (.02) mm; .07 (.00) in.  
Range: 19-39 mm; .75-1.54 in.  
V = 6.07 (.07)% N = 4061

Figure V-2m

## ARM REACH ENVELOPES

Useful limits for arm reach should be based on those of the small man. In the accompanying graphs selected data for a man with a 5th percentile arm reach are shown. In the first plot the subject was in shirtsleeves and not restricted by shoulder harness. In the second, he was restricted by shoulder harness.

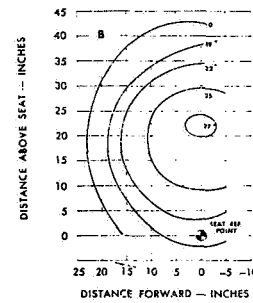
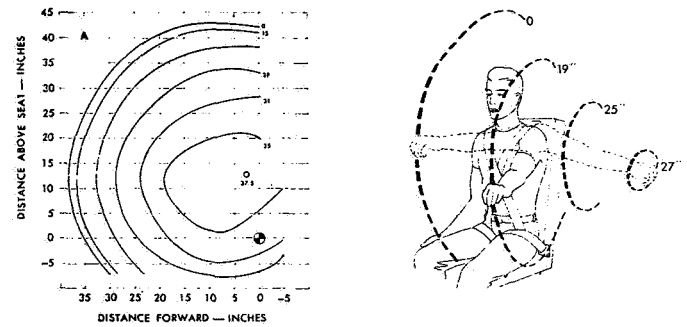


Figure V-3

## 2. Human Arm Kinesthesia and Tactual Discrimination

In the design of a position controller that has force feedback, the operator will be required to exert forces on the manipulator for extended periods of time and at various angles. To derive this force level design criteria for a controller, one must first look at man's capabilities. The data and text in this section was extracted from "Human Engineering" E. J. McCormick.

The strength that can be exerted varies with the position of the arm and with the direction of the movement. Because of this, the maximum forces to be overcome in making arm movements should depend upon the position of the arm and direction of the movement.

Information relating to strength of such movements for seated operators comes from a study by Hunsicker. In this study, 55 male subjects made movements in each of various directions, with the upper part of the arm in each of several positions. The arm positions and directions of movement are illustrated in Figures V-4a and V-4b. Figure V-4a shows a side view with the arm in each of the five positions, namely  $180^{\circ}$  (straight forward),  $150^{\circ}$ ,  $120^{\circ}$ ,  $90^{\circ}$  (straight down), and  $60^{\circ}$  (back at an angle). In each such position of the upper arm, movements were made as follows: push, pull, up, down (as shown in Figure V-4a), and in (adduction) and out (abduction) (as shown in Figure V-4b). The strength of each subject for each movement was recorded and some of the results are given in Table V-1. This table shows, for each movement, the maximum strength of the 5th percentile, and the mean maximum strength. The data for the 5th percentile are shown, since they represent values that most of the subjects (95 percent) exceeded. Forces greater than these normally should not have to be overcome in work situations, unless the operators are to be specially selected on the basis of strength. Even these forces should not be required if it is possible to avoid them, because of the possible fatigue which some operators would experience in overcoming them.

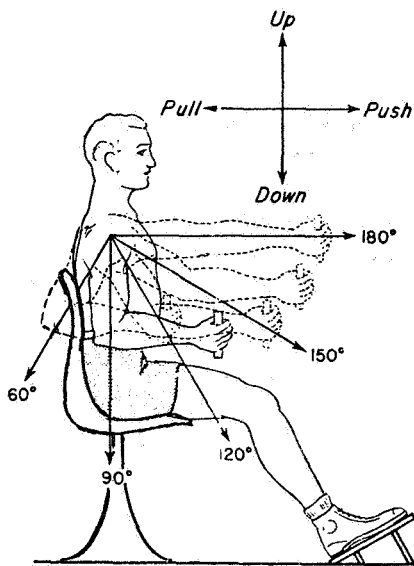


Figure V-4a Arm Positions and Directions of Movement, Side View

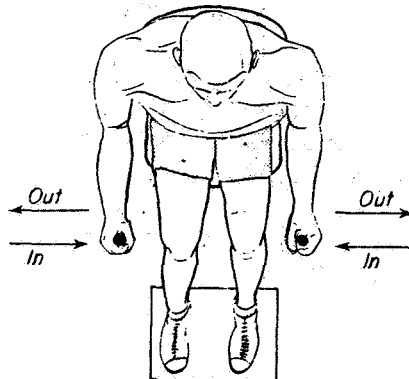


Figure V-4b Arm Positions and Directions of Movement, Top View



Table V-1 Arm Strength in Pounds

Angle of arm, degrees	5th Percentile		Mean		5th Percentile		Mean	
	Left	Right	Left	Right	Left	Right	Left	Right
	Pull				Push			
180	50	52	116	120	42	50	126	138
150	42	56	112	122	30	42	111	123
120	34	42	94	104	26	36	99	103
90	32	37	80	88	22	36	83	86
60	26	24	64	63	22	34	80	92
	Up				Down			
180	9	14	41	43	13	17	35	41
150	15	18	52	56	18	20	41	47
120	17	24	54	60	21	26	51	58
90	17	20	52	56	21	26	49	53
60	15	20	44	49	20	20	46	51
	In				Out			
180	13	20	43	50	8	14	30	34
150	15	20	47	54	8	15	29	33
120	20	22	45	53	10	15	30	34
90	16	18	48	50	10	16	33	37
60	17	20	50	52	12	17	32	42

These results show the maximums for the 5th percentiles are noticeably lower than for the means. For any given movement (such as a pull, or a push), the relative strengths of the 5th percentiles for the various arm angles fall in approximately the same rank order as the relative strengths of the means for the corresponding angles. The left hand values are consistently below those for the right hand, the difference being approximately 10 percent.

Considering the individual movements in relationship to the arm angle, it can be seen that both pushes and pulls are somewhat stronger when the arm is extended forward (at 180° or 150°) than when it is more down to the side. With up and down movements, however, greater strength can be exerted with the arm more to the side (around 120° or 90°) than extended forward. For inward and outward movements, the arm position seems to have little influence, except that there seems to be a slight advantage for outward movements in a

side position ( $90^{\circ}$  or  $60^{\circ}$ ).

Comparing the various movements with each other, it can be seen that greater force can be exerted by pulling or pushing actions than by up, down, in, or out movements. There is a slight advantage for pushing movements over pulling. Otherwise, the relative strengths of the various movements, in descending order, are up, down, in (adduction), and out (abduction). The out movement was, on the average, less than a third as strong as the strongest movement, the push.

The pulling and pushing movements in this study were made in a horizontal plane. For position controller activities, pulling or pushing movements are made at an angle, either oblique with the floor, or off to the left or right. Information based on small samples implies that, with upward pulling action at an oblique angle with the floor, the strength that can be exerted is related to the height of the hand grip. With the hand grip 6 in below the seat level, the strength exerted was greater than with the hand grip 13 in above seat level. A higher hand grip (+ 19 in) made the action especially difficult. In a horizontal pushing action, it was found that greater strength could be exerted if the direction of the movement was straight ahead, rather than at right or left angles from the shoulder. The right angle, in particular, loses in mechanical advantage.

In connection with a pushing action, it has been found that greater force can be exerted if the feet are placed forward with the legs at an oblique angle, rather than being placed flat on the floor right in front of the seat. For example, men with their feet against a pedal nearly straight ahead from the seat could exert as much as 135 lb, whereas when seated normally, they could exert only about 75 lb.

#### Push and Pull by Hand from Standing Position

Since some pushing and pulling is done in a standing position, the relationship between the position of the control device, direction of movement, and the force that can be exerted was examined. A study by Garry utilized equipment consisting of a 30-in lever that rotated in a vertical plane. It was so devised that it was possible to position the lever at any given angle and to determine the amount of force applied to the lever at each angular position. As the handle of the lever was positioned at any given angle from the center,

the center itself moved up or down so that the handle of the lever could be set at any given distance above or below shoulder height. The level was varied from 30 in below shoulder height to 24 in. above shoulder height. Depending on the height of the handle, the angle from the center, and whether the handle was being pushed or pulled, the subject then would assume whatever posture or stance was appropriate for the action.

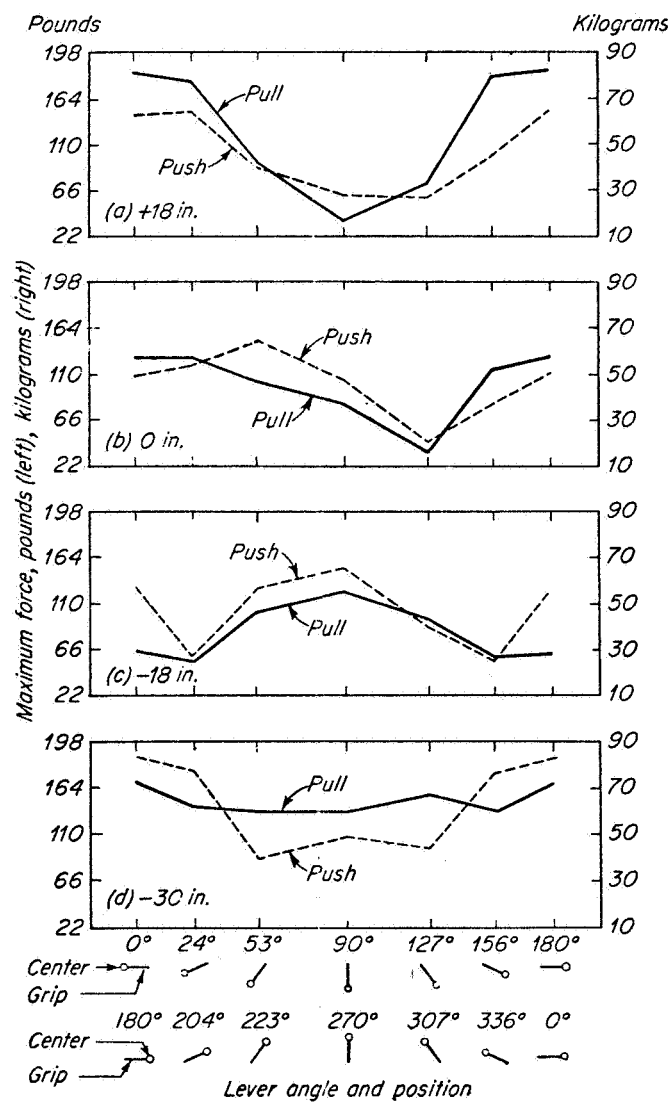


Figure V-5 Maximum Push and Pull Force

The resulting data are given in Figure V-5. These data are for selected grip levels (+ 18 in, 0. - 18 in, and - 30 in from shoulder level). The angular positions are represented as follows:  $0^{\circ}$ ,  $90^{\circ}$ ,  $180^{\circ}$ , and  $270^{\circ}$ , or, respectively, 3, 12, 9, and 6 o'clock positions. For above shoulder levels of + 18 in the maximum forces could be exerted with the lever angle approaching horizontal ( $0^{\circ}$  and  $180^{\circ}$ ). In such positions a pulling-down action was stronger than a pushing-up action. At shoulder height the  $127^{\circ}$  and corresponding  $307^{\circ}$  positions were weakest. Generally speaking, the - 30-in level resulted in greater pulling and pushing force than the - 18-in level; the exception was for pushing actions in approximately vertical positions ( $90^{\circ}$  and  $270^{\circ}$ ), where apparently pushing was more forceful if the grip level was about waist height (- 18 in). At horizontal positions below shoulder height, pushing was generally stronger than pulling, particularly at the - 30-in level, where the operator presumably could really bear down on the lever.

#### Grip Strength and Endurance

Control devices which are to be manipulated, must be grasped with the hand, and the hand must be contracted in a gripping action. The strength required for such action should be within the limits of grip strength of people who are to use the equipment in question. Hand strengths vary from a force of about 75 lb to about 170 lb, with an average of about 125 lb.

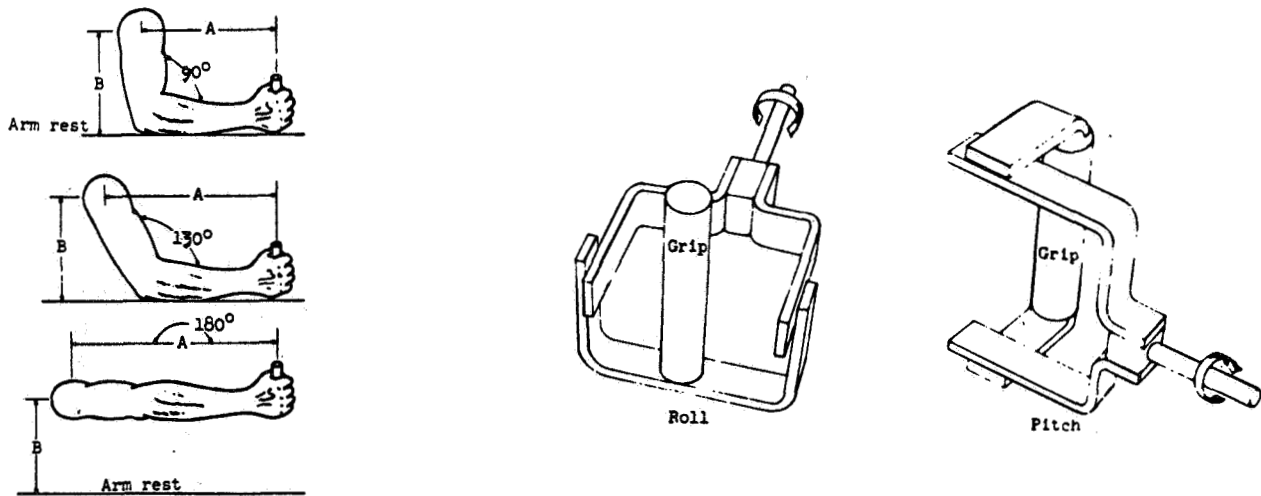
Comparative data are available for a group of 200 university male students. These data include both grip strength and endurance. Endurance was also measured in terms of a strength-endurance index, specifically the average strength in pounds that could be sustained for 1 min. The results, summarized in Table V-2, include not only the averages but also the standard deviations (SD) of the group. Strength and endurance were correlated ( $r = .67$  and  $.66$  for right and left hands, respectively). Such correlations mean that people with greater maximum strength also tend to have more staying power.

Table V-2 Grip Strength & Endurance

	Right hand		Left Hand	
	Av.	SD	Av.	SD
Average maximum strength (lb)	108	21	95	18
Average strength endurance index	62	12	55	10

### 3. Side Stick Controller Forces and Travel

The data and text in this section was extracted from the "Bioastronautics Data Book", NASA SP-3006 and "Human Engineering" by E. J. McCormick. Measurements were made of pilots arms, using a side stick mockup, to determine the unconstrained angular deflections they could achieve in roll and pitch. Data was taken with the arm straight or flexed as shown. The preferred neutral position for the controller was found to be  $8^{\circ}$  to the right and  $15^{\circ}$  forward of the vertical. The preferred arm position was a slight extension forward from  $90^{\circ}$ . Average pilot data is shown in Figure V-6 .



Average Pilot	Distance A in.			Distance B in.		Maximum controller angle (unconstrained), deg							
						Right Roll		Left Roll		Forward Pitch		Rearward Pitch	
	Measured at elbow angle of -												
	90°	130°	180°	90°	130°	90°	130°	90°	130°	90°	130°	90°	130°
Average Pilot	13.35	18.30	26.30	13.15	12.63	91.8	96	91.4	97.3	61.8	60.4	34.5	35.0

Figure V-6 Pilots Average Arm Movements

	Elbow Angle	Roll (Grip Position)										Pitch (Grip Position)									
		L 90°		L 45°		0°		R 45°		R 90°		Down 60°		Down 30°		0°		Up 50°			
		L	R	L	R	L	R	L	R	L	R	U	D	U	D	U	D	U	D	U	D
Operational Force Level	90°	11	13.5	12	11	12.5	12.5	12	12.5	6.5	7	14	12	18	17	17	15	12	14		
	130°	2	6	9.5	9.5	12	12	12	12	10	9.5	12	17	18	20	17	20	18	17.5		
Max. Oper. Force Level	90°	22	24.5	24	23	26	27	20.5	26	11	8	22	30	31	38	28	28	20	28		
	130°	10	4	19	20	26	25.5	21	25	11	21	17	29	33	34	38	37	35	34		
Max. Force Level	90°	85	88	78	85	70	75	50	48	27	25	95	82	112	95	75	75	26	32		
	130°	18	10	35	30	67	65	83	75	80	80	53	58	73	81	130	106	120	120		

Table V-3 Angular Torques (in.-lbs.)

### Elbow and Shoulder Strength

There are many varieties of elbow and shoulder actions, but two aspects of these actions may be of particular consequence in movements involving strength.

Flexion versus extension of elbow. Can flexion (bending) or extension (straightening) of the elbow result in greater force? This question was investigated with force applied to a handle connected to a strain gauge. Since the handle moved under force, it was possible to measure force exerted at each of various positions. With the upper arm adducted (in at the side) and the elbow joint at one of three degrees of flexion (45°, 90°, and 135°), 12 subjects attempted elbow-flexion (bending) and extension (streightening).

Three results in particular are pertinent: In the first place, flexion (bending) turned out to be about half again as strong as extension (straightening). In the second place, the force was greater when the elbow was at about a 90° bend than when the bend was greater or less than this angle. In the third place, the force was greater with the forearm in a medial position (palm turned toward center) than in a prone or supine position.

Elbow versus shoulder forces. In another study, a comparison was made of the relative force that can be generated by the elbow as opposed to the shoulder. For this purpose a 17-in. handwheel was used. This had a handle that could be grasped in either of two ways, namely, at right angles to the

forearm (as a streetcar conductor grasps his control lever), or parallel to the arm (like grasping the end of a fishing pole). The wheel was placed in six different positions, so that the arm positions and hand grasps were as shown in Table V-4 (the elbow being bent at  $90^{\circ}$  in all cases). Positions 1, 2, and 3 primarily required an elbow action, and 4, 5, and 6, a shoulder action. The actions were of extension or flexion depending on the arm used and direction of attempted rotation. The handwheel hardly moved under force, and force was measured by a strain gauge. Twelve subjects were tested, each one being tried on each of the six positions.

Table V-4 Hand Grasp Data

Type of hand grasp	Action	Upper-arm position		
		At side	Flexed forward at $45^{\circ}$	Flexed forward at $90^{\circ}$
Streetcar conductor	Elbow	1	2	3
Fishing pole	Shoulder	4	5	6

Without giving the details of the results, we may state the principal conclusion to be drawn from them. A rotation action of the shoulder has approximately 1-1/2 times the force of a rotation action of the elbow, and it has nearly 3 times as much staying power (the ability to maintain a force). Position and direction of rotation were not of major consequence.

Another related study indicated that shoulder extension (an upward push) is more forceful than flexion (a downward action) from a seated position.

#### Force in Controls and Reaction Time

The need to overcome the force of a control may have accompanying costs, especially in speed of response. Hence, force is interrelated with reaction time. Reaction time to simple stimuli seldom is less than 0.12 sec, and perhaps more typically is as much as 0.25 sec. To complex stimuli, such as are encountered in automobile traffic, the typical time may be as high as 0.60 sec. Excessive resistance in a control device also can increase the reaction time.

A British study yielding data on this point was carried

out with a cockpit mockup, in which the control stick was moving freely. The reaction time to a simple stimulus was about 0.20 sec, but with a loaded stick the reaction time shot up to 0.60 sec. Further evidence on this point comes from a flight situation in which it was reported that reaction time in moving a control stick increased from 0.16 to 0.75 sec as the load on the stock was increased from 37 to 97 lb.

#### Feedback from Forces in Control Devices

In case a control device such as a lever, steering wheel, or pedal is being operated by "feel" without visual cues, there are two types of feedback that can provide cues to guide the operation of the control: One of these is the pressure that is experienced in overcoming the force inherent in the system; this is sensed largely through the tactual, or touch, sensation. A moderate amount of inertia in cranks can improve tracking performance. The other cue is distance, or length of movement, which is experienced through the kinesthetic sense (from the proprioceptors in the muscles and joints), which keeps us informed of the position of parts of the body (arms, legs, etc).

Where pressure is used as a cue, the operator may apply what he considers to be the "right" amount of pressure. But how is he to know what is the "right" amount? The answer to this is, of course, experience. But how accurate are human judgements regarding amount of pressure? Can people reproduce a previously experienced pressure? And do these judgements depend somewhat on the amount of force to be overcome?

In a study designed to answer some of these questions, the subjects operated a stick type control. This control was so arranged that varying degrees of pressure could be exerted with very little movement of the control device itself. After some training and practice in "reproducing" various forces, a series of trials was attempted by each subject. Measures of actual pressure exerted were then compared with the pressures that the subjects attempted to reproduce. The "difference limens" by pounds of pressure for the various types of controls are shown in Figure V-7. Since the difference limen is the average difference that can just barely be detected, two pressures have to differ by an amount greater than the limen in order to be detected as being different. In the case in question, it is shown as a ratio, specifically the proportion of the standard pressure (the one to be reproduced) that can just barely be detected.



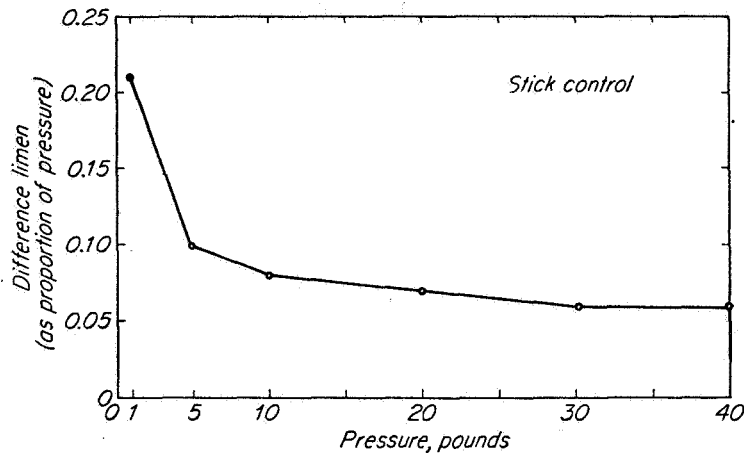


Figure V-7 "Difference limens" for various control types

It can be seen that the limen drops off markedly between 6 and 10 lb, and that it becomes relatively constant beyond that. In more practical terms, the results mean that in attempting to reproduce pressures under about 5 lb or possibly 10, the errors are proportionately greater than they are for heavier pressures. If differences in pressures are to be used as a basis for judging the operation of control devices, the pressures used preferably should be above 5 or 10 lb in order that more accurate discriminations can be made.

Pressure versus distance in feedback. In the operation of controls that involve a reasonable amount of displacement or movement of the control devices, the kinesthetic sense comes into play. There is some rather persuasive evidence that distance of movement (based on kinesthesia) is a better feedback source than pressure (based on tactual sense). Without going into this study in any detail, it may be said that the subjects operated a lever in a blind positioning task, with varying pressures to be overcome and with varying distances of movement. In general, it was found that the distance the lever traveled (detected through the kinesthetic sense) was a much better cue for positioning the lever accurately than was the amount of pressure to be overcome. Positioning errors were greater for short movements, however, than for long movements.

In designing controls that are to be operated by "feel", it then seems desirable to provide as much distance for movement as can be conveniently exercised. No particular pressure then needs to be provided. If a control is to be moved over a reasonably short range, however, pressure cues may be very useful.

The conclusions that pressure cues may be more useful for short movements than for long movements is confirmed by another study in which an "arm control" was used. This control consisted of a lever type of device on which the forearm could rest in a horizontal position beside the subject. The control was pivoted under the elbow, and had a knob to grasp at the hand end. The control could then be rotated to the side. The subjects were instructed to make rapid positioning movements to three angular positions, namely,  $17.5^{\circ}$ ,  $35^{\circ}$ , and  $70^{\circ}$ , and return.

Various torque relationships were introduced into the system. In some cases the torque was constant from beginning to end, and in other cases it increased throughout the movement. The combinations of torques used (in inch-pounds) are given in Table V-5 .

At beginning	At terminal
0	0, 50, 100, 200
25	0, 50
50	50, 100
100	50, 100
200	200

Table V-5 Torque Relationships

The results, summarized in Figure V-8 indicate that changes in torque (increases in torque as the movement continues) aided in accurate positioning for the short movements (the angular excursions of  $17.5^{\circ}$  and  $35^{\circ}$ ) but not for the longer movements ( $70^{\circ}$ ).

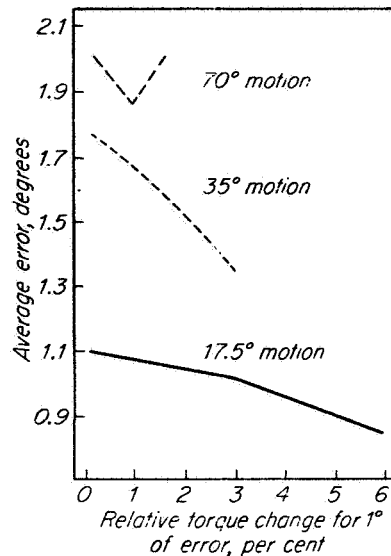


Figure V-8 Average Error in Degrees

#### Summary

1. When an operator is seated, the relative strengths of arm movements in various directions, in descending order, are push (horizontal), pull (horizontal), up, down, in, and out. The strength of arm movements is related to the position of the upper arm as follows: (a) Push and pull movements are somewhat stronger when the upper arm is extended forward (at an oblique angle or straight ahead) than when it is down to the side; (b) up and down movements are somewhat stronger when the upper arm is at the side; and (c) the strengths of in and out movements are not markedly related to arm position.

2. Greater strength can be exerted in a pulling action from a seated position if the direction of pull is upward from an oblique angle of about  $45^{\circ}$  than if the direction of pull is horizontal. Strength of upward pulls, however, is related to height of the lever grip, a low level (6 in below seat level) being better than higher levels.

3. Greater strength can be exerted in a pushing action from a seated position if the feet are placed forward with the legs at an oblique angle than if the legs are at right angles to the floor.

4. In a horizontal pushing movement, greater strength can be exerted straight ahead than at an angle to the side.

5. The strength that can be exerted in a standing position depends upon the position of the hand and the direction of movement (see Figure V-5 ). For above-shoulder levels, maximum force can be exerted with a downward pulling action. For most hand positions and movement directions below shoulder levels, force is greater at about 30 in below shoulder level than at about 18 in below.

6. Hand-grip strength and endurance are correlated to a considerable degree. (Correlations for one sample were .67 and .66 for right and left hands, respectively.)

7. In hand-turning action, exertible force is related to hand position and direction of turn. For a pronation (turning-in) direction of turn, force is greatest when the hand is at a turned-out position; for a supination (turning-out) direction of turn, force is greatest when the hand is at a turned-in position.

8. In elbow movements, a flexion action (bending) is considerably stronger than an extension action (straightening). The flexion force is maximum with the elbow bent at about a right angle.

9. A shoulder action is generally stronger than an elbow action. In a seated position, shoulder extension (an upward push) is more forceful than flexion (a downward pull).

10. In activating lever-type control devices, reaction time increases when the resistance in the control device is increased.

11. In the operation of control devices such as levers, wheels, and pedals, differences in pressure can best be discriminated when the pressures are between about 5 or 10 lb and 30 or 40 lb. Discriminations of pressure differences less than 5 or 10 lb.

12. When control devices such as levers are to be moved some distance, distance of movement generally serves as a better cue for accurate operation than changes in pressure. With short movements, however, changes in pressure improve accuracy of operation.

#### 4. Controller Deadspace and Backlash

The data and text in this section was extracted from the "Bioastronautics Data Book" NASA SP-3006 and "Human Engineering" by E. J. McCormick.

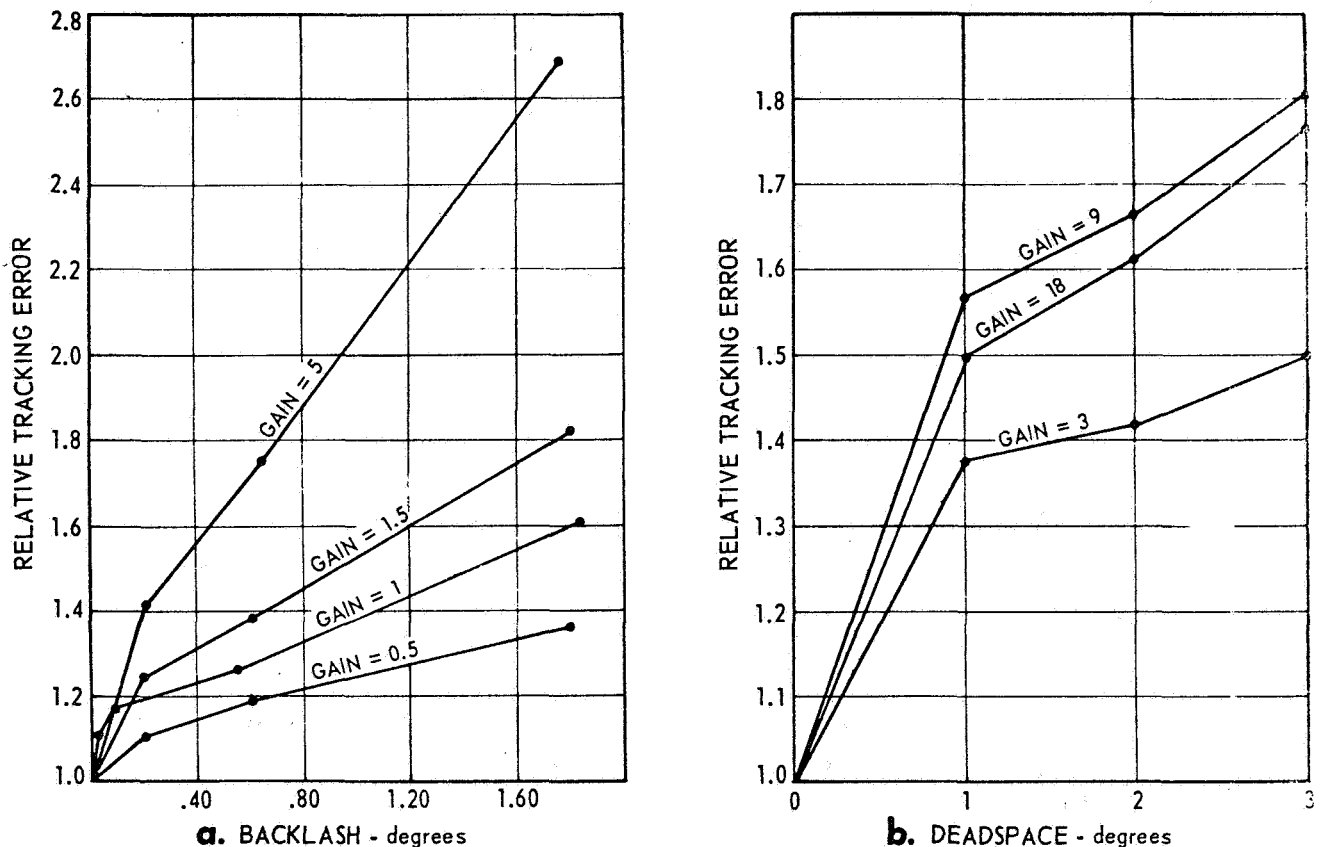


Figure V-9 Controller Nonlinearities

In most physical systems, the intended relationship between input and output is often complicated by the presence of nonlinearities such as friction, stiction, backlash, and deadspace. In a control system with a human operator, these nonlinearities act to degrade performance. The curves above show the extent of degradation as a function of amplitude of two nonlinearities, deadspace and backlash. Deadspace is a range of input. In general it exists at only one position in the input range, ordinarily the center. Backlash is a deadspace that moves with the input, being encountered with each reversal of direction.

Figure V-9a shows the integrated absolute tracking error relative to that with zero backlash for various values of gain in the controlled system (longitudinal short period dynamics of the Northrup F-89 interceptor).

Figure V-9b shows the increase in time off target relative to that for zero deadspace. The controlled system was an exponential lag with 0.125 second time constant. The curves are labeled with the values of gain in the controlled system.

In both cases, the controlled system and the variable deadspace or backlash were generated on an analog computer. The actual control sticks used were spring loaded to reduce backlash and deadspace to negligible levels.

#### 5. Motor Activities

In the performance of human motor activities, certain positions, angles, directions, speeds, or other conditions are "optimum" in terms of human performance. Degrees or levels of such variables that are greater than, or less than, these optimums typically result in poorer performance. The following is a summary of data and studies reviewed in the area of human motor characteristics:

1. The various types of sensory nerves serve as sources of information to the central nervous system. The motor nerves are the pathways through which action signals are transmitted to the muscles.
2. In some motor activities information about the progress of the activity is transmitted back to the central nervous system by the sensory nerves, to aid in continuing the activity. This is called "feedback".
3. Fatigue reduces or stops the transmission of signals through the motor nerves.
4. Motor activities can be grouped in the following classes: (a) positioning movements; (b) repetitive movements; (c) continuous movements; (d) serial movements; and (e) static reactions.
5. Simple reaction time is the time required to respond to a single stimulus (signal). Complex reaction time is the time required to react when a discrimination must be made from

among various stimuli.

6. Long movements can be made in proportionately less time in relation to length than short movements.

7. Movements terminated by mechanical devices take less time than those which are terminated exclusively by visual cues.

8. Inward or outward visually controlled positioning movements are slightly faster than lateral movements, and right-to-left lateral movements are slightly faster than left-to-right.

9. One-handed visually controlled positioning movements are performed best in terms of combined accuracy and speed when at about  $60^{\circ}$  angle right from a straight-ahead position, and when they are reasonably short.

10. Two-handed positioning movements made simultaneously are slightly faster at approximately  $30^{\circ}$  angles right and left from a straight-ahead position, and are distinctly most accurate straight ahead ( $0^{\circ}$  angle).

11. In executing blind positioning movements, people tend to overshoot long distances. With vertical movements from top to bottom there is a tendency to overshoot both short and long movements.

12. Continuous movements in a horizontal plane are most accurate in the directions represented by the 1:30 and 7:30 o'clock positions.

13. In serial movements consisting of travel and manipulation actions, travel time is affected by the nature of the manipulation task.

14. Maintaining static posture is generally more fatiguing than some kind of adjustive posture.

15. Tremor can be reduced by (a) use of visual reference; (b) support of body or body member, (c) having hand near heart level; and (d) having moderate friction in devices used.

16. In a two-dimensional setting task with a joy stick, performance is most rapid when the tip of the joy stick moves 2.5 or 3.0 times the distance of the target. Length of lever

or joy stick is of little importance if the optimum ratios are maintained.

17. A moderate amount of inertia improves the smoothness of tracking operations.



## B. CONTROLLER DESIGN EVALUATIONS

Four candidate controller configurations were studied during this program and are described below.

a. Bilateral 6-DOF Position - This configuration is generally thought of as a 6-DOF single controller in which the controller grip position, in its movement volume, relates to the manipulator TD position. Bilateral relates to a dual control loop between the controller and the manipulator. A command signal is sent from the controller to the manipulator and the dynamics of the manipulator are reflected back to the controller for an electrically induced operator "feel". Hence, the terms "force reflection" or "force feedback" are applied to a bilateral position controller. This configuration is a non-replica controller in which each controller joint movement does not necessarily relate one-to-one with the corresponding manipulator joint movements. This controller "flies" the manipulator terminal device (TD) as though it were a free flyer. A variety of controller to TD movement ratios can be utilized. Ratios from 1:1 to 30:1 appear operationally feasible. Since low movement ratios will require gross controller movements, in excess of control station volumes and the operator's arm length, indexing becomes necessary. Indexing allows the controller to be electrically disconnected from the manipulator system and be repositioned to any point the operator wishes in the movement volume. The concept is similar to a ratcheting wench. Indexing is done for both position and attitude repositioning.

Bilateral position controller type manipulators have been used for years, for handling radioactive materials. These controllers are generally mechanically linked (tape drive) to the manipulator which provides force reflection. Electrical and hydraulic systems are also available. However, all of these manipulator systems have one thing in common. The controller must be an exact replica of the manipulator and a single, fixed, movement ratio between the controller and the manipulator is determined by the controller size.

A 6 DOF bilateral position controller, as envisioned for the Shuttle manipulator system, with indexing and variable control ratios, is a developmental item.

b. Unilateral 6-DOF Position - Unilateral relates to a single data flow, from the controller to the manipulator only. The controller can be an identical design to the bilateral type as far as indexing and control ratios, except there is no force feedback. The controller can be limp, completely free to move, however, this is a totally unacceptable mode from an operator's standpoint. This can be demonstrated on the CAM 1400. The operator can "get ahead" of the manipulator and then prediction of where the TD will go is difficult. Arm and muscle induced jitter is noticeable with a limp controller.

The second mode for a unilateral controller, is one with artificial feel induced. This type was used in our man-in-the-loop dynamic simulations. It was as close as we could get to a true bilateral system at the time. Artificial feel can be induced by driving servo motors in each of the controllers joints. The force can be constant or proportional to the commanded manipulator velocity.

c. Geometrically Similar Replica - The replica controller is simply a miniature of the manipulator. Joint for joint it is identical. For laboratory work this concept is acceptable since the manipulators movement volume is generally small and the system can be designed around a specific task. However, for the Shuttle manipulator system a replica controller has some serious drawbacks. First, the replica can have only one movement ratio which is dictated by the size ratio between the controller and the manipulator. For example, with a 50 ft manipulator and an operator with an average arm length of 28", and ratio 20:1 seems reasonable. This dictates a controller approximately 32 inches long which must have free movement volume at the operator's console in a 64 in dia half sphere from its mounting base, which is significant from a crew station volume standpoint. Larger single control ratios, such as 30 or 40:1 which make the controller smaller, make vernier manipulator control difficult.

The lack of an "indexing" capability grossly affects operator performance. Our simulations show indexing is done as much or more for controller attitude corrections than for translational corrections. Most manipulator tasks require long translations with attitude changes along the way and then vernier attitude and translations at, for example, a work site. With a replica controller this generally means the operator's arm is extended at some odd angle and the wrist is bent around in an uncomfortable position. This grossly degrades operator performance.

d. 6-DOF Rate - This control configuration utilizes two 3-DOF Apollo type controllers. There is no force feedback. The TD of the manipulator is "flown" as though it were a free flyer and there is no direct interaction between the controllers and the manipulator joints. The right hand controller commands attitude changes of the manipulator wrist and the left hand controller commands translational changes at the TD. Both controllers must be proportional type. This means the commanded angular or translational velocity of the manipulator is proportional to the displacement of the controller grip, up to the manipulator's maximum velocity. The Apollo controller cannot be used for manipulator control, as-is. Both are designed for pressure suit operation and the "feel" characteristics should be changed. The attitude controller is a proportional type, however, the translation controller is not. It is simply an on-off type and would have to be redesigned if used. Rate controllers do have the advantage of allowing the attitude and translation commands to be singled out in separate controllers. No one is sure the rate controllers can control the manipulator adequately for the proposed tasks, especially where rapid non-uniform attitude changes are required such as capturing a rotating, nutating satellite. There is also, no direct feedback to the operator to indicate hitting an object or how much force is being applied to a task. However, force information can be given to the operator visually, with meters and lights.

## Master Controller Configuration Alternatives (Joint Ordering) Analysis

a. Introduction - The AMS master controller configuration must be commensurate with a restricted control station volume, while at the same time maintaining the customary isotropicity and uniformity of the friction inertia and feedback forces.

In commercial bilateral force reflecting manipulators, both in the articulated and the telescoping motion varieties, moment arms are kept sufficiently uniform by restricting motion ranges. In the majority of devices, moment arms in any direction will vary less than a factor of two from minimum to maximum. Friction and feedback forces at the TD are inversely proportional to these moments ratios, while drive train inertias are inversely proportional to the square of them. The result of this approach is often a quite large manipulator master which is not suitable for Shuttle applications. Even the smallest of the presently existing bilateral manipulators, the Brookhaven National Laboratories (BNL) arm, is too large for this applications.

In fact, a thorough and fundamental study of master configurations has never been made as existing devices lean strongly on mechanical through the wall master slave configurations, which by their very nature of application are constrained to a relatively small selection of possible motions.

b. Procedure - For ease of analysis wrist motions can be separated from translational motions. Wrist motions are assumed to consist of three orthogonal rotations in a sequence adapted to the chosen translational motions such as to minimize motion singularities. It is then sufficient to examine the properties of the translational DOF.

An attempt will be made to formulate the beginnings of selection rules that will systemize the search and assure as much as possible that no possibilities are overlooked. To ease the discussion of the many configurations possible a short hand notation is used. For rotational motions the familiar terms P (pitch), Y (yaw), and R (roll) will be used starting from the motion fixed to ground and proceeding toward the terminal device (TD). Thus the master shown in Figure V-10a and b would be  $(Y-P-P)_T$   $(Y-P-R)_R$  which would read (yaw-pitch-pitch) for translational motions, (yaw-pitch-roll) for rotational motions. A sliding motion is designated by  $S_Y$ ,  $S_P$ , or  $S_R$ , where the subscript designates the direction of the slides which is taken to be along the axis of rotation of the subscript rotational motion. Thus the

prototype would be  $(S_R - Y - P)_T (Y - P - R)_R$ .

All configurations will be examined for the following criteria:

1. Capability of true three dimensional motion
2. Absence of motion singularities or motion redundancies
3. Force uniformity and isotropicity
4. Magnitude of offset forces
5. Coverage of required volume
6. Interface with operator configuration
7. Interface with shuttle cockpit configuration
8. Weight and complexity figure of merit
9. Low inertia configuration

Failure to meet criteria 1 and 2 will result in immediate rejection of configuration a procedure which will probably leave a manageable small number of configurations to examine.

#### Candidate Configuration Selection

##### a) Three rotational DOF.

Of the 27 ways three variables can be permuted, a great number can be discarded easily. (This incidentally leads to the beginnings of motion selection rules).

1. Use of the same motion three times in succession is excluded. Reason: All three varieties lead to singularities and P-P-P as well as Y-Y-Y result in planar motion.
2. Two successive R's result in singularity and are excluded. (Eliminates R-R-Y, R-R-P, Y-R-R, P-R-R)
3. R-Y-R and R-P-R are constrained to move on the surface of a sphere and therefore have not true three dimensional motion.

4. Each of the six double Y configurations is equivalent to a double P configuration rotated by  $90^\circ$ . More or less arbitrarily we will examine only the double P configurations for criteria 1 to 4 and may rotate back to double Y configurations if criteria 5 to 7 favor it.
  5. Of the six remaining double P configurations P-P-Y and P-P-R seem not suitable as they lead to frequent singularities with any possible wrist configurations. (It looks like the motion closest to the wrist wants to be a P).
  6. Of the remaining four double P configurations we have Y-P-P, the configuration shown in Figure V-10a & b as well as that of the BNL arm. R-P-P is the BNL arm configuration with alternate mount orientation and P-R-P is the NAL E-2, E-3, E-4 configuration. These three should be examined further. The remaining P-Y-P may also be a candidate if the first P and Y axis are made to intersect.
  7. Of the six configurations containing one each of P, Y, and R, the four not having a P closest to the wrist should be eliminated since they form singularities with wrist motion as in point 5.
  8. Both the remaining Y, R, P and R, Y, P are not truly three dimensional as the wrist point describes a surface but is incapable to cover the interior volume.
- b) Three DOF with Slides.
1. All slides must be orthogonal
  2. The six possible three slide configurations are identical as far as criteria 1 to 4 are concerned. The arrangement to be chosen will be governed by the remaining criteria.
  3. S configurations may not contain an R. R-S-S and S-S-R are not three dimensional and S-R-S alters the slide-slide orthogonality.
  4. There is a Y-P similarity again so that only P-S-S, S-P-S, and S-S-P need to be considered.

5. The 18 configurations which combine one slide with two similar rotational motions are either planar or have singularities.
6. The 18 configurations which combine a slide with two different rotating motions contain 10 configurations that do not have a S or P as a last motion before the wrist. These lead to singularities with the wrist and are eliminated.
7. The remaining eight single slide configurations must be examined further.

Out of 78 configurations examined, the following 16 remain:

P-Y-P, P-R-P, Y-P-P, R-P-P,  
 S-S-S, P-S-S, S-P-S, S-S-P,  
 $S_Y$ -R-P,  $S_Y$ -Y-P, Y- $S_Y$ -P, R-S-P,  
 Y-P- $S_Y$ , Y-R- $S_Y$ , R-Y- $S_R$ , R-P- $S_Y$ .

Further examination of the single slide configuration reveals the following:

Y-R- $S_Y$  is really planar.

R-Y- $S_R$  is sequentially planar, that is all points in its volume can be reached but in general a linear motion between arbitrary points cannot be described by the wrist point.

R-S-P it is seen that a direction cannot be assigned to the slide as it changes with the position of R. This configuration is also sequentially planar.

Further reduction in the number of configurations acceptable can be made by considering volume covered to volume occupied ( $V_c/V_u$ ) ratios. The only reason rotating joints have been introduced to manipulator configurations is because in general they have a much better  $V_c/V_u$  ratios. There are however some specific exceptions where slides are acceptable.

1. Slides that can be executed by use of telescoping tubes give reasonable  $V_c/V_u$  if they are the last motion before the wrist. (Many mechanical master slaves use this).

2. For specific space configurations pseudo-slides can be attractive. These are rotating joints with very long moment arms allowed to travel through a small angle, and therefore have good linearity. Pseudo-slides are generally only useful if they are the first or the first and second motion. A pseudo-slide following a rotational motion leads to control difficulties on the latter. This eliminates  $Y-S_Y-P$ . In the narrow control volume of the shuttle, substituting a pseudo-slide for  $S_Y$  does not seem feasible nor does a true  $S_Y$ , thus eliminating  $S_Y-R-P$  and  $S_Y-Y-P$ . So, of the one slide mechanisms only  $Y-P-S_Y$  and  $R-P-S_Y$  are left.

Looking now at the two-slide mechanisms we eliminate  $P-S-S$  since a middle slide is not suitable for a pseudo-slide. In  $S-S-P$  one  $S$  must be an  $S_Y$ , which is a pseudo-slide, and not attractive in the shuttle volume.  $S-P-S$  can only be accomplished if the last slide is a true  $S_Y$  which requires the first one to be an  $S_P$  done as a pseudo-slide.

The three-slide configuration is a possibility with the first two as pseudo-slides and the last as a true  $S_Y$ . This could be done as  $S_P-S_R-S_Y$  or  $S_R-S_P-S_Y$ . However, as pseudo-slides  $S_P-S_R$  and  $S_R-S_P$  are identical balljoints. At this point it might be worthwhile to change notation and describe pseudo-slides as long rotational motions. So that if the pseudo-slides motions we have left are:  $R_L-P_L-S_Y$ , or  $P_L-R_L-S_Y$ , and  $R_L-P_L-S_Y$ . We now notice that of the four motions left involving slides or pseudo-slides three are  $R-P-S_Y$ ,  $R_L-P_L-S_Y$ , and  $R_L-P_L-S_Y$ , that is differing only by moment arm length. But the length of moment arm which we are free to adjust is the length of the telescoping arm. This moment arm wants to be as long as possible anyway in order to be able to cover vertical motion with a minimum of moment arm variation in  $R$  and  $P$ . We then arrive at  $R_L-P_L-S_Y$  as one possible final candidate. Roll (Long Moment Arm Simulating a Slide) - Pitch (Long Moment Arm) - Slide (Along the Yaw Axis Vertical).

While intuitively the other five remaining motions do not look nearly as good as  $R_L-P_L-S_Y$  it is worthwhile to make the final selection after comparison for force uniformity and isotropicity.

#### Uniformity and Isotropicity of Forces

The entire group having rotational motions only has a common feature of two  $P$  motions either in succession or separated by another rotational motion. In order for these



articulated configurations to fit and be capable of maneuvering in the A defined shuttle control space the arms between the P joints must remain quite short, 12". Yet in order to cover the desired control volume it is necessary to let the included elbow angle vary from  $15^{\circ}$  to  $150^{\circ}$ . Without analyzing all the possible positions showing force anisotropy, the top hand position of figure V-10 was evaluated. In this position the moment arm for up and down motion is approximately 1/10 that for fore and aft motion. That means that for the up and down motion friction is about 10 times nominal friction force, feedback forces are 10 times too high (80 lbs), and inertia forces due to shoulder actuator and drive train components are 100 times the nominal ones. Yet these same components are quite near nominal for fore and aft movements. While only one example has been detailed, things are nearly as bad for some other TD locations. This is highly undesirable.

At this point, the configurations left for consideration are:

1. A family of four configurations having rotational joints only.
2. A group of configurations which converged to  $P_L-R_L-S_Y$ .
3.  $Y - P - S_Y$

It is possible to eliminate the  $Y - P - S_Y$  configuration as in some positions it has no lateral displacement as well as allowing zero moment arms on the Y motion right in the middle of the covered volume.

The remaining two families are  $R_L-P_L-S_Y$  and  $Y-P-P$ . As can be seen the  $R_L-P_L-S_Y$  configuration has much better force uniformity and isotropy than the  $Y-P-P$  family. Furthermore, all three shoulder actuators can be located near the cockpit floor yielding a low inertia configuration with nearly stationary actuator packages. If cockpit configuration allows, these actuators might even be located below the cockpit floor even further reducing force ratios.

The price to be paid for this is slightly larger weight due to the long telescoping tube and the somewhat larger gear ratios required for the  $R_L$  and  $P_L$  motions. Since the vertical boom never is more than about  $17^{\circ}$  from the vertical no large unbalance occurs on the master. If necessary even this can be further improved by simple means. Also, when used for

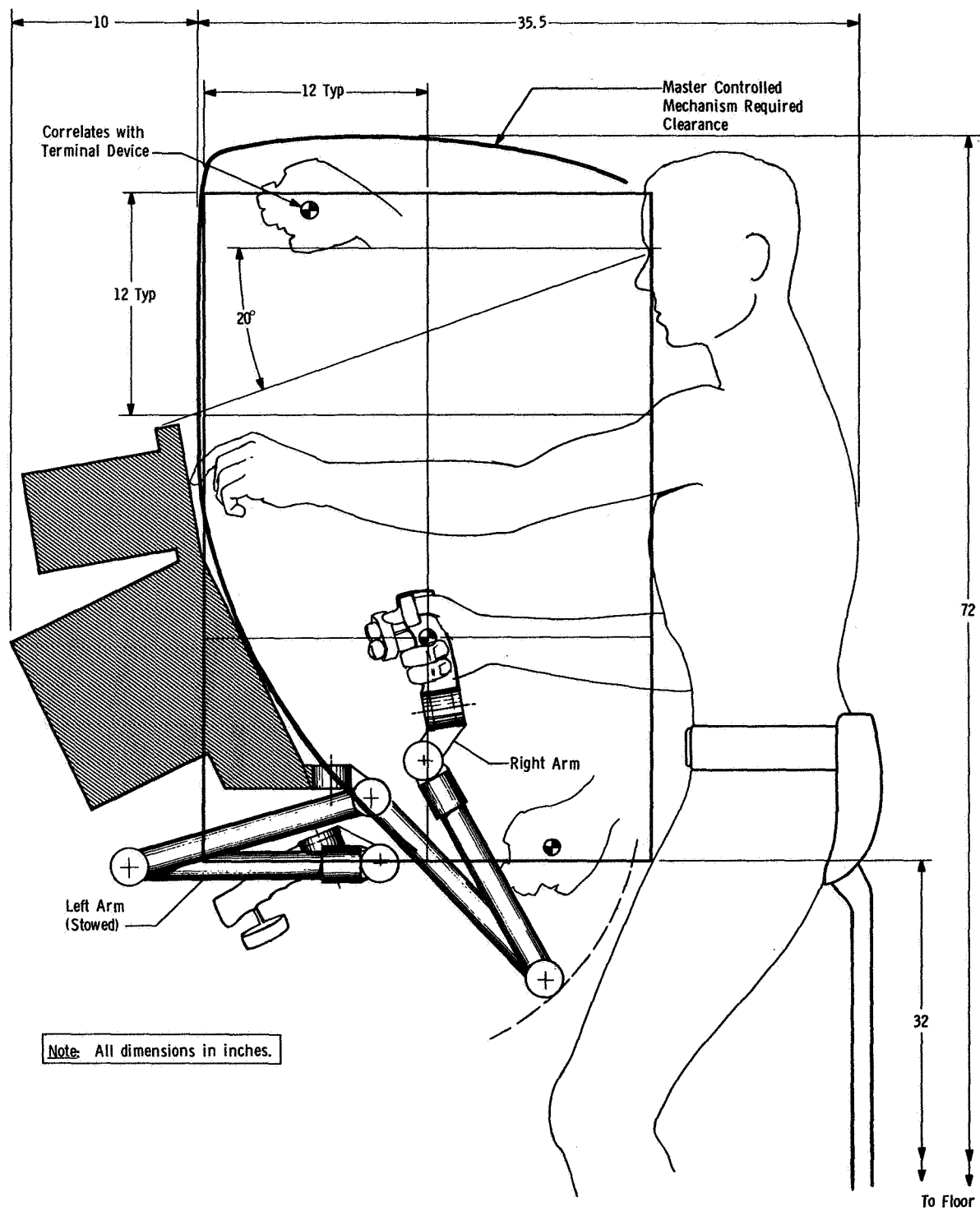


Figure V-10a Elbow Type 6 DOF Position Controller

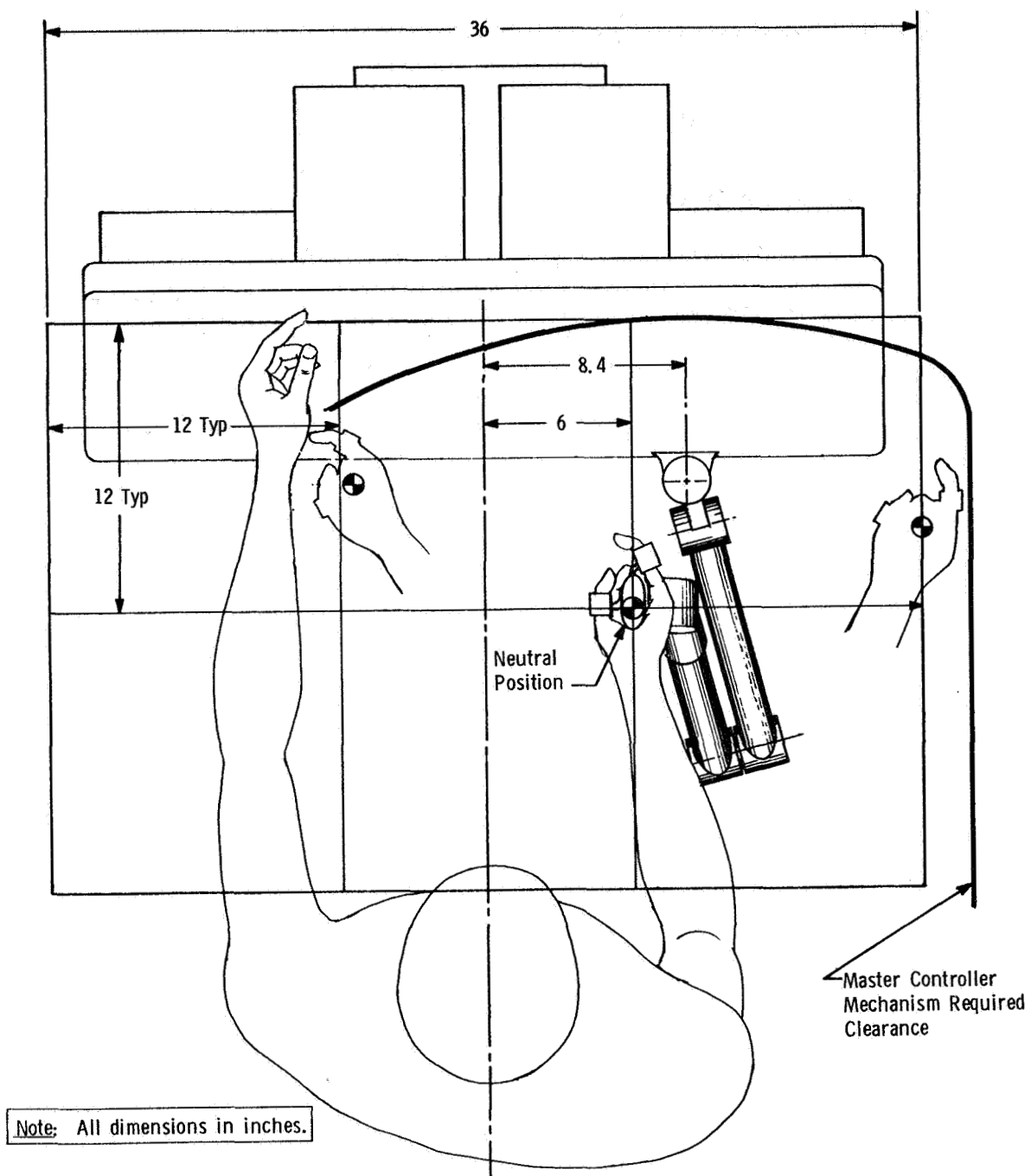


Figure V-10b Elbow Type 6 DOF Position Controller

one "G" simulation, no counterbalance is needed for the pitch and roll at base.

An appropriate wrist configuration for the  $R_L-P_L-S_Y$  configuration seems to be Y-P-R. This can be achieved in a well balanced arrangement as no vertical arm exists to cause operator elbow interference.

The configuration of  $R_L-P_L-S_Y$  is shown in figures V-11 a and b.

This master is also suitable for rate control experiments. By limiting motion to approximately 1 inch in R, P, and S and center-zero spring loading these motions, what looks like a very suitable rate control master is created.

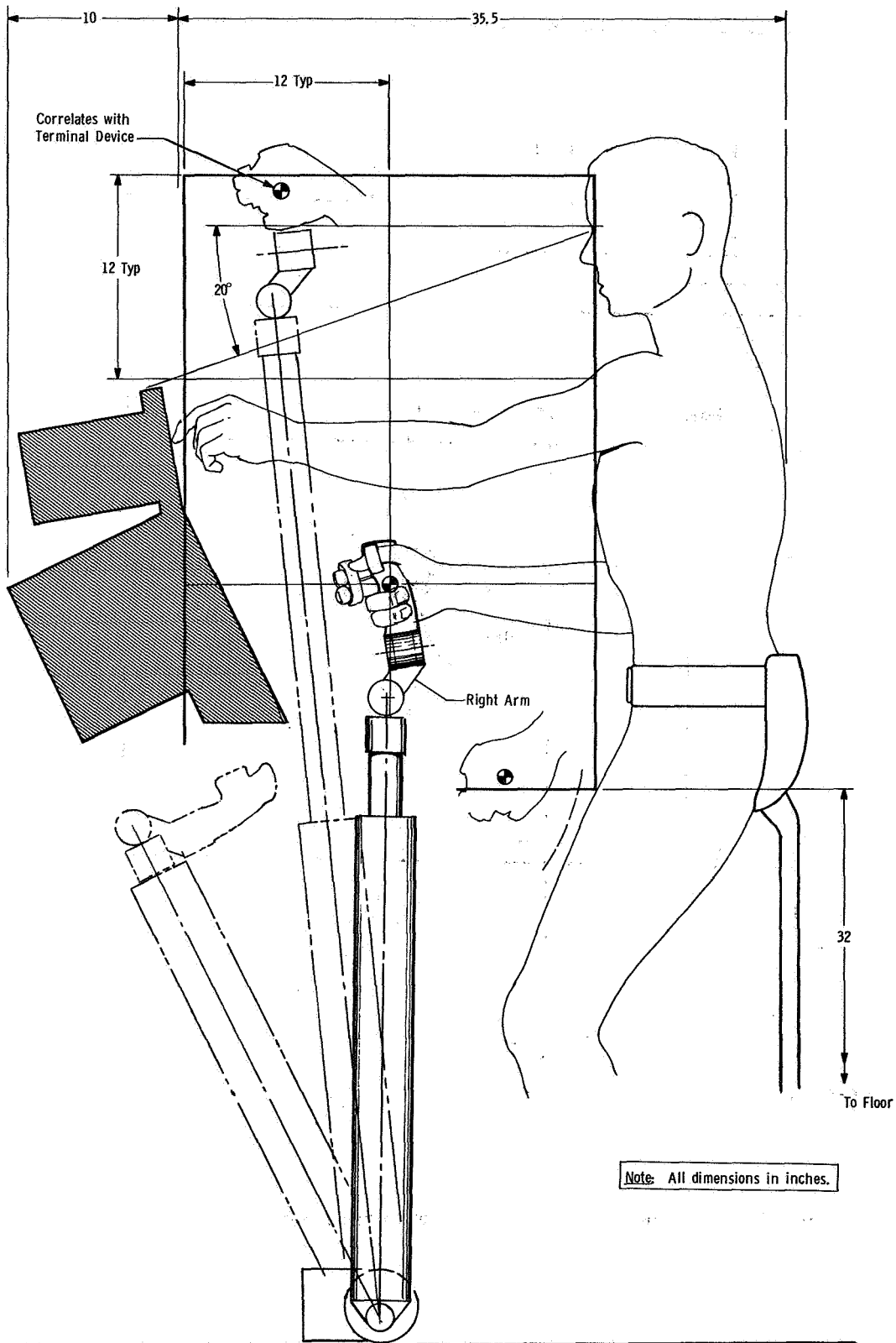


Figure V-11a 6 DOF Vertical Slider Position Controller

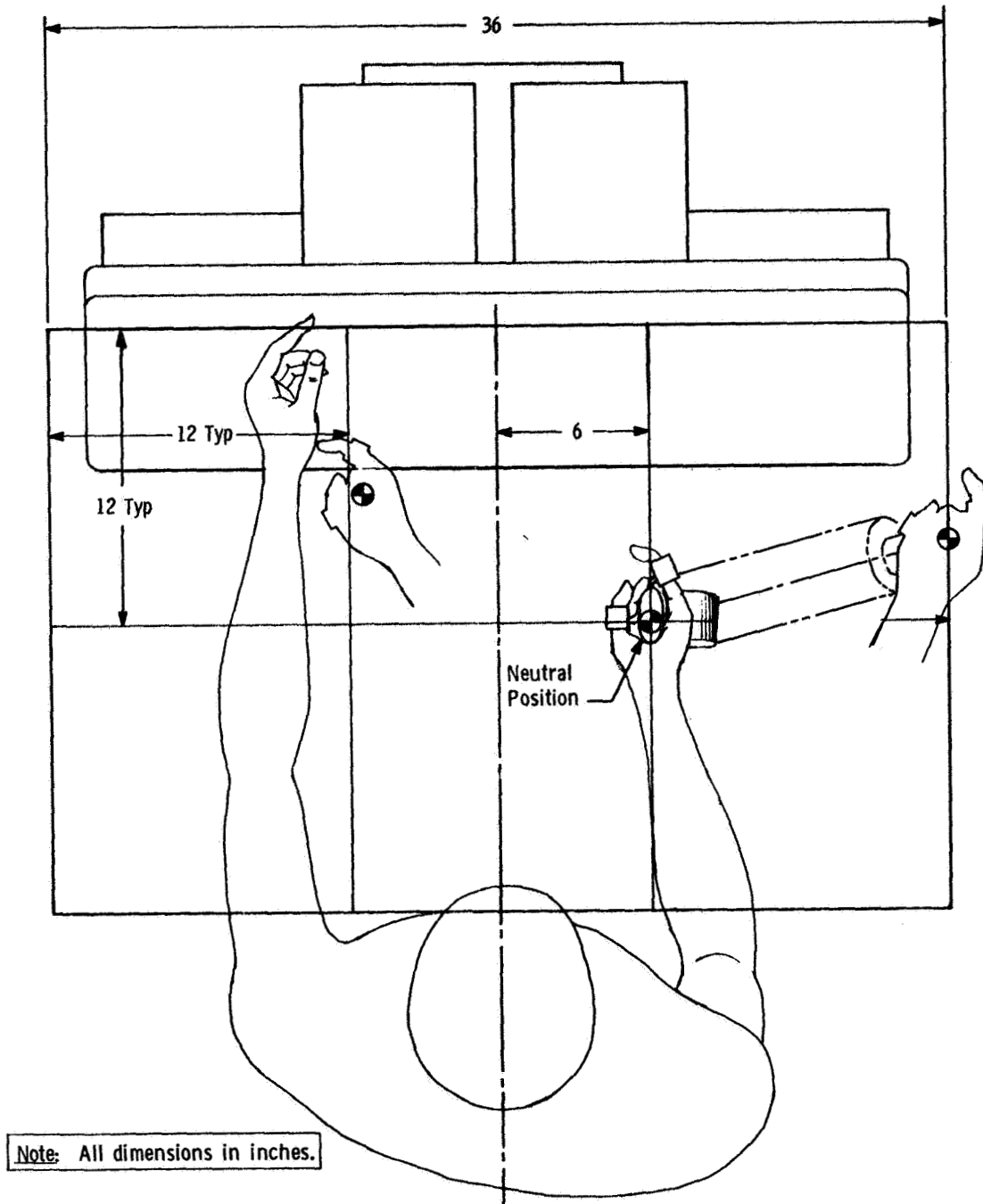


Figure V-11b 6 DOF Vertical Slider Position Controller

### Man-In-The-Loop-Simulations

Simulations were performed in Martin Marietta's Space Operations Simulator (SOS) facility, a six degree-of-freedom (DOF), moving base, servo controlled motion generating system. The simulations were divided into two phases, corresponding to two types of Shuttle tasks: Phase I, payload tracking and capture and Phase II, payload retrieval and cargo bay stowage. In the first Phase the task was primarily one of tracking the target receptacle with the terminal device, although the TD was actually inserted into the receptacle during a run. However, physical capture or contact dynamics were not simulated. The Phase II task consisted of first translating and rotating the captured payload to a position near, and aligned with, the cargo bay, and then maintaining alignment while lowering the cargo into the bay. The task was terminated when two pins on the cargo were seated into two receptacles in the bottom of the cargo bay.

The modeled manipulator arm had the following characteristics: two main segments of length 25 ft each, wrist length of 2 ft, and gimbal sequence of yaw, pitch at the shoulder, pitch at the elbow, and pitch, yaw, roll at the wrist. The arm shoulder is assumed to be attached to the Shuttle at the forward right corner of the Cargo Bay. For this simulation, the TD television camera is placed "outside" the 3 wrist gimbals; i.e., so that the 3 gimbals are between the camera and the elbow.

The control laws derived for the simulations have the following features: (1) coordinated translational and rotational control, (2) rotations about any point, (3) positional and rotational indexing, (4) automatic tip attitude hold (hawk mode), and (5) multiple gain ratios for translational motion. Both rate and position type control systems were developed so that in the simulations a good operational comparison between the two could be made.

The two most important relative motion effects were included in this simulation: target flyby velocities, and terminal device motions due to the commands sent to the joint servos. The servos were accurately modeled to include their response characteristics when accelerating and decelerating for presently conceived arm joint designs. Two models were developed, one for the tracking task (essentially no load), and one for the cargo stowage task (65,000 lb load).

Past simulations have shown that the other relative motion effects, due to Shuttle limit cycles and arm flexibility, do not greatly effect the operator's control for the joint torques used in the simulated arm model. It is believed that not including these motion effects in this simulation did not change the basic conclusions drawn concerning unilateral position systems.

Input commands from the controller are sent to the hybrid computer facility (EAI 8900), which is programmed with the control laws, manipulator arm models, and other equations or logic required by the simulation. The computer calculates the commands for the SOS servo motors which produce proper relative motion between the viewing camera and the task mock-ups in all 6 degrees-of-freedom (DOF). Video information from the cameras is then sent back to TV monitors on the operators console.

Over 100 runs were made using the SOS facility with parameter variations covering control gains or ratios, target velocities, control modes and different input controllers.



### Position Controller Design Evaluations

The goal of this evaluation phase is to evolve a bilateral position controller configuration which would be built into an operational model. Our goal at the time was to come up with an acceptable tool which would have interchangeable parts to allow a wide variety of manipulator configurations to be evaluated.

The first step was to construct several wood/metal controller mockups Figure V-12, to derive criteria on segment lengths, joint ordering, movement volumes and controller attach points in relation to the operator. At this point in the evaluation, the elbow controller was a prime contender. Emphasis was placed on joint ordering, particularly for attitude control. Figure V-13 shows movement volumes associated with this type of controller. It was thought, at the time, that large movement volumes would be desirable, which our simulations proved incorrect. If an elbow type controller was desirable with a "stacked" or unbalanced gimbal attitude control then the 6-DOF configuration shown in Figure V-14 is the most desirable. This gimbal order, starting at the grip, is pitch, yaw, roll, pitch at the elbow and yaw and pitch at the shoulder.

A functional model of this configuration was constructed of aluminum and steel with pots on each joint (Figure V-14) to further evaluate this concept. The segment lengths are variable and each joint is interchangeable. This model is described in detail in Appendix B. Various configurations of the operational elbow controller were evaluated against a simulated manipulator tracking and alignment task presented on a stereo color TV system. The stereo system is described in Appendix C, however, it is essentially a 5 DOF dot and cross-hair tracking task which did provide a dynamic evaluating technique to test controller characteristics against. It was determined that gimbal "stacking" for attitude control was a poor design since it produced cross-coupling between the attitude gimbals themselves and also between the translation gimbals. Because the gimbals are stacked and the drive motors are large, several inch long lever arms exist between upper and lower gimbals. Gross hand/arm movements were also required for attitude control. It became obvious a better manipulator design was required. A second, significant problem exists with an "elbow" type controller. This relates to the "toggle" effect. As the elbow angle changes, the force required to backdrive the joints changes significantly. Figure V-15

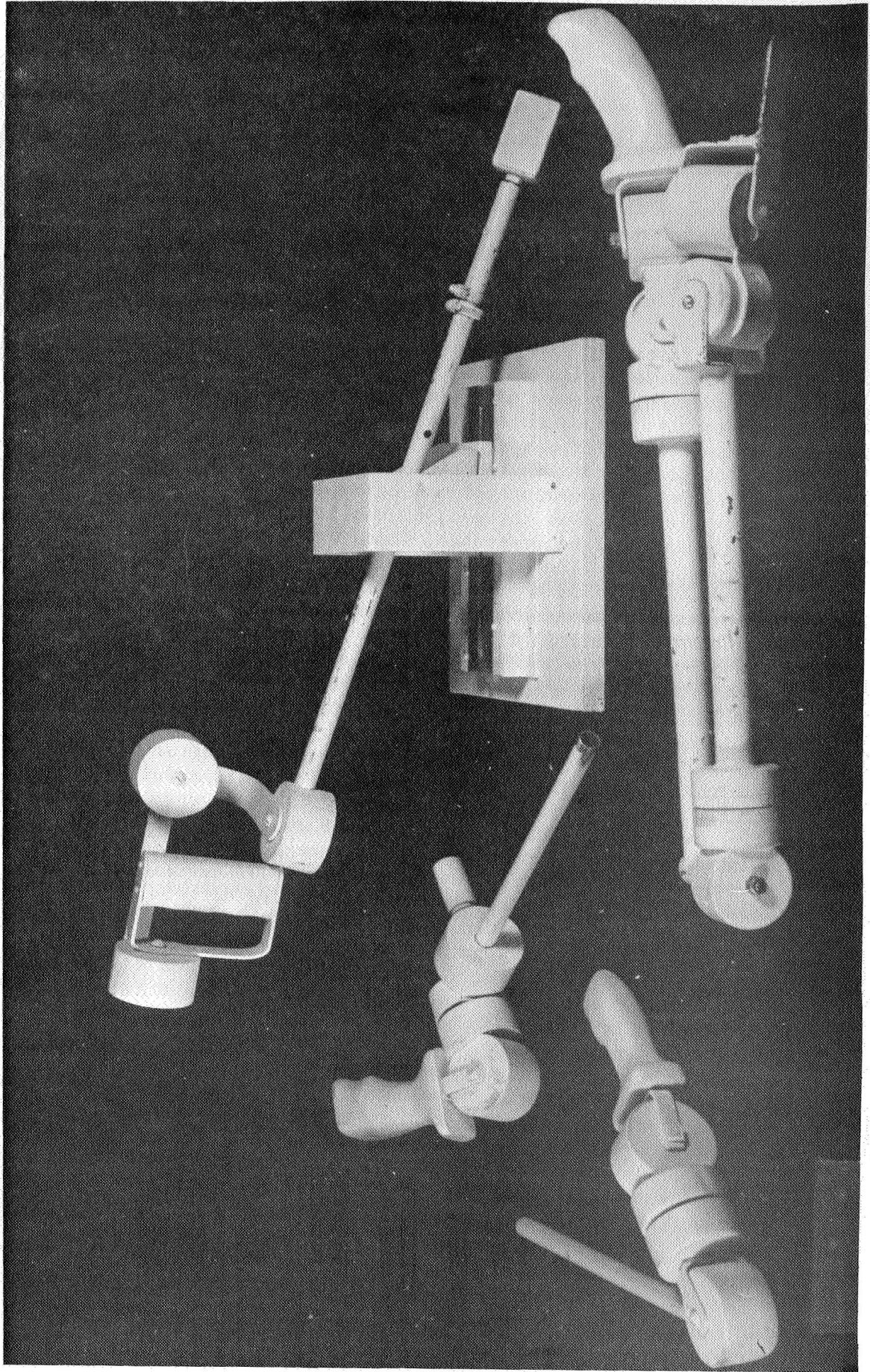


Figure V-12 Controller Mockups

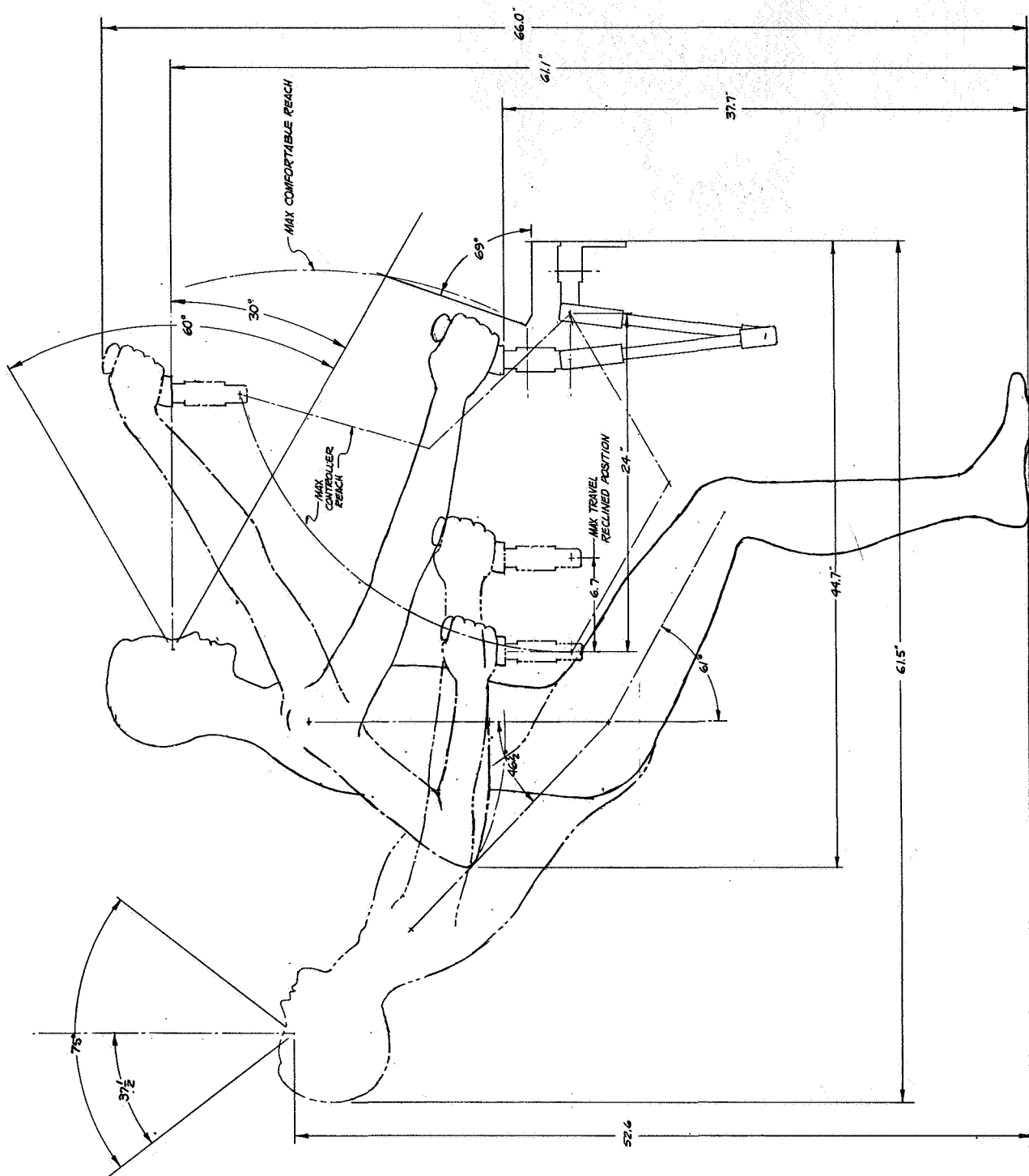


Figure V-13 6-DOF Elbow Type Controller Movement Volume



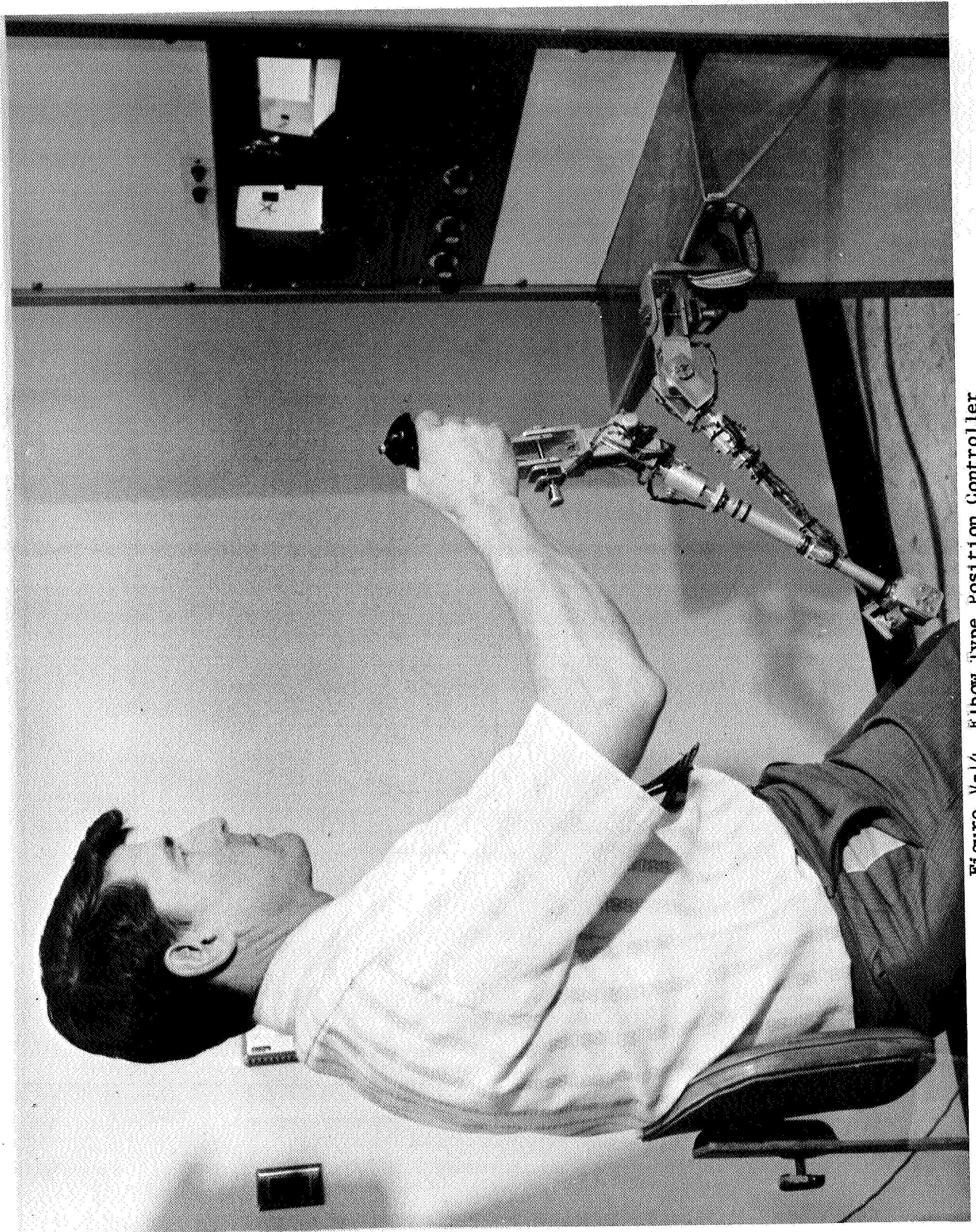
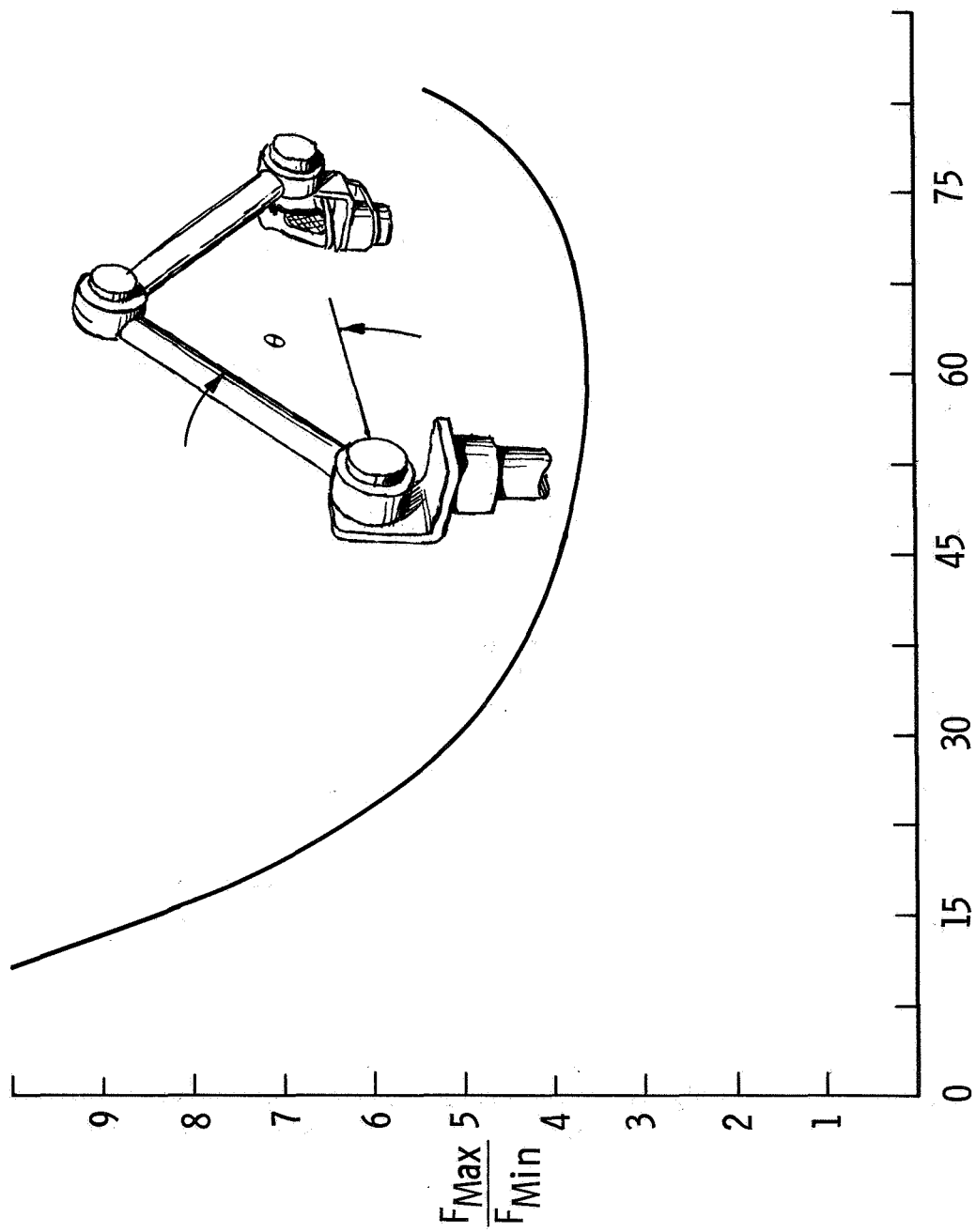


Figure V-14 Elbow type Position Controller



Shoulder Angle ( $\theta$ )

Figure V-15 Replica Stiction Force Ratio

shows this force relationship for a typical replica. It can be seen that for a force ratio of say 4 or less, the  $\theta$  must remain between  $45^\circ$  and  $75^\circ$ , an undesirable restriction. If larger angles are used the backdriving force variations can be misinterpreted as real manipulator tip forces by the operator in a force reflecting system.

The next major position controller configuration concept to evolve is called the "sliding base" and is shown in Figure V-16. The pitch and yaw attitude gimbals are balanced at the operator's wrist. Roll is balanced on the center of the grip. Y and Z translation is controlled by two gimbals attached to a sliding mechanism which controls X translation. This controller was configured into a fully operational, force reflecting system which was used as the primary position controller during our dynamic simulations on the Space Operations Simulator. The controller is counterbalanced so the operator does not have to hold the weight of the mechanism against gravity.

Extensive use of this controller configuration resulted in several significant conclusions:

1. The force feedback levels could be varied between 0 and approximately 16 lbs. The full gamut of maximum force levels was tried from very limp to levels in the 10 to 16 lb range. It was found that for typical tracking tasks, levels up to 2 lbs were too light. Since the operator's arm is not supported, muscle tremor and jitter were pronounced at the low levels. Vernier movements were difficult. It was found that the operator needed a force feedback in the 3-5 lb range, depending on the position of the operator's arm in relation to his body and the direction the force is applied. Higher forces 8-12 lbs quickly fatigued the arm and some operators resorted to using two hands to accomplish the tracking tasks at these high force levels.

2. This gimbaling concept, allowed cross-coupling between the pitch/yaw gimbals and X/Y translations. The extent of the cross-coupling varied with the force levels selected at the various joints, however, it was always present to some extent. This is caused by the moment arm resulting from controller grip being offset from the pivot point by approximately 4 in. The coupling went both ways, between attitude and translation, and translation and attitude. For example, if a straight Y translation was commanded by pushing the controller



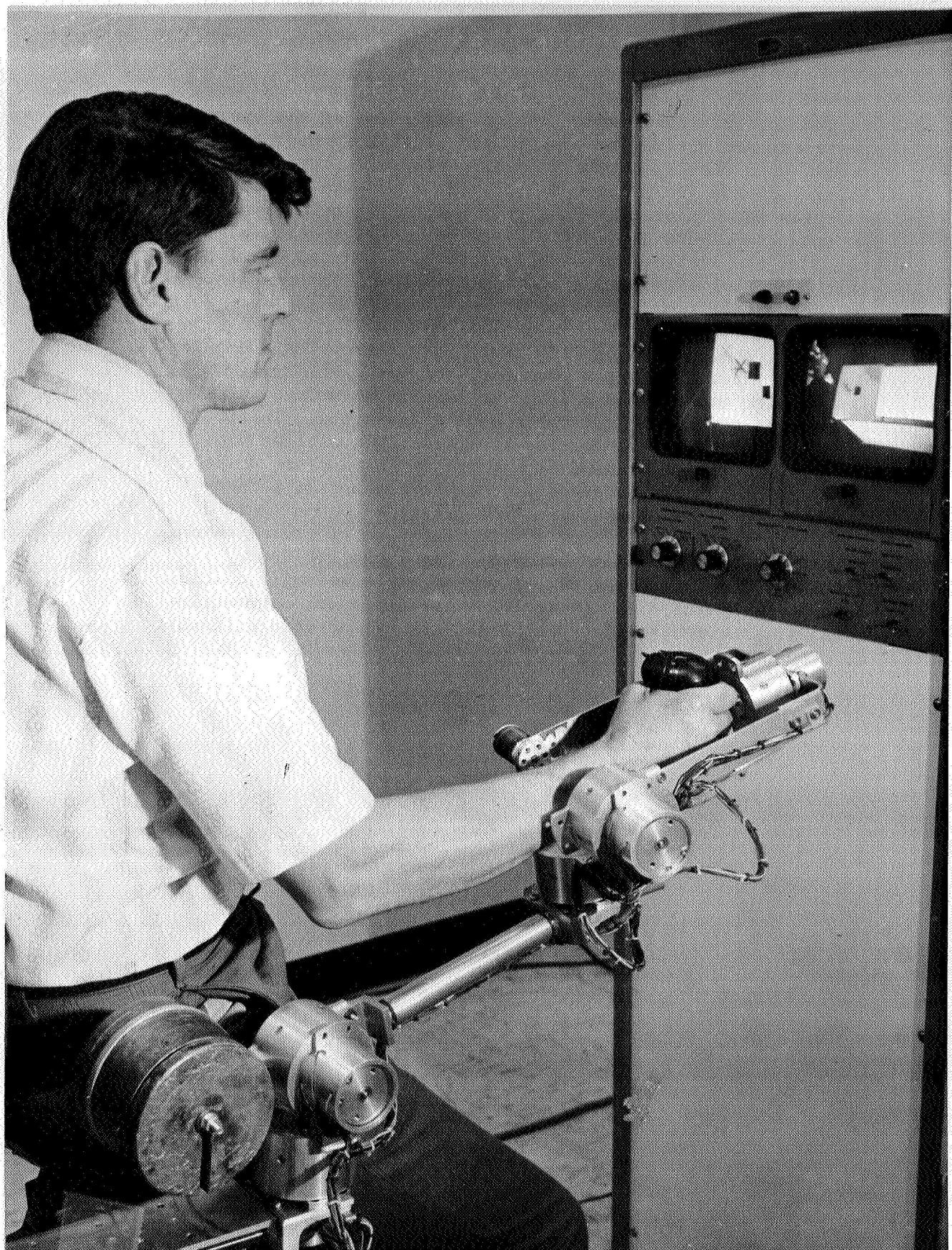


Figure V-16 6-DOF Sliding Base Position Controller

to the left or right, some portion (depending on the operator's awareness and ability to compensate) of that input would result in a rotation about the yaw gimbal axis. The same thing happened for pitch and Z translation. The obvious solution to this problem is a grip balanced attitude control as shown in Figures V-17a and V-17b. This configuration places all 3 of the attitude pivot points through the center of the grip, thereby, eliminating attitude control induced moments on the translational gimbals.

3. The sliding base concept, for X direction commands, was poor. For straight X commands, the mechanism worked well. The problem arose, when a large translational offset was created by commanding a large Y or Z translation. This rotated the forward arm of the controller off at some significant angle in relation to the sliding mechanism, 45 to 60°. X translation became difficult to control at or near these angles. As can be seen from Figure V-18 the control grip has shifted significantly off its plane of travel which, not only creates coupling between X and Y but the force required to position the slider varies with the angle of the upper arm segment. As the angle of the upper arm segment increases, combined X and Y/Z translations become more difficult to command.

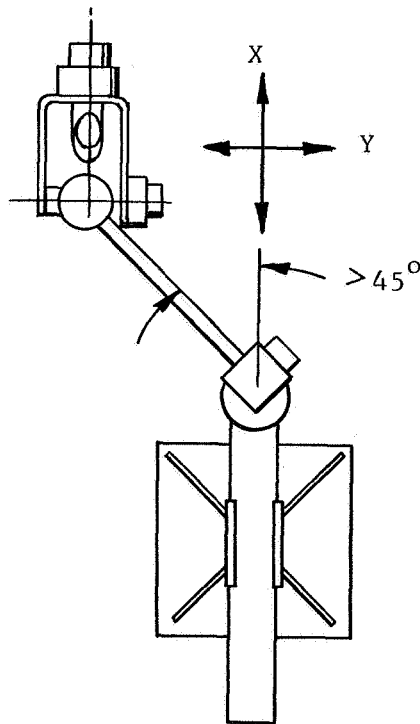


Figure V-18 Sliding Base Controller, Top View



4. At the onset of our controller evaluations we assumed indexing the controller, during a dynamic task, would be difficult and distracting. This assumption was incorrect. Even with the inertia created from the counterbalance weights, indexing the controller became an automatic reflex, similar to shifting a car. Indexing was accomplished by pressing a small button on the controller grip which electrically disconnected the controller from the manipulator control electronics. While the button was depressed, the controller could be quickly repositioned to any point in its movement volume that the operator selected.

The manipulator was engaged to the control electronics by releasing the button. Indexing times ranged from 1 to 2 sec depending on the movement involved. Indexing was required as much, or more for attitude correction as translation. Most operators indexed the controller at a convenient time during the task, rather than waiting until the controller at a convenient time during the task, rather than waiting until the controller was fully extended. The operators also preferred to keep the control grip close to the body which kept the operator's arm in a more comfortable position. This allowed for more precise movements and less arm fatigue.

5. The combination of indexing capability and a variety of control ratios allows the operator to work the position controller in a rather small volume (approx. 4 cu ft). The control ratio is the displacement ratio between the manipulator tip movement and the position controller movement. Ratios from 30:1 down to .5:1 were evaluated for tracking and cargo handling tasks. For tracking tasks, where the target velocity was .25 ft/sec, a high and low ratio was found necessary. The operators were allowed to select the ratios they wanted and most found 20 or 25:1 desirable for the high or gross movement tasks and 6 or 8:1 for vernier, close in, capture tasks. A medium range of 10 to 15:1 was used until the operators became proficient at the task and then it was dropped in favor of a single high/low ratio combination. During a dynamic tracking task, a 30:1 control ratio tended to produce very quick, erratic responses at the manipulator tip. Any extraneous arm or muscle tremor was unnecessarily amplified. Unless specifically requested, none of the operators used or wanted a ratio above 25:1. Vernier movement, while tracking at the same time, is readily controlled in the 6 to 8:1 range. Lower ratios require too many indexes and disrupts the tracking continuity.

6. The primary mode of operation, during the simulations, was to stop the manipulator tip travel during a controller index. Since the indexing sequence took place very quickly, this did not present a problem. However, it was decided to evaluate the same tracking tasks and allow the manipulator tip to continue on at the velocity commanded just before indexing. For close-in tasks, this mode is disastrous. During several runs, the target was inadvertently hit before control was regained, which never happened when the tip was stopped during indexing. Allowing the manipulator to maintain a velocity may be desirable while moving large payloads or for gross, unloaded, maneuvers where the tip is not near an obstacle. It may be desirable to give the operator the option to select whether tip velocity is maintained or not during indexing. Further simulations are required.

7. The controller interaction with the visual system is critical. The visual scene used for control of the task must be aligned with the controllers movement axis. For example, the X movement of the controller, fore and aft, must move the TD in and out of the picture. Slight, consistent, off-axis situations can be learned and compensated for, by the operator, with a corresponding small degradation in task performance. However, any gross axis misalignment or especially an inconsistent misalignment, makes many tasks nearly impossible. The operator resorts to a frustrating, guessing game where sometimes he is successful and many times not. No consistency is experienced, however.

8. In a position system, the operator derives tactile and kinesthetic feedback relative to the commanded manipulator tip velocity. The operator's sensory capability is not keen enough in the low force levels 1-2 lbs. to accurately determine the specific velocity he is commanding. Primarily, the operator needs to know when he is commanding near or at maximum tip velocities. This could be done through the controller by having a step function force increase when a command exceeded the manipulators capability. However, this method would increase the controllers motor sizes significantly since a rather sizable force is needed. Another approach, which we employed successfully, was to place two warning lights above the operator's TV monitor. A yellow light comes on when 75% of the maximum tip velocity was commanded. The red light came on when 100% is commanded. Information feedback to the operator at these two data points proved adequate during our simulations.

## C. RECOMMENDATIONS AND CONCLUSIONS

The primary purpose of this section is to describe the rationale for and recommend a bilateral master controller configuration. However, the controller is intimately tied to the total manipulator system characteristics. Therefore, the conclusions and recommendations will relate to not only the controller design but also to the associated desirable system characteristics.

### Recommended Controller Configuration

The recommended controller configuration is shown in Figures V-17 thru V-19. The configuration has the following advantages and features:

1. The attitude gimbals are balanced at the center of the operator's grip. This technique, when associated with a vertical sliding base, eliminates unwanted cross-coupling between the attitude and translation control inputs. Controller rotations rarely exceeded  $\pm 45^\circ$  in any axis, before indexing. However, design limits should be  $\pm 90^\circ$  in each attitude axis.

2. Translation control consists of a vertical telescoping member attached to pitch and yaw gimbals at the base. This design is unique, when compared with the other concepts evaluated, in that the controller can be positioned through its movement volume and not build up unwanted forces unique to its position. Pure Z translations are made by positioning the controller straight up or down. X and Y (fore/aft and right/left) translations consist of a combination of the pitch and/or yaw gimbal, and the vertical telescoping member. The mass of the vertical telescoping member can be kept low, since all three translation drives can be mounted on the base. There are no lever arms in the attitude gimbals and these drive motors can be small. Controller mass is especially important during indexing, when the unpowered controller is rapidly repositioned. A desirable movement envelope is created when the vertical slider has an upward movement of 12 inches and downward of 6 in. This is measured from the operator's hand (forward) with the elbow bent  $90^\circ$  (about waist level). The P&X base gimbal travel need not exceed  $\pm 45^\circ$  measured from vertical.

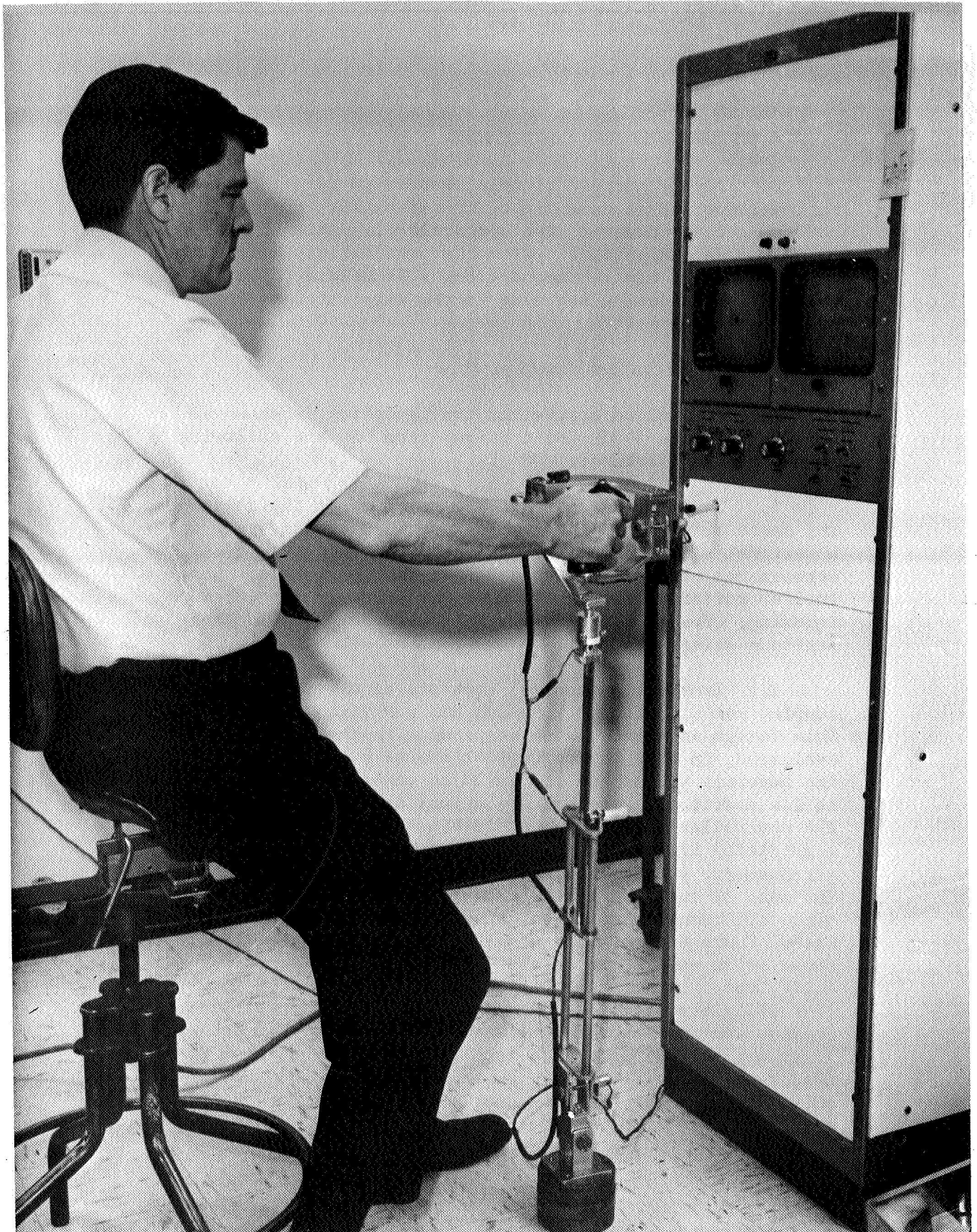


Figure V-17a 6-DOF Vertical Slider Position Controller Front Mounted





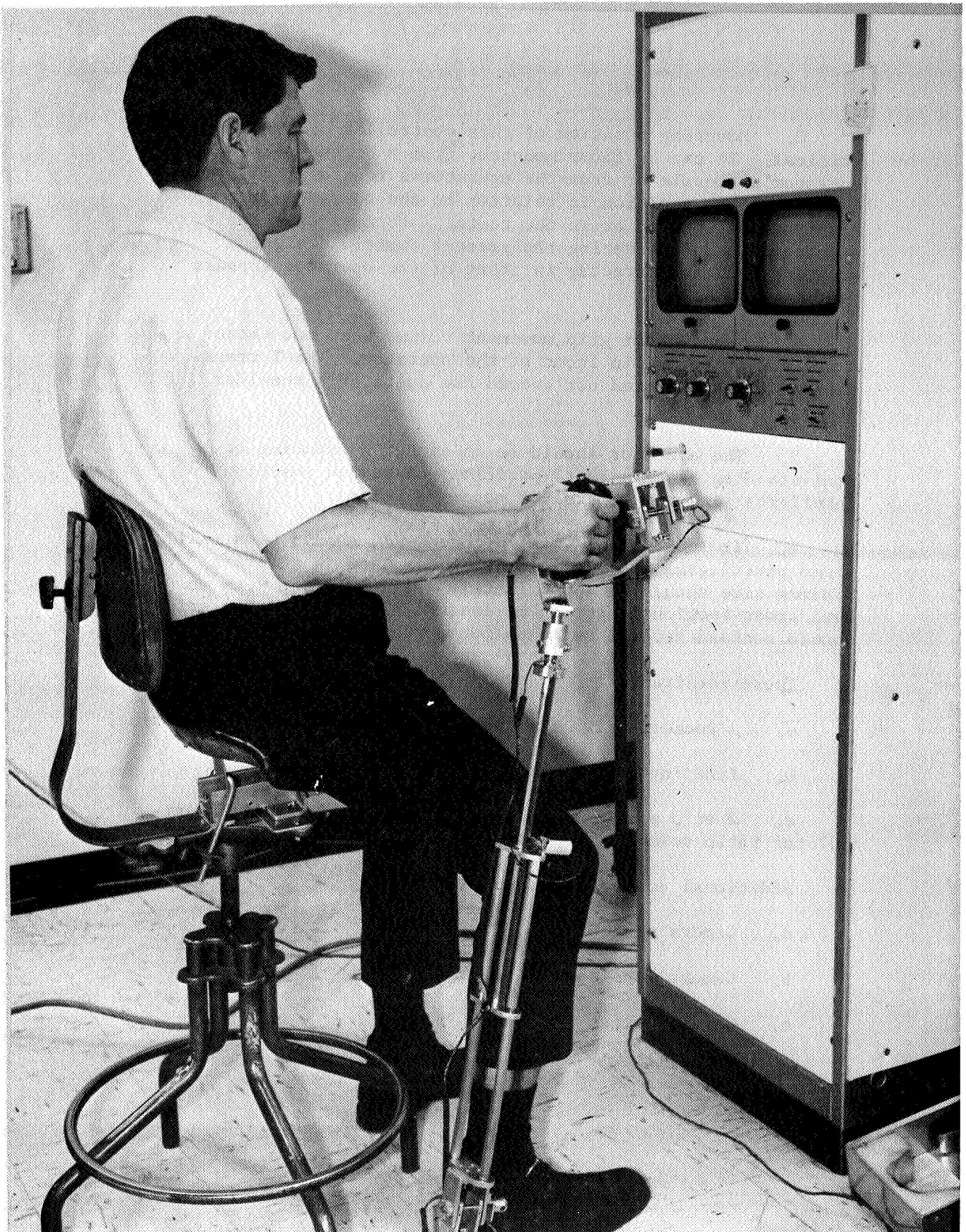


Figure V-17b 6-DOF Vertical Slider Position Controller Side Mounted

3. Mounting position of this controller concept is not critical. It can be floor mounted, from a bracket off the operator's console or from the operator's restraint. It can be used in any position in relation to the operator, i.e., right or left handed or in the center. From an operator's standpoint and considering the present Shuttle design, a mounting position directly in front of the operator appears best.

4. The control grip movement volume need not exceed a 2 x 2 x 2 ft volume in front of the operator. The Y translation dimensions need not exceed the operator's shoulder width.

5. The operator should be in either a standing or semi-standing (knee's bent) position. A seated position interferes with the controller movement volume.

6. The controller grip, Figure V-20, should be a full sized pistol grip type, similar to those used in aircraft. Minimum size should be approximately 4-1/2 in. long with an oval cross-section measuring at least 1 x 1-1/2 in. The grip should contain several switches for system control.

Those required are:

- a. A rocker switch for terminal device opening and closing.
- b. Indexing push button.
- c. 2 or 3 position selector switch for controller/manipulator ratio select.

Additional control may include:

- a. Camera pan/tilt
- b. Camera lens zoom
- c. Camera select
- d. Lighting

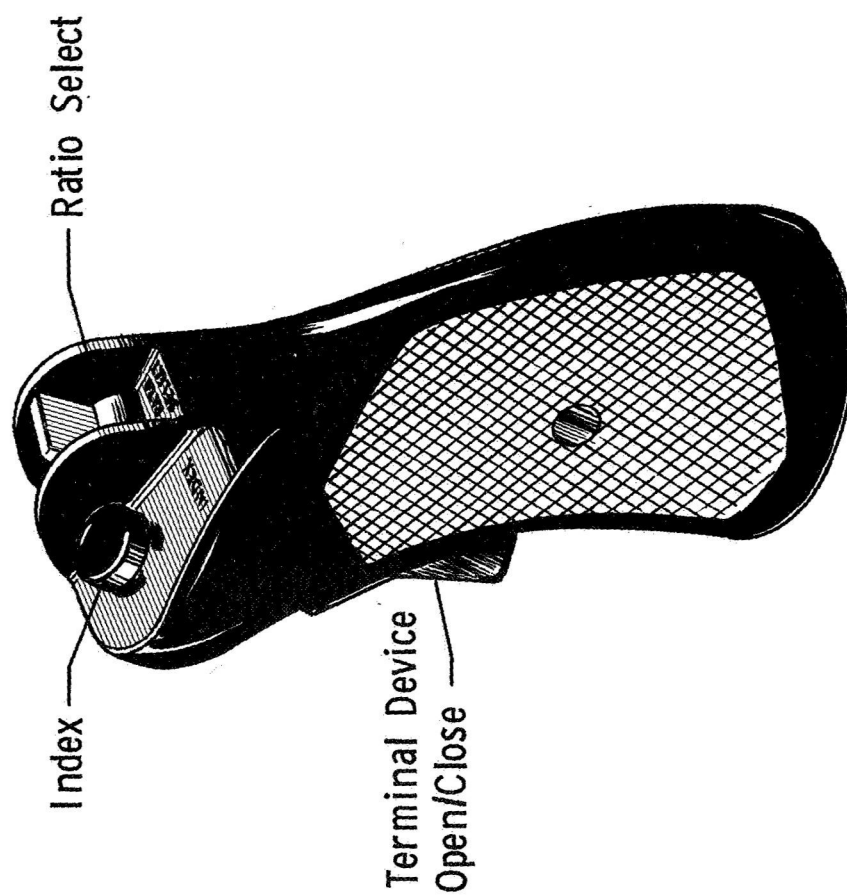


Figure V-20 Controller Hand Grip



### Recommended Manipulator System Characteristics

- A. As discussed earlier a range of manipulator/controller movement ratios of 25:1 to 4:1 were found to be the most desirable from an operator's standpoint, and related to the tasks evaluated. Since these tasks were extremes, worst case, it is felt that these end points are accurate for the full gamut of manipulator tasks.
- B. The system must allow the controller to be indexed rapidly, to any position in the movement volume.
- C. Manipulator controller axis alignment with the visual system is mandatory.
- D. Two TV monitors are required for the operator. One for a detailed view and one for an overall scene. Switching cameras on a monitor during a specific task is distracting and undesirable.
- E. Unless stereo TV is used or a side view is provided, visual aids are required to aid the operator during alignment tasks and help determine positions in the X direction. Our simulations showed that a standoff cross was required to accurately position the TD in a receptacle. Various methods such as mirrors, perpendicular lines and vertical feelers were evaluated with some success.

## VI. DYNAMICS

There are two primary objectives for conducting a dynamical analysis of an Attached Manipulator System. The first is to gather basic design data such as the torque and load requirements associated with the various manipulator tasks, and the second is to obtain a mathematical description of the pertinent dynamical (flexible body) phenomena of the AMS. The second objective is necessary for the control system design and any simulations or demonstrations of AMS dynamical behavior.

The AMS dynamics effort is divided into three parallel programs: (1) a generalized rigid body dynamics model to obtain the preliminary design data (torques and loads) for the AMS, (2) a vibrations analysis to study the mode shapes and frequencies of the AMS as it vibrates about a particular equilibrium position, and (3) a modification of a generalized n-body digital computer program previously developed by Martin Marietta. The third program is capable of simulating the flexible behavior of the AMS as the joints undergo large non-linear excursions and is being used to examine the interaction between the control system and the flexible arm.

Section A of this chapter is devoted to the rigid body analyses including the development of the mathematical model and corresponding computer program. Results for a number of payload deployment tasks are presented, and these are used to arrive at the joint torque requirements for the AMS.

Section B contains a discussion of two vibration analyses of the AMS along with results based on preliminary design data.

Section C is devoted to the generalized n-flexible body computer program, and a simplified payload handling task is used to compare the rigid and flexible behavior of the AMS.

Finally, the findings of this work are summarized in Section D along with some recommendations for future work.

## A. RIGID BODY ANALYSIS \*

For purposes of obtaining load requirements and simulation facility design requirements, the AMS was modelled as six interconnected rigid bodies. Throughout the analysis, sufficient generality was maintained to arrive at a single set of equations describing both the Shuttle Attached Manipulator System (SAMS) and the earth-based Attached Manipulator System. To maintain continuity, the description of the generalized AMS model and a detailed derivation of the equations of motion are contained in Appendix A.

### 1. Computer Program

The equations developed in Appendix A constitute the main body of a digital computer simulation which is programmed to calculate pertinent design data associated with various AMS tasks. The utility of this program is best described in terms of its input and output.

First, one selects the appropriate geometry and inertia properties describing a payload and either the SAMS or the AMS. Next, a particular task is chosen and included in the program by means of time dependent functions for the various joint angles. Finally, the user can specify any set of external forces and torques acting on any or all the bodies involved (gravitational forces are automatically included simply by specifying the components of the gravity vector in inertial space).

When the computer program is used to simulate the SAMS, the primary output consists of: interaction forces and torques acting on the SAMS, Shuttle, and payload; joint motor torques required to execute the SAMS task; and finally, the Shuttle motion which is induced by the SAMS task. By exercising the option to include external forces and torques (in particular, the ACS thrusters on the Shuttle) this program can easily be used to study the interactions between the Shuttle ACS and the motion of the SAMS.

When the program is applied to the AMS, the output is the same as for the space version, with one exception: the motion of the Shuttle is replaced by the forces and torques acting on the ground-based support structure of the AMS. In this case, selection of appropriate external forces and torques (or simply by misaligning the gravity vector from the vertical), the computer program can be used to study the effects

\* The work presented in this Section was performed under Independent Research and Development Task No. D-05R entitled "Teleoperator Manned Control and Mission Simulation".

of perturbations forces due to imperfections in the simulation facility, such as floor slope or air bearing drag forces.

## 2. Check Cases

Before applying the rigid body program to AMS behavior, it was validated by means of several check cases. It was decided to divide the check cases into two groups: those not involving the presence of external forces and torques and those that do. For the first group of check cases, all but one of the gimbal angles of the AMS are held fixed and the remaining one is prescribed as a function of time. This results in (by proper choice of inertia properties) the planar motion of two interconnected rigid bodies; the motion of one body relative to the other being prescribed. This relative motion of the two bodies will induce a motion of the second body relative to inertial space. The solution for this motion is known (see Reference 3), and with it, one can easily determine the joint forces and torques which are developed between the two bodies. Now it is precisely the computation of the motion induced in the Shuttle by the AMS prescribed motion and, with it, the computation of joint forces and torques that is the primary function of the rigid body AMS computer program. Thus, by prescribing the motion of one gimbal at a time and repeating this for all of the AMS joints, one can check out the accuracy of the computer program for all possible AMS motions.

For motion involving external forces and torques, two check cases were used. The first involved specifying a gravity vector and assigning essentially infinite inertia properties to the sixth body. The joint angles were all fixed thereby resulting in a simple statics problem of the AMS fixed to the ground. It was then an easy matter to compute the joint forces and torques to compare with those predicted by the computer program.

To check the accuracy of the program to predict the motion of the Shuttle caused by external forces and torques acting on both the AMS and the Shuttle, all six of the bodies were modeled as spheres of equal diameter and mass, acted upon by external forces and torques. The joint angles were fixed at values such that the six spheres occupied a common center resulting in the problem of a single rigid body acted upon by external forces and torques. Because of the spherical symmetry it is a straight-forward matter to determine the body components of the angular velocity. Rather than appeal to the classical solution of the kinematical equations (the attitude angles) it

was easier to solve them by numerical integration and compare these results with those of the rigid body program.

It is noted here that exact agreement between all of the check cases and the corresponding computer solutions was obtained.

### 3. Inertia Properties

In arriving at the inertia properties for the AMS, a separate computer program was developed to optimize the AMS counterbalance design. This program and the corresponding analysis are described in detail in Chapter IV. The AMS model shown in Figure IV-39 served as the basis for computing the inertia properties for use in the rigid body dynamics program. Once again, a computer program was developed for this purpose. The inputs to this program are the quantities defined in Figure IV-39 and the output consists of the masses, principal moments of inertia and the hinge vectors defined in Appendix A. Using the design data contained in Chapter IV, the input data for the rigid body dynamics program are shown in Table VI-1. Note that the data for the SAMS reflect the absence of the counterbalance and the presence of the Shuttle (bodies 1 and 6, respectively). On the other hand, the AMS data includes the 2900 lb counterbalance and the steel connecting rods (see Chapter IV). The large values for the inertia properties of body 6 in this case, are used to effectively fix the AMS to an inertial platform. In both cases, the data for body 5 represents a 15 ft diameter, 60 ft long, 65,000 lb cylindrical payload.

Table VI-1 Inertia and Geometry Data for Rigid Body Dynamics Program

Mass M (Slugs) and Principal Moments of Inertia  $I_{\lambda}$ , (Slug-Ft<sup>2</sup>)

$\lambda$	1	2	3	4	5	6
$M_{\lambda}$	0	13.74	3.33	1.55	$2.02 \times 10^3$	$1 \times 10^4$
$I_{\lambda 1}$	0	4.01	.781	0.109	$5.67 \times 10^4$	$2.3 \times 10^6$
$I_{\lambda 2}$	0	644.	127	1.22	$6.35 \times 10^5$	$1.51 \times 10^7$
$I_{\lambda 3}$	0	644.	127	1.22	$6.35 \times 10^5$	$1.51 \times 10^7$

Hinge Vector Components  $H_{\lambda j K}$  (Ft)

$\lambda j$	11	21	22	23	33	34	44	45	55	62
K 1	0	-4.84	-4.84	13.6	-5.78	12.7	-1.5	1.5	0	-32.8
K 2	0	0	0	0	0	0	0	0	0	10.0
K 3	0	0	0	0	0	0	0	0	-7.50	-17.8

(a) SAMS DATA

Mass M (Slugs) and Principal Moments of Inertia  $I_{\lambda j}$  (Slug-Ft<sup>2</sup>)

$\lambda$	1	2	3	4	5	6
$M_{\lambda}$	90.9	29.6	3.33	1.55	$2.02 \times 10^3$	$1 \times 10^{10}$
$I_{\lambda 1}$	116	6.73	2.53	0.109	$5.67 \times 10^4$	$1 \times 10^{10}$
$I_{\lambda 2}$	116	$1.24 \times 10^3$	$1.29 \times 10^2$	1.22	$6.35 \times 10^5$	$1 \times 10^{10}$
$I_{\lambda 3}$	28.7	$1.24 \times 10^3$	$1.29 \times 10^2$	1.22	$6.35 \times 10^5$	$1 \times 10^{10}$

Hinge Vector Components  $H_{\lambda j K}$  (Ft)

$\lambda j$	11	21	22	23	33	34	44	45	55	62
K 1	.527	-6.86	-4.42	14.1	-5.78	12.7	-1.50	1.50	0	-32.8
K 2	0	0	0	0	0	0	0	0	0	10.0
K 3	0	0	0	0	0	0	0	0	-7.50	-17.8

(b) AMS DATA

#### 4. Results of Rigid Body Dynamics Analysis

In order to determine the dynamic torque requirements for the AMS it was decided to investigate several 90° deployment tasks of the 65,000 lb payload. These tasks are illustrated in Figure VI-1.

The inertia properties of the payload and shuttle are those for bodies 5 and 6 in Table VI-1(a). For simplicity, it was assumed that the payload and shuttle mass center are initially coincident, and the longitudinal axis of the payload is initially parallel to the roll axis of the shuttle. The location of the shoulder joint relative to the shuttle mass center is given by  $\bar{H}_{62}$  in Table VI-1(a). Finally, it is presumed that the wrist extension is perpendicular to the longitudinal axis of the payload and the attach point is directly above the payload mass center.

Under the foregoing assumptions, the initial configuration of the AMS is defined by the following joint angles (see Appendix A for definition of joint angles):

$$\theta_{21} = \theta_{23} = 0, \theta_{22} = -12.1^\circ$$

$$\theta_{13} = \theta_{33} = -32.8^\circ$$

$$\theta_{41} = 0, \theta_{42} = -77.4^\circ, \theta_{43} = 32.8^\circ$$

$$\theta_{51} = \theta_{53} = 0, \theta_{52} = -90^\circ$$

All of the joint angles with the exception of the shoulder pitch angle ( $\theta_{22}$ ) are maintained at their initial values. The shoulder pitch angle is increased by 90° during the payload deployment. The net result is that the payload mass center moves on a circular arc in the shuttle pitch plane. The time histories of  $\theta_{22}$ ,  $\dot{\theta}_{22}$  and  $\ddot{\theta}_{22}$  are prescribed such that the tangential velocity of the payload mass center assumes the profile illustrated in Figure VI-1. In each case, the payload moves through the same 90° arc. What distinguishes one task from another is the task time, TT, during which the maneuver must take place; and the distance traveled while braking the payload to a stop. (It is assumed that the accelerations during the initial and final stages of motion are equal in magnitude and opposite in direction). Task times of 3, 5

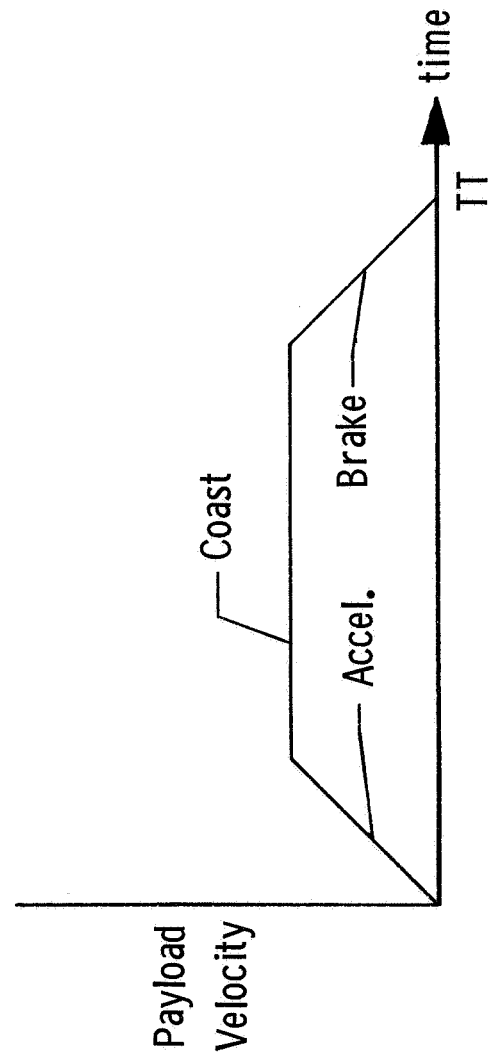
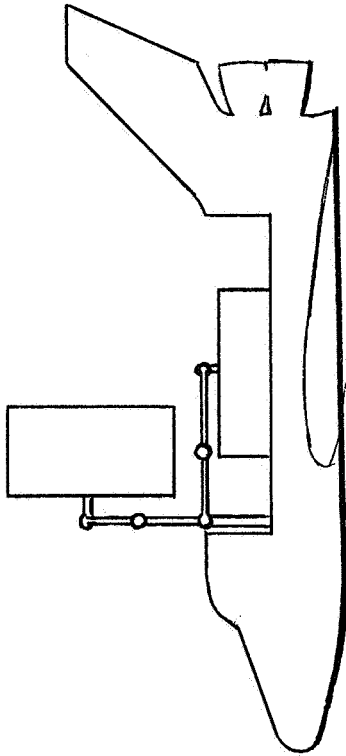


Figure VI-1 Rigid Body Payload Deployment Task



and 7 min. were investigated, and for each of these, stopping distances of 1.0, 1.5, 2.0, and 3.75 ft were assumed.

The payload and shoulder pitch motion for the 3 min. task time and the 2 ft stopping distance are shown in Figures VI-2 and VI-3. The motion induced in the shuttle during this task is shown in Figure VI-4. It is noted that the shuttle pitches approximately  $7^\circ$  during the payload deployment.

The task described above was repeated once with the shuttle assumed fixed in inertial space and again for the counterbalanced AMS attached to an inertial platform with the direction of gravity perpendicular to the pitch plane. The required pitch joint torques at the shoulder, elbow, and wrist for the first two cases are shown in Figure VI-5. The joint torques for the counterbalanced AMS are illustrated in Figure VI-6. Comparison of the joint torques shows that the torques required to execute the task using the counterbalanced AMS is almost identical to those required when the SAMS is attached to an inertially fixed shuttle. However, both of these cases require approximately 25% more torque over those required to execute the same task when the manipulator is attached to a free shuttle. The conclusion to be drawn is that more torque will be required to execute a task on the ground (using the counterbalanced AMS) than will be required to execute the same task in space (using the SAMS attached to a free shuttle). The amount of extra torque required will be directly proportional to the mass of the payload for a particular task.

The torques required during all of the tasks (using the counterbalanced AMS) are summarized in Figure VI-7, where they are plotted as functions of stopping distance (i.e., the distance traversed by the payload during the braking phase of the maneuver). Also shown in these graphs are the static torque requirements defined as those required to exert a 30 lb static tip force (tangential direction) when the AMS is fully extended. Comparison of the three curves shows that the wrist joints require the greatest increase in torque over the static requirement. This effect diminishes in the direction of the shoulder joint.

Finally, using the 5 min. deployment time and the 2 ft stopping distance as defining the dynamic torque requirement, the static torque requirements and dynamic torque requirements are shown in Figure VI-8 along with the joint torques selected to meet both of these requirements.

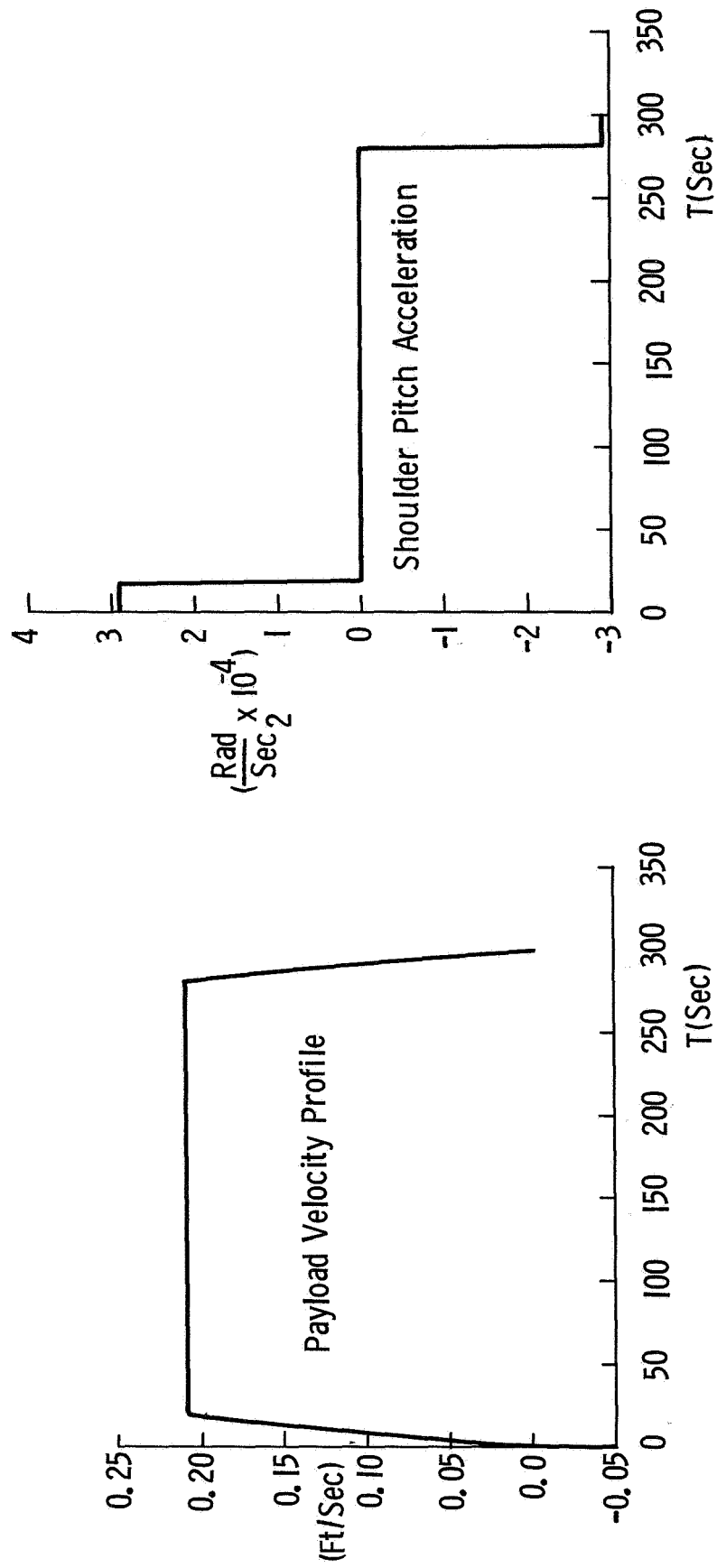


Figure VI-2 Payload Velocity and Shoulder Pitch Acceleration for 3 Min, Task Time and 2 ft Stopping Distance

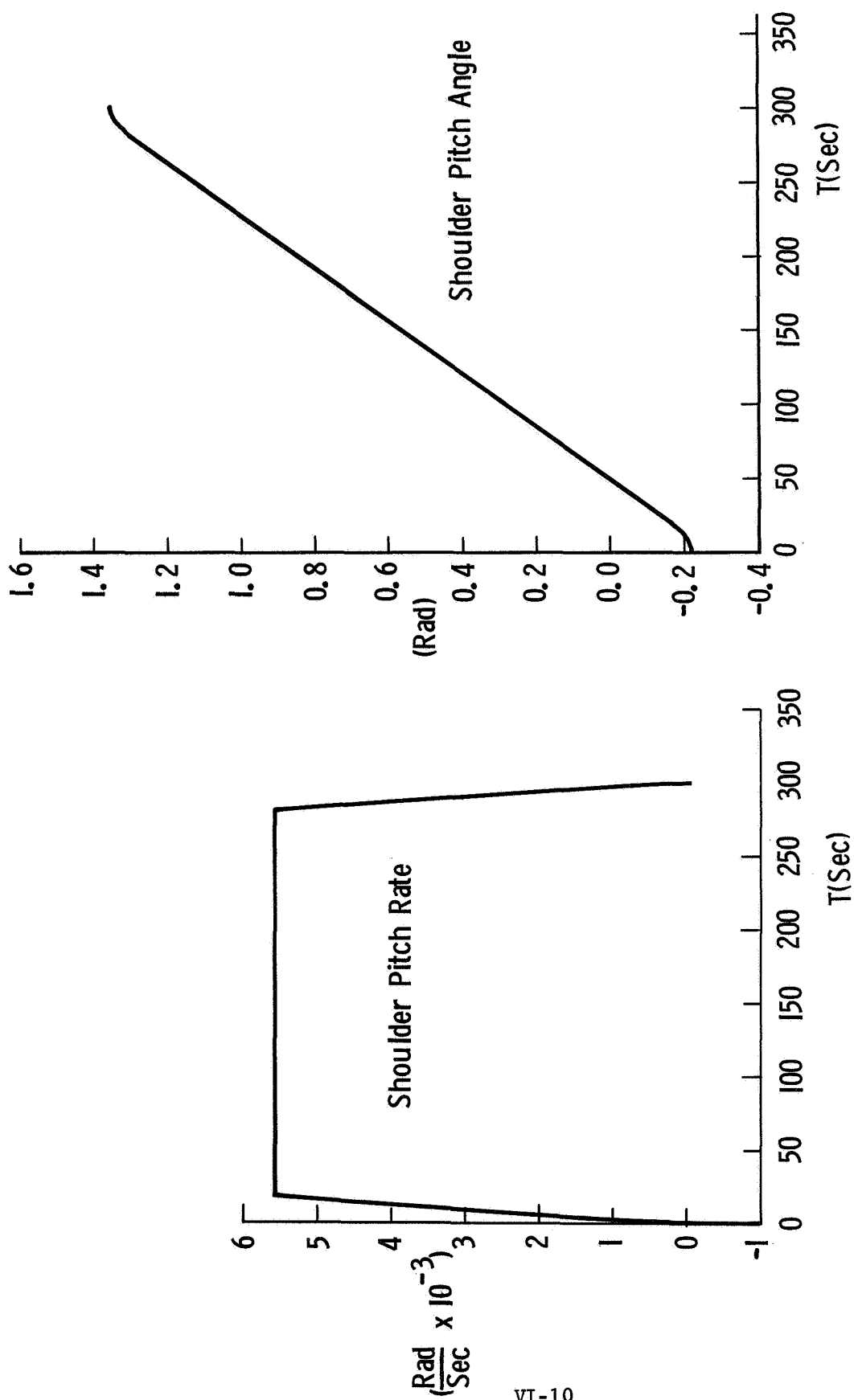


Figure VI-3 Shoulder Pitch Rate and Angle for 3 Min.  
Task Time and 2 ft Stopping Distance

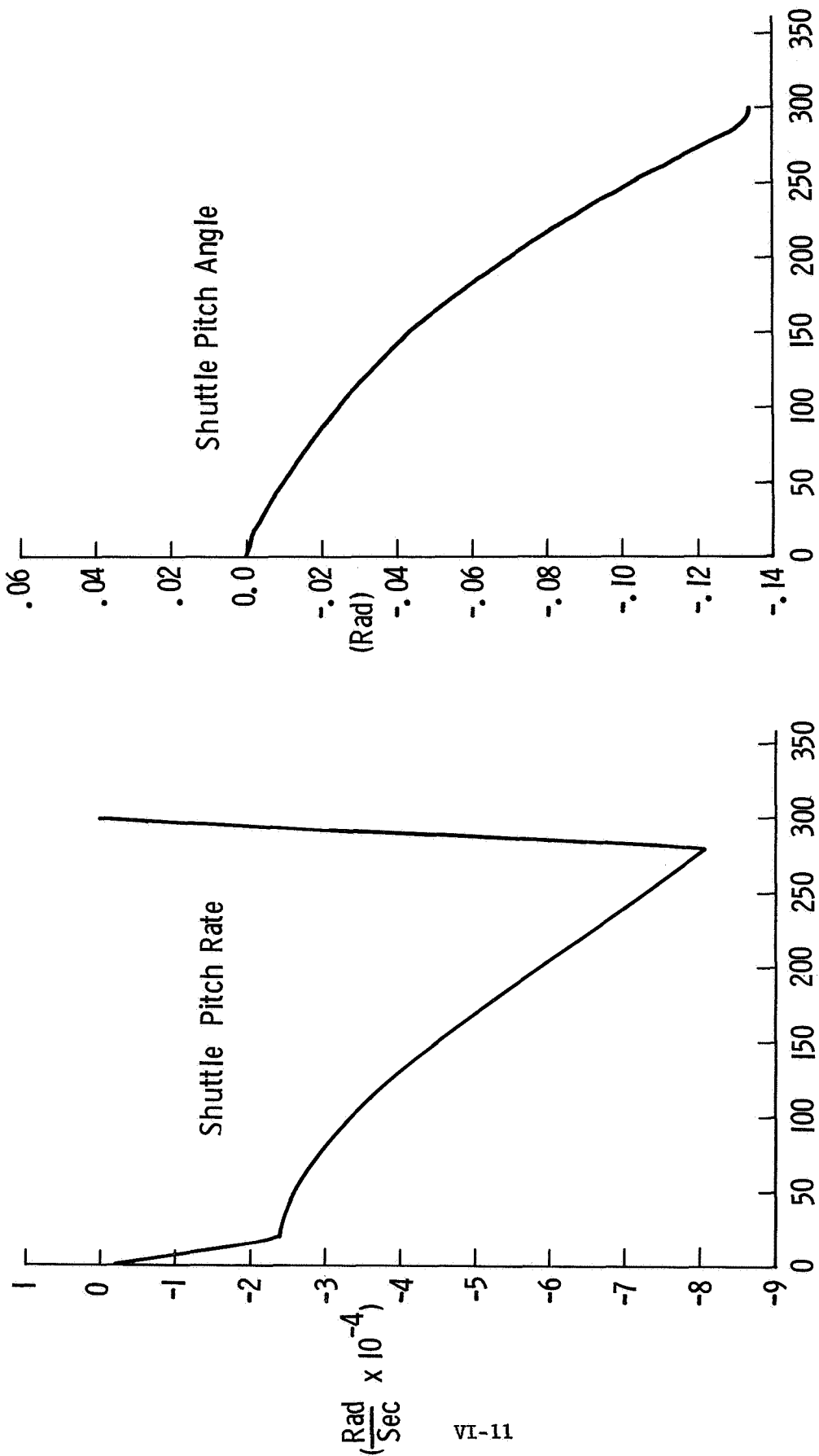


Figure VI-4 Shuttle Pitch Rate and Angle

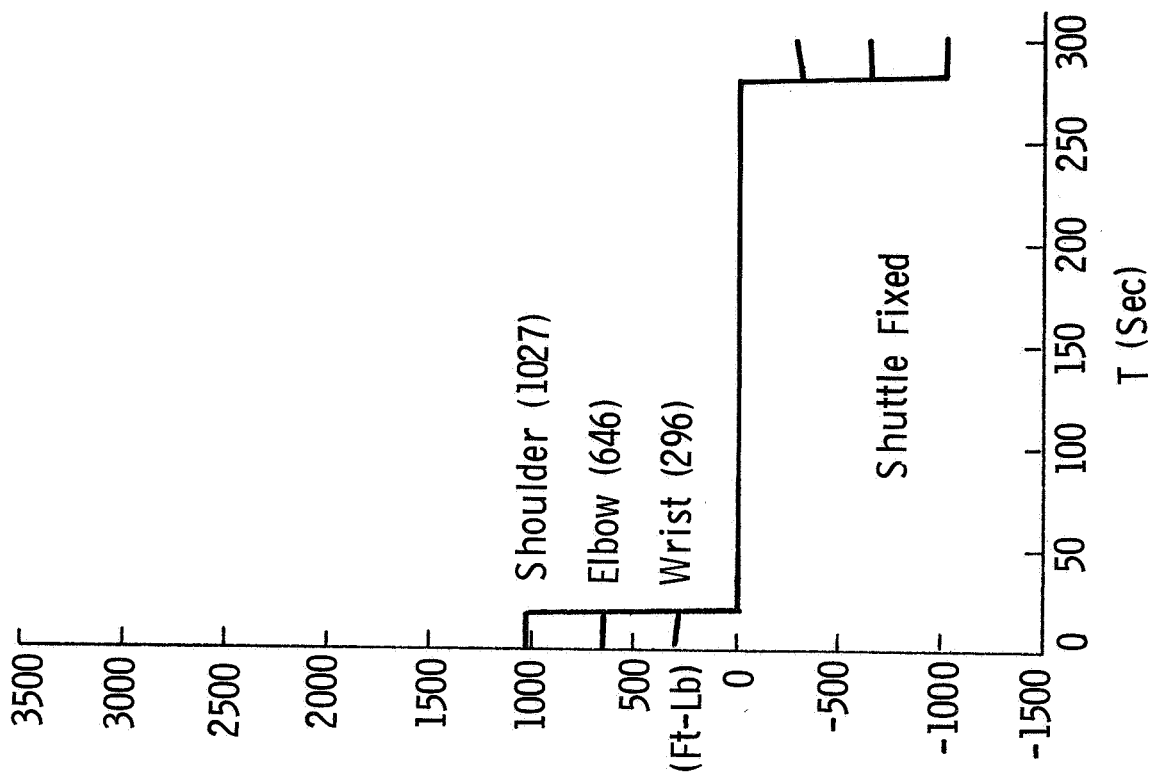
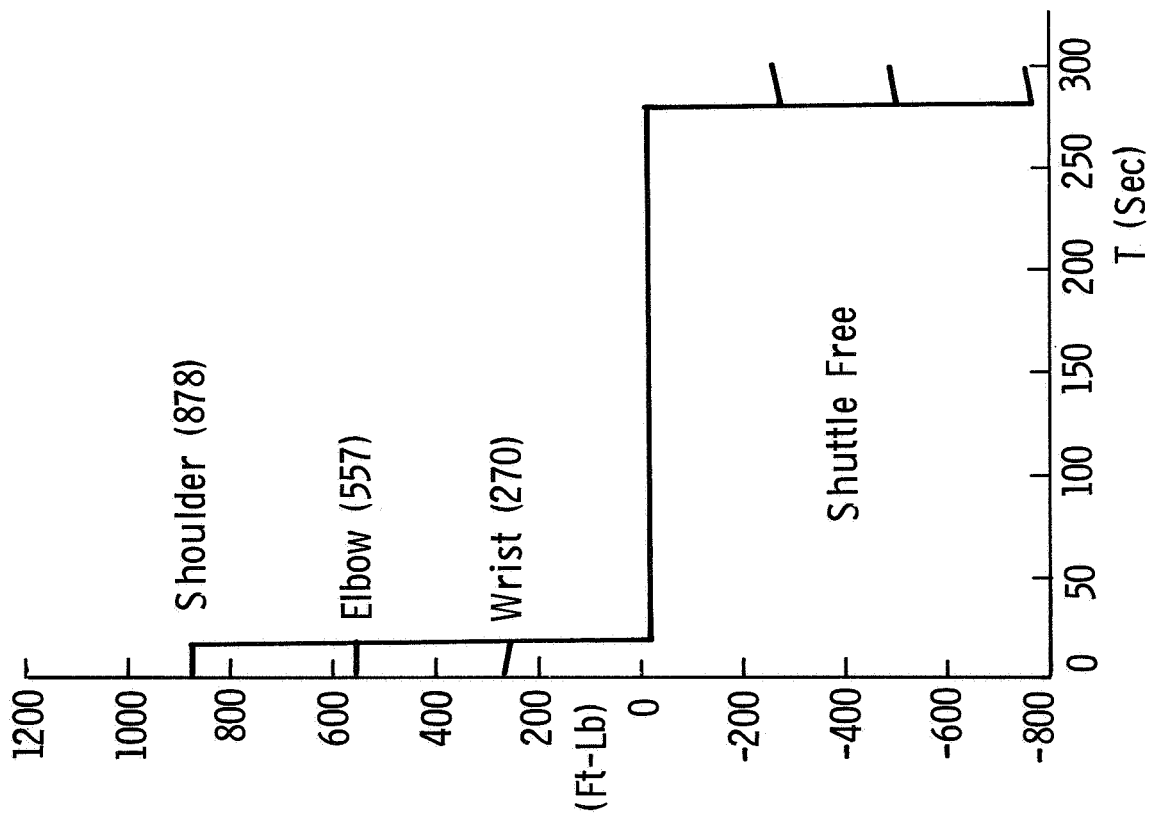


Figure VI-5 SAMS Joint Torques

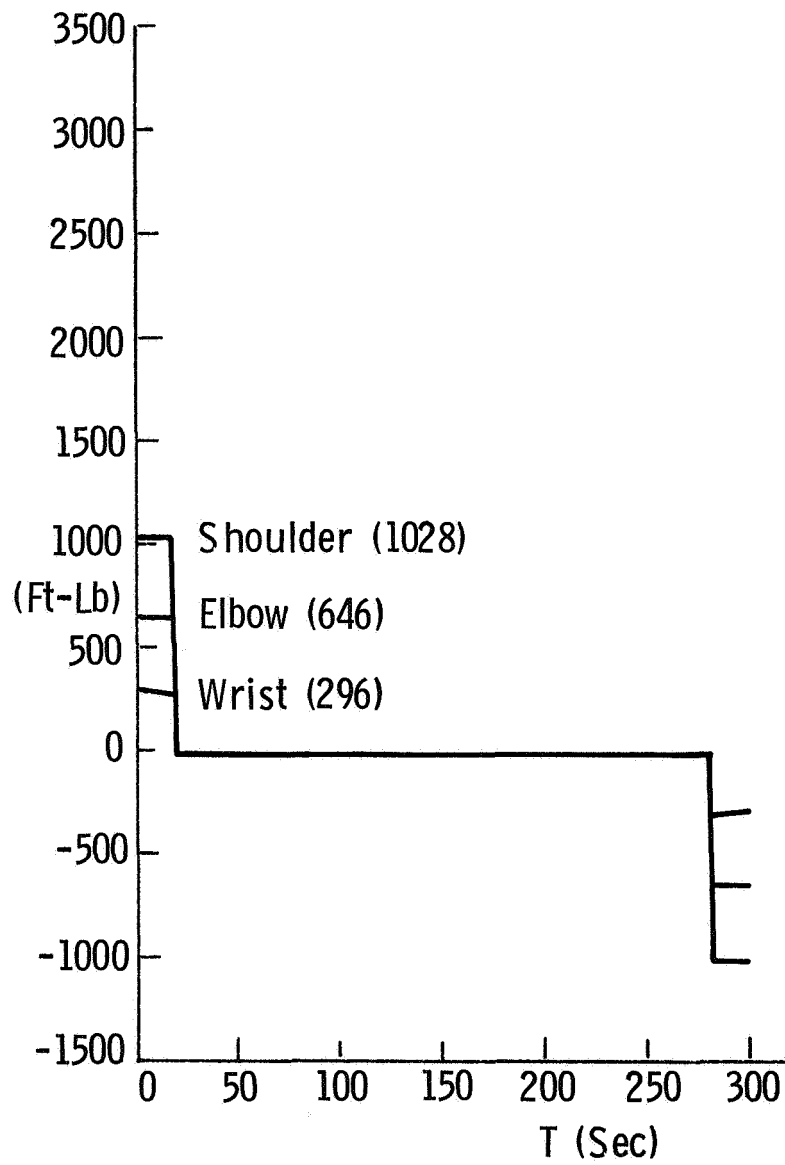


Figure VI-6 AMS Joint Torques

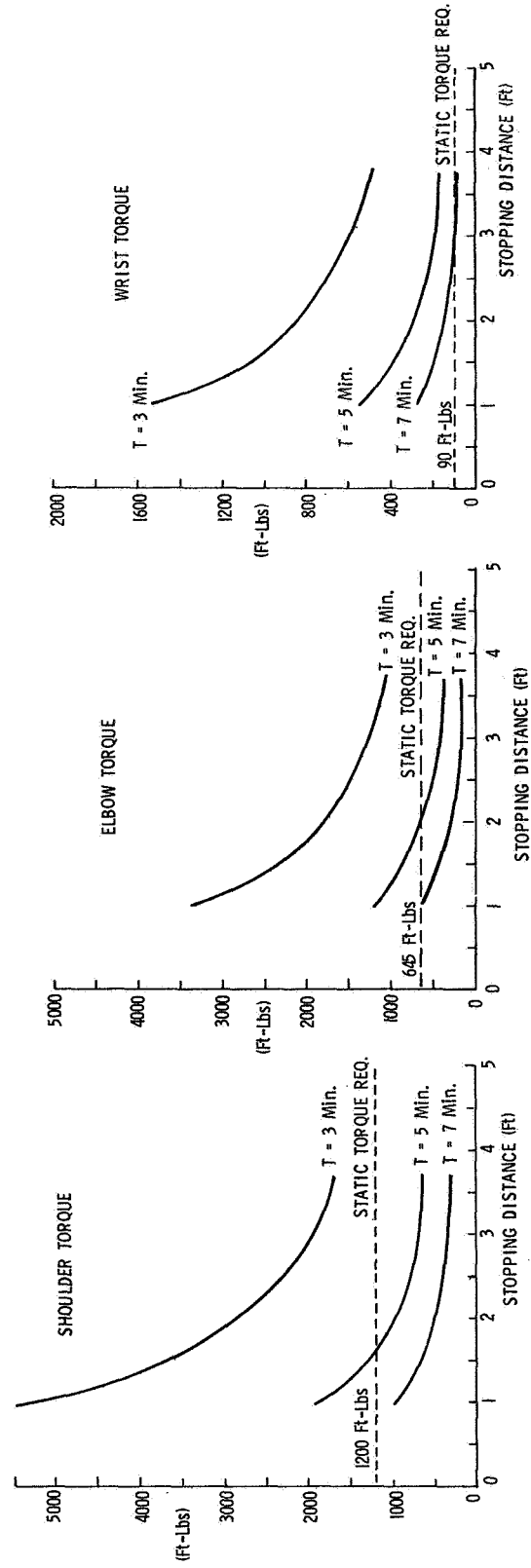


Figure VI-7 Joint Torques vs Stopping Distance

### STATIC TORQUE REQUIREMENT

Arm Fully Extended - 30 Lb Tip Force

Shoulder	1200 Ft-Lbs
Elbow	645 Ft-Lbs
Wrist	90 Ft-Lbs

### DYNAMIC TORQUE REQUIREMENT

5 Min. Deployment Time  
2-Ft Stopping Distance

Shoulder	1028 Ft-Lbs
Elbow	646 Ft-Lbs
Wrist	296 Ft-Lbs

### JOINT TORQUE SELECTION

Shoulder	1200 Ft-Lbs
Elbow	650 Ft-Lbs
Wrist	300 Ft-Lbs

Figure VI-8 Joint Torque Selection



## B. VIBRATION ANALYSIS

The reasons for conducting a vibration analysis of the AMS are twofold. First, one concerned with designing a control system for the AMS (including active damping techniques), would benefit from the knowledge of mode shapes and frequencies of the AMS as it vibrates about an equilibrium position; and second, such a study provides the elastic behavior of the major AMS segments for use in the nonlinear dynamic response program (see Section C).

The first of these objectives is achieved by analyzing the AMS as a single structure including the elastic constraints at the joints. In what follows, this type of analysis will be called a coupled vibration analysis. The second goal is realized by examining the major components of the AMS separately without regard to the flexibility at the joints. This type of analysis will be referred to as an uncoupled vibration analysis.

In the early stages of this contract a coupled vibration analysis was conducted of an AMS design concept involving a flexible Elgiloy tape as the means by which torque is transmitted from the elbow motor to the counterbalance mass. Later, an uncoupled vibration analysis was performed with the Elgiloy tape being replaced by pivoted steel rods. Both of these investigations are presented in what follows.

### 1. Coupled Vibration Analysis of AMS with Elgiloy Tape

a. Mathematical Model and Physical Constants - Elements of the mathematical model are shown schematically in Figure VI-9 for the counterbalanced AMS. The AMS is shown with the arm extended aft and parallel to the orbiter longitudinal axis. Each element has bending, torsional, and axial compliance in addition to distributed mass and inertial properties. Node points have six degree of freedom and the geometry is defined precisely in Table VI-2. The model of the space version is a simple counterbalanced model without Nodes G, H, I, and J. Elements G-I and J-D are rigid elements representing pulleys of the counterbalanced system and element I-J represents the Elgiloy tape. The pulley at Node D is integral to that joint; whereas, the pulley at Node G is connected to the second counterbalance arm only. Bending moment about the Y axis cannot be transmitted between elements C-G and G-H. The tape is allowed to experience both tension and compression to take advantage of counterbalance symmetry.

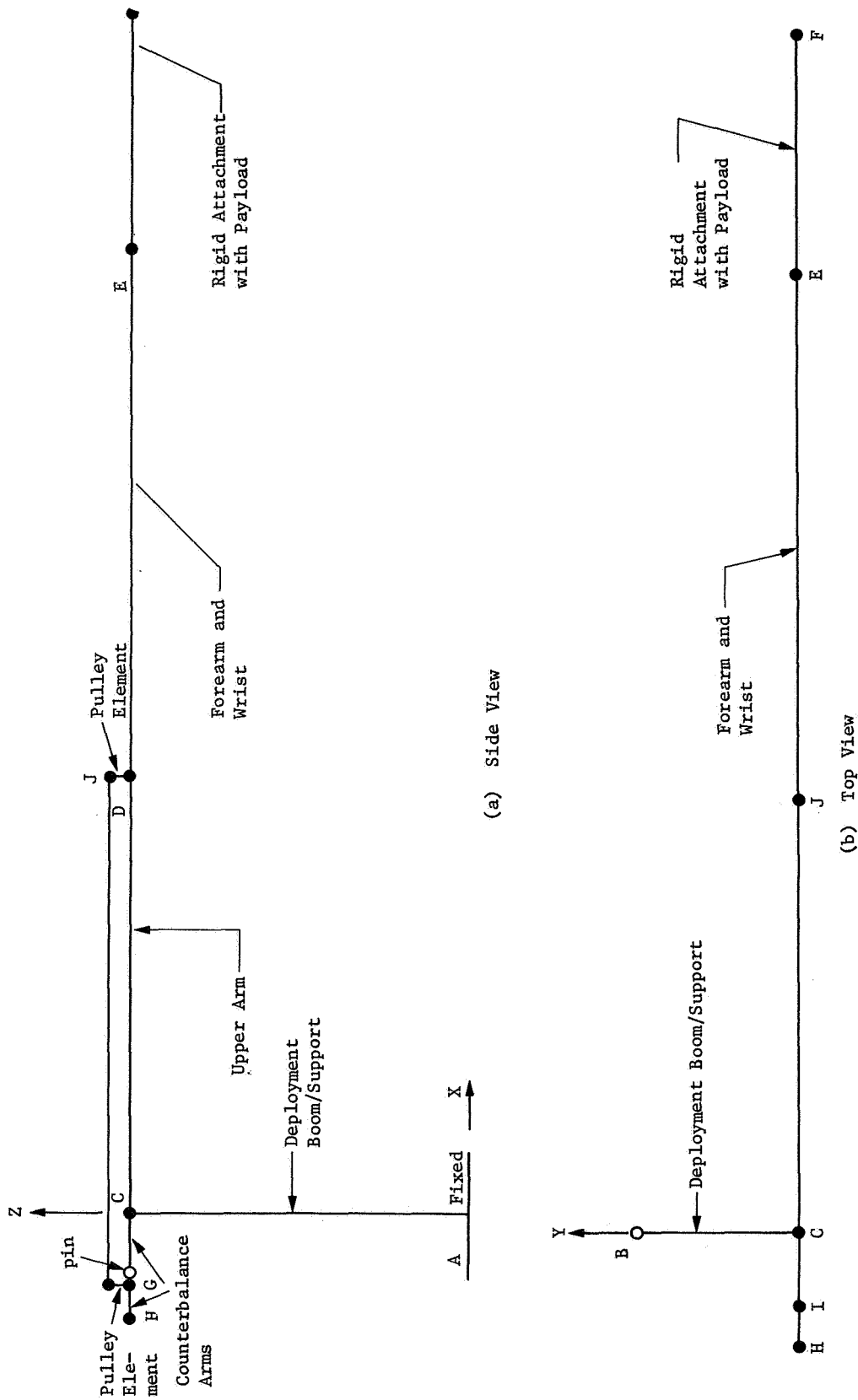


Figure VI-9 Mathematical Model of Structural Elements

Table VI-2 Degree of Freedom Table

Node Ident	Degree of Freedom						Node Location (in.)		
	X	Y	Z	TX	TY	TZ	X	Y	Z
A	56	57	58	59	60	61	0.	60.0000	0.
B	25	26	27	28	29	30	0.	60.0000	128.0000
C	19	20	21	22	23	24	0.	0.	128.0000
D	13	14	15	16	17	18	162.0000	0.	128.0000
E	7	8	9	10	11	12	360.0000	0.	128.0000
F	1	2	3	4	5	6	450.0000	0.	128.0000
G	37	38	39	40	41	42	-27.7200	0.	128.0000
H	31	32	33	34	35	36	-39.9600	0.	128.0000
I	43	44	45	46	47	48	-27.7200	0.	132.0000
J	49	50	51	52	53	54	162.0000	0.	132.0000

Table VI-3 Beam Stiffness Data (Stiffness Parameter  $\times 10^6$ )

Member	$EI_x$ (lb-in. <sup>2</sup> )	$EI_y$ (lb-in. <sup>2</sup> )	$EI_z$ (lb-in. <sup>2</sup> )	GJ (lb-in. <sup>2</sup> )	AE (lb)
A-B	100000.0	100000.0	---	100000.0	100000.0
B-C	100000.0	---	100000.0	100000.0	100000.0
C-D	---	1239.1	1239.1	926.4	139.74
D-E	---	470.8	470.8	352.0	52.75
E-F	---	100000.0	100000.0	100000.0	100000.0
C-G	---	1239.1	1239.1	926.4	139.74
G-H	---	1239.1	1239.1	926.4	139.74
G-I	100000.0	100000.0	---	100000.0	100000.0
D-I	100000.0	100000.0	---	100000.0	100000.0
I-J	---	1.0	1.0	1.0	1.5557

Stiffness parameters, based on preliminary design data, for each component beam are given in Table VI-3. Because the members supporting the counterbalance weights are undefined, their stiffnesses were assumed identical to those for the upper arm. Stiffnesses of the deployment/support mechanism, pulley elements, and payload attachment element were assumed rigid relative to the rest of the structure. Bending and torsional stiffness of the tape is negligible. The Elgiloy tape was assumed to be 2 in. wide and to be in tension over a 237.6 in. length (96 in. single layer over the pulleys and a 141.6 in. triple layer between the pulleys). Tape stiffness (K) is, then, 8200 lb/in. for an elastic modulus of  $29.5 \times 10^6$  psi. As defined in the model, the tape is only 189.72 in. long; therefore, the equivalent AE value is equal to that length times the stiffness. Because joint drives and gear trains are not defined for this configuration, they are assumed to be similar to, but stiffer than, those defined in Reference 1. That study recommended harmonic drives (USM\* #4M at the shoulder and elbow and USM #2M for the wrist joints). Stiffness of the joints is assumed to be four times the stiffness specified for harmonic drive assemblies in Reference 3. The stiffness values are:  $3.36 \times 10^6$  in.-lb/rad for the shoulder and elbow joints and  $1.88 \times 10^6$  in.-lb/rad for the wrist joints. For ease in modeling, compliances for the three shoulder joint mechanisms were all assumed to be located in the upper arm, 2-1/2 in. outboard of the deployment boom centerline. The orientation of the arm was assumed such that the elbow drive acts in pitch. Wrist mechanisms are: Pitch at X Sta 162, yaw at X Sta 180, and roll at X Sta 185.5.

Mass and inertia data are defined in Tables VI-4 and VI-5. Distributed inertias were based on upper arm and forearm outside diameters of 12 in. and wall thickness of 0.1785 and 0.0827 in., respectively. Distributed mass was chosen arbitrarily for the deployment boom/support and was considered negligible for the counterbalance mechanism. The outboard counterbalance weight was chosen so that its moments about Node G balanced the forearm and wrist gravity moment about Node D. The other counterbalance weight was chosen so that it and the outboard counterbalance weight would balance the gravity moment of

---

\* United Shoe Machinery Corporation.

Table VI-4 Distributed Mass

Section	X Sta (in.)	Mass [lb-sec <sup>2</sup> /in.)/in.]	Inertia about Bending Axes [lb-sec <sup>2</sup> in.)/in.]	Inertia about Torsional Axis [lb-sec <sup>2</sup> in./in.]
A-B	---	0.006	---	---
B-C	---	0.006	---	---
C-D	0 to 162.0	0.001845	0.030988	0.031722
D-E	162.0 to 202.0	0.0016175	0.028399	0.029117
	202.0 to 311.0	0.0011373	0.014295	0.014430
	311.0 to 360.0	0.0044471	0.029762	0.00081385
E-F	360.0 to 450.0	0.00002	---	---
C-G	0 to -27.72	0.00002	---	---
G-H	-27.72 to -39.96	0.00002	---	---
G-I	---	0.00002	---	---
J-D	---	0.00002	---	---
I-J	-27.72 to 162.0	0.00002	---	---

Table VI-5 Concentrated Mass

Location	Item	Mass lb-sec <sup>2</sup> in.	Inertia about Each Axis (lb-sec <sup>2</sup> in.)		
			X	Y	Z
F	Payload	155.28	6.982 x 10 <sup>6</sup>	6.982 x 10 <sup>6</sup>	0.5478 x 10 <sup>6</sup>
D	Drive Mechanism	0.12940	0.53917	0.53917	0.53917
G	1st Counter- balance Weight	0.261716	---	---	---
H	2nd Counter- balance Weight	4.15163	563.58	563.58	563.58
*This weight is assumed to be free hanging.					

the total arm. The payload inertias were defined to orient the payload with its longitudinal axis parallel to the Z axis. The inertias were based on a homogeneous circular cylinder (15 x 50 ft).

b. Analysis - The analysis consisted of developing the homogeneous equations of motion and solving them for the mode shape vectors and modal frequencies. The solutions were obtained with the use of the Martin Marietta computer program VIB3. VIB3 was also used to form the mass and stiffness matrices.

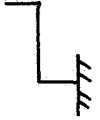
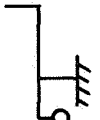

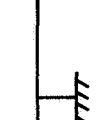
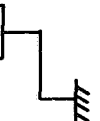
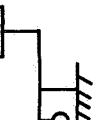
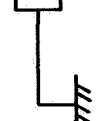

Solutions were obtained for both the counterbalanced (CB) and the space version of the AMS in four configurations (a total of eight solutions). The eight cases are depicted below and consist of both loaded and unloaded configurations, each with the arm fully extended along the X axis and with the elbow rotated 90° up.

Unloaded				Loaded			
90° Elbow		Extended		90° Elbow		Extended	
Space	CB	Space	CB	Space	CB	Space	CB

c. Results - Results from this study include: mass matrices, stiffness matrices, flexibility matrices, generalized mass matrices, mode shapes, and frequencies. These data are stored in detail on magnetic tape and presented in summary form in this report. The first 10 natural frequencies are presented in Table VI-6 and some selected mode shapes are depicted in Figures VI-10 and VI-11.

d. Discussion - By comparing the frequencies shown in Table VI-6, one can conclude that the dynamical behavior of the AMS is sensitive (to some extent) to payload mass, geometrical configuration, and counterbalance mechanism. It can

Table VI-6 Modal Frequencies (cps)

Mode Number	Unloaded Configurations				Loaded Configurations			
								
1	1.1863	1.1863	0.90515	0.90033	0.02474	0.03055	0.02226	0.03083
2	1.3909	1.3947	0.96098	0.96424	0.04267	0.04273	0.03073	0.05972
3	2.8371	2.5471	4.8596	2.5909	0.10737	0.10641	0.09633	0.07882
4	3.8119	2.9217	9.5199	4.8915	0.18337	0.18324	0.26944	0.26962
5	20.657	3.8135	22.141	9.5074	0.26937	0.26980	3.0653	2.5666
6	22.440	17.610	24.224	17.514	3.4992	2.5960	4.8039	3.0450
7	49.930	18.702	41.482	18.389	12.063	3.5001	8.5331	4.8471
8	63.828	20.656	63.298	22.154	47.766	12.061	10.169	8.5198
9	77.372	22.738	75.669	24.226	55.786	17.612	57.640	10.171
10	83.654	30.064	88.593	29.586	59.750	18.825	64.220	17.628

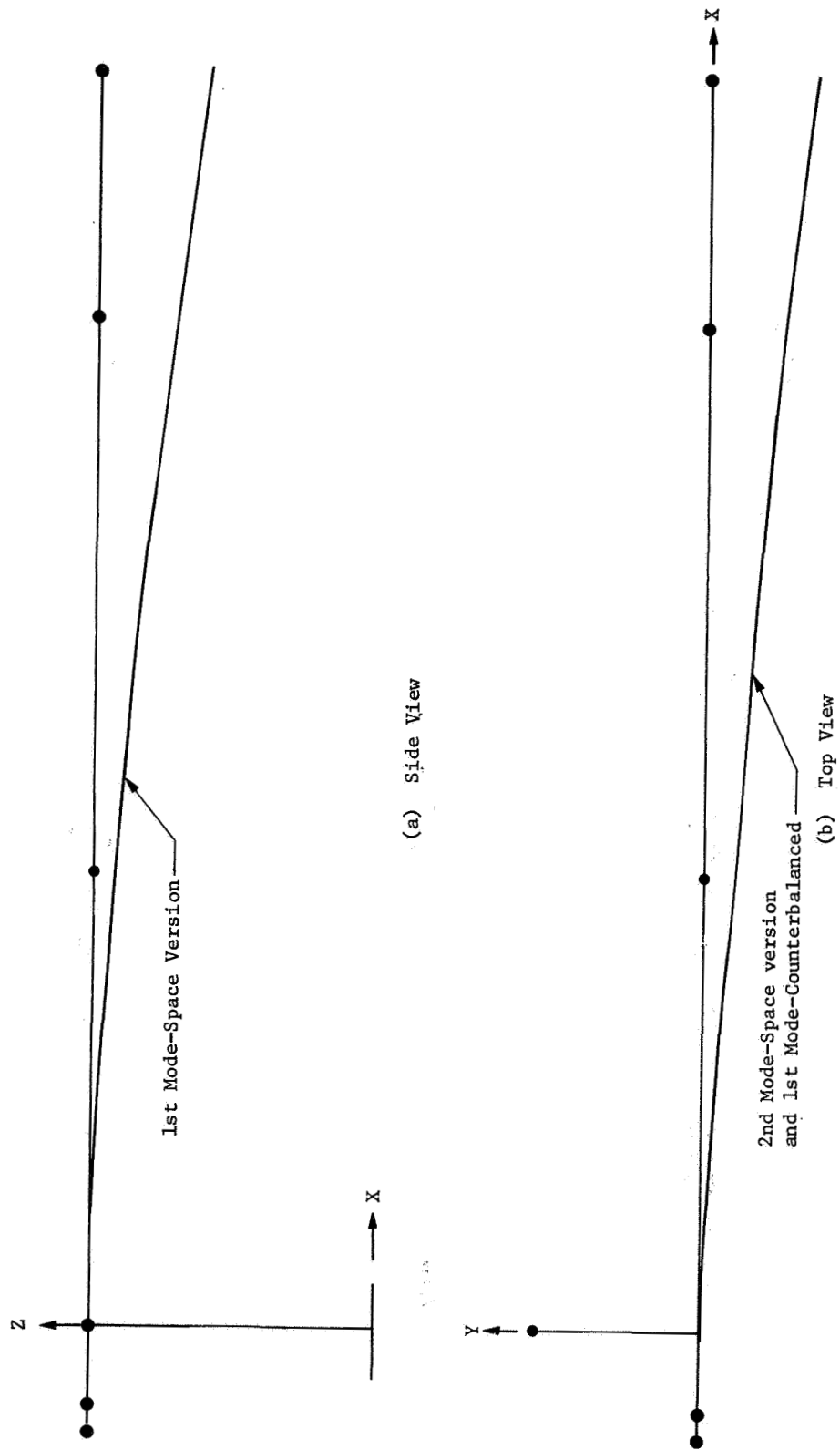


Figure VI-10 Normalized Mode Shapes, AMS Loaded and Extended



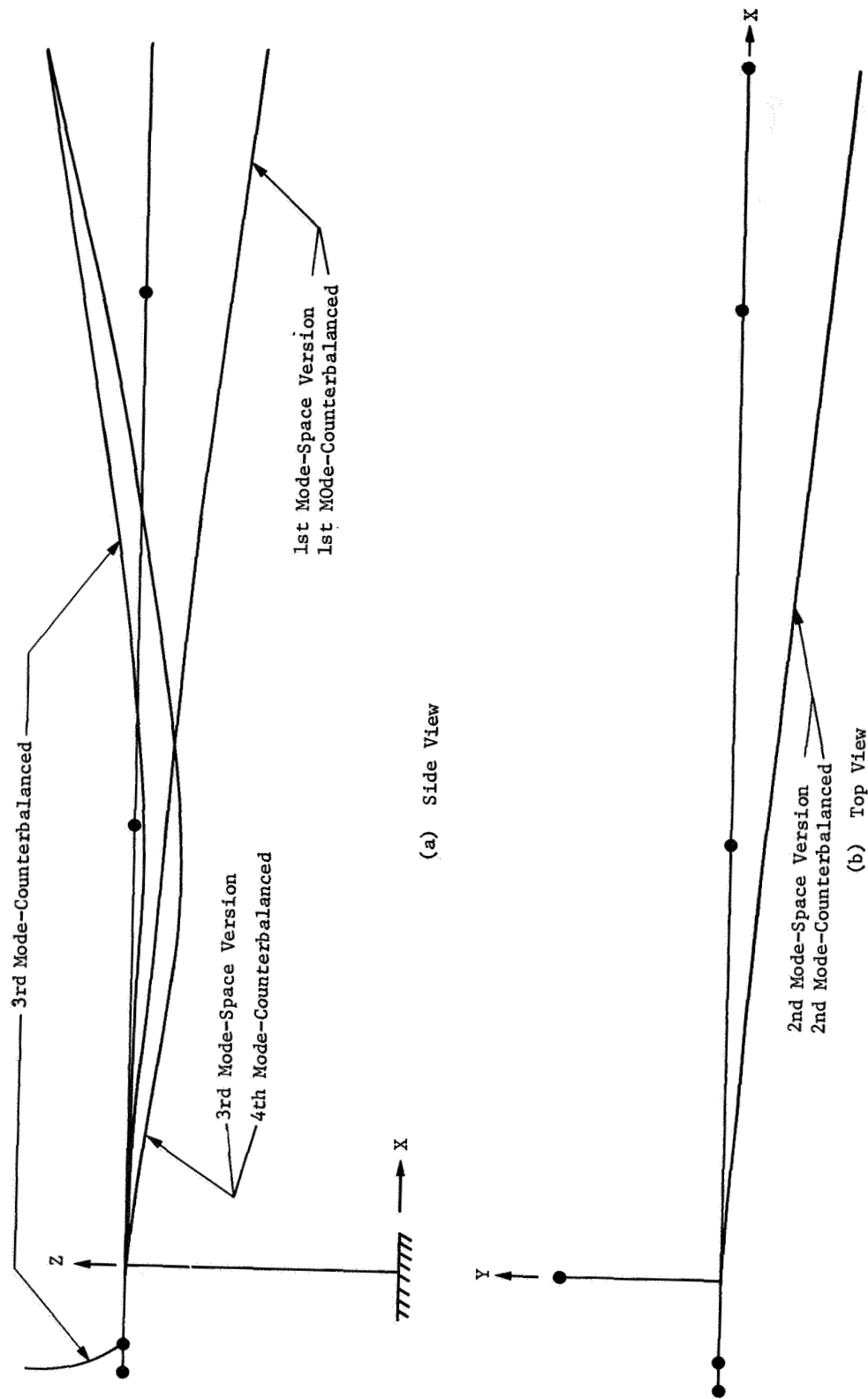


Figure VI-11 Normalized Mode Shapes, AMS Unloaded and Extended

also be seen that payload mass is the most significant parameter and geometry configuration the least. It should be noted, however, that a large payload (60,000 lb) was used in the loaded cases; and, therefore, for the smaller payloads, one could expect a smaller change in frequencies between the loaded and unloaded cases. The foregoing observations apply to both the space and counterbalanced versions of the AMS.

By comparing the frequencies in Table VI-6 for the AMS in the extended, unloaded configuration, it can be seen that the first two frequencies are the same, but a new modal frequency (lying between the second and third frequencies of the space version) is introduced by the addition of the counterbalance mechanism. Further, inspection of the last two columns of Table VI-6 reveals that the behavior of the loaded, extended configuration of the AMS is more severely affected by the addition of the counterbalance mechanism; in that, the fundamental mode of the space version is eliminated.

The similarities and differences in behavior of the space and counterbalanced versions of the AMS are further illustrated by the mode shapes depicted in Figures VI-10 and VI-11. Figure VI-11 illustrates that, for those frequencies retained by the counterbalanced system, the mode shapes of the space and counterbalanced versions in the unloaded, extended configuration are very nearly identical. From Figure VI-10 it can be seen that, in the loaded extended configuration, the second mode of the space version is identical to the first mode of the counterbalanced AMS, the motion taking place in the horizontal or X-Y plane. Figure VI-10 also shows the first mode of the loaded extended configuration of the space version of the AMS (i.e., that mode which is eliminated by the addition of the counterbalance).

Since the vibration analysis presented above was conducted, the Elgiloy tape has been replaced by steel connecting rods, the counterbalance mechanism has become better defined, and stiffness data has been obtained for the gear trains. In light of these developments, the coupled vibration analysis should be updated to reflect such design changes.

While conducting the uncoupled vibration analysis (presented in the next section), it became apparent that a major contributor to the differences in vibrations between the SAMS and the AMS was the constraint conditions assumed at the shoulder. For this reason, when the vibration analyses are

updated, greater emphasis should be placed on computing the stiffness of the support structure.

## 2. Uncoupled Vibration Analysis of AMS with Steel Rods

As mentioned earlier, the uncoupled vibration study deals with the major components of the AMS as individual structures. The necessary constraints (including the flexible joints) to properly connect these components are provided in the flexible body dynamics program (see Section D). The results of this analysis provide a mathematical description of the elastic behavior of the corresponding AMS components modelled in the dynamics program.

The uncoupled structural models are shown in Figure VI-12. The 18.5 ft lower arm is an aluminum tube with a 12 inch diameter and a .08 inch wall thickness; it is assumed to be cantilevered at the elbow. The tip of the lower arm is loaded with the mass and reflected inertia of the 3 ft wrist connected to the 65,000 lb payload. The length and diameter of the upper arm is identical to those of the lower arm; the wall thickness is 0.18 inch in this case. The mass and inertia of the steel connecting rods between the elbow and counterbalanced elbow are included in the model. It was decided that these rods do not contribute to the bending stiffness of the upper arm. The upper arm is assumed cantilevered at the shoulder and is loaded at the elbow joint with the mass and reflected inertia of the payload, wrist, and lower arm. Finally, the counterbalanced upper arm (to the left of the shoulder) is simply a 29.25 in extension of the upper arm (including steel rods) and is loaded with the mass and reflected inertia of the 2900 lb counterbalance weight. Finally, to monitor the elastic deformations, both the upper and lower arms were assigned 5 reference points as shown in Figure VI-12.

The first three frequencies and modes for the upper and lower arms are shown in Figures VI-13 and VI-14, respectively. It is noted that the frequencies corresponding to the higher modes are more than two orders of magnitude greater than these. It can be seen in Figure VI-13 that the counterbalance upper arm does not participate in these low frequency modes. This is due to the six degree of freedom constraint at the shoulder. Thus, for the structural model assumed in this case, the counterbalanced and noncounterbalanced versions of the manipulator will exhibit the same vibrational characteristics.

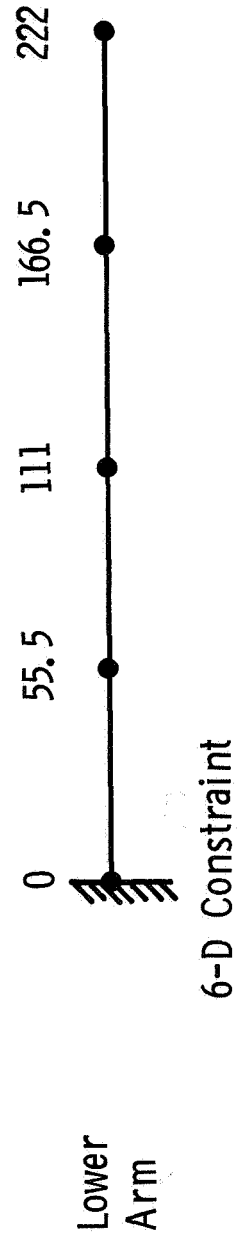
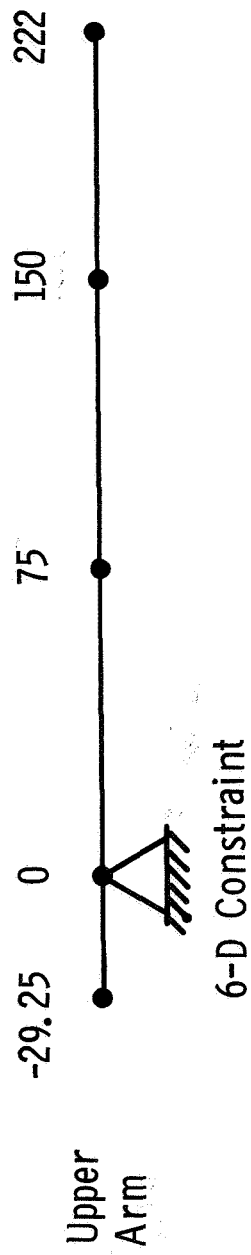


Figure VI-12 Uncoupled Vibrational Analysis Structural Model

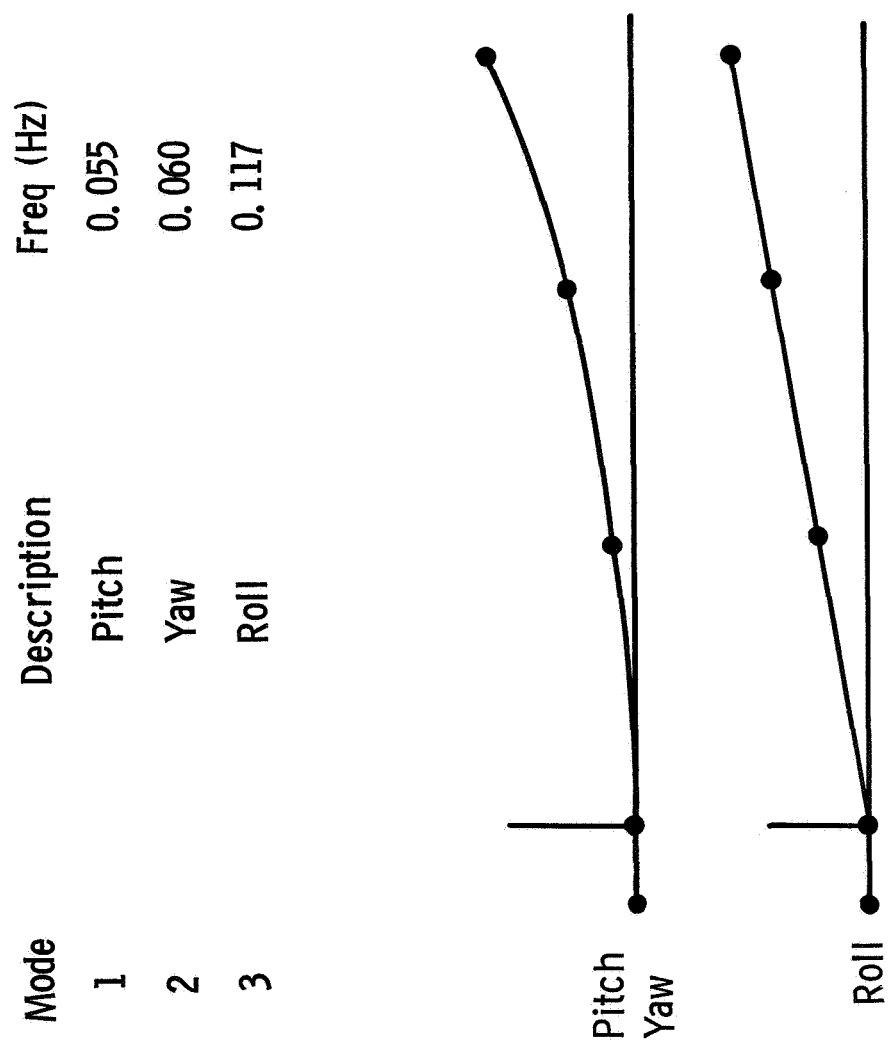


Figure VI-13 Frequencies and Modes of Upper Arm

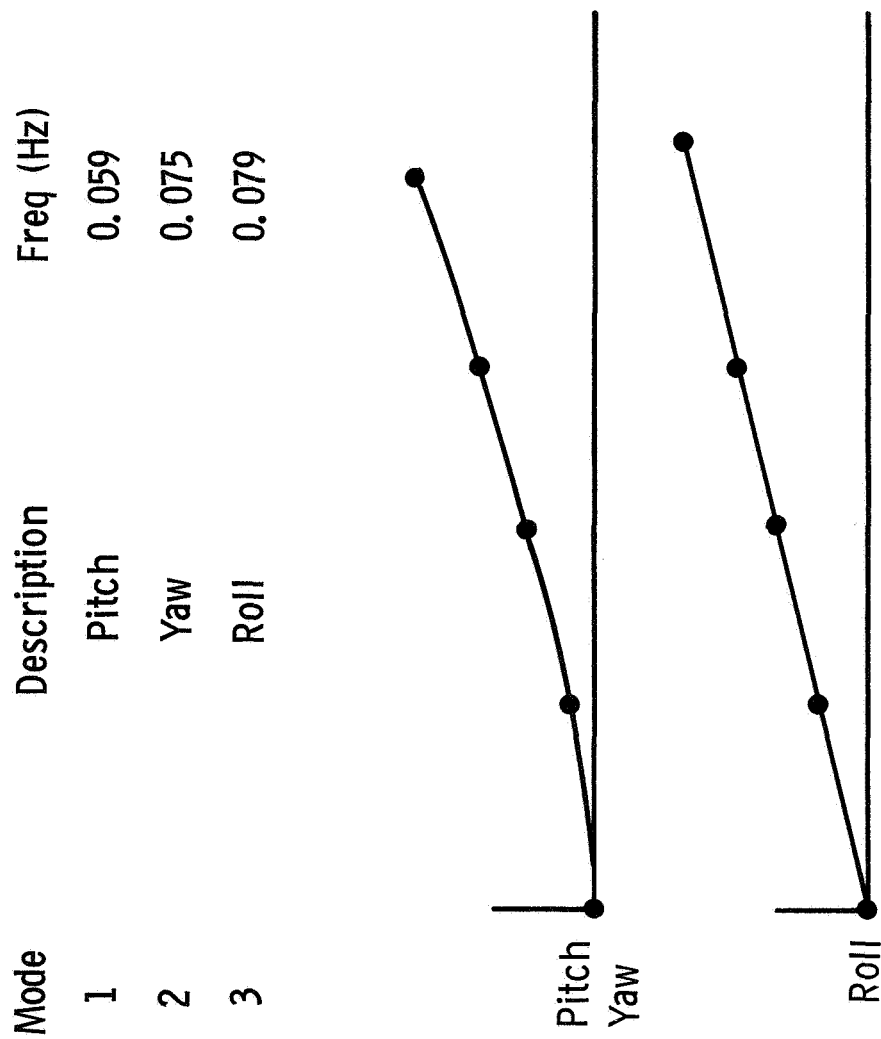


Figure VI-14 Frequencies and Modes of Lower Arm

The next section deals with a comparison of rigid and flexible body behavior of the counterbalanced AMS during a payload handling task. The uncoupled vibration data presented above was incorporated in the dynamics program to provide the elastic effects.

## C. NONLINEAR FLEXIBLE BODY ANALYSIS\*

Dynamic response analyses of the AMS is currently being performed through application of a generalized n-body digital computer program developed by the Martin Marietta Corporation. The underlying assumption of this program is that any physical system can be realistically modelled as an assemblage of n-interconnected bodies, some or all of these being flexible.

### 1. Mathematical Model and Computer Program

a. Equations of Motion - The equations of motion for an individual body are developed thru application of Lagrange equations with constraints. The resulting nonlinear, first order differential equations include elastic characteristics via normal vibration modes. These modes are provided by the uncoupled vibration analysis described in section C.

Coupling between two or more bodies is accounted for by using Lagrange multipliers to describe the kinematic constraint conditions. This formulation allows individual bodies to undergo large excursions relative to the other bodies. The n-body system is not restricted to the form of a topological tree; some similar analytical techniques which have appeared in the literature do have this restriction.

b. State Equations - The first order, nonlinear equations of motion define a state space. The state variables, for each of the n-bodies are:

- 1) Generalized momenta corresponding to 3 translations, 3 rotations, and M elastic modes.
- 2) Elastic normal coordinates for each of the M modes.
- 3) Inertial position and attitude by means of 3 position coordinates and 4 Euler quaternion elements (Euler parameters are used to eliminate possible singularities that may occur when considering large relative excursions).

Additional state variables include:

- 1) Relative position coordinates describing the attitude of any body with respect to any other.
- 2) Control system variables as defined by the user's special control laws.

\*The work presented in this Section was performed under Independent Research and Development Task No. D-05R entitled "Teleoperator Manned Control and Mission Simulation".



c. Numerical Integration - Currently, numerical integration of the state variable time derivatives is accomplished thru implementation of the 4th order Runge-Kutta algorithm with a fixed time step. The possibility of implementing a predictor - corrector algorithm will be investigated in an effort to reduce computation time.

d. Users' Options - The digital computer program has been designed to be as versatile as possible and therefore several options are available to the user:

1) Prescribed External Force/Torque Field - A prescribed time dependent, external force/torque field can be applied to any of the n-bodies in the system.

2) Initial Positions/Rates - An individual body may be assigned initial conditions describing position and/or rate.

3) Relative Motion - The relative motion between any two bodies can either be prescribed by the user as a time dependent function or can be controlled by an appropriate control law. A universal interface has been included in this program to allow the user to specify control logic applicable to his particular problem.

e. Applications - The versatility of the generalized computer program has been demonstrated thru application to several problems:

1) A hypothetical dual spin space station consisting of a stator (hub) and two counterrotating appendages was modelled. The bodies were assumed rigid with prescribed initial rates.

2) The Skylab T027 boom, yoke camera experiment package was investigated. The boom was considered elastic; the yoke and camera were rigid. Both prescribed and controlled motions were investigated. Comparison of analytical and test results was excellent.

3) The 6-body rigid AMS model described in section B was modelled with relative motion at the joints being prescribed. Exact agreement of the results from the two programs was obtained.

## 2. Comparison of Rigid and Flexible AMS Behavior

The flexible body dynamics program described above was used to obtain a comparison between the rigid and flexible behavior of the counterbalanced AMS for the same payload handling task. The task considered is depicted in Figure VI-15 and involves the 65,000 lb payload with its longitudinal axis perpendicular to the manipulator arms. The AMS is initially fully extended along the x-axis, and the shoulder and elbow yaw angles are prescribed identical counterclockwise rotation,  $\phi$ , as shown. The resulting motions of the AMS and payload occur entirely in the yaw plane. The time history of  $\phi$  is also shown in Figure VI-15 and reflects a 20 sec acceleration, a 60 sec coast phase, and a 20 sec braking period. The acceleration and braking magnitude of  $1.31 \times 10^{-4} \text{ rad/sec}^2$  is equivalent to a 20 lb tangential tip force when the arm is fully extended.

Because the motion takes place in the yaw plane, only the fundamental yaw modes shown in Figures VI-13 and VI-14 were used to provide the flexible body effects. To keep matters simple, ideal (rigid) joints were assumed for the wrist, elbow, and shoulder. Finally, because the elbow and shoulder joint angles are prescribed as functions of time, the task can be thought of as involving an ideal control system (i.e., one that involves no delays between commands and response).

The trajectory of the payload mass center resulting from the joint angle prescription is shown in Figure VI-16. The payload follows the same trajectory in both the rigid and flexible cases. This means that, for the flexible case, the oscillations take place along the trajectory. The differences between the rigid and flexible motions are more apparent in Figures VI-17 and VI-18.

Looking first at the X motion, there is no perceptible difference between the rigid and flexible case until the joint motion has stopped (at  $T = 100 \text{ sec}$ ). Beyond 100 sec, the X position of the payload mass center for the flexible AMS oscillates about that of the rigid case (not shown beyond 100 sec). As shown in Figure VI-17, these oscillations are approximately 0.6 in peak-to-peak with a frequency of 0.05 Hz (20 sec period).

Because the motion of the payload is predominantly in the Y direction, one could expect greater differences in this

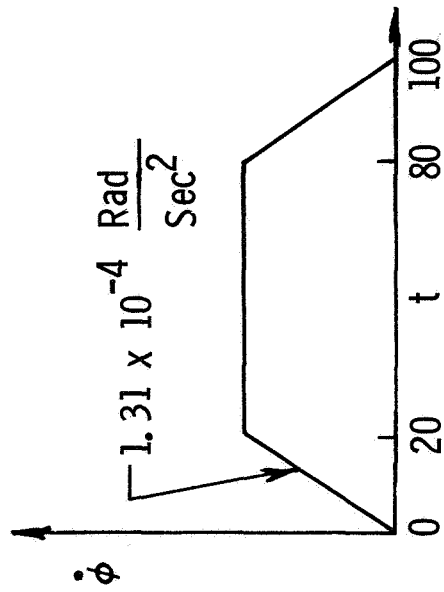
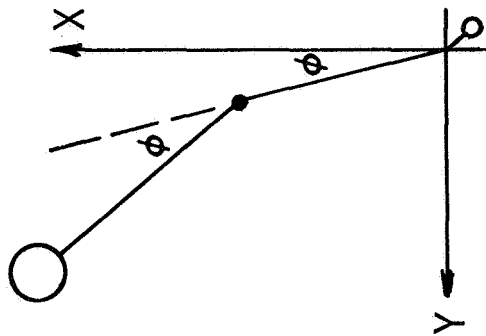


Figure VI-15 Payload Handling Task for Rigid/Flexible AMS Comparison

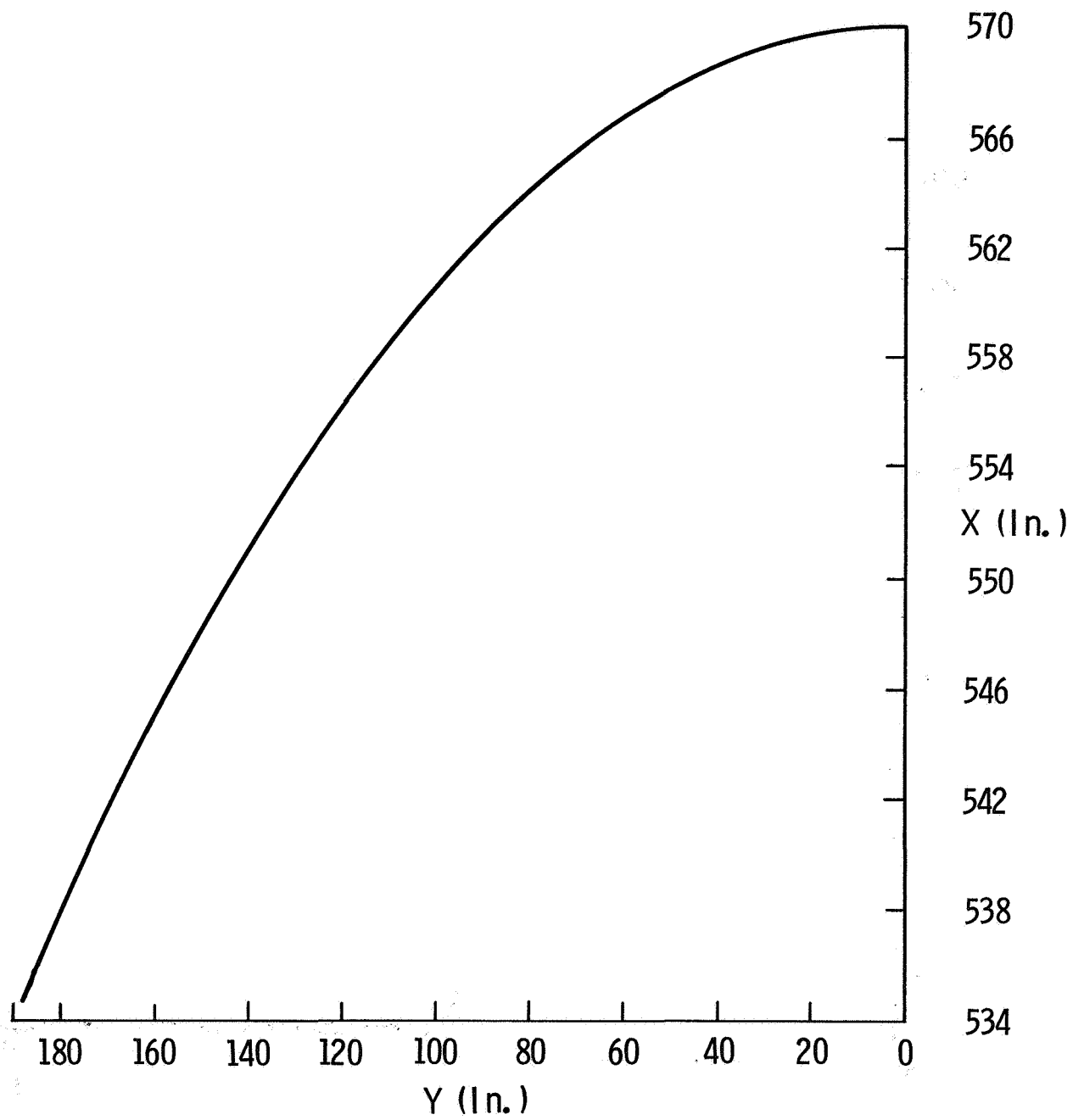


Figure VI-16 Payload Trajectory for Rigid and Flexible AMS

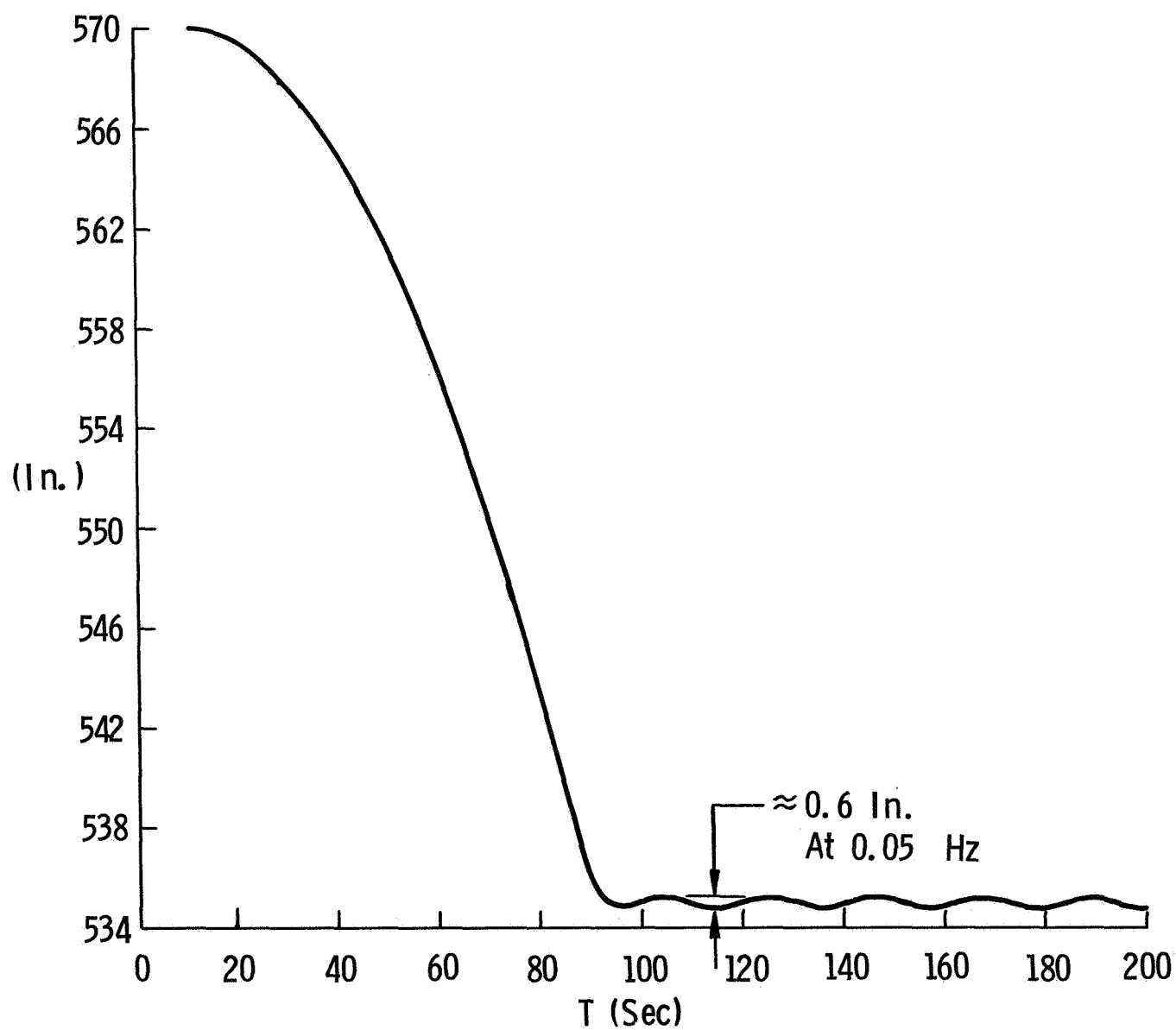


Figure VI-17 Payload X Position vs Time

coordinate when comparing results for the rigid and flexible cases. This is born out in Figure VI-18 where it is seen that the Y position in the flexible case lags by as much as 2.7 in behind that of the rigid case during the acceleration phase (first 20 sec). It appears that, between 20 and 100 sec, the Y position for the flexible and rigid case are identical. There is reason to believe however, that small oscillations do occur (in the flexible case) during this phase of the task; they are simply too small to be visible in Figure VI-18. As with the X position, it is seen that Y coordinate (flexible case) oscillates about that of the rigid case after 100 sec. In this case, the amplitude is approximately 3 in (peak-to-peak) with a 0.05 Hz frequency. Although not apparent from the X and Y curves, there is a small amount of damping present resulting from an assumed 1% structural damping in the computer program.

The shoulder, elbow, and wrist, joint torques required for the task are shown in Figures VI-19, VI-20, and VI-21, respectively. In each case, the flexible body torque is initially less than the corresponding rigid body torque. After about 5 sec however, the flexible torque requirement exceeds its rigid counterpart, peaking at approximately twice the latter after 10 sec. During the remainder of the acceleration phase the flexible requirement decreases to a zero value about which it oscillates until the braking phase begins. The braking period follows the same pattern as the acceleration phase. It is the torque oscillations during the coasting period (20-80 sec) that indicate similar oscillations in payload position during this time (it is recalled that such oscillations were not visible in the curves showing X and Y vs time).

One should not interpret the foregoing results to mean that a flexible manipulator requires approximately twice the torque capability of a rigid AMS. This is true if one desires identical joint motions in both cases. However, if one is willing to accept flexible AMS payload trajectories involving oscillations about the rigid body trajectory, then the rigid body torque capabilities will suffice.

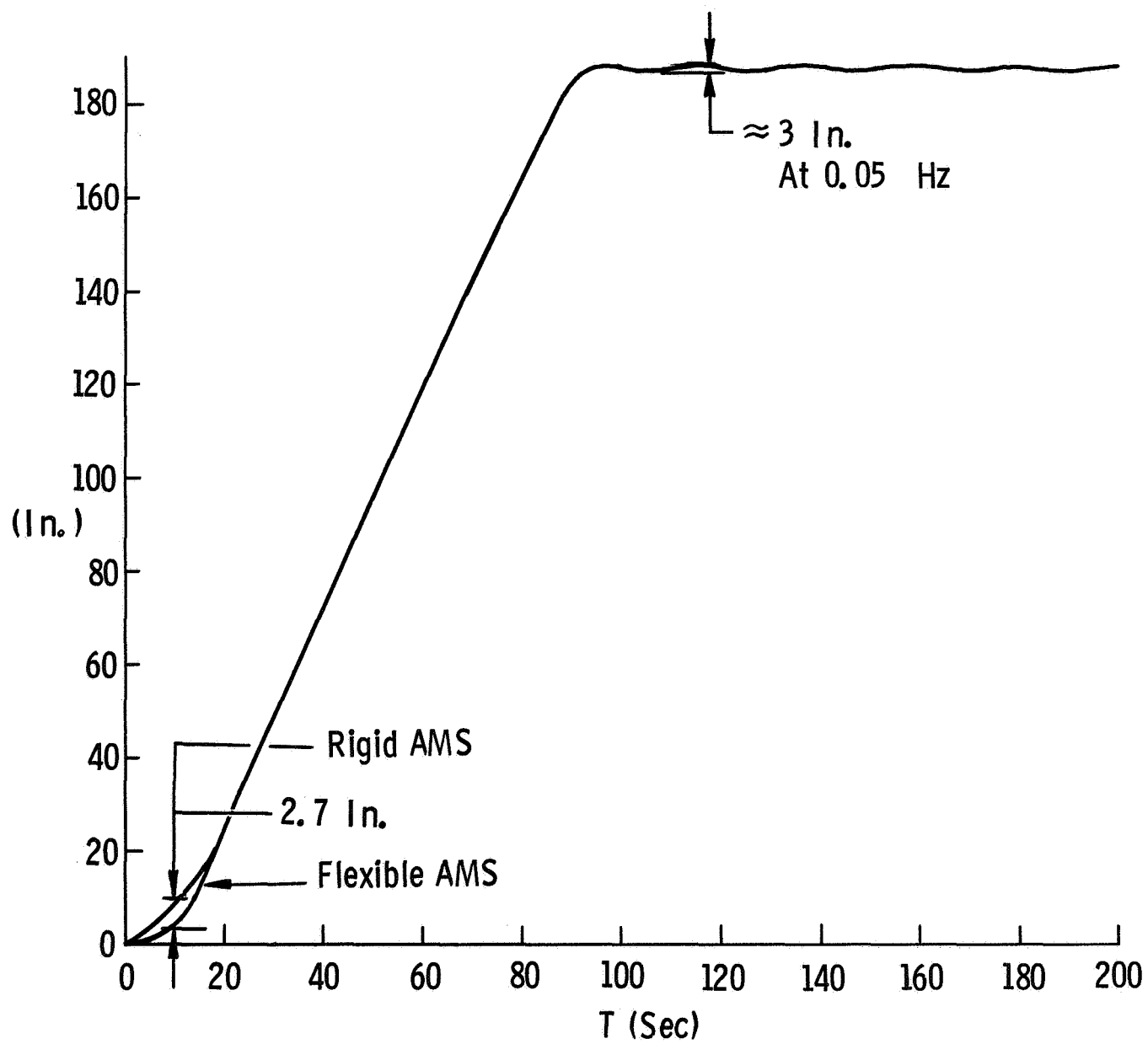


Figure VI-18 Payload Y Position vs Time

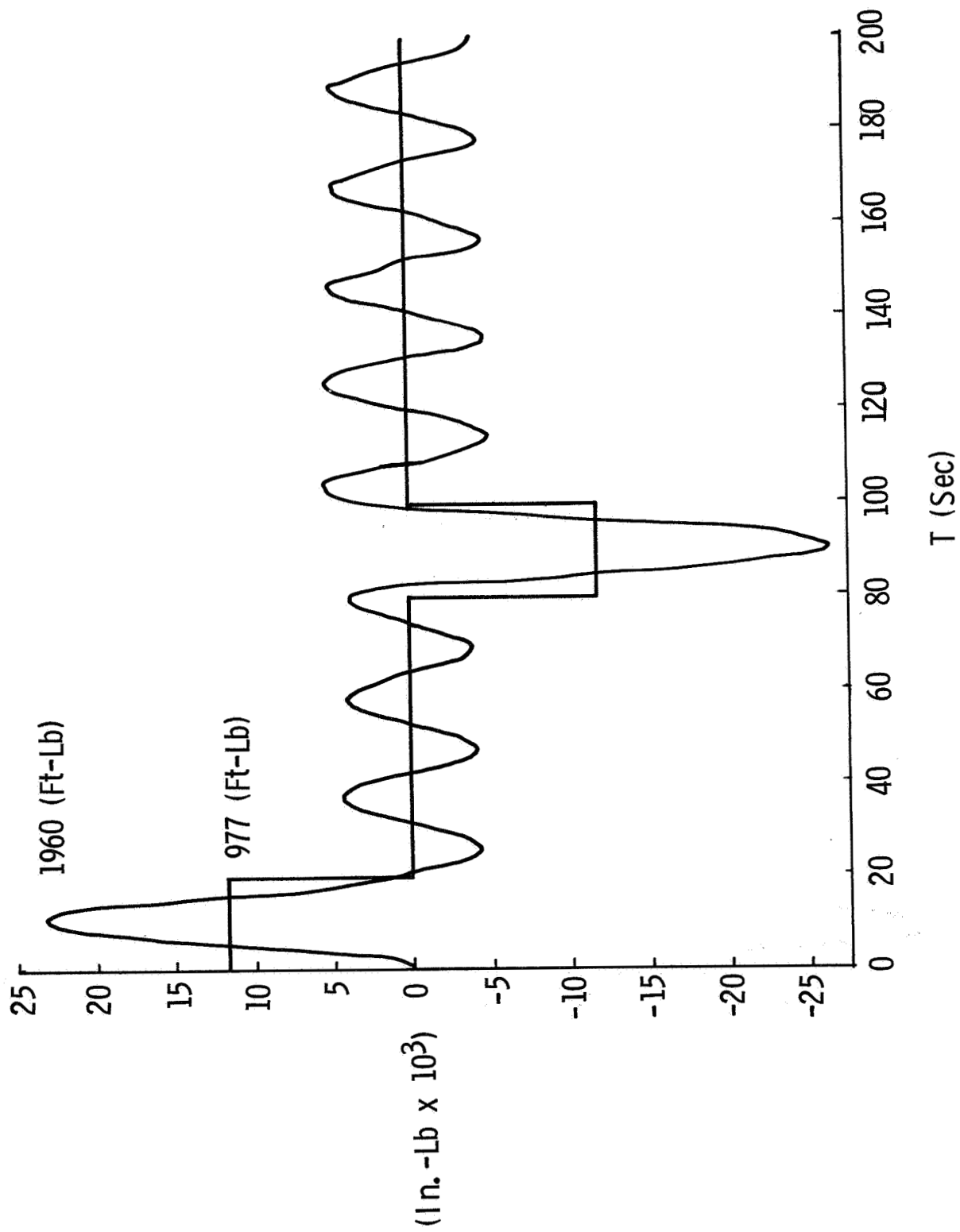


Figure VI-19 Rigid and Flexible AMS Shoulder Torque Requirement



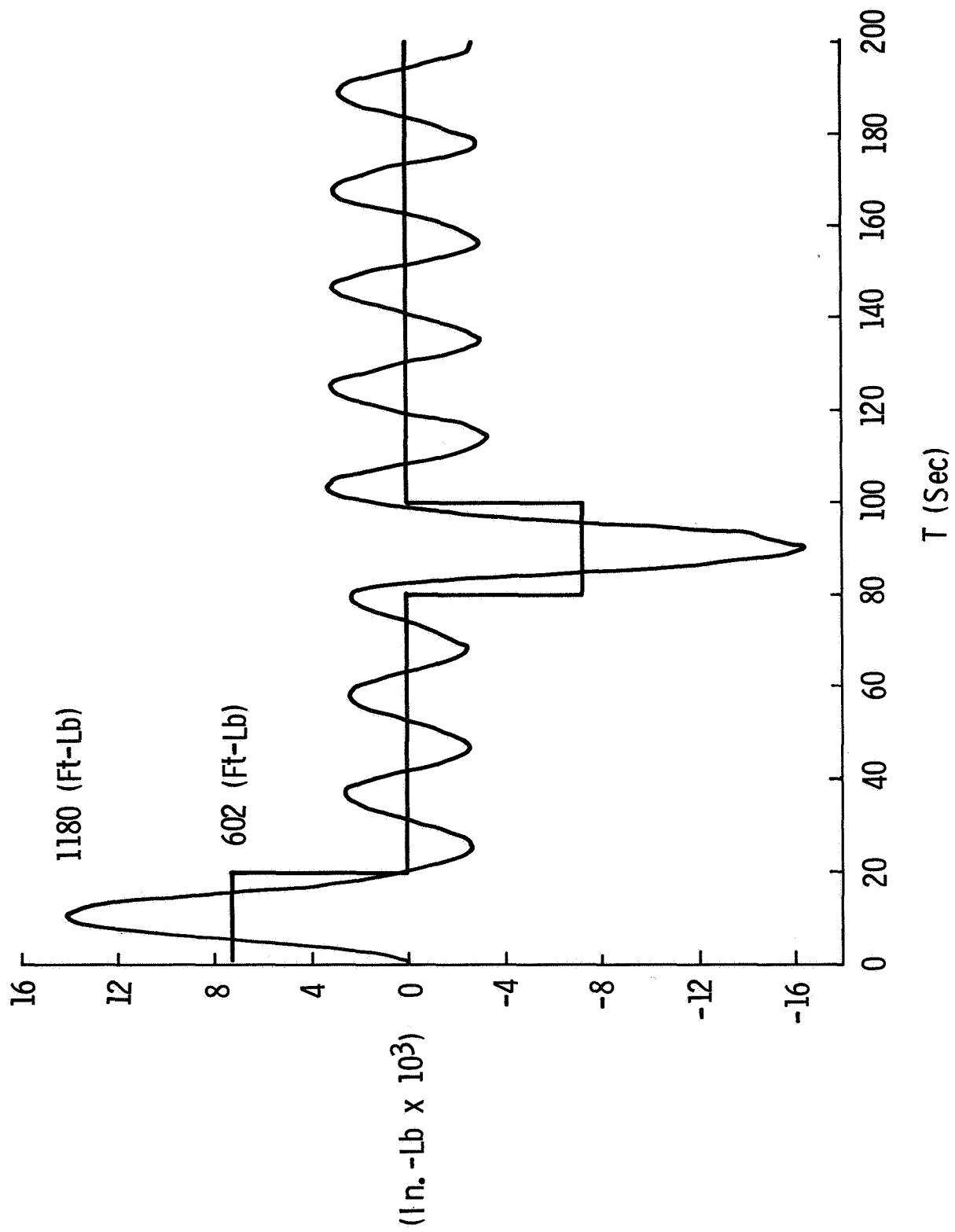


Figure VI-20 Rigid and Flexible AMS Elbow Torque Requirement

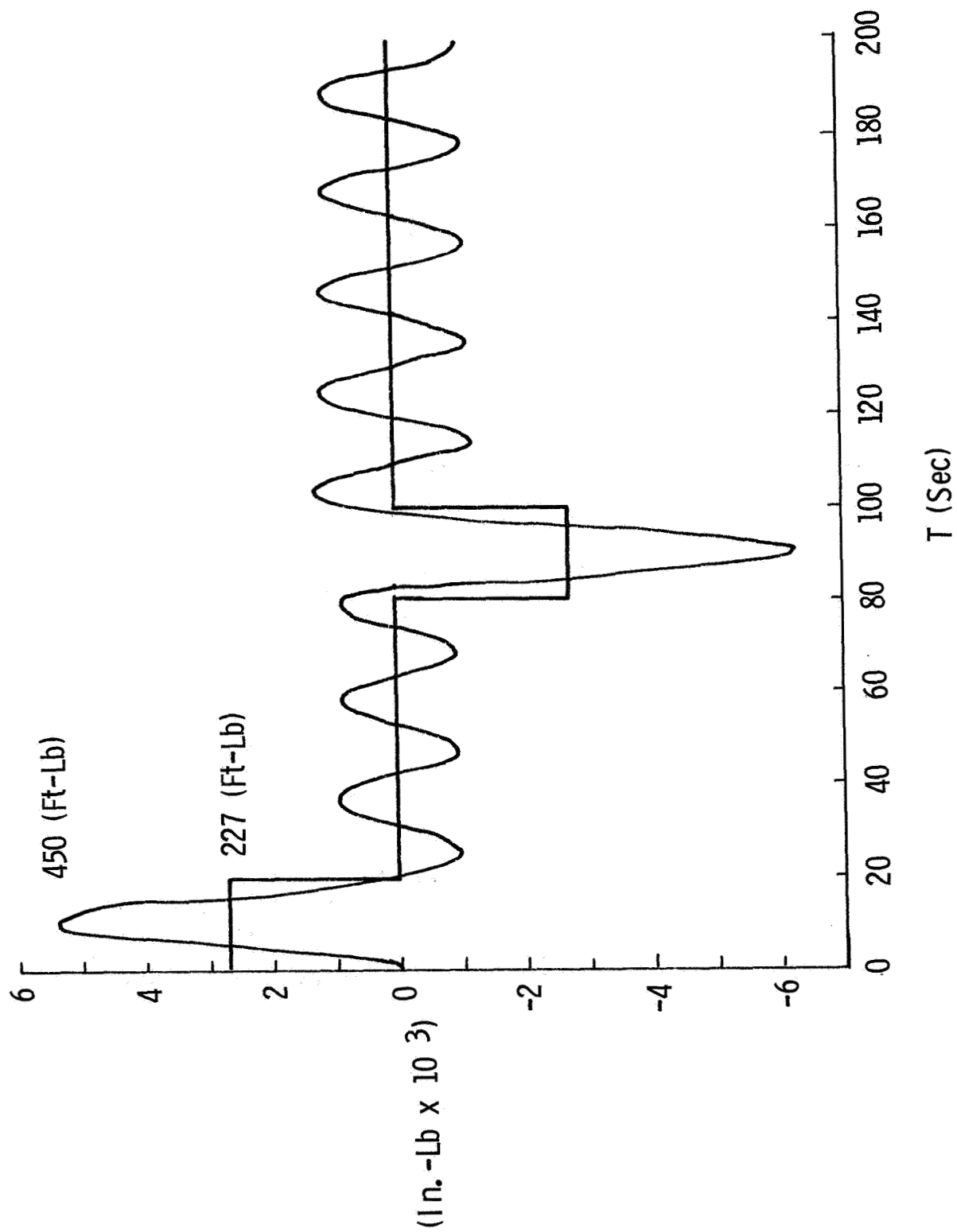


Figure VI-21 Rigid and Flexible AMS Wrist Torque Requirement

## D. SUMMARY AND RECOMMENDATIONS

### 1. Rigid Body Analysis

The rigid body dynamics model and corresponding computer program have been derived and validated by means of several check cases. Supplementary to the dynamics program, there is an additional computer program which accepts AMS design data (e.g. tube diameter, joint weight, etc.) and computes the necessary inertia properties for use in the dynamics model.

Together, these programs have been used (by specifying several payload handling tasks) to arrive at joint torque requirements of 1200, 650, and 300 ft-lbs for the shoulder, elbow, and wrist joints, respectively. In the process, it was shown that, for identical tasks, the AMS will require more torque than the SAMS; this is due to the fact that the AMS is attached to an inertial platform while the SAMS is attached to the shuttle. This effect will become less noticeable for payloads smaller than the maximum (65,000 lbs). It was also shown (for the maximum payload), that the added inertia of the counterbalance mechanism is sufficiently small as to result in no significant additional torque requirement over the non-counterbalanced manipulator. However, this may not be the case for smaller payloads. Finally, it was found that a 90° deployment of the 65,000 lb payload will result in a 7° counterrotation of the shuttle; for smaller payloads, the shuttle rotation will likewise be smaller.

For future work, it is recommended that the rigid body analysis be used primarily to measure the fidelity of 1-g simulations with the AMS. This would include a study of the interaction between the manipulator and the shuttle attitude control system for various size payloads. If such interactions are found to be significant, an investigation would be conducted to arrive at the means to include such effects in the 1-g simulations. Along the same line, the influence of orbital effects (e.g., gravity gradient torques) should be investigated and a determination made as to the inclusion of these effects in the 1-g simulations. Regarding the simulation facility itself, a systematic study should be conducted to determine for what range of payloads is the added inertia of the counterbalance significant and for what payloads is fixing the AMS to an inertial platform a serious consideration. Finally, the impact of typical simulation facility error forces (e.g. slanted floor, airpad drag, etc.) on AMS performance should be investi-

gated in order to define the tolerances for the simulation facility.

## 2. Vibration Analysis

A vibration analysis of an earlier version of the AMS (30 ft manipulator, 60,000 lb payload) resulted in fundamental frequencies on the order of 1 Hz for the unloaded AMS (both counterbalanced and space version) and fundamental frequencies of .02 - .03 Hz for the loaded (60,000 lb payload) manipulator.

As could be expected, the vibrational behavior of both the counterbalanced and non-counterbalanced versions of the AMS is sensitive to payload mass and arm configuration. Significant differences and similarities were found to exist between the vibration behavior of counterbalanced and non-counterbalanced AMS. It is felt that the differences in behavior are due, in large part, to the constraint conditions at the shoulder.

It is recommended that the vibration analysis be updated to include the latest design changes with careful attention given to the shoulder joint and the support structure.

## 3. Nonlinear Flexible Body Analysis

The generalized flexible body dynamics program was used to compare rigid and flexible AMS behavior for a planar payload handling task. The motion of the 65,000 lb payload was obtained by prescribing identical time histories for the shoulder and elbow yaw joints. The results for the flexible AMS revealed oscillations (about the rigid body trajectory) with approximately a 3 in amplitude (peak-to-peak) and a frequency of 0.05 Hz.

It is recommended that the flexible body dynamics program be updated along with the vibration analysis and, in the process, joint flexibility should be included. This program should be used primarily to verify the control system design and any active damping techniques that are developed. The program is also well suited to establish the validity of any simplified dynamics program that might be used for man-in-the-loop simulations.

#### E. REFERENCES

1. "Preliminary Design of a Shuttle Docking and Cargo Handling System". MSC-05218. Martin Marietta Corporation, Denver, Colorado, December 1971.
2. "Harmonic Drive Designers Manual", Revision 2. USM Corporation, Gear Systems Division, Wakefield, Massachusetts.
3. Yatteau, J. D. and Kane, T. R., "Experimental Investigation of Planar Motions of a Human Being Under the Action of a Body-Fixed Thrust", Stanford University Technical Report No. 202, Stanford University; Stanford, California, January 1971.

## APPENDIX A. Derivation of the Rigid Body Equations of Motion

### A. INTRODUCTION

This appendix presents a detailed derivation of the equations of motion of six interconnected rigid bodies. A detailed description of the generalized (AMS) model along with some remarks as to how this model is reduced to the space and 1-G versions of the AMS are presented in Section B. The vector form of the equations of motion are developed in Section C, and scalar form of these equations are derived in Section D.

### B. SYSTEM DESCRIPTION

The generalized AMS model consists of six rigid bodies interconnected by five hinges as shown in Fig. A-1. It is assumed that the motion takes place in the presence of an arbitrary gravitational acceleration denoted by the vector  $\underline{g}$ . Each body is presumed to have arbitrary inertia properties and hinge locations. Finally, although not shown in Fig. A-1, each body is acted upon by arbitrary, external, non-gravitational forces and torques.

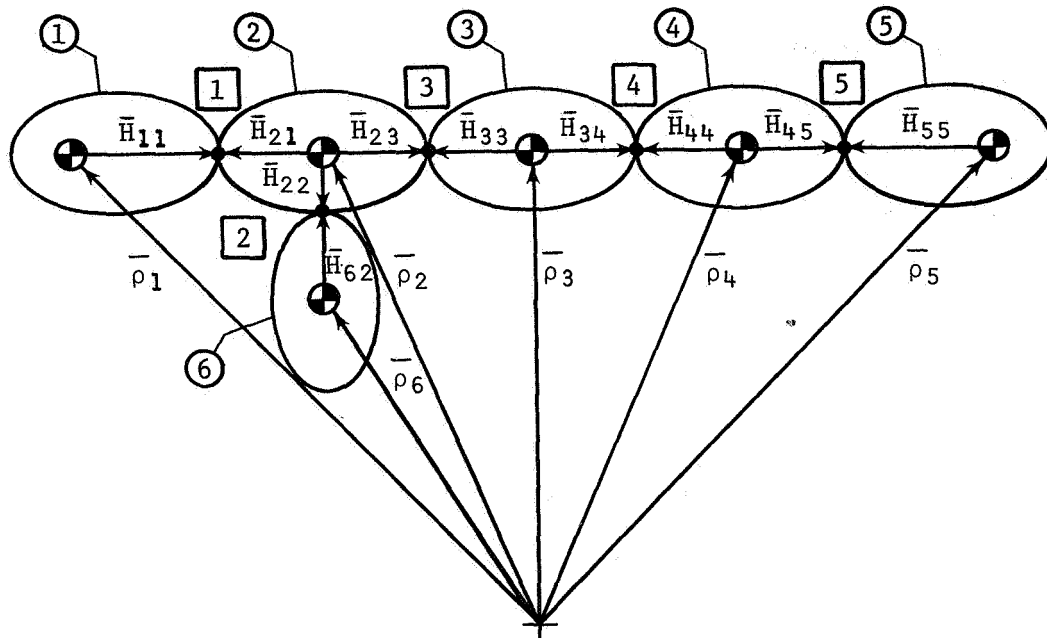
With the generalized model just described, it is a simple matter to extract both the 1-G and space versions of the AMS. First, to obtain the space version (without orbital effects included) one merely has to choose zero inertia properties for body 1, assign the Shuttle inertia properties to body 6, and select zero magnitude for the gravitational vector  $\underline{g}$ . On the other hand, to extract the 1-G,  $\underline{g}$  is assumed to be parallel to the vertical, and body 6 is assumed fixed in the inertial reference frame.

### C. VECTOR EQUATIONS OF MOTION

Newton's second law, for each of the bodies shown in Fig. A-1, can be written:

$$\bar{\mathbf{F}}_1 + \bar{\mathbf{F}}_{11}^H = m_1 \ddot{\rho}_1 \quad (\text{A-1})$$

$$\bar{\mathbf{F}}_2 + \bar{\mathbf{F}}_{21}^H + \bar{\mathbf{F}}_{22}^H + \bar{\mathbf{F}}_{23}^H = m_2 \ddot{\rho}_2 \quad (\text{A-2})$$




(1) Counterbalance Lower Arm	( $\lambda$ ) Body Label
(2) Counterbalance and Slave Upper Arm	[j] Hinge Label
(3) Slave Lower Arm	 Mass Center
(4) Wrist	$\bar{H}_{\lambda j}$ Position Vector of Hinge j relative to mass center of body $\lambda$
(5) Payload	0 Origin of inertial reference frame
(6) Body to which Arm is attached	$\bar{\rho}_{\lambda}$ Position vector of mass center of body $\lambda$ relative to 0
	$\bar{g}$ Gravity Vector

Figure A-1 Generalized AMS Model

$$\bar{F}_3 + \bar{F}_{33}^H + \bar{F}_{34}^H = m_3 \ddot{\rho}_3 \quad (A-3)$$

$$\bar{F}_4 + \bar{F}_{44}^H + \bar{F}_{45}^H = m_4 \ddot{\rho}_4 \quad (A-4)$$

$$\bar{F}_5 + \bar{F}_{55}^H = m_5 \ddot{\rho}_5 \quad (A-5)$$

$$\bar{F}_6 + \bar{F}_{62}^H = m_6 \ddot{\rho}_6 \quad (A-6)$$

where  $\bar{F}_\lambda$  ( $\lambda = 1, 2, \dots, 6$ ) is the resultant force, exclusive of hinge interaction forces, acting on body  $\lambda$ ;  $\bar{F}_{\lambda j}^H$  is the hinge interaction force on body  $\lambda$  at hinge  $j$ ; and  $m_\lambda$  is the mass of body  $\lambda$ .

Euler's dynamical equations for the six bodies are:

$$\bar{I}_1 \cdot \dot{\bar{\omega}}_1 + \bar{\omega}_1 \times \bar{I}_1 \cdot \bar{\omega}_1 = \bar{T}_1 + \bar{T}_{11}^H + \bar{H}_{11} \times \bar{F}_{11}^H \quad (A-7)$$

$$\begin{aligned} \bar{I}_2 \cdot \dot{\bar{\omega}}_2 + \bar{\omega}_2 \times \bar{I}_2 \cdot \bar{\omega}_2 = & \bar{T}_2 + \bar{T}_{21}^H + \bar{T}_{22}^H + \bar{T}_{23}^H + \bar{H}_{21} \times \bar{F}_{21}^H + \bar{H}_{22} \\ & \times \bar{F}_{22}^H + \bar{H}_{23} \times \bar{F}_{23}^H \end{aligned} \quad (A-8)$$

$$\bar{I}_3 \cdot \dot{\bar{\omega}}_3 + \bar{\omega}_3 \times \bar{I}_3 \cdot \bar{\omega}_3 = \bar{T}_3 + \bar{T}_{33}^H + \bar{T}_{34}^H + \bar{H}_{33} \times \bar{F}_{33}^H + \bar{H}_{34} \times \bar{F}_{34}^H \quad (A-9)$$

$$\bar{I}_4 \cdot \dot{\bar{\omega}}_4 + \bar{\omega}_4 \times \bar{I}_4 \cdot \bar{\omega}_4 = \bar{T}_4 + \bar{T}_{44}^H + \bar{T}_{45}^H + \bar{H}_{44} \times \bar{F}_{44}^H + \bar{H}_{45} \times \bar{F}_{45}^H \quad (A-10)$$

$$\bar{I}_5 \cdot \dot{\bar{\omega}}_5 + \bar{\omega}_5 \times \bar{I}_5 \cdot \bar{\omega}_5 = \bar{T}_5 + \bar{T}_{55}^H + \bar{H}_{55} \times \bar{F}_{55}^H \quad (A-11)$$

$$\bar{I}_6 \cdot \dot{\bar{\omega}}_6 + \bar{\omega}_6 \times \bar{I}_6 \cdot \bar{\omega}_6 = \bar{T}_6 + \bar{T}_{62}^H + \bar{H}_{62} \times \bar{F}_{62}^H \quad (A-12)$$



where  $\bar{\bar{I}}$  ( $\lambda = 1, 2, \dots, 6$ ) is the inertia dyadic of body  $\lambda$  for its mass center;  $\omega_\lambda$  is the angular velocity of body  $\lambda$  in inertial space;  $\bar{T}_\lambda$  is the resultant torque exclusive of hinge interaction torques acting on body  $\lambda$ ; and  $\bar{T}_{\lambda j}^H$  is the hinge interaction torque on body  $\lambda$  at joint  $j$ .

From Fig. A-1 it can be seen that knowledge of the attitude of each of the six bodies is sufficient to determine the configuration and attitude of the system. For this reason, it must be possible to combine Eqs. (A-1) - (A-12) to obtain six equations for the rotational motion which are uncoupled from the translational equations. A detailed description of this reduction in the equations of motion is given by Hooker and Margulies for the general  $n$ -body problem in reference 1. The development presented by Hooker and Margulies is fairly involved even when applied to six bodies. For this reason, only the results in reference 1 pertinent to the problem at hand will be presented here.

The following definitions prove useful in the sequel:

$$m_{\lambda j} = \sum_{\mu \in S_{\lambda j}} m_\mu \quad (A-13)$$

$$\bar{D}_\lambda = -\frac{1}{M} \sum_{j \in J_\lambda} m_{\lambda j} H_{\lambda j} \quad (A-14)$$

$$\bar{D}_{\lambda j} = \bar{D}_\lambda + \bar{H}_{\lambda j}$$

$$\begin{aligned} \bar{\bar{I}}_\lambda^* = \bar{\bar{I}}_\lambda + \left[ m_\lambda (\bar{D}_\lambda \cdot \bar{D}_\lambda) + \sum_{j \in J_\lambda} m_{\lambda j} (\bar{D}_{\lambda j} \cdot \bar{D}_{\lambda j}) \right] \bar{\bar{I}} \\ - \left[ m_\lambda \bar{D}_\lambda \bar{D}_\lambda + \sum_{j \in J_\lambda} m_{\lambda j} \bar{D}_{\lambda j} \bar{D}_{\lambda j} \right] \end{aligned} \quad (A-15)$$

where  $S_{\lambda j}$  denotes the set of (labels of) bodies connected to body  $\lambda$  at joint  $j$ ,  $J_\lambda$  is the set of labels for hinges in body  $\lambda$ , and  $\bar{I}$  is the identity dyadic. The physical significance of the quantities defined above is best described in terms of Fig. A-2

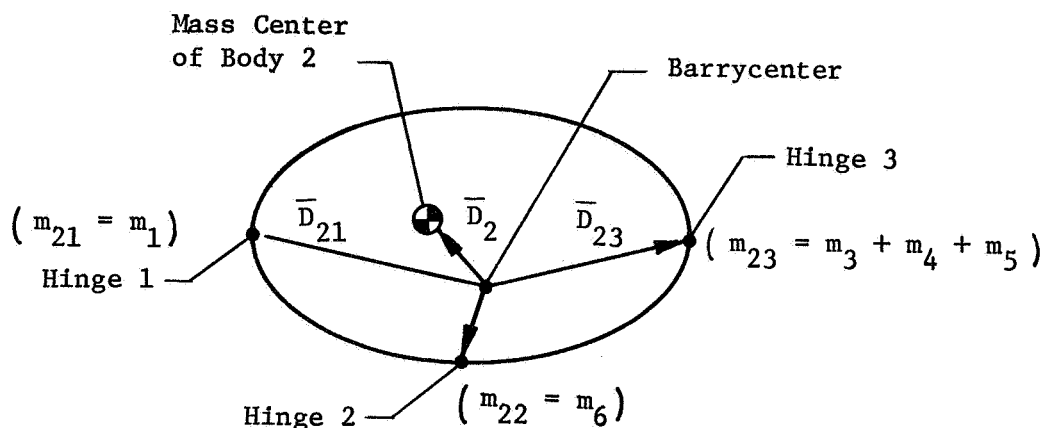


Figure A-2 Augmented Body 2

First, the mass distribution of each body is augmented by point masses at each hinge of the body (as shown for body 2 in Fig. A-2). The amount of mass concentrated at hinge  $j$  of body  $\lambda$  is called  $M_{\lambda j}$  and is equal to the sum of the masses of all those bodies (excluding body  $\lambda$ ) connected to hinge  $j$ , either directly or indirectly. The mass distribution of the body in question along with the point masses at the hinges define a new mass center which is called the "barrycenter" (see Fig. A-2). Now the vector,  $\bar{D}_\lambda$ , appearing in Eqs. (A-14) and (A-15) denotes the position vector of the mass center of body  $\lambda$  relative to the barrycenter of body  $\lambda$ . The  $\bar{D}_{\lambda j}$  vector represents the position vector of hinge  $j$  of body  $\lambda$  from the barrycenter of body  $\lambda$ . Finally,  $\bar{I}_\lambda^*$  denotes the inertia dyadic of the augmented body  $\lambda$  about its barrycenter.

The first step in obtaining the desired set of rotational equations is to solve Eqs. (A-1) - (A-6) for the hinge interaction forces  $\bar{F}_{\lambda j}^H$ . The result can be expressed in terms of the mass center acceleration of body  $\mu$ ,  $\ddot{\rho}_\mu$  and the system mass center acceleration,  $\ddot{\rho}$ , as follows

$$\bar{F}_{\lambda j}^H = \sum_{\mu \in S_{\lambda j}} \left[ \bar{F}_\mu - \frac{m_\mu}{M} \bar{F}_T - m_\mu \left( \ddot{\rho}_\mu - \ddot{\rho} \right) \right] \quad (A-17)$$

where  $M = \sum_{\lambda=1}^6 M_\lambda$  is the total mass of the system and  $\bar{F}_T = \sum_{\lambda=1}^6 \bar{F}_\lambda$

is the total external force acting on the system. Now it is shown in reference 1 that

$$\ddot{\rho}_\mu - \ddot{\rho} = \ddot{D}_\mu - \sum_{v \neq \mu} \ddot{D}_v K_v(\mu) \quad (A-18)$$

where  $K_v(\mu)$  is that joint of body  $v$  which leads to body  $\mu$ . Now, since

$$\ddot{D}_\lambda = \dot{\omega}_\lambda \times \bar{D}_\lambda + \bar{\omega}_\lambda \times (\bar{\omega}_\lambda \times \bar{D}_\lambda) \quad (A-19)$$

$$\ddot{D}_{\lambda j} = \dot{\omega}_\lambda \times \bar{D}_{\lambda j} + \bar{\omega}_\lambda \times (\bar{\omega}_\lambda \times \bar{D}_{\lambda j}) \quad (A-20)$$

it is possible, by means of (A-17) - (A-20), to obtain an expression for each of the  $\bar{F}_{\lambda j}^H$  in terms of the rotational motion. When these expressions are substituted into Eqs (A-7) - (A-12), there results (after considerable simplification);

$$\begin{aligned} \bar{\bar{I}}_1^* \cdot \dot{\bar{\omega}}_1 + \bar{\omega}_1 \times \bar{\bar{I}}_1^* \cdot \bar{\omega}_1 &= \bar{T}_1 + \bar{T}_{11}^H + \bar{D}_1 \times \bar{F}_1 + \bar{D}_{11} \times (\bar{F}_2 + \ddot{M}\bar{D}_{21} \\ &+ \bar{F}_3 + \ddot{M}\bar{D}_{33} + \bar{F}_4 + \ddot{M}\bar{D}_{44} + \bar{F}_5 + \ddot{M}\bar{D}_{55} + \bar{F}_6 + \ddot{M}\bar{D}_{62}) \end{aligned} \quad (A-21)$$

$$\begin{aligned} \bar{\bar{I}}_2^* \cdot \dot{\bar{\omega}}_2 + \bar{\omega}_2 \times \bar{\bar{I}}_2^* \cdot \bar{\omega}_2 &= \bar{T}_2 + \bar{T}_{21}^H + \bar{T}_{22}^H + \bar{T}_{23}^H + \bar{D}_2 \times \bar{F}_2 + \bar{D}_{21} \\ &\times (\bar{F}_1 + \ddot{M}\bar{D}_{11}) + \bar{D}_{23} \times (\bar{F}_3 + \ddot{M}\bar{D}_{33} + \bar{F}_4 + \ddot{M}\bar{D}_{44} + \bar{F}_5 + \ddot{M}\bar{D}_{55}) \\ &+ \bar{D}_{22} \times (\bar{F}_6 + \ddot{M}\bar{D}_{62}) \end{aligned} \quad (A-22)$$

$$\begin{aligned} \bar{\bar{I}}_3^* \cdot \dot{\bar{\omega}}_3 + \bar{\omega}_3 \times \bar{\bar{I}}_3^* \cdot \bar{\omega}_3 &= \bar{T}_3 + \bar{T}_{33}^H + \bar{T}_{34}^H + \bar{D}_3 \times \bar{F}_3 + \bar{D}_{33} \times (\bar{F}_1 + \ddot{M}\bar{D}_{11} \\ &+ \bar{F}_2 + \ddot{M}\bar{D}_{23} + \bar{F}_6 + \ddot{M}\bar{D}_{62}) + \bar{D}_{34} \times (\bar{F}_4 + \ddot{M}\bar{D}_{44} + \bar{F}_5 + \ddot{M}\bar{D}_{55}) \end{aligned} \quad (A-23)$$

$$\begin{aligned} \bar{\bar{I}}_4^* \cdot \dot{\bar{\omega}}_4 + \bar{\omega}_4 \times \bar{\bar{I}}_4^* \cdot \bar{\omega}_4 &= \bar{T}_4 + \bar{T}_{44}^H + \bar{T}_{45}^H + \bar{D}_4 \times \bar{F}_4 + \bar{D}_{44} \times (\bar{F}_1 + \ddot{M}\bar{D}_{11} \\ &+ \bar{F}_2 + \ddot{M}\bar{D}_{23} + \bar{F}_3 + \ddot{M}\bar{D}_{34} + \bar{F}_6 + \ddot{M}\bar{D}_{62}) + \bar{D}_{45} \times (\bar{F}_5 + \ddot{M}\bar{D}_{55}) \end{aligned} \quad (A-24)$$

$$\begin{aligned} \bar{\bar{I}}_5^* \cdot \dot{\bar{\omega}}_5 + \bar{\omega}_5 \times \bar{\bar{I}}_5^* \cdot \bar{\omega}_5 &= \bar{T}_5 + \bar{T}_{55}^H + \bar{D}_5 \times \bar{F}_5 + \bar{D}_{55} \times [\bar{F}_1 + \bar{F}_2 + \bar{F}_3 \\ &+ \bar{F}_4 + \bar{F}_6 + M(\ddot{D}_{11} + \ddot{D}_{23} + \ddot{D}_{62} + \ddot{D}_{34} + \ddot{D}_{45})] \end{aligned} \quad (A-25)$$

$$\begin{aligned} \bar{\mathbf{I}}_6^* \cdot \dot{\bar{\boldsymbol{\omega}}}_6 + \bar{\boldsymbol{\omega}}_6 \times \bar{\mathbf{I}}_6^* \quad \bar{\boldsymbol{\omega}}_6 = \bar{\mathbf{T}}_6 + \bar{\mathbf{T}}_{62}^H + \bar{\mathbf{D}}_6 \times \bar{\mathbf{F}}_6 + \bar{\mathbf{D}}_{62} \times [\bar{\mathbf{F}}_1 + \bar{\mathbf{F}}_2 + \bar{\mathbf{F}}_3 \\ + \bar{\mathbf{F}}_4 + \bar{\mathbf{F}}_5 + M (\ddot{\mathbf{D}}_{11} + \ddot{\mathbf{D}}_{22} + \ddot{\mathbf{D}}_{33} + \ddot{\mathbf{D}}_{44} + \ddot{\mathbf{D}}_{55})] \end{aligned} \quad (\text{A-26})$$

which are the desired set of uncoupled rotational equations.

Now, for purposes of this study, it is assumed that the motion of bodies 1-5 relative to body 6 is specified, and it remains to determine the resulting motion induced in body 6 along with the forces,  $\bar{\mathbf{F}}_{\lambda j}^H$ , and torques,  $\bar{\mathbf{T}}_{\lambda j}^H$ , of interaction occurring at the joints. To facilitate this determination, the following quantities are defined:

$$\bar{\mathbf{M}}_\lambda = M \sum_{\mu \neq \lambda} \bar{\mathbf{D}}_{\lambda K_\lambda(\mu)} \times \ddot{\mathbf{D}}_{\mu K_\mu(\lambda)} \quad , \quad (\lambda = 1, 2, \dots, 6) \quad (\text{A-27})$$

$$\bar{\mathbf{L}}_\lambda = \bar{\mathbf{T}}_\lambda + \bar{\mathbf{D}}_\lambda \times \bar{\mathbf{F}}_\lambda + \sum_{\mu \neq \lambda} \bar{\mathbf{D}}_{\lambda K_\lambda(\mu)} \times \bar{\mathbf{F}}_\mu \quad , \quad (\lambda = 1, 2, \dots, 6) \quad (\text{A-28})$$

$$\bar{\mathbf{N}}_\lambda = \bar{\mathbf{I}}_\lambda^* \cdot \dot{\bar{\boldsymbol{\omega}}}_\lambda + \bar{\boldsymbol{\omega}}_\lambda \times \bar{\mathbf{I}}_\lambda^* \cdot \bar{\boldsymbol{\omega}}_\lambda \quad (\lambda = 1, 2, \dots, 6) \quad (\text{A-29})$$

Eqs. (A-21) - (A-22) can be rewritten in terms of the above quantities as:

$$\bar{\mathbf{T}}_{11}^H = \bar{\mathbf{N}}_1 - \bar{\mathbf{L}}_1 - \bar{\mathbf{M}}_1 \quad (\text{A-30})$$

$$\bar{\mathbf{T}}_{55}^H = \bar{\mathbf{N}}_5 - \bar{\mathbf{L}}_5 - \bar{\mathbf{M}}_5 \quad (\text{A-31})$$

$$\bar{\mathbf{T}}_{44}^H = \bar{\mathbf{N}}_4 - \bar{\mathbf{L}}_4 - \bar{\mathbf{M}}_4 + \bar{\mathbf{T}}_{55}^H \quad (\text{A-32})$$

$$\bar{\mathbf{T}}_{33}^H = \bar{\mathbf{N}}_3 - \bar{\mathbf{L}}_3 - \bar{\mathbf{M}}_3 + \bar{\mathbf{T}}_{44}^H \quad (\text{A-33})$$

$$\bar{T}_{22}^H = \bar{N}_2 - \bar{L}_2 - \bar{M}_2 + \bar{T}_{11}^H + \bar{T}_{33}^H \quad (A-34)$$

$$\bar{N}_6 - \bar{L}_6 - \bar{M}_6 + \bar{T}_{22}^H = 0 \quad (A-35)$$

where advantage has been taken of the fact that the torques on either side of a joint are equal in magnitude and opposite in direction (e.g.,  $\bar{T}_{21}^H = -\bar{T}_{11}^H$ ). Equation (A-35) is the differential equation for  $\bar{\omega}_6$  which must be integrated before the torques in Eqs. (A-31) - (A-34) can be evaluated; the reason being that the right hand sides of the torque equations are dependent upon  $\bar{\omega}_6$  and  $\dot{\bar{\omega}}_6$ .

The proper kinematical equations must be added to Eqs. (A-30) - (A-35) to complete the description of the rotational motion; these equations are given in the next section where the various vector quantities are put in component form.

#### D. KINEMATICS AND SCALAR FORM OF THE EQUATIONS OF MOTION

##### 1. Reference Frames and Transformation Equations

In order to assign values to the vector quantities appearing in Equations (A-30) - (A-35), reference frames are defined by fixing mutually perpendicular unit vectors  $\bar{e}_{\lambda j}$  ( $j = 1, 2, 3$ ) in body  $\lambda$  as shown in Figure A-3. An inertial reference frame, R, is defined by the  $e_{Rj}$  ( $j = 1, 2, 3$ ) unit vectors. It is assumed that the  $\bar{e}_{\lambda j}$  unit vectors are parallel to the principal axes of body  $\lambda$  for its mass center.

Now it is possible to express the relationships between the various reference frames by means of the following transformation equations\*:

$$\left\{ \bar{e}_{\lambda i} \right\} = \left[ \begin{matrix} \lambda \\ E \end{matrix} \right] \left\{ \bar{e}_{\mu i} \right\}, \quad (\lambda, \mu = R, 1, 2, \dots, 6) \quad (A-36)$$

---

\*Unless otherwise specified, {} represents a 3 x 1 column matrix and [] indicates a 3 x 3 square matrix.

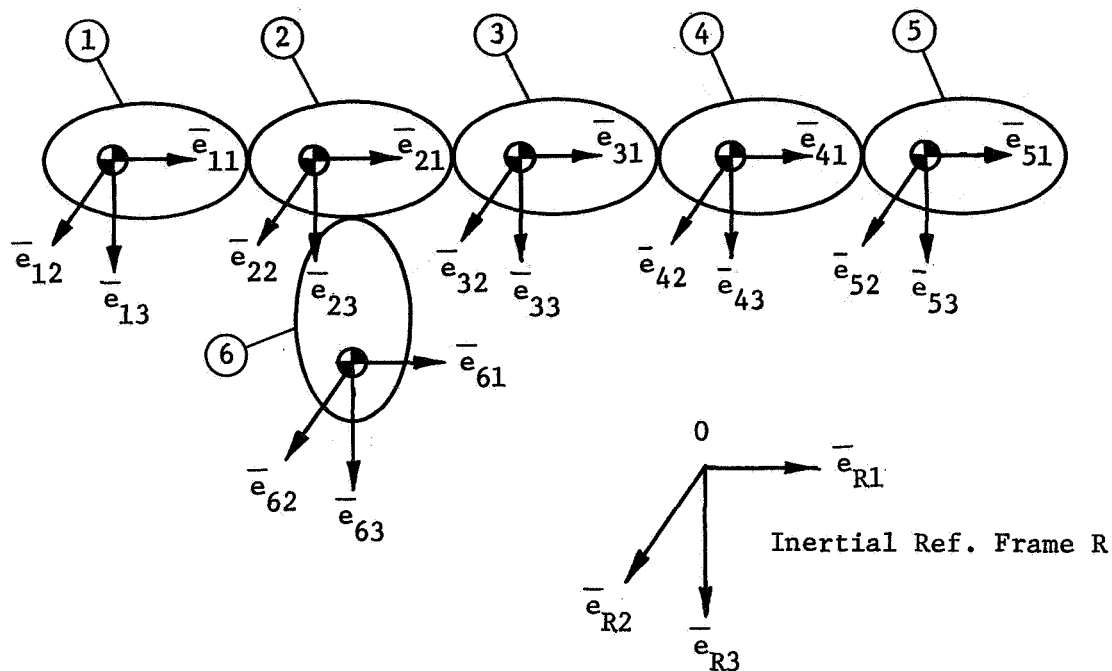


Figure A-3 Reference Frames

The elements of  ${}^{\lambda}E^{\mu}$  are determined by the means one chooses to describe orientations. In this case, Euler angles are used because they are easily related to gimbal angles which are assumed to exist at the joints of the AMS. It remains to specify the gimbal order present at each of the joints. To this end, the following convention is adopted for each body  $\lambda$ :

Roll: A rotation of amount  $\theta_{\lambda 1}$  about an axis parallel to  $\bar{e}_{\lambda 1}$

Pitch: A rotation of amount  $\theta_{\lambda 2}$  about an axis parallel to  $\bar{e}_{\lambda 2}$ .

Yaw: A rotation of amount  $\theta_{\lambda 3}$  about an axis parallel to  $\bar{e}_{\lambda 3}$ .

Based on the latest design of the AMS, the relative orientation of body  $\mu$  to body  $\lambda$  is assumed to be a result of the following rotation sequences of body  $\mu$  about axes parallel to the  $\bar{e}_{\mu i}$  unit vectors:

Body 6 to Inertial Ref. Frame R: Roll, Pitch, Yaw ( $\theta_{61}, \theta_{62}, \theta_{63}$ )

Body 2 to Body 6: Pitch, Yaw, Roll ( $\theta_{22}, \theta_{23}, \theta_{21}$ )

Body 1 and 3 to Body 2\*: Yaw only ( $\theta_{33}$ )

Body 4 to Body 3: Yaw, Pitch, Roll ( $\theta_{43}, \theta_{42}, \theta_{41}$ )

Body 5 to Body 4\*\*: Roll, Pitch, Yaw ( $\theta_{51}, \theta_{52}, \theta_{53}$ )

Having specified the necessary rotations, it is now possible to write the transformation matrices  ${}^\lambda E^\mu$  in equation (A-36). These are:

$$[{}^R_E]^6 = \begin{bmatrix} C_{62}C_{63} & -C_{62}S_{63} & S_{62} \\ C_{61}S_{63} + S_{61}S_{62}C_{63} & C_{61}C_{63} - S_{61}S_{62}S_{63} & -S_{61}C_{62} \\ S_{61}S_{63} - C_{61}S_{62}C_{63} & S_{61}C_{63} + C_{61}S_{62}S_{63} & C_{61}C_{62} \end{bmatrix} \quad (A-37)$$

$$[{}^6_E]^2 = \begin{bmatrix} C_{22}C_{23} & -C_{22}S_{23}C_{21} + S_{22}S_{21} & C_{22}S_{23}S_{21} + S_{22}C_{21} \\ S_{23} & C_{23}C_{21} & -C_{23}S_{21} \\ -S_{22}C_{23} & S_{22}S_{23}C_{21} + C_{22}S_{21} & -S_{22}S_{23}S_{21} + C_{22}C_{21} \end{bmatrix} \quad (A-38)$$

$$[{}^2_E]^3 = \begin{bmatrix} C_{33} & -S_{33} & 0 \\ S_{33} & C_{33} & 0 \\ 0 & 0 & 1 \end{bmatrix} = [{}^2_E]^1 \quad (A-39)$$

\* Because Body 1 counterbalances Body 3, these two bodies will always have the same orientation relative to Body 2, and hence only one set of Euler angles need be specified.

\*\*Body 5 (payload) is assumed fixed to Body 4 but may have an arbitrary orientation relative to same.



$$\begin{bmatrix} 3 \\ E \\ 4 \end{bmatrix} = \begin{bmatrix} C_{43}C_{42} & C_{43}S_{42}S_{41} - S_{43}C_{41} & C_{43}S_{42}C_{41} + S_{43}S_{41} \\ S_{43}C_{42} & S_{43}S_{42}S_{41} + C_{43}C_{41} & S_{43}S_{42}C_{41} - C_{43}S_{41} \\ -S_{42} & C_{42}S_{41} & C_{42}C_{41} \end{bmatrix} \quad (A-40)$$

$$\begin{bmatrix} 4 \\ E \\ 5 \end{bmatrix} = \begin{bmatrix} C_{52}C_{53} & -C_{52}S_{53} & S_{52} \\ C_{51}S_{53} + S_{51}S_{52}S_{53} & C_{51}C_{53} - S_{51}S_{52}S_{53} & -S_{51}C_{52} \\ S_{51}S_{53} - C_{51}S_{52}C_{53} & S_{51}C_{53} + C_{51}S_{52}C_{53} & C_{51}C_{52} \end{bmatrix} \quad (A-41)$$

Where  $S_{\lambda j} = \sin \theta_{\lambda j}$  and  $C_{\lambda j} = \cos \theta_{\lambda j}$ . Because the  ${}^{\lambda}E^{\mu}$  matrices are orthogonal (i.e., because  ${}^{\mu}E^{\lambda} = [{}^{\lambda}E^{\mu}]^{-1} = [{}^{\lambda}E^{\mu}]^T$ ), it is an easy matter to obtain the other transformations implied by Equation (A-36) and hence are not written here.

## 2. Kinematical Equations

It can be seen from Equations (A-27) - (A-29) that Equations (A-30) - (A-35) are functions of the angular velocities of the various bodies relative to the inertial reference frame R. Because the  $\bar{D}_{\lambda}$  vectors and the inertia dyadics,  $\bar{I}_{\lambda}^*$ , are constant in the body  $\lambda$ , it is advantageous to project the angular velocity vectors along axes parallel to the  $\bar{e}_{\lambda i}$  vectors. In other words we let

$$\omega_{\lambda i} = \bar{\omega}_{\lambda} \cdot \bar{e}_{\lambda i} \quad (A-42)$$

and to be consistent with the preceding orientation specifications, we write:

$$\{\omega_{2i}\} = \{{}^2E^6\} \left[ \omega_{6i} \right] + \{{}^6\omega_{2i}\} \quad (A-43)$$

$$\{\omega_{1i}\} = \{\omega_{3i}\} = \begin{bmatrix} 3E^2 \end{bmatrix} \{\omega_{2i}\} + \{\omega_{3i}^2\} \quad (A-44)$$

$$\{\omega_{4i}\} = \begin{bmatrix} 4E^3 \end{bmatrix} \{\omega_{3i}\} + \{\omega_{4i}^3\} \quad (A-45)$$

$$\{\omega_{5i}\} = \begin{bmatrix} 5E^4 \end{bmatrix} \{\omega_{4i}\} \quad (A-46)$$

where the  ${}^\mu\omega_{\lambda i}$  ( $i = 1,2,3$ ) are the projections of the angular velocity of body  $\lambda$  relative to body  $\mu$ ,  ${}^\mu\omega_{\lambda}^-$ , on the  $\bar{e}_{\lambda i}$  unit vectors, or

$${}^\mu\omega_{\lambda i} = {}^\mu\omega_{\lambda}^- \cdot \bar{e}_{\lambda i} \quad (i = 1,2,3) \quad (A-47)$$

The  $\omega_{6i}$  and  ${}^\mu\omega_{\lambda i}$  are determined by the so-called kinematical equations relating the quantities to the appropriate Euler angle rates. For the aforementioned rotation sequences, the equations are:

$$\{\omega_{6i}\} = \begin{bmatrix} R_6 \end{bmatrix} \{\dot{\theta}_{6i}\} \quad (A-48)$$

$$\{\omega_{2i}^6\} = \begin{bmatrix} R_2 \end{bmatrix} \{\dot{\theta}_{2i}\} \quad (A-49)$$

$$\{\omega_{3i}^2\} = \begin{bmatrix} R_3 \end{bmatrix} \{\dot{\theta}_{3i}\} \quad (A-50)$$

$$\{\omega_{4i}^3\} = \begin{bmatrix} R_4 \end{bmatrix} \{\dot{\theta}_{4i}\} \quad (A-51)$$

where

$$\begin{bmatrix} R_6 \end{bmatrix} = \begin{bmatrix} C_{63}C_{62} & S_{63} & 0 \\ -S_{63}C_{62} & C_{63} & 0 \\ S_{62} & 0 & 1 \end{bmatrix} \quad (A-52)$$

$$\begin{bmatrix} R_2 \end{bmatrix} = \begin{bmatrix} \bar{1} & s_{63} & 0 \\ 0 & c_{23}c_{21} & s_{21} \\ 0 & -c_{23}s_{21} & c_2 \end{bmatrix} \quad (A-53)$$

$$\begin{bmatrix} R_3 \end{bmatrix} = \begin{bmatrix} \bar{0} & 0 & \bar{0} \\ 0 & 0 & 0 \\ 0 & 0 & \bar{1} \end{bmatrix} = \begin{bmatrix} R_1 \end{bmatrix} \quad (A-54)$$

$$\begin{bmatrix} R_4 \end{bmatrix} = \begin{bmatrix} \bar{1} & 0 & -s_{42} \\ 0 & c_{41} & s_{41}c_{42} \\ 0 & -s_{41} & c_{41}c_{42} \end{bmatrix} \quad (A-55)$$

Now, as mentioned at the end of Section C, Equation (A-35) must be integrated before Equations (A-30) - (A-34) can be evaluated, and to do this numerically, Equation (A-35) must be put into the following form:

$$\dot{\omega}_{6i} = f(\omega_{6i}) \quad (i = 1, 2, 3) \quad (A-56)$$

which means that when those terms in Equations (A-30) - (A-35), which are dependent upon the  $\dot{\omega}_{6i}$ , are written; the dependence on the  $\dot{\omega}_{6i}$  must be shown explicitly. For this reason, the derivatives of the angular velocity vectors are written as follows:

$$\left\{ \dot{\omega}_{\lambda i} \right\} = \left[ W_{\lambda} \right] \left\{ \dot{\omega}_{6i} \right\} + \left\{ W'_{\lambda} \right\} \quad (A-57)$$

where

$$\dot{\omega}_{\lambda i} = \dot{\bar{\omega}}_{\lambda} \cdot \bar{e}_{\lambda i} \quad (A-58)$$

It follows from Equations (A-43) - (A-46) that

$$\begin{bmatrix} W_2 \end{bmatrix} = \begin{bmatrix} 2_E^6 \end{bmatrix} \quad (A-59)$$

$$\begin{Bmatrix} W_2' \end{Bmatrix} = \begin{bmatrix} 2_E^6 \end{bmatrix} \begin{Bmatrix} \omega_{6i} \end{Bmatrix} + \begin{Bmatrix} 6_{2i}^{\dot{\omega}} \end{Bmatrix} \quad (A-60)$$

$$\begin{bmatrix} W_1 \end{bmatrix} = \begin{bmatrix} W_3 \end{bmatrix} = \begin{bmatrix} 3_E^2 \end{bmatrix} \begin{bmatrix} W_2 \end{bmatrix} \quad (A-61)$$

$$\begin{Bmatrix} W_1' \end{Bmatrix} = \begin{Bmatrix} W_3' \end{Bmatrix} = \begin{bmatrix} 3_E^2 \end{bmatrix} \begin{Bmatrix} \omega_{2i} \end{Bmatrix} + \begin{bmatrix} 3_E^2 \end{bmatrix} \begin{Bmatrix} W_2' \end{Bmatrix} + \begin{Bmatrix} 2_{3i}^{\dot{\omega}} \end{Bmatrix} \quad (A-62)$$

$$\begin{bmatrix} W_4 \end{bmatrix} = \begin{bmatrix} 4_E^3 \end{bmatrix} \begin{bmatrix} W_3 \end{bmatrix} \quad (A-63)$$

$$\begin{Bmatrix} W_4' \end{Bmatrix} = \begin{bmatrix} 4_E^3 \end{bmatrix} \begin{Bmatrix} \omega_{3i} \end{Bmatrix} + \begin{bmatrix} 4_E^3 \end{bmatrix} \begin{Bmatrix} W_3' \end{Bmatrix} + \begin{Bmatrix} 3_{4i}^{\dot{\omega}} \end{Bmatrix} \quad (A-64)$$

$$\begin{bmatrix} W_5 \end{bmatrix} = \begin{bmatrix} 5_E^4 \end{bmatrix} \begin{bmatrix} W_4 \end{bmatrix} \quad (A-65)$$

$$\begin{Bmatrix} W_5' \end{Bmatrix} = \begin{bmatrix} 5_E^4 \end{bmatrix} \begin{Bmatrix} W_4' \end{Bmatrix} \quad (A-66)$$

where the  $\begin{Bmatrix} \mu_{\lambda i}^{\dot{\omega}} \end{Bmatrix}$  are obtained by differentiating Equations (A-49) - (A-51).

### 3. Inertia Dyadics and the $\bar{N}_\lambda$ Vectors

The inertia dyadics,  $\bar{I}_\lambda^*$ , appearing in Equation (A-29) can be evaluated directly from (A-16), but first, the components of the  $\bar{D}_\lambda$  and  $\bar{D}_{\lambda j}$  vectors are defined by

$$D_{\lambda j} = \bar{D}_\lambda \cdot \bar{e}_{\lambda i} \quad (i = 1, 2, 3) \quad (A-67)$$

$$D_{\lambda ji} = \bar{D}_{\lambda j} \cdot \bar{e}_{\lambda i} \quad (i = 1, 2, 3) \quad (\text{A-68})$$

and the elements of the inertia dyadic  $\bar{\bar{I}}_{\lambda}$  are defined by

$$\bar{\bar{I}}_{\lambda} = \sum_{i=1}^3 I_{\lambda i} \bar{e}_{\lambda i} \bar{e}_{\lambda i} \quad (\lambda = 1, 2, \dots, 6) \quad (\text{A-69})$$

since it was assumed the  $\bar{e}_{\lambda i}$  are parallel to the principal axes of body  $\lambda$  for its mass center. Finally, the elements of  $\bar{\bar{I}}_{\lambda}^*$  inertia dyadics are given by:

$$\bar{\bar{I}}_{\lambda}^* = \sum_{j=1}^3 \sum_{K=1}^3 I_{\lambda jK}^* \bar{e}_{\lambda j} \bar{e}_{\lambda K} \quad (\text{A-70})$$

and an associated matrix is defined by

$$[\bar{\bar{I}}_{\lambda}^*] = \begin{bmatrix} I_{\lambda 11}^* & I_{\lambda 12}^* & I_{\lambda 13}^* \\ I_{\lambda 21}^* & I_{\lambda 22}^* & I_{\lambda 23}^* \\ I_{\lambda 31}^* & I_{\lambda 32}^* & I_{\lambda 33}^* \end{bmatrix} \quad (\text{A-71})$$

Using the definitions given by Equation (A-29) and Equations (A-67) - (A-71), the following expressions are obtained for the elements of the  $[\bar{\bar{I}}_{\lambda}^*]$  matrices:

Body 1

$$I_{111}^* = I_{11} + m_1 (D_{12}^2 + D_{13}^2) + m_{11} (D_{112}^2 + D_{113}^2)$$

$$I_{112}^* = - \left[ m_1 D_{11} D_{12} + m_{11} D_{111} D_{112} \right]$$

$$I_{113}^* = - \left[ m_1 D_{11} D_{13} + m_{11} D_{111} D_{113} \right]$$

$$I_{121}^* = I_{112}^*$$

$$I_{122}^* = I_{12} + m_1 (D_{11}^2 + D_{13}^2) + m_{11} (D_{111}^2 + D_{113}^2)$$

$$I_{123}^* = - \left[ m_1 D_{12} D_{13} + m_{11} D_{112} D_{113} \right]$$

$$I_{131}^* = I_{113}^*$$

$$I_{132}^* = I_{123}^*$$

$$I_{133}^* = I_{13} + m_1 (D_{11}^2 + D_{12}^2) + m_{11} (D_{111}^2 + D_{112}^2)$$

(A-72)

Body 2

$$I_{211}^* = I_{21} + m_2 (D_{22}^2 + D_{23}^2) + m_{21} (D_{212}^2 + D_{213}^2) + m_{22} (D_{221}^2 + D_{223}^2) + m_{23} (D_{232}^2 + D_{233}^2)$$

$$I_{212}^* = - \left[ m_2 D_{21} D_{22} + m_{21} D_{211} D_{212} + m_{22} D_{221} D_{222} + m_{23} D_{231} D_{232} \right]$$

$$I_{213}^* = - \left[ m_2 D_{21} D_{23} + m_{21} D_{211} D_{213} + m_{22} D_{221} D_{223} + m_{23} D_{231} D_{233} \right]$$

$$I_{221}^* = I_{212}^*$$

(A-73)

$$\begin{aligned}
I_{222}^* &= I_{22} + m_2 \left( D_{21}^2 + D_{23}^2 \right) + m_{21} \left( D_{211}^2 + D_{213}^2 \right) + m_{22} \left( D_{221}^2 + D_{223}^2 \right) \\
&\quad + m_{23} \left( D_{231}^2 + D_{233}^2 \right) \\
I_{223}^* &= - \left[ m_2 D_{22} D_{23} + m_{21} D_{212} D_{213} + m_{22} D_{222} D_{223} + m_{23} D_{232} D_{233} \right] \\
I_{231}^* &= I_{213}^* \\
I_{232}^* &= I_{223}^* \\
I_{233}^* &= I_{23} + m_2 \left( D_{21}^2 + D_{22}^2 \right) + m_{21} \left( D_{211}^2 + D_{212}^2 \right) + m_{22} \left( D_{221}^2 + D_{222}^2 \right) \\
&\quad + m_{23} \left( D_{231}^2 + D_{232}^2 \right)
\end{aligned}
\tag{A-73}$$

(cont)

Body 3

$$\begin{aligned}
I_{311}^* &= I_{31} + m_3 \left( D_{32}^2 + D_{33}^2 \right) + m_{33} \left( D_{332}^2 + D_{333}^2 \right) + m_{34} \left( D_{342}^2 + D_{343}^2 \right) \\
I_{312}^* &= - \left[ m_3 D_{31} D_{32} + m_{33} D_{331} D_{332} + m_{34} D_{341} D_{342} \right] \\
I_{313}^* &= - \left[ m_3 D_{31} D_{33} + m_{33} D_{331} D_{333} + m_{34} D_{341} D_{343} \right] \\
I_{321}^* &= I_{312}^* \\
I_{322}^* &= I_{32} + m_3 \left( D_{31}^2 + D_{33}^2 \right) + m_{33} \left( D_{331}^2 + D_{333}^2 \right) + m_{34} \left( D_{341}^2 + D_{343}^2 \right) \\
I_{323}^* &= - \left[ m_3 D_{32} D_{33} + m_{33} D_{332} D_{333} + m_{34} D_{342} D_{343} \right] \\
I_{331}^* &= I_{313}^*
\end{aligned}
\tag{A-74}$$

$$I_{332}^* = I_{323}^*$$

(A-74)

$$I_{333}^* = I_{33} + m_3 (D_{31}^2 + D_{32}^2) + m_{33} (D_{331}^2 + D_{332}^2) + m_{34} (D_{341}^2 + D_{342}^2)$$

(cont)

Body 4

$$I_{411}^* = I_{41} + m_4 (D_{42}^2 + D_{43}^2) + m_{44} (D_{442}^2 + D_{443}^2) + m_{45} (D_{452}^2 + D_{453}^2)$$

$$I_{412}^* = - \left[ m_4 D_{41} D_{42} + m_{44} D_{441} D_{442} + m_{45} D_{451} D_{452} \right]$$

$$I_{421}^* = I_{412}^*$$

$$I_{422}^* = I_{42} + m_4 (D_{41}^2 + D_{43}^2) + m_{44} (D_{441}^2 + D_{443}^2) + m_{45} (D_{451}^2 + D_{453}^2)$$

(A-75)

$$I_{423}^* = - \left[ m_4 D_{42} D_{43} + m_{44} D_{442} D_{443} + m_{45} D_{452} D_{453} \right]$$

$$I_{431}^* = I_{413}^*$$

$$I_{432}^* = I_{423}^*$$

$$I_{433}^* = I_{43} + m_4 (D_{41}^2 + D_{42}^2) + m_{44} (D_{441}^2 + D_{442}^2) + m_{45} (D_{451}^2 + D_{452}^2)$$

Body 5

$$I_{511}^* = I_{51} + m_5 (D_{52}^2 + D_{53}^2) + m_{55} (D_{552}^2 + D_{553}^2)$$

$$I_{512}^* = - \left[ m_5 D_{51} D_{52} + m_{55} D_{551} D_{552} \right]$$

$$I_{513}^* = - \left[ m_5 D_{51} D_{53} + m_{55} D_{551} D_{553} \right]$$

(A-76)

$$I_{521}^* = I_{512}^*$$



$$I_{522}^* = I_{52} + m_5 \left( D_{51}^2 + D_{53}^2 \right) + m_{55} \left( D_{551}^2 + D_{533}^2 \right)$$

$$I_{523}^* = - \left[ m_5 D_{52} D_{53} + m_{55} D_{552} D_{553} \right]$$

$$I_{531}^* = I_{513}^*$$

$$I_{532}^* = I_{523}^*$$

$$I_{533}^* = I_{53} + m_5 \left( D_{51}^2 + D_{52}^2 \right) + m_{35} \left( D_{551}^2 + D_{552}^2 \right)$$

(A-76)  
(cont)

Body 6

$$I_{611}^* = I_{61} + m_6 \left( D_{62}^2 + D_{63}^2 \right) + m_{62} \left( D_{622}^2 + D_{623}^2 \right)$$

$$I_{612}^* = - \left[ m_6 D_{61} D_{62} + m_{62} D_{621} D_{622} \right]$$

$$I_{613}^* = - \left[ m_6 D_{61} D_{63} + m_{62} D_{621} D_{623} \right]$$

(A-77)

$$I_{621}^* = I_{612}^*$$

$$I_{622}^* = I_{62} + m_6 \left( D_{61}^2 + D_{63}^2 \right) + m_{62} \left( D_{621}^2 + D_{623}^2 \right)$$

$$I_{623}^* = - \left[ m_6 D_{62} D_{63} + m_{62} D_{622} D_{623} \right]$$

$$I_{631}^* = I_{613}^*$$

$$I_{632}^* = I_{623}^*$$

$$I_{623}^* = I_{63} + m_6 \left( D_{61}^2 + D_{62}^2 \right) + m_{62} \left( D_{621}^2 + D_{622}^2 \right)$$

With the inertia dyadics  $\bar{\bar{I}}_\lambda^*$  defined, it is possible to evaluate the  $\bar{N}_\lambda$  vectors in Equation (A-29). Once again, to show the dependence on  $\dot{\omega}_6$  explicitly, we write:

$$\{N_{\lambda i}\} = [\mathcal{N}_\lambda] \{\dot{\omega}_{6i}\} + \{\mathcal{N}_\lambda^i\} \quad (\text{A-78})$$

where

$$N_{\lambda i} = \bar{N}_\lambda \cdot \bar{e}_{\lambda i} \quad (\text{A-79})$$

Before writing the  $[\mathcal{N}_\lambda]$  and  $\{\mathcal{N}_\lambda^i\}$  expressions, it is helpful to define a "cross product" matrix as follows: Consider two vectors  $\bar{A}$  and  $\bar{B}$  with components in a reference frame  $\lambda$  given by:

$$\begin{aligned} A_i &= \bar{A} \cdot \bar{e}_{\lambda i} \\ B_i &= \bar{B} \cdot \bar{e}_{\lambda i} \end{aligned} \quad (i = 1, 2, 3)$$

where the  $\bar{e}_{\lambda i}$  ( $i = 1, 2, 3$ ) are mutually perpendicular unit vectors. The cross product matrix associated with  $\bar{A}$  is denoted by  $[\hat{A}]$  and is given by

$$[\hat{A}] = \begin{bmatrix} 0 & -A_3 & A_2 \\ A_3 & 0 & -A_1 \\ -A_2 & A_1 & 0 \end{bmatrix} \quad (\text{A-80})$$

Now if a third vector  $\bar{C}$  is defined by

$$\bar{C} = \bar{A} \times \bar{B}$$

it follows that

$$\{C_i\} = [\hat{A}] \{B_i\}$$

where

$$C_i = \bar{C} \cdot \bar{e}_{\lambda i} \quad (i = 1, 2, 3)$$

Using the above convention along with Equations (A-29), (A-57), (A-71) and (A-78) we have

$$[\mathcal{N}_\lambda] = [I_\lambda^*] [W_\lambda] \quad (\lambda = 1, 2, \dots, 5) \quad (A-82)$$

$$\{\mathcal{N}_\lambda^i\} = [I_\lambda^*] [W_\lambda^i] + [\tilde{\omega}_\lambda] [I_\lambda^*] \{\omega_{\lambda i}\}, \quad (\lambda = 1, 2, \dots, 5) \quad (A-83)$$

and

$$[\mathcal{N}_6] = [I_6^*] \quad (A-84)$$

$$\{\mathcal{N}_6^i\} = [\tilde{\omega}_6] [I_6^*] \{\omega_{6i}\} \quad (A-85)$$

#### 4. The $\ddot{D}_{\lambda j}$ and $\bar{M}_\lambda$ Vectors

The  $\bar{M}_\lambda$  vectors in Equation (A-27) depend on the  $\ddot{D}_{\lambda j}$  which, in turn, depend on  $\dot{\omega}_6$  as seen from Equations (A-20) and (A-61). Because of this the  $\ddot{D}_{\lambda j}$  are written as

$$\{\ddot{D}_{\lambda j i}\} = [\mathcal{D}_{\lambda j}] \{\dot{\omega}_{6i}\} + \{\mathcal{D}'_{\lambda j}\}, \quad j \in J(\lambda), \quad (\lambda = 1, 2, \dots, 5) \quad (A-86)$$

where

$$\ddot{D}_{\lambda j i} = \ddot{D}_{\lambda j} \cdot \bar{e}_{\lambda i} \quad (i = 1, 2, 3) \quad (A-87)$$

Using the cross product matrix defined by Equations (A-80) and (A-81) and Equations (A-20) and (A-47), the  $[\mathcal{D}_{\lambda j}]$  and  $\{\mathcal{D}'_{\lambda j}\}$  can be written

$$[\mathcal{D}_{\lambda j}] = - [\tilde{D}_{\lambda j}] [W_\lambda] \quad j \in J(\lambda), \quad (\lambda = 1, 2, \dots, 5) \quad (A-88)$$

$$\{\mathcal{D}'_{\lambda j}\} = - \left[ \tilde{\mathcal{D}}_{\lambda j} \right] \{W'_\lambda\} + \left[ \tilde{\omega}_\lambda \right] \left[ \tilde{\omega}_\lambda \right] \{D_{\lambda j i}\} \quad j \in J(\lambda) \quad (\lambda = 1, 2, \dots, 5) \quad (\text{A-89})$$

and

$$[\mathcal{D}'_{62}] = - \left[ \tilde{\mathcal{D}}_{62} \right] \quad (\text{A-90})$$

$$\{\mathcal{D}'_{62}\} = \left[ \tilde{\omega}_6 \right] \left[ \tilde{\omega}_6 \right] \{D_{62 i}\} \quad (\text{A-91})$$

Having the  $\ddot{\mathcal{D}}_{\lambda j}$  in hand, the  $\bar{M}_\lambda$  vectors can be written as

$$\{M_{\lambda i}\} = [\mathcal{M}_\lambda] \{\dot{\omega}_{6i}\} + \{\mathcal{M}_\lambda\}, \quad (\lambda = 1, 2, \dots, 6) \quad (\text{A-92})$$

where

$$M_{\lambda i} = \bar{M}_\lambda \cdot \bar{e}_{\lambda i} \quad (i = 1, 2, 3) \quad (\text{A-93})$$

Combining Equations (A-27), (A-86) and (A-92) we arrive at

$$\begin{aligned} [\mathcal{M}_1] = & M \left[ \tilde{\mathcal{D}}_{11} \right] \left[ \left[ {}^3E^2 \right] [\mathcal{D}_{21}] + [\mathcal{D}_{33}] + \left[ {}^3E^4 \right] [\mathcal{D}_{44}] + \left[ {}^3E^5 \right] [\mathcal{D}_{55}] \right. \\ & \left. + \left[ {}^3E^6 \right] [\mathcal{D}_{62}] \right] \end{aligned} \quad (\text{A-94})$$

$$\begin{aligned} [\mathcal{M}_2] = & M \left[ \tilde{\mathcal{D}}_{21} \right] \left[ {}^2E^3 \right] [\mathcal{D}_{11}] + M \left[ \tilde{\mathcal{D}}_{23} \right] \left[ \left[ {}^2E^3 \right] [\mathcal{D}_{33}] + \left[ {}^2E^4 \right] [\mathcal{D}_{44}] \right. \\ & \left. + \left[ {}^2E^5 \right] [\mathcal{D}_{55}] \right] + M \left[ \tilde{\mathcal{D}}_{22} \right] \left[ {}^2E^6 \right] [\mathcal{D}_{62}] \end{aligned} \quad (\text{A-95})$$

$$\begin{aligned} [\mathcal{M}_3] = & M \left[ \tilde{\mathcal{D}}_{33} \right] \left[ [\mathcal{D}_{11}] + \left[ {}^3E^2 \right] [\mathcal{D}_{23}] + \left[ {}^3E^6 \right] [\mathcal{D}_{62}] \right] \\ & + M \left[ \tilde{\mathcal{D}}_{34} \right] \left[ \left[ {}^3E^4 \right] [\mathcal{D}_{44}] + \left[ {}^3E^5 \right] [\mathcal{D}_{55}] \right] \end{aligned} \quad (\text{A-96})$$

$$\begin{aligned}
[\mathcal{M}_4] = M[\overset{\sim}{D}_{44}] & \left[ \begin{bmatrix} 4_E^1 \end{bmatrix} [\mathcal{D}_{11}] + \begin{bmatrix} 4_E^2 \end{bmatrix} [\mathcal{D}_{23}] + \begin{bmatrix} 4_E^6 \end{bmatrix} [\mathcal{D}_{62}] \right. \\
& \left. + \begin{bmatrix} 4_E^3 \end{bmatrix} [\mathcal{D}_{34}] \right] + M[\overset{\sim}{D}_{45}] \begin{bmatrix} 4_E^5 \end{bmatrix} [\mathcal{D}_{55}]
\end{aligned} \tag{A-97}$$

$$\begin{aligned}
[\mathcal{M}_5] = M[\overset{\sim}{D}_{55}] & \left[ \begin{bmatrix} 5_E^1 \end{bmatrix} [\mathcal{D}_{11}] + \begin{bmatrix} 5_E^2 \end{bmatrix} [\mathcal{D}_{23}] + \begin{bmatrix} 5_E^6 \end{bmatrix} [\mathcal{D}_{62}] \right. \\
& \left. + \begin{bmatrix} 5_E^3 \end{bmatrix} [\mathcal{D}_{34}] + \begin{bmatrix} 5_E^4 \end{bmatrix} [\mathcal{D}_{45}] \right]
\end{aligned} \tag{A-98}$$

$$\begin{aligned}
[\mathcal{M}_6] = M[\overset{\sim}{D}_{62}] & \left[ \begin{bmatrix} 6_E^3 \end{bmatrix} [\mathcal{D}_{11}] + \begin{bmatrix} 6_E^2 \end{bmatrix} [\mathcal{D}_{22}] + \begin{bmatrix} 6_E^3 \end{bmatrix} [\mathcal{D}_{33}] \right. \\
& \left. + \begin{bmatrix} 6_E^4 \end{bmatrix} [\mathcal{D}_{44}] + \begin{bmatrix} 6_E^5 \end{bmatrix} [\mathcal{D}_{55}] \right]
\end{aligned} \tag{A-99}$$

The expressions for  $\{\mathcal{M}'_\lambda\}$  defined by Equation (A-92) are obtained from the  $[\mathcal{M}_\lambda]$  equations above simply by replacing the  $[D_{\lambda j}]$  matrices with  $\{D'_{\lambda j}\}$  matrices.

### 5. External Forces and Torques and the $\bar{L}$ Vectors

To evaluate the components of the  $\bar{L}_\lambda$  vectors in Equation (A-28), the external forces and torques,  $\bar{F}_\lambda$  and  $\bar{T}_\lambda$ , must be specified. The components of the external torque vector,  $\bar{T}_\lambda$ , are defined by

$$T_{\lambda i} = \bar{T}_\lambda \cdot \bar{e}_{\lambda i} \quad (i = 1, 2, 3) \tag{A-100}$$

The external force acting on body  $\lambda$ ,  $\bar{F}_\lambda$ , is written

$$\bar{F}_\lambda = \bar{F}_{\lambda g} + \bar{F}'_\lambda \quad (\lambda = 1, 2, \dots, 6) \tag{A-101}$$

where  $\bar{F}_{\lambda g}$  is the gravitational force and  $\bar{F}'_\lambda$  is any other external force acting on body  $\lambda$ . If the components of the  $\bar{F}_{\lambda g}$  are defined by

$$F_{\lambda gi} = \bar{F}_{\lambda g} \cdot \bar{e}_{\lambda i} \quad (i = 1, 2, 3) \tag{A-102}$$

and if the components of the gravitational acceleration vector,  $\bar{g}_R$ , in inertial space, are defined by

$$g_{Ri} = \bar{g}_R \cdot \bar{e}_{Ri} \quad (i = 1, 2, 3) \quad (A-103)$$

it follows that

$$\{F_{\lambda gi}\} = m_\lambda \left[ {}^\lambda E^R \right] \{g_{Ri}\}, \quad (\lambda = 1, 2, \dots, 6) \quad (A-104)$$

The components of  $\bar{F}'_\lambda$  are written

$$\bar{F}'_{\lambda i} = \bar{F}'_\lambda \cdot \bar{e}_{\lambda i} \quad (i = 1, 2, 3) \quad (A-105)$$

Finally, the components of the total external force vector acting on body  $\lambda$  is given by

$$\{F_{\lambda i}\} = \{F_{\lambda gi}\} + \{F'_{\lambda i}\} \quad (\lambda = 1, 2, \dots, 6) \quad (A-106)$$

where

$$F_{\lambda i} = \bar{F}_\lambda \cdot \bar{e}_{\lambda i} \quad (i = 1, 2, 3) \quad (A-107)$$

Thus, by specifying the  $T_{\lambda i}$ ,  $F'_{\lambda i}$ , and  $g_{Ri}$ , one is able to apply any set of external force and torques to each of the bodies as well as specify an arbitrary gravitational force (including zero).

By means of Equation (A-28), the components of the  $\bar{L}_\lambda$  vectors can be written in terms of  $F_{\lambda i}$  and  $T_{\lambda i}$  as follows:

$$\begin{aligned} \{L_{1i}\} &= \{T_{1i}\} + \left[ \begin{smallmatrix} \gamma \\ D \end{smallmatrix} \right]_1 \{F_{1i}\} + \left[ \begin{smallmatrix} \gamma \\ D \end{smallmatrix} \right]_{11} \left\{ \left[ {}^3 E^2 \right] \{F_{2i}\} + \{F_{3i}\} + \left[ {}^3 E^4 \right] \{F_{4i}\} \right. \\ &\quad \left. + \left[ {}^3 E^5 \right] \{F_{5i}\} + \left[ {}^3 E^6 \right] \{F_{6i}\} \right\} \end{aligned} \quad (A-108)$$

$$\begin{aligned} \{L_{2i}\} &= \{T_{2i}\} + \left[ \begin{smallmatrix} \gamma \\ D \end{smallmatrix} \right]_2 \{F_{2i}\} + \left[ \begin{smallmatrix} \gamma \\ D \end{smallmatrix} \right]_{21} \left[ {}^2 E^3 \right] \{F_{1i}\} + \left[ \begin{smallmatrix} \gamma \\ D \end{smallmatrix} \right]_{23} \left\{ \left[ {}^2 E^3 \right] \{F_{3i}\} \right. \\ &\quad \left. + \left[ {}^2 E^4 \right] \{F_{4i}\} + \left[ {}^3 E^5 \right] \{F_{5i}\} \right\} + \left[ \begin{smallmatrix} \gamma \\ D \end{smallmatrix} \right]_{22} \left[ {}^2 E^6 \right] \{F_{6i}\} \end{aligned} \quad (A-109)$$

$$\begin{aligned} \{L_{3i}\} &= \{T_{3i}\} + [\tilde{D}_3] \{F_{3i}\} + [\tilde{D}_{33}] \left\{ \{F_{1i}\} + [{}^3_E{}^2] \{F_{2i}\} \right. \\ &\quad \left. + [{}^3_E{}^6] \{F_{6i}\} \right\} + [\tilde{D}_{34}] \left\{ [{}^3_E{}^4] \{F_{4i}\} + [{}^3_E{}^5] \{F_{5i}\} \right\} \end{aligned} \quad (A-110)$$

$$\begin{aligned} \{L_{4i}\} &= \{T_{4i}\} + [\tilde{D}_4] \{F_{4i}\} + [\tilde{D}_{44}] \left\{ [{}^4_E{}^1] \{F_{1i}\} + [{}^4_E{}^2] \{F_{2i}\} \right. \\ &\quad \left. + [{}^4_E{}^3] \{F_{3i}\} + [{}^4_E{}^6] \{F_{6i}\} \right\} + [\tilde{D}_{45}] \{F_{5i}\} \end{aligned} \quad (A-111)$$

$$\begin{aligned} \{L_{5i}\} &= \{T_{5i}\} + [\tilde{D}_5] \{F_{5i}\} + [\tilde{D}_{55}] \left\{ [{}^5_E{}^1] \{F_{1i}\} + [{}^3_E{}^2] \{F_{2i}\} \right. \\ &\quad \left. + [{}^5_E{}^3] \{F_{3i}\} + [{}^5_E{}^4] \{F_{4i}\} + [{}^5_E{}^6] \{F_{6i}\} \right\} \end{aligned} \quad (A-112)$$

$$\begin{aligned} \{L_{6i}\} &= \{T_{6i}\} + [\tilde{D}_6] \{F_{6i}\} + [\tilde{D}_{62}] \left\{ [{}^6_E{}^3] \{F_{1i}\} + [{}^6_E{}^2] \{F_{2i}\} \right. \\ &\quad \left. + [{}^6_E{}^3] \{F_{3i}\} + [{}^6_E{}^4] \{F_{4i}\} + [{}^6_E{}^5] \{F_{5i}\} \right\} \end{aligned} \quad (A-113)$$

where

$$L_{\lambda i} = \bar{L}_\lambda \cdot \bar{e}_{\lambda i}, \quad (i = 1, 2, 3) \quad (A-114)$$

## 6. Joint Torques and the Differential Equations for $\bar{\omega}_6$

Having expressions for the components of the  $\bar{M}_\lambda$ ,  $\bar{L}_\lambda$ , and  $\bar{N}_\lambda$  vectors, it is now possible to evaluate the joint torques given by Equations (A-30) - (A-35). First the components of the joint torques are written

$$\{T_{\lambda j}^H\} = [\tau_{\lambda j}] \{\dot{\omega}_{6i}\} + \{\tau'_{\lambda j}\} \quad j \in J(\lambda), \quad (\lambda = 1, 2, \dots, 6) \quad (A-115)$$

where

$$T_{\lambda j i}^H = \bar{T}_{\lambda j}^H \cdot \bar{e}_{\lambda i} \quad (i = 1, 2, 3) \quad (\text{A-116})$$

and using Equations (A-30) - (A-34), (A-78), (A-92), and (A-114), the  $\tau_{\lambda j}$  and  $\tau'_{\lambda j}$  can be written:

$$[\tau_{11}] = [\mathcal{N}_1] - [\mathcal{M}_1] \quad (\text{A-117})$$

$$\{\tau'_{11}\} = \{\mathcal{N}'_1\} - \{L_{11}\} - \{\mathcal{M}'_1\} \quad (\text{A-118})$$

$$[\tau_{55}] = [\mathcal{N}_5] - [\mathcal{M}_5] \quad (\text{A-119})$$

$$\{\tau'_{55}\} = \{\mathcal{N}'_5\} - \{L_{51}\} - \{\mathcal{M}'_5\} \quad (\text{A-120})$$

$$[\tau_{45}] = - [{}^4_E{}^5] [\tau_{55}] \quad (\text{A-121})$$

$$\{\tau'_{45}\} = - [{}^4_E{}^5] \{\tau'_{55}\} \quad (\text{A-122})$$

$$[\tau_{44}] = [\mathcal{N}_4] - [\mathcal{M}_4] - [\tau_{45}] \quad (\text{A-123})$$

$$\{\tau_{44}\} = \{\mathcal{N}'_4\} - \{L_{41}\} - \{\mathcal{M}'_4\} - \{\tau'_{45}\} \quad (\text{A-124})$$

$$[\tau_{33}] = [\mathcal{N}_3] - [\mathcal{M}_3] - [\tau_{34}] \quad (\text{A-125})$$

$$\{\tau'_{33}\} = \{\mathcal{N}'_3\} - \{L_{31}\} - \{\mathcal{M}'_3\} - \{\tau'_{34}\} \quad (\text{A-126})$$

$$[\tau_{21}] = [{}^2_E{}^3] [\tau_{11}] \quad (\text{A-127})$$

$$\{\tau'_{21}\} = - [{}^2_E{}^3] \{\tau'_{11}\} \quad (\text{A-128})$$



$$\begin{bmatrix} \tau_{23} \end{bmatrix} = - \begin{bmatrix} 2_E^3 \end{bmatrix} \begin{bmatrix} \tau_{33} \end{bmatrix} \quad (\text{A-129})$$

$$\left\{ \tau'_{23} \right\} = - \begin{bmatrix} 2_E^3 \end{bmatrix} \left\{ \tau'_{33} \right\} \quad (\text{A-130})$$

$$\begin{bmatrix} \tau_{22} \end{bmatrix} = \begin{bmatrix} \mathcal{N}_2 \end{bmatrix} - \begin{bmatrix} \mathcal{M}_2 \end{bmatrix} - \begin{bmatrix} \tau_{21} \end{bmatrix} - \begin{bmatrix} \tau_{23} \end{bmatrix} \quad (\text{A-131})$$

$$\left\{ \tau'_{22} \right\} = \left\{ \mathcal{N}'_2 \right\} - \left\{ \mathcal{L}_{2i} \right\} - \left\{ \mathcal{M}'_2 \right\} - \left\{ \tau'_{21} \right\} - \left\{ \tau'_{23} \right\} \quad (\text{A-132})$$

$$\begin{bmatrix} \tau_{62} \end{bmatrix} = - \begin{bmatrix} 6_E^2 \end{bmatrix} \begin{bmatrix} \tau_{22} \end{bmatrix} \quad (\text{A-133})$$

$$\left\{ \tau'_{62} \right\} = - \begin{bmatrix} 6_E^2 \end{bmatrix} \left\{ \tau'_{22} \right\} \quad (\text{A-134})$$

The differential equation (A-35) for  $\bar{\omega}_6$  can now be written as follows:

$$\begin{bmatrix} W_6 \end{bmatrix} \left\{ \dot{\omega}_{6i} \right\} - \left\{ W'_6 \right\} = 0 \quad (\text{A-135})$$

where

$$\dot{\omega}_{6i} = \dot{\bar{\omega}}_6 \cdot \bar{e}_{6i} \quad (i = 1, 2, 3) \quad (\text{A-136})$$

and

$$\begin{bmatrix} W_6 \end{bmatrix} = \begin{bmatrix} \mathcal{N}_6 \end{bmatrix} - \begin{bmatrix} \mathcal{M}_6 \end{bmatrix} - \begin{bmatrix} \tau_{62} \end{bmatrix} \quad (\text{A-137})$$

$$\left\{ W'_6 \right\} = \left\{ \mathcal{L}_{6i} \right\} + \left\{ \mathcal{M}'_6 \right\} + \left\{ \tau'_{62} \right\} - \left\{ \mathcal{N}'_6 \right\} \quad (\text{A-138})$$

Finally, solving (A-135) for  $\dot{\omega}_{6i}$ ,

$$\left\{ \dot{\omega}_{6i} \right\} = \begin{bmatrix} W_6 \end{bmatrix}^{-1} \left\{ W'_6 \right\} \quad (\text{A-139})$$

which is the desired form for numerical integration.

Now, once the  $\omega_{6i}$  are obtained by integration of Equation (A-139), the Euler angles,  $\theta_{6i}$ , can be determined by integrating Equation (A-48) as follows:

$$\left\{ \dot{\theta}_{6i} \right\} = \left[ R_6 \right]^{-1} \left\{ \omega_{6i} \right\} \quad (\text{A-140})$$

which completes the determination of the rotational motion of body 6.

Finally, the joint torques,  $\bar{T}_{\lambda j}^H$ , are now easily obtained by substitution of the  $\omega_{6i}$  and  $\dot{\omega}_{6i}$  into Equation (A-43).

#### 7. Joint Forces

The forces of interaction at the joints,  $\bar{F}_{\lambda j}^H$ , can now be determined in the following way: First, the  $\ddot{\bar{D}}_{\lambda j}$  vectors are determined from Equation (A-86). Then from the definition of the barrycenter vectors  $\bar{D}_{\lambda}$  and  $\bar{D}_{\lambda\mu}$  we can write

$$m_{\mu} \bar{D}_{\mu} + \sum_{v \neq \mu} m_v \bar{D}_{\mu K_{\mu}(v)} = \bar{0} \quad (\text{A-141})$$

or

$$\ddot{\bar{D}}_{\mu} = - \frac{1}{m_{\mu}} \sum_{v \neq \mu} m_v \ddot{\bar{D}}_{\mu K_{\mu}(v)} \quad (\text{A-142})$$

which enables one to determine the  $\ddot{\bar{D}}_{\lambda}$  from the  $\ddot{\bar{D}}_{\lambda j}$ . At this point, the  $\ddot{\rho}_{\mu} - \ddot{\rho}$  accelerations can be determined from Equation (A-18); they are

$$\left\{ \ddot{\rho}_{R1i} \right\} = - \frac{m_{11}}{m_1} \left\{ \ddot{D}_{11i} \right\} + \left[ {}^3E^2 \right] \left\{ \ddot{D}_{21i} \right\} + \left\{ \ddot{D}_{33i} \right\} + \left[ {}^3E^4 \right] \left\{ \ddot{D}_{44i} \right\} \\ \left[ {}^3E^5 \right] \left\{ \ddot{D}_{55i} \right\} + \left[ {}^3E^6 \right] \left\{ \ddot{D}_{62i} \right\} \quad (\text{A-143})$$

$$\begin{aligned} \left\{ \ddot{\rho}_{R2i} \right\} = & \frac{m_{21}}{m_2} \left\{ \ddot{D}_{21i} \right\} - \frac{m_{22}}{m_2} \left\{ \ddot{D}_{22i} \right\} - \frac{m_{23}}{m_2} \left\{ \ddot{D}_{23i} \right\} + \left[ {}^2_E 3 \right] \left\{ \ddot{D}_{11i} \right\} \\ & + \left[ {}^2_E 3 \right] \left\{ \ddot{D}_{33i} \right\} + \left[ {}^2_E 6 \right] \left\{ \ddot{D}_{62i} \right\} + \left[ {}^2_E 4 \right] \left\{ \ddot{D}_{44i} \right\} + \left[ {}^2_E 5 \right] \left\{ \ddot{D}_{55i} \right\} \end{aligned} \quad (A-144)$$

$$\begin{aligned} \left\{ \ddot{\rho}_{R3i} \right\} = & - \frac{m_{33}}{m_3} \left\{ \ddot{D}_{33i} \right\} - \frac{m_{24}}{m_3} \left\{ \ddot{D}_{34i} \right\} + \left\{ \ddot{D}_{11i} \right\} + \left[ {}^3_E 6 \right] \left\{ \ddot{D}_{62i} \right\} \\ & + \left[ {}^3_E 2 \right] \left\{ \ddot{D}_{23i} \right\} + \left[ {}^3_E 4 \right] \left\{ \ddot{D}_{44i} \right\} + \left[ {}^3_E 5 \right] \left\{ \ddot{D}_{55i} \right\} \end{aligned} \quad (A-145)$$

$$\begin{aligned} \left\{ \ddot{\rho}_{R4i} \right\} = & - \frac{m_{44}}{m_4} \left\{ \ddot{D}_{44i} \right\} - \frac{m_{45}}{m_4} \left\{ \ddot{D}_{45i} \right\} + \left[ {}^4_E 3 \right] \left\{ \ddot{D}_{11i} \right\} + \left[ {}^4_E 2 \right] \left\{ \ddot{D}_{23i} \right\} \\ & + \left[ {}^4_E 3 \right] \left\{ \ddot{D}_{34i} \right\} + \left[ {}^4_E 5 \right] \left\{ \ddot{D}_{55i} \right\} + \left[ {}^4_E 6 \right] \left\{ \ddot{D}_{62i} \right\} \end{aligned} \quad (A-146)$$

$$\begin{aligned} \left\{ \ddot{\rho}_{R5i} \right\} = & - \frac{m_{55}}{m_5} \left\{ \ddot{D}_{55i} \right\} + \left[ {}^5_E 3 \right] \left\{ \ddot{D}_{11i} \right\} + \left[ {}^5_E 2 \right] \left\{ \ddot{D}_{23i} \right\} + \left[ {}^5_E 6 \right] \left\{ \ddot{D}_{62i} \right\} \\ & + \left[ {}^5_E 3 \right] \left\{ \ddot{D}_{34i} \right\} + \left[ {}^5_E 4 \right] \left\{ \ddot{D}_{45i} \right\} \end{aligned} \quad (A-147)$$

$$\begin{aligned} \left\{ \ddot{\rho}_{R6i} \right\} = & - \frac{m_{62}}{m_6} \left\{ \ddot{D}_{62i} \right\} + \left[ {}^6_E 3 \right] \left\{ \ddot{D}_{11i} + \ddot{D}_{33i} \right\} + \left[ {}^6_E 2 \right] \left\{ \ddot{D}_{22i} \right\} \\ & + \left[ {}^6_E 4 \right] \left\{ \ddot{D}_{44i} \right\} + \left[ {}^6_R 5 \right] \left\{ \ddot{D}_{55i} \right\} \end{aligned} \quad (A-148)$$

where

$$\ddot{\rho}_{R\lambda i} = \left( \ddot{\rho}_{\lambda} - \ddot{\rho} \right) \cdot \bar{e}_{\lambda i} \quad (i = 1, 2, 3; \lambda = 1, 2, \dots, 6) \quad (A-149)$$

Finally, by expanding Equation (A-17) we have for the hinge interaction forces

$$\begin{aligned} \{F_{11i}^H\} &= \frac{m_1}{M} \{F_{T3i}\} - \{F_{1i}\} - m_2 \begin{bmatrix} 3_E^2 \end{bmatrix} \{\ddot{\rho}_{R2i}\} - m_3 \{\ddot{\rho}_{R3i}\} \\ &\quad - m_4 \begin{bmatrix} 3_E^4 \end{bmatrix} \{\ddot{\rho}_{R4i}\} - m_5 \begin{bmatrix} 3_E^5 \end{bmatrix} \{\ddot{\rho}_{R5i}\} - m_6 \begin{bmatrix} 3_E^6 \end{bmatrix} \{\ddot{\rho}_{R6i}\} \end{aligned} \quad (A-150)$$

$$\{F_{21i}^H\} = - \begin{bmatrix} 2_E^3 \end{bmatrix} \{F_{11i}^H\} \quad (A-151)$$

$$\begin{aligned} \{F_{62i}^H\} &= \frac{m_6}{M} \begin{bmatrix} 6_E^3 \end{bmatrix} \{F_{T3i}\} - \{F_{3i}\} - \begin{bmatrix} 6_E^3 \end{bmatrix} \{m_1 \ddot{\rho}_{R1i} + m_3 \ddot{\rho}_{R3i}\} \\ &\quad - m_2 \begin{bmatrix} 6_E^2 \end{bmatrix} \{\ddot{\rho}_{R2i}\} - m_4 \begin{bmatrix} 6_E^4 \end{bmatrix} \{\ddot{\rho}_{R4i}\} - m_5 \begin{bmatrix} 6_E^5 \end{bmatrix} \{\ddot{\rho}_{R5i}\} \end{aligned} \quad (A-152)$$

$$\{F_{22i}^H\} = - \begin{bmatrix} 2_E^6 \end{bmatrix} \{F_{62i}^H\} \quad (A-153)$$

$$\begin{aligned} \{F_{55i}^H\} &= \frac{m_5}{M} \begin{bmatrix} 5_E^3 \end{bmatrix} \{F_{T3i}\} - \{F_{5i}\} - \begin{bmatrix} 5_E^3 \end{bmatrix} \{m_1 \ddot{\rho}_{R1i} + m_3 \ddot{\rho}_{R3i}\} \\ &\quad - m_2 \begin{bmatrix} 5_E^2 \end{bmatrix} \{\ddot{\rho}_{R2i}\} - m_4 \begin{bmatrix} 5_E^4 \end{bmatrix} \{\ddot{\rho}_{R4i}\} - m_6 \begin{bmatrix} 5_E^6 \end{bmatrix} \{\ddot{\rho}_{R6i}\} \end{aligned} \quad (A-154)$$

$$\{F_{45i}^H\} = - \begin{bmatrix} 4_E^5 \end{bmatrix} \{F_{55i}^H\} \quad (A-155)$$

$$\begin{aligned} \{F_{44i}^H\} &= \frac{m_4 + m_5}{M} \begin{bmatrix} 4_E^3 \end{bmatrix} \{F_{T3i}\} - \{F_{4i}\} - \begin{bmatrix} 4_E^5 \end{bmatrix} \{F_{5i}\} \\ &\quad - \begin{bmatrix} 4_E^3 \end{bmatrix} \{m_1 \ddot{\rho}_{R1i} + m_3 \ddot{\rho}_{R3i}\} - m_2 \begin{bmatrix} 4_E^2 \end{bmatrix} \{\ddot{\rho}_{R2i}\} \\ &\quad - m_6 \begin{bmatrix} 4_E^6 \end{bmatrix} \{\ddot{\rho}_{R6i}\} \end{aligned} \quad (A-156)$$

$$\{F_{34i}^H\} = - \begin{bmatrix} 3_E^4 \end{bmatrix} \{F_{44i}^H\} \quad (A-157)$$

$$\begin{aligned} \{F_{33i}^H\} = & \left( \frac{m_3 + m_4 + m_5}{M} \right) \{F_{T3i}\} - \{F_{3i}\} - \begin{bmatrix} 3_E^4 \end{bmatrix} \{F_{4i}\} - \begin{bmatrix} 3_E^5 \end{bmatrix} \{F_{5i}\} \\ & - m_1 \{\ddot{\rho}_{R1i}\} - m_2 \begin{bmatrix} 3_E^2 \end{bmatrix} \{\ddot{\rho}_{R2i}\} - m_6 \begin{bmatrix} 3_E^6 \end{bmatrix} \{\ddot{\rho}_{R6i}\} \end{aligned} \quad (A-158)$$

$$\{F_{23i}^H\} = - \begin{bmatrix} 2_E^3 \end{bmatrix} \{F_{33i}^H\} \quad (A-159)$$

where

$$F_{\lambda ji}^H = \bar{F}_{\lambda j}^H \cdot \bar{e}_{\lambda i} \quad (i = 1, 2, 3) \quad (A-160)$$

and

$$F_{T3i} = \left( \sum_{\lambda=1}^6 \bar{F}_{\lambda} \right) \cdot \bar{e}_{3i} \quad (i = 1, 2, 3) \quad (A-161)$$

## 8. Motor Torques

Torque motors are assumed to drive the various gimbals at Joints 2, 3 and 4. The motor torques to produce the specified motion are determined by projecting the appropriate hinge interaction torques along the motor axes. The results are:

### Joint 2

(Pitch Motor Torque,  $M_{21}$ )

$$M_{21} = \frac{C_{21} T_{222}^H = S_{21} T_{223}^H}{C_{23}} \quad (A-162)$$

(Yaw Motor Torque,  $M_{22}$ )

$$M_{22} = S_{21} T_{222}^H + C_{21} T_{223}^H \quad (A-163)$$

(Roll Motor Torque,  $M_{23}$ )

$$M_{23} = T_{221}^H - S_{23}M_{-1} \quad (A-164)$$

### Joint 3

The motor at Joint 3 must drive the pitch motion of both bodies 1 and 3 and hence the required pitch motor torque is

$$M_{33} = T_{333}^H + T_{113}^H \quad (A-165)$$

### Joint 4

(Yaw Motor Torque,  $M_{41}$ )

$$M_{41} = \left( T_{442}^H S_{41} + T_{443}^H C_{41} \right) / C_{42} \quad (A-166)$$

(Pitch Motor Torque,  $M_{42}$ )

$$M_{42} = T_{442}^H C_{41} - T_{443}^H S_{41} \quad (A-167)$$

(Roll Motor Torque,  $M_{43}$ )

$$M_{43} = T_{441}^H + M_{41}S_{42} \quad (A-168)$$

Equations (A-162) - (A-164) and (A-166) - (A-168) for joints 2 and 4 are valid only in the absence of external forces and torques. When such influences are present, it is necessary to identify that portion of the  $\bar{T}_{\lambda j}^H$  due to external forces and torques and that portion necessitated by inertia forces (the motion). To this end, we define  $\bar{T}_{\lambda j E}^H$  as that part of  $\bar{T}_{\lambda j}^H$  due to external forces and torques and  $\bar{T}_{\lambda j I}^H$  as that part of  $\bar{T}_{\lambda j}^H$  due to inertia forces. It follows that

$$\bar{T}_{\lambda j I}^H = \bar{T}_{\lambda j}^H - \bar{T}_{\lambda j E}^H \quad (A-169)$$

Now it can be seen from Equations (A-27) - (A-35) that the contribution of external forces and torques to the  $\bar{T}_{\lambda j}^H$  is contained in the  $\bar{L}_{\lambda}$  vectors only. It therefore follows from Equations (A-30) - (A-35) that

$$\bar{T}_{11E}^H = - \bar{L}_1 \quad (A-170)$$

$$\bar{T}_{55E}^H = - \bar{L}_5 \quad (A-171)$$

$$\bar{T}_{44E}^H = - \bar{L}_4 + \bar{T}_{55E}^H \quad (A-172)$$

$$\bar{T}_{33E}^H = - \bar{L}_3 + \bar{T}_{44E}^H \quad (A-173)$$

$$\bar{T}_{22E}^H = - \bar{L}_2 + \bar{T}_{11E}^H + \bar{T}_{33E}^H \quad (A-174)$$

Equation (A-169) can now be used to determine the  $\bar{T}_{\lambda j I}^H$ . We now define

$$T_{\lambda j E i}^H = \bar{T}_{\lambda j E}^H \cdot \bar{e}_{\lambda i} \quad (i = 1, 2, 3) \quad (A-175)$$

$$T_{\lambda j I i}^H = \bar{T}_{\lambda j I}^H \cdot \bar{e}_{\lambda i} \quad (i = 1, 2, 3) \quad (A-176)$$

Now, for the three gimbal joints (joints 2 and 4), only that component of  $\bar{T}_{\lambda j E}^H$  which is parallel to a particular gimbal axis at joint  $j$  contributes to the motor torque associated with that gimbal axis. The remaining two components are absorbed as constraint torques. On the other hand the entire  $\bar{T}_{\lambda j I}^H$  vector must be produced by the torque motors at a three gimbal hinge  $j$ . This requirement results in equations like (A-162) - (A-164) and (A-166) - (A-168) with the  $T_{\lambda j i}^H$  replaced by  $T_{\lambda j I i}^H$ .

Thus when external forces are present, the motor torque equations for joints 2 and 4 become

$$M_{21} = T_{62E1}^H + \frac{C_{21}T_{22I2}^H - S_{21}T_{22I3}^H}{C_{23}} \quad (A-177)$$

$$M_{22} = S_{21}T_{222}^H + C_{21}T_{223}^H \quad (A-178)$$

$$M_{23} = T_{22E1}^H + T_{22I1}^H - S_{23} \left( M_{21} - T_{62E1}^H \right) \quad (A-179)$$

$$M_{41} = T_{34E3}^H + \frac{S_{41}T_{44I2}^H + C_{41}T_{44I3}^H}{C_{42}} \quad (A-180)$$

$$M_{42} = C_{41}T_{442}^H - S_{41}T_{443}^H \quad (A-181)$$

$$M_{43} = T_{44E1}^H + T_{44I1}^H + S_{42} \left( M_{41} - T_{34E3}^H \right) \quad (A-182)$$

#### E. REFERENCES

1. W. Hooker & G. Margulies: "The Dynamical Attitude Equations for an N-Body Satellite." Journal of Astronautical Sciences, Vol. XII, No. 4, pp 123 - 128, Winter, 1965.



## APPENDIX B - 7-DOF JOINT ORDERING CONTROLLER BREADBOARD

A mechanism was devised which allowed examination of various control device configurations of a 6-DOF bilateral, non-counterbalance, geometrically similar master controller. The configurations were evaluated for joint ordering segment lengths, joint travel and overall configuration.

This section presents the configuration and design of a joint ordering controller; next it is shown how the erector set type joints were first used as a slave manipulator; and then finally the apparatus was reconfigured as a controller. Incidentally, another variation resulted which required some modification of the basics by addition of a vertical translation mode. This final scheme was then converted into a recommended final floor mounted 6-DOF controller.

### 1. Requirements for Breadboards

The following lists the guidelines for this test tool.

- (1) Device to represent full scale controller with some telescoping capability for length extensions.  
Lengths to be compatible with SAMS control area.
- (2) Device to have a minimum of six joints, each of which represents an approximate length required for a force feedback servomechanism.
- (3) Device to sense position (angular) only for each joint.
- (4) Joints to be interchangeable to allow any order of yaw, pitch, roll, etc.
- (5) Locking or braking was provided to either lock out any joint or represent a frictional drag.
- (6) Device to use light weight aluminum material where feasible, ball bearing joints, yoke design, common flange mounts.

### 2. Design of the Joint Ordering Test Mechanism

It was decided to provide seven degrees of freedom (i.e., 7 joints) for utmost versatility. Drawing RES3156200,

shows these joints assembled. There are four identical yaw or pitch joints. Assembly Drawing RES3156201, and three identical roll joints assembly Drawing RES3156202. RES 3156200 installment drawing shows these joints in the following order starting from the handle:

- (1) Wrist Roll Control (using pitch type yoke joint)
- (2) Wrist Pitch Control (using pitch type yoke joint)
- (3) Wrist Yaw Control (using rotary type joint)
- (4) Elbow (using rotary type joint)
- (5) Shoulder Yaw (using rotary type joint)
- (6) Shoulder Pitch (using pitch type joint)
- (7) Shoulder Roll (using pitch type joint)

Sum = 4 pitch type yoke joints +  
3 rotary type joints.

Telescoping is provided as shown, from 4 1/8 to 8 inches on 2 segments.

All flanges have the same bolt circles and by orienting two pitch hinge assemblies 90° apart they become a pitch-yaw, etc.

One half inch plastic, single stage, continuous, infinite resolution potentiometers are used throughout and are easily indexed.

Braking on the roll joints is provided by a brake shoe (oilite bearing) which is clamped by 3 equispaced locking screws on the housing circumference.

Braking on the pitch hinges is provided by split ring collars using an adjustment screw to increase shaft friction.

Prior to design joint motors and gearing were investigated so that the breadboard joint sizes could be representative of actual joint sizes.

### 3. Joint Ordering Breadboard Mechanism as a Slave Manipulator

As soon as the mechanism parts were completed and the joints were assembled it was decided to use the mechanism, first as a manipulator model for evaluating cargo deployment. See Section II B&C. Figure B-1 shows the first assembly using the first telescoping tubes. These tubes were extended to represent a scaled slave arm. Naturally the control handle was not used.

### 4. Joint Ordering Breadboard Mechanism as a Master Controller

Upon completion of the manipulator joint angle and reach study the parts were reassembled in the form of Dwg. RES 3156200 with the handle added and was used to evaluate the order of joints has a master controller. Figure B-2 shows one position that the controller was evaluated.

### 5. Modified 6-DOF Bilateral Controller Breadboard (Final Version)

Evaluation of the controllers described previously led to the modified arrangement as discussed here. The controller was mounted on the floor rather than on the control console or armrest. This produced the joint order as follows:

#### Handle

- Wrist roll
- Wrist pitch
- Wrist yaw
- Vertical elbow translation
- Shoulder yaw
- Shoulder pitch

The advantages and evaluation of this design are discussed in section V.

This section discusses the design and hardware aspect of this controller. Figure B-3 shows the breadboard. The "shoulder" joints are at floor level. Dual rods offered a simple method for producing linear bearing support which is nonrotatable. A crossplate containing linear bushings, the translational rod and a gear rack are capable of being extended approximately 15 inches. The rack is used to drive a pinion upon whose shaft another 1/2 inch (10 turn) potentiometer is attached. This is used to read translational position. All joints excepting the translational are the same ones used in

the original joint ordering breadboard, except they are assembled in a different order with revised bracketry. The handle has been repositioned from that described in the 6-DOF Bilateral Force Feedback controller, in that the three axis intercept is at the center of the hand rather than at the operator's wrist pivot point.

For this configuration joint scaling is no longer completely valid. Those joints at the floor must be capable of larger torques because of the longer total arm length. However, for preliminary studies the breadboard, with its potentiometers at each joint, provide a useful evaluation tool.

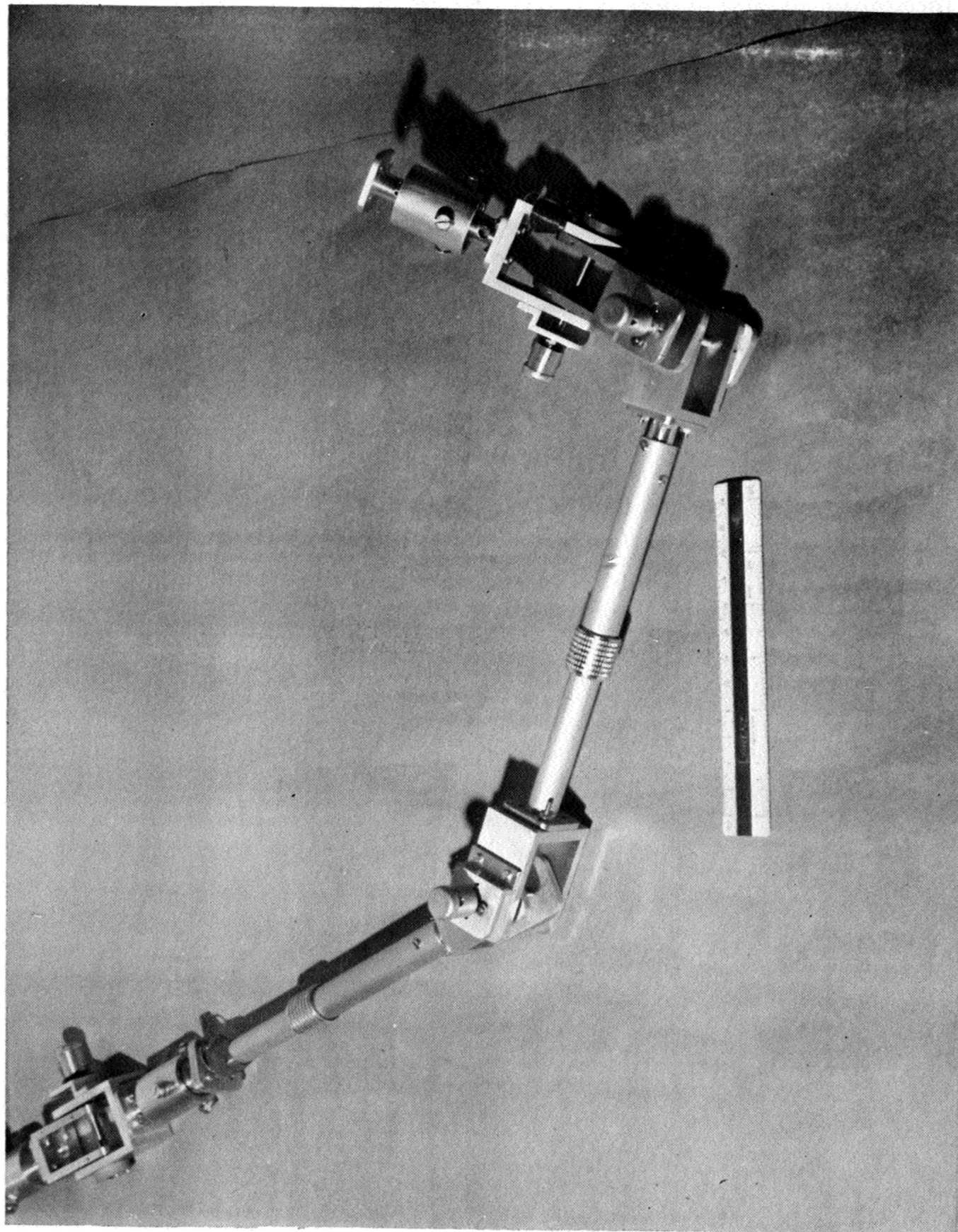


Figure B-1 Joint Ordering Mechanism

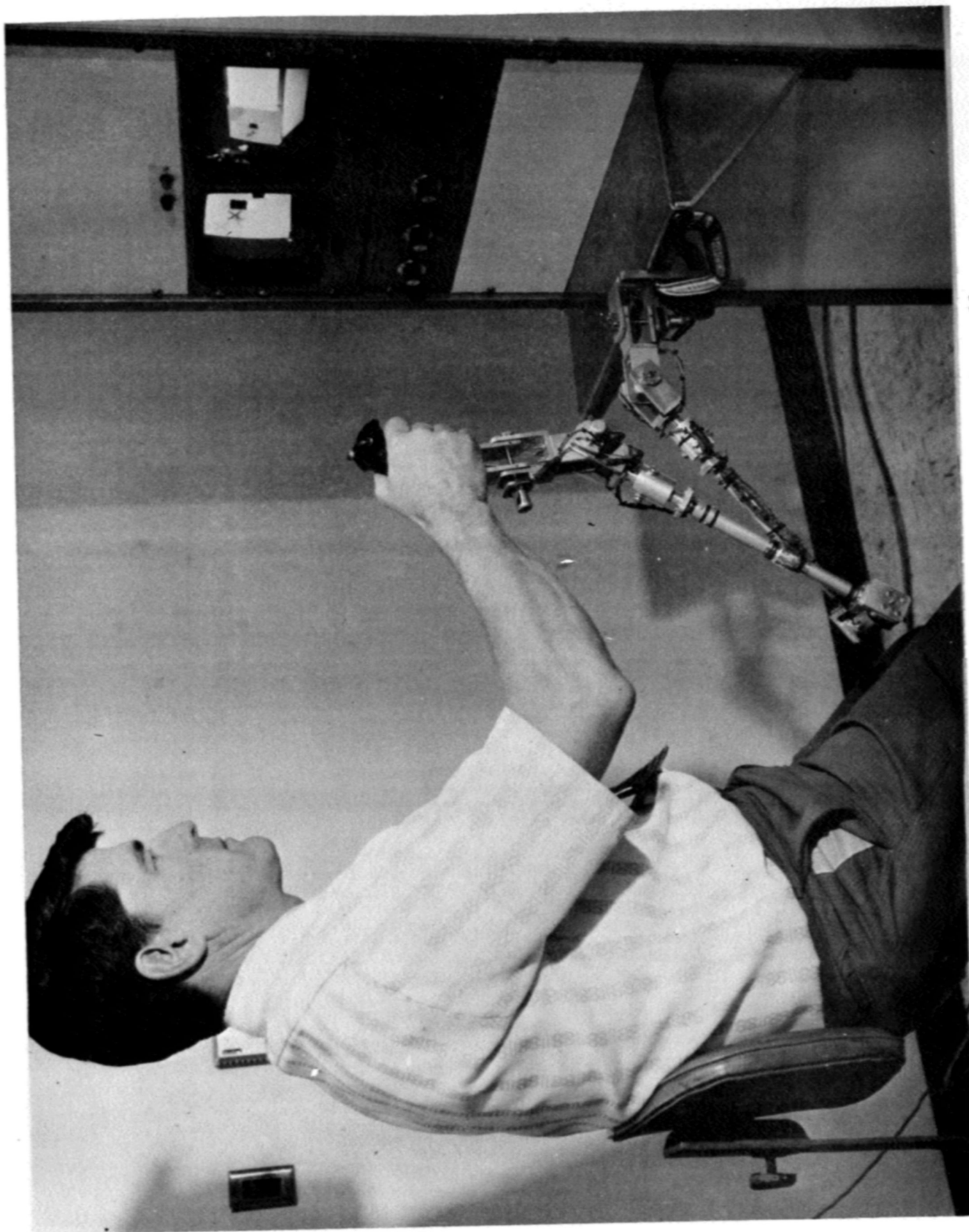


Figure B-2 Joint Ordering Mechanism as a Master Controller



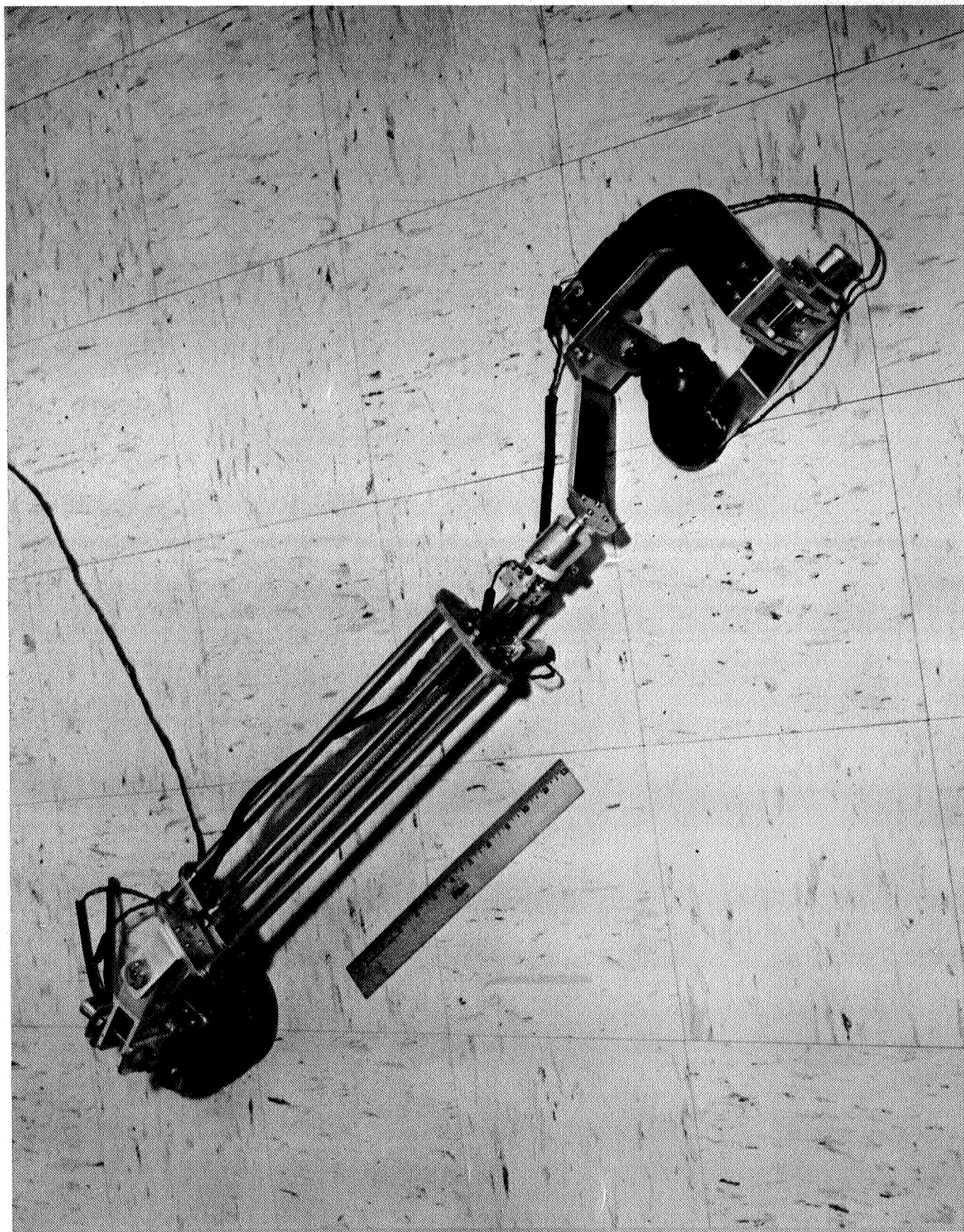


Figure B-3 Telescoping 6 DOF Controller (Modified from  
6 DOF Joint Ordering Mechanism)

## APPENDIX C. VIDEO SYNTHESIZER

In order to evaluate various master controller configurations without involvement of the moving base simulator, a general purpose Video Synthesizer (VS) was constructed. The VS provides a display of 4 dots and 2 crosshairs which are displaced from the center of the screen (0, 0, 0 position) by dc command voltages. The VS may be configured to provide any of the following presentation modes:

1. Planar
  - a. Monochrome
  - b. Color
2. Stereo
  - a. Dual monitor (Fresnel, lenticular, etc.)
    - 1) Monochrome
    - 2) Color
  - b. Single monitor--split screen
    - 1) Monochrome
    - 2) Color
  - c. Single monitor--color separation

In the simulation system, one dot represented the target; the other two dots are used to show end effector translational position; the crosshair represented the end effector orientation (pitch and yaw) and was considered pointing at the target when the crosshairs and the target dot were coincident.

The VS was first used in the dual monitor stereo mode. This mode, however, proved unsatisfactory from a human factors standpoint. It was found difficult to converge on spots of light in different planes. An alternative method based upon a color depth indication was devised.



The target in this configuration was represented by a single blue dot on a color monitor. The end effector position was represented by a white cross. The end effector translation was represented by two dots -- one red and one green -- the horizontal separation of which represented the distance from the depth plane of the target. When the manipulator end effector was closer to the "camera" than the target the green dot was to the left of the red dot as in Figure C-1a. As the end effector moved out, the green and red dots would move closer together until, as in Figure C-1b, the dots would merge into a single yellow dot when the end effector and target were in the same depth plane. If the end effector were moved farther out, the two dots would reappear; this time the red dot would be to the left of the green as in Figure C-1c. Thus, the necessary depth information was displayed without the convergence difficulties encountered using stereo. This method was used for the controller evaluations.

Figure-C-2 is the VS block diagram. The inputs are analog voltages from a computer. The generation of the crosshair is the simplest. The X command for the crosshair to be seen by the left eye is  $X_L^C$ . When the input from the Horizontal Sweep Generator is more negative than  $X_L^C$  the Comparator output is zero. The Horizontal Sweep Generator produces a linear sawtooth which starts at -10 volts and sweeps in a positive direction to +10 volts. This process is repeated 15,750 times per second. Each sweep corresponds to one horizontal line on the face of the monitors. Assume  $X_L^C = 5.0$  volts. As soon as the output of the Horizontal Sweep Generator becomes more positive than 5.0 volts the Comparator output goes high and triggers the Pulse Generator. The pulse produced causes a white spot to appear on the otherwise dark monitor screen. Since this process occurs once during each horizontal line, at the same X displacement on each line, the result is a white vertical line on the screen.

Now let us see how the horizontal line of the crosshair is developed. A similar comparison is used to determine the Y component of the crosshair. The Vertical Sweep Generator produces the same kind of -10 volt to +10 volt sawtooth except that it occurs 60 times per second and corresponds to the monitor vertical scan. As soon as the sweep voltage goes positive with respect to the  $Y^C$  command the Comparator switches from zero to high. However, the Gate holds the Comparator output from triggering the Pulse Generator until the beginning of the

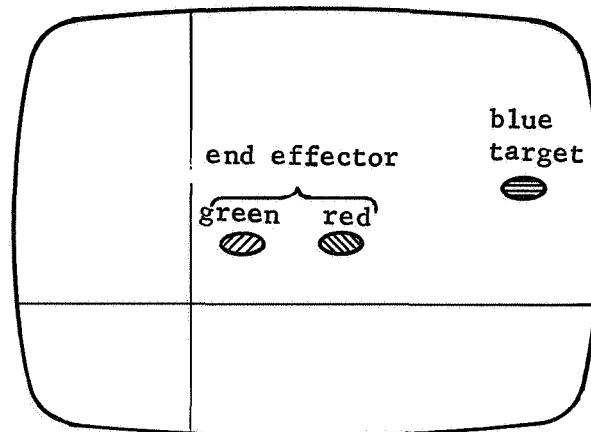
next horizontal scan line, to avoid a scan line which is partially black, partially white. During the horizontal blanking interval the Gate opens and triggers the Pulse Generator. The pulse duration allows one scan line to appear white -- the horizontal portion of the crosshair.

The dot generation is similar except that the output of the Y Pulse Generator is used to gate the X pulses. For example, the  $X_L^T$  Comparator will produce an output during each horizontal line. However, it does not trigger a pulse because the Gate is held closed by the output of the  $Y^T$  Pulse Generator. When the  $Y^T$  Comparator goes high and the next horizontal line begins, the  $X_L^T$  Gate opens and allows the  $X_L^T$  Comparator output to trigger the Pulse Generator and produce a dot on the monitor screen. At the end of that horizontal line the  $Y^T$  goes back to zero and closes the  $X_L^T$  gate. Thus only one dot appears on the screen rather than a whole sequence as in the case of the crosshair.

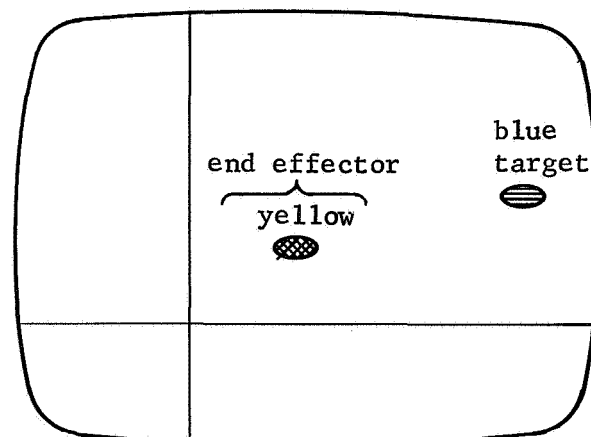
Timing for the Horizontal and Vertical Sweep Generators is provided by the crystal-controlled Sync Generator. A synchronizing signal which becomes part of the composite video is sent from the Sync Generator to the Output Summing Amplifiers.

The Output Summing Amplifiers are an array of 12 video amplifiers with an input matrix which provides the proper combination of signals -- including sync -- at the output. All the outputs can be used simultaneously or separately.

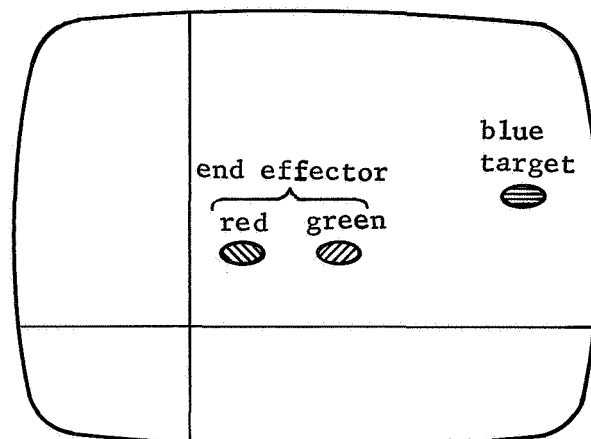
Figure C-1 Color Video Monitor Displays



a. End effector closer than target plane



b. End effector in target plane



c. End effector farther out than target plane

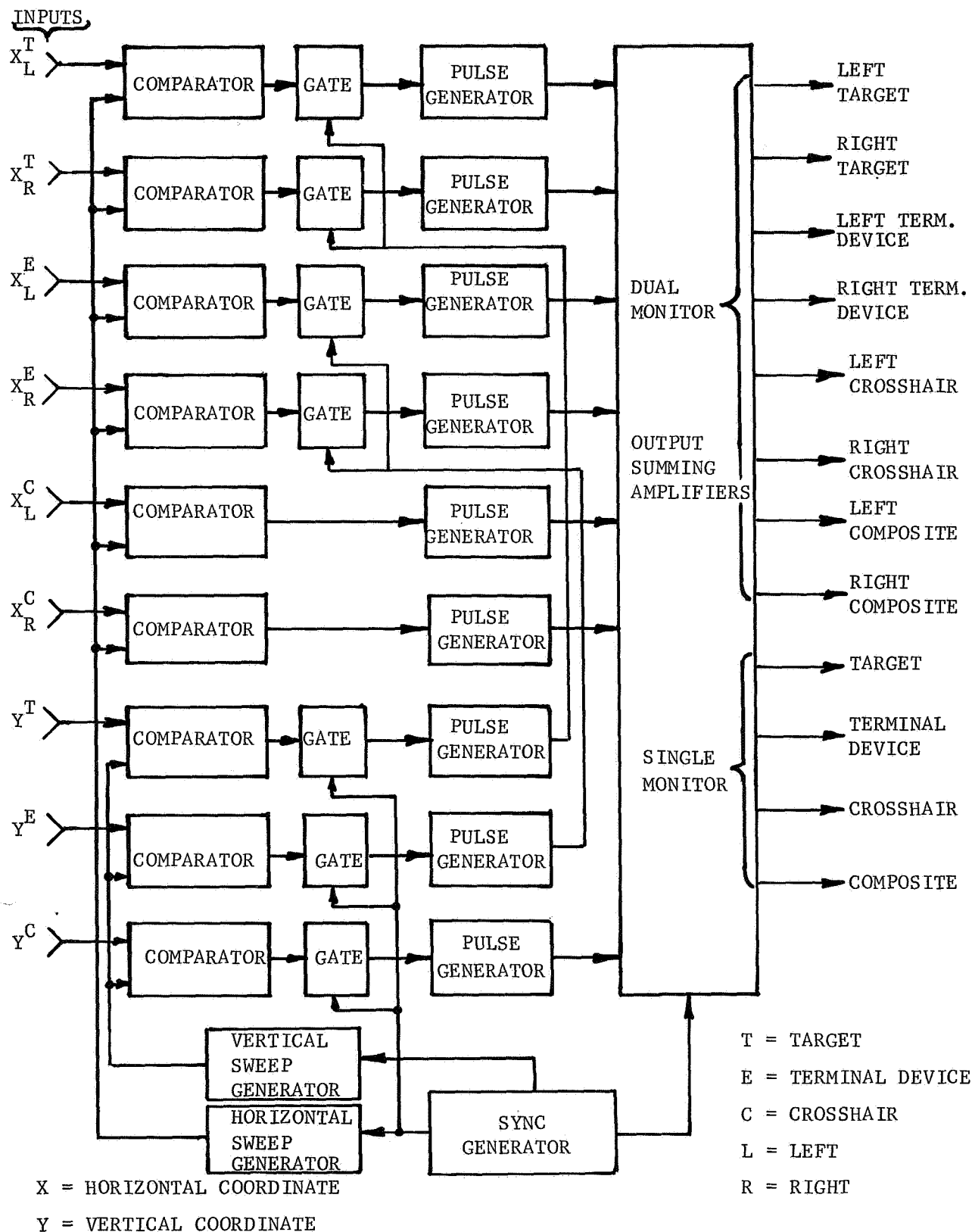


FIGURE C-2 VIDEO SYNTHESIZER BLOCK DIAGRAM

## APPENDIX D - BREADBOARD DIGITAL PROGRAM

This appendix presents a listing of the Fortran IV digital program that was used as a time domain design tool in the servo system fabrication of the two DOF breadboard manipulator.

# Appendix D - Two D.O.F. Bilateral Control System Digital Program

```

PROGRAM BILAT(INPUT,OUTPUT,TAPE5=INPUT,TAPE6=OUTPUT,FILMPL)
C
C***MAIN PROGRAM FOR 4 JOINT BILATERAL FORCE REFLECTING SYSTEM
C
  DIMENSION X(8),DX(8),KT(4),RT(4),KG(4),CV(2),MV(2),J1(2,2),
1          J2(2,2),JM(4),KB(4),
2          PT(1020),PX1(1020),PX2(1020),PX3(1020),PX4(1020),
3          PX5(1020),PX6(1020),PX7(1020),PX8(1020),PXC1(1020),
4          PXC2(1020),PXM1(1020),PXM2(1020),PXC01(1020),
5          PXC02(1020),PXM01(1020),PXM02(1020),XC(2),XM(2),XCD(2),
6          XMD(2),PTQ1(1020),PTQ2(1020),PTQ3(1020),PTQ4(1020)
  COMMON/BLK1/KFB(4),KEI(4),K1(2,2),K2(2,2),K3(2,2),K4(2,2),K5(2,2),
1          K6(2,2),MM(2,2),PI(2),RR(2),CT(2,2),CTI(2,2),GS(4),
2          CA(2,2),MA(2,2),FC(2),FM(2),DTC,DTM,LC,LM,KFL(4),
3          RL(4),TL(4),TQ(4)
  REAL KFL,KFB,KEI,K1,K2,K3,K4,K5,K6,MM,MA,LC,LM,KT,KG,JM,MV,J1,J2,
1  KB
  EXTERNAL FIRDER
C***READ IN ALL DATA
  READ (5,1) K1
1  FORMAT (4F10.3)
52  FORMAT (4F10.5)
  READ (5,1) K2
  READ (5,1) K3
  READ (5,1) K4
  READ (5,1) K5
  READ (5,1) K6
  READ (5,52) CA
  READ (5,52) MA
  READ (5,1) MM
  READ (5,1) GS
  READ (5,2) PI
2  FORMAT (2F10.3)
  READ (5,2) RR
  READ (5,1) KT
  READ (5,1) RL
  READ (5,1) TL
  READ (5,1) RT
  READ (5,1) KG
  READ (5,52) KB
  READ (5,1) JM
  READ (5,3) RA
3  FORMAT (F10.3)
  READ (5,2) LC,LM
  READ (5,3) STIME
  READ (5,4) NEQ,STEP
4  FORMAT (I2,F10.3)
  READ (5,3) T

```

```

      READ (5,5) X
      5 FORMAT (8F10.3)
      READ (5,2) FC
      READ (5,2) FM
C***WRITE ALL INPUT DATA TO VERIFY
      WRITE (6,6)
      6 FORMAT (1H1,5X,*TWO DIMENSIONAL BILATERAL MANIPULATOR PROGRAM*/)
      WRITE (6,7)
      7 FORMAT (5X,*INPUT DATA*/)
      WRITE (6,8)
      8 FORMAT (5X,*K1*,28X,*K2*)
      DO 9 I=1,2
      9 WRITE (6,10) (K1(I,J),J=1,2),(K2(I,J),J=1,2)
      10 FORMAT (5X,2(F10.3,3X,F10.3,7X))
      53 FORMAT (5X,2(F10.5,3X,F10.5,7X))
      WRITE (6,11)
      11 FORMAT (/5X,*K3*,28X,*K4*)
      DO 12 I=1,2
      12 WRITE (6,10) (K3(I,J),J=1,2),(K4(I,J),J=1,2)
      WRITE (6,80)
      80 FORMAT (/5X,*K5*,28X,*K6*)
      DO 81 I=1,2
      81 WRITE (6,10) (K5(I,J),J=1,2),(K6(I,J),J=1,2)
      WRITE (6,82)
      82 FORMAT (/5X,*CA*,28X,*MA*)
      DO 83 I=1,2
      83 WRITE (6,53) (CA(I,J),J=1,2),(MA(I,J),J=1,2)
      WRITE (6,84)
      84 FORMAT (/5X,*MM*)
      DO 85 I=1,2
      85 WRITE (6,86) (MM(I,J),J=1,2)
      86 FORMAT (5X,F10.3,3X,F10.3)
      WRITE (6,13)
      13 FORMAT (/5X,*GS*)
      WRITE (6,14) (GS(I),I=1,4)
      14 FORMAT (5X,4(F10.3,3X))
      54 FORMAT (5X,4(F10.5,3X))
      WRITE (6,15)
      15 FORMAT (/5X,*PI*)
      WRITE (6,16) (PI(I),I=1,2)
      16 FORMAT (5X,2(F10.3,3X))
      WRITE (6,17)
      17 FORMAT (/5X,*RR*)
      WRITE (6,16) (RR(I),I=1,2)
      WRITE (6,19)
      19 FORMAT (/5X,*KT*)
      WRITE (6,14) (KT(I),I=1,4)
      WRITE (6,21)
      21 FORMAT (/5X,*RL*)
      WRITE (6,14) (RL(I),I=1,4)
      WRITE (6,23)
      23 FORMAT (/5X,*TL*)
      WRITE (6,14) (TL(I),I=1,4)

```

```

WRITE (6,25)
25 FORMAT (/5X,*RT*)
WRITE (6,14) (RT(I),I=1,4)
WRITE (6,26)
26 FORMAT (/5X,*KG*)
WRITE (6,14) (KG(I),I=1,4)
WRITE (6,40)
40 FORMAT (/5X,*KB*)
WRITE (6,54) (KB(I),I=1,4)
WRITE (6,27)
27 FORMAT (/5X,*JM*)
WRITE (6,14) (JM(I),I=1,4)
WRITE (6,28) RA
28 FORMAT (/5X,*RA = *,F10.3)
WRITE (6,29) LC,LM
29 FORMAT (/5X,*LC = *,F10.3,3X,*LM = *,F10.3)
WRITE (6,30) STIME
30 FORMAT (/5X,*STIME = *,F10.3)
WRITE (6,31) NEQ,STEP
31 FORMAT (/5X,*NEQ = *,I2,3X,*STEP =*,F10.3)
WRITE (6,32) T
32 FORMAT (/5X,*T = *,F10.3)
WRITE (6,33)
33 FORMAT (/5X,*X(1)*,9X,*X(2)*,9X,*X(3)*,9X,*X(4)*)
WRITE (6,34) (X(I),I=1,4)
34 FORMAT (5X,4(F10.3,3X))
WRITE (6,87)
87 FORMAT (/5X,*X(5)*,9X,*X(6)*,9X,*X(7)*,9X,*X(8)*)
WRITE (6,34) (X(I),I=5,8)
WRITE (6,35)
35 FORMAT (/5X,*FC*)
WRITE (6,16) (FC(I),I=1,2)
WRITE (6,36)
36 FORMAT (/5X,*FM*)
WRITE (6,16) (FM(I),I=1,2)
WRITE (6,37)
37 FORMAT (5X,*END OF INPUT DATA*)
C***COORDINATE TRANSFORMATION MATRIX
CT(1,1)=COS(RA)
CT(1,2)=-SIN(RA)
CT(2,1)=SIN(RA)
CT(2,2)=COS(RA)
C***INVERSE COORDINATE TRANSFORMATION MATRIX
CTI(1,1)=CT(1,1)
CTI(1,2)=CT(2,1)
CTI(2,1)=CT(1,2)
CTI(2,2)=CT(2,2)
C***CALCULATION OF COMPOSITE SERVO PARAMETERS
DO 38 I=1,4
38 KFL(I)=KT(I)*KG(I)
DO 39 I=1,4
39 KFB(I)=KG(I)*KB(I)
KEI(1)=1.0/(0.8426+JM(1))

```



```

      KEI(2)=1.0/(0.5971+JM(2))
      KEI(3)=1.0/(1.8981+JM(3))
      KEI(4)=1.0/(0.6798+JM(4))
      WRITE (6,41)
41  FORMAT (1H1,5X,*COMPOSITE SERVO PARAMETER VALUES*/)
      WRITE (6,42)
42  FORMAT (5X,*KFL*)
      WRITE (6,43) (KFL(I),I=1,4)
43  FORMAT (5X,4(F10.3,3X))
      WRITE (6,44)
44  FORMAT (/5X,*KFB*)
      WRITE (6,43) (KFB(I),I=1,4)
      WRITE (6,45)
45  FORMAT (/5X,*KEI*)
      WRITE (6,43) (KEI(I),I=1,4)
C***CALCULATION OF CID AND MANIP. (X,Y) TIP POSITION
      XC(1)=LC*COS(X(1))+LC*COS(X(1)+X(3))
      XC(2)=LC*SIN(X(1))+LC*SIN(X(1)+X(3))
      XM(1)=LM*COS(X(5))+LM*COS(X(5)+X(7))
      XM(2)=LM*SIN(X(5))+LM*SIN(X(5)+X(7))
C***JOINT VELOCITY VECTORS
      CV(1)=X(2)
      CV(2)=X(4)
      MV(1)=X(6)
      MV(2)=X(8)
C***JACOBIAN MATRICES
      J1(1,1)=LC*(-SIN(X(1))-SIN(X(1)+X(3)))
      J1(1,2)=LC*(-SIN(X(1)+X(3)))
      J1(2,1)=LC*(COS(X(1))+COS(X(1)+X(3)))
      J1(2,2)=LC*(COS(X(1)+X(3)))
      J2(1,1)=LM*(-SIN(X(5))-SIN(X(5)+X(7)))
      J2(1,2)=LM*(-SIN(X(5)+X(7)))
      J2(2,1)=LM*(COS(X(5))+COS(X(5)+X(7)))
      J2(2,2)=LM*(COS(X(5)+X(7)))
C***CID AND MANIP. TIP VELOCITY
      CALL MMPROD(J1,CV,XCD,2,2,1)
      CALL MMPROD(J2,MV,XMD,2,2,1)
      M=1
      PT(M)=T
      PX1(M)=X(1)
      PX2(M)=X(2)
      PX3(M)=X(3)
      PX4(M)=X(4)
      PX5(M)=X(5)
      PX6(M)=X(6)
      PX7(M)=X(7)
      PX8(M)=X(8)
      PXC1(M)=XC(1)
      PXC2(M)=XC(2)
      PXM1(M)=XM(1)
      PXM2(M)=XM(2)
      PXCD1(M)=XCD(1)
      PXCD2(M)=XCD(2)

```

```

    PXMD1(M)=XMD(1)
    PXMD2(M)=XMD(2)
    PTQ1(M)=0.0
    PTQ2(M)=0.0
    PTQ3(M)=0.0
    PTQ4(M)=0.0
    STIME=STIME-1.0E-06
C***KUTTA-MERSON NUMERICAL INTEGRATION ROUTINE
    50 CALL DFEQKM(NEQ,T,STEP,X,FIRDER,+1.0E-06,+1.0E-06,20,EXIT,.TRUE.)
    IF (EXIT.EQ.0.0) GO TO 90
C***CALCULATION OF CID AND MANIP. (X,Y) TIP POSITION
    XC(1)=LC*COS(X(1))+LC*COS(X(1)+X(3))
    XC(2)=LC*SIN(X(1))+LC*SIN(X(1)+X(3))
    XM(1)=LM*COS(X(5))+LM*COS(X(5)+X(7))
    XM(2)=LM*SIN(X(5))+LM*SIN(X(5)+X(7))
C***JOINT VELOCITY VECTORS
    CV(1)=X(2)
    CV(2)=X(4)
    MV(1)=X(6)
    MV(2)=X(8)
C***JACOBIAN MATRICES
    J1(1,1)=LC*(-SIN(X(1))-SIN(X(1)+X(3)))
    J1(1,2)=LC*(-SIN(X(1)+X(3)))
    J1(2,1)=LC*(COS(X(1))+COS(X(1)+X(3)))
    J1(2,2)=LC*(COS(X(1)+X(3)))
    J2(1,1)=LM*(-SIN(X(5))-SIN(X(5)+X(7)))
    J2(1,2)=LM*(-SIN(X(5)+X(7)))
    J2(2,1)=LM*(COS(X(5))+COS(X(5)+X(7)))
    J2(2,2)=LM*(COS(X(5)+X(7)))
C***CID AND MANIP. TIP VELOCITY
    CALL MMPRDU(J1,CV,XCD,2,2,1)
    CALL MMPRDU(J2,MV,XMD,2,2,1)
    M=M+1
    PT(M)=T
    PX1(M)=X(1)
    PX2(M)=X(2)
    PX3(M)=X(3)
    PX4(M)=X(4)
    PX5(M)=X(5)
    PX6(M)=X(6)
    PX7(M)=X(7)
    PX8(M)=X(8)
    PXC1(M)=XC(1)
    PXC2(M)=XC(2)
    PXM1(M)=XM(1)
    PXM2(M)=XM(2)
    PXCD1(M)=XCD(1)
    PXCD2(M)=XCD(2)
    PXMD1(M)=XMD(1)
    PXMD2(M)=XMD(2)
    PTQ1(M)=TQ(1)
    PTQ2(M)=TQ(2)
    PTQ3(M)=TQ(3)

```

```

PTQ4(M)=TQ(4)
IF (T.LT.STIME) GO TO 50
WRITE (6,46)
46 FORMAT (1H1,5X,*OUTPUT DATA*)
C***WRITING JOINT POSITIONS AND VELOCITIES
WRITE (6,47)
47 FORMAT (5X,*MASTER AND SLAVE JOINT POSITIONS AND VELOCITIES*//)
WRITE (6,48)
48 FORMAT (5X,*TIME*,8X,*X(1)*,11X,*X(2)*,11X,*X(3)*,11X,*X(4)*,11X,
1      *X(5)*,11X,*X(6)*,11X,*X(7)*,11X,*X(8)*)
DO 49 I=1,M
49 WRITE (6,100) PT(I),PX1(I),PX2(I),PX3(I),PX4(I),PX5(I),PX6(I),
1      PX7(I),PX8(I)
100 FORMAT (5X,F6.3,8(6X,F9.5))
C***WRITING X TIP POSITIONS AND RATES
WRITE (6,101)
101 FORMAT (1H1,5X,*MASTER AND SLAVE X TIP POSITIONS AND RATES*//)
WRITE (6,102)
102 FORMAT (5X,*TIME*,8X,*XC(1)*,10X,*XC(2)*,10X,*XM(1)*,10X,*XM(2)*,
1      10X,*XCD(1)*,9X,*XCD(2)*,9X,*XMD(1)*,9X,*XMD(2)*)
DO 103 I=1,M
103 WRITE (6,100) PT(I),PXC1(I),PXC2(I),PXM1(I),PXM2(I),PXCD1(I),
1      PXCD2(I),PXMD1(I),PXMD2(I)
C***WRITING JOINT TORQUES
WRITE (6,104)
104 FORMAT (1H1,5X,*MASTER AND SLAVE JOINT TORQUES*//)
WRITE (6,105)
105 FORMAT (5X,*TIME*,8X,*TQ(1)*,10X,*TQ(2)*,10X,*TQ(3)*,10X,*TQ(4)*)
DO 106 I=1,M
106 WRITE (6,107) PT(I),PTQ1(I),PTQ2(I),PTQ3(I),PTQ4(I)
107 FORMAT (5X,F6.3,4(6X,F9.5))
WRITE (6,51) M
51 FORMAT (/5X,*M =*,I4)
C***FINDING MIN. AND MAX. SCALE VALUES FOR PLOTTING
CALL MINMAX(M,PT,PTS,PTL)
CALL MINMAX(M,PX1,PX1S,PX1L)
CALL MINMAX(M,PX2,PX2S,PX2L)
CALL MINMAX(M,PX3,PX3S,PX3L)
CALL MINMAX(M,PX4,PX4S,PX4L)
CALL MINMAX(M,PX5,PX5S,PX5L)
CALL MINMAX(M,PX6,PX6S,PX6L)
CALL MINMAX(M,PX7,PX7S,PX7L)
CALL MINMAX(M,PX8,PX8S,PX8L)
CALL MINMAX(M,PXC1,PXC1S,PXC1L)
CALL MINMAX(M,PXC2,PXC2S,PXC2L)
CALL MINMAX(M,PXM1,PXM1S,PXM1L)
CALL MINMAX(M,PXM2,PXM2S,PXM2L)
CALL MINMAX(M,PXCD1,PXCD1S,PXCD1L)
CALL MINMAX(M,PXCD2,PXCD2S,PXCD2L)
CALL MINMAX(M,PXMD1,PXMD1S,PXMD1L)
CALL MINMAX(M,PXMD2,PXMD2S,PXMD2L)
CALL MINMAX(M,PTQ1,PTQ1S,PTQ1L)
CALL MINMAX(M,PTQ2,PTQ2S,PTQ2L)

```

```

CALL MINMAX(M,PTQ3,PTQ3S,PTQ3L)
CALL MINMAX(M,PTQ4,PTQ4S,PTQ4L)
CALL SCALE(PTL,PTS,10,PTG,PTT,S1)
CALL SCALE(PX1L,PX1S,10,PX1G,PX1T,S2)
CALL SCALE(PX2L,PX2S,10,PX2G,PX2T,S3)
CALL SCALE(PX3L,PX3S,10,PX3G,PX3T,S4)
CALL SCALE(PX4L,PX4S,10,PX4G,PX4T,S5)
CALL SCALE(PX5L,PX5S,10,PX5G,PX5T,S6)
CALL SCALE(PX6L,PX6S,10,PX6G,PX6T,S7)
CALL SCALE(PX7L,PX7S,10,PX7G,PX7T,S8)
CALL SCALE(PX8L,PX8S,10,PX8G,PX8T,S9)
CALL SCALE(PXC1L,PXC1S,10,PXC1G,PXC1T,S10)
CALL SCALE(PXC2L,PXC2S,10,PXC2G,PXC2T,S11)
CALL SCALE(PXM1L,PXM1S,10,PXM1G,PXM1T,S12)
CALL SCALE(PXM2L,PXM2S,10,PXM2G,PXM2T,S13)
CALL SCALE(PXCD1L,PXCD1S,10,PXCD1G,PXCD1T,S14)
CALL SCALE(PXCD2L,PXCD2S,10,PXCD2G,PXCD2T,S15)
CALL SCALE(PXMD1L,PXMD1S,10,PXMD1G,PXMD1T,S16)
CALL SCALE(PXMD2L,PXMD2S,10,PXMD2G,PXMD2T,S17)
CALL SCALE(PTQ1L,PTQ1S,10,PTQ1G,PTQ1T,S18)
CALL SCALE(PTQ2L,PTQ2S,10,PTQ2G,PTQ2T,S19)
CALL SCALE(PTQ3L,PTQ3S,10,PTQ3G,PTQ3T,S20)
CALL SCALE(PTQ4L,PTQ4S,10,PTQ4G,PTQ4T,S21)
C***PLOT OF MASTER SHOULDER POSITION
CALL BPLT(0,2HLC)
CALL SPLT(0.0,S1,4HTIME,24HMASTER SHOULDER POSITION,0.,1.,PX1T,
1      PX1G,4HX(1))
DO 60 I=1,M
60 CALL FPLT(PT(I),PX1(I))
CALL EPLT(0)
C***PLOT OF MASTER SHOULDER VELOCITY
CALL SPLT(0.0,S1,4HTIME,24HMASTER SHOULDER VELOCITY,0.,1.,PX2T,
1      PX2G,4HX(2))
DO 61 I=1,M
61 CALL FPLT(PT(I),PX2(I))
CALL EPLT(0)
C***PLOT OF MASTER ELBOW POSITION
CALL SPLT(0.0,S1,4HTIME,21HMASTER ELBOW POSITION,0.,1.,PX3T,
1      PX3G,4HX(3))
DO 62 I=1,M
62 CALL FPLT(PT(I),PX3(I))
CALL EPLT(0)
C***PLOT OF MASTER ELBOW VELOCITY
CALL SPLT(0.0,S1,4HTIME,21HMASTER ELBOW VELOCITY,0.,1.,PX4T,
1      PX4G,4HX(4))
DO 63 I=1,M
63 CALL FPLT(PT(I),PX4(I))
CALL EPLT(0)
C***PLOT OF SLAVE SHOULDER POSITION
CALL SPLT(0.0,S1,4HTIME,23HSLAVE SHOULDER POSITION,0.,1.,PX5T,
1      PX5G,4HX(5))
DO 64 I=1,M
64 CALL FPLT(PT(I),PX5(I))

```

```

      CALL EPLT(0)
C***PLOT OF SLAVE SHOULDER VELOCITY
      CALL SPLT(0.0,S1,4HTIME,23HSLAVE SHOULDER VELOCITY,0.,1.,PX6T,
1          PX6G,4HX(6))
      DO 65 I=1,M
65  CALL FPLT(PT(I),PX6(I))
      CALL EPLT(0)
C***PLOT OF SLAVE ELBOW POSITION
      CALL SPLT(0.0,S1,4HTIME,20HSLAVE ELBOW POSITION,0.,1.,PX7T,
1          PX7G,4HX(7))
      DO 66 I=1,M
66  CALL FPLT(PT(I),PX7(I))
      CALL EPLT(0)
C***PLOT OF SLAVE ELBOW VELOCITY
      CALL SPLT(0.0,S1,4HTIME,20HSLAVE ELBOW VELOCITY,0.,1.,PX8T,
1          PX8G,4HX(8))
      DO 67 I=1,M
67  CALL FPLT(PT(I),PX8(I))
      CALL EPLT(0)
C***PLOT OF MASTER X TIP POSITION
      CALL SPLT(0.0,S1,4HTIME,21HMASTER X TIP POSITION,0.,1.,PXC1T,
1          PXC1G,5HXC(1))
      DO 68 I=1,M
68  CALL FPLT(PT(I),PXC1(I))
      CALL EPLT(0)
C***PLOT OF MASTER X TIP VELOCITY
      CALL SPLT(0.0,S1,4HTIME,21HMASTER X TIP VELOCITY,0.,1.,PXCD1T,
1          PXCD1G,6HXC(1))
      DO 69 I=1,M
69  CALL FPLT(PT(I),PXCD1(I))
      CALL EPLT(0)
C***PLOT OF MASTER Y TIP POSITION
      CALL SPLT(0.0,S1,4HTIME,21HMASTER Y TIP POSITION,0.,1.,PXC2T,
1          PXC2G,5HXC(2))
      DO 70 I=1,M
70  CALL FPLT(PT(I),PXC2(I))
      CALL EPLT(0)
C***PLOT OF MASTER Y TIP VELOCITY
      CALL SPLT(0.0,S1,4HTIME,21HMASTER Y TIP VELOCITY,0.,1.,PXCD2T,
1          PXCD2G,6HXC(2))
      DO 71 I=1,M
71  CALL FPLT(PT(I),PXCD2(I))
      CALL EPLT(0)
C***PLOT OF SLAVE X TIP POSITION
      CALL SPLT(0.0,S1,4HTIME,20HSLAVE X TIP POSITION,0.,1.,PXM1T,
1          PXM1G,5HXM(1))
      DO 72 I=1,M
72  CALL FPLT(PT(I),PXM1(I))
      CALL EPLT(0)
C***PLOT OF SLAVE X TIP VELOCITY
      CALL SPLT(0.0,S1,4HTIME,20HSLAVE X TIP VELOCITY,0.,1.,PXMD1T,
1          PXMD1G,6HXM(1))
      DO 73 I=1,M

```

```

73 CALL FPLT(PT(I),PXMD1(I))
   CALL EPLT(0)
C***PLOT OF SLAVE Y TIP POSITION
   CALL SPLT(0.0,S1,4HTIME,20HSLAVE Y TIP POSITION,0.,1.,PXM2T,
1       PXM2G,5HXM(2))
   DO 74 I=1,M
74 CALL FPLT(PT(I),PXM2(I))
   CALL EPLT(0)
C***PLOT OF SLAVE Y TIP VELOCITY
   CALL SPLT(0.0,S1,4HTIME,20HSLAVE Y TIP VELOCITY,0.,1.,PXMD2T,
1       PXMD2G,6HXM(2))
   DO 75 I=1,M
75 CALL FPLT(PT(I),PXMD2(I))
   CALL EPLT(0)
C***PLOT OF MASTER SHOULDER TORQUE
   CALL SPLT(0.0,S1,4HTIME,22HMASTER SHOULDER TORQUE,0.,1.,PTQ1T,
1       PTQ1G,5HTQ(1))
   DO 76 I=1,M
76 CALL FPLT(PT(I),PTQ1(I))
   CALL EPLT(0)
C***PLOT OF MASTER ELBOW TORQUE
   CALL SPLT(0.0,S1,4HTIME,19HMASTER ELBOW TORQUE,0.,1.,PTQ2T,
1       PTQ2G,5HTQ(2))
   DO 77 I=1,M
77 CALL FPLT(PT(I),PTQ2(I))
   CALL EPLT(0)
C***PLOT OF SLAVE SHOULDER TORQUE
   CALL SPLT(0.0,S1,4HTIME,21HSLAVE SHOULDER TORQUE,0.,1.,PTQ3T,
1       PTQ3G,5HTQ(3))
   DO 78 I=1,M
78 CALL FPLT(PT(I),PTQ3(I))
   CALL EPLT(0)
C***PLOT OF SLAVE ELBOW TORQUE
   CALL SPLT(0.0,S1,4HTIME,18HSLAVE ELBOW TORQUE,0.,1.,PTQ4T,
1       PTQ4G,5HTQ(4))
   DO 79 I=1,M
79 CALL FPLT(PT(I),PTQ4(I))
   CALL EPLT(0)
   GO TO 99
90 WRITE (6,91)
91 FORMAT (5X,*SOLUTION NOT ATTAINABLE FROM DFEQKM*)
99 STOP
   END

```

```

SUBROUTINE DFEQKM(NEQ,X,STEP,Y,F,EPS,AB,NCUTS,EXIT,STPSZ)
C
C
C*****
C* SUBROUTINE DFEQKM *
C*****

```

```

C      INTEGER NEQ, NCUTS
      REAL X, STEP, Y(NEQ), F, EPS, AB
      EXTERNAL F
      LOGICAL STPSZ

C
      REAL FINAL, H2, H3, H6, H8, ERR, TEST, T, H, EPSL,
1      Y1(30), Y2(30), F0(30), F1(30), F2(30), TEMP
      INTEGER I, CUT
      LOGICAL DBL
50  FORMAT (* *,*THE STEPSIZE IS NOW *,G12.4,* AT T =*,G12.4)
60  FORMAT(* THE STEPSIZE HAS BEEN HALVED *,I5,* TIMES*)
      HC=0.0
      EXIT=1.0
C *** CHECK FOR INITIAL ENTRY AND ADJUST HC, IF NECESSARY.
      IF(NEQ.NE.0) GO TO 10
      HC = STEP
      RETURN
10     IF(STEP.EQ.0) RETURN
      IF(HC.EQ.0) HC = STEP
C *** SET LOCAL VARIABLES.
      FINAL = X+STEP
      H = STEP
      EPSL = EPS
C *** CHANGE DIRECTION, IF REQUIRED.
      IF(EPS.EQ.0 .OR. ABS(H) .LE. ABS(HC)) GO TO 15
      IF(H*HC.LE.0) HC = -HC
      H = HC
15     T = X+H
      CUT = NCUTS
      X = FINAL
      H2 = H/2.
      H3 = H/3.
      H6 = H/6.
      H8 = H/8.
C *** MAIN KUTTA-MERSON STEP
20     IF(H.GT.0 .AND. T.GT.FINAL .OR. H.LT.0.AND.T.LT.FINAL) GOTO 40
21     CALL F(T-H, Y, F0)
      DO 22 I = 1,NEQ
22         Y1(I) = F0(I)*H3+Y(I)
      CALL F(T-2.*H3, Y1, F1)
      DO 23 I = 1,NEQ
23         Y1(I) = (F0(I)+F1(I))*H6+Y(I)
      CALL F(T-2.*H3, Y1, F1)
      DO 24 I = 1,NEQ
24         Y1(I) = (F1(I)*3.+F0(I))*H8+Y(I)
      CALL F(T-H2, Y1, F2)
      DO 25 I = 1,NEQ
25         Y1(I) = (F2(I)*4.-F1(I)*3.+F0(I))*H2 +Y(I)
      CALL F(T, Y1, F1)
      DO 26 I = 1,NEQ
26         Y2(I) = (F2(I)*4.+F1(I)+F0(I))*H6 +Y(I)
C *** DOES THE STEP SIZE H NEED TO BE CHANGED.

```

```

        IF(EPSL.EQ.0) GO TO 38
        DBL = .TRUE.
        DO 35 I = 1,NEQ
            ERR = ABS(Y1(I)-Y2(I))*0.2
            TEST = ABS(Y1(I))*EPSL
            IF(ERR.LE.TEST .OR. ERR.LT.AB) GO TO 34
C *** HALVE THE STEP SIZE.
            H = H2
            T = T-H2
            IF (.NOT.STPSZ) GO TO 30
            TEMP = T-H2
            WRITE (6,50) H, TEMP
30          CUT = CUT + 1
            IF (CUT .GE. 0) GO TO 31
            X = T - H2
            WRITE (6,60) NCUTS

            EXIT=0.0
            RETURN
31          IF(T+H.NE.T) GO TO 33
            X = T

            EXIT = 0.0
            RETURN
C*** STEP SIZE TOO SMALL RELATIVE TO T, SET EXIT=0 AND RETURN
33          H2 = H/2.
            H3 = H/3.
            H6 = H/6.
            H8 = H/8.
            GO TO 21
34          IF(64.0*ERR.GT.TEST) DBL = .FALSE.
35          CONTINUE
C *** DOUBLE THE STEP SIZE, MAYBE.
            IF(.NOT.DBL) GO TO 38
            H2 = H
            H = 2.*H
            IF (STPSZ) WRITE (6,50) H,T
            H3 = H/3.
            H6 = H/6.
            H8 = H/8.
            CUT = NCUTS
38          DO 39 I = 1,NEQ
39          Y(I) = Y2(I)
            T = T+H
            GO TO 20
40          IF(EPSL.EQ.0) RETURN
C *** NOW BE SURE TO HAVE T = FINAL.
            HC = H
            H = FINAL-(T-H)
            IF(ABS(H).LE.ABS(FINAL)*9.536744 E-7) RETURN
            T= FINAL
            EPSL = 0
            H2 = H/2.
            H3 = H/3.
            H6 = H/6.

```



H8 = H/8.  
GO TO 20

END

C \*\*\* LAST CARD OF SUBROUTINE DFEQ1

SUBROUTINE FIRDER(I,X,DX)

C

C

C\*\*\*SUBROUTINE FOR FINDING FIRST DERIVATIVES

C

```

      DIMENSION CV(2),MV(2),TC(2,2),TM(2,2),J1(2,2),J2(2,2),TCI(2,2),
1      TMI(2,2),R1(2),R2(2),R4(2),R6(2),PE1(2),PE2(2),R3(2),
2      R8(2),R14(2),R16(2),R30(2),R5(2),R10(2),R7(2),R12(2),
3      CF(2),MF(2),R9(2),R11(2),R18(2),R20(2),R22(2),TA(2),
4      TB(2),TI(4),TR(4),X(8),DX(8),XC(2),XM(2),XCD(2),XMD(2)
      COMMON/BLK1/KFB(4),KEI(4),K1(2,2),K2(2,2),K3(2,2),K4(2,2),K5(2,2),
1      K6(2,2),MM(2,2),PI(2),RR(2),CT(2,2),CTI(2,2),GS(4),
2      CA(2,2),MA(2,2),FC(2),FM(2),DTC,DTM,LC,LM,KFL(4),
3      RL(4),TL(4),TQ(4)
      REAL MV,J1,J2,MF,KFB,KEI,K1,K2,K3,K4,K5,K6,MM,MA,LC,LM,KFL

```

C

C\*\*\*EFFECTS OF SERVO RATE LIMITS

```

      IF (ABS(X(2)).GT.RL(1)) 50,51
50  X(2)=SIGN(RL(1),X(2))
51  IF (ABS(X(4)).GT.RL(2)) 52,53
52  X(4)=SIGN(RL(2),X(4))
53  IF (ABS(X(6)).GT.RL(3)) 54,55
54  X(6)=SIGN(RL(3),X(6))
55  IF (ABS(X(8)).GT.RL(4)) 56,57
56  X(8)=SIGN(RL(4),X(8))

```

C\*\*\*DEFINING JOINT VELOCITIES

```

57  CV(1)=X(2)
      CV(2)=X(4)
      MV(1)=X(6)
      MV(2)=X(8)

```

C

C\*\*\*CALCULATION OF CID AND MANIPULATOR TIP POSITION

C

```

      XC(1)=LC*COS(X(1))+LC*COS(X(1)+X(3))
      XC(2)=LC*SIN(X(1))+LC*SIN(X(1)+X(3))
      XM(1)=LM*COS(X(5))+LM*COS(X(5)+X(7))
      XM(2)=LM*SIN(X(5))+LM*SIN(X(5)+X(7))

```

C\*\*\*CALCULATION OF TORQUE MATRICES

```

      TC(1,1)=-LC*(SIN(X(1))+SIN(X(1)+X(3)))
      TC(1,2)=LC*(COS(X(1))+COS(X(1)+X(3)))
      TC(2,1)=-LC*(SIN(X(1)+X(3)))
      TC(2,2)=LC*(COS(X(1)+X(3)))
      TM(1,1)=-LM*(SIN(X(5))+SIN(X(5)+X(7)))
      TM(1,2)=LM*(COS(X(5))+COS(X(5)+X(7)))
      TM(2,1)=-LM*(SIN(X(5)+X(7)))

```

```

      TM(2,2)=LM*(COS(X(5)+X(7)))
C***CALCULATION OF JACOBIAN MATRICES
      J1(1,1)=LC*(-SIN(X(1))-SIN(X(1)+X(3)))
      J1(1,2)=LC*(-SIN(X(1)+X(3)))
      J1(2,1)=LC*(COS(X(1))+COS(X(1)+X(3)))
      J1(2,2)=LC*(COS(X(1)+X(3)))
      J2(1,1)=LM*(-SIN(X(5))-SIN(X(5)+X(7)))
      J2(1,2)=LM*(-SIN(X(5)+X(7)))
      J2(2,1)=LM*(COS(X(5))+COS(X(5)+X(7)))
      J2(2,2)=LM*(COS(X(5)+X(7)))
C***CALCULATION OF INTERNAL VECTORS IN SIGNAL CHANNELING LOOP
      DO 100 I=1,2
100   R1(I)=XC(I)-PI(I)
      CALL MPRDU(CT,XM,R2,2,2,1)
      DO 101 I=1,2
101   R4(I)=R2(I)*MM(I,I)
      DO 102 I=1,2
102   R6(I)=R4(I)-RR(I)
      DO 103 I=1,2
103   PE1(I)=R6(I)-R1(I)
      DO 104 I=1,2
104   PE2(I)=R1(I)-R6(I)
      DO 105 I=1,2
105   R3(I)=PE1(I)*K1(I,I)
      DO 106 I=1,2
106   R8(I)=PE2(I)*K4(I,I)
      CALL MPRDU(J1,CV,XCD,2,2,1)
      CALL MPRDU(J2,MV,XMD,2,2,1)
      CALL MPRDU(CT,XMD,R14,2,2,1)
      DO 107 I=1,2
107   R16(I)=R14(I)*MM(I,I)
      DO 108 I=1,2
108   R30(I)=XCD(I)-R16(I)
      DO 109 I=1,2
109   R5(I)=R30(I)*K3(I,I)
      DO 110 I=1,2
110   R10(I)=R30(I)*K6(I,I)
      DO 111 I=1,2
111   R7(I)=XCD(I)*K2(I,I)
      DO 112 I=1,2
112   R12(I)=R16(I)*K5(I,I)
      DO 113 I=1,2
113   CF(I)=R3(I)-R5(I)+R7(I)
      DO 114 I=1,2
114   MF(I)=R8(I)+R10(I)+R12(I)
      CALL MPRDU(TC,CF,R9,2,2,1)
      DO 115 I=1,2
115   R11(I)=R9(I)*CA(I,I)
      CALL MPRDU(CTI,MF,R18,2,2,1)
      CALL MPRDU(TM,R18,R20,2,2,1)
      DO 116 I=1,2
116   R22(I)=R20(I)*MA(I,I)
C***CALCULATION OF INPUT TORQUES FROM INPUT FORCES

```

```

      CALL MMPRDU(TC,FC,TA,2,2,1)
      CALL MMPRDU(TM,FM,TB,2,2,1)
      TQ(1)=(R11(1)-KFB(1)*X(2))*KFL(1)
      TQ(2)=(R11(2)-KFB(2)*X(4))*KFL(2)
      TQ(3)=(R22(1)-KFB(3)*X(6))*KFL(3)
      TQ(4)=(R22(2)-KFB(4)*X(8))*KFL(4)
C***EFFECTS OF SERVO TORQUE LIMITS
      DO 71 I=1,4
        IF (ABS(TQ(I)).GT.TL(I)) 70,71
      70 TQ(I)=SIGN(TL(I),TQ(I))
      71 CONTINUE
      DO 72 I=1,2
      72 TI(I)=TQ(I)+TA(I)
      DO 73 I=1,2
      73 TI(I+2)=TQ(I+2)+TB(I)
C***NO GEAR STICTION INCLUDED
      DO 74 I=1,4
      74 TR(I)=TI(I)
C***DETERMINATION OF FIRST DERIVATIVES
      125 DX(1)=X(2)
          DX(2)=KEI(1)*TR(1)
          DX(3)=X(4)
          DX(4)=KEI(2)*TR(2)
          DX(5)=X(6)
          DX(6)=KEI(3)*TR(3)
          DX(7)=X(8)
          DX(8)=KEI(4)*TR(4)
          RETURN
      END
C***END OF SUBROUTINE FIRDER

```

```

      SUBROUTINE MINMAX(M,XI,XMIN,XMAX)
C***SUBROUTINE FOR FINDING MIN. AND MAX. VALUES OF VECTORS
      DIMENSION XI(1020)
      XMIN=XI(1)
      XMAX=XI(1)
      DO 1 I=2,M
        IF(XMIN.GT.XI(I)) XMIN=XI(I)
      1 IF(XMAX.LT.XI(I)) XMAX=XI(I)
      RETURN
      END
C***LAST CARD OF SUBROUTINE MINMAX

```

```

      SUBROUTINE SCALE(XPMAX,XPMIN, NSQ,XSMAX,XSMIN,S)
C      XPMAX=MAXIMUM VALUE TO BE PLOTTED
C      XPMIN=MINIMUM VALUE TO BE PLOTTED
C      NSQ =NUMBER OF PLOT MAJOR GRIDS = 10

```

```

C      XSMAX=MAXIMUM SCALE VALUE
C      XSMIN=MINIMUM SCALE VALUE
C      S      =SCALE FACTOR PER MAJOR GRID
      FNSQ=NSQ
      XSMIN =0.0
      IF(XPMAX-XPMIN) 12,12,13
12     XPMIN=XPMIN-5.0
      XPMAX=XPMAX+5.0
13     XDIF=XPMAX-XPMIN
      DO 1 I=1,66
      DO 1 J=1,3
      T=2.0** (J-2)*FNSQ/10.0
      IF(XDIF-T*10.0** (I-33)) 2,2,1
1     CONTINUE
2     S=T*10.0** (I-33)/FNSQ
      IF(XPMIN) 3,7,4
3     XSMIN=XSMIN-S
      IF(XSMIN-XPMIN) 7,7,3
4     XSMIN=XSMIN+S
      IF(XSMIN-XPMIN) 4,7,6
6     XSMIN=XSMIN-S
7     XSMAX=XSMIN+ S*FNSQ
      IF(XSMAX-XPMAX) 8,11,11
8     IF(J-3) 10,9,9
9     J=0
      I=I+1
10    J=J+1
      T=2.0** (J-2)*FNSQ/10.0
      XSMIN=0.0
      GO TO 2
11    XSMIN=XSMAX-10.0*S
      RETURN
      END

```

## APPENDIX E - MANIPULATOR TRAJECTORY DATA

A digital computer program was written to calculate the manipulator position and attitude from the joint angle data recorded during the manipulator trajectory definition task. The analog data defining the joint angles were transcribed into digital format for use as input data to the program. The following pages list the results obtained with this program. The X, Y, Z information defines the position of the wrist of the manipulator relative to the shoulder joint, in the Shuttle axis system. Likewise, the Roll, Pitch, Yaw information defines the attitude of the terminal device relative to the Shuttle, for a standard Yaw-Pitch-Roll Euler angle sequence. The corresponding manipulator joint angles are then listed, along with comments describing the position of the manipulator at significant points along the trajectory. The manipulator shoulder location, in relation to the shuttle, is shown in Figure II-5.

CAPTURE CONCEPT NUMBER 1 (7-DOF)

LINE	X	Y	Z	ROLL	PITCH	YAW	M-ROLL	M-PITCH	M-YAW	ELBOW	S-ROLL	S-YAW	S-PITCH	COMMENTS
1	47.00	0.	0.	0.	0.	0.	0.	0.	0.	0.	0.	0.	0.	IC CONDITION ALL JOINTS = 0 DEG
2	44.51	-2.32	-6.44	26.54	31.68	-25.40	39.6	27.0	0.	-33.3	-9.0	0.	0.	
3	21.56	-3.28	-12.59	4.93	71.38	-86.23	100.8	57.6	63.0	-115.2	-31.5	13.5	10.8	
4	2.81	-3.46	-13.82	56.12	82.36	-33.60	117.0	0.	82.8	-144.0	-43.2	47.7	56.7	
5	-17.53	-8.57	-14.91	-57.50	75.56	-161.03	90.0	-30.6	82.8	-117.0	18.0	36.0	120.6	
6	-32.23	-9.03	-13.82	-53.07	81.73	-157.77	75.6	-50.4	76.5	-79.2	22.5	22.5	123.3	
7	-40.59	-8.76	-13.61	-64.68	70.37	-154.72	73.8	-54.0	54.0	-43.2	10.0	9.0	142.2	
8	-43.32	-9.36	-11.84	-42.70	75.67	-138.18	72.0	-58.5	41.4	-25.2	20.7	0.	154.8	
9	-42.91	-9.73	-12.97	-70.58	73.69	-166.41	73.8	-58.5	43.2	-25.2	13.5	0.	160.2	FWD CAPTURE POSITION
10	-42.76	-9.52	-13.60	-60.06	73.48	-161.21	73.8	-55.8	46.8	-25.2	18.0	0.	150.4	
11	-39.94	-9.33	-14.54	-58.93	78.55	-154.16	72.0	-54.0	52.2	-67.5	18.0	9.0	153.0	
12	-34.54	-9.79	-15.44	-67.62	81.59	-141.33	72.0	-52.2	64.8	-94.5	16.2	18.0	146.7	
13	-26.00	-10.02	-14.86	-75.99	84.54	-111.33	72.0	-45.0	90.0	-115.2	18.0	32.4	136.8	
14	-17.93	-9.94	-14.63	-84.35	82.42	-153.39	72.0	-36.0	90.0	-127.8	16.2	36.0	120.6	
15	-11.28	-9.08	-15.67	-42.55	85.51	-135.66	81.0	-25.2	90.0	-135.0	16.2	36.0	109.8	
16	-4.64	-8.86	-14.95	-7.82	80.02	-104.93	85.5	-9.0	90.0	-135.0	16.2	36.0	90.0	
17	-1.81	-8.42	-15.01	-42.37	79.00	-139.50	90.0	4.5	90.0	-136.8	9.0	38.7	87.3	
18	1.79	-9.26	-14.50	-62.45	79.41	-163.68	90.0	18.0	97.2	-136.8	1.8	38.0	81.0	
20	9.55	-9.41	-15.68	-27.20	82.47	-130.87	90.0	19.8	97.2	-133.2	0.	38.0	83.7	
22	19.18	-9.63	-16.31	-81.56	85.18	-178.88	109.8	32.4	90.0	-127.8	-10.8	36.0	69.3	
23	25.88	-9.73	-16.97	-106.93	84.79	-156.71	90.0	45.0	81.0	-122.4	0.	36.0	63.0	
24	31.03	-10.59	-16.69	-18.57	84.33	-121.54	117.0	48.6	90.0	-109.8	-13.5	32.4	52.2	
25	37.34	-10.41	-16.71	-57.67	85.40	-155.72	126.0	52.2	90.0	-92.7	-18.0	27.0	46.8	
26	40.57	-10.67	-16.36	-9.32	80.15	-107.86	135.0	54.0	81.0	-76.5	-23.4	18.0	43.2	
27	42.02	-8.62	-16.48	.86	82.78	-99.23	144.0	54.0	81.0	-52.2	-27.0	9.0	36.0	
							140.7	54.0	70.2	-33.3	-34.2	0.	31.5	REAR POSITION
							142.2	58.5	58.5	-24.3	-27.0	0.	27.0	

POSITION (FT)

DEGREES

CAPTURE CONCEPT NUMBER 1 (6-DOF)

LINE	X	Y	Z	ROLL	PITCH	YAW	M-ROLL	M-PITCH	M-YAW	ELBOW	S-ROLL	S-YAW	S-PITCH	COMMENTS
1	47.00	0.	0.	0.	0.	0.	0.	0.	0.	0.	0.	0.	0.	IC CONDITION ALL JOINTS = 0 DEG
2	44.51	-2.32	-6.44	26.54	31.68	-25.40	39.6	27.0	0.	-33.3	-9.0	0.	0.	
3	21.56	-3.28	-12.59	4.93	71.38	-86.23	100.8	57.6	63.0	-115.2	-31.5	13.5	10.8	
4	2.81	-3.46	-13.82	56.12	82.36	-33.60	117.0	0.	82.8	-144.0	-43.2	47.7	56.7	
5	-17.53	-8.57	-14.91	-57.50	75.56	-161.03	90.0	-30.6	82.8	-117.0	18.0	36.0	120.6	
6	-32.23	-9.03	-13.82	-53.07	81.73	-157.77	75.6	-50.4	76.5	-79.2	22.5	22.5	123.3	
7	-40.59	-8.76	-13.61	-64.68	70.37	-154.72	73.8	-54.0	54.0	-43.2	10.0	9.0	142.2	
8	-43.32	-9.36	-11.84	-42.70	75.67	-138.18	72.0	-58.5	41.4	-25.2	20.7	0.	154.8	
9	-42.91	-9.73	-12.97	-70.58	73.69	-166.41	73.8	-58.5	43.2	-25.2	13.5	0.	160.2	FWD CAPTURE POSITION
10	-42.76	-9.52	-13.60	-60.06	73.48	-161.21	73.8	-55.8	46.8	-25.2	18.0	0.	150.4	
11	-39.94	-9.33	-14.54	-58.93	78.55	-154.16	72.0	-54.0	52.2	-67.5	18.0	9.0	153.0	
12	-34.54	-9.79	-15.44	-67.62	81.59	-141.33	72.0	-52.2	64.8	-94.5	16.2	18.0	146.7	
13	-26.00	-10.02	-14.86	-75.99	84.54	-111.33	72.0	-45.0	90.0	-115.2	18.0	32.4	136.8	
14	-17.93	-9.94	-14.63	-84.35	82.42	-153.39	72.0	-36.0	90.0	-127.8	16.2	36.0	120.6	
15	-11.28	-9.08	-15.67	-42.55	85.51	-135.66	81.0	-25.2	90.0	-135.0	16.2	36.0	109.8	
16	-4.64	-8.86	-14.95	-7.82	80.02	-104.93	85.5	-9.0	90.0	-135.0	16.2	36.0	90.0	
17	-1.81	-8.42	-15.01	-42.37	79.00	-139.50	90.0	4.5	90.0	-136.8	9.0	38.7	87.3	
18	1.79	-9.26	-14.50	-62.45	79.41	-163.68	90.0	18.0	97.2	-136.8	1.8	38.0	81.0	
20	9.55	-9.41	-15.68	-27.20	82.47	-130.87	90.0	19.8	97.2	-133.2	0.	38.0	83.7	
22	19.18	-9.63	-16.31	-81.56	85.18	-178.88	109.8	32.4	90.0	-127.8	-10.8	36.0	69.3	
23	25.88	-9.73	-16.97	-106.93	84.79	-156.71	90.0	45.0	81.0	-122.4	0.	36.0	63.0	
24	31.03	-10.59	-16.69	-18.57	84.33	-121.54	117.0	48.6	90.0	-109.8	-13.5	32.4	52.2	
25	37.34	-10.41	-16.71	-57.67	85.40	-155.72	126.0	52.2	90.0	-92.7	-18.0	27.0	46.8	
26	40.57	-10.67	-16.36	-9.32	80.15	-107.86	135.0	54.0	81.0	-76.5	-23.4	18.0	43.2	
27	42.02	-8.62	-16.48	.86	82.78	-99.23	144.0	54.0	81.0	-52.2	-27.0	9.0	36.0	
							140.7	54.0	70.2	-33.3	-34.2	0.	31.5	REAR POSITION
							142.2	58.5	58.5	-24.3	-27.0	0.	27.0	

POSITION (FT)

DEGREES

## CAPTURE CONCEPT NUMBER 2 (7-DOF)

LINE	X	Y	Z	ROLL	PITCH	YAW	W-ROLL	W-PITCH	M-YAW	ELBOW	S-ROLL	S-YAW	S-PITCH	COMMENTS
1	47.00	0.00	0.00	0.00	0.00	0.00	0.00	0.00	0.00	0.00	0.00	0.00	0.00	IC CONDITION ALL JOINTS = 0 DEG
2	43.61	6.99	-0.91	36.26	22.38	-9.47	37.8	13.5	0.00	-36.0	0.00	27.0	9.0	
3	27.49	7.54	-10.91	46.98	68.13	-45.75	63.0	36.0	4.5	-99.0	16.2	63.0	9.0	
4	13.42	11.57	-10.66	61.37	66.39	-41.97	94.5	36.0	13.5	-127.8	27.0	99.0	9.0	
5	-26	14.62	-15.74	54.92	61.96	-37.03	117.0	19.8	1.8	-126.0	54.0	138.5	7.2	
6	-14.12	17.78	-15.74	86.09	56.55	6.16	130.5	0.00	-22.5	-108.0	58.5	153.0	16.2	
7	-35.50	11.57	-14.54	109.96	58.68	63	184.5	-13.5	-57.5	-53.0	90.0	168.2	10.8	
8	-43.58	10.30	-10.04	92.20	77.30	-15.70	184.5	-19.8	-76.5	-27.0	109.8	162.0	0.00	
9	-43.83	11.26	-11.44	37.50	74.15	-76.22	184.5	-19.8	-76.5	-13.5	126.0	162.0	-9.0	
10	-44.86	6.83	-8.14	41.25	83.19	-65.02	184.5	-19.8	-72.0	-22.5	116.2	166.5	0.00	
11	-36.67	6.01	-8.04	37.79	84.55	-56.32	171.0	-19.8	-45.0	-72.0	106.2	157.5	22.5	FWD CAPTURE POSITION
12	-21.40	7.42	-7.71	62.44	86.09	-28.29	153.0	-28.0	-13.5	-118.0	91.8	139.5	45.0	
13	-10.44	7.32	-6.96	72.40	84.13	-31.36	144.0	-31.5	9.0	-14.0	63.0	126.0	67.5	
14	-7.77	5.95	-6.93	-17.03	83.81	-116.79	117.0	13.5	36.2	-157.5	31.5	126.0	54.0	
15	6.40	7.15	-8.41	-12.05	78.81	-107.99	112.5	54.0	45.0	-146.5	43.2	117.0	0.00	
16	17.53	7.03	-9.93	-81.00	85.50	171.00	99.0	63.0	36.0	-126.0	31.5	81.0	0.00	
17	33.46	10.68	-11.34	-124.48	85.46	140.12	72.0	78.2	0.00	-76.5	18.0	54.0	7.2	
18	43.25	10.05	-10.05	-158.53	85.29	112.98	72.0	76.5	-13.5	-28.8	9.0	27.0	10.8	REAR POSITION
19	44.48	6.96	-9.92	-165.37	85.36	100.64	76.5	76.5	-13.5	-22.5	9.0	19.8	10.8	

POSITION (FT)

DEGREES

## CAPTURE CONCEPT NUMBER 2 (6-DOF)

LINE	X	Y	Z	ROLL	PITCH	YAW	W-ROLL	W-PITCH	M-YAW	ELBOW	S-ROLL	S-YAW	S-PITCH	COMMENTS
1	47.00	0.00	0.00	0.00	0.00	0.00	0.00	0.00	0.00	0.00	0.00	0.00	0.00	IC CONDITION ALL JOINTS = 0 DEG
2	40.83	13.61	-13.14	58.50	36.00	0.00	58.5	18.0	0.00	-36.0	0.00	36.0	18.0	
3	7.56	13.34	-14.84	82.45	72.75	-21.31	101.7	10.8	16.0	-126.0	0.00	181.7	63.0	
4	-11.55	16.86	-10.12	-28.04	83.80	-134.11	110.7	-45.0	7.2	-121.5	0.00	108.0	139.5	
5	-29.50	15.09	-9.3	-77.21	71.97	-168.17	101.7	-78.2	7.2	-90.0	0.00	72.0	178.2	
6	-42.51	13.81	-0.00	-85.50	72.00	175.50	94.5	-72.0	4.5	-36.0	0.00	36.0	180.0	
7	-42.32	13.95	-0.00	-81.00	72.00	176.40	99.0	-72.0	1.8	-32.4	0.00	36.2	180.0	
8	-42.32	13.95	-0.00	-81.00	72.00	176.40	99.0	-72.0	1.8	-32.4	0.00	36.2	180.0	
9	-42.51	13.81	-0.00	-90.00	73.74	171.00	90.0	-76.5	9.0	-36.0	0.00	36.0	180.0	
10	-37.86	6.61	-1.19	-76.70	73.74	164.07	101.7	-72.0	10.8	-78.2	0.00	45.0	178.2	
11	-26.99	11.57	-4.27	-71.13	78.96	-162.29	100.8	-70.2	18.0	-191.7	0.00	73.8	171.8	
12	-15.04	9.80	-6.23	-91.70	78.29	-177.51	90.0	-55.8	36.0	-191.7	0.00	97.2	157.5	
13	-4.90	7.13	-6.75	-93.60	78.30	-180.00	86.4	-24.3	36.0	-132.3	0.00	117.0	126.0	
14	-1.58	8.12	-7.25	-81.00	77.40	-180.00	99.0	1.8	28.8	-133.0	0.00	124.2	100.8	
15	-1.59	7.88	-7.54	-104.22	74.63	159.30	96.3	5.4	36.0	-133.0	0.00	124.2	99.0	
16	-1.19	7.88	-7.54	-104.22	74.63	159.30	96.3	5.4	36.0	-133.0	0.00	124.2	99.0	
17	-1.19	7.88	-7.54	-112.12	73.49	150.42	97.2	5.4	38.7	-133.0	0.00	122.4	99.0	
18	-1.19	7.88	-7.54	-101.52	74.63	159.30	99.0	5.4	36.0	-133.0	0.00	122.4	99.0	
19	3.31	8.66	-8.76	-85.50	74.70	-180.00	94.5	36.0	31.5	-133.0	0.00	124.2	69.3	
20	11.82	9.25	-11.10	-94.13	73.52	171.34	99.0	63.0	42.3	-133.0	0.00	96.3	43.2	
21	17.84	9.85	-12.82	-90.56	71.51	170.36	108.0	72.0	45.0	-118.8	0.00	83.7	36.0	
22	27.57	10.59	-10.42	-103.42	76.75	159.17	114.3	74.0	45.0	-91.8	0.00	64.8	27.0	
23	36.52	9.89	-14.05	-103.42	73.83	163.84	126.0	81.0	45.0	-91.8	0.00	43.2	23.4	
24	40.86	10.49	-15.44	-101.64	76.13	165.01	118.8	81.0	29.7	-84.2	0.00	30.6	20.7	
25	42.47	10.84	-15.29	-107.59	75.85	164.46	118.8	82.8	27.0	-84.2	0.00	22.5	19.8	REAR POSITION

POSITION (FT)

DEGREES

SHOULDER CENTERLINE

## CAPTURE CONCEPT NUMBER 3 (7-DOF)

LINE	X	Y	Z	ROLL	PITCH	YAW	M-ROLL	M-PITCH	M-YAW	ELBOW	S-ROLL	S-YAW	S-PITCH	COMMENTS
1	47.00	0.	0.	0.	0.	0.	0.	0.	0.	0.	0.	0.	0.	IC CONDITION ALL JOINTS = 0 DEG
2	46.42	0.	-1.35	0.	9.08	0.	0.	0.	0.	0.	0.	0.	0.	
3	14.52	0.	-40.70	0.	72.08	0.	0.	0.	0.	0.	0.	0.	0.	
4	3.09	-3.63	-40.61	-118.32	56.68	-108.97	0.	0.	0.	0.	0.	0.	0.	
5	-6.46	-10.66	-43.97	-146.82	80.14	-152.77	9.0	0.	22.5	-9.0	0.	0.	0.	
6	-6.12	-10.64	-40.83	-148.29	80.27	-152.44	9.0	0.	22.5	-27.0	0.	0.	0.	
7	-6.46	-10.86	-43.97	-146.82	80.14	-152.77	9.0	0.	22.5	-27.0	0.	0.	0.	
8	-6.46	-10.64	-40.83	-148.29	80.27	-152.44	9.0	0.	22.5	-27.0	0.	0.	0.	
9	-6.46	-10.64	-40.83	-148.29	80.27	-152.44	9.0	0.	22.5	-27.0	0.	0.	0.	
10	-6.46	-10.64	-40.83	-148.29	80.27	-152.44	9.0	0.	22.5	-27.0	0.	0.	0.	
11	-6.46	-10.64	-40.83	-148.29	80.27	-152.44	9.0	0.	22.5	-27.0	0.	0.	0.	
12	-6.46	-10.64	-40.83	-148.29	80.27	-152.44	9.0	0.	22.5	-27.0	0.	0.	0.	
13	-6.46	-10.64	-40.83	-148.29	80.27	-152.44	9.0	0.	22.5	-27.0	0.	0.	0.	
14	-6.46	-10.64	-40.83	-148.29	80.27	-152.44	9.0	0.	22.5	-27.0	0.	0.	0.	
15	-6.46	-10.64	-40.83	-148.29	80.27	-152.44	9.0	0.	22.5	-27.0	0.	0.	0.	
16	-6.46	-10.64	-40.83	-148.29	80.27	-152.44	9.0	0.	22.5	-27.0	0.	0.	0.	
17	-6.46	-10.64	-40.83	-148.29	80.27	-152.44	9.0	0.	22.5	-27.0	0.	0.	0.	
18	-6.46	-10.64	-40.83	-148.29	80.27	-152.44	9.0	0.	22.5	-27.0	0.	0.	0.	
19	-6.46	-10.64	-40.83	-148.29	80.27	-152.44	9.0	0.	22.5	-27.0	0.	0.	0.	
20	-6.46	-10.64	-40.83	-148.29	80.27	-152.44	9.0	0.	22.5	-27.0	0.	0.	0.	
21	-6.46	-10.64	-40.83	-148.29	80.27	-152.44	9.0	0.	22.5	-27.0	0.	0.	0.	
22	-6.46	-10.64	-40.83	-148.29	80.27	-152.44	9.0	0.	22.5	-27.0	0.	0.	0.	
23	-6.46	-10.64	-40.83	-148.29	80.27	-152.44	9.0	0.	22.5	-27.0	0.	0.	0.	
24	-6.46	-10.64	-40.83	-148.29	80.27	-152.44	9.0	0.	22.5	-27.0	0.	0.	0.	
25	-6.46	-10.64	-40.83	-148.29	80.27	-152.44	9.0	0.	22.5	-27.0	0.	0.	0.	
26	-6.46	-10.64	-40.83	-148.29	80.27	-152.44	9.0	0.	22.5	-27.0	0.	0.	0.	

POSITION (FT)

DEGREES

25 FT ABOVE CREW STATION

FULL DOWN

FULL UP

## CAPTURE CONCEPT NUMBER 3 (6-DOF)

LINE	X	Y	Z	ROLL	PITCH	YAW	M-ROLL	M-PITCH	M-YAW	ELBOW	S-ROLL	S-YAW	S-PITCH	COMMENTS
1	47.00	0.	0.	0.	0.	0.	0.	0.	0.	0.	0.	0.	0.	IC CONDITION ALL JOINTS = 0 DEG
2	17.99	0.	-43.42	0.	67.50	0.	0.	0.	0.	0.	0.	0.	0.	
3	-7.29	-4.44	-46.01	-138.27	74.78	-136.59	0.	0.	0.	0.	0.	0.	0.	
4	-7.23	-7.59	-45.82	-127.19	72.14	-125.28	0.	0.	0.	0.	0.	0.	0.	
5	-7.13	-10.94	-45.88	-180.00	78.30	-180.00	0.	0.	0.	0.	0.	0.	0.	
6	-7.13	-10.94	-45.88	-180.00	78.30	-180.00	0.	0.	0.	0.	0.	0.	0.	
7	-7.13	-10.94	-45.88	-180.00	78.30	-180.00	0.	0.	0.	0.	0.	0.	0.	
8	-7.13	-10.94	-45.88	-180.00	78.30	-180.00	0.	0.	0.	0.	0.	0.	0.	
9	-7.13	-10.94	-45.88	-180.00	78.30	-180.00	0.	0.	0.	0.	0.	0.	0.	
10	-7.13	-10.94	-45.88	-180.00	78.30	-180.00	0.	0.	0.	0.	0.	0.	0.	
11	-7.13	-10.94	-45.88	-180.00	78.30	-180.00	0.	0.	0.	0.	0.	0.	0.	
12	-7.13	-10.94	-45.88	-180.00	78.30	-180.00	0.	0.	0.	0.	0.	0.	0.	
13	-7.13	-10.94	-45.88	-180.00	78.30	-180.00	0.	0.	0.	0.	0.	0.	0.	
14	-7.13	-10.94	-45.88	-180.00	78.30	-180.00	0.	0.	0.	0.	0.	0.	0.	
15	-7.13	-10.94	-45.88	-180.00	78.30	-180.00	0.	0.	0.	0.	0.	0.	0.	
16	-7.13	-10.94	-45.88	-180.00	78.30	-180.00	0.	0.	0.	0.	0.	0.	0.	
17	-7.13	-10.94	-45.88	-180.00	78.30	-180.00	0.	0.	0.	0.	0.	0.	0.	

POSITION (FT)

DEGREES

25 FT ABOVE CREW STATION

FULL DOWN

FULL UP

IC CONDITION ALL JOINTS = 0 DEG



## CAPTURE CONCEPT NUMBER 4 (17-DOF)

LINE	X	Y	Z	ROLL	PITCH	YAW	M-ROLL	M-PITCH	M-YAW	ELBOW	S-ROLL	S-YAW	S-PITCH	COMMENTS
1	47.00	0.00	0.00	0.00	0.00	0.00	0.00	0.00	0.00	0.00	0.00	0.00	0.00	IC CONDITION ALL JOINTS = 0 DEG
2	46.05	-3.63	-7.00	7.48	10.29	-9.03	0.00	0.00	0.00	-9.00	9.00	0.00	9.00	
3	42.36	-17.26	-10.41	-4.32	57.74	-27.69	-1.80	45.00	0.00	-45.00	4.50	0.00	13.50	
4	26.82	-32.76	-9.64	-7.17	64.79	-39.90	-13.50	72.00	0.00	-45.00	10.80	-18.00	13.50	
5	28.52	-32.80	-12.73	129.02	82.77	125.06	-36.00	81.00	21.60	-23.40	14.40	-35.00	19.80	FULL STARBOARD
6	28.47	-33.74	-13.02	123.66	84.21	116.74	-40.50	79.20	14.40	-23.40	16.20	-35.00	19.80	
7	28.86	-33.74	-12.12	104.86	84.76	98.92	-41.40	79.20	14.40	-23.40	16.20	-35.00	19.80	
8	28.86	-33.74	-12.12	111.88	83.19	107.39	-43.20	81.00	14.40	-23.40	16.20	-35.00	19.80	
9	29.44	-28.73	-13.91	145.75	80.22	138.35	-45.00	81.00	16.20	-27.00	14.40	-19.80	18.00	
10	29.85	-21.44	-13.27	170.90	79.80	-174.98	-47.70	77.40	16.20	-27.00	9.00	0.00	18.00	
11	29.35	-20.78	-12.48	164.64	78.03	-172.89	-45.00	79.20	16.20	-27.00	9.00	2.70	18.00	
12	28.02	-19.86	-12.88	173.59	83.25	-149.00	-81.00	72.00	28.80	-77.40	9.00	5.40	18.00	
13	27.33	-14.99	-12.94	155.88	84.95	134.43	-36.00	72.00	30.60	-88.20	15.30	17.00	13.50	
14	27.20	-10.16	-12.55	137.89	83.19	148.49	-36.00	72.00	30.60	-95.40	10.80	27.00	10.80	
15	27.21	-9.53	-11.60	143.61	81.58	131.37	-27.00	74.70	30.60	-97.20	18.00	28.80	9.00	
16	26.69	-9.72	-12.63	162.42	80.43	150.25	-27.00	74.70	30.60	-97.20	15.30	28.80	13.50	SHUTTLE CENTERLINE
17	26.61	-9.80	-12.72	165.10	80.36	159.72	-29.70	74.70	30.60	-97.20	18.00	28.80	11.70	
18	26.64	-9.53	-12.87	154.76	82.64	145.72	-30.60	73.80	28.80	-97.20	18.00	31.50	10.80	
19	27.25	-8.17	-12.53	154.76	82.64	147.13	-32.40	66.60	18.00	-99.00	27.00	49.00	3.60	
20	27.92	-6.61	-12.32	130.47	80.27	161.41	-32.40	63.00	0.00	-97.20	37.80	57.60	-1.80	
21	27.00	7.48	-13.45	178.94	72.77	170.91	-32.40	59.40	-25.20	-82.80	55.00	63.00	-9.00	
22	26.87	17.34	-14.84	178.94	72.77	165.47	-27.00	54.00	-32.40	-84.80	51.30	64.80	-5.40	
23	27.74	24.66	-14.05	168.80	79.22	165.47	-27.00	54.00	-39.60	-66.80	37.80	64.80	5.40	
24	27.99	30.06	-13.19	162.96	83.26	156.31	-16.20	54.00	-43.20	-87.80	27.00	83.00	15.20	
25	26.16	35.28	-12.64	124.59	81.78	122.59	-9.00	54.00	-46.80	-9.00	9.00	83.00	23.40	FULL PORT
26	27.67	35.66	-13.60	137.60	84.57	131.97	1.80	63.00	-46.80	-9.00	9.00	83.00	23.40	
27	27.75	35.64	-12.45	157.39	84.22	151.59	2.70	66.60	-46.80	-9.00	6.30	54.00	23.40	

POSITION (FT)

DEGREES

## CAPTURE CONCEPT NUMBER 4 (16-DOF)

LINE	X	Y	Z	ROLL	PITCH	YAW	M-ROLL	M-PITCH	M-YAW	ELBOW	S-ROLL	S-YAW	S-PITCH	COMMENTS
1	47.00	0.00	0.00	0.00	0.00	0.00	0.00	0.00	0.00	0.00	0.00	0.00	0.00	IC CONDITION ALL JOINTS = 0 DEG
2	40.22	-6.55	-9.66	-8.03	10.89	-36.77	0.00	0.00	0.00	-54.00	0.00	18.00	13.50	
3	30.83	-19.87	-10.02	-13.63	38.07	-44.03	0.00	24.30	30.60	-72.00	0.00	4.50	18.00	
4	29.27	-32.69	-12.12	161.11	74.69	-162.93	-27.00	81.00	30.60	-28.80	0.00	-31.50	22.50	
5	28.88	-34.27	-13.04	180.27	83.41	-165.32	0.00	72.00	48.60	-13.50	0.00	-40.50	24.30	FULL STARBOARD
6	28.88	-34.27	-13.04	180.27	83.41	-165.32	0.00	72.00	48.60	-13.50	0.00	-40.50	24.30	
7	28.88	-34.27	-13.04	159.99	83.28	-160.92	-1.80	72.00	46.80	-13.50	0.00	-40.50	24.30	
8	27.62	-29.37	-12.47	138.37	81.46	-144.51	-9.00	72.00	54.00	-52.20	0.00	-18.00	24.30	
9	27.57	-18.67	-12.97	163.83	82.54	-167.06	-1.80	72.00	66.60	-81.00	0.00	9.00	25.20	
10	27.52	-12.04	-12.95	169.43	82.62	169.12	4.50	72.00	72.00	-91.80	0.00	24.30	25.20	
11	27.08	-11.04	-12.74	173.93	82.62	169.12	9.00	72.00	72.00	-94.50	0.00	27.00	25.20	
12	27.08	-11.04	-12.74	179.77	82.62	169.12	15.30	72.00	72.00	-94.50	0.00	27.00	25.20	
13	27.08	-11.04	-12.74	179.77	82.62	169.12	15.30	72.00	72.00	-94.50	0.00	27.00	25.20	
14	27.78	-10.75	-13.03	179.32	79.81	171.77	13.50	78.60	72.00	-92.70	0.00	38.70	25.20	SHUTTLE CENTERLINE
15	27.13	-5.72	-12.77	178.32	82.73	173.39	1.80	72.00	63.00	-99.00	0.00	54.00	25.20	
16	27.53	2.39	-12.96	171.00	78.30	180.00	9.00	76.50	45.00	-99.00	0.00	66.60	24.30	
17	27.43	10.57	-12.39	153.22	85.07	-158.23	0.00	70.20	22.50	-81.00	0.00	72.00	24.30	
18	27.77	18.67	-12.54	150.27	82.93	-156.88	-1.80	72.00	0.00	-61.20	0.00	72.00	24.30	
19	27.66	26.75	-12.49	177.07	80.98	176.97	1.80	78.70	-9.00	-45.00	0.00	58.40	24.30	
20	27.54	31.18	-12.44	171.07	83.41	165.32	1.80	72.00	-18.00	-45.00	0.00	57.60	24.30	
21	27.54	35.38	-12.44	178.17	83.41	165.32	9.90	72.00	-36.00	-16.20	0.00	57.60	24.30	FULL PORT
22	27.73	35.63	-12.52	172.43	83.50	167.64	9.00	72.00	-40.50	-9.00	0.00	54.00	24.30	

POSITION (FT)

DEGREES

## CAPTURE CONCEPT NUMBER 5 (7-DOF)

LINE	X	Y	Z	ROLL	PITCH	YAW	M-ROLL	M-PITCH	M-YAW	ELBOW	S-ROLL	S-YAW	S-PITCH	COMMENTS
1	47.00	0.0	0.0	0.0	0.0	0.0	0.0	0.0	0.0	0.0	0.0	0.0	0.0	IC CONDITION ALL JOINTS = 0 DE
2	46.92	-1.11	-2.21	-1.13	2.78	-2.70	0.0	0.0	0.0	-2.7	0.0	0.0	0.0	
3	32.20	-12.78	-12.75	-18.65	11.09	-60.33	0.0	0.0	0.0	-76.5	0.0	0.0	21.6	
4	13.14	-11.80	-17.06	-41.73	16.86	-104.13	0.0	0.0	0.0	-117.0	24.3	25.2	28.8	
5	5.43	-25.33	-17.18	-50.58	-2.28	-112.76	0.0	0.0	0.0	-97.2	16.2	-33.3	51.3	
6	13.83	-35.76	-7.55	-27.65	5.45	-100.66	-15.3	0.0	1.8	-67.5	9.0	-45.0	72.0	
7	2.60	-39.96	-16.07	-83.37	32.03	-94.72	-15.3	10.8	29.7	-46.8	9.0	-45.0	81.0	
8	0.05	-39.97	-16.96	-83.37	32.03	-94.72	-15.3	10.8	29.7	-46.8	9.0	-45.0	81.0	
9	-2.28	-39.92	-15.37	-83.78	85.13	-106.96	130.6	9.0	88.2	-48.6	9.0	-45.0	88.2	
10	-2.80	-39.89	-14.93	-83.36	82.63	-133.92	180.0	10.8	88.2	-48.6	9.0	-45.0	90.0	FULL STARBOARD
11	-2.28	-39.92	-15.37	-83.78	85.13	-106.96	130.6	9.0	88.2	-48.6	9.0	-45.0	88.2	
12	-3.01	-35.61	-14.76	-95.92	73.82	-93.26	166.5	20.7	82.8	-69.3	18.0	-36.0	74.7	
13	-6.53	-31.09	-14.12	-54.61	71.58	-145.76	157.5	40.5	81.0	-69.3	28.8	-32.4	68.4	
14	-3.59	-22.21	-16.03	-58.63	80.77	-135.72	135.0	40.5	81.0	-18.0	35.0	-18.0	49.5	
15	-3.64	-14.96	-17.77	-14.97	77.66	-175.93	128.0	40.5	81.0	-18.0	35.0	-18.0	49.5	
16	-2.45	-8.79	-14.30	-51.97	81.28	-137.17	122.4	22.5	81.0	-137.7	54.2	-7.2	45.0	
17	-2.65	-8.38	-14.50	-45.56	81.96	-163.53	130.5	22.5	81.0	-137.7	54.2	-7.2	45.0	
18	-3.11	-7.99	-14.63	-29.69	74.98	-163.53	130.5	22.5	81.0	-137.7	54.2	-7.2	45.0	SHUTTLE CENTERLINE
19	-2.67	-5.60	-13.90	-33.60	76.67	-159.69	127.8	16.2	76.5	-142.2	61.2	13.5	37.8	
20	-3.21	-1.07	-14.12	-24.17	85.48	-166.41	121.5	0.0	81.0	-144.0	79.2	18.0	33.3	
21	-2.92	5.45	-13.14	-12.19	76.78	-164.55	108.2	-18.0	67.5	-144.0	108.0	18.0	25.2	
22	-3.78	3.56	-17.22	-43.65	60.13	-88.49	99.0	-43.2	67.5	-135.0	148.5	38.0	32.4	
23	-8.59	17.17	-4.32	-43.65	48.82	-165.50	73.8	-54.0	63.0	-130.5	148.5	38.0	49.5	
24	-3.86	35.55	-10.39	-43.65	75.93	-177.78	72.0	-63.0	56.7	-66.6	144.0	45.0	54.0	
25	-2.56	36.79	-15.69	-12.75	73.07	-177.58	81.0	-63.0	56.7	-66.6	144.0	45.0	54.0	
26	-1.07	39.74	-15.11	-2.50	54.98	-171.72	81.0	-67.5	27.0	-50.4	153.0	49.5	61.2	FULL PORT
27	-5.17	41.33	-14.06	-5.36	69.60	-170.13	90.0	-66.6	24.3	-41.4	135.0	61.2	63.0	

DEGREES

POSITION (FT)

## CAPTURE CONCEPT NUMBER 5 (6-DOF)

LINE	X	Y	Z	ROLL	PITCH	YAW	M-ROLL	M-PITCH	M-YAW	ELBOW	S-ROLL	S-YAW	S-PITCH	COMMENTS
1	47.00	0.0	0.0	0.0	0.0	0.0	0.0	0.0	0.0	0.0	0.0	0.0	0.0	IC CONDITION ALL JOINTS = 0 DE
2	46.03	5.89	-7.29	-1.14	9.00	-9.1	0.0	0.0	-6.3	0.0	0.0	0.0	0.0	
3	34.03	-8.34	-7.05	-10.45	5.28	-63.48	0.0	0.0	-9.0	-3.6	0.0	0.0	9.0	
4	29.74	-19.17	-9.66	-17.51	2.82	-67.79	0.0	18.0	9.0	-3.0	0.0	27.0	11.7	
5	19.83	-32.79	-11.73	-22.43	58.00	-39.72	0.0	31.5	63.0	-53.0	0.0	-23.4	30.6	
6	5.01	-39.40	-13.27	-122.72	81.99	-125.53	0.0	25.2	90.0	-54.0	0.0	-43.2	69.3	
7	1.78	-39.40	-14.07	-129.15	79.26	-139.56	9.0	15.3	90.0	-54.0	0.0	-43.2	82.8	
8	0.00	-39.56	-16.02	-14.18	80.61	-163.44	167.4	9.0	90.0	-54.0	0.0	-43.2	90.0	
9	-8.1	-39.59	-17.11	-7.20	81.00	-180.00	187.2	6.3	90.0	-54.0	0.0	-43.2	92.7	
10	-1.34	-39.58	-17.85	-2.35	80.82	-168.71	189.0	6.3	90.0	-54.0	0.0	-43.2	92.7	
11	-1.34	-39.59	-17.08	-15.93	83.45	-164.03	180.0	1.8	91.8	-46.8	0.0	-43.2	94.5	
12	-1.35	-38.17	-17.18	-21.38	83.15	-156.76	181.8	1.8	95.4	-46.8	0.0	-43.2	94.5	
13	-1.29	-36.22	-16.44	-25.22	82.75	-158.28	184.5	1.8	100.8	-53.0	0.0	-38.2	94.5	
14	-8.3	-30.27	-17.56	-23.63	78.27	-147.61	189.0	7.2	108.0	-53.7	0.0	-18.8	92.7	
15	0.00	-25.25	-17.16	-7.78	80.61	-163.44	189.0	9.0	108.0	-53.7	0.0	-18.8	92.7	
16	0.00	-22.76	-17.66	-14.94	80.61	-163.44	189.0	9.0	108.0	-53.7	0.0	-18.8	92.7	
17	0.00	-22.35	-16.24	9.00	81.00	-180.00	189.0	9.0	108.0	-53.7	0.0	-18.8	92.7	
18	0.00	-16.47	-16.47	-24.96	79.73	-152.08	183.6	11.7	111.6	-120.6	0.0	15.3	90.0	
19	0.00	-12.27	-15.80	-40.69	81.71	-139.44	180.0	4.5	108.0	-129.6	0.0	27.0	91.8	
20	-1.44	-9.40	-15.27	-141.37	85.51	-136.49	181.8	-9.0	101.7	-135.0	0.0	38.0	95.4	
21	-1.68	-9.40	-15.24	-159.78	81.48	-17.93	181.8	-14.4	101.7	-135.0	0.0	38.0	95.4	
22	-1.20	-9.40	-15.29	-27.30	84.75	-148.99	183.6	0.0	101.7	-135.0	0.0	38.0	95.4	
23	-7.2	-9.40	-15.32	-4.50	85.50	-150.00	184.5	1.8	99.0	-135.0	0.0	38.0	95.4	
24	-4.8	-9.40	-15.33	17.67	82.58	-165.99	183.6	5.4	97.2	-135.0	0.0	38.0	95.4	
25	-4.7	-5.63	-14.89	33.04	81.14	-156.10	189.0	6.3	87.3	-140.4	0.0	49.5	91.8	
26	0.0	1.02	-14.41	-50.15	79.95	-116.71	193.5	4.5	73.8	-140.4	0.0	79.2	90.0	
27	0.0	14.61	-15.55	-36.09	83.64	-135.09	189.0	4.5	24.3	-126.0	0.0	106.2	90.0	
28	-5.1	20.51	-16.16	-22.10	83.96	-153.45	184.5	3.6	7.2	-12.5	0.0	108.0	91.8	
29	-6.6	35.35	-13.98	-46.82	79.74	-127.85	180.0	3.6	-24.3	-36.0	0.0	104.4	92.7	
30	-6.5	42.51	-13.80	-55.50	79.51	-128.90	183.6	2.7	-45.0	-36.0	0.0	88.2	94.5	
31	-9.5	44.08	-12.02	-72.45	74.28	-105.11	181.8	0.0	-45.0	-27.0	0.0	88.2	94.5	
32	-1.02	44.58	-12.91	-75.12	69.72	-102.29	181.8	0.0	-45.0	-18.0	0.0	88.2	94.5	

DEGREES

POSITION (FT)

## CAPTURE CONCEPT NUMBER 6 (7-DOF)

LINE	X	Y	Z	ROLL	PITCH	YAW	W-ROLL	W-PITCH	W-YAW	ELBOW	S-ROLL	S-YAW	S-PITCH	COMMENTS
1	47.00	0.	0.	0.	0.	0.	0.	0.	0.	0.	0.	0.	0.	IC CONDITION ALL JOINTS = 0 DEG
2	37.17	-11.74	-12.74	-12.27	13.92	-47.68	0.	0.	0.	-58.5	0.	0.	0.	
3	16.89	-14.87	-16.03	-35.02	12.47	-96.80	0.	0.	0.	-108.0	14.4	19.8	18.0	
4	-2.83	-21.03	-19.48	-73.34	-15.28	-15.11	0.	0.	1.8	-104.4	22.5	0.	72.0	
5	-13.42	-25.16	-12.75	-79.74	13.35	-102.26	0.	-26.5	32.4	-99.0	37.8	-9.0	87.3	
6	-25.50	-29.01	-10.83	-61.62	29.76	-112.89	76.5	-36.0	39.6	-72.0	36.8	-14.4	126.0	
7	-32.04	-31.12	-12.63	29.19	67.47	-114.48	153.0	-36.0	63.0	-34.2	36.0	-27.0	148.5	
8	-33.37	-30.11	-13.24	3.93	77.11	-117.24	153.8	-36.0	63.0	-18.0	27.0	-34.2	153.0	
9	-33.92	-30.94	-11.33	15.32	76.84	-123.03	163.8	-32.4	64.8	-9.0	27.0	-36.0	155.7	FULL STARBOARD
10	-33.02	-26.22	-11.48	21.14	73.35	-182.84	145.8	-18.0	72.0	-25.2	40.5	-33.3	149.4	
11	-33.75	-19.85	-10.54	22.95	76.15	-188.76	135.0	-9.0	82.8	-43.2	52.2	-25.2	139.5	
12	-34.52	-10.98	-11.73	27.00	74.38	-197.59	123.3	-2.7	90.0	-61.2	63.0	-18.0	131.4	
13	-34.70	-10.36	-11.60	34.89	76.51	-195.76	108.0	1.8	92.7	-72.0	79.2	-12.6	124.2	
14	-34.44	-8.07	-10.53	9.80	78.85	-172.43	103.5	9.0	94.5	-72.0	82.8	-14.4	124.2	SHUTTLE CENTERLINE
15	-35.52	-0.01	-10.02	7.20	76.50	-169.26	103.8	2.7	94.5	-76.5	81.0	-9.0	124.2	
16	-35.79	10.91	-10.53	11.55	80.94	-179.74	90.0	-18.4	99.0	-76.5	90.0	0.	126.0	
17	-35.61	18.10	-15.03	41.19	85.79	-188.18	81.0	-23.5	90.0	-68.4	92.7	18.0	127.8	
18	-32.82	26.39	-17.74	-10.88	88.12	-159.50	72.0	-23.4	76.5	-49.5	91.8	27.0	129.6	
19	-34.17	27.13	-15.85	-11.84	84.34	-161.19	67.5	-19.8	72.0	-27.0	91.8	36.0	135.0	FULL PORT
20										-18.0	91.8	36.0	144.0	

POSITION (FT)

DEGREES

## CAPTURE CONCEPT NUMBER 6 (6-DOF)

LINE	X	Y	Z	ROLL	PITCH	YAW	W-ROLL	W-PITCH	W-YAW	ELBOW	S-ROLL	S-YAW	S-PITCH	COMMENTS
1	47.00	0.	0.	0.	0.	0.	0.	0.	0.	0.	0.	0.	0.	IC CONDITION ALL JOINTS = 0 DEG
2	23.93	-14.00	-21.78	-39.47	16.65	-70.81	0.	0.	0.	-82.0	0.	0.	0.	
3	3.86	-15.40	-24.39	-80.93	-7.11	-91.13	0.	0.	-13.5	-103.5	0.	19.8	42.3	
4	-14.68	-23.45	-20.21	-126.41	-8.00	-84.14	0.	0.	13.5	-86.4	0.	0.	81.0	
5	-19.78	-31.42	-18.00	-141.68	19.48	-12.87	0.	0.	18.0	-87.6	0.	-20.7	126.0	
6	-26.67	-32.38	-13.59	-178.63	32.97	-176.97	0.	0.	64.0	-80.5	0.	-27.0	137.7	
7	-30.20	-30.98	-13.07	-143.72	47.46	-170.27	40.5	-24.3	66.6	-82.4	0.	-27.0	153.0	
8	-32.43	-30.94	-13.43	-35.77	74.86	-145.96	165.6	-54.0	61.2	-72.0	0.	-36.0	156.6	
9	-33.39	-29.98	-13.83	-2.59	80.96	-174.00	181.8	-58.5	45.0	-7.2	0.	-36.0	157.5	
10	-33.39	-29.98	-13.83	7.20	81.00	-180.00	181.8	-58.5	45.0	-7.2	0.	-36.0	157.5	
11	-33.37	-29.41	-13.82	25.97	83.41	-180.77	190.8	-61.2	42.3	-15.3	0.	-31.5	157.5	FULL STARBOARD
12	-32.65	-29.24	-13.52	44.23	82.40	-181.22	194.4	-61.2	42.3	-25.2	0.	-27.0	157.5	
13	-33.90	-20.17	-14.04	44.28	79.95	-137.11	193.5	-59.4	42.3	-54.0	0.	-1.8	157.5	
14	-33.08	-16.17	-13.70	54.16	77.51	-113.93	193.5	-59.4	36.0	-86.6	0.	9.0	157.5	
15	-33.41	-11.75	-13.84	5.40	83.70	-180.00	185.4	-61.2	54.0	-72.0	0.	18.0	157.5	
16	-32.84	-11.48	-13.00	7.06	82.76	-173.10	181.8	-61.2	54.0	-75.6	0.	19.8	158.4	
17	-33.23	-11.48	-11.96	6.59	80.97	-174.47	182.7	-61.2	54.0	-75.6	0.	19.8	160.2	
18	-33.25	-7.90	-11.97	27.10	80.15	-151.04	187.2	-59.4	42.3	-79.2	0.	27.0	160.2	SHUTTLE CENTERLINE
19	-33.33	-2.00	-12.59	15.41	79.92	-166.81	186.3	-59.4	40.5	-81.0	0.	36.0	159.3	
20	-32.81	9.81	-12.48	20.64	78.53	-155.74	184.5	-58.5	27.0	-81.0	0.	45.0	159.3	
21	-32.81	9.81	-12.48	1.57	77.29	-177.62	180.0	-57.6	24.3	-79.2	0.	54.0	159.3	
22	-32.27	13.44	-12.57	4.07	76.45	-173.51	180.0	-55.8	12.6	-72.0	0.	56.7	159.3	
23	-33.40	18.19	-12.62	5.98	74.66	-170.02	180.0	-54.0	0.	-86.0	0.	58.5	159.3	
24	-33.01	24.88	-12.47	-3.61	76.55	-174.00	180.0	-54.0	-9.0	-68.0	0.	54.5	159.3	
25	-33.49	27.32	-12.65	-7.67	73.51	-173.51	176.4	-55.8	-18.0	-33.3	0.	52.0	159.3	
26	-33.06	29.24	-12.49	-0.00	76.50	-180.00	180.0	-55.8	-27.0	-25.2	0.	54.0	159.3	
27	-33.89	29.02	-12.81	15.24	77.98	-183.68	184.5	-57.6	-36.0	-18.0	0.	47.7	159.3	

POSITION (FT)

DEGREES

CAPTURE CONCEPT NUMBER 7 (7-DOF)

LINE	X	Y	Z	ROLL	PITCH	YAW	W-ROLL	W-PITCH	W-YAW	ELBOW	S-ROLL	S-YAW	S-PITCH	COMMENTS
1	47.00	0.0	0.0	0.0	0.0	0.0	0.0	0.0	0.0	0.0	0.0	0.0	0.0	IC CONDITION ALL JOINTS = 0 DEG
2	46.43	-2.21	-5.87	-9.91	7.14	-7.26	0.0	0.0	0.0	-9.0	0.0	1.8	7.2	
3	37.30	-1.98	-16.50	-15.31	18.82	-34.42	0.0	0.0	0.0	-59.4	-2.7	27.0	25.2	
4	13.71	-5.34	-16.35	-44.31	28.79	-92.22	0.0	0.0	0.0	-124.2	23.4	45.0	28.8	
5	9.96	-7.05	-18.35	-76.00	9.99	-118.99	0.0	0.0	1.8	-130.5	37.8	34.2	50.4	
6	-9.33	-17.91	-13.97	-114.11	12.87	-133.46	0.0	-1.8	33.3	-117.0	9.0	18.8	112.5	
7	-25.08	-26.82	-9.87	-150.02	4.85	-115.73	0.0	-31.5	34.2	-72.0	4.5	-38.0	154.8	
8	-30.25	-30.76	-5.32	-30.75	52.75	-182.60	144.0	-45.0	34.2	-23.4	-1.8	-22.5	171.0	
9	-31.25	-32.96	-7.45	-22.42	83.11	164.21	198.0	-76.5	34.2	-34.0	-4.8	-34.2	169.2	
10	-31.32	-33.23	-7.64	85.71	88.81	-76.90	189.0	-79.2	29.7	-19.8	-4.5	-36.0	167.4	FULL STARBOARD
11	-31.92	-32.81	-7.72	82.65	89.14	-81.73	189.0	-79.2	29.7	-16.0	-4.5	-36.0	167.4	
12	-31.08	-33.40	-7.50	-13.29	85.45	-174.49	189.0	-76.5	29.7	-20.7	-7.2	-38.0	168.3	
13	-31.85	-29.58	-6.57	54.52	84.16	-111.51	189.0	-76.5	29.7	-41.4	-1.8	-21.8	169.2	
14	-31.61	-23.54	-7.22	36.78	87.92	-138.65	189.0	-76.5	54.0	-83.0	-1.8	-4.5	168.3	
15	-30.30	-14.44	-8.04	37.10	84.82	-142.74	183.6	-70.2	63.0	-85.0	1.8	21.6	162.0	SHUTTLE CENTERLINE
16	-31.01	-12.50	-6.22	33.96	88.63	-145.92	171.0	-67.5	72.0	-87.3	9.0	21.6	162.0	
17	-31.00	-12.31	-6.63	44.52	84.09	-147.40	171.0	-67.5	83.7	-87.3	11.7	21.6	159.3	
18	-31.95	-8.35	-6.29	10.88	81.84	-178.50	166.5	-65.7	83.7	-90.0	11.7	29.7	168.2	
19	-32.43	1.07	-7.20	1.19	83.57	-183.64	154.8	-65.7	83.7	-90.0	28.7	45.0	153.0	
20	-33.93	10.37	-7.41	12.10	88.80	-173.89	147.6	-67.5	72.0	-81.0	28.8	54.0	148.5	
21	-34.33	19.53	-7.17	25.93	81.89	-184.77	131.4	-72.0	58.5	-83.0	34.2	57.6	148.5	
22	-34.91	26.86	-5.11	23.10	78.51	-187.36	110.7	-72.0	58.5	-88.7	36.0	54.0	157.5	FULL PORT
23	-35.29	29.98	-6.53	21.26	76.17	-189.90	100.8	-67.5	52.2	-12.6	36.0	45.0	164.7	

DEGREES

POSITION (FT)

CAPTURE CONCEPT NUMBER 7 (6-DOF)

LINE	X	Y	Z	ROLL	PITCH	YAW	W-ROLL	W-PITCH	W-YAW	ELBOW	S-ROLL	S-YAW	S-PITCH	COMMENTS
1	47.00	0.0	0.0	0.0	0.0	0.0	0.0	0.0	0.0	0.0	0.0	0.0	0.0	IC CONDITION ALL JOINTS = 0 DEG
2	43.54	-5.66	-10.45	-5.45	12.37	-23.99	0.0	0.0	0.0	-32.4	0.0	9.0	13.5	
3	21.26	-17.47	-14.45	-33.99	14.04	-84.04	0.0	0.0	0.0	-97.2	0.0	14.4	34.2	
4	3.22	-16.65	-16.88	-78.90	-13.26	-92.58	0.0	0.0	0.0	-118.8	0.0	15.3	79.2	
5	-16.61	-24.24	-16.61	-135.00	0.00	-90.00	0.0	0.0	0.0	-88.2	0.0	-1.8	135.0	
6	-27.24	-30.51	-9.08	-24.67	134.15	87.51	0.0	-42.3	1.8	-52.2	0.0	-19.8	162.0	
7	-28.87	-33.99	-4.54	-169.11	82.56	-168.31	0.0	-73.8	58.5	-36.0	0.0	-31.5	171.0	
8	-29.07	-33.23	-5.67	-167.81	84.41	-161.68	0.0	-73.8	58.5	-34.2	0.0	-30.6	169.2	
9	-30.92	-34.27	-6.91	-22.30	86.23	160.54	172.8	-73.8	58.5	-13.5	0.0	-40.5	167.4	
10	-31.30	-34.16	-7.00	-2.62	84.55	171.18	183.6	-72.0	54.0	-9.0	0.0	-42.3	167.4	
11	-31.44	-33.77	-7.03	7.43	82.80	177.57	189.0	-70.2	54.0	-3.5	0.0	-39.6	167.4	FULL STARBOARD
12	-30.02	-33.80	-6.71	24.94	84.29	-157.11	189.0	-72.0	54.0	-27.0	0.0	-38.2	167.4	
13	-30.97	-17.45	-6.92	56.03	84.95	-128.81	198.0	-73.8	54.0	-79.2	0.0	18.8	167.4	
14	-30.93	-11.43	-6.93	44.94	85.65	-140.76	195.3	-73.8	54.0	-88.2	0.0	24.3	167.4	SHUTTLE CENTERLINE
15	-30.99	-11.43	-6.93	44.94	85.65	-140.76	195.3	-73.8	54.0	-88.2	0.0	24.3	167.4	
16	-30.85	-10.27	-6.89	41.07	85.77	-143.71	193.5	-73.8	54.0	-90.0	0.0	27.0	167.4	
17	-32.44	3.65	-7.21	-18.59	84.36	-159.82	175.5	-72.0	45.0	-90.0	0.0	51.3	167.4	
18	-32.51	12.63	-7.80	-3.82	83.68	-174.45	180.0	-70.2	21.6	-81.0	0.0	61.2	166.5	
19	-32.57	22.00	-7.82	18.87	82.63	-164.96	189.0	-69.3	21.6	-53.0	0.0	64.8	166.5	
20	-33.22	29.17	-7.97	11.67	85.49	-176.46	189.0	-72.0	-7.2	-34.2	0.0	57.6	166.5	
21	-33.39	31.24	-8.82	6.74	81.00	-177.86	185.4	-67.5	-34.2	-18.0	0.0	51.3	166.5	FULL PORT

DEGREES

POSITION (FT)

# PLACEMENT IN CARGO BAY - CONCEPT NUMBER 1 (6-DOF)

LINE	X	Y	Z	ROLL	PITCH	YAW	W-ROLL	W-PITCH	W-YAW	ELBOW	S-ROLL	S-YAW	S-PITCH	COMMENTS
1	26.86	-4.78	-13.69	-119.24	70.75	-123.54	-37.8	67.5	12.6	-99.0	0.	40.5	27.0	I C CONDITION-75 PER OF FULL FWD TRAVEL
2	29.13	-2.48	-12.07	-104.93	65.08	-109.25	-52.2	63.0	-9.0	-95.4	0.	43.2	22.5	
3	30.67	1.57	-12.70	-89.10	21.73	-96.57	-54.8	22.5	-45.0	-90.0	0.	47.7	25.2	
4	33.17	4.34	-15.61	-89.52	-21.97	-94.29	-63.0	-18.0	-72.0	-76.5	0.	45.0	23.4	
5	33.85	-7.45	-14.65	-91.55	-53.87	-85.31	-45.0	-49.5	-74.7	-76.5	0.	36.0	23.5	
6	34.66	-2.36	-14.35	-98.52	-66.06	-72.53	-45.0	-63.0	-81.0	-73.8	0.	33.3	22.5	
7	36.06	-5.95	-10.48	-151.17	-80.65	-27.64	-27.0	-81.0	-105.2	-72.0	0.	27.0	16.2	
8	34.93	-8.14	-4.41	-176.40	-82.80	-8.00	-76.5	-90.0	-18.0	-61.0	0.	30.6	7.2	
9	32.22	-7.76	-2.54	-175.50	-85.50	-8.00	-100.0	-90.0	-18.0	-90.0	0.	31.5	4.5	
10	32.22	-7.76	-2.54	-129.91	-82.98	50.31	-90.0	-95.4	-31.5	-90.0	0.	31.5	4.5	SATELLITE IN CARGO BAY
11	32.22	-7.76	-2.54	122.63	-81.22	54.95	-68.2	-97.2	-36.0	-90.0	0.	31.5	4.5	

DEGREES

POSITION (FT)

# PLACEMENT IN CARGO BAY - CONCEPT NUMBER 2 (6-DOF)

LINE	X	Y	Z	ROLL	PITCH	YAW	W-ROLL	W-PITCH	W-YAW	ELBOW	S-ROLL	S-YAW	S-PITCH	COMMENTS
1	28.16	10.27	-14.35	113.72	77.69	156.31	-11.7	72.0	49.5	-90.0	0.	63.0	27.0	I C CONDITION-75 PER OF FULL FWD TRAVEL
2	28.80	10.27	-13.46	-101.90	66.90	-110.58	-40.5	63.0	-27.0	-90.0	0.	63.0	25.2	
3	29.86	7.76	-13.63	-86.73	19.34	-98.49	-63.0	18.0	-51.3	-90.0	0.	58.5	22.5	
4	32.92	2.80	-12.63	-88.43	-29.94	-91.22	-63.0	-27.0	-67.5	-81.0	0.	45.0	22.5	
5	32.92	2.80	-13.63	-96.54	-44.08	-76.44	-64.0	-45.0	-63.0	-81.0	0.	45.0	19.0	
6	33.52	2.80	-12.07	-181.90	-51.25	-59.22	-69.3	-59.4	-59.4	-81.0	0.	36.0	18.0	
7	33.99	-2.80	-11.01	-118.36	-69.07	-55.36	-63.0	-72.0	-63.0	-81.0	0.	36.0	10.8	
8	32.22	-4.76	-6.26	167.55	-79.80	14.49	-108.0	-92.7	-18.0	-88.2	0.	31.5	4.5	
9	32.22	-7.76	-2.54	122.03	-85.00	56.33	-118.3	-98.5	-9.0	-90.0	0.	29.7	4.5	SATELLITE IN CARGO BAY
10	33.52	-8.00	-2.61	113.37	-80.40	68.78	-94.5	-99.0	-27.0	-86.4	0.	29.7	4.5	
11	33.52	-7.79	-2.64	123.33	-79.22	55.22	-81.0	-99.0	-45.0	-85.5	0.	29.7	4.5	

DEGREES

POSITION (FT)

# PLACEMENT IN CARGO BAY - CONCEPT NUMBER 3 (6-DOF)

LINE	X	Y	Z	ROLL	PITCH	YAW	W-ROLL	W-PITCH	W-YAW	ELBOW	S-ROLL	S-YAW	S-PITCH	COMMENTS
1	-97	-6.73	-6.15	-143.06	61.58	-161.79	18.0	18.0	117.0	-157.5	0.	31.5	99.0	I C CONDITION-75 PER OF FULL UP TRAVE
2	-4.9	-6.73	-6.20	-144.09	62.45	-161.67	16.2	21.6	117.0	-157.5	0.	31.5	94.5	
3	1.28	-6.63	-6.20	-145.77	61.60	-163.62	13.5	38.7	115.2	-157.5	0.	32.4	78.3	
4	3.79	-7.13	-7.43	-153.61	62.28	-168.63	9.0	54.0	108.0	-153.0	0.	36.0	63.0	
5	5.29	-7.45	-7.29	-143.05	61.21	-164.75	9.0	63.0	99.0	-151.2	0.	36.0	54.0	
6	12.75	-8.66	-9.26	-165.18	62.96	-179.84	9.0	81.0	91.8	-135.0	0.	38.7	35.0	
7	18.22	-7.01	-10.78	-169.96	63.90	-179.84	9.0	89.5	79.2	-123.3	0.	43.2	30.6	
8	24.00	-7.71	-11.30	-174.68	64.80	-180.00	9.0	90.0	73.8	-123.3	0.	37.0	25.2	
9	25.44	-6.16	-10.54	-167.40	67.50	-180.00	7.2	90.0	60.3	-106.2	0.	40.5	22.5	
10	28.72	-0.00	-10.34	-99.12	63.79	-180.26	-54.0	63.0	-18.0	-90.0	0.	49.5	19.8	
11	31.51	2.61	-18.24	-94.19	35.35	-98.55	-72.0	36.0	-45.0	-90.0	0.	49.5	18.0	
12	31.56	3.18	-10.38	-94.62	36.57	-93.09	-76.5	7.2	-52.2	-68.2	0.	46.8	16.4	
13	32.17	1.04	-8.26	-93.01	-23.54	-91.06	-77.4	-22.5	-54.0	-90.0	0.	45.0	13.5	
14	32.32	0.00	-7.76	-97.75	-53.91	-80.28	-74.7	-54.0	-50.4	-90.0	0.	37.0	9.0	
15	32.57	-4.17	-5.16	-105.74	-71.79	-74.75	-76.5	-72.0	-50.4	-90.0	0.	29.7	9.0	
16	31.66	-8.77	-5.01	143.08	-79.78	37.50	-97.2	-96.3	-22.5	-90.0	0.	29.7	9.0	SATELLITE IN CARGO BAY
17	31.36	-10.27	-3.96	128.22	-78.32	50.55	-90.0	-99.0	-28.8	-90.0	0.	27.0	7.2	

DEGREES

POSITION (FT)

# PLACEMENT IN CARGO BAY - CONCEPT NUMBER 4 (6-DOF)

LINE	X	Y	Z	ROLL	PITCH	YAW	W-ROLL	W-PITCH	W-YAW	ELBOW	S-ROLL	S-YAW	S-PITCH	COMMENTS
1	24.07	26.09	-14.19	86.45	82.79	177.26	-30.0	67.5	-9.0	-66.6	0.	76.5	29.7	I C CONDITION-75 PER OF FULL STARBOARD TRAVEL
2	24.08	26.03	-13.73	95.40	82.88	180.00	-34.6	67.5	-7.2	-72.0	0.	79.2	29.7	
3	23.17	23.21	-14.20	132.98	80.57	-165.15	-67.5	67.5	-6.3	-81.0	0.	81.0	31.5	
4	21.82	19.36	-13.25	167.32	84.02	-142.15	-57.6	63.0	1.8	-94.5	0.	84.5	31.5	
5	21.84	18.27	-12.88	-117.09	83.13	-80.15	-47.7	57.6	0.	-97.2	0.	84.5	30.6	
6	25.83	14.26	-12.96	-108.97	81.85	-98.83	-27.0	63.0	2.7	-94.5	0.	73.8	27.8	
7	28.68	10.27	-12.46	-115.89	79.45	-121.08	-16.0	68.4	1.8	-90.0	0.	63.0	29.2	
8	29.29	9.27	-12.67	-94.26	69.20	-103.56	-36.0	63.0	-20.7	-90.0	0.	55.8	23.4	
9	30.86	7.79	-13.35	-98.44	51.02	-98.44	-54.0	48.6	-40.5	-85.0	0.	55.8	23.4	
10	31.79	7.69	-13.17	-88.35	27.53	-94.56	-63.0	27.0	-54.0	-82.0	0.	54.0	24.3	
11	31.67	8.34	-14.30	-88.06	13.84	-94.41	-63.0	14.4	-61.2	-81.0	0.	52.2	24.3	
12	31.00	7.25	-14.43	-87.47	-6.56	-87.02	-63.0	7.2	-63.0	-81.0	0.	49.5	19.8	
13	33.21	5.59	-11.96	-87.45	-18.42	-87.92	-66.6	-18.0	-63.0	-79.2	0.	45.0	18.0	
14	34.29	3.41	-11.14	-86.97	-42.54	-88.38	-63.0	-40.5	-70.2	-72.0	0.	33.3	18.0	
15	36.12	-4.79	-11.74	-102.33	-75.13	-66.33	-36.0	-72.0	-91.8	-72.0	0.	25.2	12.6	
16	36.37	-6.61	-8.56	-138.81	-84.88	-36.42	-14.4	-81.0	-115.2	-70.2	0.	27.0	5.4	
17	39.77	-3.14	-3.76	-146.78	-85.88	-17.16	-28.8	-88.2	-99.0	-63.0	0.	27.0	4.5	
18	34.84	-8.34	-2.73	-174.60	-85.98	-0.0	-12.6	-90.0	-108.0	-61.0	0.	27.0	4.5	SATELLITE IN CARGO BAY
19	34.68	-8.34	-2.18	-174.60	-86.40	-0.0	-12.6	-90.0	-108.0	-61.0	0.	27.0	3.6	

POSITION (FT)

# PLACEMENT IN CARGO BAY - CONCEPT NUMBER 5 (6-DOF)

LINE	X	Y	Z	ROLL	PITCH	YAW	W-ROLL	W-PITCH	W-YAW	ELBOW	S-ROLL	S-YAW	S-PITCH	COMMENTS
1	-1.36	29.84	-17.28	48.77	80.44	-131.06	180.0	1.8	-24.3	-85.5	0.	102.6	94.5	I C CONDITION-75 PER OF FULL PORT TRAVEL
2	-0.0	27.62	-17.53	36.80	80.44	-139.02	175.5	7.2	-18.0	-91.8	0.	183.5	90.0	
3	5.62	14.56	-17.28	22.89	87.48	-122.61	-67.5	67.5	-6.3	-81.0	0.	81.0	31.5	
4	11.41	16.93	-18.61	-0.0	48.31	-110.39	136.8	28.8	0.	-120.6	0.	99.0	72.0	
5	14.89	11.67	-18.00	-1.8	19.08	-101.58	81.0	36.0	-34.2	-108.0	0.	91.8	58.5	
6	22.06	18.79	-20.08	-3.98	19.11	-93.32	54.0	20.7	-52.2	-112.5	0.	82.8	50.4	
7	27.85	16.63	-19.65	-2.14	17.27	-85.32	40.5	16.2	-63.0	-86.2	0.	72.0	42.3	
8	31.49	8.82	-21.40	-4.21	-10.43	-88.89	34.2	9.0	-70.2	-81.0	0.	61.2	36.0	
9	33.51	3.37	-13.82	-5.93	-29.32	-85.88	30.6	-10.8	-72.0	-67.5	0.	46.8	34.2	
10	35.60	-1.14	-18.14	-18.82	-58.94	-79.90	28.8	-27.0	-73.8	-63.0	0.	38.7	30.6	
11	36.95	-7.58	-14.63	-21.99	-75.67	-71.49	36.0	-52.2	-82.8	-63.0	0.	27.0	27.8	
12	38.96	-8.00	-10.00	-23.05	-81.80	-66.18	49.5	-68.4	-99.0	-61.2	0.	19.8	21.6	
13	38.96	-8.00	-10.00	-23.05	-81.80	-66.18	49.5	-68.4	-99.0	-61.2	0.	19.8	21.6	
14	35.88	-11.75	-4.53	-96.95	-84.39	-7.60	54.0	-76.5	-101.7	-58.5	0.	18.0	14.4	
15	36.16	-11.75	8.	-117.00	-88.20	-24.30	61.2	-88.2	-101.7	-72.0	0.	18.0	7.2	SATELLITE IN CARGO BAY

POSITION (FT)

# PLACEMENT IN CARGO BAY - CONCEPT NUMBER 6 (6-DOF)

LINE	X	Y	Z	ROLL	PITCH	YAW	W-ROLL	W-PITCH	W-YAW	ELBOW	S-ROLL	S-YAW	S-PITCH	COMMENTS
1	-31.20	20.68	-11.23	-150.60	82.13	-152.15	9.0	-63.0	-6.3	-67.5	0.	65.7	180.2	I C CONDITION-75 PER OF FULL PORT TRAVEL
2	-22.70	20.08	-11.57	-139.95	81.68	-116.16	-10.8	-58.5	-6.3	-92.7	0.	84.6	153.8	
3	-12.25	16.81	-13.05	145.99	72.52	-155.30	-54.0	-27.0	7.2	-117.8	0.	101.7	133.2	
4	-6.52	15.78	-12.80	142.87	74.44	-156.48	-58.5	-12.6	9.0	-129.6	0.	115.2	99.0	
5	-2.00	15.42	-12.60	127.81	66.39	-162.28	-70.2	13.5	7.2	-129.6	0.	115.2	99.0	
6	4.48	17.81	-13.79	117.92	65.59	-165.18	-81.0	41.4	1.8	-121.5	0.	111.6	72.0	
7	8.39	21.83	-14.71	127.00	63.44	-144.77	-103.5	49.5	-21.6	-108.0	0.	106.2	68.3	
8	13.94	20.48	-16.33	150.53	44.13	-189.84	-141.3	39.6	-54.0	-101.7	0.	94.5	49.5	
9	20.41	16.47	-20.41	151.63	29.45	-186.49	-155.7	31.5	-63.0	-98.0	0.	74.7	45.0	
10	24.79	15.45	-22.86	161.90	5.69	-89.10	-155.7	3.6	-72.0	-76.5	0.	63.0	42.3	
11	30.67	6.73	-22.14	166.54	-13.13	-88.10	-155.7	-11.7	-74.7	-69.3	0.	47.7	36.0	
12	33.96	4.40	-20.81	161.83	-48.61	-88.97	-133.0	-34.2	-88.2	-63.0	0.	37.8	31.5	
13	35.71	0.0	-18.13	-158.99	-95.23	-76.75	-100.8	-58.5	-97.2	-63.0	0.	31.5	27.0	
14	37.88	-4.40	-12.31	-171.66	-79.93	-68.76	-88.2	-73.8	-108.0	-63.0	0.	25.2	18.0	
15	37.09	-5.95	-8.87	-154.37	-85.15	-36.37	-81.0	-84.6	-108.0	-72.0	0.	27.0	9.0	
16	37.26	-5.95	-4.71	136.88	-84.26	-36.44	-81.0	-84.6	-103.5	-72.0	0.	27.0	7.2	SATELLITE IN CARGO BAY

POSITION (FT)

CARGO DEPLOYMENT - TO SPACE (6-DOF)										COMMENTS				
LINE	X	Y	Z	ROLL	PITCH	YAW	W-ROLL	W-PITCH	W-YAW	ELBOW	S-ROLL	S-YAW	S-PITCH	
1	34.30	-7.69	-2.70	139.59	-74.33	40.81	-54.0	-102.6	-72.0	-82.6	0.0	28.8	4.5	I C CONDITION- ATTACHED TO CARGO IN BAY
2	33.19	-5.13	-7.97	174.50	-76.50	-0.0	-55.8	-90.0	-67.5	-85.5	0.0	34.2	13.5	
3	31.66	-0.06	-13.12	127.71	-70.13	-50.61	-54.0	-72.0	-72.0	-85.5	0.0	36.0	22.5	
4	30.73	1.35	-15.66	-99.96	-45.62	-77.21	-61.2	-45.0	-64.8	-85.5	0.0	45.0	27.0	
5	29.92	4.61	-12.39	-92.98	-95.02	-88.19	-70.2	-9.0	-54.0	-91.8	0.0	54.0	22.5	
6	28.94	2.39	-9.48	-94.93	36.74	-94.38	-72.0	36.0	-36.0	-99.0	0.0	54.0	18.0	
7	28.63	2.39	-10.31	-111.83	65.25	-104.93	-65.7	63.0	-18.0	-99.0	0.0	54.0	19.8	
8	27.05	-0.69	-10.71	-126.56	75.15	-130.74	-37.8	73.8	9.0	-103.5	0.0	50.4	21.6	
9	24.96	-8.87	-15.25	-151.18	73.35	-153.65	-19.8	72.0	36.0	-101.7	0.0	41.4	31.5	
10	20.35	-8.33	-20.35	-156.61	68.76	-154.88	-18.0	63.0	40.5	-103.5	0.0	43.2	45.0	
11	19.95	-5.18	-21.95	-121.80	71.72	-132.32	-2.7	46.8	45.0	-108.0	0.0	43.2	54.0	
12	8.43	-8.43	-25.95	-162.89	76.11	-167.11	2.7	31.5	59.4	-108.0	0.0	45.0	72.0	
13	4.72	-4.72	-29.78	172.09	75.37	170.14	2.7	23.4	61.2	-99.0	0.0	40.5	81.0	
14	2.58	-2.58	-32.72	174.91	75.88	162.29	13.5	18.0	58.5	-90.0	0.0	36.0	89.5	
15	0.0	-0.0	-38.07	157.91	78.00	-167.19	9.0	11.7	40.5	-78.2	0.0	27.0	98.0	
16	-3.39	-4.76	-43.03	175.96	76.38	172.43	3.6	9.0	38.6	-45.0	0.0	16.2	94.5	
17	-5.73	-8.05	-45.38	180.00	79.20	180.00	0.0	3.6	18.0	-23.4	0.0	5.4	97.2	
18	-5.77	-5.82	-45.63	189.73	79.94	169.65	0.0	2.7	18.0	-18.0	0.0	1.8	97.2	
19	-4.35	-5.84	-46.06	167.48	79.94	167.44	0.0	2.7	16.2	-14.4	0.0	0.0	95.4	
20	-3.64	-5.49	-46.21	159.45	82.31	159.41	0.0	2.7	16.2	-13.5	0.0	8.0	94.5	SATELLITE DEPLOYED TO SPACE

CARGO DEPLOYMENT TO DOCKING PORT - UPPER (6-DOF)										COMMENTS				
LINE	X	Y	Z	ROLL	PITCH	YAW	W-ROLL	W-PITCH	W-YAW	ELBOW	S-ROLL	S-YAW	S-PITCH	
1	35.02	-5.59	-4.42	149.98	-75.55	30.48	-54.0	-99.0	-76.5	-81.0	0.0	31.5	7.2	I C CONDITION- ATTACHED TO CARGO IN BAY
2	35.02	-5.59	-4.42	144.95	-75.51	30.27	-64.8	-99.0	-63.0	-81.0	0.0	31.5	7.2	
3	33.33	-4.06	-8.00	163.75	-75.09	21.38	-81.0	-95.4	-45.0	-85.5	0.0	36.0	13.5	
4	32.86	-1.45	-16.74	-183.78	-69.45	-32.59	-43.2	-75.6	-90.0	-76.5	0.0	36.0	27.0	
5	32.42	0.00	-23.55	-128.03	-67.11	-43.41	-27.0	-65.7	-108.0	-63.0	0.0	31.5	36.0	
6	30.38	6.0	-23.57	-125.20	-58.11	-52.36	-46.8	-60.3	-88.2	-63.0	0.0	36.0	37.8	
7	28.28	2.44	-26.56	-136.24	-47.37	-42.84	-61.2	-61.2	-76.5	-68.4	0.0	37.8	43.2	
8	26.67	4.77	-26.67	-146.87	-41.73	-29.54	-75.6	-68.4	-63.0	-72.0	0.0	43.2	45.0	
9	22.85	2.21	-26.76	-162.84	-35.26	-21.89	-96.3	-72.0	-48.3	-82.8	0.0	45.0	49.5	
10	22.07	5.21	-26.68	-154.16	-17.42	-17.42	-108.0	-45.0	-45.0	-83.7	0.0	50.4	50.4	
11	21.84	7.79	-25.57	-162.19	-9.18	-66.98	-12.5	-23.4	-52.2	-85.5	0.0	59.5	49.5	
12	18.88	6.13	-25.99	-177.08	-1.74	-71.16	-12.4	-16.2	-45.0	-91.8	0.0	56.7	54.0	
13	13.57	6.19	-26.63	165.08	2.12	-74.70	-133.2	-12.6	-63.2	-99.0	0.0	61.2	63.0	
14	8.39	5.18	-25.81	165.64	1.97	-76.07	-123.3	-12.6	-40.5	-108.0	0.0	64.8	72.0	
15	3.10	4.72	-24.54	169.98	4.16	-80.37	-108.0	-9.0	-37.8	-115.2	0.0	68.4	82.8	
16	2.26	4.98	-23.94	167.82	2.88	-82.48	-108.0	-7.2	-39.6	-117.0	0.0	70.2	84.6	
17	2.95	4.48	-23.32	169.42	3.11	-85.97	-108.0	-3.6	-17.8	-118.8	0.0	70.2	82.8	
18	3.52	4.48	-22.25	171.09	2.38	-87.80	-108.0	-1.8	-37.8	-121.5	0.0	72.8	81.8	CARGO POSITIONED AT DOCKING PORT

MODULE REPLACEMENT (7-DOF)										COMMENTS				
LINE	X	Y	Z	ROLL	PITCH	YAW	W-ROLL	W-PITCH	W-YAW	ELBOW	S-ROLL	S-YAW	S-PITCH	
1	46.14	3.68	-7.31	0.0	9.00	0.00	0.0	0.0	0.0	-9.0	0.0	9.0	9.0	I C CONDITION- ALL JOINTS=0 DEG
2	41.39	-2.20	-6.38	-20.59	-4.46	-25.75	0.0	0.0	0.0	-54.0	-20.7	25.2	18.0	
3	36.61	-2.26	-7.10	147.85	-134.11	142.18	0.0	-36.0	-20.7	-74.7	-27.0	30.6	27.0	
4	34.85	-4.80	-2.37	147.22	-118.66	130.39	0.0	-38.0	-27.0	-82.8	-36.0	27.0	27.0	
5	32.62	-6.27	-1.12	-73.83	-77.44	-20.17	-7.2	-54.0	-27.0	-90.0	-36.8	25.2	22.5	
6	32.51	-6.16	3.05	-94.25	-84.69	9.0	-7.2	-54.0	-27.0	-90.0	-40.5	25.2	22.5	
7	32.51	-6.16	3.05	-94.25	-84.69	9.0	-7.2	-54.0	-27.0	-90.0	-40.5	25.2	22.5	
8	32.62	-6.27	-1.12	-91.07	-80.36	-4.83	-7.2	-54.0	-27.0	-90.0	-36.0	27.0	27.0	T O AT MODULE- CENTER OF CARGO BAY LEVEL 3
9	32.62	-6.27	-1.12	-78.78	-78.49	-30.66	-7.2	-59.5	-45.0	-88.2	-27.0	28.8	31.5	
10	32.52	-8.18	-7.42	-70.81	-75.37	-35.36	-7.2	-59.5	-45.0	-90.0	-27.0	31.5	31.5	
11	32.59	-4.32	-7.66	-66.33	-45.48	-82.65	-27.0	-27.0	-45.0	-88.2	-22.5	34.2	28.8	
12	31.81	-8.65	-8.91	-30.91	5.34	-98.84	-15.3	18.0	-45.0	-90.0	-13.5	37.8	25.2	
13	27.89	-1.43	-12.32	-1.89	7.43	-143.60	12.6	27.0	-87.3	-99.0	-1.8	48.0	25.2	
14	24.91	8.7	-11.91	-4.67	-1.15	-151.31	9.0	21.6	-97.2	-108.0	-1.8	55.8	27.0	
15	19.89	-1.18	-10.13	-4.02	3.05	-153.76	9.0	27.0	-88.2	-123.3	0.0	61.2	27.0	
16	16.32	-2.20	-10.77	-3.28	-1.98	-160.55	13.5	27.0	-83.7	-130.5	9.0	58.5	25.2	
17	14.49	-2.71	-10.38	-5.69	-2.67	-157.47	13.5	27.0	-75.6	-135.0	9.0	58.5	27.0	MODULE PLACED IN DOCKED SATELLITE

LINE	MODULE REPLACEMENT	X	Y	Z	SHOULDER ROLL AT -45 DEG	PITCH	YAW	W-ROLL	W-PITCH	W-YAW	ELBOW	S-ROLL	S-YAW	S-PITCH	COMMENTS
1	46.00	6.84	-6.76	-81.57	7.65	7.79	-37.8	0.	0.	-1.8	-45.0	9.0	9.0	9.0	I C CONDITION- 6 JOINTS AT 0 DEG.
2	42.73	1.74	-9.00	-30.72	-1.47	-14.84	-34.2	1.8	0.	-43.2	-45.0	18.0	27.0	27.0	SHOULDER ROLL LOCKEE
3	37.54	-2.41	7.95	-37.72	-18.45	-23.41	12.6	9.0	0.	-70.2	-45.0	22.5	22.5	22.5	AT -45 DEG
4	32.46	-6.36	-3.86	157.25	-106.61	127.89	20.7	-36.0	-36.0	-90.0	-45.0	18.0	18.0	36.0	
5	32.09	-8.54	1.32	25.31	-86.71	-113.24	18.0	-43.2	-42.3	-90.0	-45.0	18.0	18.0	28.8	
6	32.03	-8.54	2.33	129.68	-86.74	-133.56	99.0	-43.2	-42.3	-90.0	-45.0	18.0	18.0	27.8	
7	32.52	-8.31	3.54	144.21	-84.50	-142.24	10.5	-43.2	-42.3	-88.2	-45.0	18.0	18.0	24.3	
8	32.46	-8.31	4.05	144.79	-83.76	-147.29	99.0	-43.2	-42.3	-88.2	-45.0	18.0	18.0	23.4	
9	32.57	-8.31	3.03	154.47	-86.52	-152.57	103.5	-45.0	-45.0	-42.3	-45.0	18.0	18.0	25.2	
10	32.56	-8.31	-3.13	54.66	-79.93	-50.64	108.2	-38.7	-38.7	-42.3	-45.0	18.0	18.0	36.0	
11	32.55	-4.71	-8.76	132.23	-45.99	-123.06	126.0	-4.8	-4.8	-73.8	-88.2	-45.0	25.2	45.0	
12	32.71	-2.86	-12.13	92.43	-1.64	-119.30	90.0	43.2	43.2	-81.0	-83.7	-45.0	27.8	48.6	
13	31.29	-1.89	-11.95	-4.15	10.89	-120.25	-4.5	52.2	52.2	-81.0	-90.0	-45.0	31.5	49.5	
14	28.03	-8.82	-12.05	-8.73	3.14	-131.74	18.0	43.2	43.2	-91.8	-99.0	-45.0	37.8	55.8	
15	25.79	1.02	-9.84	-12.16	-4.41	-145.11	-27.0	27.0	-101.7	-108.0	-45.0	46.8	46.8	55.8	
16	21.59	.70	-10.29	-6.74	2.55	-146.94	-18.0	36.0	36.0	-99.0	-118.8	-45.0	52.2	63.8	
17	16.56	-3.11	-10.13	-4.04	.64	-149.72	-18.0	45.0	45.0	-90.0	-130.5	-45.0	48.0	72.0	
18	14.76	-4.06	-9.44	-2.52	2.19	-152.17	-20.7	49.5	49.5	-90.0	-135.0	-45.0	48.3	77.7	MODULE PLACED IN DOCKED SATELLITE

LINE	MODULE REPLACEMENT (6-DOF)			T D AT MODULE- CENTER OF CARGO BAY LEVEL 3										COMMENTS
	X	Y	Z	ROLL	PITCH	YAW	W-ROLL	W-PITCH	W-YAW	ELBOW	S-ROLL	S-YAW	S-PITCH	
1	46.81	2.95	0.	0.	0.	.00	0.	0.	C.	-7.2	0.	7.2	0.	I C CONDITION- ALL JOINTS= 0 DEG
2	43.61	-2.74	0.	0.	-27.00	-25.20	0.	-27.0	0.	-43.2	0.	16.0	0.	
3	40.36	-2.54	0.	0.	-45.00	-47.70	0.	-45.0	0.	-61.2	0.	27.0	0.	
4	34.73	-6.06	0.	14.40	-49.50	-20.70	1.4	-49.5	-13.5	-82.8	0.	31.5	0.	
5	30.15	-7.13	3.33	21.14	-60.07	-17.03	18.0	-54.0	46.8	-97.2	0.	36.0	-6.3	
6	29.32	-6.78	4.64	23.84	-68.96	-18.79	18.0	-60.3	49.5	-99.0	0.	38.0	-9.0	
7	29.18	-9.14	5.57	70.05	-84.99	-52.58	33.3	-75.6	49.5	-97.2	0.	31.5	-10.8	
8	29.18	-9.14	5.57	54.75	-84.99	-52.58	18.0	-75.6	49.5	-97.2	0.	31.5	-10.8	
9	29.18	-9.14	5.57	49.35	-84.99	-52.58	1.6	-75.6	49.5	-97.2	0.	31.5	-10.8	
10	29.02	-9.43	.91	47.38	-88.87	-47.36	18.0	-87.3	49.5	-99.0	0.	34.2	5.4	
11	29.31	-8.05	-2.77	3.60	-84.60	-0.00	2.6	-90.0	46.8	-99.0	0.	38.5	-1.8	
12	28.68	-6.54	-4.57	-14.09	-70.92	-58.29	14.4	-73.8	-22.5	-100.8	0.	37.8	9.8	
13	29.80	-3.35	-5.69	25.40	-46.50	-165.15	28.8	-36.0	-111.6	-99.0	0.	43.2	18.8	
14	30.25	-3.41	-6.26	-5.10	-34.74	-164.89	-1.8	-23.4	-111.6	-97.2	0.	42.3	11.7	
15	26.76	-2.21	-8.69	-15.75	.67	-164.61	-10.8	18.0	-106.2	-106.2	0.	48.6	18.0	
16	20.53	-1.38	-7.76	-17.41	6.13	-158.01	-9.0	25.2	-93.0	-134.2	0.	58.5	20.7	
17	17.97	-2.71	-9.62	-9.62	1.63	-160.84	0.	27.0	-86.4	-128.7	0.	56.7	27.0	
18	14.93	-4.30	-7.61	-3.21	3.68	-159.59	7.2	28.8	-73.8	-136.8	0.	54.0	27.0	MODULE PLACED IN DOCKED SATELLITE

POSITION (FT)

DEGREES

LINE	PLACEMENT IN CARGO BAY - CONCEPT NUMBER 7 (6-DOF)				COMMENTS
	X	Y	Z	ROLL	
1	-29.54	22.35	-8.58	-180.00	180.00
2	-18.50	22.58	-9.53	153.00	-180.00
3	-9.97	20.53	-9.07	137.73	78.00
4	-1.84	22.26	-11.64	122.10	71.45
5	3.93	23.15	-12.10	94.50	165.90
6	3.33	23.53	-12.10	100.80	180.00
7	15.96	16.94	-15.80	133.06	72.00
8	21.39	13.23	-15.96	134.64	71.34
9	26.09	13.68	-20.24	165.26	69.37
10	29.68	11.75	-20.28	167.39	43.59
11	33.42	6.21	-21.48	165.23	3.04
12	36.89	-5.65	-14.61	-14.49	-30.71
13	38.64	-7.58	-9.28	108.07	-181.53
14	37.36	-7.80	-4.72	80.10	85.19
15	36.69	-7.62	-2.89	80.10	-32.86
				-95.50	-82.80
					-00
					-00

I C CONDITION- 75 PER OF FULL PORT TRAVEL

SATELLITE IN CARGO BAY

POSITION (FT)

DEGREES



## APPENDIX F - MECHANICAL DESIGN OF MASTER AND SLAVE OF 2 DOF BREADBOARD

Two simple, breadboard-type test mechanism arms were designed to provide a tool for proving the control equations of a six degree-of-freedom, bilateral, force-reflecting tele-operator/manipulator system. The requirements were stipulated by the control system engineers as a minimum for proving the feasibility of the concept.

The master arm has two 11-in. segments and the slave, two 22-in. segments. All joints are similar. Design details are shown in Figure III-21, and the final product is depicted in Figure III-5.

Normally the devices will be mounted with the arm plates parallel to the floor or ground. The arms are not designed to take any additional vertical tip load, only the weight of the arm itself. In the horizontal plane, a tip force of up to about 8 lb can be developed on the short (master) arm and about 7 lbs on the large (slave) arm when both arms are in the fully extended position, neglecting small friction losses. These forces will be sufficient to demonstrate the bilateral servo control system. The joints themselves were designed using 100:1 or less simple spur gearing to assure a backdriving capability. No brake system or limit stops were provided.

Many motors and generators were investigated. It was concluded that a self-contained, packaged motor and generator unit available from Inland Motor Company would be the least expensive, yet provide suitable torque and speed characteristics for use with the servo control electronics. The selected motors have a torque rating of 54 in-oz at stall.

The gears have been designed to accommodate 30% greater loads than the motor stall torque, but they will not take severe impact loads.

Inertias of the joint members and outer arm have been calculated and frictional characteristics were also investigated.

The maximum backdriving torque at any joint has been calculated to be between 1.5 and 2.2 ft-lb based on a motor starting frictional torque of 3.3 in-oz. The dynamic friction should be less than half of this.

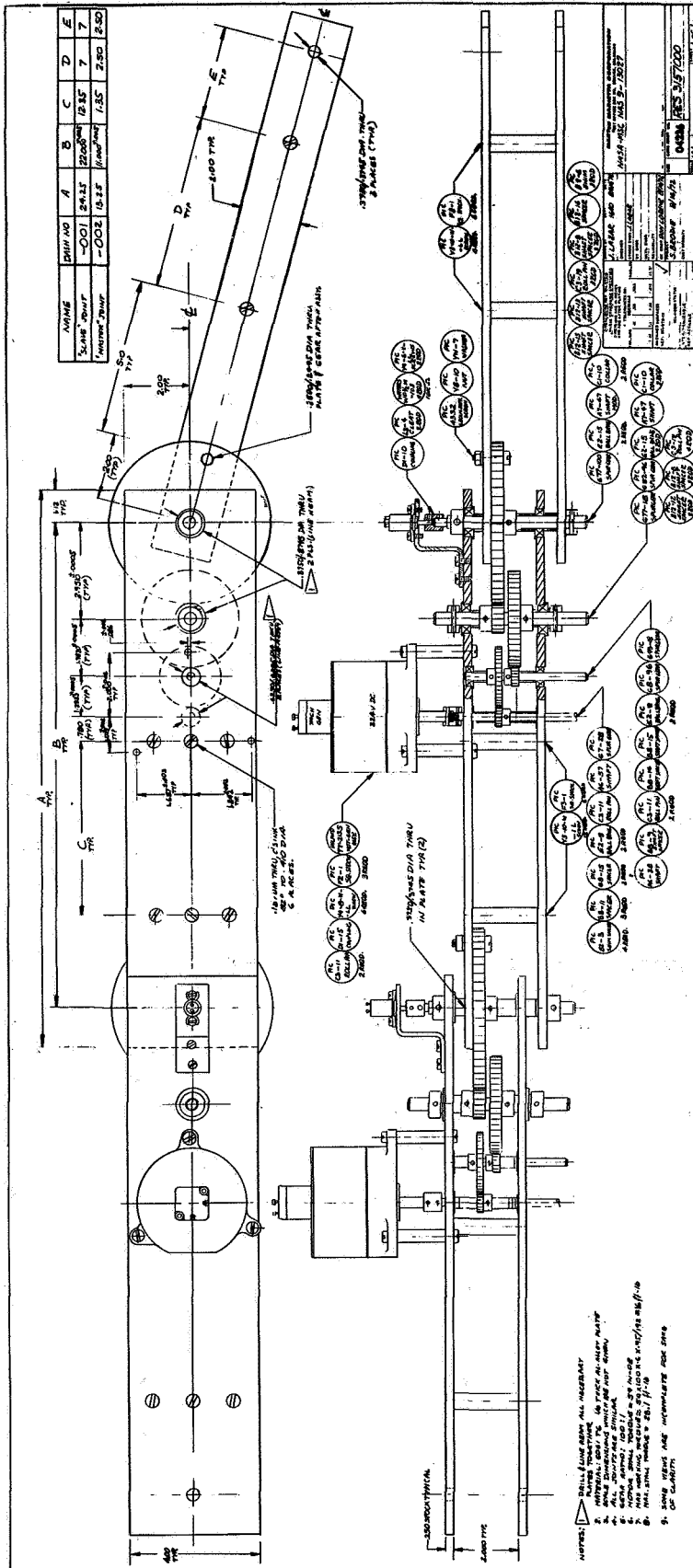


Figure III-21 Schematic of Two Degree of Freedom Breadboard Arms

## 1. Requirements

A list of requirements for mechanically designing the breadboard arms and joints is presented below. Some of the items were generated at the outset of the program; others evolved as the design progressed.

1. The design shall include two simple breadboard manipulator arms, one master and one slave, each of which is electrically driven.
2. The master shall be capable of controlling the slave's tip position within  $\pm 1/16$  in., excluding gear backlash effects. This is equivalent to an accuracy of approximately 10 minutes of arc and relates primarily to the selection of position potentiometers and control electronics.
3. To obtain size disparity, the slave arm shall be at least twice as long as the master arm.
4. Arms shall operate only in the horizontal plane (no motion against gravity).
5. No terminal device is required.
6. Torques at joints shall be at least 25 ft-lb.
7. The master arm shall be capable of exerting a tip force of at least 8 lb.
8. When no load is applied, the shaft speed at the rated output capability of the gear train shall be 1.5 rad/sec.
9. Backlash should be kept to a minimum.

## 2. Design Summary

### a. Components:

Motor: Inland Motor Company Model NT2173; operating voltage = 22.8 V. - Integrally packaged.

Tach. Generator: Inland Motor Company Model TG0714

Potentiometers: Slave-20 turn, infinite resolution;  
Master 20 turn, infinite resolution

Gears: Straight spur gears

Gear Ratio:

Master Shoulder - 62:1  
Master Elbow - 29:1  
Slave Shoulder - 100:1  
Slave Elbow - 100:1

Gear Meshes: Output gears: Pitch = 20, pressure  
angle = 20°, Ratio = 5.56:1  
Intermediate gears: Pitch = 32,  
pressure angle = 20°, Ratio = 5.33:1  
Input (motor) gears: Pitch = 48,  
pressure angle = 20°, Ratio = 3.42:1

Bearings: Flanged ball bearings  
Double shield

Arm Plates: 6061 T-6 aluminum alloy, 1/4 in. thick.

Standoffs: 2-in.-long x 0.50-in. x 0.50-in. aluminum  
alloy

Mounting: Optional - Clamped or bolted to table or wall

3. Design Data

Inertias: Look-in or backdrive inertia of gear train  
joint = 7.08 in.-lb sec<sup>2</sup>

Torques/Forces: Maximum stall torque = 28 ft-lb

Calculated Data: Full load condition (not including  
motor stiction)

Static Efficiency: Backdrive = 92.8%  
Forward drive = 98.0%

Dynamic Efficiency: Backdrive = 95.6%  
Forward drive = 98.5%

Backlash: 3.7 minutes of arc, calculated

Estimated Backdriving Torque:

Static: 1.7 to 2.2 ft-lb with motor

Dynamic: 0.5 - 1.0 ft-lb with motor

4. Test Data (Using Torque Watches)

Actual Backdriving Torque:

Static: Approximately 10 to 11 in. oz without motor; 315-350 in oz with motor and tach gen.

Drive Shaft (Less Motor):

Static: Approximately 0.1 in. oz breakaway

Backlash: (See Page III-104)

5. Design Approach

a. Design Philosophy - The basic approach was to develop a simple design with standard components. In our design, both the master and slave arms use similar joints. The gears are housed between two flat plates whose bearing holes were simultaneously line-reamed to ensure parallel mounting of the shafts. These plates were used not only to support the gear train, but also to act as arm segments and provide structural support. Both the master and slave arms were built so that they can accept extra degrees of freedom if the necessity arises during the later stages of the control study. A disadvantage of the system is that the connecting plates produce a high arm inertia.

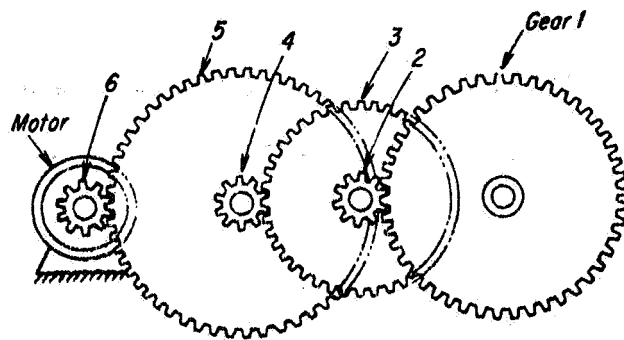
b. Accessibility and/or Interchangeability - Should the requirement arise, the gears can easily be exchanged to achieve a joint gear ratio higher or lower than the present 100:1. The joints are not encased and the gears can easily be cleaned if necessary.

c. Lubrication - We anticipate that the gear teeth and ball bearings may require periodic light lubrication.

1. Bearings are to be greased with MIL-G3278
2. Gears are to be lubricated with MIL-L6085A or an equivalent light oil.

d. Theoretical Gear Train Efficiency Under Full Load

Note: All gears have a 20° pressure angle.



100:1

Name	No.	Pitch Diameter, in.	Outside Diameter, in.	Face Width, in.	Gear Material	Ratio
Gear	1	5.000	5.100	0.375	CRS*	5.560
Pinion	2	0.900	1.000	0.375	CRS	
Gear	3	3.000	3.062	0.375	Bronze	5.333
Pinion	4	0.5625	0.625	0.187	CRS	
Gear	5	2.000	2.042	0.187	Aluminum	3.452
Pinion	6	0.5833	0.625	0.187	CRS	
* Corrosion-resistant steel						

### Theoretical Forward Drive Efficiency

$$K = \frac{W_t}{FD} \left( \frac{N+1}{N} \right)$$

$$V = 0.2618 DN$$

$$H_s = \left( \frac{N+1}{N} \right) \left( \sqrt{\frac{r_o}{r} - \cos^2 \theta} - \sin \theta \right)$$

$$H_t = (N+1) \left( \sqrt{\frac{R_o}{R} - \cos^2 \theta} - \sin \theta \right)$$

$$P = \frac{50F}{\cos \theta} \left( \frac{H_s^2 + H_t^2}{H_s + H_t} \right)$$

$$E = 100 - P$$

where

K = load factor

$W_t$  = tangential tooth load, lbs

N = gear ratio of mesh

n = pinion speed

F = face width of gear, in.

D = diameter of gear, in.

V = pitch line velocity, ft/minute

$H_s$  = sliding velocity to pitch line velocity ratio (start to approach)

$H_t$  = sliding velocity to pitch line velocity ratio (recess action)

$r_o$  = radius of pinion, in.

r = pitch radius of pinion, in.

$\theta$  = pressure angle of gear ( $20^\circ$  for all joints)

$R_o$  = Radius of gear, in.

R = pitch radius of gear, in.

f = coefficient of friction

P = power loss, %

E = efficiency, %

\*E.E. Shipley: "How to Predict Efficiency of Gear Trains." Product Engineering Journal

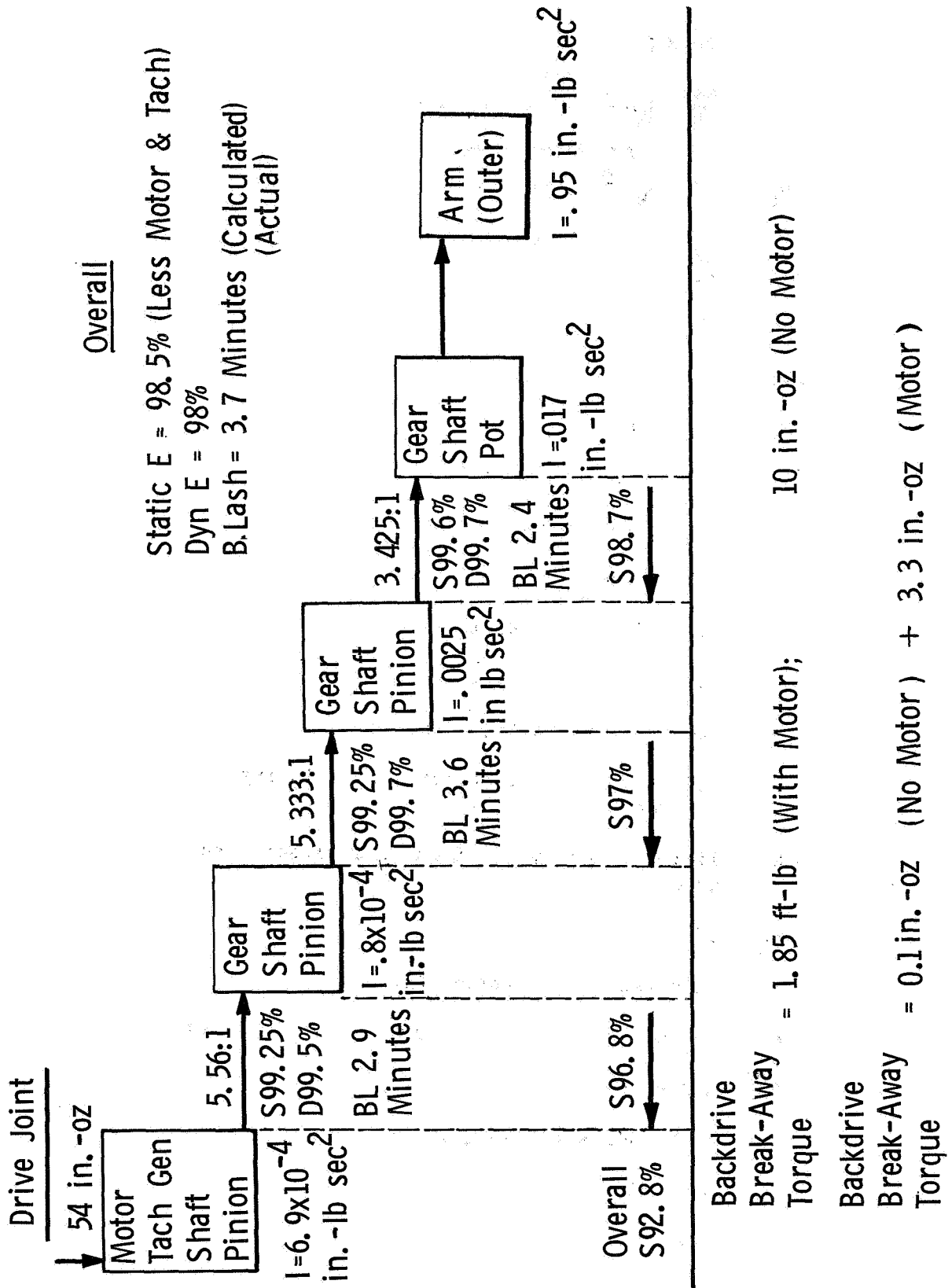


Figure III-22 Gearing Characteristics of Two DOF Breadboard Arms



e. Forward Drive Dynamic Efficiency

Mesh 1,2 :  $V_{\text{Rated}} = 11.2 \text{ ft/minute}$ ; using Shipley's chart,

$$K_{\text{Rated}} = 600, f = 0.053$$

$$\left. \begin{array}{l} H_s = 0.151 \\ H_t = 0.496 \end{array} \right\} \text{At maximum rated load \& speed}$$

$$P = 0.496$$

$$E = 99.50\%$$

Mesh 3,4 :  $K = 583, V = 37 \quad f = 0.051$

$$H_s = 0.162$$

$$H_t = 0.1835$$

$$P = 0.47\%$$

$$E = 99.53\%$$

Mesh 5,6 :  $K = 173, V = 134 \quad f = 0.043$

$$H_t = 0.1371$$

$$H_s = 0.123$$

$$P = 0.298\%$$

$$E = 99.7\%$$

Overall dynamic efficiency at full-load (rated) condition = 98.5%

f. Forward Drive Efficiency at Startup (slow speed) considering  
higher friction factors:

$$\text{Mesh 1,2} = 99.25\%$$

$$\text{Mesh 3,4} = 99.25\%$$

$$\text{Mesh 5,6} = 99.60\%$$

$$\text{Overall static efficiency} = 98\%$$

g. Backdrive Efficiency (At a rated load of 28 ft-lb and an angular  
velocity of 0.90 rad/sec for dynamic consideration)

Mesh 1,2 :  $K = 80$ ,  $V = 0$ ,  $f = 0.070$ ; ( $f$  includes static friction additive of 0.025)

$$H_s = 0.0354$$

$$H_t = 0.890$$

$$P = 3.17\%$$

$$E = 96.83\%$$

Mesh 3,4 :

$$E = 96.97\%$$

Mesh 5,6 :  $f = 0.060$

$$P_L = 1.245\%$$

$$E = 98.75\%$$

Overall static efficiency of gear train = 92.8%

#### h. Backdrive Dynamic Efficiency

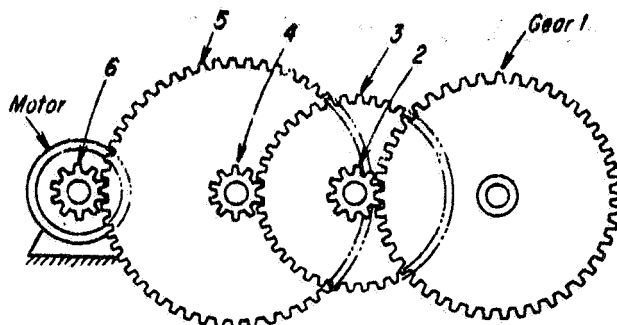
$$\text{Mesh 1,2} = 98.76\%$$

$$\text{Mesh 3,4} = 97.0\%$$

$$\text{Mesh 5,6} = 96.8\%$$

Overall dynamic efficiency = 95.6%

#### i. Projected Backlash Calculations



$\Delta C$  = Center Distance Change (Bending + Tolerances)

$$\Delta C_1 = 0.003 \text{ in.}$$

$$\Delta C_2 = 0.002 \text{ in.}$$

$$\Delta C_3 = 0.002 \text{ in.}$$

$$B = \frac{2 \tan \phi \Delta C}{R_G} \times 180 \times 60$$

where  $B$  = backlash, arc-minutes

Consider rated load:

$$\text{Mesh 1} \quad B_1 = \frac{0.728}{2.5} \times 0.003 \times 3438 = 2.90$$

$$\text{Mesh 2} \quad B_2 = \frac{0.728}{1.5} \times 0.002 \times 3438 = 3.57$$

$$\text{Mesh 3} \quad B_3 = \frac{0.728}{1.0} \times 0.002 \times 3438 = 2.37$$

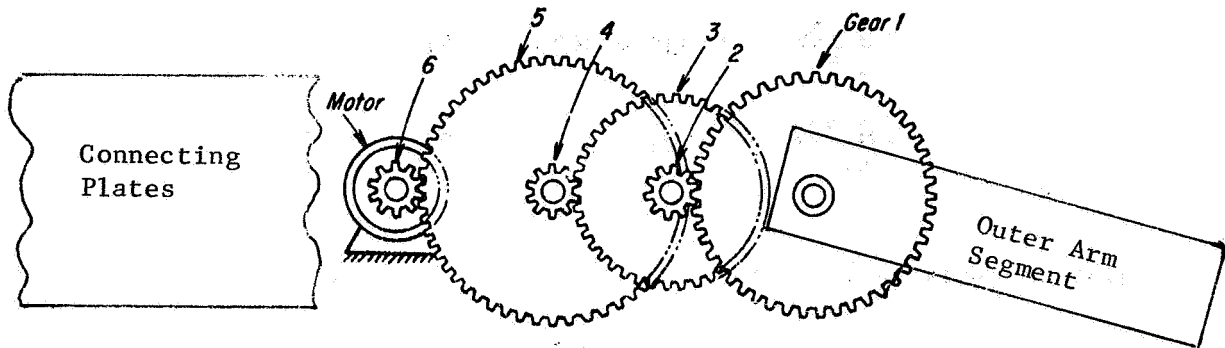
Backlash of power gear:

$$B_{1-3} = 2.90 + \frac{3.57}{5.56} + \frac{2.37}{5.56 \times 5.33}$$

$$= 3 \text{ minutes } 40 \text{ seconds.}$$

## 6. Calculated Inertias (Summary)

The inertia calculations included herein do not include all members.



$$I_1 \text{ (Power Shaft)} = 170.5 \times 10^{-4} \text{ in-lb-sec}^2 \text{ (arm not included)}$$

$$I_2 \text{ (Gears 2 \& 3 + Shaft)} = 24.75 \times 10^{-4} \text{ in-lb-sec}^2$$

$$I_4 \text{ (Gear 4 \& 5 + Shaft 4)} = 0.80 \times 10^{-4} \text{ in-lb-sec}^2$$

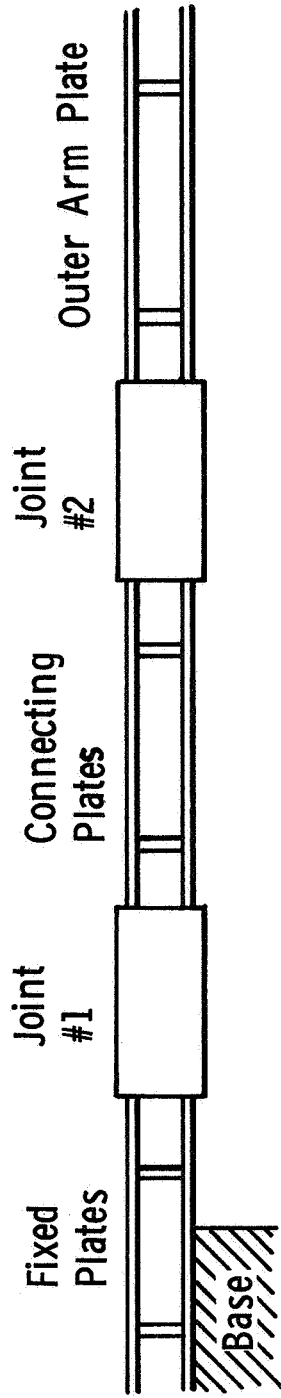
$$I_6 \text{ (Motor Rotor + Shaft)} = 6.92 \times 10^{-4} \text{ in-lb-sec}^2$$

To obtain  $I$  ("look-in" inertia) we multiply by the square of the gear ratio;

$$I \text{ ("look-in-" inertia)} = \{ 170.5 + 24.7 (5.56)^2 + 0.8 (5.56 \times 5.33)^2 + 6.9 (100)^2 \} \times 10^{-4} = 7.08 \text{ in lb sec}^2$$

$$I \text{ (Outer Arm Segment)} = 0.95 \text{ in-lb-sec}^2 \text{ (about power shaft) (slave)}$$

Weight Summary			
Slave Arm, lb		Master Arm, lb	
Power Shaft + Gear 1 =	2.264		2.26
Shaft 2 + Gears =	1.1		1.1
Shaft 4 + Gears =	0.13		0.13
Shaft 6 + Gear =	0.13		0.12
Motor + Generator =	3.00		3.00
Arm + Spacer =	2.40		1.31
Connecting Plates + Bars	5.16		2.82
Total	14.18 lb		10.74 lb



F-13

$$\text{Slave:} \quad 5.16 + 3(\text{Motor}) + 5.16 + 3(\text{Motor}) + 2.4 = 25.96 \text{ lb}$$

$$3.62 (\text{Other}) + 3.62 (\text{Other})$$

$$\text{Master:} \quad 2.82 + 3(\text{Motor}) + 2.82 + 3(\text{Motor}) + 1.31 = 20.19 \text{ lb}$$

$$3.62 (\text{Other}) + 3.62 (\text{Other})$$

Figure III-23 Weight Summary of Two DOF Breadboard Arms

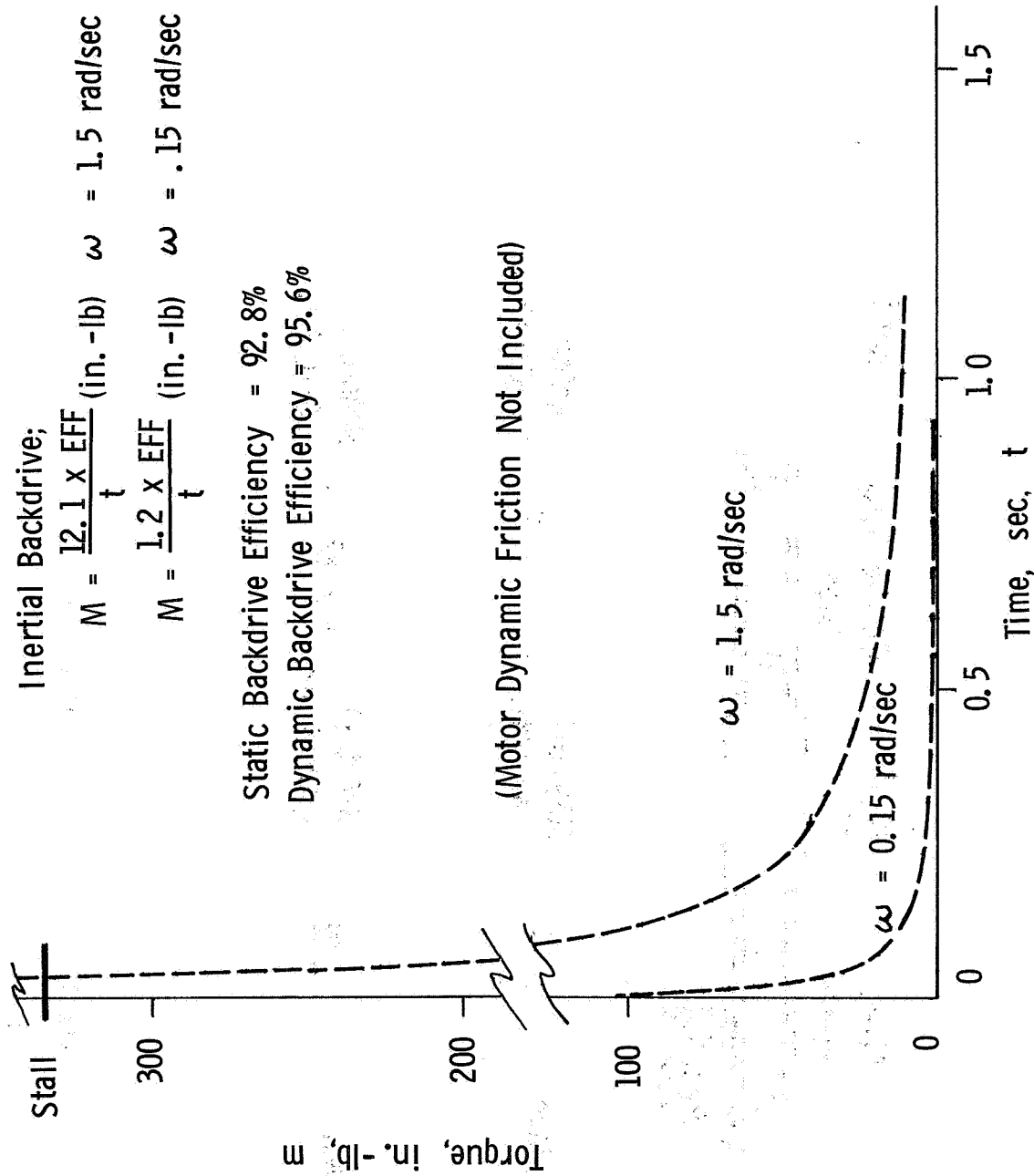


Figure III-24 Backdrive Characteristics of Breadboard Arm Joint

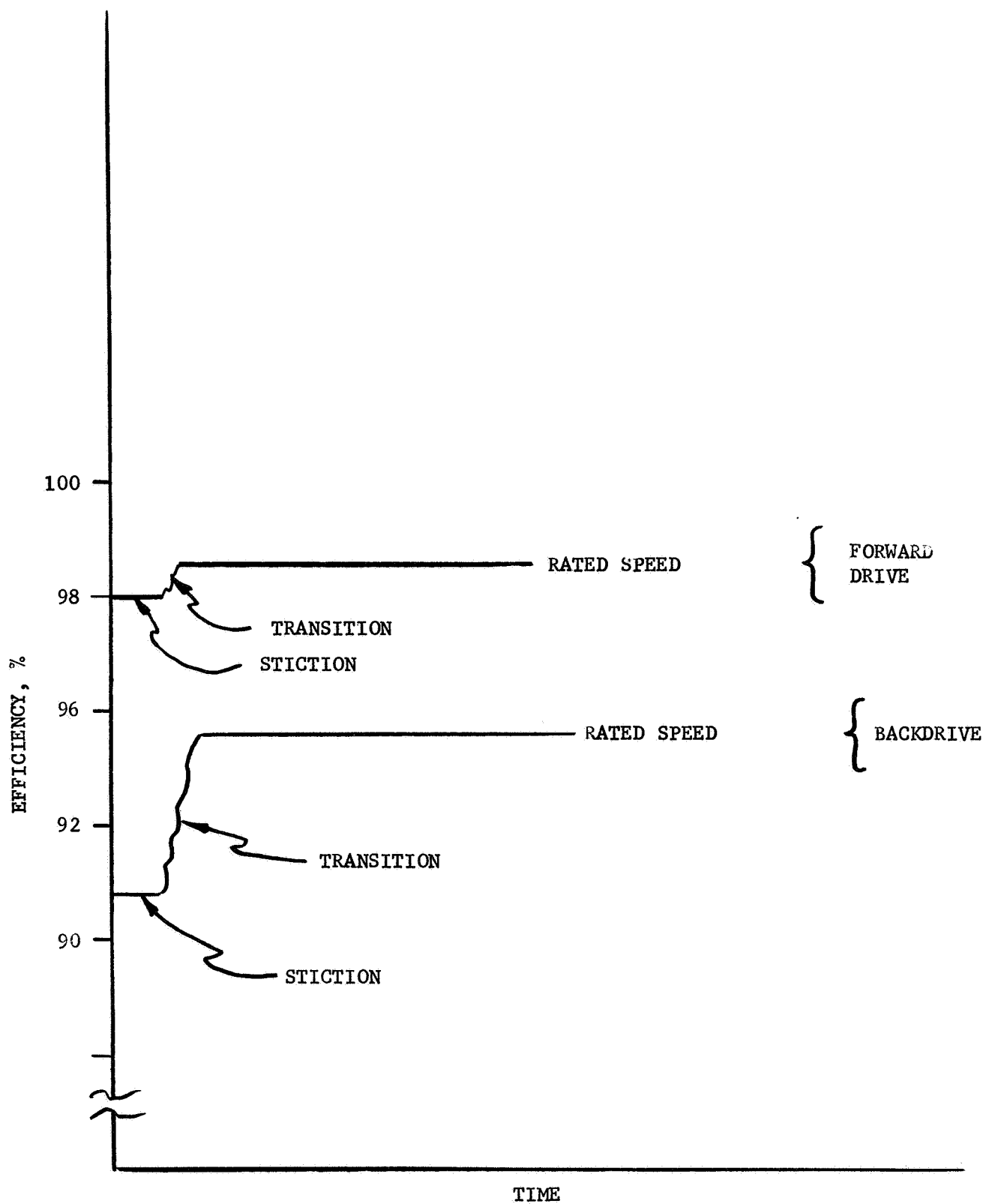


Figure III-25 Forward and Backdrive Characteristics of Breadboard Arm Joint

## 8. Air Bearing Inertia Load

An inertia load of approximately 300 lbs as free from friction as possible was required to simulate payloads on the end of the 2 DOF Breadboard manipulator arm. It was desired to employ this load for horizontal use on the same table area that the 2 DOF system was installed.

Ball bearings, air bearings and a suspended counterbalanced support system were considered. Ideally, a three air bearing system would be desirable however space on the table was limited and small air pads are not readily available. It was questionable that a single air bearing would give sufficient stability, however, a simple test of a proven air pad from one of our existing air pad simulators showed that with careful air supply regulation the stability was excellent.

The following design evolved which allowed the mass to be used on the existing test table and beneath the arm tip.



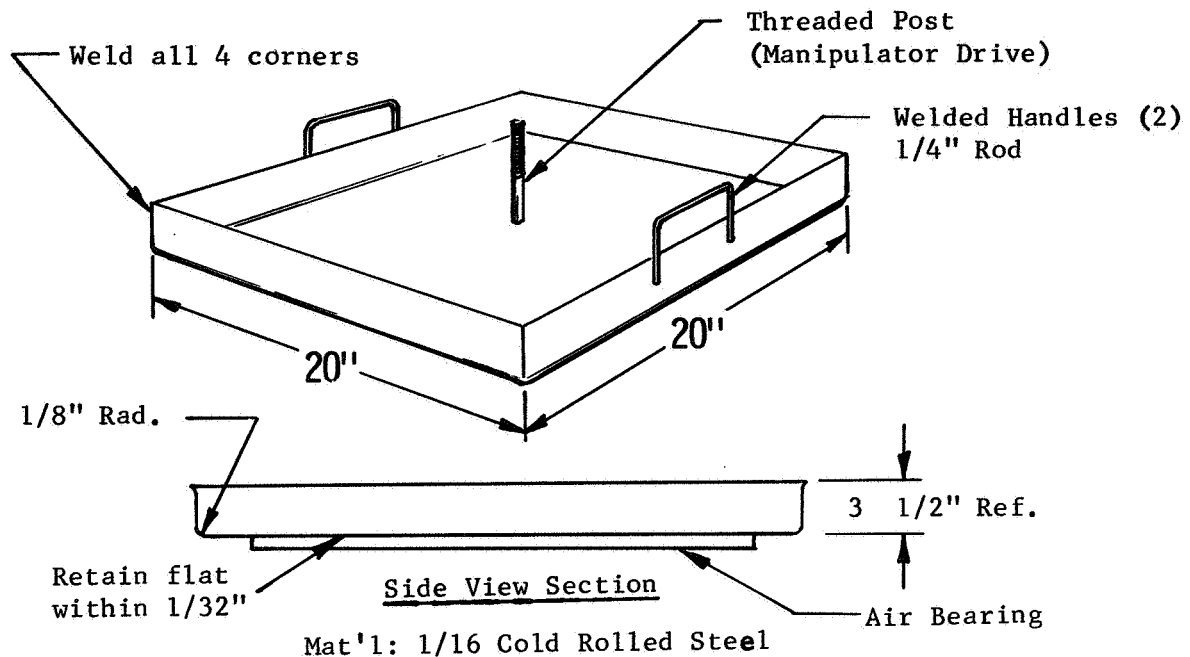


Figure III-26 Pan and Air Bearing Design

Weight (Lead Shot)

$$= .215 \text{ lb/in}^3 \text{ (density for lead shot)}$$

$$\text{Required } \frac{300 \text{ lb}}{.215 \frac{\text{lb}}{\text{in}^3}} = 1400 \text{ in}^3$$

$$\text{Pan Volume} = 20 \text{ in} \times 20 \text{ in} \times 3.5 \text{ in} = 1400 \text{ in}^3$$

Air Bearing Pad

$$\text{Effective diameter} = 12 \text{ in}$$

$$\text{Area} = 113 \text{ in}^2$$

$$\text{Air pressure required} = \frac{300}{113} = 2.65 \text{ psi}$$

This is easily supplied and regulated from shop air. Travel capability on the Masonite covered table is approximately  $\pm 18$  in. in X and Y axes.